ACS SYMPOSIUM SERIES 1119

# Nanomaterials for Biomedicine

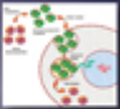

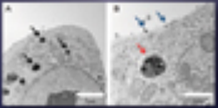

EDITED BY

**Ramanathan Nagarajan**

Downloaded by UNIV OF ALABAMA BIRMINGHAM on December 8, 2012 | http://pubs.acs.org
Publication Date (Web): December 7, 2012 | doi: 10.1021/bk-2012-1119.fw001

# Nanomaterials for Biomedicine

In Nanomaterials for Biomedicine; Nagarajan, R.;
ACS Symposium Series; American Chemical Society: Washington, DC, 2012.

Downloaded by UNIV OF ALABAMA BIRMINGHAM on December 8, 2012 | http://pubs.acs.org
Publication Date (Web): December 7, 2012 | doi: 10.1021/bk-2012-1119.fw001

ACS SYMPOSIUM SERIES **1119**

# Nanomaterials for Biomedicine

**Ramanathan Nagarajan**, Editor
*Molecular Sciences and Engineering Team*
*Natick Soldier Research Development & Engineering Center*
*Natick, Massachusetts*

Downloaded by UNIV OF ALABAMA BIRMINGHAM on December 8, 2012 | http://pubs.acs.org
Publication Date (Web): December 7, 2012 | doi: 10.1021/bk-2012-1119.fw001

**Sponsored by the**
**ACS Division of Colloid and Surface Chemistry**

American Chemical Society, Washington, DC

Distributed in print by Oxford University Press, Inc.

Downloaded by UNIV OF ALABAMA BIRMINGHAM on December 8, 2012 | http://pubs.acs.org
Publication Date (Web): December 7, 2012 | doi: 10.1021/bk-2012-1119.fw001

**Library of Congress Cataloging-in-Publication Data**

Nanomaterials for biomedicine / Ramanathan Nagarajan, editor ; Molecular Sciences and Engineering Team, Natick Soldier Research Development & Engineering Center, Natick, Massachusetts ; sponsored by the ACS Division of Colloid and Surface Chemistry.
pages cm. -- (ACS symposium series ; 1119)
Includes bibliographical references and index.
ISBN 978-0-8412-2718-7
1. Nanomedicine. 2. Nanostructured materials--Health apects. 3. Biomedical engineering. I. Nagarajan, R. (Ramanathan), editor of compilation. II. U.S. Army Natick Soldier Research Development & Engineering Center. Molecular Sciences and Engineering Team. III. American Chemical Society. Division of Colloid and Surface Chemistry, sponsoring body.
R857.N34N352 2013
610.28--dc23
2012042532

The paper used in this publication meets the minimum requirements of American National Standard for Information Sciences—Permanence of Paper for Printed Library Materials, ANSI Z39.48n1984.

Copyright © 2012 American Chemical Society

Distributed in print by Oxford University Press, Inc.

All Rights Reserved. Reprographic copying beyond that permitted by Sections 107 or 108 of the U.S. Copyright Act is allowed for internal use only, provided that a per-chapter fee of $40.25 plus $0.75 per page is paid to the Copyright Clearance Center, Inc., 222 Rosewood Drive, Danvers, MA 01923, USA. Republication or reproduction for sale of pages in this book is permitted only under license from ACS. Direct these and other permission requests to ACS Copyright Office, Publications Division, 1155 16th Street, N.W., Washington, DC 20036.

The citation of trade names and/or names of manufacturers in this publication is not to be construed as an endorsement or as approval by ACS of the commercial products or services referenced herein; nor should the mere reference herein to any drawing, specification, chemical process, or other data be regarded as a license or as a conveyance of any right or permission to the holder, reader, or any other person or corporation, to manufacture, reproduce, use, or sell any patented invention or copyrighted work that may in any way be related thereto. Registered names, trademarks, etc., used in this publication, even without specific indication thereof, are not to be considered unprotected by law.

PRINTED IN THE UNITED STATES OF AMERICA

Downloaded by UNIV OF ALABAMA BIRMINGHAM on December 8, 2012 | http://pubs.acs.org
Publication Date (Web): December 7, 2012 | doi: 10.1021/bk-2012-1119.fw001

# Foreword

The ACS Symposium Series was first published in 1974 to provide a mechanism for publishing symposia quickly in book form. The purpose of the series is to publish timely, comprehensive books developed from the ACS sponsored symposia based on current scientific research. Occasionally, books are developed from symposia sponsored by other organizations when the topic is of keen interest to the chemistry audience.

Before agreeing to publish a book, the proposed table of contents is reviewed for appropriate and comprehensive coverage and for interest to the audience. Some papers may be excluded to better focus the book; others may be added to provide comprehensiveness. When appropriate, overview or introductory chapters are added. Drafts of chapters are peer-reviewed prior to final acceptance or rejection, and manuscripts are prepared in camera-ready format.

As a rule, only original research papers and original review papers are included in the volumes. Verbatim reproductions of previous published papers are not accepted.

**ACS Books Department**

Downloaded by UNIV OF ALABAMA BIRMINGHAM on December 8, 2012 | http://pubs.acs.org
Publication Date (Web): December 7, 2012 | doi: 10.1021/bk-2012-1119.pr001

# Preface

This book results from the symposium "Nanomaterials for Biological, Pharmaceutical and Biomedical Applications" held at the 240th ACS National Meeting in Boston, MA on August 22–26, 2010. The symposium was sponsored by the ACS Division of Colloid and Surface Chemistry as part of its continuing symposia series on nanoscience and nanotechnology. The symposium included technical sessions devoted to synthesis of nanoparticles, biomolecular functionalization of nanoparticles, nanoparticle for detection of biomolecules and cells, applications of gold nanoparticles, applications of magnetic nanomaterials, nanoparticle-cell interactions, polymer nanoparticles for drug delivery, and nanoparticle applications in gene delivery, diagnostic imaging, molecular diagnostics, therapeutics, etc. Over 90 papers were presented at this symposium, and the book chapters represent a sampling of problems addressed.

The application of nanoparticles to biomedicine has become a distinct and extremely active area of scientific and technological development over the last ten years. A Web of Science keyword search reveals the dramatic increase in the number of studies related to applications of nanoparticles for drug delivery and imaging over the last decade, the correspondingly increasing investigations of nanoparticle toxicity, and a growing interest in nanoparticles for combined diagnostics and therapeutics. The entry for 2012 in Table 1 covers only the first nine months and indicates that the growth in research publications continues at the same rapid rate.

The use of nanomaterials for biomedicine seeks to take advantage of the size, shape, and large specific surface area characteristics that are intrinsic to nanomaterials. The large enough volume of nanoparticles compared to the molecular scale of typical drugs allows the nanoparticles to be carriers of a large load of drugs or imaging agents. The large specific surface area of the nanoparticles and our ability to functionalize and modify the surface properties allows for many advantages to be derived from use of nanomaterials. Drugs or imaging agents can be easily conjugated chemically to the nanoparticles to improve the stability of the drug in the nanocarriers. Nanoparticles can incorporate more than one kind of imaging or therapeutic agents, making them potential multifunctional systems for both medical diagnosis and therapy. Specific targeting of tissues and organs can be realized with multiple targeting agents connected to the nanoparticle surface, providing strength of target binding as well as high specificity for the target. Many methods of surface modification have been developed to improve the circulation time of nanoparticles and to prevent their uptake and removal by the reticuloendothelial system. The use of nanomaterials as carriers is also stimulated by the potential for improved drug stability, solubility, and bioavailability, improved pharmacokinetics, and reduced immunogenicity.

**Table 1. Web of Science Keyword Search**

| *Key Words for Search* | *Web of Science Hits for Search Year* | | | | | | |
|---|---|---|---|---|---|---|---|
| | *2001* | *2003* | *2005* | *2007* | *2009* | *2011* | *2012* |
| Nanoparticles AND Drug Delivery | 126 | 215 | 504 | 1034 | 2062 | 3405 | 2889 |
| Nanoparticles AND Imaging | 158 | 319 | 639 | 1297 | 2143 | 3260 | 2353 |
| Nanoparticles AND Diagnostics | 19 | 30 | 101 | 177 | 337 | 518 | 410 |
| Nanoparticles AND Therapeutics | 1 | 6 | 39 | 91 | 182 | 361 | 271 |
| Nanoparticles AND Theranostics | 0 | 0 | 0 | 0 | 8 | 56 | 59 |
| Nanoparticles AND Toxicity | 7 | 31 | 103 | 320 | 834 | 1545 | 1274 |

A wide variety of nanomaterials, incorporating numerous types of surface modifications, has been developed and advanced for biomedical applications. Examples include dendrimers, fullerenes, liposomes, superparamagnetic particles, colloidal gold particles, polymeric nanoparticles, block copolymer micelles, gold nanoshells, quantum dots, polyelectrolyte multilayer capsules, virus particles, etc. Given the extent of research intensity in this field, no single book can pretend to summarize the state of the art or be comprehensive to cover all advances. The present book takes a snapshot of research in this vibrant field and gives a sampling of important nanomaterials that are being developed and their applications.

Chapter 1 describes a novel nanostructure, named the spherical nucleic acid (SNA), investigated for over 15 years by the Mirkin group. Spherical nucleic acids consist of a metal or metal oxide nanoparticle core and a densely functionalized, highly oriented nucleic acid (DNA or RNA) shell. They display a sharp melting transition compared to free nucleic acids, significantly higher binding constants for free complementary oligonucleotide strands compared to free DNA of the same sequence, enhanced resistance to many forms of enzymatically enhanced cleavage, and ease of cell entry. Their highly oriented and densely packed spherical structures renders them capable of interacting with biological materials in unique ways, allowing for their use in molecular diagnostics, gene regulation, and nanomedicine. This chapter descries the methods of preparation of SNAs, their characterization, and potential nanomedicine applications.

Downloaded by UNIV OF ALABAMA BIRMINGHAM on December 8, 2012 | http://pubs.acs.org
Publication Date (Web): December 7, 2012 | doi: 10.1021/bk-2012-1119.pr001

Downloaded by UNIV OF ALABAMA BIRMINGHAM on December 8, 2012 | http://pubs.acs.org
Publication Date (Web): December 7, 2012 | doi: 10.1021/bk-2012-1119.pr001

In Chapter 2, Qian Wang group describe their studies on hierarchical assemblies of viruses and other protein-based nanoparticles for biomedical applications. The virus begins with a single coat protein, which can be chemically and genetically altered with biologically relevant groups. Inorganic nanocrystals can be deposited on the surface of the viral particles and cell binding sequences can be added at high surface densities. The authors discuss the scope of applications of these protein-based nanoparticles for drug/gene delivery, tissue engineering scaffolds, and as anchor sites for cell adhesion to promote bone marrow stem cells differentiation.

Soto and Ostroff discuss in Chapter 3, their development of a drug delivery system based on glucan microparticles that are designed to target macrophage and dendritic cells that express β-glucan receptors. In addition to this targeting, the glucan microparticles serve as carriers of other nanoparticles with a drug payload that are either bound to or encapsulated in the microparticles. They describe various glucan microparticle hybrids such as quantum dots for imaging, gold nanoparticles for drug delivery, magnetic nanoparticles for cell purification, imaging and drug delivery and adeno-associated virus for gene therapy. Ahmed and Narain have developed a wide range of nanoparticles based on carbohydrates, motivated by the fact that biological cell surface and extracellular matrix contain a variety of carbohydrates in the form of glycoproteins and glycolipids, which play a key role in cell-cell interactions, communication, and recognition of antibodies. In Chapter 4, they report on the preparation of glyconanoparticles by modification of polymeric nanoparticles, liposomes, gold and magnetic nanoparticles, quantum dots, and carbon nanotubes with carbohydrate residues. The chapter discusses the gene delivery efficacies of the different types of glyconanoparticles synthesized.

Paresh Ray and collaborators show in Chapter 5 that the plasmonic properties of the gold nanoparticles are useful for labeling, imaging, and diagnosis and that, in the presence of suitable light, these bioconjugated nanoparticles are capable of selectively killing the multidrug resistance bacteria. Since the photothermal bacterial destruction mechanism is completely different from antibiotic-based killing, they speculate that the bacteria will be unlikely to develop resistance. In Chapter 6, Liu et al. present an overview of the evolution of bactericidal agents. Emphasis is placed on silver nanoparticles and nanoporous materials such as zeolites and metal organic frameworks.

Simmons et al. present a novel nanocomposite material prepared from single-wall carbon nanotubes and the polymer polyvinylpyrrolidone for applications in wound healing in Chapter 7. The carbon nanotubes are employed as substrates for cell growth while the antibacterial protection is provided by iodine.

In Chapter 8, Suzuki, Lee, and Sakai report on stimuli responsive action of liposomes using laser light as the trigger. The rupture of liposomes causes the encapsulated drug to be released while the laser light offers the option of photodynamic therapy. From microscopic snapshots of the liposomes subjected to the laser trigger, they have identified implosion and microscopic cavitation as mechanisms involved in the liposome rupture process. Beyond drug delivery and photodynamic therapeutics, they suggest the potential exploitation of the cavitation for medical ultrasonics.

Downloaded by UNIV OF ALABAMA BIRMINGHAM on December 8, 2012 | http://pubs.acs.org
Publication Date (Web): December 7, 2012 | doi: 10.1021/bk-2012-1119.pr001

In Chapter 9, Miyamoto et al. describe the development of a three-dimensional cell array cytotoxicity test system and the preparation of polysaccharide-based magnetic iron oxide nanoparticles for the purposes of cell tracking and monitoring. The magnetic nanoparticles are taken into transplanted cells to visualize therapeutic cells, and the transplanted cells are tracked using the nuclear magnetic resonance. The test method is intended for evaluating transplanted cells and tissues at the very early stages of transplantation where no direct methods are available to monitoring the success of transplantation.

In Chapter 10, Ward, DeWitt, and Davis present their work on halloysite nanoclays for controlled delivery applications. One of the most common morphologies of this nanoclay is a tubular structure consisting of many concentric layers, one of silica and the other of alumina. The tubular cavities can be compartments for incorporating drugs, and the nanoclays can be blended with polymers to create nanocomposite controlled release devices. In the Chapter 11, the loading and release of a model drug, from micro porous zeolite-Y with varying silica/alumina ratios and from mesoporous silica functionalized with amine groups are discussed. These porous nanomaterials are proposed as potential candidates for positron emission tomography (PET) imaging applications.

Sans and Fuente present a comprehensive description of nanostructures modified with nucleic acids in Chapter 12. The DNA and RNA conjugated nanomaterials provide biological recognition capability and also act as a cargo for delivery purposes. Applications of these nucleic acid conjugated particles to biosensing and gene delivery are reviewed. In Chapter 13 from Anjana Jain group discusses current nanomaterials-based diagnostic and therapeutic strategies applied to central nervous system (CNS) injuries. Nanoparticles-based biosensors, nanoparticle drug carriers, nanoparticle imaging agents, and nanofiber scaffolds for reconstruction and regeneration of damaged spinal cord and brain are described.

The contributing authors for this book come from a wide cross-section of international institutions. The multiplicity of authors of each chapter and their disciplinary backgrounds reveal the interdisciplinary emphasis of this field and the role chemical sciences plays at the center. The affiliations of the authors are also representative of the broad pervasive interest in the development of nanomaterials designed for applications in nanomedicine. The editor is thankful to the numerous reviewers. The reviewers of individual chapters contributed prompt critical reviews that have helped improve the quality of the manuscripts. The editor acknowledges support from ACS Books, especially Tim Marney and Ashlie Carlson, with the use of the newly introduced online manuscript submissions process. The editor acknowledges the support from Natick Soldier Research, Development & Engineering Center, that allowed him to organize the symposium and develop this book based on selected contributions.

**R. Nagarajan**
Molecular Sciences and Engineering Team
Natick Soldier Research, Development & Engineering Center
Natick, Massachusetts

# Editor's Biography

## Ramanathan Nagarajan

Dr. Nagarajan is Emeritus Professor of Chemical Engineering at The Pennsylvania State University and is currently a research scientist at the Natick Soldier Research, Development & Engineering Center. His research interests span the fundamentals and applications of soft nanoparticles generated by self-assembly of surfactant and block copolymer molecules, multifunctional nanomaterials, computational chemistry, and colloid and polymer science. He has authored approximately 100 publications, which have been cited over 3,000 times with an H index of 30. Nagarajan is the Program Chair of ACS Division of Colloid and Surface Chemistry and has served as the Guest Editor of *Colloids and Surfaces and Advances in Colloid and Interface Science* and as an editorial board member of *Journal of Colloid and Interface Science*, *Encyclopedia of Surface and Colloid Science*, and *Journal of Macromolecular Science Part A. Pure and Applied Chemistry*. Nagarajan is co-editor of the ACS Symposium Series books *Nanoparticles: Synthesis, Stabilization, Passivation and Functionalization*, published in 2008, and *Nanoscience and Nanotechnology for Chemical and Biological Defense*, published in 2009; he is editor of the book *Amphiphiles: Molecular Assembly and Applications*, published in 2011. Dr. Nagarajan was elected a Fellow of the American Chemical Society in 2012.

In Nanomaterials for Biomedicine; Nagarajan, R.;
ACS Symposium Series; American Chemical Society: Washington, DC, 2012.

Downloaded by ILLINOIS STATE UNIV on December 8, 2012 | http://pubs.acs.org
Publication Date (Web): December 7, 2012 | doi: 10.1021/bk-2012-1119.ch001

## Chapter 1

# Biochemistry and Biomedical Applications of Spherical Nucleic Acids (SNAs)

**Will Briley,[1] Tiffany L. Halo,[1,2] Pratik S. Randeria,[1] Ali H. Alhasan,[1]
Evelyn Auyeung,[1] Sarah J. Hurst,[1] and Chad A. Mirkin*,[1]**

**[1]Department of Chemistry and International Institute
for Nanotechnology, Northwestern University,
2145 Sheridan Road, Evanston, Illinois 60208-3113, United States
[2]AuraSense LLC, 8045 Lamon Avenue, Suite 410,
Skokie, Illinois 60077, United States
*E-mail: chadnano@northwestern.edu. Fax: (+1) 847-467-5123**

Careful observation of cellular processes has revealed exquisite examples of how the architecture of DNA and RNA can confer unique and complex functionality upon nucleic acid sequences. DNA superhelices, tRNA, and other intracellular ribozymes are essential components of life processes which require higher ordered structure for proper function. The realization that higher order nucleic acid architectures can afford unique functionality has ignited a new field of research that attempts to exploit such structures for a vast array of applications. In this chapter, we describe a novel three-dimensional nucleic acid architecture, referred to as the spherical nucleic acid (SNA), which possesses a number of exceptional properties not observed with any other nucleic acid structural motif. We then discuss how the unique properties of SNAs are being exploited in many next generation extra- and intra- cellular diagnostic and therapeutic applications.

Downloaded by ILLINOIS STATE UNIV on December 8, 2012 | http://pubs.acs.org
Publication Date (Web): December 7, 2012 | doi: 10.1021/bk-2012-1119.ch001

## Dimensionality in Nature

Nature has shown us that the higher order structures of biomolecules allow them to carry out specific and often complex functions that are essential to life processes. Intricate molecular architectures can be assembled from simple building blocks that interact in predictable patterns. In an almost gestalt fashion, the resulting two- and three-dimensional structures often have properties and functions that are distinct from those of their lower dimensional components. The chromophoric core of Green Fluorescent Protein (GFP), for instance, is composed of just three amino acids, but the structure and function of this core are maintained by the massive β-barrel structural motif that surrounds it (*1*). Much like that of their protein counterparts, the architecture of nucleic acids has proven to be profoundly important for life processes. For example, the cloverleaf shape of tRNA enables this nucleic acid to act as an adaptor molecule that can both bind and deliver amino acids to ribosomal machinery during protein translation (*2*). Also, DNA strands are composed of four nucleotide building blocks linked together to form single-stranded structures, which can then hybridize with complementary strands to form helical secondary structures. Certain helices form superhelical coils around histone proteins to form a spool-and-thread structure called chromatin (*3*). Chromatin is 40,000 times shorter than its unpacked components and allows for the storage of large eukaryotic genomes inside a nucleus that spans less than 10 μm in diameter. Storage of such a massive amount of genetic information in a micron-scale space would not be possible without this sort of structural manipulation.

The concept that higher order nucleic acid architectures afford unique functionality has ignited a new field of research that attempts to exploit such structures for a vast array of applications, spanning the materials (*4–6*), electronics (*7*) and biomedical fields (*8–10*). One such novel structure that has been heavily researched in the last 15 years is the spherical nucleic acid (SNA) (Figure 1). Our recent studies, as well as those of several other research groups, have shown that these structures, which typically consist of nanoparticle cores densely functionalized with a monolayer of highly oriented nucleic acids, are extremely efficacious as agents for both disease diagnosis (*8*) and treatment (*9*). Further, they have been used to probe several fundamental biological questions pertaining to nanomaterial-cell interactions. Their utility in such schemes is due to their distinctive architecture-dependent properties, including their ability to enter live cells rapidly and efficiently (over 50 cell lines tested to date) (*9*) with minimal toxicity and immunogenicity (*11*). In this chapter, we describe the synthesis, chemical and physical properties, and biological activity of SNAs, as well as some of their use in several important extra- and intracellular applications as diagnostic probes and therapeutic agents.

## Synthesis of Spherical Nucleic Acids (SNAs)

Spherical nucleic acids typically consist of: 1) a nanoparticle core (~ 2-250 nm in diameter; silver (*12*), gold (*13*), silica (*14*), iron oxide (*15*), quantum dots (*16*), hollow (*17*)) and 2) a densely functionalized, highly oriented nucleic acid

Downloaded by ILLINOIS STATE UNIV on December 8, 2012 | http://pubs.acs.org
Publication Date (Web): December 7, 2012 | doi: 10.1021/bk-2012-1119.ch001

shell (nucleic acids typically between 10-50 bases in length; single and double stranded DNA (*18*), small interfering RNA (siRNA) (*19*), micro-RNA (miRNA) (*20*), and modified nucleic acids, such as locked nucleic acids (LNA)).

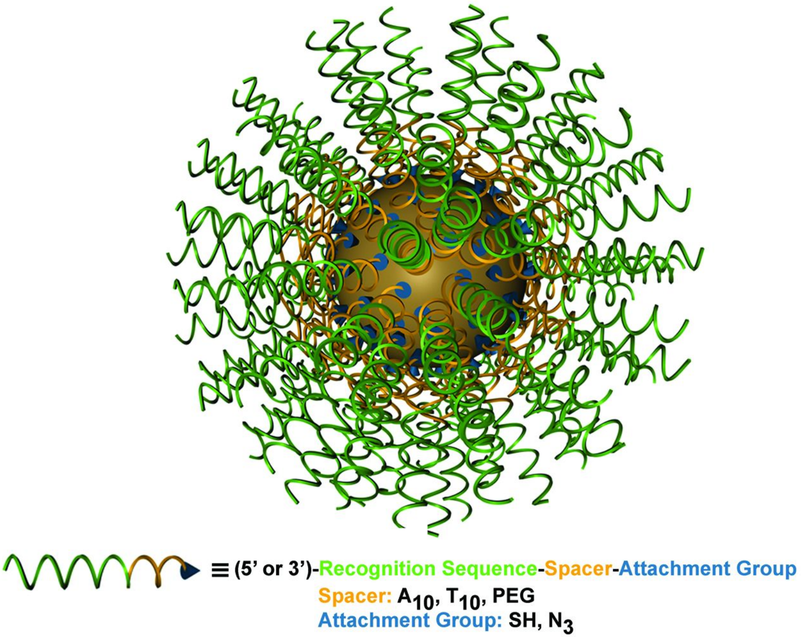

*Figure 1. Structure of a spherical nucleic acid-gold nanoparticle conjugate (SNA-AuNP). (Reproduced with permission from reference (17). Copyright 2012 American Chemical Society.)*

To date, the most common type of SNA used in biomedical applications has consisted of a gold nanoparticle core and an oligonucleotide shell (SNA-AuNP), and the synthetic route to this type of SNA structure is discussed below. Several classes of well-documented synthetic routes exist for making the monodisperse colloidal gold nanoparticles typically used to make SNA-AuNPs. The most widely used method was developed by Enustun and Turkevich and later refined by Frens (*21*, *22*). This solution phase reduction method can be used to prepare citrate-capped gold nanoparticles 5 to 150 nm in diameter in an aqueous environment through the reduction of chloroauric acid ($HAuCl_4$). Larger nanoparticles up to 300 nm in diameter can be made using a modified method that uses hydroquinone to catalyze the reduction of ionic gold onto the surface of gold nanoparticle seeds (*23*). Different sizes of particles are useful for different purposes, and biological parameters, such as cellular uptake, are often dependent on nanoparticle and nanoconjugate size (*24*). Thus, it is advantageous that such facile synthetic routes exist to access high-quality nanoparticles of a range of sizes.

The short, synthetic oligonucleotides used to construct SNA-AuNPs are synthesized via well-established solid phase methodologies (*25*). They typically consist of three regions: 1) a chemical tethering group (e.g., alkylthiol in the case of gold particles; often at the 3' end) that can be used to link the oligonucleotides to the nanoparticle surface, 2) a recognition element that is complementary to the target biomolecule of interest, and 3) a spacer region that can be modulated in length to tune the distance between the recognition element and the nanoparticle surface; extending the recognition element away from the particle surface gives it more free volume to interact with incoming strands due to the high curvature of the nanoparticle (*26*). The spacer chemistry can be modulated to vary the DNA density of the SNA nanostructure. Common spacers utilized are poly-adenine (poly-A), poly-thyamine (poly-T), or oligo-ethylene glycol (OEG). OEG spacers are less highly charged and have a lower affinity for the gold surface than the nucleotide spacers. Therefore, strands containing OEG spacers are capable of packing more tightly into the crowded area immediately surrounding the NP surface than poly-A or poly-T spacers, allowing higher surface coverage to be achieved (*26–30*).

Downloaded by ILLINOIS STATE UNIV on December 8, 2012 | http://pubs.acs.org
Publication Date (Web): December 7, 2012 | doi: 10.1021/bk-2012-1119.ch001

After the synthesis of the inorganic and organic building blocks, SNA-AuNPs are formed by mixing alkylthiol-terminated oligonucleotides with citrate-capped gold nanoparticles (*27*). The alkylthiol-modified oligonucleotides displace citrate ions from the gold surface making a stable gold-thiol linkage; unlike some other natural (*31*) and synthetic (*32*) higher-order forms of nucleic acids, SNAs are synthesized using covalent bonds, not hybridization interactions. Unless a monovalent salt, such as sodium chloride is added to the solution, only a sparse monolayer of nucleic acids is formed on the SNA. Sodium chloride is added to screen the negatively charged phosphate-sugar backbones of the closely-packed oligonucleotides, significantly increasing the number of strands that can be adsorbed onto the gold surface. By changing the amount of NaCl (0.05-1.0 M) added to the mixture, it is possible to tailor the density of the oligonucleotide monolayer (*27*). In fact, we have shown that by adding 1.0 M NaCl, up to 250 alkylthiol-modified oligonucleotides with oligo-ethylene glycol (OEG) spacers can be chemisorbed onto 15 nm gold particles, resulting in the creation of a dense polyvalent structure (up to 56 pmol/cm$^2$) (*27*). The unique spherical, three-dimensional architecture of SNA-AuNPs results in many unusual and biologically relevant properties, which will be described in the next section (*27*).

## Chemical and Physical Properties of Spherical Nucleic Acids

SNAs exhibit a number of interesting chemical and physical properties that make them extremely effective as probes in high sensitivity detection systems and agents in intracellular diagnostic and therapeutic schemes.

Downloaded by ILLINOIS STATE UNIV on December 8, 2012 | http://pubs.acs.org
Publication Date (Web): December 7, 2012 | doi: 10.1021/bk-2012-1119.ch001

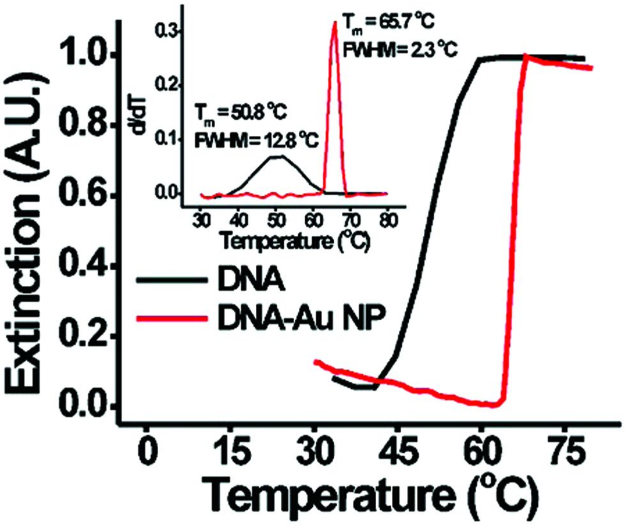

*Figure 2. Under identical conditions, aggregates of SNAs (red line) have a sharper melting transition and a higher melting temperature compared to the same sequence of free duplex DNA. Sequences used: 5'-alkanethiol-$A_{10}$ ATC CTT TAC AAT ATT 3' and 5' alkanethiol-$A_{10}$ AAT ATT GTA AAG GAT 3'. (Adapted with permission from reference (35). Copyright 2012 American Chemical Society.)*

First, SNAs behave unlike any other form of nucleic acid in binding experiments. When two sets of SNAs functionalized with complementary single stranded DNA are mixed together below the melting temperature of the duplex strands, the DNA hybridizes, and an extended network structure of aggregated nanoparticles is formed (*13*). This assembly event is accompanied by a concomitant red-to-blue color change, resulting from a red-shifting and dampening of the nanoparticle surface plasmon resonance (SPR) band. This assembly process is reversible, and upon heating above the melting temperature of the duplex, a sharp melting transition and a blue-to-red color change is observed as the DNA linking the particles dehybridizes, and the particles return to the dispersed state (Figure 2) (*13*). For both linear duplexes and aggregates of SNAs, the melting temperature ($T_m$) of the system is defined as the temperature at which half of the DNA duplexes in solution are dehybridized, and it is indicative of the strength of the duplex interaction (*33*). As the salt concentration of the solution, the number of complementary bases in the duplex, and the G-C content increases, an increase in the melting temperature is observed for both systems. Melting transitions for aggregates of SNAs occur at a higher temperature ($T_m$ ~66 °C, SNA-Au NPs; ~51 °C, free DNA) than free duplex DNA of the same sequence and occur over a narrower temperature range (full width at half maximum (fwhm) of the first derivative ~2 °C, SNA-AuNPs; vs. ~13 °C, free DNA) (*33*). This sharp melting transition results from the cooperativity between multiple duplex links between particles in the networked aggregate (*34*, *35*). The duplexes in close proximity to each other on the particle surface share the salt cloud of the neighboring strands, and when one duplex breaks releasing its associated ions, adjacent duplexes are destabilized, ultimately leading to a catastrophic dissociation of all duplexes in the networked structure that occurs over a very narrow temperature range (*34*).

In addition, SNAs also have significantly higher binding constants for free complementary oligonucleotide strands than free DNA of the same sequence (~100 times higher) (*36*). This enhanced binding strength was found to be directly related to the high density of DNA strands on and high local salt concentration around the nanoparticle surface rather than the absolute amount of bound DNA (*37*). Further, the presence of a spacer element was shown to be important, with the binding constant of nanoparticle systems without a spacer group significantly diminished (*36*). The increase in binding strength exhibited by the SNAs in comparison to the free molecular probes directly translates into lower limits of detection for target sequences, and allows for the differentiation of fully complementary and mismatched DNA targets that vary by as little as a single nucleotide (*38*). Other modifications of the SNA architecture can be made to restrict the possible conformations that the attached oligonucleotide strands can adopt and vary the rate of duplex formation with incoming free complementary strands (*39*).

Another intriguing property of SNAs is the facile nature with which they cross cell membranes (shown in over 50 cell lines to date) (*9*). This is surprising because the surface of these nanostructures is functionalized with a densely packed monolayer of polyanionic DNA. Generally, negatively charged species such as linear DNA require positively charged transfection agents in order to be internalized. However, our group has demonstrated that rapid (within five minutes) (*40*) uptake of high quantities of SNAs (on the order of $10^6$) into cells occurs without the need for cationic, often cytotoxic, transfection agents (*41*). This internalization is believed to be mediated by scavenger receptors, which are found on the surface of cells and are known to widely recognize and take up macromolecules having a negative charge density (*41*, *42*). A proposed model for the scavenger receptor uptake mechanism is that the dense monolayer of oligonucleotides exposed on the SNA surface mimics the conformation of the scavenger receptor-binding ligand, poly-1. In serum containing media, it has been shown that SNAs become coated in proteins, which can interfere with the scavenger receptor binding process (Figure 3). Thus, the interaction of SNAs and scavenger receptors is inversely related to the amount of serum proteins in solution, and directly related to the density of oligonucleotides conjugated to the nanoparticle (*41*).

Another unique property of SNA nanostructures is their enhanced resistance to many forms of enzymatically-enhanced cleavage. Historically, intracellular nucleic acid-based therapies have been hampered by the high susceptibility of free nucleic acids to degradation by nucleases. While the endonuclease DNAse-1 is very effective at cleaving free DNA strands, it has been shown to be much less potent at degrading DNA strands densely packed on the surface of a SNA nanostructure (*18*). Specifically, experiments show that DNA organized on the surface of a SNA architecture is degraded by wild-type nucleases at a rate 4.3 times

Downloaded by ILLINOIS STATE UNIV on December 8, 2012 | http://pubs.acs.org
Publication Date (Web): December 7, 2012 | doi: 10.1021/bk-2012-1119.ch001

slower than free linear DNA. The proposed explanation for this enhanced stability is that the steric congestion and high local salt concentration associated with the densely packed DNA in this architecture inhibits enzyme activity (*43*), because when nucleases engineered to tolerate high monovalent salt concentrations are used, the rates of degradation of free and nanoparticle-bound DNA become very similar (*11*).

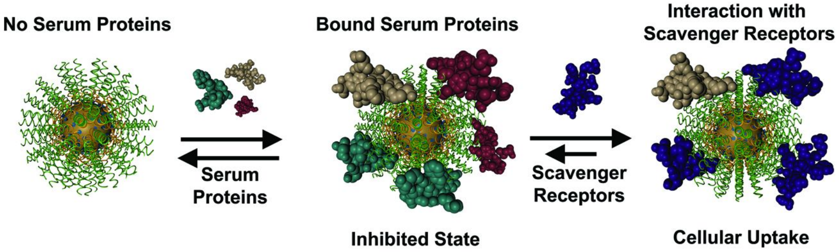

*Figure 3. SNAs are taken into cells via scavenger receptor-mediated endocytosis. Serum proteins nonspecifically coat the nanoconjugate, preventing binding to the receptors and inhibiting cellular uptake.*

Downloaded by ILLINOIS STATE UNIV on December 8, 2012 | http://pubs.acs.org
Publication Date (Web): December 7, 2012 | doi: 10.1021/bk-2012-1119.ch001

Also, unlike their linear nucleic acid counterparts, SNA nanostructures do not elicit an immune response when taken up into cells (*11*). Our group has demonstrated that interferon-beta (IFN-β), a protein associated with the triggering of a protective immune response, is produced in 25-fold lower quantities when nucleic acids in the SNA architecture are delivered into cells versus free nucleic acids of the same sequence delivered using common lipid-based transfection agents. The magnitude of this innate immune response can be regulated by modifying the DNA surface density on the nanoparticle; the more densely packed the DNA strands on the nanoconjugate, the lower the IFN-β response (*44*). Since lipoplexes were found to contribute negligibly to the level of the cellular immune response, it can be concluded that the spherical, three-dimensional architecture of the SNA nanostructure plays a critical role in its interaction with biological systems and significantly affects how cells respond to foreign genetic material. Further, analysis of whole-genome expression profiles of cells treated with SNAs made from single-stranded DNA, double-stranded DNA, or double-stranded RNA showed no significant up- or down-regulation of genes when compared to untreated cells or those treated with nanoparticle functionalized with bovine serum albumin (BSA). This result is in contrast to the considerable transcriptional response of cells treated with citrate-capped gold nanoparticles in which 127 genes had significantly altered expression (119 up-regulated, 8 down-regulated) (Figure 4) (*45*).

Downloaded by ILLINOIS STATE UNIV on December 8, 2012 | http://pubs.acs.org
Publication Date (Web): December 7, 2012 | doi: 10.1021/bk-2012-1119.ch001

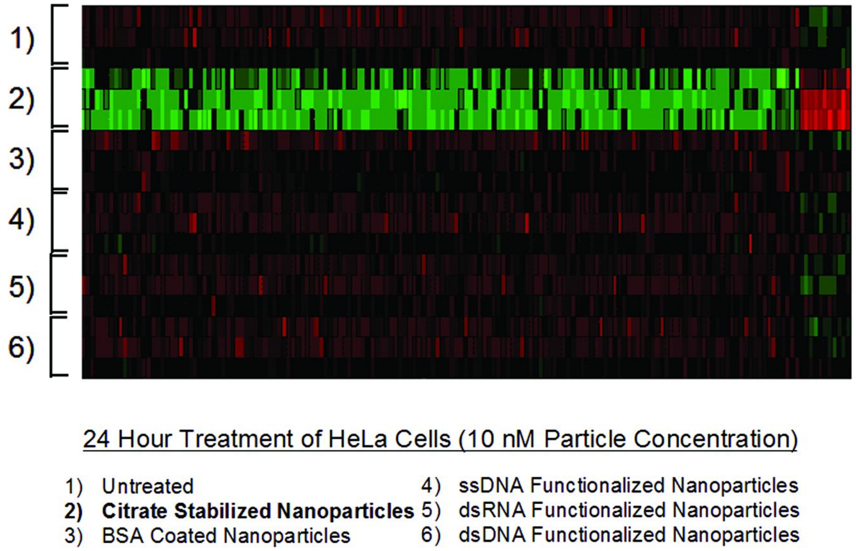

*Figure 4. Whole genome expression analysis indicating that SNA-AuNPs did not cause significant up- or down-regulation of genes investigated. Alternatively, citrate-capped (unfunctionalized) gold nanoparticles alter expression of 127 genes (119 up-regulated, 8 down-regulated). (Adapted with permission from reference (45). Copyright 2010 American Chemical Society.)*

## Extracellular Diagnostic Applications of SNA-AuNPs

SNAs, particularly those comprised of oligonucleotides and gold nanoparticles, have been utilized in a number of important biomedical applications, and we focus our discussion specifically on these materials in the next two sections.

SNAs have been utilized to develop many extracellular solution-phase and surface-based diagnostic assays for detecting biomarkers for cancers and other diseases that overcome many shortcomings associated with conventionally-used methods (*13*, *38*). In 1996, our group introduced the first simple, yet powerful, colorimetric assay in which the optical properties of SNA-AuNPs were used to detect the presence DNA duplexes with sticky ends in a “sandwich” type assay (*13*). The target binding event was accompanied by a change in the color of the colloidal solution from red to blue that was discernible with the naked eye (*vida supra)* (*38*, *46*). Since this initial proof-of-concept demonstration, similar SNA-AuNP-based colorimetric assays have been developed for the detection of other types of nucleic acid targets (*47*, *48*), proteins (*49*, *50*), mercuric ion (*51*), and small molecule intercalators (*52*). Similar nanoparticle-binding based diagnostic assays for nucleic acids and proteins also have been developed that rely on surface enhanced Raman scattering (SERS) (*53*, *54*), electrical conductivity (*55*), and silver (*56*) and gold (*57*) staining for readout.

Colorimetric assays are often advantageous in terms of their simplicity, robustness, and potential for point-of-care use in remote locations, but in certain cases, they are not sensitive enough to detect the ultra-low quantities of biomolecules that would make them relevant for use in biomedicine. The bio-barcode assay (BCA) however, which employs SNAs as probes, is a signal amplification strategy that can be used to detect the presence of protein (*49*) and nucleic acid (*58*) targets at levels comparable to or exceeding those attainable using enzyme-linked immunosorbant assay (ELISA) (*49*) and polymerase chain reaction (PCR) (*58*). The ultrahigh sensitivity of the BCA is mainly derived from: 1) the simple enrichment and purification of the targets that are present in the sample of interest using a magnetic field, 2) the signal amplification of the target strand by the hundreds of bio-barcode DNA strands on the particle surface, and 3) a light scattering-based read-out methodology called the scanometric assay that relies on the catalytic amplification of the optical signature of individual Au NPs on a chip via silver (*56*) or gold (*57*) staining (*vida infra*).

The first iteration of the BCA was developed for protein detection and introduced by our group in 2003. In a typical experiment, magnetic microparticle (MMP) probes functionalized with monoclonal antibodies are used to capture the antigen of interest from solution (Figure 5). These structures are then washed to remove excess target and mixed with SNAs functionalized with both polyclonal antibodies, which are used to sandwich the captured biomarker targets, and single-stranded bio-barcode oligonucleotides (100s per particle), which serve downstream as markers for the presence of the protein target. After thorough washing steps to separate the MMP-SNA complexes from the other species in solution, the barcode strands on the gold nanoparticle surface are dehybridized, and the scanometric assay is used to quantify them (*56*). In the scanometric assay, a capture nucleic acid, complementary to one part of the barcode is attached to the surface of a glass slide. As an aside, the placement of these capture nucleic acids can be coded allowing one to sort barcodes to specific locations on the array, which is highly useful for the simultaneous detection of multiple targets. The barcodes are then hybridized to the surface of this chip, and subsequently exposed to another set of SNA-Au NP probes, complementary to the other end of the barcode DNA. Next, a silver staining reaction (i.e., catalytic reduction of silver in the presence of hydroquinone (*56*) at the surface of the gold particle) is used to amplify the light scattering of the gold nanoparticle, and the scattering signal is measured and used to quantify the concentration of the original protein target (Figure 6A). This system was initially demonstrated for the prostate cancer biomarker, prostate specific antigen (PSA), and the bio-barcode assay was found to be $10^6$ times more sensitive than conventional ELISA assays for the same target with a limit of detection (LOD) of 30 aM (*49*). Since this initial demonstration, the bio barcode assay (when coupled to the scanometric assay) has been adapted for the detection of nucleic acids (*59*), Alzheimer's disease markers in cerebral spinal fluid (*60*), and bacterial genomic DNA (*61*) with LODs of 500 zM, 100 aM, and 2.5 fM, respectively. It has also been demonstrated to be useful in a

Downloaded by ILLINOIS STATE UNIV on December 8, 2012 | http://pubs.acs.org
Publication Date (Web): December 7, 2012 | doi: 10.1021/bk-2012-1119.ch001

multiplexed format for the simultaneous detection of more than one protein (*62*) or nucleic acid (*63*) target, and to be compatible in both a microfluidic format (*64*) and an automated format for the analysis of cancer recurrence in patient samples in a clinical pilot study (*65*).

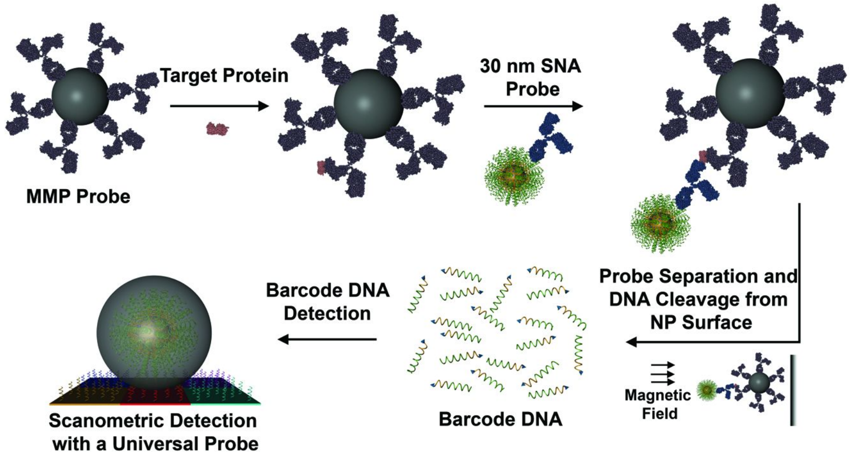
Target Protein
30 nm SNA Probe
MMP Probe
Probe Separation and DNA Cleavage from NP Surface
Barcode DNA Detection
Magnetic Field
Barcode DNA
Scanometric Detection with a Universal Probe

*Figure 5. General schematic of the biobarcode assay.*

In addition to its use in conjunction with the biobarcode assay, the scanometric assay has been developed on its own to improve its sensitivity and capabilities. For example, it has been redesigned to detect thousands of micro-RNAs (small non-coding RNA molecules) in a single experiment (*66*). This novel platform, termed the scanometric micro-RNA (scano-miR) platform, has been applied to high density array formats for high throughput microRNA (miRNA) profiling from various biological samples, including human serum. The scano-miR platform is able to detect 1 fM concentrations of miRNA in human serum with single nucleotide mismatch resolution (*66*). Importantly, this system has been successfully utilized to screen hundreds of miRNA markers that are specific to aggressive forms of prostate cancer (Gleason score 9) with 98.8% accuracy, highlighting its utility in identifying novel disease biomarkers. The scano-miR system employs a gold-based staining methodology, which utilizes tetrachloroaurate and hydroxylamine, instead of the traditional silver staining method. Studies have shown that, after three rounds of gold deposition, the surface-bound gold coated particle probes were approximately five times larger (2700 nm vs. 550 nm for the silver deposition strategy) and more highly faceted than the silver coated structures, which resulted in significant enhancement of the scattered light (Figure 6B) (*57*). Finally, the scanometric system has even been developed commercially by Nanosphere (www.nanosphere.us; the Verigene® ID System) and forms the basis of seven (to-date) FDA cleared panel assays for, for instance, *Staphylococcus aureus* and Warfarin metabolism.

Downloaded by ILLINOIS STATE UNIV on December 8, 2012 | http://pubs.acs.org
Publication Date (Web): December 7, 2012 | doi: 10.1021/bk-2012-1119.ch001

Downloaded by ILLINOIS STATE UNIV on December 8, 2012 | http://pubs.acs.org
Publication Date (Web): December 7, 2012 | doi: 10.1021/bk-2012-1119.ch001

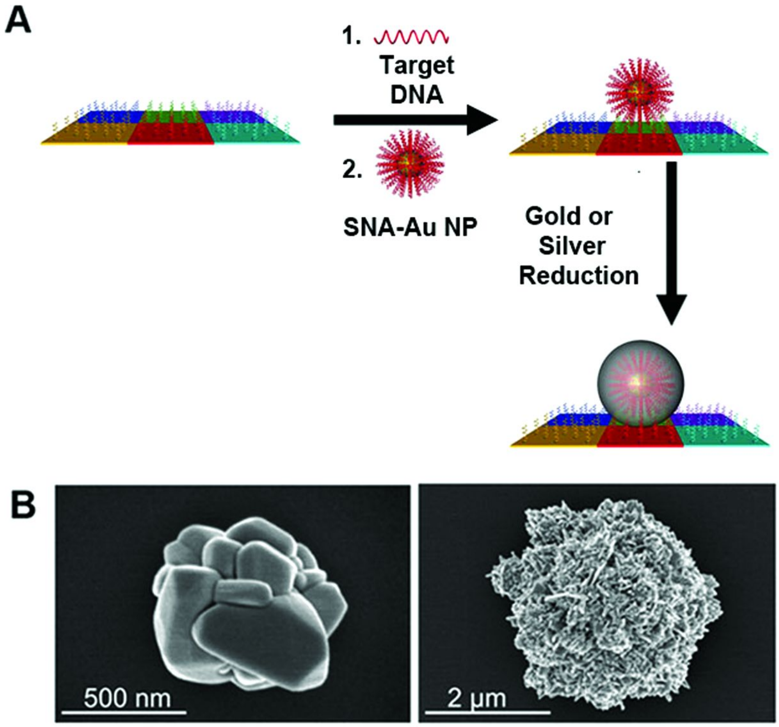

*Figure 6. The Scanometric Assay. A) General scheme of the scanometric assay. B) SEM images of amplified SNA-Au NPs using silver reduction (Left) or gold enhancement (Right) solutions. (Adapted with permission from reference (57). Copyright 2009 American Chemical Society.)*

## Intracellular Applications of SNA-AuNPs

SNA-Au NPs have been developed as highly efficacious agents for intracellular detection and gene regulation via both antisense and RNAi pathways in part due to their ability to rapidly and efficiently enter cells and to bind tightly with complementary biomolecule targets (*18*, *19*). SNAs can function in the antisense pathway by base-pairing with complementary mRNA targets and removing them from the pool of translationally-available transcripts, thus preventing the synthesis of the corresponding protein (Figure 7). Additionally, this mRNA binding event leads to rapid degradation of the DNA/RNA duplex, since the activity of RNAse-H is selectively enhanced near the nanoparticle surface (the activity of most other nucleases (i.e., DNAases) is decreased) (*67*).

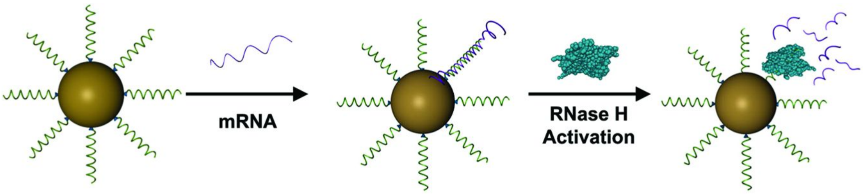

*Figure 7. SNA-Au NPs bind with target mRNA, which is then enzymatically degraded.*

Downloaded by ILLINOIS STATE UNIV on December 8, 2012 | http://pubs.acs.org
Publication Date (Web): December 7, 2012 | doi: 10.1021/bk-2012-1119.ch001

When tested with C166-EGFP, a endothelial cell line which stably expresses high levels of enhanced green fluorescent protein (EGFP), the antisense SNA nanoconjugates significantly outperformed linear nucleic acids complexed with commercially available lipoplex delivery systems in total EGFP knock-down (*19*). Further, the inclusion of locked nucleic acids (LNA) into the antisense strand nearly doubled the efficacy of the SNAs (*68*) likely because LNA has a greater binding affinity for mRNA targets than does DNA, and is also more resistant to nuclease degradation. Advantageously, the incorporation of the LNA bases did not negatively impact the high rate of cellular uptake compared to that observed with DNA functionalized gold nanoparticles.

The high rate of cellular entry and complementary base-pairing by SNA-Au NPs has also been exploited to create a novel intracellular detection and gene regulation system – the nanoflare platform. A nanoflare is an SNA-AuNP conjugate with a short complementary DNA strand containing a terminal fluorophore (the reporter flare) hybridized to the thiolated DNA (*69*) or DNA/LNA hybrid (*19*) antisense strand attached to the particle surface. When bound in close proximity to the gold particle, the fluorescence of the fluorophore is quenched (*70*). However, in the presence of an mRNA target complementary to the antisense sequence, the nanoflare forms a longer, more stable duplex and the shorter flare strand is displaced. Since the displaced fluorophore is no longer quenched by the gold nanoparticle surface, increased fluorescence is observed (Figure 8A). In proof-of-principle experiments, the nanoflare construct was used to detect intracellular mRNA transcripts of survivin, an anti-apoptotic gene which is upregulated in many cancers (Figure 8B) (*71*). Importantly, the nanoflare was able to provide fluorescence readout for this gene in a matter of hours without noticeably disrupting cellular function.

Because the SNA architecture is a highly modular and highly tailorable scaffold which can be functionalized with many different types of nucleic acids strands, it is also possible to design nanoflare systems in which multiple intracellular targets can be simultaneously detected using a single nanoflare construct (*72*). Importantly, such a nanoflare can be used to detect a constitutively expressed housekeeping gene, such as actin, in addition to a variable target sequence. This type of internal control can be used to normalize for cell-to-cell variations that may arise from external factors such as heterogeneous nanoparticle uptake. This technique greatly improves the ability of the nanoflare to quantify relative mRNA expression, to the point that it is comparable to real time PCR (RT-PCR), and allows for the identification and separation of live cells based on their genetic expression profiles.

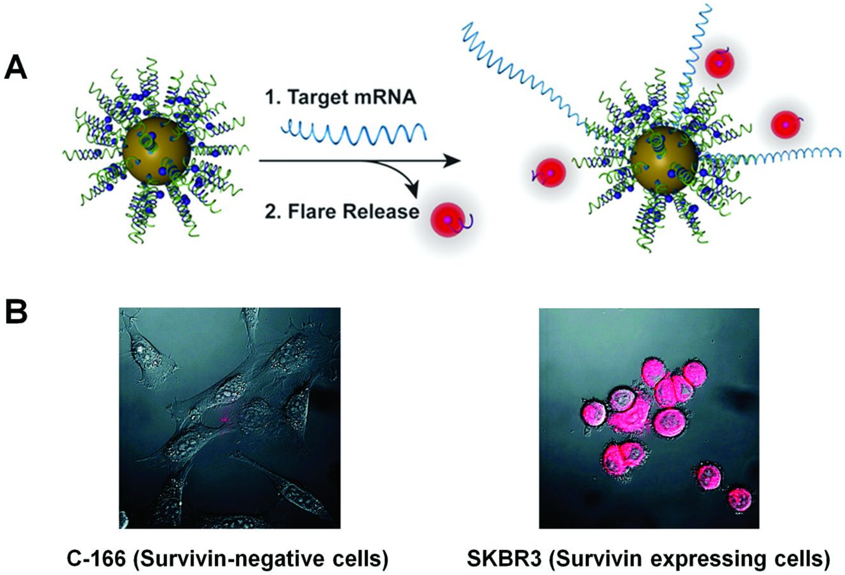
A
1. Target mRNA
2. Flare Release
B
C-166 (Survivin-negative cells)
SKBR3 (Survivin expressing cells)

*Figure 8. General schematic showing nanoflare technology operation. A) Binding of an mRNA target displaces a short, fluorophore labeled flare. B) Expression of the target results in detectable fluorescence within cells. (Adapted with permission from reference (69). Copyright 2007 American Chemical Society.)*

In 2010, Harry et al. developed a nanoconjugate architecture, similar to the nanoflare, for the intracellular detection of tyrosinase mRNA in cultured melanoma cells. In this scheme, gold nanoparticles were functionalized with hairpin strands containing fluorophores (*73*). In the absence of target, these hairpin strands stayed tightly folded, holding the fluorophore at close proximity to the gold quenching its fluoresence. Upon binding target intracellular mRNA the hairpin strand unraveled, moving the fluorophore away from the surface of the gold and resulting in a measurable and sequence-specific fluorescence response (*73*).

The nanoflare approach can be used to detect other important intracellular analytes. For instance, our group has shown that the antisense DNA strands on the nanoflare surface can be replaced with aptamer sequences known to bind relevant intracellular small molecules such as adenosine triphosphate (ATP), a cellular coenzyme which functions as an energy carrier and is typically present in high

Downloaded by ILLINOIS STATE UNIV on December 8, 2012 | http://pubs.acs.org
Publication Date (Web): December 7, 2012 | doi: 10.1021/bk-2012-1119.ch001

levels in cancer cells (*74*). In this system, ATP binding alters the structure of the aptamer on the particle surface and induces the displacement of the flare strand. The measurement of the resultant fluorescence levels is indicative of the amount of ATP present in the live cells. This aptamer nanoflare was highly selective for ATP binding even in the presence of uridine triphosphate (UTP), guanosine triphosphate (GTP), and cytidine triphosphate (CTP). Aptamer-functionalized Au NPs can also be used to guide nanoparticle uptake. For instance, gold nanoparticles functionalized with an aptamer for a cell surface marker (epidermal growth factor (EGFR)), often overexpressed on cancer cells, were shown by Li and co-workers to exhibit a greater rate of uptake onto EGFR-expressing cell types compared to the equivalent, non-targeting particles (*75*).

Importantly, nanoflares also can be used as a theranostic tool, capable of detecting the presence of an intracellular mRNA target via the sequence-specific displacement of a fluorophore-labeled flare, while simultaneously knocking down the expression of that target transcript (*19*). The hybridization of a short internal complementary DNA strand (sicDNA), such as the reporter flare, to the antisense sequence on the nanoparticle was even shown to increase the rate of target binding by up to five-fold (*39*). While the inclusion of a sicDNA may intuitively seem to provide competitive inhibition to the binding of an mRNA target, the formation of the short duplex actually extends the antisense strand away from the surface, inducing a conformation that more favorably binds incoming complementary mRNA strands.

Downloaded by ILLINOIS STATE UNIV on December 8, 2012 | http://pubs.acs.org
Publication Date (Web): December 7, 2012 | doi: 10.1021/bk-2012-1119.ch001

## Other Types of Spherical Nucleic Acid Architectures

Thus far, all of the applications discussed herein have involved SNA-Au-NPs comprised of DNA bound to the surface of gold nanoparticles. However, extremely useful versions of SNAs have been synthesized that consist of short RNA duplexes (*19*) or microRNA (*20*) strands that are capable of regulating gene expression via RNA interference (RNAi) pathways. These RNA materials are architecturally similar to their DNA counterparts, and they are also extremely efficient gene regulation agents. Just as with their DNA analogs, RNA versions of SNAs are considerably more resistant to degradation by nucleases than free RNA; they have a half-life of up to six times greater than that of free double-stranded RNA in serum-containing media (*19*). This type of finding is potentially even more important in the RNA cases, as the extremely short half-life of functional linear RNA has been a significant barrier to its efficacy in gene regulation.

SNAs that incorporate non-nucleotide based modifications to the nanoparticle surface have also have been synthesized. Specifically, other types of biomolecules can be incorporated with, or complexed to, the nucleic acid layer to provide added functionality to the SNA-AuNP nanostructure. For instance, short peptide sequences and short, alkylthiol modified oligonucleotide sequences can be co-assembled on the surface of gold nanoparticles to create a heterofunctionalized nanoconjugate structure. In one study, an N-teminal cysteine was added to the transactivator of transcription (Tat) and Nuclear Localization Signal (NLS) peptide sequences, allowing them to be conjugated to the nanoparticle surface in combination with a glyceraldehyde phosphate dehydrogenase (GAPDH) antisense DNA sequence (Figure 9A) (*76*). The dual-functionalized SNA was capable of effecting significantly higher knockdown of GAPDH in HeLa cells than the same SNA without peptides (Figure 9B).

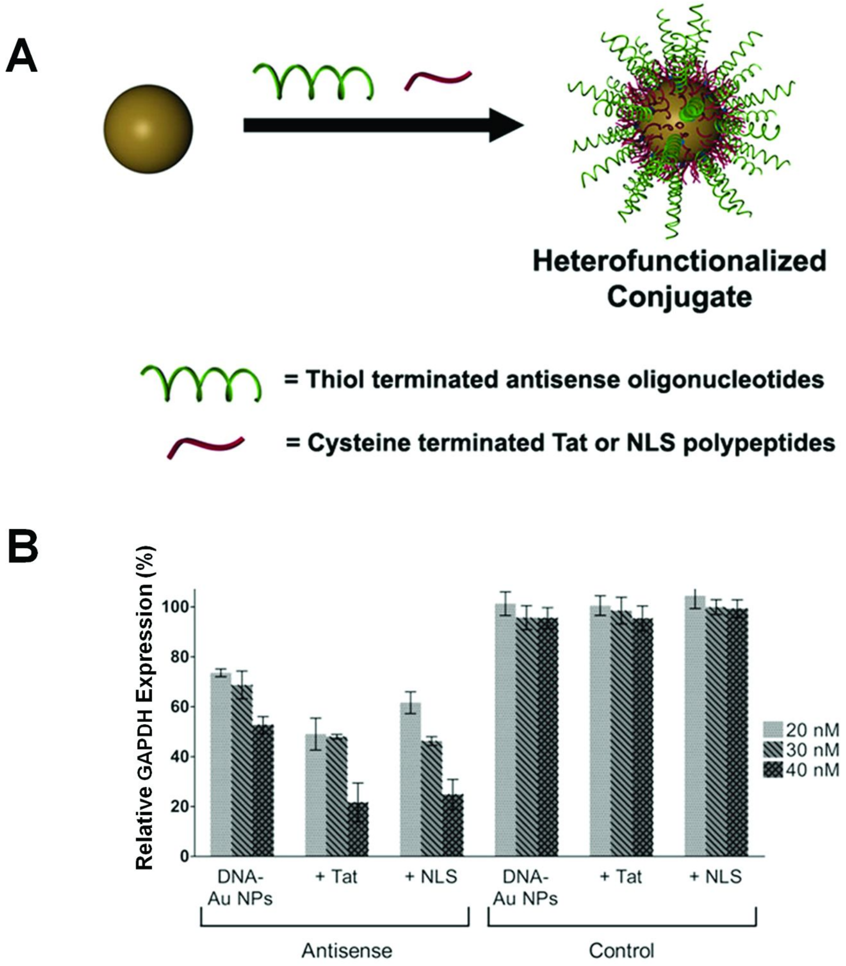

*Figure 9. Peptide-Antisense SNAs. A) Cystein-terminated peptides can be incorporated with the SNA nucleotide monolayer. B) Functionalization of Au-NPs with antisense GAPDH DNA and either Tat or NLS peptide sequences increases the efficacy of knock-down, as measured by western blot. (Adapted with permission from reference (76). Copyright 2008 by The National Academy of Sciences of the U.S.A.)*

Downloaded by ILLINOIS STATE UNIV on December 8, 2012 | http://pubs.acs.org
Publication Date (Web): December 7, 2012 | doi: 10.1021/bk-2012-1119.ch001

When the peptide antisense nanoparticles were labeled with a fluorescent reporter these nanoconjugates were found to be consistently localized directly outside the nucleus, while nanoparticles functionalized with only antisense oligonucleotides were evenly distributed throughout the cytoplasm.

In addition, chemotherapeutic versions of SNAs have been synthesized. To form such a structure, cis-Pt(IV) was covalently linked to the ends of DNA strands on the surface of gold nanoparticles to create a dense, highly oriented, surface-bound monolayer of Pt(IV) prodrugs (*77*). The dense oligonucleotide layer allowed these particles to be endocytosed efficiently into cells, whereupon the relatively low pH of endosomes released the platinum in the form of cytotoxic cis-platin, one of the most common anti-tumor drugs used today. This delivery of Pt(IV) showed similar (and in some cases superior) killing ability in several cancerous cell lines when compared to the common treatment with cis-platin, and was hypothesized to have fewer side effects due to the utilization of the otherwise bioinactive Pt(IV).

Downloaded by ILLINOIS STATE UNIV on December 8, 2012 | http://pubs.acs.org
Publication Date (Web): December 7, 2012 | doi: 10.1021/bk-2012-1119.ch001

## Future Directions and Conclusions

SNAs take one of the most important and highly studied molecules known – linear nucleic acids – and organize them in such a way that novel chemical and physical properties are conferred upon the conjugate. Some of the most striking properties of these materials have been discovered while studying and understanding their interactions with biological structures both *in vitro* and *in vivo* in live cellular models and living organisms. Due to this and to the fact that SNAs are easily synthesized, extremely robust, and highly modular and tailorable (in terms of their composition, surface derivatization, charge, and size), these structures have been developed in a number of important extra- and intra-cellular biodiagnostic and therapeutic strategies that have the potential to revolutionize the biotechnology and biomedical industries.

Currently, we and other groups are using SNA-Au NP nanoconjugates to tackle some of the most important challenges in biology and medicine, and are also moving these SNA systems from the laboratory setting toward clinical applications. Such work represents the combined cross-disciplinary efforts of teams of researchers operating at the crossroads of chemistry, materials science, cell biology, and clinical medicine. For example, SNAs have been shown to enter cells and tissues that are historically difficult to transfect. Our group has recently shown that SNA-Au NPs can traverse the lipid-rich stratum corneum of the skin to enter the epidermis and effect gene knockdown. This system is the only topically applied gene regulation agent for the skin, and as such represents an important a new lead for melanoma, psoriasis, and wound healing therapies (*78*). The ability of these nanoconjugates to enter areas of the body normally off-limits to conventional therapies promises exciting results in the future for some of the most persistent and destructive diseases.

Further, SNA-based nanoflare technology provides the only way to perform intracellular genetic testing via bulk treatment of entire populations of live cells. This technology is now being explored as a potential diagnostic and prognostic for aggressive, metastatic forms of cancer. Currently, metastatic cancer is most often diagnosed by identifying secondary tumors. At this stage, patient prognosis is often poor. Early detection of circulating tumor cells with upregulated genes associated with metastasis would enable systemic treatment prior to the formation of distal tumors. Nanoflares for several important metastatic marker genes are currently being investigated for their ability to pull circulating tumor cells out of whole blood and sort them using fluorescence for readout. Preliminary results indicate that this technique may prove exceptionally useful in the field of cancer diagnostics, and may offer an efficient, accurate proxy for assessing patient treatment progression.

The research discussed in this chapter provides only a glimpse into the diverse range of potential applications for SNAs in biology and medicine. Further, research groups investigating non-nucleic acid based nanoconjugates have also demonstrated other exciting, clinically relevant properties from a wide variety of three-dimensional structures (*79–90*). Together, we anticipate the prominence and use of these structures in these fields will continue to grow as studies involving them move further beyond cell-based analysis to animal models and, ultimately, clinical trials involving humans and human samples. Given the success seen thus far, we feel SNAs hold promise toward initiating exciting advances in the coming years and will be used to overcome some of the most persistent challenges in the detection and treatment of disease.

Downloaded by ILLINOIS STATE UNIV on December 8, 2012 | http://pubs.acs.org
Publication Date (Web): December 7, 2012 | doi: 10.1021/bk-2012-1119.ch001

## References

1. Chudakov, D. M.; Matz, M. V.; Lukyanov, S.; Lukyanov, K. A. *Physiol. Rev.* **2010**, *90*, 1103.
2. Florentz, C.; Sohm, B.; Tryoen-Tóth, P.; Pütz, J.; Sissler, M. *Cell. Mol. Life Sci.* **2003**, *60*, 1356.
3. McGhee, J. D.; Felsenfeld, G. *Annu. Rev. Biochem.* **1980**, *49*, 1115.
4. Macfarlane, R. J.; Lee, B.; Jones, M. R.; Harris, N.; Schatz, G. C.; Mirkin, C. A. *Science* **2011**, *334*, 204.
5. Niemeyer, C. M. *Angew. Chem., Int. Ed.* **2001**, *40*, 4128.
6. Yan, H.; Zhang, X.; Shen, Z.; Seeman, N. C. *Nature* **2002**, *415*, 62.
7. Willner, I.; Patolsky, F.; Wasserman, J. *Angew. Chem., Int. Ed.* **2001**, *40*, 1861.
8. Rosi, N. L.; Mirkin, C. A. *Chem. Rev.* **2005**, *105*, 1547.
9. Giljohann, D. A.; Seferos, D. S.; Daniel, W. L.; Massich, M. D.; Patel, P. C.; Mirkin, C. A. *Angew. Chem., Int. Ed.* **2010**, *49*, 3280.
10. Farokhzad, O. C.; Jon, S.; Khademhosseini, A.; Tran, T.-N. T.; LaVan, D. A.; Langer, R. *Cancer Res.* **2004**, *64*, 7668.
11. Prigodich, A. E.; Seferos, D. S.; Massich, M. D.; Giljohann, D. A.; Lane, B. C.; Mirkin, C. A. *ACS Nano* **2009**, *3*, 2147.
12. Lee, J.-S.; Lytton-Jean, A. K. R.; Hurst, S. J.; Mirkin, C. A. *Nano Lett.* **2007**, *7*, 2112.
13. Mirkin, C. A.; Letsinger, R. L.; Mucic, R. C.; Storhoff, J. J. *Nature* **1996**, *382*, 607.

14. Young, K. L.; Scott, A. W.; Hao, L.; Mirkin, S. E.; Liu, G.; Mirkin, C. A. *Nano Lett.* **2012**.
15. Cutler, J. I.; Zheng, D.; Xu, X.; Giljohann, D. A.; Mirkin, C. A. *Nano Lett.* **2010**, *10*, 1477.
16. Mitchell, G. P.; Mirkin, C. A.; Letsinger, R. L. *J. Am. Chem. Soc.* **1999**, *121*, 8122.
17. Cutler, J. I.; Auyeung, E.; Mirkin, C. A. *J. Am. Chem. Soc.* **2012**, *134*, 1376.
18. Rosi, N. L.; Giljohann, D. A.; Thaxton, C. S.; Lytton-Jean, A. K.; Han, M. S.; Mirkin, C. A. *Science* **2006**, *312*, 1027.
19. Giljohann, D. A.; Seferos, D. S.; Prigodich, A. E.; Patel, P. C.; Mirkin, C. A. *J. Am. Chem. Soc.* **2009**, *131*, 2072.
20. Hao, L.; Patel, P. C.; Alhasan, A. H.; Giljohann, D. A.; Mirkin, C. A. *Small* **2011**, *7*, 3158.
21. Frens, G. *Nature (London), Phys. Sci.* **1973**, *241*, 20.
22. Enustun, B. V.; Turkevich, J. *J. Am. Chem. Soc.* **1963**, *85*, 3317.
23. Perrault, S. D.; Chan, W. C. W. *J. Am. Chem. Soc.* **2009**, *131*, 17042.
24. Chithrani, B. D.; Ghazani, A. A.; Chan, W. C. W. *Nano Lett.* **2006**, *6*, 662.
25. Beaucage, S. L.; Iyer, R. P. *Tetrahedron* **1992**, *48*, 2223.
26. Hill, H. D.; Millstone, J. E.; Banholzer, M. J.; Mirkin, C. A. *ACS Nano* **2009**, *3*, 418.
27. Hurst, S. J.; Lytton-Jean, A. K.; Mirkin, C. A. *Anal Chem* **2006**, *78*, 8313.
28. Demers, L. M.; Ostblom, M.; Zhang, H.; Jang, N. H.; Liedberg, B.; Mirkin, C. A. *J. Am. Chem. Soc.* **2002**, *124*, 11248.
29. Kimura-Suda, H.; Petrovykh, D. Y.; Tarlov, M. J.; Whitman, L. J. *J. Am. Chem. Soc.* **2003**, *125*, 9014.
30. Storhoff, J. J.; Elghanian, R.; Mirkin, C. A.; Letsinger, R. L. *Langmuir* **2002**, *18*, 6666.
31. Hall, K. B.; Sampson, J. R.; Uhlenbeck, O. C.; Redfield, A. G. *Biochemistry* **1989**, *28*, 5794.
32. Rothemund, P. W. K. *Nature* **2006**, *440*, 297.
33. Lytton-Jean, A. K. R.; Mirkin, C. A. *J. Am. Chem. Soc.* **2005**, *127*, 12754.
34. Jin, R.; Wu, G.; Li, Z.; Mirkin, C. A.; Schatz, G. C. *J. Am. Chem. Soc.* **2003**, *125*, 1643.
35. Hurst, S. J.; Hill, H. D.; Mirkin, C. A. *J. Am. Chem. Soc.* **2008**, *130*, 12192.
36. Lytton-Jean, A. K.; Mirkin, C. A. *J. Am. Chem. Soc.* **2005**, *127*, 12754.
37. Long, H.; Kudlay, A.; Schatz, G. C. *J. Phys. Chem. B* **2006**, *110*, 2918.
38. Elghanian, R.; Storhoff, J. J.; Mucic, R. C.; Letsinger, R. L.; Mirkin, C. A. *Science* **1997**, *277*, 1078.
39. Prigodich, A. E.; Lee, O.-S.; Daniel, W. L.; Seferos, D. S.; Schatz, G. C.; Mirkin, C. A. *J. Am. Chem. Soc.* **2010**, *132*, 10638.
40. Giljohann, D. A.; Seferos, D. S.; Patel, P. C.; Millstone, J. E.; Rosi, N. L.; Mirkin, C. A. *Nano Lett.* **2007**, *7*, 3818.
41. Patel, P. C.; Giljohann, D. A.; Daniel, W. L.; Zheng, D.; Prigodich, A. E.; Mirkin, C. A. *Bioconjugate Chem.* **2010**, *21*, 2250.
42. Doi, T.; Higashino, K.; Kurihara, Y.; Wada, Y.; Miyazaki, T.; Nakamura, H.; Uesugi, S.; Imanishi, T.; Kawabe, Y.; Itakura, H. *J. Biol. Chem.* **1993**, *268*, 2126.

Downloaded by ILLINOIS STATE UNIV on December 8, 2012 | http://pubs.acs.org
Publication Date (Web): December 7, 2012 | doi: 10.1021/bk-2012-1119.ch001

43. Seferos, D. S.; Prigodich, A. E.; Giljohann, D. A.; Patel, P. C.; Mirkin, C. A. *Nano Lett* **2009**, *9*, 308.
44. Massich, M. D.; Giljohann, D. A.; Seferos, D. S.; Ludlow, L. E.; Horvath, C. M.; Mirkin, C. A. *Mol. Pharmaceutics* **2009**, *6*, 1934.
45. Massich, M. D.; Giljohann, D. A.; Schmucker, A. L.; Patel, P. C.; Mirkin, C. A. *ACS Nano* **2010**, *4*, 5641.
46. Jin, R.; Wu, G.; Li, Z.; Mirkin, C. A.; Schatz, G. C. *J. Am. Chem. Soc.* **2003**, *125*, 1643.
47. Elghanian, R.; Storhoff, J. J.; Mucic, R. C.; Letsinger, R. L.; Mirkin, C. A. *Science* **1997**, *277*, 1078.
48. Storhoff, J. J.; Elghanian, R.; Mucic, R. C.; Mirkin, C. A.; Letsinger, R. L. *J. Am. Chem. Soc.* **1998**, *120*, 1959.
49. Nam, J. M.; Thaxton, C. S.; Mirkin, C. A. *Science* **2003**, *301*, 1884.
50. Nam, J. M.; Jang, K. J.; Groves, J. T. *Nat. Protoc.* **2007**, *2*, 1438.
51. Lee, J. S.; Han, M. S.; Mirkin, C. A. *Angew. Chem., Int. Ed.* **2007**, *46*, 4093.
52. Xin, A.; Dong, Q.; Xiong, C.; Ling, L. *Chem. Commun. (Cambridge, U.K.)* **2009**, 1658.
53. Cao, Y. C.; Jin, R.; Mirkin, C. A. *Science* **2002**, *297*, 1536.
54. Grubisha, D. S.; Lipert, R. J.; Park, H. Y.; Driskell, J.; Porter, M. D. *Anal. Chem.* **2003**, *75*, 5936.
55. Park, S. J.; Taton, T. A.; Mirkin, C. A. *Science* **2002**, *295*, 1503.
56. Taton, T. A.; Mirkin, C. A.; Letsinger, R. L. *Science* **2000**, *289*, 1757.
57. Kim, D.; Daniel, W. L.; Mirkin, C. A. *Anal. Chem.* **2009**, *81*, 9183.
58. Nam, J. M.; Stoeva, S. I.; Mirkin, C. A. *J Am Chem Soc* **2004**, *126*, 5932.
59. Nam, J. M.; Stoeva, S. I.; Mirkin, C. A. *J. Am. Chem. Soc.* **2004**, *126*, 5932.
60. Georganopoulou, D. G.; Chang, L.; Nam, J. M.; Thaxton, C. S.; Mufson, E. J.; Klein, W. L.; Mirkin, C. A. *Proc. Nat. Acad. Sci. U.S.A.* **2005**, *102*, 2273.
61. Hill, H. D.; Vega, R. A.; Mirkin, C. A. *Anal. Chem.* **2007**, *79*, 9218.
62. Stoeva, S. I.; Lee, J. S.; Smith, J. E.; Rosen, S. T.; Mirkin, C. A. *J. Am. Chem. Soc.* **2006**, *128*, 8378.
63. Stoeva, S. I.; Lee, J. S.; Thaxton, C. S.; Mirkin, C. A. *Angew. Chem., Int. Ed.* **2006**, *45*, 3303.
64. Goluch, E. D.; Stoeva, S. I.; Lee, J. S.; Shaikh, K. A.; Mirkin, C. A.; Liu, C. *Biosens. Bioelectron.* **2009**, *24*, 2397.
65. Thaxton, C. S.; Elghanian, R.; Thomas, A. D.; Stoeva, S. I.; Lee, J. S.; Smith, N. D.; Schaeffer, A. J.; Klocker, H.; Horninger, W.; Bartsch, G.; Mirkin, C. A. *Proc. Nat. Acad. Sci. U.S.A.* **2009**, *106*, 18437.
66. Alhasan, A. H.; Kim, D. Y.; Daniel, W. L.; Watson, E.; Meeks, J. J.; Thaxton, C. S.; Mirkin, C. A. *Anal. Chem.* **2012**, *84*, 4153.
67. Prigodich, A. E.; Alhasan, A. H.; Mirkin, C. A. *J. Am. Chem. Soc.* **2011**, *133*, 2120.
68. Seferos, D. S.; Giljohann, D. A.; Rosi, N. L.; Mirkin, C. A. *ChemBioChem* **2007**, *8*, 1230.
69. Seferos, D. S.; Giljohann, D. A.; Hill, H. D.; Prigodich, A. E.; Mirkin, C. A. *J. Am. Chem. Soc.* **2007**, *129*, 15477.
70. Dubertret, B.; Calame, M.; Libchaber, A. J. *Nat. Biotechnol.* **2001**, *19*, 365.
71. Altieri, D. C. *Nat. Rev. Cancer* **2008**, *8*, 61.

Downloaded by ILLINOIS STATE UNIV on December 8, 2012 | http://pubs.acs.org
Publication Date (Web): December 7, 2012 | doi: 10.1021/bk-2012-1119.ch001

72. Prigodich, A. E.; Randeria, P. S.; Briley, W. E.; Kim, N. J.; Daniel, W. L.; Giljohann, D. A.; Mirkin, C. A. *Anal. Chem.* **2012**, *84*, 2062.
73. Harry, S. R.; Hicks, D. J.; Amiri, K. I.; Wright, D. W. *Chem. Commun.* **2010**, *46*, 5557.
74. Zheng, D.; Seferos, D. S.; Giljohann, D. A.; Patel, P. C.; Mirkin, C. A. *Nano Lett.* **2009**, *9*, 3258.
75. Li, N.; Larson, T.; Nguyen, H. H.; Sokolov, K. V.; Ellington, A. D. *Chem. Commun.* **2010**, *46*, 392.
76. Patel, P. C.; Giljohann, D. A.; Seferos, D. S.; Mirkin, C. A. *Proc. Nat. Acad. Sci. U.S.A.* **2008**, *105*, 17222.
77. Dhar, S.; Daniel, W. L.; Giljohann, D. A.; Mirkin, C. A.; Lippard, S. J. *J. Am. Chem. Soc.* **2009**, *131*, 14652.
78. Zheng, D.; Giljohann, D. A.; Chen, D. L.; Massich, M. D.; Wang, X.-Q.; Iordanov, H.; Mirkin, C. A.; Paller, A. S. *Proc. Nat. Acad. Sci. U.S.A.* **2012**.
79. Lee, N. S.; Sun, G.; Neumann, W. L.; Freskos, J. N.; Shieh, J. J.; Dorshow, R. B.; Wooley, K. L. *Adv. Mater.* **2009**, *21*, 1344.
80. Qian, X.; Peng, X.-H.; Ansari, D. O.; Yin-Goen, Q.; Chen, G. Z.; Shin, D. M.; Yang, L.; Young, A. N.; Wang, M. D.; Nie, S. *Nat. Biotechnol.* **2008**, *26*, 83.
81. Fuller, J. E.; Zugates, G. T.; Ferreira, L. S.; Ow, H. S.; Nguyen, N. N.; Wiesner, U. B.; Langer, R. S. *Biomaterials* **2008**, *29*, 1526.
82. DeVries, G. A.; Brunnbauer, M.; Hu, Y.; Jackson, A. M.; Long, B.; Neltner, B. T.; Uzun, O.; Wunsch, B. H.; Stellacci, F. *Science* **2007**, *315*, 358.
83. Sandhu, K. K.; McIntosh, C. M.; Simard, J. M.; Smith, S. W.; Rotello, V. M. *Bioconjugate Chem.* **2001**, *13*, 3.
84. Kelly, J. Y.; DeSimone, J. M. *J. Am. Chem. Soc.* **2008**, *130*, 5438.
85. Tkachenko, A. G.; Xie, H.; Coleman, D.; Glomm, W.; Ryan, J.; Anderson, M. F.; Franzen, S.; Feldheim, D. L. *J. Am. Chem. Soc.* **2003**, *125*, 4700.
86. Kim, J. S.; Rieter, W. J.; Taylor, K. M. L.; An, H.; Lin, W.; Lin, W. *J. Am. Chem. Soc.* **2007**, *129*, 8962.
87. Santra, S.; Zhang, P.; Wang, K.; Tapec, R.; Tan, W. *Anal. Chem.* **2001**, *73*, 4988.
88. Loo, C.; Lowery, A.; Halas, N.; West, J.; Drezek, R. *Nano Lett.* **2005**, *5*, 709.
89. Lu, Y.; Yin, Y.; Mayers, B. T.; Xia, Y. *Nano Lett.* **2002**, *2*, 183.
90. Lewin, M.; Carlesso, N.; Tung, C.-H.; Tang, X.-W.; Cory, D.; Scadden, D. T.; Weissleder, R. *Nat. Biotechnol.* **2000**, *18*, 410.

Downloaded by ILLINOIS STATE UNIV on December 8, 2012 | http://pubs.acs.org
Publication Date (Web): December 7, 2012 | doi: 10.1021/bk-2012-1119.ch001

## Chapter 2

# Assembly of Virus Particles and Virus-like Particles as Templates for Biomedical Applications

**L. Andrew Lee,*,[1,2] Elizabeth Balizan,[1] Yuan Lin,[3] and Qian Wang[1]**

**[1]University of South Carolina, Department of Chemistry & Biochemistry,
631 Sumter St., Columbia, South Carolina 29208
[2]A&Q NanoDesigns, LLC., Columbia, South Carolina 29206
[3]State Key Laboratory of Polymer Physics and Chemistry,
Changchun Institute of Applied Chemistry, Chinese Academy of Sciences,
Changchun 130022, PR China
*E-mail: lee@aqnano.com**

Several groups have utilized viruses as primary building blocks to generate functional nanomaterials for a variety of applications. In essence, the virus embodies the nature-derived protein based polymers. A large number of these obligate organisms have been cloned and engineered to function as drug/gene delivery vehicles, vaccines, and polymeric co-assemblies. These studies have contributed valuable insights on the viruses and their potential as nanotemplates. Batch consistency, time honored purification process, well-characterized three-dimensional structures at near-atomic resolutions, and its genetic and chemical malleabilities confer certain advantages that are not feasible with other materials in this nanometer range. Recent studies have shifted the focus on translating these viruses and their hierarchical assemblies beyond conventional applications. For instance, genetically modified viruses have been co-assembled with polymers to provide unique anchor sites for cell adhesion and promote bone marrow stem cells differentiation. The use of viruses as tissue engineering scaffolds is still in its infancy in comparison to polymeric scaffolds. This chapter is to outline some of the key concepts along with the future directions of this field.

In Nanomaterials for Biomedicine; Nagarajan, R.;
ACS Symposium Series; American Chemical Society: Washington, DC, 2012.

# Introduction

Viruses and other protein-based nanoparticles (PBNs) have sparked the interests of scientists beyond its conventional realm of virology. These macro-building blocks are no longer just associated as gene transfection agents, but as promising building materials for applications as novel multifunctional particles for nanomedicine and diagnostic assays (*1–8*). For the scope of this chapter, these bio-inspired nanoparticles are broadly defined to encompass not only viruses, but also other similar protein-based assemblies, which include virus-like particles, ferritins, enzyme complexes, stressosomes, heat shock proteins and other supramolecular protein assemblies (Figure 1). The two major characteristics that unify the PBNs are; 1) the biological origins (hence genetically programmable) and 2) the natural ability to precisely arrange tens to hundreds of proteins into metastable supramolecular complexes within the nanometer range (10 to 300 nm).

There are several advantages bestowed on PBNs. One of the major advantages is the particle uniformity. Biological systems possess unsurpassed fidelity that churn out replicas with unmatched speeds. This provides the narrow size distributions of PBNs, batch to batch consistencies, and economic scale production potentials. And like any uniform proteins, the structural features can be analyzed at near atomic resolutions by x-ray crystallography. The structural information is an invaluable asset when it comes to reconfiguring the PBNs either by chemical or genetic modifications by using a structure based approach. Another advantage is the genetic flexibility of the proteins to generate a tremendous number of variables. One prominent example of this molecular tool and its genetic flexibility is M13 bacteriophage (*9*). This platform utilizes permissivity of the bacteriophage to its pIII minor coat protein gene (*9*), allowing peptides and even large proteins to be genetically fused to the coat protein. This system has provided robust high throughput screening of protein interactions, discovery of high affinity antibodies, functional selection of an enzyme, metal binding peptide sequences, and therapeutic proteins (*10–14*).

The disadvantages of PBNs are typical of many protein based systems. Low stabilities in organic solvents, limitation to 20 natural amino acids, susceptibility to proteases, pH extremes, low/high ionic conditions, high temperatures and large scale production yields are often limited to a few species of viruses. However, each of these factors can be seen as an obstacle rather than an impediment, and virus particles often exhibit a wider range of stabilities than most proteins. For instance, CPMV can tolerate aqueous/organic cosolvents in which the organic solvent volume ratio can reach up to 50-60%. *Tobacco mosaic virus* (TMV) tolerates temperatures up to 60°C, and can be stored for weeks at 4°C or prolonged storage at or below -20°C. The incorporation of non-natural amino acids, i.e. propargylglycine (*15–18*), or specific recognition sequences for post-translational modifications (*19*, *20*) have expanded the repertoire of primary building units. These approaches have further expanded the possible modifications available to the viruses and PBNs. Alternatively, conjugating with hydrophobic oligomers (*21*), extending polymeric chains (*22*, *23*), or co-assemblies with polymers (*24–26*) are possible chemical routes to alter its properties. In addition, evolutionary designs to genetically generate more stable mutants (*27–29*), or seeking thermophilic viruses (*30*, *31*) are possible routes to adjust these protein templates for strategic applications.

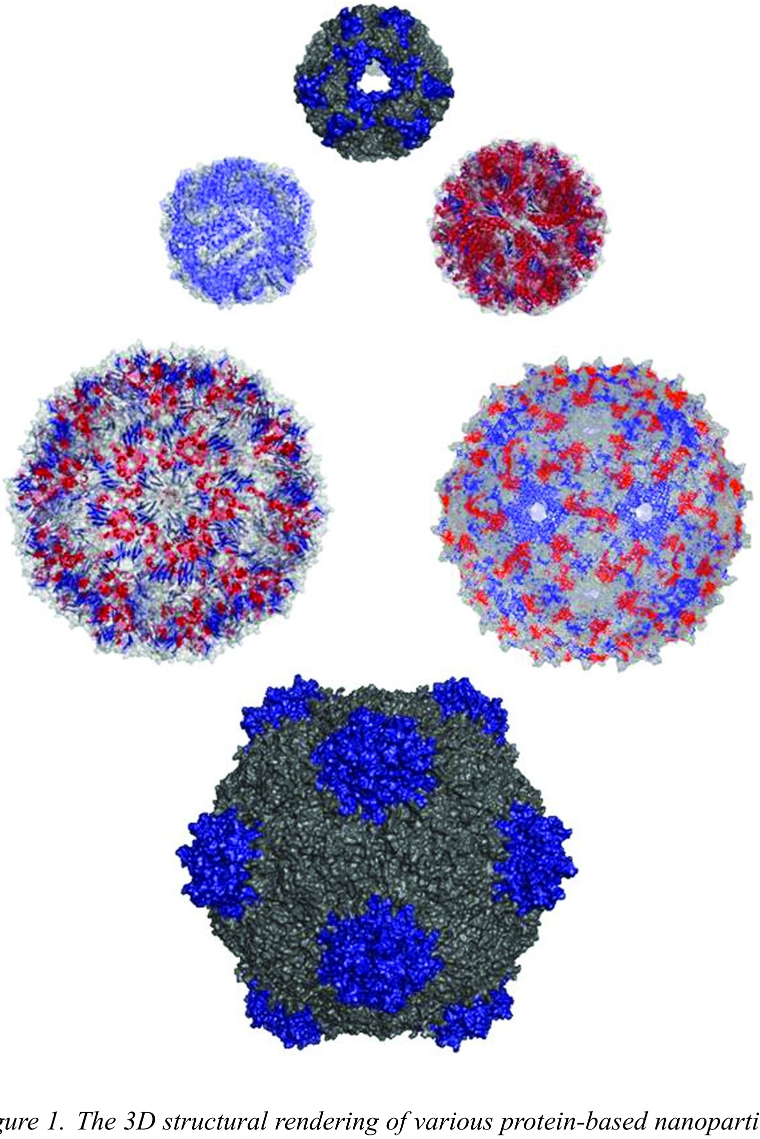

*Figure 1. The 3D structural rendering of various protein-based nanoparticles reported in literature. Heat shock protein, lumazine synthase, MS2 bacteriophage, Cowpea mosaic virus, Cowpea chlorotic mosaic virus and horse spleen ferritin (from top moving clockwise). The protein coordinates are from RCSB Protein Data Bank (www.rcsb.org/pdb) and the structures are rendered with PyMol (www.pymol.org).*

In Nanomaterials for Biomedicine; Nagarajan, R.;
ACS Symposium Series; American Chemical Society: Washington, DC, 2012.

In this chapter, we focus on the recent progress with the hierarchical assemblies of viruses and the adaptation of these macrostructures to elicit various cellular responses (Figure 2). The rationale for using virus-based assemblies as molecular tools for cell studies stems from the tissue itself. A tissue is comprised of several cell types and glycoproteins (or extracellular matrix – ECM) to execute a specialized function. This ECM is an amalgamation of various proteins that begin at the nanometer level, or at a subcellular level to provide structural and mechanical support to the cells (*32–34*). A bone tissue, for example, contains calcium phosphate nanocrystals to provide mechanical strength and collagen bundles to anchor the cells (*35*). Analogous to these hierarchical assemblies, the virus begins with a single coat protein which can be chemically and genetically altered with biologically relevant groups. The single coat protein is then assembled to larger scale macromolecule with nanometer sizes, well-defined ligand arrangements, and with molecular consistency. Inorganic nanocrystals can be deposited on the surface of viral particles, cell binding sequences can be added at high densities, and these final materials are biodegradable. However, unlike the other natural materials, isolation of virus-based materials is highly scalable to near industrial levels within a laboratory setting (kilogram yields). Rather than seeing the virus as its native infectious agent, we envision these particles as well-defined protein macromolecules that can be modified and characterized with relative ease.

One major concern is the immediate negative association of viruses in the public mindset with pathogenic strains. Human immunodeficiency virus, Ebola virus, avian flu virus, and the many more infectious agents have debilitating effects. The plant viruses reduce crop yields and food supplies. Overcoming this common preception of viruses is a great barrier to the research. CPMV has been well studied as intravital imaging agents with little to no cytotoxic effects in mice and in chick embryos (*36*, *37*). The plant viruses and bacteriophages have co-existed with mammalian hosts for ages without causing epidemics. Ongoing studies with subcutaneous implants of virus-polymer composite hydrogels in murine models indicate no detectable changes to white blood cell counts nor immunoglobulin titers against the virus (*38*). While it is unlikely to completely alter the public perception of viruses, these innocuous plant virus systems can provide a unique niche of molecular tools to study the role of ligand valency and hierarchical structures in cellular functions.

The following sections in this chapter are to elaborate on some of the basics of the virus-based materials within the last ten years. The chapter starts with a brief overview of the virus-based chemistry, which has been extensively reviewed by several groups (*39–41*). An expanded section has been dedicated to the use of genetic engineering to introduce biorelevant ligands on the surface of the virus, followed by the section describing the assembly of higher ordered structures and its use in cell studies. The last section provides open ended questions and discusses possible future directions in this field of virus-based nanotechnology. The highlighted works summarized in this chapter are by no means a comprehensive list of the recent achievements in this field, and many of the leading research groups have made significant contributions that are beyond the scope of this chapter's theme.

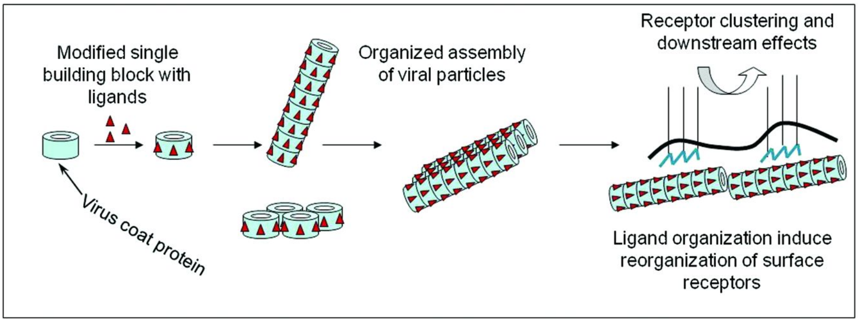
Modified single building block with ligands
Virus coat protein
Organized assembly of viral particles
Receptor clustering and downstream effects
Ligand organization induce reorganization of surface receptors

*Figure 2. Schematic illustration of using viral particles and its intrinsic assembly behaviors to generate higher ordered structures for cell studies.The smallest building unit, the virus coat protein, is chemically or genetically modified with biologically relevant ligands (i.e. cell binding ligands, dyes, drugs) and the particles are assembled into long rod-like structures or 2D arrays. These smaller macromolecules are then bundled to larger macrostructures to guide cell growth, migration, and differentiation.*

## Regioselective Chemical Modifications

Series of review articles have been published within the last ten years regarding the regioselective modifications of viruses and PBNs (*39–41*). Readers are encouraged to follow up on these review articles for in-depth discussion, and the primary literature as the field continues to blossom. This section is to briefly highlight the chemical modality of the virus and protein nanoparticles. In brief, the amines, thiols, phenols and carboxylates from lysines, cysteines, tyrosines and the two acidic residues (aspartic and glutamic acids) are well established conjugation techniques for viruses (*5*, *6*, *39*, *42*). An added flavor is the combination of molecular designing the chemically reactive groups (i.e. amine or thiol) based on the structural information of the virus and subsequently modifying the specific residue with expanded functionalities. This approach is a powerful means for designing novel nanomaterials. For example, the original strain of *Cowpea mosaic virus* (CPMV) possesses no reactive sulfhydryl groups on the outer surface, thereby allowing cysteine residues to be placed with molecular precision to display another chemically reactive group (*43*, *44*). On the other hand, CPMV has five reactive lysines exposed on the outer surface, two of which account for the majority of the reactivities towards N-hydroxysuccimide esters and isothiocynates (*44–46*). Conversed substitution mutations of the selected lysines with unreactive arginines permitted a unique mutant strain with single lysine groups positioned around the virus protein shell (capsid). The reduction of reactive groups can provide a predetermined ligand distribution around the capsid. The cysteine mutant and unique lysine mutant of CPMV are examples of combining genetic engineering with pre-designed bioconjugation approach. Many similar designs can also be conceived for other PBNs.

The examples of virus-based materials engineering are extensive. CPMV has been one of the earlier role models of virus-based materials, with enormous amount of work in the chemical and physical characterizations and its potential therapeutic use as a multifunctional nanocarrier for imaging and tumor targeting (*36*, *47–49*). The syntheses of inorganic nanoparticles with ferritin, *Cowpea chlorotic mottle virus* (CCMV) and other protein cages (*31*, *50*, *51*) as a nanosized tumor theranostic agent (*52*, *53*), and the light harvesting arrays with TMV coat proteins modified with flurophores are some of the highlighted developments in recent years (*54–56*). In another study, the same type of plant virus (TMV) has been assembled on silicon anode as nanocomposite electrodes with potential application as high performance lithium-ion batteries (*57*). Bacteriophage P22 exhibits unique self-assembly behaviors that provide large pores to shuttle materials within the viral capsid and the use of scaffolding proteins to release a portion of the scaffolding protein upon heating and protease treatment has been a clever approach to design temperature and enzyme triggered protein release nanocarriers (*58*). Filamentous M13 bacteriophage have been designed to bind and align inorganic nanocrystals in an ordered array exemplary models of a biological system for materials development (*59–62*).

## Genetic Modifications

### Multivalent Nanosized Vaccines

Since the 1990s, several studies involving peptide insertions on the coat protein of plant viruses has been reported for vaccine development (*3*, *7*, *63–66*). Configuring non-lethal plant viruses to prime the immune system against a lethal challenge of pathogens has been an attractive alternative to current recombinant technologies with mammalian pathogens. These non-replicating plant viruses pose little potential for re-integrating into the host genome, display the peptide inserts in multiple copies in a high density array, and can directly stimulate antigen presenting cells to provide protection against tumor challenges in mice (*67*). Multiple copies of the influenza virus antigens displayed on the *Potato virus X* (PVX) coat proteins have been shown to activate antigen specific CD8+ T-cells without co-administration of an adjuvant (*68*). Intramucosal administration of chimeric CPMV particles displaying the D2 peptide of fibronectin-binding protein B of Staphylococcus aureus had primed T-cells and generated high titers of antigen specific immunoglobulin G in mouse sera (*69*). Fluorescence activated cell sorting studies indicate rapid uptake within two hours of incubation of TMV particles by primary mouse splenocytes and bone marrow cells *in vitro* (*67*). Mice immunization with chimeric TMV particles activated peptide-specific T-cells by IFNy secretion and protected the mice from two different tumor models in both preventive and therapeutic settings (*67*). Translating the plant virus-based vaccines to the market will require extensive examinations involving effectiveness of the immunizations, long term storage, administration routes, bio-containment in the plant fields and other regulatory issues. Moreover, these earlier studies paved the road for genetic modifications on plant viruses, and simplified the transition of plant viruses to tissue engineering applications.

## Inserting RGD Motifs for Cell Adhesion

Initiating attachment, and regulating cell migration, growth and differentiation are crucial factors for engineering functional tissues. The classic approach has been to insert the minimal fragment, arginine – glycine – aspartic acid (RGD) amino acid residues, which is based on the integrin binding sequence of fibronectin (*70*, *71*). However, the minimal sequence has broad receptor affinities (*72*) and has been reported to interact strongly with integrin $\alpha_v\beta_3$, rather than integrin $\alpha_5\beta_1$ receptors as indicated by decreased cell attachments when blocked with anti-$\alpha_v$ antibody (*73*, *74*). In comparison to the RGDS peptide alone, the recombinant fibronectin fragment showed selective binding to $\alpha_5\beta_1$ integrin receptors, increased cell attachment strengths and improved titanium implant integration in rat models (*75*). Phage display studies with sequence extensions and incorporation of auxiliary binding sequence with varying linker lengths suggest that selective binding of integrins could be achieved (*76–80*). Cyclization of the RGD peptide via a disulfide bridge to mimic the natural loop in fibronectin resulted in greater potency inhibiting cell attachment than its linear form (*81*, *82*). These experimental results indicate that engineering the appropriate ligands can provide specific receptor targeting, which can be crucial in guiding stem cell differentiation. Studies show that $\alpha_5\beta_1$ specific engagement facilitates mesenchymal stem cell differentiation towards bone tissues (*83*) with increasing amounts of fibronectin and collagen synthesis and deposition over the 28 day time course (*84*). The results from these studies indicate the importance of ECM and its corresponding integrin specificities to influence osteogenic differentiation in mesenchymal stem cells.

Earlier studies with plant viruses demonstrated that the viruses were not toxic to the mesenchymal stem cells and had significantly accelerated bone differentiation *in vitro* (*85–87*). To further explore the potential of virus-based cell scaffolds, TMV coat protein was genetically modified with a 7-mer and 12-mer RGD containing peptide sequences to generate non-infectious, multivalent ECM mimetics (*88*, *89*) (Table 1).

**Table 1. RGD sequences inserted to TMV coat protein**

| *Mutants* | *Insert Sequence* | *Insertion Site* |
|---|---|---|
| RGD1 | GRGDSPG (7-mer) | Fused to the carboxyl end of viral coat protein |
| RGD7 | AVTGRGDSPASS (12-mer) | Inserted between residues Ser155-Gly156 of coat protein |

The goals were to obtain consistent ligand distribution and structural regularity of cell binding ligands by using a virus as a scaffold. Slightly longer peptide inserts were fused near or at the carboxy end of the coat protein to display the ligands to the outer surface.

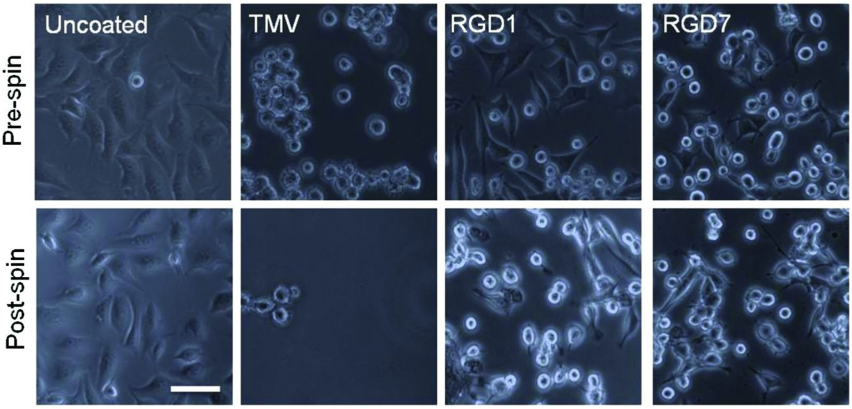

*Figure 3. Phase contrast microscopy of cells prior and post inverted centrifugation indicate poor binding to native TMV. The uncoated wells promoted cell attachment, however, the cells seeded on TMV coated wells remain rounded prior to subjecting the cells to the inverted spin. Cells seeded on TMV-RGD1 (abbreviated as RGD1) show well spread cells as well as some rounded cells, and similarly for the cells on TMV-RGD7 (noted as RGD7,) the mixed morphologies of cells are observed prior to centrifugation. After a 10 g inverted spin for 5 minutes, the majority of the cells on TMV coated wells are removed. Both RGD1 and RGD7 coated wells retain the cells. Images adapted with permission from ref. (88). Copyright (2012) American Chemical Society. Scale bar is 50 microns.*

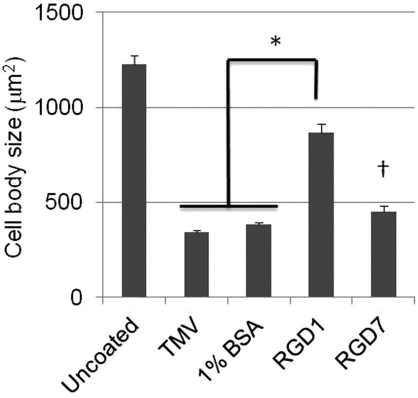

*Figure 4. Cell body sizes measured prior to spin indicate cells spread on the TMV mutants with the RGD sequence inserts, and not on native TMV. Error bars denote ± SEM (n = 50). p values < 0.05 were considered statistically significant based on two-tailed Student t-test. *p value < 0.005 and †p value < 0.05. Data adapted from ref (88).*

X-ray crystal structure and previous mutagenesis studies indicate that the carboxy end of the TMV coat protein is a highly flexible region exposed to the outer surface (*65*). The native and mutant viruses were screened by coating 96-well plates and allowing the cells to adhere for one hour in serum-free conditions. Afterwards the cells were subjected to an inverted centrifugation to remove weakly attached cells in a consistent manner. The adherent cells were visualized by phase contrast microscopy prior to and after centrifugation (Figure 3).The cells seeded on uncoated wells adhered similar to standard tissue culture plastic with similar morphologies (broad, pyramidal cell shape). The cells on TMV coated surfaces remained rounded and in suspension, whereas the cells on TMV mutants exhibited long and thin filopodial extensions (Figure 3). As indicated by the pre-spin cell body sizes, which can also be correlated to cell spreading, the average cell size significantly decreased from 1200 $\mu m^2$ (uncoated) to 300 $\mu m^2$ for cells on TMV-coated surfaces. The cell sizes were partially restored for the cells seeded on surfaces coated with TMV-RGD1 to 800 $\mu m^2$ (Figure 4), and a modest increase from 300 to 450 $\mu m^2$ was measured for BHK cells seeded on surfaces coated with TMV-RGD7 (Figure 4). Quantitative cell attachment measurements with fluorescently labeled cells validate these observations that native TMV lack specific cell binding moieties for the two mammalian cell lines.

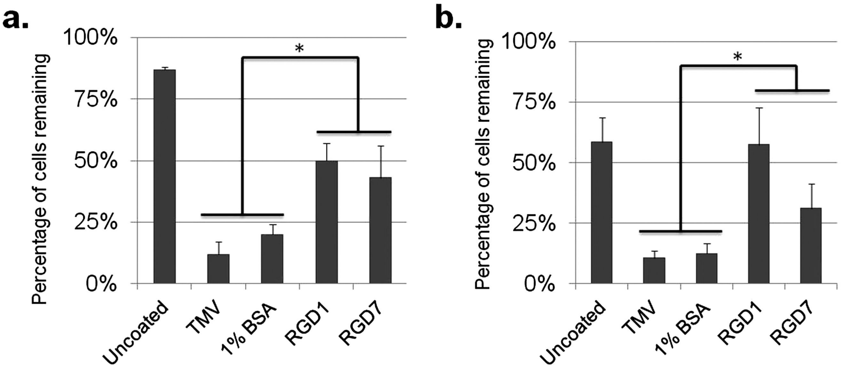

*Figure 5. Inverted centrifugal assay indicate differential adhesion for the native TMV and TMV mutants. After subjecting the cells to an inverted spin of 10 g (1.2 pN/cell) for 5 minutes (**a**) approximately 50% of the BHK cells remain attached to the TMV-RGD1 and –RGD7 coated wells, whereas (**b**) over 50% of CHO cells remain attached only on TMV-RGD1 coated wells. Error bars denote ± SEM (n = 6) from three separate experiments. p values < 0.05 were considered statistically significant based on unpaired Student t-test. *p < 0.05. Adapted with permission from ref (88). Copyright (2012) American Chemical Society.*

Inverted centrifugal assay indicated the original viral capsid having similar cell attachment profiles to the negative controls (1% BSA coated), supporting the argument that BHK (Figure 5a) and CHO cells (Figure 5b) do not bind to TMV coated surfaces. On the other hand, both TMV mutants retained 50% cell attachment for both cell lines after an inverted spin at 10 *g* (Figure 5a, b).

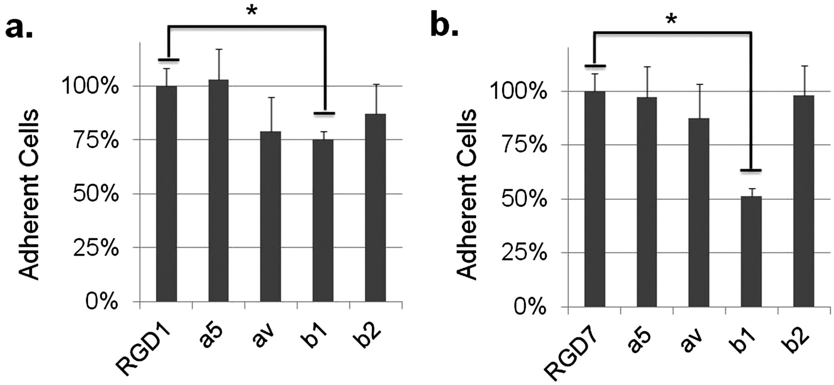

*Figure 6. TMV RGD mutants with different flanking sequences are partially inhibited by anti- $\beta_1$ antibodies. (**a**) Blocking the integrin subunits with monoclonal antibodies indicate TMV-RGD1 mutant partially mediates cell attachment via $\beta_1$ subunit whereas (**b**) TMV-RGD7 has more preferential binding to $\beta_1$ subunit. *$p < 0.05$ ($n = 4$, two-tailed Student t-test). Data adapted from ref (88).*

Receptor specificities were determined by blocking integrin subunits $\alpha_5$, $\alpha_v$, $\beta_1$, and $\beta_2$. Neither of the antibodies against α subunits inhibited cell attachment, but cells incubated with anti-$\beta_1$ showed partial reduction in cell binding towards TMV-RGD1 coated substrates (Figure 6a) with greater reduction in attachment to TMV-RGD7 coated substrates (Figure 6b). Based on these results, one could argue that the TMV-RGD7 mutant has preferential binding to the $\beta_1$ subunit whereas the TMV-RGD1 mutant mediates its binding through other receptors, $\alpha_v\beta_3$ and $\alpha_v\beta_5$ being highly possible candidates among the different integrin receptors. The results also support the initial design of the inserts, in which both 7-mer and 12-mer inserts were based on the tenth fibronectin type III repeat, but a slightly longer flanking region improves selectivity. Additional studies with purified $\alpha_5\beta_1$ and $\alpha_v\beta_3$ receptors would shed light to the actual binding affinities and selectivity of the two receptors towards these two mutants.

Clues to designing novel peptide ligands can be found by analyzing other ECM proteins that possess the RGD cell attachment sites (*90*) (Table 2). Within the bone tissue, the non-collagenous matrix proteins such as bone sialoprotein (BSP), osteopontin (OPN), and dentin share the RGD mediated cell attachment sequences

(*91*, *92*). Although the peptide sequences alone cannot completely recapitulate the natural ECM proteins, providing auxiliary domains, distal secondary binding sites and structural conformations to assist the cell binding sequences may enhance selective receptor binding and cell functions.

The attachment of animal viruses (i.e. penton base of adenovirus, foot and mouth disease virus) to the various cell surface receptors offers insight to the structural and functional properties involving virus-receptor complexes. The GH loop of the structural viral protein VP1 contains the integrin binding sequence for Foot-and-mouth disease virus (FDMV) that has most likely evolved to bind to $\alpha_v\beta_6$ with higher affinity than other integrin receptors (*93*). Extensive knowledge of adenoviruses and its distinct interactions with the cell surface receptors are promising models for improving the other virus based scaffolds. Majority of the studies involving adenovirus in biomedical applications are presented in the context of gene therapy, but the extensive mutational analyses of the virus capsid (*94*, *95*) are important experimental designs that could guide future mutational designs for the purpose of tissue engineering.

**Table 2. Non-collagenous matrix proteins with RGD sequences**

| *Protein* | *Sequence flanking RGD* |
|---|---|
| Bone sialoprotein | ENGEP – RGD - NYRAY (*96*) |
| Dentin | VVSES – RGD - NPDPT (*97*) |
| Osteopontin | DTYDG – RGD - SVVYG (*98*) |
| 10th type 3 repeat of fibronectin | YAVTG – RGD - SPASS (*99*) |
| Vitronectin | KPQVT – RGD - VFTMP (*100*) |
| Tenascin C | SLISR – RGD - MSSNP (*101*) |
| Laminin P1 fragment | GTFAL – RGD - NPQGC (*102*, *103*) |

## Alternative Surface Receptor Binding Repertoire

Alternative cell attachment peptide sequences lacking the RGD sequences exist in the natural ECM proteins and have been reviewed by other groups (*104*, *105*). For the purpose of future designs and discussions, a very limited description of the various ligands are listed in this section. Collagen is known to interact with integrin $\alpha_2\beta_1$ receptors (*106*, *107*). Other peptide sequences derived from fibronectin synergy site (PHSRN) (*108*, *109*) and post-translational conversion of Asn-Gly-Arg (NGR) sites to isoasparatyl groups to result isoAsp-Gly-Arg (isoDGR) (*110*, *111*) has been shown to promote integrin recognition and cell binding. The polypeptide with the repeat sequence of GFOGER (O = hydroxyproline) forms a similar triple helix bundle (*112*) and mimic its effects for supporting osteoblastic differentiation (*106*). Other collagen mimetic sequences

(DGEA, P15, GEFYFDLRLKGDK) have been displayed as peptides on different bioactive surfaces (*113*, *114*) or on viruses to promote cell attachment and differentiation (*88*, *115*). The peptide sequences, YIGSR and IKVAV, are derived from laminin and have been reported as active sequences to induce cell attachment and neurite outgrowth (*116–120*).

Native mammalian viruses also possess non-RGD containing cell binding motifs to infect the host through receptor-mediated endocytosis. In the case of adeno-associated virus serotype 2, integrin receptors $\alpha_V\beta_5$ have been identified as cell surface receptors that mediate virus entry through LDV sequence (*121*), whereas the cell attachment is mediated through heparin sulfate proteoglycans (*122*). By no means are integrin receptors the sole source of ECM and cell signaling interactions; these receptors interact with multiple signals from growth factors and glycoproteins to input external signals. Growth factor sequences and other receptor binding peptide sequences beyond the integrin receptors are crucial tools to engineering the hospitable niche. The dissection and re-integration of these multiple cues as essential extracellular components to guide and determine stem cell outcomes will be necessary. One of the future studies could revolve around the role of the multi-component ligands expressed on virus particles versus dissociated particles in promoting cell attachment, migration, growth, and differentiation.

## Hierarchical Assembly of Viruses

The recent works discussed in this section describe how the innate structural properties of viruses are exploited to generate higher ordered structures, which in turn are used to direct cellular functions. In the earlier works, the chemical modifications of different types of viral particles had been reported by Wang *et al* (*123–126*), along with the structural and mechanical features of one and two dimensional virus assemblies (nanofibers, thin films, Pickering emulsions and microspheres) (*127–133*). Recent studies have shifted the focus on translating these assemblies for biological applications. Some of these coatings support and sustain mammalian cells with no measurable cytotoxicity (*124*, *134*). Previous sections discussed how the virus particles can be primed with biochemical cues to interact with integrin receptors. The following three sections are recent studies involving assembly strategies with viral particles for potential use in biomedicine. These modified virus particles are arranged with well-known assembly strategies to display as two dimensional and three dimensional scaffolds for cell growth. These materials in turn are used to revisit some of the fundamental questions in cell biology (adhesion and migration).

### Electrospun Virus−Polymer Composite Nanofibers

The plant virus, TMV, were electrospun with PVA, poly(vinyl alcohol), to generate nanofibers with diameters ranging 200-400 nm as non-woven mats for potential use as a tissue supporting substrate (Figure 7) (*89*). PVA is approved for use in the biomedical field as transdermal patches or as part of slow releasing ophthalmic and oral drug tablet formulations (*135–138*). The polymer can be directly modified by targeting the hydroxyl groups of PVA (*139*), or alternatively by blending a co-polymer or proteins (*140–143*). The mixing of viral particles was a proof-of-concept study for functionalizing the polymer blends. No major differences could be observed by scanning electron microscopy between TMV-PVA fibers versus the PVA only fibers (Figure 7a, b). The composite TMV-PVA electrospun nanofibers were continuous and uniform strands without beading (Figure 7b). Within the tested concentration range, increasing the concentration of the viral particles resulted in no observable morphological differences between the composite nanofibers based on SEM imaging (Figure 7b-f). Similarly, incorporating the viral particles to the fibers did not significantly impair the tensile strength of the fibers. The calculated Young's modulus for TMV-PVA nanofibers was 315.0 ± 51.4 MPa, which was comparable with that of the as-spun PVA nanofiber (*89*). The result suggests that the incorporation of TMV at the reported concentrations in PVA solution provided sufficient viscosity and electrostatic charge to generate long continuous fibers without significantly impairing the mechanical properties of the electrospun fibers.

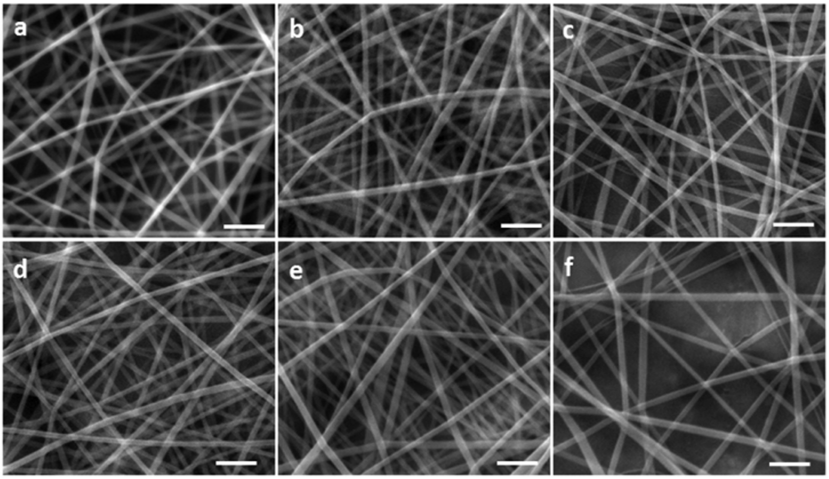

*Figure 7. SEM images show as-spun TMV-PVA nanofibers at 12 wt% PVA and TMV concentration of (**a**) 0.0 mg/mL, (**b**) 0.17 mg/mL, (**c**) 0.34 mg/mL, (**d**) 0.68 mg/mL, (**e**) 1.20 mg/mL, and (**f**) 1.70 mg/mL. Scale bars are 2 μm. Reproduced from ref. (144) by permission of The Royal Society of Chemistry. Copyright (2011).*

A major disadvantage of the system was that both the virus and polymer were highly soluble in water, and would immediately disperse in cell culture medium unless the composite fibers were stabilized with chemical crosslinking reagents or crystallization of PVA by dehydration. We have conducted a series of tests to improve the water resistance of PVA-virus composite nanofibers by dehydration (*144*). The fibers were treated with methanol or ethanol to induce the partial crystallization of PVA and thereby increase the stability of the composite nanofibers in aqueous solutions (*144*). X-ray diffraction indicated the partial dehydration process by resulted in a transition from amorphorous to a more ordered fiber, whereas repeated freeze-thaw only provided a slight change with a narrow diffraction peak appearing at about $2\Theta = 2°$ (*144*). Incubation of the dehydrated composite fibers resisted water salvation up to 3 days in complete media.

The incorporation of viral particles in polymers as electrospun fibers was suggested as a novel approach towards modifying the polymeric system with a multivalent scaffold. As a proof of concept, baby hamster kidney (BHK) cells were cultured on the non-woven mat of composite fibers comprised of genetically modified virus (TMV-RGD1) and PVA. The experimental results showed that the cells were poorly adherent on substrates with PVA and TMV-PVA composite fibers, typically forming rounded cell bodies and low cell densities even after 12 hours of culture in serum-free media. The substrate comprised of TMV-RGD1 and PVA, on the other hand, provided anchor points for the cells to attach and spread (*144*).

The reported method can be used in the fabrication of a broad range of composite nanofibers using synthetic polymers and bionanoparticles as starting materials. Since TMV as a building block can be tailored with various functional groups by both chemical conjugation and mutagenesis, the co-electrospin process can incorporate a variety of functionalities into PVA fibers. The mutant TMV-RGD1 co-spun with PVA into nanofibers, which could be used as substrates for cell adhesion studies. The reported study demonstrates the great potential of this method in fabricating bioactive fibrillar materials as degradable biomaterials in tissue engineering applications.

## Assemblies To Direct Cell Outgrowth

For years, bacteriophages and other viruses have been utilized as drug delivery vehicles and vaccines (*5*, *48*, *63*, *64*, *67*, *69*). The straight forward bioconjugate chemistries (*145*) and genetic modularity of viruses facilitated the generation of novel materials (*57*, *62*, *146*). M13 bacteriophage, in particular, has been extensively characterized over the past years for use in phage display and inorganic material deposition (*62*, *147*, *148*). Its innate ability to organize into liquid crystalline, along with well-defined nanostructures, standardized molecular cloning strategy, and rapid production in large quantities, the bacteriophage possessed many key features as a powerful building material (*59*, *149–152*). In one study, the M13 phage's natural tendency to form well-ordered films were exploited to generate thin films to dictate cell adhesion and outgrowth (*153*).

A single-step assembly process was introduced for depositing aligned arrays of viral particles over several centimeter length scales, in which all the rods align parallel to a single direction (*154*). The coating thickness and directionality is controlled by the operational parameters of withdrawal speed and substrate wettablity (Figure 8) (*154–156*). Similar to drop casting, dip coating and convective assembly, the mechanism driving the surface organization is based on the receding liquid front and the resulting shear forces create dense packaging of the particles (*156*). These assembly techniques are well-studied in colloidal science, as large number of particles has been deposited on surfaces as "bottom-up" techniques to achieve highly consistent and controlled surface coatings (*154*, *157–162*).

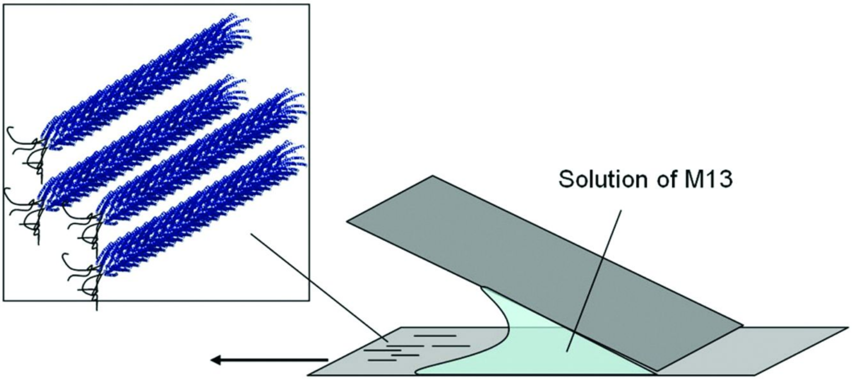

*Figure 8. Scheme of convective assembly of M13 bacteriophage on glass surface to induce aligned virus film. The bottom plate and top plate move in opposite directions to drag the meniscus of virus solution across the bottom plate. Reproduced from (153) by permission of The Royal Society of Chemistry. Copyright (2008).*

Using this convective assembly technique, long range ordered M13 bacteriophage and TMV particles were presented as thin coatings (*153*, *154*, *156*). The M13 virus films provided a protein-based substrate to guide cell alignment and orient the cell outgrowth along defined directions, while still retaining the chemical and genetic malleabilities of a biological scaffold (*115*, *120*, *163*). Rong *et al* targeted the surface exposed amino groups on M13 bacteriophage to tether the classic cell binding peptide sequence, Arg-Gly-Asp, to promote fibroblast adhesion and outgrowth (Figure 9) (*153*). Other groups have genetically engineered the major coat protein of phages to display peptide sequences from collagen, laminin, osteocalcin and osteogenic growth peptide to control cell differentiation (*115*, *120*, *163*).

These studies have demonstrated that these virus-based materials can be effectively used as materials to govern the cell morphologies and migratory behaviors. A more in-depth analysis of the underlying features revealed topographical patterns at the nanometer level (*89*). The height profiles along the length of the viral film ranged from 40 to 80 nm with a median of 60 nm, whereas the heights across the virus film ranged from 60 nm to 110 nm with a median height of 100 nm (*89*). These measurements suggest that the convective assembly with the bacteriophage solution provides "peaks" and "valleys", and such patterns provide topographical cues to dictate the cell migration. The hypothesis that these physical barriers are forcing the cells to migrate in a uniform manner appears to be in line with reports using controlled topographical features (*164–169*). Previous studies have indicated that varying ridge width and depth appear to be important factors for cell elongation, with different critical groove depths being reported for different cell types (*170–173*).

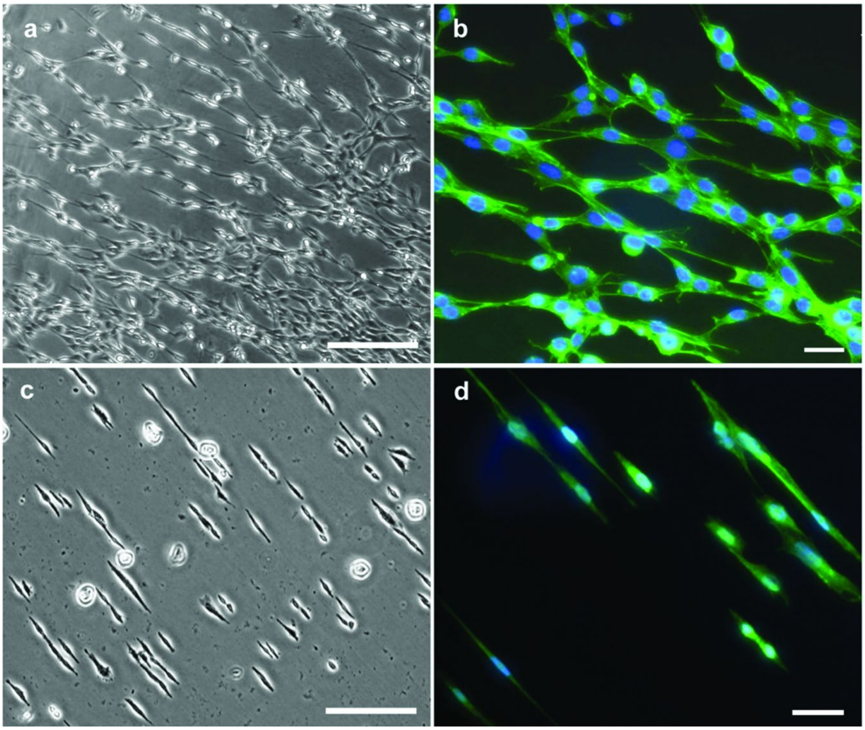

*Figure 9. Optical images using an inverted phase contrast microscope.* ***(a)*** *Optical image of NIH-3T3 cells cultured on an aligned M13 thin film by the slow dragging method.* *(**b**) Fluorescence image of NIH-3T3 cells.* *(**c**) Optical image of CHO cells cultured on an aligned M13 thin film by the slow dragging method.* *(**d**) Fluorescence image of CHO cells . β-actin is labeled with green fluorescent phalloidin, and the nuclei with 4′,6-diamidino-2-phenylindole (DAPI). Scale bars: 100 μm. Reproduced from ref (153) by permission of The Royal Society of Chemistry. Copyright (2008).*

Similar to our previous report, when 3T3 and BHK cells were cultured for 24 h on the aligned M13 films, the majority of the cells displayed elongated, spindle-like morphologies. The cells grown on coverslips were randomized with stellate morphologies (Figure 10a, d). In contrast, the cells were aligned parallel to the convective assembly direction of M13 viruses rather than traversing the ridge and groove, (Figure 10b, e). This tendency of the cell orientation suggests that the presence of contact cues between cells and the patterned M13 scaffolds plays an important role in cell morphology and spreading. Such observations have also been documented for cells cultured on nanopatterned substrates with varying heights and ridge widths. When the cells were incubated for longer time period (72 h), 3T3 fibroblasts appeared less elongated and lost their overall orientation (Figure 10c). More cells began to exhibit stellate morphologies rather than a spindle-like morphology. On the contrary, BHK cells remained to their original orientation and appeared to be more significantly elongated (Figure 10f). The cell alignment was measured using previously reported method to compare elongation factor and degree of orientation for the two cell lines.

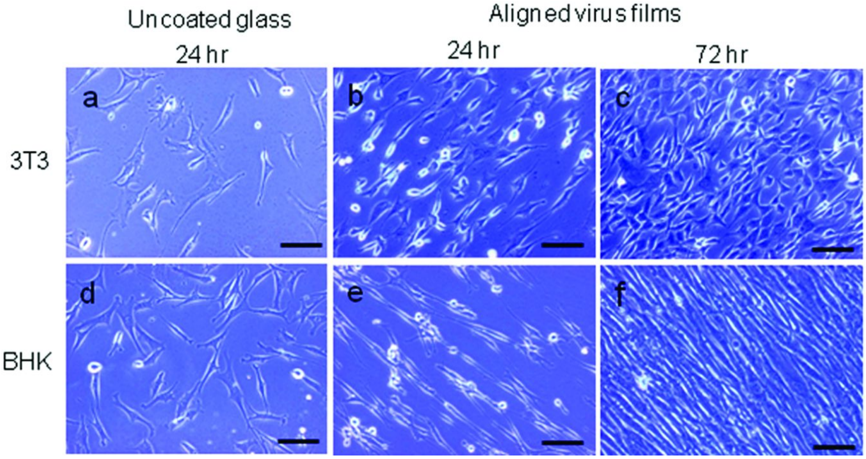

*Figure 10. Phase contrast images of mammalian cell lines cultured on plain, uncoated glass versus on aligned virus films. Optical images of NIH-3T3 cells (incubated for24 h) on plain coverslip (**a**) and on M13 films after 24 h (**b**) and after 72 h (**c**). Optical images of BHK cells grown on coverslip for 24 h (**d**) and on M13 films for24 h (**e**) and for 72 h (**f**). Reprinted with permission from (89). Copyright (2011) American Chemical Society.*

As shown in Figure 11a, the orientation angle (θ) refers to alignment of the long axis of the cell body (X-axis) to the general direction of the virus film. An angle of 0° denotes a perfect parallel alignment of cell to the direction of the virus film whereas orientation angles of > 45° would note random orientation. The ratio of X/Y represents the elongation factor, where the higher values indicate longer and thinner morphologies, which are typically observed with spindle-shaped cells that are aligned within grooved substrates. Based on these measurements, the elongation factors and orientation angles of 3T3 and BHK cells were calculated (Figure 11b). The measured values indicate an incremental loss of alignment and reduced elongation factor for NIH-3T3 cells over longer culture period, but the inverse for BHK cells with increased alignment and higher elongation factor after 3 day cultures. Sequential imaging analyses at micro- and nano- scale levels of aligned cells and fibrillar matrix proteins were documented using scanning electron microscopy (SEM) and immunofluorescence microscopy (*89*). The results from this study provide a crucial insight into the topographical features of a biological thin film, which can be utilized to control the cell orientation and its surrounding ECM.

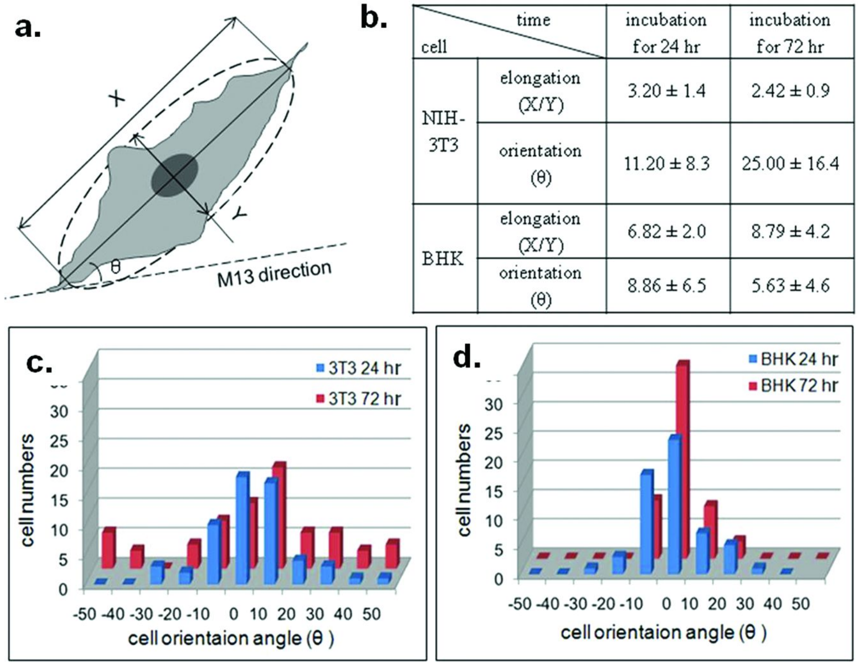

| time<br>cell | | incubation for 24 hr | incubation for 72 hr |
|---|---|---|---|
| NIH-3T3 | elongation (X/Y) | 3.20 ± 1.4 | 2.42 ± 0.9 |
| | orientation (θ) | 11.20 ± 8.3 | 25.00 ± 16.4 |
| BHK | elongation (X/Y) | 6.82 ± 2.0 | 8.79 ± 4.2 |
| | orientation (θ) | 8.86 ± 6.5 | 5.63 ± 4.6 |

*Figure 11. The orientation angle and elongation factor of mammalian cells on patterned M13 films. (**a**) Schematic illustration of orientation angle θ and elongation factor X/Y. (**b**) Representative table of the elongation factors and orientation angles of 3T3 and BHK cells incubated on the M13 film, with mean ± S.D. Orientation of (**c**) NIH-3T3 cells and (**d**) BHK cells on M13 films when cultured for 24 h and 72 h, respectively (0° degree represents perfect alignment and >45° represents random orientation). Reprinted with permission from (89). Copyright (2011) American Chemical Society.*

The coupling of a convective assembly process to the lyotropic crystallinity of viruses provides a unique bottom-up fabrication approach to generate well defined thin film coatings on surfaces. A thin film of M13 bacteriophage can be readily generated to support cells (*89*, *153*). The resulting virus coating directed NIH-3T3 fibroblasts along a predictable manner, and the thin virus coatings could be further stabilized by chemical crosslinking. In addition, the surface of M13 has been chemically modified with an alkynyl group which had been used as a universal handle to introduce various functionalities by copper(I) catalyzed alkyne-azide cycloaddition "click" reaction (*145*). The study by Li *et al* extensively documents the accessibility and reactivity of the bacteriophage coat protein. The bioconjugation approach expands other synthetic functional groups to be displayed on the virus. Furthermore, this concept can be extended in similar manner to other rod-like viruses (TMV and PVX) to generate the nanometer topographical features generated by M13 bacteriophage crystalline film.

### Alignment of TMV under Confined Space To Form Striped Patterns

Drying nanosized colloidal suspensions is a relatively simple fabrication process for large scale pattern formation in which as the solvent containing the nanoparticles evaporate, the organization of the nanoparticles can be controlled by rate of evaporation, ionic strengths, and particle concentration (*174–176*). Different pattern formations using this phenomenon can also be obtained by confining the solvent in a geometrically defined container (Figure 12) (*177*, *178*). The general principle that governs the pattern formation lies with the pinning and depinning process (stick-slip motion) at the contact line (*158*). Usually, spherical colloidal particle suspensions and polymer solutions are two widely used systems for theoretical and experimental studies. However, a systematic study of the orientation of anisotropic particles, such as nanorods, at the contact line during the drying process can further improve the theoretical understanding of pattern formation induced by solvent evaporation. TMV is an ideal candidate to initiate these studies due to its rod-like morphology and high monodispersity. We studied the formation of diverse patterns resulting from drying a solution of rod-like TMV particles in glass capillary tube and two horizontally stacked glass slides (*179*). The concentration of TMV, the salt concentration in aqueous solution and surface properties are three key factors that govern such a combined self-assembly behavior. One direct application of the patterned structure in the capillary tube is to direct the orientation of smooth muscle cells perpendicular to long axis of the tube, which renders it great potential in the development of enhanced vascular grafts.

The phenotypic switching in smooth muscle cells (SMCs), from contractile to synthetic and vice versa, has been recognized as an important regulating point in a number of vasculature related diseases (i.e. atherosclerosis) (*180*). Synthetic phenotype are defined by epithelioid or rhomboid morphology, often described as cobble stone, whereas the contractile form of SMCs are long and spindle shaped with more contractile filaments. The proliferation and migration rates of the synthetic SMCs are higher than its contractile counterpart. They also have a larger number of organelles dedicated to protein synthesis (*181*).

There has been considerable research in the mechanisms of SMC phenotypic regulation (*182*, *183*), migration (*184*), and differentiation (*180*). Ultimately the regulatory mechanisms involved with SMC phenotype switching will play a significant role in atherosclerosis (*184*, *185*). Atherosclerosis is the underlying cause of a group of diseases, characterized by a thickening of artery walls (*186*). Atherothrombotic diseases are currently and are projected to be the leading cause of death worldwide by 2020 (*187*). Coronary atherosclerosis results in approximately $44 billion in expenses for the American public each year (*188*). This thickening of artery wall is attributed to dramatically increased proliferation, differentiation, and migration of SMCs to occupy the intima (*184*). The primary functions of aortic SMCs are regulation of blood vessel tone-diameter, blood pressure, and blood flow distribution (*189*). However they also play important roles during vascular remodeling i.e. during pregnancy, exercise, or after vascular injury (*190*). In response to these environmental cues, SMCs produce large amounts of extracellular matrix and undergo a dramatic increase in proliferation and migration (*191*). Thus understanding the response of SMCs towards various micro- and nano-environmental cues are important in short-term regulation as well as long-term adaptation (*182*).

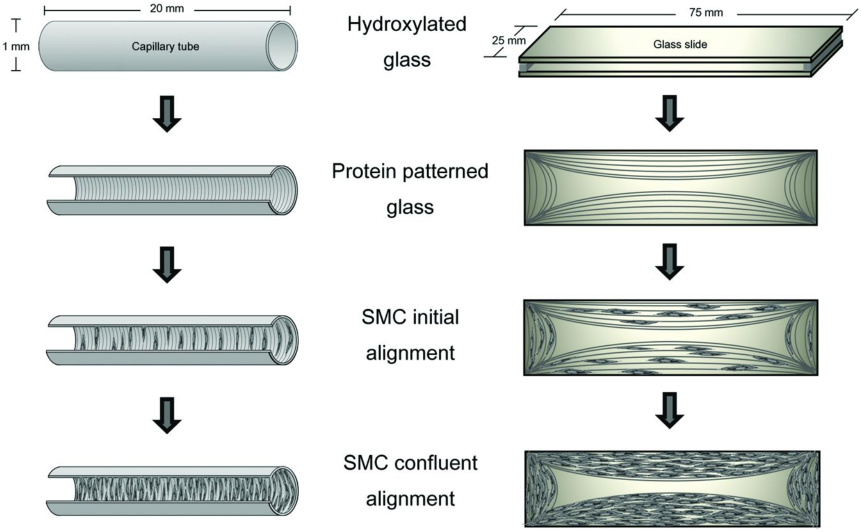

*Figure 12. The virus particles self-assemble in capillary tube and between two glass slides by water evaporation. A hydrophilic surface is generated on the glass surface by treating with piranha solution. The virus is pinned to the surface along the water/surface contact line as the liquid slowly. As the contact line retreats, the hierarchical structures of stripes are formed along the axis of the water receding line.*

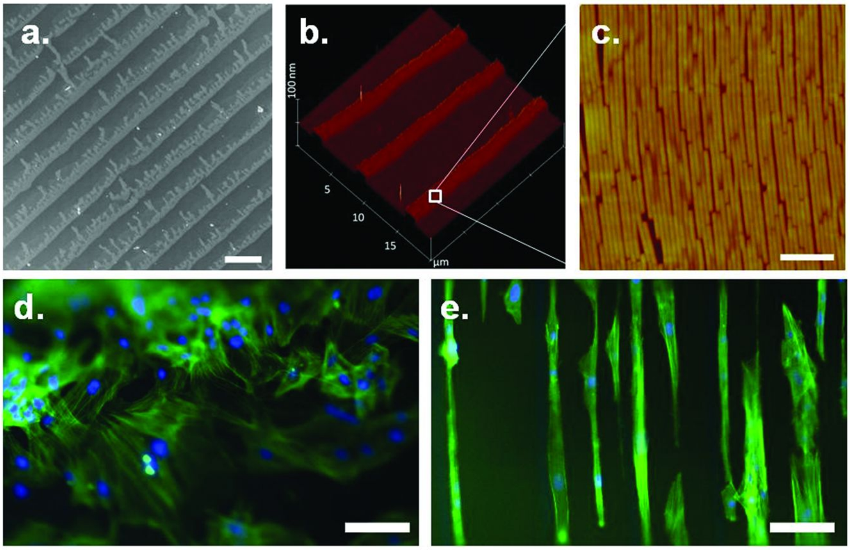

*Figure 13. The alignment of virus particles inside the capillary tube generates striped patterns. (**a**) Scanning electron microscopy (SEM) image of stripe patterns after drying 0.1 mg/mL TMV solution in capillary tube. (**b**) 3D atomic force microscopy height image of aligned TMV particles. (**c**) An enlarged region of highlighted box in (**b**). (**d**) Fluorescence images of rat aortic smooth muscle cells cultured inside the capillary without stripe patterns, (**e**) the same cells cultured inside the capillary tubes with patterned surface. Scale bars: **a**, 20 µm; **c**, 200 nm; **d** and **e**, 50 µm. Adapted with permission from ref. (179). Copyright 2010 John Wiley and Sons.*

The synthetic modeling of the microenvironment for SMC cultures has been approached with virus-based assemblies by using the similar slow drying method as previously described. In this study, TMV solutions were dried in an open-ended horizontally laid capillary tube (length 2.2 cm, inner diameter 0.15 cm) under ambient conditions. Symmetrical patterns were formed at each side of the tube, as indicated by SEM imaging (Figure 13a). The patterns are generated based on the pinning and de-pinning of TMV particles at the air/liquid/surface interface. The height profile of the atomic force microscopy (AFM) image (Figure 13b) shows a single layer of TMV particles can be deposited on the surface as striped patterns by controlling the virus concentration, ionic strength of the solvent, and surface wettability (*179*). As the solvent meniscus recedes within the capillary, the particles form a close-packed structure, in which TMVs orient parallel to the contact line while perpendicular to the long axis of the capillary tube (Figure 13c). The formation of hierarchical structure is determined by preferred orientation of TMV at the air/liquid interface as well as the pinning-depinning process. At low concentration of TMV with salts, individual TMV orients parallel to the plane of the interface to maximize the interfacial coverage per particle. One direct application of the patterned structure in the capillary tube is to direct the smooth muscle cells (SMCs) orientation perpendicular to long axis of the tube. Within the body, SMCs are spindle shaped and align their long axis circumferential to the long axis of the blood vessels. This alignment is crucial for proper blood vessel function to provide the proper elasticity (*192*). In a diseased or damaged blood vessel SMCs change to a synthetic phenotype and exhibit an increased proliferation rate. Most current efforts have focused on either stress induced SMCs alignment or 2D patterns generated by lithography method or mechanical stress (*27*, *28*). Compared to the SMCs cultured in glass capillary tubes (Figure 13d), SMCs cultured inside the TMV patterned capillary tubes align perpendicular to the capillary tube (Figure 13e). In glass capillary tubes without TMV patterns (Figure 13d), morphology of SMCs was epithelioid or rhomboid, typical of the rapidly proliferating, synthetic phenotype (*29*). However, SMCs cultured in the tube with stripe patterns tended to be spindle shaped, typical of the contractile phenotype (Figure 13e).

## Conclusion

Nature designs many biogenic systems with exquisite symmetries and complexities at nanometer scales. Viruses, ferritins, enzyme complexes, chaperonines and carboxysomes range widely in shapes and sizes with diverse chemical and physical properties, thereby presenting an extensive selection of primary building blocks. These particles possess astounding thermal and pH stabilities along with tremendous resistance to denaturation at high ionic concentrations. Such features, in combination with superb symmetry and size uniformity, have been exploited as templates for material synthesis, structural analysis. The system modularity is further strengthened in combination with genetic engineering to position additional functionalities with molecular precision. Our recent discoveries with these PBNs will be discussed here with brief discussion on modification with biologically-relevant moieties, and largely focusing on controlled assembly patterns, and their application for directing cell adhesion, spreading, proliferation and differentiation.

There are yet more hurdles to overcome as this field progresses. A major limitation of plant viruses is the time required to generate novel functionalities via moleulcar cloning. The plant host often requires two or three months to cultivate and mutations that may seem innocous by design may wreak havoc on the virus replication and infection pathways, which would translate to low or even possibly no viruses. Diverting the virus to recombinant bacterial expression system could shorten this time frame, however there are some viruses with post-translational modifications (acetylation of N-terminal residue) can disrupts the virus assembly process. Furthermore, not all virus coat proteins are compilant in the bacteria host. For plant viruses, we have looked at the potential of *Arabidopsis thaliana* and other plant protoplasts to shorten the turnover. These protoplasts require septic cultures and nutrients with a quicker turnover in generating plant viruses with the proper post-translational modifications with reduced contaminations or cross-overs.

One other hurdle to overcome is the generation of libraries with these viral nanoparticles and their screening process. A voluminous pool with various functional groups will be required as more and more of these protein systems are sought for cell-targeting. Previous peptide sequences derived from phage display do not display the ligands with the same geometric symmetries as the other viruses. How much of these ligand organizations will affect cell-binding remains much to be explored. Tapping into this reservoir of viruses that comes in diverse shapes and sizes, along with remarkable physical and chemical stabilities and relative ease of processibility seems to be only limited by our ability to detect, isolate, and produce the viruses.

## References

1. Manchester, M.; Singh, P. Virus-based nanoparticles (VNPs): platform technologies for diagnostic imaging. *Adv. Drug Delivery Rev.* **2006**, *58* (14), 1505–22.
2. Franzen, S.; Lommel, S. A. Targeting cancer with ‘smart bombs’: equipping plant virus nanoparticles for a ‘seek and destroy’ mission. *Nanomedicine (London)* **2009**, *4* (5), 575–88.
3. Destito, G.; Schneemann, A.; Manchester, M. Biomedical nanotechnology using virus-based nanoparticles. *Curr. Top. Microbiol. Immunol.* **2009**, *327*, 95–122.
4. Park, J. S.; Cho, M. K.; Lee, E. J.; Ahn, K. Y.; Lee, K. E.; Jung, J. H.; Cho, Y.; Han, S. S.; Kim, Y. K.; Lee, J. A highly sensitive and selective diagnostic assay based on virus nanoparticles. *Nat. Nanotechnol.* **2009**, *4* (4), 259–64.
5. Lee, L. A.; Wang, Q. Adaptations of nanoscale viruses and other protein cages for medical applications. *Nanomedicine* **2006**, *2* (3), 137–49.
6. Li, K.; Nguyen, H. G.; Lu, X.; Wang, Q. Viruses and their potential in bioimaging and biosensing applications. *Analyst* **2010**, *135* (1), 21–7.
7. Steinmetz, N. F.; Lin, T.; Lomonossoff, G. P.; Johnson, J. E. Structure-based engineering of an icosahedral virus for nanomedicine and nanotechnology. *Curr. Top. Microbiol. Immunol.* **2009**, *327*, 23–58.
8. Sapsford, K. E.; Soto, C. M.; Blum, A. S.; Chatterji, A.; Lin, T.; Johnson, J. E.; Ligler, F. S.; Ratna, B. R. A cowpea mosaic virus nanoscaffold for multiplexed antibody conjugation: application as an immunoassay tracer. *Biosens. Bioelectron.* **2006**, *21* (8), 1668–73.
9. Smith, G. P. Filamentous fusion phage: novel expression vectors that display cloned antigens on the virion surface. *Science* **1985**, *228* (4705), 1315–7.
10. Terskikh, A. V.; Le Doussal, J. M.; Crameri, R.; Fisch, I.; Mach, J. P.; Kajava, A. V. “Peptabody”: a new type of high avidity binding protein. *Proc. Natl. Acad. Sci. U.S.A.* **1997**, *94* (5), 1663–8.
11. Barbas, C. F., 3rd; Kang, A. S.; Lerner, R. A.; Benkovic, S. J. Assembly of combinatorial antibody libraries on phage surfaces: the gene III site. *Proc. Natl. Acad. Sci. U.S.A.* **1991**, *88* (18), 7978–82.

12. Pfistermueller, D. M.; Blaas, D.; Hodits, R. A. Preferential recognition of the very low-density lipoprotein receptor ligand binding site by antibodies from phage display libraries. *FEBS Lett.* **1996**, *396* (1), 14–20.
13. Watkins, N. A.; Du, L. M.; Scott, J. P.; Ouwehand, W. H.; Hillery, C. A. Single-chain antibody fragments derived from a human synthetic phage-display library bind thrombospondin and inhibit sickle cell adhesion. *Blood* **2003**, *102* (2), 718–24.
14. Ting, A. Y.; Witte, K.; Shah, K.; Kraybill, B.; Shokat, K. M.; Schultz, P. G. Phage-display evolution of tyrosine kinases with altered nucleotide specificity. *Biopolymers* **2001**, *60* (3), 220–8.
15. Dieterich, D. C.; Lee, J. J.; Link, A. J.; Graumann, J.; Tirrell, D. A.; Schuman, E. M. Labeling, detection and identification of newly synthesized proteomes with bioorthogonal non-canonical amino-acid tagging. *Nat. Protoc.* **2007**, *2* (3), 532–40.
16. Johnson, J. A.; Lu, Y. Y.; Van Deventer, J. A.; Tirrell, D. A. Residue-specific incorporation of non-canonical amino acids into proteins: recent developments and applications. *Curr. Opin. Chem. Biol.* **2010**, *14* (6), 774–80.
17. Pastrnak, M.; Schultz, P. G. Phage selection for site-specific incorporation of unnatural amino acids into proteins in vivo. *Bioorg. Med. Chem.* **2001**, *9* (9), 2373–9.
18. Neumann, H.; Wang, K.; Davis, L.; Garcia-Alai, M.; Chin, J. W. Encoding multiple unnatural amino acids via evolution of a quadruplet-decoding ribosome. *Nature* **2010**, *464* (7287), 441–4.
19. Lin, C. W.; Ting, A. Y. Transglutaminase-catalyzed site-specific conjugation of small-molecule probes to proteins in vitro and on the surface of living cells. *J. Am. Chem. Soc.* **2006**, *128* (14), 4542–3.
20. Chen, I.; Howarth, M.; Lin, W.; Ting, A. Y. Site-specific labeling of cell surface proteins with biophysical probes using biotin ligase. *Nat. Methods* **2005**, *2* (2), 99–104.
21. Bruckman, M. A.; Liu, J.; Koley, G.; Li, Y.; Benicewicz, B.; Niu, Z.; Wang, Q. Tobacco mosaic virus based thin film sensor for detection of volatile organic compounds. *J. Mater. Chem.* **2010**, *20*, 5715–5719.
22. van Rijn, P.; Mougin, N. C.; Franke, D.; Park, H.; Boker, A. Pickering emulsion templated soft capsules by self-assembling cross-linkable ferritin-polymer conjugates. *Chem. Commun. (Cambridge, U.K.)* **2011**, *47* (29), 8376–8.
23. Laga, R.; Konak, C.; Subr, V.; Ulbrich, K.; Suthiwangcharoen, N.; Niu, Z.; Wang, Q. Chemical conjugation of cowpea mosaic viruses with reactive HPMA-based polymers. *J. Biomater. Sci., Polym. Ed.* **2010**, *21* (12), 1669–85.
24. Niu, Z.; Bruckman, M.; Kotakadi, V. S.; He, J.; Emrick, T.; Russell, T. P.; Yang, L.; Wang, Q. Study and characterization of tobacco mosaic virus head-to-tail assembly assisted by aniline polymerization. *Chem. Commun. (Cambridge, U.K.)* **2006** (28), 3019–21.
25. Niu, Z.; Bruckman, M. A.; Li, S.; Lee, L. A.; Lee, B.; Pingali, S. V.; Thiyagarajan, P.; Wang, Q. Assembly of tobacco mosaic virus into fibrous

and macroscopic bundled arrays mediated by surface aniline polymerization. *Langmuir* **2007**, *23* (12), 6719–24.

26. Li, T.; Wu, L.; Suthiwangcharoen, N.; Bruckman, M. A.; Cash, D.; Hudson, J. S.; Ghoshroy, S.; Wang, Q. Controlled assembly of rodlike viruses with polymers. *Chem. Commun. (Cambridge, U.K.)* **2009** (20), 2869–71.
27. Kadowaki, K.; Shibata, T.; Takeuchi, K.; Himeno, M.; Sakai, H.; Komano, T. Identification of a temperature-resistant bacteriophage phi X174 mutant. *J. Gen. Virol.* **1987**, *68* (Pt 9), 2443–7.
28. Middleton, J. K.; Agosto, M. A.; Severson, T. F.; Yin, J.; Nibert, M. L. Thermostabilizing mutations in reovirus outer-capsid protein mu1 selected by heat inactivation of infectious subvirion particles. *Virology* **2007**, *361* (2), 412–25.
29. Shiomi, H.; Urasawa, T.; Urasawa, S.; Kobayashi, N.; Abe, S.; Taniguchi, K. Isolation and characterisation of poliovirus mutants resistant to heating at 50 degrees Celsius for 30 min. *J. Med. Virol.* **2004**, *74* (3), 484–91.
30. Rice, G.; Tang, L.; Stedman, K.; Roberto, F.; Spuhler, J.; Gillitzer, E.; Johnson, J. E.; Douglas, T.; Young, M. The structure of a thermophilic archaeal virus shows a double-stranded DNA viral capsid type that spans all domains of life. *Proc. Natl. Acad. Sci. U.S.A.* **2004**, *101* (20), 7716–20.
31. Douglas, T.; Young, M. Viruses: Making Friends with Old Foes. *Science* **2006**, *312* (5775), 873–875.
32. Wang, N.; Tytell, J. D.; Ingber, D. E. Mechanotransduction at a distance: mechanically coupling the extracellular matrix with the nucleus. *Nat. Rev. Mol. Cell Biol.* **2009**, *10* (1), 75–82.
33. Lutolf, M. P.; Hubbell, J. A. Synthetic biomaterials as instructive extracellular microenvironments for morphogenesis in tissue engineering. *Nat. Biotechnol.* **2005**, *23* (1), 47–55.
34. Silva, E. A.; Mooney, D. J. Synthetic extracellular matrices for tissue engineering and regeneration. *Curr. Top. Dev. Biol.* **2004**, *64*, 181–205.
35. Peterlik, H.; Roschger, P.; Klaushofer, K.; Fratzl, P. From brittle to ductile fracture of bone. *Nat. Mater.* **2006**, *5* (1), 52–5.
36. Lewis, J. D.; Destito, G.; Zijlstra, A.; Gonzalez, M. J.; Quigley, J. P.; Manchester, M.; Stuhlmann, H. Viral nanoparticles as tools for intravital vascular imaging. *Nat. Med.* **2006**, *12* (3), 354–360.
37. Leong, H. S.; Steinmetz, N. F.; Ablack, A.; Destito, G.; Zijlstra, A.; Stuhlmann, H.; Manchester, M.; Lewis, J. D. Intravital imaging of embryonic and tumor neovasculature using viral nanoparticles. *Nat. Protoc.* **2010**, *5* (8), 1406–17.
38. Luckanagul, J.; Lee, L. A.; Yang, X.; You, S.; Wang, Q. In vivo response towards virus-modified porous alginate hydrogels, in preparation.
39. Lee, L. A.; Niu, Z.; Wang, Q. Viruses and virus-like protein assemblies-chemically programmable nanoscale building blocks. *Nano Res.* **2009**, *2* (5), 349–364.
40. Strable, E.; Finn, M. G. Chemical modification of viruses and virus-like particles. *Curr. Top. Microbiol. Immunol.* **2009**, *327*, 1–21 (Viruses and Nanotechnology).

41. Steinmetz, N. F.; Evans, D. J. Utilisation of plant viruses in bionanotechnology. *Org. Biomol. Chem.* **2007**, *5* (18), 2891–2902.
42. Lee, L. A.; Nguyen, H. G.; Wang, Q. Altering the landscape of viruses and bionanoparticles. *Org. Biomol. Chem.* **2011**, *9* (18), 6189–95.
43. Wang, Q.; Lin, T.; Johnson, J. E.; Finn, M. G. Natural supramolecular building blocks. Cysteine-added mutants of cowpea mosaic virus. *Chem. Biol.* **2002**, *9* (7), 813–9.
44. Chatterji, A.; Ochoa, W.; Shamieh, L.; Salakian, S. P.; Wong, S. M.; Clinton, G.; Ghosh, P.; Lin, T.; Johnson, J. E. Chemical conjugation of heterologous proteins on the surface of Cowpea mosaic virus. *Bioconjugate Chem.* **2004**, *15* (4), 807–13.
45. Wang, Q.; Kaltgrad, E.; Lin, T.; Johnson, J. E.; Finn, M. G. Natural supramolecular building blocks. Wild-type cowpea mosaic virus. *Chem. Biol.* **2002**, *9* (7), 805–11.
46. Chatterji, A.; Ochoa, W. F.; Paine, M.; Ratna, B. R.; Johnson, J. E.; Lin, T. New addresses on an addressable virus nanoblock; uniquely reactive Lys residues on cowpea mosaic virus. *Chem. Biol.* **2004**, *11* (6), 855–63.
47. Destito, G.; Yeh, R.; Rae, C. S.; Finn, M. G.; Manchester, M. Folic Acid-Mediated Targeting of Cowpea Mosaic Virus Particles to Tumor Cells. *Chem. Biol.* **2007**, *14* (10), 1152–1162.
48. Manayani, D. J.; Thomas, D.; Dryden, K. A.; Reddy, V.; Siladi, M. E.; Marlett, J. M.; Rainey, G. J. A.; Pique, M. E.; Scobie, H. M.; Yeager, M.; Young, J. A. T.; Manchester, M.; Schneemann, A. A viral nanoparticle with dual function as an anthrax antitoxin and vaccine. *PLoS Pathog.* **2007**, *3* (10), 1422–1431.
49. Steinmetz, N. F.; Manchester, M. PEGylated Viral Nanoparticles for Biomedicine: The Impact of PEG Chain Length on VNP Cell Interactions In Vitro and Ex Vivo. *Biomacromolecules* **2009**, *10* (4), 784–792.
50. Douglas, T.; Young, M. Virus particles as templates for materials synthesis. *Adv. Mater.* **1999**, *11* (8), 679–681.
51. Douglas, T.; Young, M. Host-guest encapsulation of materials by assembled virus protein cages. *Nature* **1998**, *393* (6681), 152–155.
52. Flenniken, M. L.; Liepold, L. O.; Crowley, B. E.; Willits, D.; Young, M.; Douglas, T. Selective attachment and release of a chemotherapeutic agent from the interior of a protein cage architecture. *Chem. Comm.* **2005**, 447–449.
53. Flenniken, M. L.; Willits, D. A.; Harmsen, A. L.; Liepold, L. O.; Harmsen, A. G.; Young, M. J.; Douglas, T. Melanoma and lymphocyte cell-specific targeting incorporated into a heat shock protein cage architecture. *Chem. Biol.* **2006**, *13* (2), 161–170.
54. Ma, Y. Z.; Miller, R. A.; Fleming, G. R.; Francis, M. B. Energy transfer dynamics in light-harvesting assemblies templated by the tobacco mosaic virus coat protein. *J. Phys. Chem. B* **2008**, *112* (22), 6887–92.
55. Miller, R. A.; Presley, A. D.; Francis, M. B. Self-assembling light-harvesting systems from synthetically modified tobacco mosaic virus coat proteins. *J. Am. Chem. Soc.* **2007**, *129* (11), 3104–9.

56. Miller, R. A.; Stephanopoulos, N.; McFarland, J. M.; Rosko, A. S.; Geissler, P. L.; Francis, M. B. Impact of assembly state on the defect tolerance of TMV-based light harvesting arrays. *J. Am. Chem. Soc.* **2010**, *132* (17), 6068–74.
57. Chen, X.; Gerasopoulos, K.; Guo, J.; Brown, A.; Wang, C.; Ghodssi, R.; Culver, J. N. Virus-enabled silicon anode for lithium-ion batteries. *ACS Nano* **2010**, *4* (9), 5366–72.
58. O'Neil, A.; Reichhardt, C.; Johnson, B.; Prevelige, P. E.; Douglas, T. Genetically programmed in vivo packaging of protein cargo and its controlled release from bacteriophage P22. *Angew. Chem., Int. Ed.* **2011**, *50* (32), 7425–8.
59. Lee, S.-W.; Mao, C.; Flynn, C. E.; Belcher, A. M. Ordering of quantum dots using genetically engineered viruses. *Science* **2002**, *296* (5569), 892–895.
60. Lee, Y. J.; Yi, H.; Kim, W.-J.; Kang, K.; Yun, D. S.; Strano, M. S.; Ceder, G.; Belcher, A. M. Fabricating Genetically Engineered High-Power Lithium-Ion Batteries Using Multiple Virus Genes. *Science* **2009**, *324* (5930), 1051–1055.
61. Mao, C.; Solis, D. J.; Reiss, B. D.; Kottmann, S. T.; Sweeney, R. Y.; Hayhurst, A.; Georgiou, G.; Iverson, B.; Belcher, A. M. Virus-based toolkit for the directed synthesis of magnetic and semiconducting nanowires. *Science* **2004**, *303* (5655), 213–217.
62. Nam, K. T.; Kim, D.-W.; Yoo, P. J.; Chiang, C.-Y.; Meethong, N.; Hammond, P. T.; Chiang, Y.-M.; Belcher, A. M. Virus-Enabled Synthesis and Assembly of Nanowires for Lithium Ion Battery Electrodes. *Science* **2006**, *312* (5775), 885–888.
63. McCormick, A. A.; Palmer, K. E. Genetically engineered Tobacco mosaic virus as nanoparticle vaccines. *Expert Rev. Vaccines* **2008**, *7* (1), 33–41.
64. Montague, N. P.; Thuenemann, E. C.; Saxena, P.; Saunders, K.; Lenzi, P.; Lomonossoff, G. P. Recent advances of cowpea mosaic virus-based particle technology. *Hum. Vaccines* **2011**, *7* (3), 383–90.
65. Smith, M. L.; Fitzmaurice, W. P.; Turpen, T. H.; Palmer, K. E. Display of peptides on the surface of tobacco mosaic virus particles. *Curr. Top. Microbiol. Immunol.* **2009**, *332*, 13–31.
66. Chatterji, A.; Burns, L. L.; Taylor, S. S.; Lomonossoff, G. P.; Johnson, J. E.; Lin, T.; Porta, C. Cowpea mosaic virus: from the presentation of antigenic peptides to the display of active biomaterials. *Intervirology* **2002**, *45* (4-6), 362–70.
67. McCormick, A. A.; Corbo, T. A.; Wykoff-Clary, S.; Nguyen, L. V.; Smith, M. L.; Palmer, K. E.; Pogue, G. P. TMV-peptide fusion vaccines induce cell-mediated immune responses and tumor protection in two murine models. *Vaccine* **2006**, *24* (40-41), 6414–23.
68. Lico, C.; Mancini, C.; Italiani, P.; Betti, C.; Boraschi, D.; Benvenuto, E.; Baschieri, S. Plant-produced potato virus X chimeric particles displaying an influenza virus-derived peptide activate specific CD8+ T cells in mice. *Vaccine* **2009**, *27* (37), 5069–76.
69. Brennan, F. R.; Bellaby, T.; Helliwell, S. M.; Jones, T. D.; Kamstrup, S.; Dalsgaard, K.; Flock, J. I.; Hamilton, W. D. Chimeric plant virus particles

administered nasally or orally induce systemic and mucosal immune responses in mice. *J. Virol.* **1999**, *73* (2), 930–8.

70. Pierschbacher, M. D.; Ruoslahti, E. Variants of the cell recognition site of fibronectin that retain attachment-promoting activity. *Proc. Natl. Acad. Sci. U.S.A.* **1984**, *81* (19), 5985–8.
71. Pierschbacher, M. D.; Ruoslahti, E. Cell attachment activity of fibronectin can be duplicated by small synthetic fragments of the molecule. *Nature* **1984**, *309* (5963), 30–3.
72. Ruoslahti, E. RGD and other recognition sequences for integrins. *Annu. Rev. Cell Dev. Biol.* **1996**, *12*, 697–715.
73. Cutler, S. M.; Garcia, A. J. Engineering cell adhesive surfaces that direct integrin alpha5beta1 binding using a recombinant fragment of fibronectin. *Biomaterials* **2003**, *24* (10), 1759–70.
74. Petrie, T. A.; Capadona, J. R.; Reyes, C. D.; Garcia, A. J. Integrin specificity and enhanced cellular activities associated with surfaces presenting a recombinant fibronectin fragment compared to RGD supports. *Biomaterials* **2006**, *27* (31), 5459–70.
75. Petrie, T. A.; Reyes, C. D.; Burns, K. L.; Garcia, A. J. Simple application of fibronectin-mimetic coating enhances osseointegration of titanium implants. *J. Cell Mol. Med.* **2009**, *13* (8B), 2602–12.
76. Kao, W. J.; Lee, D.; Schense, J. C.; Hubbell, J. A. Fibronectin modulates macrophage adhesion and FBGC formation: the role of RGD, PHSRN, and PRRARV domains. *J. Biomed. Mater. Res.* **2001**, *55* (1), 79–88.
77. Ochsenhirt, S. E.; Kokkoli, E.; McCarthy, J. B.; Tirrell, M. Effect of RGD secondary structure and the synergy site PHSRN on cell adhesion, spreading and specific integrin engagement. *Biomaterials* **2006**, *27* (20), 3863–74.
78. Rahman, S.; Aitken, A.; Flynn, G.; Formstone, C.; Savidge, G. F. Modulation of RGD sequence motifs regulates disintegrin recognition of alphaIIb beta3 and alpha5 beta1 integrin complexes. Replacement of elegantin alanine-50 with proline, N-terminal to the RGD sequence, diminishes recognition of the alpha5 beta1 complex with restoration induced by Mn2+ cation. *Biochem. J.* **1998**, *335* (Pt 2), 247–57.
79. Li, R.; Hoess, R. H.; Bennett, J. S.; DeGrado, W. F. Use of phage display to probe the evolution of binding specificity and affinity in integrins. *Protein Eng.* **2003**, *16* (1), 65–72.
80. Koivunen, E.; Gay, D. A.; Ruoslahti, E. Selection of peptides binding to the alpha 5 beta 1 integrin from phage display library. *J. Biol. Chem.* **1993**, *268* (27), 20205–10.
81. Koivunen, E.; Wang, B.; Ruoslahti, E. Phage libraries displaying cyclic peptides with different ring sizes: ligand specificities of the RGD-directed integrins. *Biotechnology* **1995**, *13* (3), 265–70.
82. Kumagai, H.; Tajima, M.; Ueno, Y.; Giga-Hama, Y.; Ohba, M. Effect of cyclic RGD peptide on cell adhesion and tumor metastasis. *Biochem. Biophys. Res. Commun.* **1991**, *177* (1), 74–82.
83. Martino, M. M.; Mochizuki, M.; Rothenfluh, D. A.; Rempel, S. A.; Hubbell, J. A.; Barker, T. H. Controlling integrin specificity and stem cell

differentiation in 2D and 3D environments through regulation of fibronectin domain stability. *Biomaterials* **2009**, *30* (6), 1089–97.

84. Kundu, A. K.; Khatiwala, C. B.; Putnam, A. J. Extracellular matrix remodeling, integrin expression, and downstream signaling pathways influence the osteogenic differentiation of mesenchymal stem cells on poly(lactide-co-glycolide) substrates. *Tissue Eng., Part A* **2009**, *15* (2), 273–83.
85. Kaur, G.; Valarmathi, M. T.; Potts, J. D.; Jabbari, E.; Sabo-Attwood, T.; Wang, Q. Regulation of osteogenic differentiation of rat bone marrow stromal cells on 2D nanorod substrates. *Biomaterials* **2010**, *31* (7), 1732–41.
86. Kaur, G.; Valarmathi, M. T.; Potts, J. D.; Wang, Q. The promotion of osteoblastic differentiation of rat bone marrow stromal cells by a polyvalent plant mosaic virus. *Biomaterials* **2008**, *29* (30), 4074–81.
87. Kaur, G.; Wang, C.; Sun, J.; Wang, Q. The synergistic effects of multivalent ligand display and nanotopography on osteogenic differentiation of rat bone marrow stem cells. *Biomaterials* **2010**, *31* (22), 5813–24.
88. Lee, L. A.; Nguyen, Q. L.; Wu, L.; Horvath, G.; Nelson, R. S.; Wang, Q. Mutant plant viruses with cell binding motifs provide differential adhesion strengths and morphologies. *Biomacromolecules* **2012**, *13* (2), 422–31.
89. Wu, L.; Lee, L. A.; Niu, Z.; Ghoshroy, S.; Wang, Q. Visualizing cell extracellular matrix (ECM) deposited by cells cultured on aligned bacteriophage M13 thin films. *Langmuir* **2011**, *27* (15), 9490–6.
90. Plow, E. F.; Haas, T. A.; Zhang, L.; Loftus, J.; Smith, J. W. Ligand binding to integrins. *J. Biol. Chem.* **2000**, *275* (29), 21785–8.
91. Young, M. F.; Kerr, J. M.; Ibaraki, K.; Heegaard, A. M.; Robey, P. G. Structure, expression, and regulation of the major noncollagenous matrix proteins of bone. *Clin. Orthop. Relat. Res.* **1992** (281), 275–94.
92. Ingram, R. T.; Clarke, B. L.; Fisher, L. W.; Fitzpatrick, L. A. Distribution of noncollagenous proteins in the matrix of adult human bone: evidence of anatomic and functional heterogeneity. *J. Bone Miner. Res.* **1993**, *8* (9), 1019–29.
93. Burman, A.; Clark, S.; Abrescia, N. G.; Fry, E. E.; Stuart, D. I.; Jackson, T. Specificity of the VP1 GH loop of Foot-and-Mouth Disease virus for alphav integrins. *J. Virol.* **2006**, *80* (19), 9798–810.
94. Asokan, A.; Conway, J. C.; Phillips, J. L.; Li, C.; Hegge, J.; Sinnott, R.; Yadav, S.; DiPrimio, N.; Nam, H. J.; Agbandje-McKenna, M.; McPhee, S.; Wolff, J.; Samulski, R. J. Reengineering a receptor footprint of adeno-associated virus enables selective and systemic gene transfer to muscle. *Nat. Biotechnol.* **2010**, *28* (1), 79–82.
95. Buning, H.; Ried, M. U.; Perabo, L.; Gerner, F. M.; Huttner, N. A.; Enssle, J.; Hallek, M. Receptor targeting of adeno-associated virus vectors. *Gene Ther.* **2003**, *10* (14), 1142–51.
96. Fisher, L. W.; Hawkins, G. R.; Tuross, N.; Termine, J. D. Purification and partial characterization of small proteoglycans I and II, bone sialoproteins I and II, and osteonectin from the mineral compartment of developing human bone. *J. Biol. Chem.* **1987**, *262* (20), 9702–8.

97. Kulkarni, G. V.; Chen, B.; Malone, J. P.; Narayanan, A. S.; George, A. Promotion of selective cell attachment by the RGD sequence in dentine matrix protein 1. *Arch. Oral Biol.* **2000**, *45* (6), 475–84.
98. Young, M. F.; Kerr, J. M.; Termine, J. D.; Wewer, U. M.; Wang, M. G.; McBride, O. W.; Fisher, L. W. cDNA cloning, mRNA distribution and heterogeneity, chromosomal location, and RFLP analysis of human osteopontin (OPN). *Genomics* **1990**, *7* (4), 491–502.
99. Main, A. L.; Harvey, T. S.; Baron, M.; Boyd, J.; Campbell, I. D. The three-dimensional structure of the tenth type III module of fibronectin: an insight into RGD-mediated interactions. *Cell* **1992**, *71* (4), 671–8.
100. Suzuki, S.; Oldberg, A.; Hayman, E. G.; Pierschbacher, M. D.; Ruoslahti, E. Complete amino acid sequence of human vitronectin deduced from cDNA. Similarity of cell attachment sites in vitronectin and fibronectin. *EMBO J.* **1985**, *4* (10), 2519–24.
101. Leahy, D. J.; Hendrickson, W. A.; Aukhil, I.; Erickson, H. P. Structure of a fibronectin type III domain from tenascin phased by MAD analysis of the selenomethionyl protein. *Science* **1992**, *258* (5084), 987–91.
102. Aumailley, M.; Gerl, M.; Sonnenberg, A.; Deutzmann, R.; Timpl, R. Identification of the Arg-Gly-Asp sequence in laminin A chain as a latent cell-binding site being exposed in fragment P1. *FEBS Lett.* **1990**, *262* (1), 82–6.
103. Sasaki, T.; Timpl, R. Domain IVa of laminin alpha5 chain is cell-adhesive and binds beta1 and alphaVbeta3 integrins through Arg-Gly-Asp. *FEBS Lett.* **2001**, *509* (2), 181–5.
104. Yamada, Y.; Hozumi, K.; Nomizu, M. Construction and activity of a synthetic basement membrane with active laminin peptides and polysaccharides. *Chemistry* **2011**, *17* (38), 10500–8.
105. Ozbek, S.; Balasubramanian, P. G.; Chiquet-Ehrismann, R.; Tucker, R. P.; Adams, J. C. The evolution of extracellular matrix. *Mol. Biol. Cell* **2010**, *21* (24), 4300–5.
106. Reyes, C. D.; Garcia, A. J. Alpha2beta1 integrin-specific collagen-mimetic surfaces supporting osteoblastic differentiation. *J. Biomed. Mater., Res A* **2004**, *69* (4), 591–600.
107. Mizuno, M.; Fujisawa, R.; Kuboki, Y. Type I collagen-induced osteoblastic differentiation of bone-marrow cells mediated by collagen-alpha2beta1 integrin interaction. *J. Cell. Physiol.* **2000**, *184* (2), 207–13.
108. Aota, S.; Nagai, T.; Yamada, K. M. Characterization of regions of fibronectin besides the arginine-glycine-aspartic acid sequence required for adhesive function of the cell-binding domain using site-directed mutagenesis. *J. Biol. Chem.* **1991**, *266* (24), 15938–43.
109. Mardon, H. J.; Grant, K. E. The role of the ninth and tenth type III domains of human fibronectin in cell adhesion. *FEBS Lett.* **1994**, *340* (3), 197–201.
110. Corti, A.; Curnis, F. Isoaspartate-dependent molecular switches for integrin-ligand recognition. *J. Cell Sci.* **2011**, *124* (Pt 4), 515–22.
111. Corti, A.; Curnis, F.; Arap, W.; Pasqualini, R. The neovasculature homing motif NGR: more than meets the eye. *Blood* **2008**, *112* (7), 2628–35.

112. Yamazaki, C. M.; Kadoya, Y.; Hozumi, K.; Okano-Kosugi, H.; Asada, S.; Kitagawa, K.; Nomizu, M.; Koide, T. A collagen-mimetic triple helical supramolecule that evokes integrin-dependent cell responses. *Biomaterials* **2010**, *31* (7), 1925–34.
113. Hennessy, K. M.; Pollot, B. E.; Clem, W. C.; Phipps, M. C.; Sawyer, A. A.; Culpepper, B. K.; Bellis, S. L. The effect of collagen I mimetic peptides on mesenchymal stem cell adhesion and differentiation, and on bone formation at hydroxyapatite surfaces. *Biomaterials* **2009**, *30* (10), 1898–909.
114. Choi, B. H.; Choi, Y. S.; Kang, D. G.; Kim, B. J.; Song, Y. H.; Cha, H. J. Cell behavior on extracellular matrix mimic materials based on mussel adhesive protein fused with functional peptides. *Biomaterials* **2010**, *31* (34), 8980–8.
115. Yoo, S. Y.; Kobayashi, M.; Lee, P. P.; Lee, S. W. Early osteogenic differentiation of mouse preosteoblasts induced by collagen-derived DGEA-peptide on nanofibrous phage tissue matrices. *Biomacromolecules* **2011**, *12* (4), 987–96.
116. Tashiro, K.; Sephel, G. C.; Weeks, B.; Sasaki, M.; Martin, G. R.; Kleinman, H. K.; Yamada, Y. A synthetic peptide containing the IKVAV sequence from the A chain of laminin mediates cell attachment, migration, and neurite outgrowth. *J. Biol. Chem.* **1989**, *264* (27), 16174–82.
117. Graf, J.; Iwamoto, Y.; Sasaki, M.; Martin, G. R.; Kleinman, H. K.; Robey, F. A.; Yamada, Y. Identification of an amino acid sequence in laminin mediating cell attachment, chemotaxis, and receptor binding. *Cell* **1987**, *48* (6), 989–96.
118. Graf, J.; Ogle, R. C.; Robey, F. A.; Sasaki, M.; Martin, G. R.; Yamada, Y.; Kleinman, H. K. A pentapeptide from the laminin B1 chain mediates cell adhesion and binds the 67,000 laminin receptor. *Biochemistry* **1987**, *26* (22), 6896–900.
119. Iwamoto, Y.; Robey, F. A.; Graf, J.; Sasaki, M.; Kleinman, H. K.; Yamada, Y.; Martin, G. R. YIGSR, a synthetic laminin pentapeptide, inhibits experimental metastasis formation. *Science* **1987**, *238* (4830), 1132–4.
120. Merzlyak, A.; Indrakanti, S.; Lee, S. W. Genetically engineered nanofiber-like viruses for tissue regenerating materials. *Nano Lett.* **2009**, *9* (2), 846–52.
121. Asokan, A.; Hamra, J. B.; Govindasamy, L.; Agbandje-McKenna, M.; Samulski, R. J. Adeno-associated virus type 2 contains an integrin alpha5beta1 binding domain essential for viral cell entry. *J. Virol.* **2006**, *80* (18), 8961–9.
122. Summerford, C.; Samulski, R. J. Membrane-associated heparan sulfate proteoglycan is a receptor for adeno-associated virus type 2 virions. *J. Virol.* **1998**, *72* (2), 1438–45.
123. Wang, Q.; Lin, T.; Tang, L.; Johnson, J. E.; Finn, M. G. Icosahedral virus particles as addressable nanoscale building blocks. *Angew. Chem., Int. Ed.* **2002**, *41* (3), 459–62.
124. Bruckman, M. A.; Kaur, G.; Lee, L. A.; Xie, F.; Sepulveda, J.; Breitenkamp, R.; Zhang, X.; Joralemon, M.; Russell, T. P.; Emrick, T.; Wang, Q. Surface modification of tobacco mosaic virus with “click” chemistry. *ChemBioChem* **2008**, *9* (4), 519–523.

125. Barnhill, H. N.; Reuther, R.; Ferguson, P. L.; Dreher, T.; Wang, Q. Turnip Yellow Mosaic Virus as a Chemoaddressable Bionanoparticle. *Bioconjugate Chem.* **2007**, *18*, 852–859.
126. Zeng, Q.; Reuther, R.; Oxsher, J.; Wang, Q. Characterization of horse spleen apoferritin reactive lysines by MALDI-TOF mass spectrometry combined with enzymatic digestion. *Bioorg. Chem.* **2008**, *36* (5), 255–260.
127. Bruckman, M. A.; Niu, Z.; Li, S.; Lee, L. A.; Varazo, K.; Nelson, T.; Lavigne, J. J.; Wang, Q. Development of Nanobiocomposite Fibers by Controlled-Assembly of Rod-Like Tobacco Mosaic Virus. *NanoBiotechnology* **2007**, *3*, 31–39.
128. Kaur, G.; He, J.; Xu, J.; Pingali, S.; Jutz, G.; Boker, A.; Niu, Z.; Li, T.; Rawlinson, D.; Emrick, T.; Lee, B.; Thiyagarajan, P.; Russell, T. P.; Wang, Q. Interfacial Assembly of Turnip Yellow Mosaic Virus Nanoparticles. *Langmuir* **2009**, *25* (9), 5168–5176.
129. Li, T.; Ye, B.; Niu, Z.; Thompson, P.; Seifert, S.; Lee, B.; Wang, Q. Closed-Packed Colloidal Assemblies from Icosahedral Plant Virus and Polymer. *Chem. Mater.* **2009**, *21* (6), 1046–1050.
130. Niu, Z.; Bruckman, M.; Kotakadi, V. S.; He, J.; Emrick, T.; Russell, T. P.; Yang, L.; Wang, Q. Study and characterization of tobacco mosaic virus head-to-tail assembly assisted by aniline polymerization. *Chem. Comm.* **2006** (28), 3019–21.
131. Niu, Z.; Liu, J.; Lee, L. A.; Bruckman, M. A.; Zhao, D.; Koley, G.; Wang, Q. Biological Templated Synthesis of Water-Soluble Conductive Polymeric Nanowires. *Nano Lett.* **2007**, *7* (12), 3729–3733.
132. Lee, B.; Lo, C.; Thiyagarajan, P.; Winans, R.; Li, X.; Niu, Z.; Wang, Q. Effect of interfacial interaction on the cross-sectional morphology of tobacco mosaic virus using GISAXS. *Langmuir* **2007**, *23* (22), 11157–11163.
133. Niu, Z.; Bruckman, M. A.; Li, S.; Lee, L. A.; Lee, B.; Pingali, S. V.; Thiyagarajan, P.; Wang, Q. Assembly of tobacco mosaic virus into fibrous and macroscopic bundled arrays mediated by surface aniline polymerization. *Langmuir* **2007**, *23* (12), 6719–24.
134. Lin, Y.; Su, Z.; Niu, Z.; Li, S.; Kaur, G.; Lee, L. A.; Wang, Q. Layer-by-layer assembly of viral capsid for cell adhesion. *Acta Biomater.* **2008**, *4* (4), 838–43.
135. DeMerlis, C. C.; Schoneker, D. R. Review of the oral toxicity of polyvinyl alcohol (PVA). *Food Chem. Toxicol.* **2003**, *41* (3), 319–26.
136. Kelly, C. M.; DeMerlis, C. C.; Schoneker, D. R.; Borzelleca, J. F. Subchronic toxicity study in rats and genotoxicity tests with polyvinyl alcohol. *Food Chem. Toxicol.* **2003**, *41* (5), 719–27.
137. Rodwell, D. E.; Kelly, C. M.; DeMerlis, C. C.; Schoneker, D. R.; Borzelleca, J. F. Effects of polyvinyl alcohol administered in the diet to rats on fertility, early embryonic development, growth and development. *Food Chem. Toxicol.* **2003**, *41* (5), 729–37.
138. Schoneker, D. R.; DeMerlis, C. C.; Borzelleca, J. F. Evaluation of the toxicity of polyvinylacetate phthalate in experimental animals. *Food Chem. Toxicol.* **2003**, *41* (3), 405–13.

139. Takasu, A.; Niwa, T.; Itou, H.; Inai, Y.; Hirabyashi, T. Chemical modification of hydroxyl groups of poly(vinyl alcohol) by glycosidation reaction. *Macromol. Rapid Commun.* **2000**, *21* (11), 764–769.

140. Kenawy el, R.; Layman, J. M.; Watkins, J. R.; Bowlin, G. L.; Matthews, J. A.; Simpson, D. G.; Wnek, G. E. Electrospinning of poly(ethylene-co-vinyl alcohol) fibers. *Biomaterials* **2003**, *24* (6), 907–13.

141. Shafiee, A.; Soleimani, M.; Chamheidari, G. A.; Seyedjafari, E.; Dodel, M.; Atashi, A.; Gheisari, Y. Electrospun nanofiber-based regeneration of cartilage enhanced by mesenchymal stem cells. *J. Biomed. Mater., Res A* **2011**, *99* (3), 467–78.

142. Jannesari, M.; Varshosaz, J.; Morshed, M.; Zamani, M. Composite poly(vinyl alcohol)/poly(vinyl acetate) electrospun nanofibrous mats as a novel wound dressing matrix for controlled release of drugs. *Int. J. Nanomed.* **2011**, *6*, 993–1003.

143. Salalha, W.; Kuhn, J.; Dror, Y.; Zussman, E. Encapsulation of bacteria and viruses in electrospun nanofibres. *Nanotechnology* **2006**, *17* (18), 4675–81.

144. Wu, L.; Zeng, J.; Lee, L. A.; Niu, Z.; Horvath, G.; Braxton, V.; Wibowo, A. C.; Bruckman, M. A.; Ghoshroy, S.; zur Loye, H. C.; Li, X.; Wang, Q. Electrospinning fabrication, structural and mechanical characterization of rod-like virus-based composite nanofibers. *J. Mater. Chem.* **2011**, *21*, 8550–8557.

145. Li, K.; Chen, Y.; Li, S.; Nguyen, H. G.; Niu, Z.; You, S.; Mello, C. M.; Lu, X.; Wang, Q. Chemical modification of M13 bacteriophage and its application in cancer cell imaging. *Bioconjugate Chem.* **2010**, *21* (7), 1369–77.

146. Yoo, S. Y.; Oh, J. W.; Lee, S. W. Phage-chips for novel optically readable tissue engineering assays. *Langmuir* **2012**, *28* (4), 2166–72.

147. Whaley, S. R.; English, D. S.; Hu, E. L.; Barbara, P. F.; Belcher, A. M. Selection of peptides with semiconductor binding specificity for directed nanocrystal assembly. *Nature* **2000**, *405* (6787), 665–8.

148. Yoo, P. J.; Nam, K. T.; Qi, J.; Lee, S.-K.; Park, J.; Belcher, A. M.; Hammond, P. T. Spontaneous assembly of viruses on multilayered polymer surfaces. *Nat. Mater.* **2006**, *5* (3), 234–240.

149. Lee, S.-W.; Wood, B. M.; Belcher, A. M. Chiral Smectic C Structures of Virus-Based Films. *Langmuir* **2003**, *19* (5), 1592–1598.

150. Lee, S.-W.; Belcher, A. M. Virus-Based Fabrication of Micro- and Nanofibers Using Electrospinning. *Nano Lett.* **2004**, *4* (3), 387–390.

151. Lee, S.-W.; Lee, S. K.; Belcher, A. M. Virus-based alignment of inorganic, organic, and biological nanosized materials. *Adv. Mater.* **2003**, *15* (9), 689–692.

152. Eric, G.; Seth, F. What is the origin of chirality in the cholesteric phase of virus suspensions? *Phys. Rev. Lett.* **2003**, *90* (19), 198302/1–198302/4.

153. Rong, J.; Lee, L. A.; Li, K.; Brandon, H.; Mello, C. M.; Niu, Z.; Wang, Q. Oriented cell growth on self-assembled bacteriophage M13 thin films. *Chem. Commun.* **2008** (41), 5185–5187.

154. Kuncicky, D. M.; Naik, R. R.; Velev, O. D. Rapid Deposition and Long-Range Alignment of Nanocoatings and Arrays of Electrically Conductive Wires from Tobacco Mosaic Virus13. *Small* **2006**, *2* (12), 1462–1466.

155. Prevo, B. G.; Velev, O. D. Controlled, rapid deposition of structured coatings from micro- and nanoparticle suspensions. *Langmuir* **2004**, *20* (6), 2099–107.

156. Wargacki, S. P.; Pate, B.; Vaia, R. A. Fabrication of 2D ordered films of tobacco mosaic virus (TMV): processing morphology correlations for convective assembly. *Langmuir* **2008**, *24* (10), 5439–44.

157. Lin, K.; Crocker, J. C.; Prasad, V. V.; Schofield, A.; Weitz, D. A.; Lubensky, T. C.; Yodh, A. G. Entropically driven colloidal crystallization on patterned surfaces. *Phys. Rev. Lett.* **2000**, *85* (8), 1770–3.

158. Adachi, E.; Dimitrov, A. S.; Nagayama, K. Stripe Patterns Formed on a Glass Surface during Droplet Evaporation. *Langmuir* **1995**, *11* (4), 1057–60.

159. Meng, L.; Wei, H.; Nagel, A.; Wiley, B. J.; Scriven, L. E.; Norris, D. J. The role of thickness transitions in convective assembly. *Nano Lett.* **2006**, *6* (10), 2249–53.

160. Dimitrov, A. S.; Nagayama, K. Continuous convective assembling of fine particles into two-dimensional arrays on solid surfaces. *Langmuir* **1996**, *12* (5), 1303–1311.

161. Denkov, N.; Velev, O. D.; Kralchevski, P.; Ivanov, I.; Yoshimura, H.; Nagayama, K. Mechanism of formation of two-dimensional crystals from latex particles on substrates. *Langmuir* **1992**, *8*, 3183–3190.

162. Prevo, B. G.; III, J. C. F.; Velev, O. D. Rapid deposition of gold nanoparticle films with controlled thickness and structure by convective assembly. *Chem. Mater.* **2005**, *17* (2), 28–35.

163. Zhu, H.; Cao, B.; Zhen, Z.; Laxmi, A. A.; Li, D.; Liu, S.; Mao, C. Controlled growth and differentiation of MSCs on grooved films assembled from monodisperse biological nanofibers with genetically tunable surface chemistries. *Biomaterials* **2011**, *32* (21), 4744–52.

164. Flemming, R. G.; Murphy, C. J.; Abrams, G. A.; Goodman, S. L.; Nealey, P. F. Effects of synthetic micro- and nano-structured surfaces on cell behavior. *Biomaterials* **1999**, *20* (6), 573–88.

165. Teixeira, A. I.; Abrams, G. A.; Bertics, P. J.; Murphy, C. J.; Nealey, P. F. Epithelial contact guidance on well-defined micro- and nanostructured substrates. *J. Cell Sci.* **2003**, *116* (Pt 10), 1881–92.

166. Fraser, S. A.; Ting, Y. H.; Mallon, K. S.; Wendt, A. E.; Murphy, C. J.; Nealey, P. F. Sub-micron and nanoscale feature depth modulates alignment of stromal fibroblasts and corneal epithelial cells in serum-rich and serum-free media. *J. Biomed. Mater. Res., Part A* **2008**, *86* (3), 725–35.

167. Liliensiek, S. J.; Wood, J. A.; Yong, J.; Auerbach, R.; Nealey, P. F.; Murphy, C. J. Modulation of human vascular endothelial cell behaviors by nanotopographic cues. *Biomaterials* **2010**, *31* (20), 5418–26.

168. McKee, C. T.; Raghunathan, V. K.; Nealey, P. F.; Russell, P.; Murphy, C. J. Topographic modulation of the orientation and shape of cell nuclei and their influence on the measured elastic modulus of epithelial cells. *Biophys. J.* **2011**, *101* (9), 2139–46.

169. den Braber, E. T.; de Ruijter, J. E.; Smits, H. T.; Ginsel, L. A.; von Recum, A. F.; Jansen, J. A. Effect of parallel surface microgrooves and surface energy on cell growth. *J. Biomed. Mater. Res.* **1995**, *29* (4), 511–8.

170. Dalton, B. A.; Walboomers, X. F.; Dziegielewski, M.; Evans, M. D.; Taylor, S.; Jansen, J. A.; Steele, J. G. Modulation of epithelial tissue and cell migration by microgrooves. *J. Biomed. Mater. Res.* **2001**, *56* (2), 195–207.
171. Matsuzaka, K.; Walboomers, X. F.; de Ruijter, J. E.; Jansen, J. A. The effect of poly-L-lactic acid with parallel surface micro groove on osteoblast-like cells in vitro. *Biomaterials* **1999**, *20* (14), 1293–301.
172. Lamers, E.; Walboomers, X. F.; Domanski, M.; te Riet, J.; van Delft, F. C.; Luttge, R.; Winnubst, L. A.; Gardeniers, H. J.; Jansen, J. A. The influence of nanoscale grooved substrates on osteoblast behavior and extracellular matrix deposition. *Biomaterials* **2010**, *31* (12), 3307–16.
173. Lamers, E.; van Horssen, R.; te Riet, J.; van Delft, F. C.; Luttge, R.; Walboomers, X. F.; Jansen, J. A. The influence of nanoscale topographical cues on initial osteoblast morphology and migration. *Eur. Cell Mater.* **2010**, *20*, 329–43.
174. Huang, J.; Kim, F.; Tao, A. R.; Connor, S.; Yang, P. Spontaneous formation of nanoparticle stripe patterns through dewetting. *Nat. Mater.* **2005**, *4* (12), 896–900.
175. Velev, O. D.; Gupta, S. Materials Fabricated by Micro- and Nanoparticle Assembly - The Challenging Path from Science to Engineering. *Adv. Mater. (Weinheim, Ger.)* **2009**, *21* (19), 1897–1905.
176. Deegan, R. D.; Bakajin, O.; Dupont, T. F.; Huber, G.; Nagel, S. R.; Witten, T. A. Contact line deposits in an evaporating drop. *Phys. Rev. E* **2000**, *62* (1-B), 756–765.
177. Xu, J.; Xia, J.; Hong, S. W.; Lin, Z.; Qiu, F.; Yang, Y. Self-Assembly of Gradient Concentric Rings via Solvent Evaporation from a Capillary Bridge. *Phys. Rev. Lett.* **2006**, *96* (6), 066104/1–066104/4.
178. Lin, Z.; Granick, S. Patterns Formed by Droplet Evaporation from a Restricted Geometry. *J. Am. Chem. Soc.* **2005**, *127* (9), 2816–2817.
179. Lin, Y.; Balizan, E.; Lee, L. A.; Niu, Z.; Wang, Q. Self-assembly of rodlike bio-nanoparticles in capillary tubes. *Angew. Chem., Int. Ed.* **2010**, *49* (5), 868–72.
180. Owens, G. K.; Kumar, M. S.; Wamhoff, B. R. Molecular regulation of vascular smooth muscle cell differentiation in development and disease. *Physiol. Rev.* **2004**, *84* (3), 767–801.
181. Hao, H.; Gabbiani, G.; Bochaton-Piallat, M. L. Arterial smooth muscle cell heterogeneity: implications for atherosclerosis and restenosis development. *Arterioscler., Thromb., Vasc. Biol.* **2003**, *23* (9), 1510–20.
182. Rensen, S. S.; Doevendans, P. A.; van Eys, G. J. Regulation and characteristics of vascular smooth muscle cell phenotypic diversity. *Neth. Heart J.* **2007**, *15* (3), 100–8.
183. Villacorta, L.; Zhang, J.; Garcia-Barrio, M. T.; Chen, X. L.; Freeman, B. A.; Chen, Y. E.; Cui, T. Nitro-linoleic acid inhibits vascular smooth muscle cell proliferation via the Keap1/Nrf2 signaling pathway. *Am. J. Physiol. Heart Circ. Physiol.* **2007**, *293* (1), H770–6.
184. Gerthoffer, W. T. Mechanisms of vascular smooth muscle cell migration. *Circ. Res.* **2007**, *100* (5), 607–21.

185. Osterud, B.; Bjorklid, E. Role of monocytes in atherogenesis. *Physiol. Rev.* **2003**, *83* (4), 1069–112.

186. Rosamond, W.; Flegal, K.; Furie, K.; Go, A.; Greenlund, K.; Haase, N.; Hailpern, S. M.; Ho, M.; Howard, V.; Kissela, B.; Kittner, S.; Lloyd-Jones, D.; McDermott, M.; Meigs, J.; Moy, C.; Nichol, G.; O'Donnell, C.; Roger, V.; Sorlie, P.; Steinberger, J.; Thom, T.; Wilson, M.; Hong, Y. Heart disease and stroke statistics--2008 update: a report from the American Heart Association Statistics Committee and Stroke Statistics Subcommittee. *Circulation* **2008**, *117* (4), e25–146.

187. Steg, P. G.; Bhatt, D. L.; Wilson, P. W.; D'Agostino, R., Sr.; Ohman, E. M.; Rother, J.; Liau, C. S.; Hirsch, A. T.; Mas, J. L.; Ikeda, Y.; Pencina, M. J.; Goto, S. One-year cardiovascular event rates in outpatients with atherothrombosis. *J. Am. Med. Assoc.* **2007**, *297* (11), 1197–206.

188. Russo, C. A.; Andrews, R. M. The National Hospital Bill: The Most Expensive Conditions, by Payer, 2004: Statistical Brief #13; 2006.

189. Yoshida, T.; Owens, G. K. Molecular determinants of vascular smooth muscle cell diversity. *Circ. Res.* **2005**, *96* (3), 280–91.

190. Herity, N. A.; Ward, M. R.; Lo, S.; Yeung, A. C. Review: Clinical aspects of vascular remodeling. *J. Cardiovasc. Electrophysiol.* **1999**, *10* (7), 1016–24.

191. Li, S.; Fan, Y. S.; Chow, L. H.; Van Den Diepstraten, C.; van Der Veer, E.; Sims, S. M.; Pickering, J. G. Innate diversity of adult human arterial smooth muscle cells: cloning of distinct subtypes from the internal thoracic artery. *Circ. Res.* **2001**, *89* (6), 517–25.

192. De, R.; Zemel, A.; Safran, S. A. Dynamics of cell orientation. *Nat. Phys.* **2007**, *3*, 655–659.

## Chapter 3

# Glucan Particles as Carriers of Nanoparticles for Macrophage-Targeted Delivery

**Ernesto Soto and Gary Ostroff***

**Program in Molecular Medicine,
University of Massachusetts Medical School,
373 Plantation Street, Worcester, Massachusetts 01605, USA
*E-mail: gary.ostroff@umassmed.edu**

Glucan particles (GP) are 2-4 μm hollow and porous microspheres derived from *Saccharomyces cerevisiae* (Baker's yeast) that provide an efficient system for encapsulation, protection, and oral or systemic macrophage-targeted delivery of macromolecules, such as DNA, siRNA and proteins using either a polyplex or layer-by-layer (LbL) synthesis methods. We have recently extended the application of GPs to the delivery of nanoparticles (NP) that are encapsulated within the hollow cavity of GPs or bound to the outer surface of chemically derivatized GPs (Soto, et al. *J. Drug Delivery,* **2012,** Article ID 143524). GP mediated delivery of nanoparticles provides the advantages of (1) encapsulation of materials that are difficult to prepare *in situ* within the glucan particles, such as nanomaterials composed of water-insoluble components, (2) β1,3-D-glucan receptor-targeted delivery of nanoparticles to phagocytic innate immune cells, (3) small molecule loaded nanoparticles for small drug molecule delivery, and (4) targeted delivery of nanoparticles with an intrinsic property, such as magnetic or gold nanoparticles, thus increasing the versatility of the GPs for theranostic applications. Examples of nanoparticles that have been formulated with GPs include magnetic iron oxide nanoparticles, gold nanoparticles, quantum dots and adeno-associated virus (AAV).

# Introduction

Advances in rational drug design and rapid screening (*1*), combined with the discovery of promising new approaches to treat diseases such as gene (*2*, *3*) and siRNA therapies (*4*, *5*), have spurred the development of an increasing number of novel drug delivery technologies. An effective drug delivery system must address several hurdles including issues of drug solubility, *in vivo* stability, efficient targeting, poor pharmacokinetics, toxicity and adverse side effects. Nanotechnology-based drug delivery systems represent a promising approach to fulfill the need for new delivery techniques. The field of nanoparticle based drug delivery has its origins in the discovery of liposomes (*6*) and polymer-drug conjugates (*7*). The development of methods for the synthesis, characterization and precise control over size and shape design (i.e. Particle Replication in Non-wetting Templates (PRINT) technology (*8*, *9*)) of nanoparticles has made it possible over the past 20 years to explore a variety of materials for nanoparticle based drug delivery (*10*, *11*), including natural and synthetic polymers, metal nanoparticles (gold, magnetic iron oxide), quantum dots, silica, dendrimers, and virus-like particles. The successful development of nanoparticle based delivery systems is exemplified by the use of nanomaterials for approved anticancer drug formulations (*12*, *13*), and it is anticipated that the number of applications using nanotechnology for drug delivery will continue to expand in the near future.

The interest in using nanoparticles for drug delivery is driven by high nanoparticle drug loading capacity, improved drug solubility and bioavailability, improved pharmacokinetics and therapeutic index, reduced immunogenicity, and the potential for targeted and controlled release (*10*, *11*, *14*). Careful synthetic design also allows for the synthesis of nanoparticles with precise size and shape and texture, key factors affecting penetration across biological barriers and cellular uptake mechanisms. More recently, research on nanoparticles has also focused on the design of nanoparticulate theranostic agents (*15*). The term theranostic, a term derived from therapeutic and diagnostic, was initially proposed by Funkhouser (*16*) in 2002, and it refers to materials that combine therapeutic drug delivery (i.e. gene therapy, chemotherapy, radiation, photodynamic therapy) and diagnostic imaging (i.e. magnetic resonance imaging (MRI), positron emission tomography/single-photon emission computed tomography (PET/SPECT), near-infrared (NIR) fluorescence functionality). These properties allow for the design of multifunctional nanoparticles that can be loaded with a therapeutic drug (i.e. siRNA) and an imaging agent (i.e. Gd(III) for MRI imaging), which can be delivered at the same time within the same dose. In the case of some nanoparticles (i.e. magnetic iron oxide, quantum dots, gold nanoparticles) the imaging application is an intrinsic property of the nanoparticle. Although the theranostics field is relatively new, significant advances have been made in the past decade to design promising nanoparticulate materials. The combination of therapeutic and diagnostic capabilities has the promise to drive the application of nanoparticle based materials in the biomedical field.

## Nanoparticle Design for Drug Delivery

Three primary parameters need to be considered for the successful design of nanoparticles as drug carriers: (1) a method to load and deliver a drug, (2) the mechanism of cell uptake, and (3) payload release. A payload can be loaded by multiple general strategies including: physical entrapment or payload absorption onto the NP using non-covalent interactions, or covalent binding to the NP using degradable or non-degradable bonds. Targeting of NPs can be achieved by three approaches: (a) passive accumulation of NPs by the enhanced permeability and retention (EPR) effect, such as the case of NP accumulation through the leaky vasculature of tumors (*13*), (b) NPs can be partially targeted by attaching ligands with specificity to receptors that are over-expressed in certain cells (i.e. folate and transferrin receptors in cancer cells (*17–21*)). However, this mechanism has the disadvantage of off-target effects as the receptors can be expressed on other types of non-target cells, and (c) targeting of cell populations with high selectivity by grafting specific targeting moieties (i.e. antibodies, aptamers, peptides, oligonucleotides) to nanoparticle surfaces recognized by cell surface receptors known to be expressed only on target cells (i.e. antibodies to target prostate-specific membrane antigen (PSMA) (*22*), or galactose to target asialoglycoprotein receptors on hepatocyte cells (*23*)). Finally, efficient payload release from NPs is accomplished by using stimuli-responsive components. Nanoparticles offer the advantage of selective chemical modification to incorporate components that will respond to an internal (reducing nature of cellular environment, change in pH) or external stimulus (applied magnetic field, radiation exposure). These stimuli activate a chemical mechanism to degrade or destabilize a carrier and release physically entrapped payloads (*24*, *25*), or to cleave a degradable bond and release molecules that are covalently bound to the NP (*26*, *27*).

The most critical challenge of current nanoparticle based drug delivery systems is the lack of optimal strategies for selective and efficient targeted delivery. Several undesired processes such as off-target accumulation in other organs tissues and cells, rapid particle clearance from *in vivo* circulation (especially particles less than 5 nm) (*28*, *29*), opsonization and macrophage clearance (*30*, *31*), and complement activation by proteins that causes hypersensitivity reactions (*32*) reduce the number of nanoparticles reaching target cells, thus resulting in using high nanoparticle concentrations to achieve a therapeutic response. Synthetic design of nanoparticles allows for specific control of nanoparticle functionalization to introduce chemical groups that reduce undesired processes. For example multifunctional NPs coated with cell surface receptor-targeting ligands combined with PEG polymer brush coats inhibit protein adsorption reducing macrophage uptake and rapid clearance by the RES; and control of particle size, shape and texture alters cellular internalization and trafficking (*32–35*).

We have developed a drug delivery system based on 1,3-β-D-glucan (β-glucan) microparticles (GP) that allows for receptor-targeted delivery to macrophage and dendritic cells that express β-glucan receptors. The combined use of GPs for binding/encapsulation of nanoparticles containing a payload drug aims to integrate the structural advantages of nanoparticles with the targeting capabilities of glucan microparticles to selectively target nanoparticles to macrophages via β-glucan mediated phagocytosis of the GP carriers.

A challenge with nanoparticle delivery is unintended partial uptake and clearance by phagocytic cells, such as macrophages. In contrast, glucan particles are selectively targeted to phagocytic macrophages by both a size (2-4 micron) and a receptor mediated uptake mechanism. GPs remain in macrophage endosomes for a longer time compared to nanoparticle uptake by pinocytosis or other non-receptor mediated mechanisms. We previous reported the kinetics of glucan particle intracellular metabolism showing that GPs remain intact in macrophages for several days and are slowly degraded into soluble β-glucan fragments (*36*). The ability of targeting GPs into macrophages and their slow degradation makes GPs an ideal drug carrier to target diseases or ameliorate symptoms in diseases in which macrophages play a significant role. Specific examples of diseases in which GP drug targeting to macrophages could play a significant role include: (1) targeting of antibiotics into alveolar macrophages to inhibit replication of *Mycobacterium tuberculosis*, (2) anti-inflammatory drug delivery to macrophages that promote pathogenic responses in inflammatory diseases such as diabetes, rheumatoid arthritis, Chrohn’s disease and psoriasis, (3) use of GPs loaded with antigens for vaccine delivery (*37*, *38*).

## β-Glucan Based Drug Delivery

1,3-β-D-glucans are a class of polysaccharides consisting of D-glucose monomers naturally found in fungi, algae, plants and some bacteria. Their most studied application is based on their ability to activate the immune system. Two receptors, dectin-1 (D1) and the Complement Receptor 3 (CR3 or CD11b/CD18), present on the surface of innate immune cells have been found to be primarily responsible for binding to 1,3-β-D-glucans (*39*) and the signaling mediated by both receptors has been characterized at the molecular level (*40–42*). In addition to immuno-stimulatory properties and their use as adjuvants in pharmaceutical formulations, glucans have been used in drug delivery systems as actual drug carriers, or in combination with other materials to form suitable drug delivery systems. The most significant applications of 1,3-β-D-glucan for drug delivery can be classified in four categories: (1) the use of 1,3-β-D-glucan (primarily curdlan, scleroglucan and their synthetic derivatives) as carriers in drug formulations consisting of hydrogels, tablets and ingestible films (*43–46*), (2) the preparation of particles coated with 1,3-β-D-glucan (i.e. use of curdlan for stabilization of liposomes (*47*, *48*), lipid nanoparticles of glyceryl caprate for entrapment of doxorubicin (*49*), superparamagnetic iron oxide nanoparticles coated with β-glucan for MRI diagnosing of liver metastasis (*50*)); (3) the use of soluble 1,3-β-D-glucan for encapsulation and delivery of macromolecules (i.e. DNA delivery with schizophyllan complexes (*51–53*)); and (4) the development of the yeast 1,3-β-D-glucan particle drug delivery technology.

In Nanomaterials for Biomedicine; Nagarajan, R.;
ACS Symposium Series; American Chemical Society: Washington, DC, 2012.

## Glucan Particles

(GPs) are highly purified, biodegradable, porous and hollow 2-4 μm microspherical particles prepared from Baker's yeast. Upon systemic administration, the GPs are internalized through a receptor-mediated process by phagocytic cells, such as monocytes, macrophages, neutrophils and dendritic cells (*36*, *37*). The use of glucan particles for macromolecule (DNA, siRNA, protein, vaccine) delivery has been demonstrated both *in vitro* and *in vivo* (*37*, *38*, *54–56*). Macromolecules such as nucleic acids can be efficiently loaded into GPs using either polyplex core or layer-by-layer synthesis approaches to produce glucan particle encapsulated DNA or siRNA polyplexes (*54*, *55*). The GPs offer protection and macrophage targeted delivery allowing a significant reduction in the amount of DNA or siRNA required for efficient transfection or gene silencing compared to the corresponding control polyplex samples prepared in the absence of GPs. A significant advance in the use of GPs for macrophage targeted delivery was the development of Glucan encapsulated siRNA particles (GeRPs) for oral and parenteral delivery of Map4k4-siRNA (*55*). These GeRPs consisted of glucan particle encapsulated tRNA/polyethylenimine cores onto which siRNA and other components were adsorbed by LbL synthesis. The GeRPs effectively suppressed lipopolysaccharide induced systemic inflammation protecting septic mice at siRNA doses 10-fold lower than required in *in vivo* studies reported using other available siRNA delivery methods (*55*). More recently, we engineered a simpler formulation method than the original multi-layered GeRPs by directly forming amphiphatic peptide (Endo-Porter (EP))/siRNA nanocomplexes in empty glucan shells. These formulations efficiently induced gene silencing in macrophages that internalized the glucan particles/siRNA-EP complexes, but not other cell types (*56*).

The advantages of GP delivery have been recognized by others for diverse applications. In independent work, Zhu (*57*) reported the use of GeRPs containing antiviral vp28-siRNA for delivery into *Marsupenaeus japonicus* shrimp to inhibit replication of white spot syndrome virus (WSSV), which is a major shrimp viral pathogen responsible for worldwide economic losses to shrimp aquaculture. Figueiredo (*58*) used glucan particles for delivery of an amphiphatic/lipophilic gadolinium MRI imaging agent (Gd-DOTAMA(C18)$_2$; DOTAMA = 1,4,7,10-tetraazacyclododecane-N,N′,N″,N‴-tetraacetic acid monoamide). Particles containing an oil/water microemulsion to trap the amphiphatic MRI agent were used for MRI imaging of mice grafted subcutaneously with B16 melanoma cells. Following 48 h post-injection of the paramagnetic GPs the particles were observed in lymph nodes near the tumor as a result of rapid macrophage uptake of GP Gd and subsequent delivery to the lymph node by migrating macrophages.

We have also used GPs for the encapsulation of small drug molecules, such as the antibiotic rifampicin (rif) (*59*). Rifampicin was loaded in soluble form into glucan particles, precipitated by a change in pH and subsequently trapped by loading of alginate or chitosan to form a hydrogel matrix to slow the release of rifampicin from the particles. These GP rif particles enhanced *in vitro* macrophage killing of TB. However, the use of glucan particles for small drug molecule delivery has been generally limited by the lack of efficient methods to load and retain small drug molecules inside GPs. The combined use of nanoparticles for drug binding and GP encapsulation of nanoparticles for targeted delivery represents a promising approach to expand the applications for GP delivery. The use of glucan particles for macrophage-targeted delivery of nanoparticles was initially reported using fluorescent polystyrene nanoparticles and mesoporous-silica nanoparticles containing the chemotherapeutic drug doxorubicin (Dox) (*60*). Nanoparticles containing Dox were loaded inside the hollow cavity of the glucan particles or non-covalently attached to the outer surface of chemically-derivatized GPs. GPs containing doxorubicin-mesoporous silica nanoparticles efficiently delivered the drug into GP phagocytic cell line 3T3-D1 expressing the dectin-1 receptor, resulting in enhanced Dox-mediated growth arrest. The advantages of combining glucan particle and existing nanoparticle drug delivery methods include: (1) 1,3-β-D-glucan receptor-targeted delivery to macrophage and dendritic cells. Although, others have reported the use of different nanoparticles coated with β-glucan for targeted delivery to cells expressing β-glucan receptors (*49*, *50*, *61*), these systems present the disadvantage of each uptake event delivering just one nanoparticle as opposed to the possibility of delivering hundreds to thousands of nanoparticles in one glucan particle uptake event due to the high loading capacity of GPs, (2) the encapsulation of payload complexes that cannot be prepared *in situ* as the synthetic conditions are not compatible with GPs, (3) the loading of nanoparticles with small neutral and hydrophobic drug molecules into GPs that is not possible to load by polyplex trapping or LbL methods, and (4) the incorporation of nanoparticles with an intrinsic property, such as magnetic nanoparticles, thus increasing the versatility of the particles and creating potential theranostic agents. A current disadvantage with theranostics is the mismatch in dose required for imaging and for therapeutic use, the dosages required for nuclear imaging and anticancer therapeutics are several orders of magnitude different. Other MRI agents, such as those based on gadolinium require considerably higher doses than the typical therapeutic drug due to the low sensitivity of MRI (*62*). A potential advantage of GPs for delivery of nanoparticles for theranostic applications is that NPs for imaging and NPs containing the therapeutic drug can be independently co-loaded in the same GP at the optimal concentration required for each function.

Here we report on the different strategies developed to efficiently create Glucan Particle – Nanoparticle (GP/NP) hybrid systems and present examples of potential applications using quantum dots, gold nanoparticles, magnetic iron oxide nanoparticles and adeno-associated virus.

## Glucan Particle-Nanoparticle Loading Strategies (GP/NP Delivery)

As previously reported (*60*), it is possible to use glucan particles for nanoparticle delivery by either encapsulation of nanoparticles inside glucan particles (GP-NP) or by binding of nanoparticles to the outer surface of chemically-modified glucan particles (NP-GP). The nanoparticle location is dependent on nanoparticle size. NPs of average diameter less than 30 nm can diffuse through the GP shell matrix and be trapped inside the cavity by physical or chemical methods. Larger nanoparticles, which are unable to penetrate into GPs must be loaded by binding to the outer surface of chemically-derivatized glucan particles. The NP-GP system offers the advantage of more rapid release due to less nanoparticle aggregation and overcomes the possible slow diffusion of a payload from the glucan particles. In contrast, the GP-NP system, encapsulating nanoparticles inside GPs is a more advantageous strategy due to (1) higher nanoparticle loading capacity, and (2) protection of NPs by the glucan shell in transit to target cells. An alternative GP nanoparticle loading strategy to overcome NP size limitation is the *in situ* synthesis of nanoparticles inside GPs for those nanoparticles that can be synthesized under conditions that are compatible with GPs.

The mechanisms by which pre-formed nanoparticles remain incorporated inside or on the surface of glucan particles include physical aggregation, physical embedment of nanoparticles in a polymer gel, covalent crosslinking of nanoparticles, non-covalent electrostatic interactions, or affinity binding (i.e. streptavidin-biotin) of nanoparticles to either surface derivatized GPs or polymers loaded inside the hollow GP cavity.

Using either commercially available nanoparticles of narrow size distribution or nanoparticles synthesized in our laboratory we developed different loading strategies to incorporate NPs inside or on the surface of GPs.

## Glucan Particle Encapsulated Nanoparticles (GP-NP)

Pre-formed nanoparticles of less than 30 nm in diameter can be loaded through the pores of glucan particles (Figure 1). Ideally, the nanoparticles are in a stable suspension to prevent aggregation outside the GPs. Nanoparticle loading is accomplished by wetting the glucan particles in a sub-hydrodynamic volume of the nanoparticle suspension to ensure complete absorption of the NP suspension into GPs by capillary action. Subsequent solvent hydration/lyophilization steps hydraulically push the nanoparticles into GPs by capillary action. In most formulations the solvent is water, although depending on the nanoparticles solvents such as 70% ethanol are more suitable to foster NP aggregation inside GPs. The nanoparticles are retained inside GPs by either particle aggregation, physical or chemical trapping. Spontaneous nanoparticle aggregation occurs with some nanoparticles during the lyophilization steps involved in GP-NP synthesis. However NPs less prone to aggregation quickly diffuse out of the GPs upon resuspension of the GP-NP sample in a volume higher than the hydrodynamic volume. To ensure that the majority of nanoparticles (either single particle or large aggregates) are effectively retained inside the GPs we have investigated the use of cationic or anionic polymers to non-covalently bind nanoparticles functionalized with corresponding anionic or cationic groups. Additionally, more stable samples can be prepared by covalent chemical crosslinking of nanoparticles with a polymer (i.e. EDC crosslinking of carboxylated labeled nanoparticles with a cationic polymer like chitosan or PEI). Other strategies include the non-covalent affinity binding of biotin-surface-modified nanoparticles interacting with biotin-modified polymers through avidin or streptavidin bridges between the nanoparticles and polymers. A click chemistry reaction is another possibility to generate stable polymer/nanoparticle aggregates inside GPs. Figure 1 shows microscopic images of GP-NP samples prepared with fluorescently labeled 20 nm carboxylated nanoparticles. The carboxylate groups on the nanoparticle surface allow for electrostatic crosslinking with polyethylenimine (PEI) or other cationic polymers forming nanoparticle aggregates or cores inside the GPs. The use of a cationic polymer to bind nanoparticles also offers the possibility of using the cationic nanoparticle core for binding of an anionic payload molecule (i.e. DNA or siRNA).

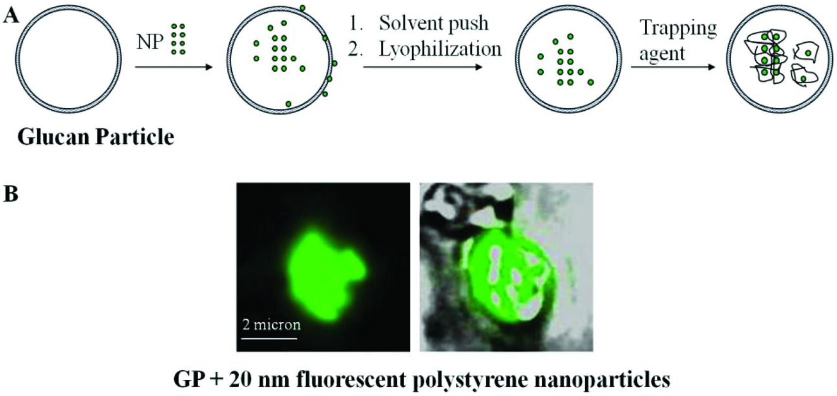

*Figure 1. (A) Schematic representation of nanoparticle loading inside GPs, (B) Microscopic image of GPs containing a core of fluorescently labeled polystyrene (20 nm) nanoparticles crosslinked with PEI (fluorescent image on the left, overlay of fluorescent and brightfield image on the right). (see color insert)*

## *In Situ* Synthesis of GP-NP

As indicated above, nanoparticle size is the key limiting factor to the preparation of encapsulated GP-NP samples. An alternative strategy to load larger nanoparticles is the *in situ* synthesis of NPs inside GPs for those NPs that can be synthesized under conditions compatible with GPs (Figure 2A). Two key parameters were identified for successful *in situ* synthesis of nanoparticles: (1) efficient loading of nanoparticle starting materials and their stability prior to (2) generation of optimal nanoparticle formation reaction conditions within glucan particles. For example, although we can efficiently load starting materials for *in situ* synthesis of mesoporous silica nanoparticles (MSN) or poly(lactic-co-glycolic acid) (PLGA) nanoparticles, it is difficult to generate exact reaction conditions (i.e. stable surfactant micelle for MSN synthesis or water/oil emulsion for synthesis of PLGA) resulting in GPs containing mixture of MSN or PLGA particles and side products (i.e. silicon dioxide from decomposition of tetraethylorthosilicate used for MSN synthesis).

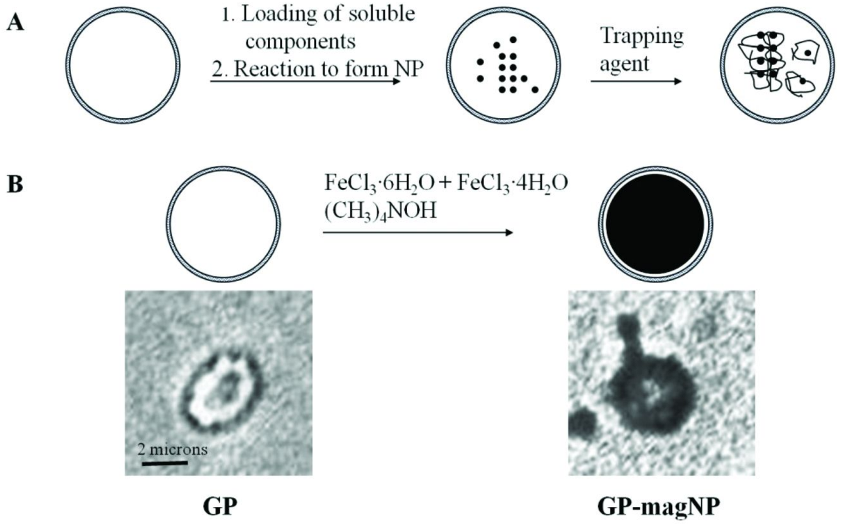
A
1. Loading of soluble components
2. Reaction to form NP
Trapping agent
B
$FeCl_3 \cdot 6H_2O + FeCl_3 \cdot 4H_2O$
$(CH_3)_4NOH$
2 microns
GP
GP-magNP

*Figure 2. (A) Schematic representation of in situ synthesis of NPs inside GPs, (B) Bright field microscopic images of empty GPs and magnetic GP $Fe_xO_y$ NPs.*

We have successfully synthesized *in situ* GP-NPs containing iron oxide nanoparticles. Colloidal iron oxide nanoparticles are of interest for their magnetic properties as MRI contrast agents. Iron oxide nanoparticle cores were prepared inside GPs by co-precipitation of acidic aqueous solutions of iron chloride (III) and iron chloride (II) in the presence of tetramethylammonium hydroxide (TMAOH). Optimal iron salts and TMAOH concentrations, as well as temperature were based on the work by Babes (*63*), to generate paramagnetic particle aggregates inside GPs (GP $Fe_xO_y$ NPs). The brightfield microscopic images in Figure 2B show the difference between empty GPs and GPs containing magnetic iron oxide nanoparticles.

## Nanoparticle Binding to the Outer GP Surface (NP-GP)

Nanoparticles of average diameter greater than 30 nm will not efficiently penetrate through the GP shell and can be chemically bound to the surface of derivatized GPs, as previously demonstrated for anionic polystyrene nanoparticles or anionic mesoporous silica nanoparticles electrostatically bound to GPs derivatized with cationic PEI (*60*). GPs are essentially neutral with exception of a small amount of positively charged chitosan. However, the chitosan is largely buried in the glucan matrix and not readily available for electrostatic binding of anionic nanoparticles. Cationic GPs can be synthesized by covalent modification of the GP surface with cationic polymers (i.e. PEI, chitosan, PLL) via a reductive amination synthetic approach. This synthetic strategy allows functionalization of the reducing terminal glucose monomers (<2%) in the β-glucan structure of the particles. Additionally, surface derivatization of GPs can be done using the same reductive amination approach to incorporate other polymers on the surface as depicted schematically in Figure 3A. For example, anionic polymers (i.e. alginate, tRNA) can be easily attached to a GP previously derivatized with a diamine molecule (i.e. diamino propane or $NH_2$-PEG-$NH_2$) onto which the anionic polymer can be covalently linked. Other covalent examples include: 1) the derivatization of GPs with molecules terminated in a biotin moiety for affinity binding to avidin or streptavidin, 2) cyclodextrin for host-guest interactions with nanoparticles derivatized with groups such as adamantane, or 3) azido/alkene groups for nanoparticle attachment using a click chemistry reaction. Figure 3B shows an example of NP-GP synthesis through GP surface derivatization with 10 kD PEI allowing for linkage to carboxylate fluorescent polystyrene NPs.

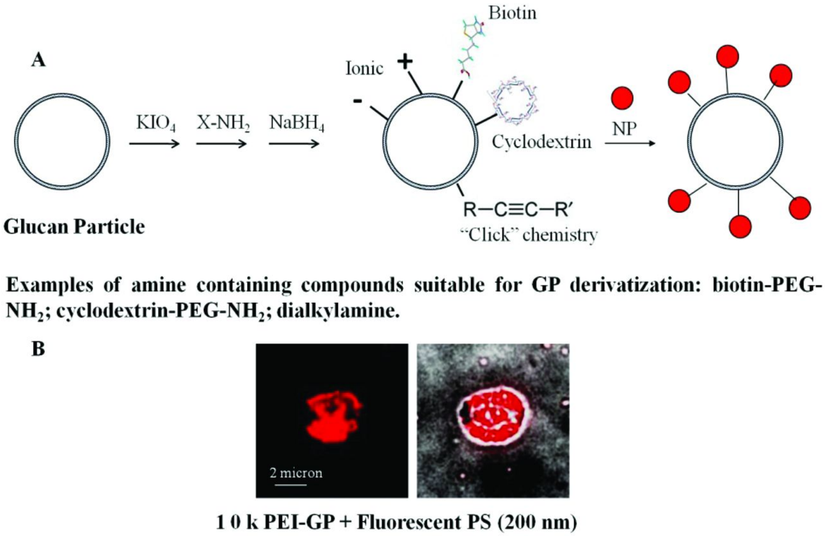

**Examples of amine containing compounds suitable for GP derivatization: biotin-PEG-$NH_2$; cyclodextrin-PEG-$NH_2$; dialkylamine.**

*Figure 3. (A) Schematic representation of GP surface derivatization methods for different nanoparticle binding strategies and (B) Microscopic images showing binding of fluorescent anionic polystyrene nanoparticles to 10 k PEI surface derivatized GPs (fluorescent image on the left, overlay of fluorescent and brightfield image on the right). (see color insert)*

## Examples of Glucan Particle/Nanoparticle Systems and Potential Applications

Using the different nanoparticle loading strategies described in the previous section we have prepared numerous GP samples containing nanoparticles for potential applications in imaging, cell purification, and drug delivery. Here, we described the most significant examples of glucan particle/nanoparticle systems containing quantum dots, gold nanoparticles, magnetic iron oxide nanoparticles, and adeno-associated virus.

## Quantum Dots

Quantum dots (QDs) have been proposed as a useful tool for molecular diagnostics due to their unique optical properties that give them advantages over fluorescent organic dyes (*64*). QDs have high extinction coefficients, reduced susceptibility to photobleaching, potential for high-resolution cellular imaging, and long-term *in vivo* tracking. However QD's *in vivo* applications are limited by their potential cytotoxicity and colloidal stability. The use of quantum dots allowed us to demonstrate the versatility of GPs for nanoparticle binding by developing GP/QD samples localized inside or outside GPs, and trapped by embedding of QDs in a polymer (i.e. calcium alginate) hydrogel, electrostatic binding (carboxylated quantum dots crosslinked with PEI) or affinity trapping (biotinylated QDs bound onto biotin-GPs or inside GPs with PEI-biotin using an avidin or streptavidin bridge).

Figure 4 shows the synthetic strategy and microscopic images of GPs containing carboxylated quantum dots (Ocean Nanotech LLC, Springdale, AR) crosslinked with PEI. These quantum dots (average hydrodynamic size of 10 nm) consist of a CdSe/ZnS core shell structure coated with a carboxylated polymer. The presence of carboxylate groups on the QD surface allowed for efficient condensation with PEI into larger aggregates, thus preventing QD leakage from the GP-QD samples. The samples efficiently delivered QDs into the phagocytic cell line 3T3-D1.

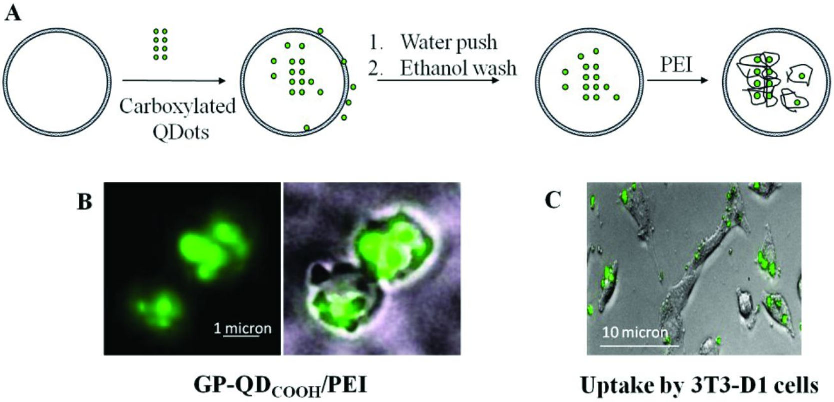

**GP-QD$_{COOH}$/PEI** **Uptake by 3T3-D1 cells**

*Figure 4. (A) Schematic representation of the method used to prepare GP samples containing electrostatically trapped quantum dots inside GPs. (B) Microscopic images showing GP-QD samples (fluorescent image on the left, overlay of fluorescent and brightfield image on the right) and (C) Overlay of fluorescent and brightfield microscopic images showing uptake of GP-QD by 3T3-D1 cells capable of phagocytosing GPs. (see color insert)*

Figure 5 illustrates two procedures to generate GPs containing QDs either inside or outside the GPs using biotin modified QDs (Invitrogen, Carlsbad, CA). For GP surface loaded samples biotin-modified GPs were used as the starting material to bind avidin or streptavidin protein followed by the binding of biotinylated QDs. The encapsulated GP-QD samples were prepared by loading QDs in the sub-hydrodynamic volume, lyophilizing the sample and repeating the loading procedure using streptavidin and then PEI functionalized with biotin. Upon resuspension of the lyophilized particles in water a core of QD-biotin-streptavidin-biotin-PEI was formed inside the GPs and unbound QDs were washed from the sample. The microscopic images shown in Figure 6 confirmed successful synthesis of QD-GP or GP-QD samples and efficient uptake by RAW264 phagocytic cells. The particle uptake of QD-GP by the murine macrophage cell line, RAW264 demonstrated the stability of the QD bound to the outer surface of modified GPs. Additionally, biotin surface modification of GPs or the binding of QD-biotin-avidin to the derivatized particles had no apparent effect on glucan-mediated phagocytosis or cellular toxicity. This is similar to our previous study showing efficient GP uptake by 3T3-D1 of GPs modified with PEI with and without anionic polystyrene nanoparticles electrostatically bound to PEI (*60*). We hypothesize that the low surface modification (<2% of reducing glucose ends are derivatized in surface GPs) does not have a significant effect on blocking accessibility of glucan receptors to the β-glucan. Coating of GPs with PEG also did not have significant effect on particle uptake likely as result of inefficient blocking of all the β-glucan by the reductive amination approach to functionalize GPs (data not shown).

The ability to encapsulate QDs inside glucan particles provides a potentially more suitable tool for *in vivo* imaging and biodistribution than original glucan particles labeled on the surface with an organic fluorescent dye (i.e. FITC). Additionally, the possibility of loading QDs of different average diameter might allow the development of formulations with control over QD release (i.e. use of a biodegradable hydrogel matrix) for studies of QD intracellular trafficking upon GP mediated uptake of QDs.

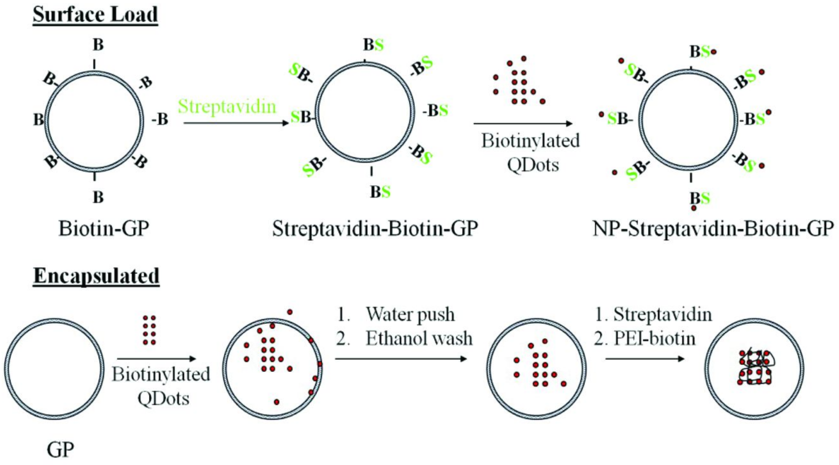

*Figure 5. Schematic representation of method to affinity trapping quantum dots on the GP surface or encapsulated in the hollow GP cavity.*

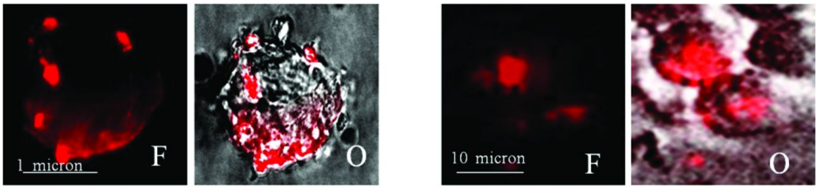

**A. GP surface loaded QDots**

**Uptake by RAW264 cells**

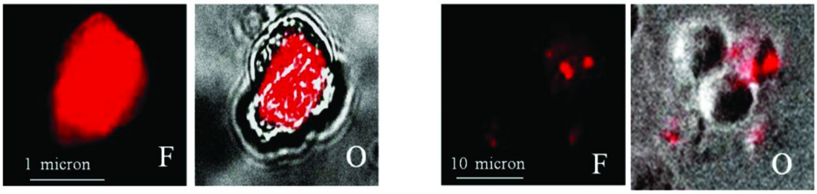

**B. GP encapsulated QDots**

**Uptake by RAW264 cells**

*Figure 6. Fluorescent microscope images (F: Fluorescent, O: Overlay) showing localization of biotinylated QDs and GP-mediated cell uptake by RAW264 cells. (A) Biotinylated QDs loaded on surface of avidin-biotin-GPs, (B) Biotinylated QDs encapsulated in GPs following trapping reaction with streptavidin-biotin-PEI. (see color insert)*

## Gold Nanoparticles

Gold nanoparticles have been extensively investigated for their potential medical use as both drug carriers and for diagnostic applications. Their application as drug carriers depends on efficiency of drug binding and release, nanoparticle uptake and biodistribution that is a function of gold nanoparticle size and shape. Gold nanoparticles have been used as carriers of anticancer drugs such as paclitaxel (*65*, *66*) and doxorubicin (*67*). The ability of gold nanoparticles to target tumors has also been used for *in vivo* detection using surface enhanced raman spectroscopy (SERS) (*68*) and as photothermal agents (*69*).

We have prepared GP samples containing gold nanoparticles (Nanoxact, San Diego, CA) of average diameter of 10, 20 and 30 nm as shown in Figure 7A. A monolayer of mercaptoundecanoic acid (MUA) on the nanoparticle surface allowed for crosslinking of the nanoparticles with a cationic polymer into larger aggregates. Figure 7B shows a microscopic image of GP-Au/PEI nanoparticle cores crosslinked with fluorescently labeled PEI (FL-PEI). These GP-Au/FL-PEI nanoparticle cores were efficiently phagocytosed by 3T3-D1 cells. The GP-Au/PEI nanoparticle cationic cores were evaluated for their ability to bind fluorescently labeled (Cy3) siRNA (Figure 7C). GP-Au nanoparticle cores without PEI do not show binding affinity for siRNA. In comparison, the efficiency of GP-Au/PEI cores to bind siRNA is similar to standard samples of GPs containing a tRNA/PEI nanoparticulate core.

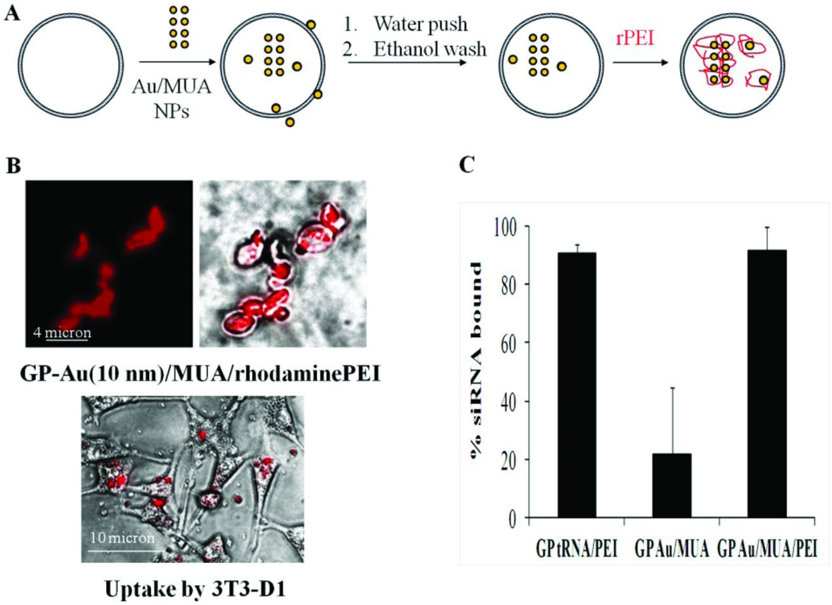

*Figure 7. (A) Schematic representation of GP-Au synthesis, (B) Microscopic images showing GP-Au nanoparticle cores crosslinked with FL-PEI (left – fluorescent, right – overlay) and uptake by 3T3-D1 cells (fluorescent-brightfield overlay), (C) siRNA binding efficiency to GP-Au control cores, and GP-Au/MUA/PEI and GP-tRNA/PEI cationic cores (experiment was done by loading 100 ng siRNA/1x10$^6$ GP). (see color insert)*

## Magnetic Iron Oxide Nanoparticles

The first generation magnetic GPs were prepared by *in situ* synthesis of magnetic iron oxide nanoparticles inside GPs as shown in Figure 2. Disadvantages of this approach to synthesize GP-$Fe_xO_y$ NPs were the formation of a fraction of GPs containing non-magnetic iron oxide and long term stability of the magnetic GP fraction. Stable magnetic GPs were prepared using pre-formed magnetic nanoparticles (magNP) of an average diameter of 10 nm. These magnetic nanoparticles (Ferrotec, Bedford, NH) contain either a cationic or anionic coat allowing for crosslinking with a polymer of opposite charge. Magnetic GPs were prepared with or without polymer crosslinking, as it was determined experimentally that the lyophilization and ethanol push treatments led to aggregation of the magnetic nanoparticles inside the GPs. These GP encapsulated aggregated magNP formulations have been shown to be stable for extended periods of time (up to 3 years). Figure 8 shows a schematic representation of GP-magNP synthesis and the results of cell purification following particle uptake by non-phagocytic NIH3T3 control fibroblasts and GP phagocytic 3T3-D1 cells. Both cell lines were incubated with either fluorescent labeled GP magNPs or fluorescent GP control (non-magnetic). Following a three hour incubation to allow for GP uptake, the cells were processed to detach them from plates and transferred to magnetic purification columns (MACS separation columns, Miltenyi Biotec Inc, Auburn, CA). The flow-through buffer containing cells without magnetic particles was collected. The columns were removed from the magnet to release the cells containing magnetic particles and these cells were collected by washing the column with the buffer solution. Both the bound and unbound fractions were centrifuged, resuspended in the same volume of buffer, and cells counted using a hematocytometer. The results in Figure 8 demonstrate that only the GP phagocytic 3T3-D1 cells containing magnetic GPs were efficiently separated in the magnetic fraction.

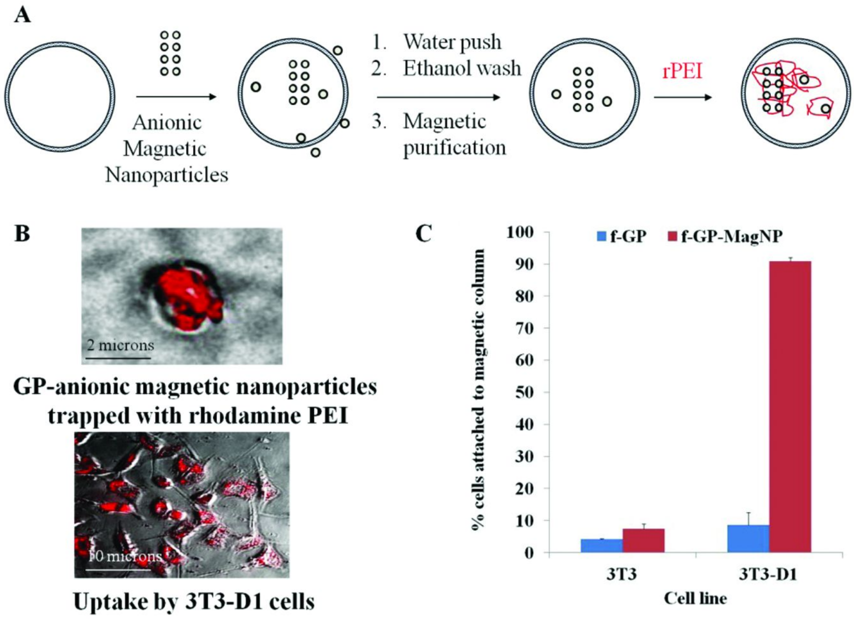

*Figure 8. (A) Schematic representation of magnetic GP synthesis (B) Microscopic images showing GPs containing anionic magnetic nanoparticles crosslinked with fluorescent PEI and their uptake by 3T3-D1 cells (fluorescent-brightfield overlay) (C) Results of magnetic cell purification using GPs containing anionic magnetic nanoparticles (without PEI coat). (see color insert)*

DNA binding to magnetic GPs was evaluated using a layer-by-layer method as previously described for GP encapsulated tRNA/PEI cores (*54*). Magnetic GPs containing anionic iron oxide nanoparticles cores were coated with PEI and used in binding experiments with a fluorescently labeled (rhodamine) DNA. The results shown in Figure 9A demonstrate that GP-magNP/PEI cores have a similar binding efficiency for DNA as GP-tRNA/PEI cores. The effect of GP-magNP/PEI on DNA transfection was evaluated using gWizGFP plasmid DNA adsorbed onto the cores and coated with an additional outer PEI layer. The results in Figure 9B show the comparable % GFP transfection values of 3T3-D1 cells at an optimal DNA concentration using GP-tRNA/PEI or GP-magNP/PEI cores. Further optimization of these materials could include the incorporation of additional components into the multilayered polyplex structure to facilitate polyplex defoliation, endosomal release and DNA nuclear uptake (*70*).

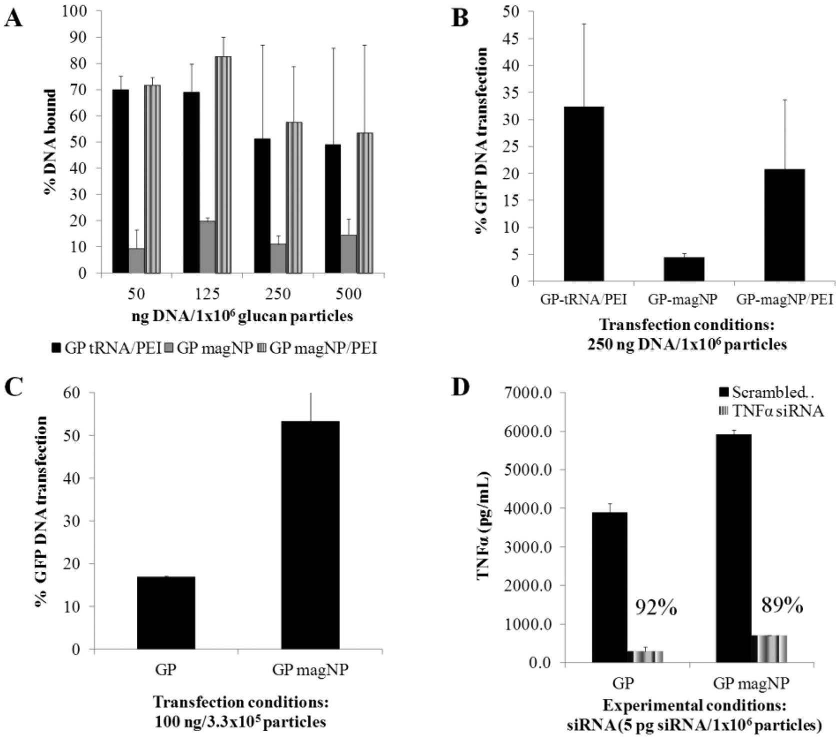

*Figure 9. Use of GP-magNPs for DNA and siRNA delivery: (A) Fluorescent (rhodamine) DNA binding efficiency to control and GP-magNP/PEI cores, (B) GFP DNA transfection efficiency in 3T3-D1 cells using LbL GP-mag/PEI and control GP cores, (C) GFP DNA transfection efficiency in 3T3-D1 cells using GP and GP-magNPs to deliver DNA-PEI polyplex cores, and (D) TNFα silencing in bone marrow macrophages using GP and GP-magNPs to deliver scrambled control siRNA or TNFα siRNA-EP polyplex cores.*

We have recently developed a simpler approach to prepare GP encapsulated nucleic acid cores. These formulations used cationic peptide (Endo-Porter (EP); Gene Tools, Philomath, OR)-siRNA polyplexes to efficiently transfect macrophage cells (*56*). The advantage of this new approach is that it reduces the number of components in the GP-DNA or siRNA formulations compared to the original, more complex GP encapsulated layer by layer core structures. Using a similar nucleic acid–cationic trapping agent approach we used empty glucan particles and glucan particles containing a core of magnetic nanoparticles (the nanoparticles held together inside the GPs by aggregation without incorporation of an additional coat) to evaluate delivery of DNA-PEI polyplexes. The results in Figure 9C show transfection results using magnetic and non-magnetic GPs containing DNA polyplexes (100 ng DNA/3.3x$10^5$ particles) prepared with sequentially added 2.5 k PEI and 25 k PEI to transfect $10^6$ 3T3-D1 cells. The transfection results indicate that GP-magNPs are significantly better at transfecting phagocytic cells than empty GPs. It is likely that a fraction of the DNA-PEI polyplexes binds to the anionic magnetic nanoparticles thus increasing the stable encapsulation of the DNA-PEI polyplexes.

Current studies are focused on the optimization of GPs for siRNA delivery into macrophages. Empty glucan particles and GPs containing magnetic NPs were used in the preparation of samples containing siRNA/EP polyplexes. The results in Figure 9D show the effect on TNFα secretion by bone marrow macrophage cells following uptake of GP or GP-magNP samples containing siRNA complexes. GP siRNA samples delivering a siRNA sequence targeting TNFα significantly silenced TNFα by ~90% compared to samples that delivered a scrambled control siRNA. The efficiency in siRNA knock down is similar for both GPs or GP-magNPs. The use of GP-magNPs for siRNA delivery will potentially provide both combined theranostic and siRNA delivery capabilities to the GP delivery system. In addition, it is possible to magnet purify cells containing GP-magNPs loaded with siRNA to selectively measure target gene silencing in transfected cells.

## Adeno-Associated Virus

Adeno-associated virus type 2 (AAV2) is a single strand DNA human parvovirus. Recombinant AAV viruses have been extensively used as gene therapy vectors as there is no known pathology and a natural propensity to persist in human cells. Several applications, primarily using AAV2 for gene therapy treatment of hemophilia B (*71*), α-1 antitrypsin deficiency (*72*), and cystic fibrosis (*73*) have reached clinical trials. A major limitation in the application of AAV gene therapy is the low resistance of the virus to neutralizing AAV antibodies, which has been shown to limit its repeated use (*74*). AAV2 has an icosohedron structure with an average diameter of 24 nm making it a suitable viral particle to test for encapsulation within GPs. It is also known that AAV2 cellular uptake takes place primarily by binding to heparin sulfate proteoglycan (HSPG) (*75*). We devised a synthetic strategy to trap AAV2 inside GPs by forming AAV2/heparin complexes as illustrated in Figure 10. Heparin was chosen as the trapping polymer for the following reasons: (1) ability of AAV2 to bind heparin to maximize AAV2 trapping efficiency within GPs, (2) to block uptake of free AAV2 virus by heparin-mediated receptor as any AAV2 not initially trapped within GPs and carried over in the formulations will most likely be associated with excess heparin and therefore blocked for cell uptake, and (3) AAV2/heparin complexes within GP should be stable and protect the virus during transport and uptake process, but the complexes will dissociate at low endosomal pH efficiently releasing the virus following the normal AAV2 infection process.

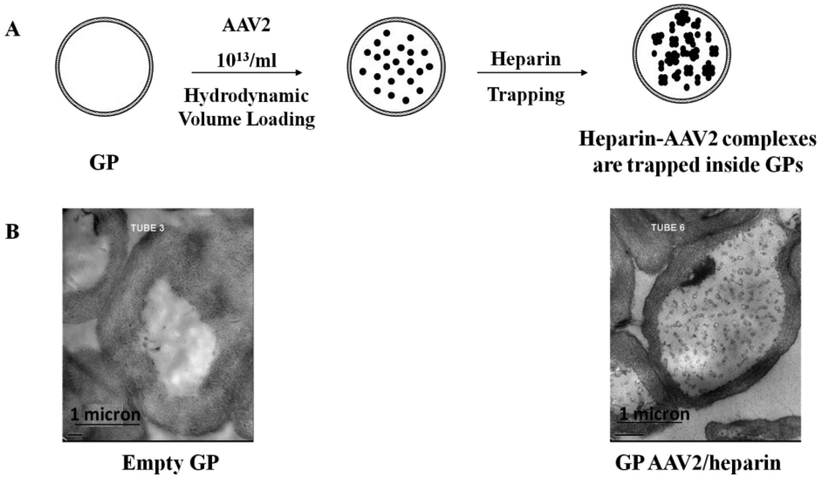
A
AAV2
10¹³/ml
Hydrodynamic
Volume Loading
GP
Heparin
Trapping
Heparin-AAV2 complexes
are trapped inside GPs
B
TUBE 3
1 micron
Empty GP
TUBE 6
1 micron
GP AAV2/heparin

*Figure 10. (A) Schematic of synthetic procedure to load AAV2 into glucan particles and (B) Transmission electron micrographs (TEM) showing empty glucan particles and glucan particles containing AAV2/heparin aggregates.*

As shown in Figure 10A, hydrodynamic volume loading of AAV2 virus followed by reaction with heparin resulted in the formation of heparin/AAV2 complexes. These complexes are large enough to be imaged inside GPs by transmission electron microscopy (Figure 10B). The efficacy of the GP-AAV2 delivery system was evaluated using an AAV2 virus containing a gene fluorescent protein (GFP) reporter gene cassette to visualize cellular delivery as monitored by GFP transduction in 3T3-D1 cells. The fluorescent microscopic images in Figure 11 show the relative GFP transduction efficiency using free AAV2-GFP virus and GP-AAV2-GFP samples. GP delivery of AAV2-GFP is as effective as free virus at transducing 3T3-D1 cells to express GFP (>50% transduction with both samples). In the presence of 100 μg/mL heparin, free virus transduction, but not GP-AAV2 transduction is more than 90% inhibited as result of binding of free AAV2 to heparin in the medium and not the heparin cell surface receptors. It is hypothesized that GP-AAV will also be resistant to neutralizing AAV antibodies overcoming a major limitation of AAV gene therapy targeting macrophages.

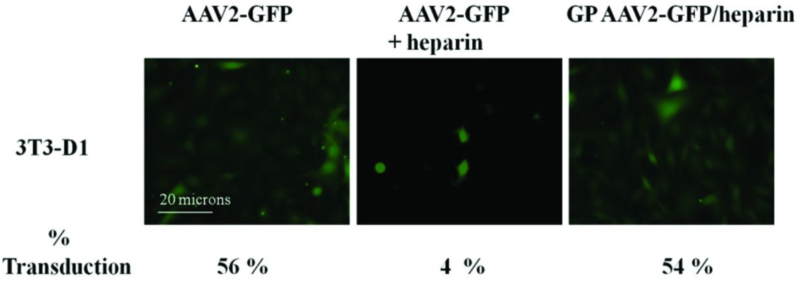

*Figure 11. Microscopic images showing AAV2-GFP +/- heparin and GP-AAV2-GFP/heparin transduction of 3T3-D1 cells. (see color insert)*

## Conclusions

We have extended the application of the glucan particle delivery technology to the macrophage-targeted delivery of nanoparticles. Nanoparticles of less than 30 nm in diameter can be encapsulated within the hollow cavity of GPs providing nanoparticle/drug protection in addition to targeted delivery. Using this encapsulation method we have developed GP formulations containing quantum dots for imaging applications; gold nanoparticles for drug delivery; magnetic nanoparticles for cell purification, imaging and drug delivery; and adeno-associated virus for gene therapy applications. Larger nanoparticles can be bound to the surface of chemically-derivatized GPs as demonstrated by the binding of biotinylated quantum dots to the outer surface of GPs, or as reported in a previous publication showing targeted delivery of GPs containing mesoporous silica nanoparticles encapsulating the chemotherapeutic doxorubicin (*60*). The ability to combine glucan particles with existing nanoparticle delivery technologies opens the possibility of developing systems for efficient macrophage-targeted drug delivery applications. The GP/NP system combines the advantages of glucan particle mediated targeted delivery into phagocytic innate immune cells and nanoparticles for high drug binding capacity (either by physisorption or chemical adsorption onto the nanoparticle surface or by drug encapsulation). In addition, the use of certain types of nanoparticles (i.e. gold nanoparticles or magnetic iron oxide) may add theranostic value to the GP/NP delivery system. A significant advantage of using GPs as a targeted delivery vehicle for nanoparticles into macrophages is that a single GP uptake event results in efficient cell delivery of a large number of nanoparticles in contrast to a single nanoparticle uptake from nanoparticles coated with β-glucan.

## Acknowledgments

We would like to thank Drs. Christian Mueller and Guanping Gao for their collaboration on the GP-AAV project. We appreciate the help of Shira Kahlon, Melissa Castle, Melissa Hauser, and Benjamin Moorehouse. This work was supported by UMass Medical School, Commonwealth Medicine and the Juvenile Diabetes Research Foundation (Grant no. 17-2009-546).

## References

1. Englebienne, P. *Front. Drug Des. Discovery* **2005**, *1*, 69–86.
2. Pack, D. W.; Hoffman, A. S.; Pun, S.; Stayton, P. S. *Nat. Rev. Drug Discovery* **2005**, *4*, 581–593.
3. Park, I.; Singha, K.; Arote, R.; Choi, Y.; Kim, W.; Cho, C. *Macromol. Rapid Commun.* **2010**, *31*, 1122–1133.
4. Stanton, M. G.; Colletti, S. L. *J. Med. Chem.* **2010**, *53*, 7887–7901.
5. Yuriko, H.; Kawakami, S.; Hashida, M. *BioDrugs* **2010**, *24*, 195–205.
6. Gregoriadis, G. *FEBS Lett.* **1973**, *36*, 292–296.
7. Kopf, H.; Joshi, R. K.; Soliva, M.; Speiser, P. *Pharm. Ind.* **1976**, *38*, 281–284.
8. Gratton, S. E.; Williams, S. S.; Napier, M. E.; Pohlhaus, P. D.; Zhou, Z.; Wiles, K. B.; Maynor, B. W.; Shen, C.; Olafsen, T.; Samulski, T. E.; DeSimone, J. M. *Acc. Chem. Res.* **2008**, *41*, 1685–1695.
9. Euliss, L. E.; Dupont, J. A.; Gratton, S.; DeSimone, J. *Chem. Soc. Rev.* **2006**, *35*, 1095–1104.
10. Suri, S. S.; Fenniri, H.; Singh, B. *J. Occup. Med. Toxicol. (London)* **2007**, *2*, 1–6.
11. Petros, R. A.; DeSimone, J. *Nat. Rev. Drug Discovery* **2010**, *9*, 615–627.
12. Ferrari, M. *Nat. Rev. Cancer* **2005**, *5*, 161–171.
13. Maeda, H.; Greish, K.; Fang, J. *Adv. Polym. Sci.* **2006**, *193*, 103–121.
14. Brewer, E.; Coleman, J.; Lowman, A. *J. Nanomater.* **2011**, 408675.
15. Kelkar, S. S.; Reineke, T. M. *Bioconjugate Chem.* **2011**, *22*, 1879–1903.
16. Funkhouser, J. *Curr. Drug Discovery* **2002**, *2*, 17–19.
17. Wang, X.; Li, J.; Wang, Y.; Cho, K. J.; Kim, G.; Gjyrezi, A.; Koenig, L.; Giannakakou, P.; Shin, H. J. C.; Tighiouart, M.; Nie, S.; Chen, Z.; Shin, D. M. *ACS Nano* **2009**, *3*, 3165–3174.
18. Low, P. S.; Henne, W. A.; Doorneweerd, D. D. *Acc. Chem. Res.* **2008**, *41*, 120–129.
19. Choi, C. H.; Alabi, C. A.; Webster, P.; Davis, M. E. *Proc. Nat. Acad. Sci. U.S.A.* **2010**, *107*, 1235–1240.
20. Han, L.; Huang, R.; Liu, S.; Huang, S.; Jiang, C. *Mol. Pharmaceutics* **2010**, *7*, 2156–2165.
21. Dowling, M. B.; Li, L.; Park, J.; Kumi, G.; Nan, A.; Ghandehari, H.; Fourkas, J. T.; DeShong, P. *Bioconjugate Chem.* **2010**, *21*, 1968–1977.
22. Patri, A. K.; Myc, A.; Beals, J.; Thomas, T. P.; Bander, N. H.; Baker, J. R. *Bioconjugate Chem.* **2004**, *15*, 1174–1181.

23. Plank, C.; Zatloukal, K.; Cotton, M.; Mechtler, K.; Wagner, E. *Bioconjugate Chem.* **1992**, *3*, 533–539.
24. Klaikherd, A.; Nagamani, C.; Thayumanavan, S. *J. Am. Chem. Soc.* **2009**, *131*, 4830–4838.
25. Ryu, J.; Jiwpanich, S.; Chacko, R.; Bickerton, S.; Thayumanavan, S. *J. Am. Chem. Soc.* **2010**, *132*, 8246–8247.
26. Saito, G.; Swanson, J. A.; Lee, K. *Adv. Drug Delivery Rev.* **2003**, *55*, 199–215.
27. Kim, B.; Han, G.; Toley, B.; Kim, C.; Rotello, V. M.; Forbes, N. S. *Nat. Nanotechnol.* **2010**, *5*, 465–472.
28. Vinogradov, S. V.; Bronich, T. K.; Kabanov, A. V. *Adv. Drug Delivery Rev.* **2002**, *54*, 135–147.
29. Choi, H. S.; Liu, W.; Misra, P.; Tanaka, E.; Zimmer, J. P.; Ipe, B. I.; Bawendi, M. G.; Frangioni, J. V. *Nat. Biotechnol.* **2007**, *25*, 1165–1170.
30. Owens, D. E., III; Peppas, N. A. *Int. J. Pharm.* **2006**, *307*, 93–102.
31. Howard, M. D.; Jay, M.; Dziublal, T. D.; Lu, X. L. *J. Biomed. Nanotechnol.* **2008**, *4*, 133–148.
32. Hamad, I.; Hunter, A. C.; Rutt, K. J.; Liu, Z.; Dai, H.; Moghimi, S. M. *Mol. Immunol.* **2008**, *45*, 3797–3803.
33. Neoh, K. G.; Kang, E. T. *Polym. Chem.* **2011**, *2*, 747–759.
34. Champion, J. A.; Katare, Y. K.; Mitragotri, S. *J. Controlled Release* **2007**, *121*, 3–9.
35. Alexis, F.; Pridgen, E.; Molnar, L. K.; Farohkzad, O. C. *Mol. Pharmaceutics* **2008**, *5*, 505–515.
36. Hong, F.; Yan, J.; Baran, J. T.; Allendorf, D. J.; Hansen, R. D.; Ostroff, G. R.; Xing, P. X.; Cheung, N. K.; Ross, G. D. *J. Immunol.* **2004**, *173*, 797–806.
37. Huang, H.; Ostroff, G. R.; Lee, C. K.; Wang, J. P.; Specht, C. A.; Levitz, S. M. *Infect. Immun.* **2009**, *77*, 1774–1781.
38. Huang, H.; Ostroff, G. R.; Lee, C. K.; Specth, C. A.; Levitz, S. M. *mBio.* **2010**, *1*, e00164–10.
39. Vetvicka, V.; Thornton, B. P.; Ross, G. D. *J. Clin. Invest.* **1996**, *98*, 50–61.
40. Thornton, B. P.; Vetvicka, V.; Pitman, M.; Goldman, R. C.; Ross, G. D. *J. Immunol.* **1996**, *156*, 1235–1246.
41. Taylor, P. R.; Brown, G. D.; Reid, D. M.; Willment, J. A.; Martinez-Pomares, L.; Gordon, S.; Wong, S. Y. C. *J. Immunol.* **2002**, *169*, 3876–3882.
42. Brown, G. D.; Gordon, S. *Nature* **2001**, *413*, 36–37.
43. Kim, B. S.; Jung, I. D.; Kim, J. S.; Lee, J. H.; Lee, I. Y.; Lee, K. B. *Biotechnol. Lett.* **2000**, *22*, 1127–1130.
44. Na, K.; Park, K. H.; Kim, S. W.; Bae, Y. H. *J. Controlled Release* **2000**, *69*, 225–236.
45. Coviello, T.; Palleschi, A.; Grassi, M.; Matricardi, P.; Bocchinfuso, G.; Alhaique, F. *Molecules* **2005**, *10*, 6–33.
46. Coviello, T.; Matricardi, P.; Marianecci, C.; Alhaique, F. *J. Controlled Release* **2007**, *119*, 5–24.
47. Kim, B.; Na, K.; Choi, H. *Eur. J. Pharm. Sci.* **2005**, *24*, 199–205.
48. Lee, C.; Lee, H.; Lee, K. *J. Biosci. Bioeng.* **2005**, *100*, 255–259.
49. Subedi, R. K.; Kang, K. W.; Choi, H. *Eur. J. Pharm. Sci.* **2009**, *37*, 508–513.

50. Vu-Quang, H.; Muthiah, M.; Lee, H. J.; Kim, Y. K.; Rhee, J.; Lee, J. H.; Lee, J.; Cho, C.; Choi, Y.; Jeong, Y.; Park, I. *Carbohydr. Polym.* **2012**, *87*, 1159–1168.
51. Sakurai, K.; Kimura, T.; Koumoto, K.; Kobayashi, R.; Shinkai, S. *Nucleic Acids Res.* **2001**, *1*, 223–224.
52. Sakurai, K.; Uezu, K.; Numata, M.; Hasegawa, T.; Li, C.; Kaneko, K.; Shinkai, S. *Chem. Commun. (London)* **2005**, *35*, 4383–4398.
53. Mochizuki, S.; Sakurai, K. *Polym. J. (Tokyo, Jpn.)* **2009**, *41*, 343–353.
54. Soto, E.; Ostroff, G R. *Bioconjugate Chem.* **2008**, *19*, 840–848.
55. Aouadi, M.; Tesz, G.; Nicoloro, S.; Wang, M.; Chouinard, M.; Soto, E.; Ostroff, G. R.; Czech, M. *Nature* **2009**, *458*, 1180–1184.
56. Tesz, G.; Aouadi, M.; Prot, M.; Nicoloro, S.; Boutet, E.; Amano, S.; Goller, A.; Wang, M.; Guo, C.; Salomon, W. E.; Virbasius, J. V.; Baum, R. A.; O’Connor, M. J.; Soto, E.; Ostroff, G. R.; Czech, M. P. *Biochem. J.* **2011**, *436*, 351–362.
57. Zhu, F.; Zhang, X. *Mar. Biotechnol.* **2011**, *14*, 63–68.
58. Figueiredo, S.; Moreira, J. N.; Geraldes, C. F.; Rizzitelli, S.; Aime, S.; Terreno, E. *Chem. Commun. (London)* **2011**, *47*, 10365–10367.
59. Soto, E.; Kim, Y.; Lee, J.; Kornfeld, H.; Ostroff, G. *Polymers* **2010**, *2*, 681–689.
60. Soto, E.; Caras, A.; Kut, L.; Castle, M.; Ostroff, G. R. *J. Drug Delivery* **2012**, 143524.
61. Huong, L. M.; Thu, H. P.; Thuy, N. T. B.; Ha, T. T. H.; Thi, H. T. M.; Trang, M. T.; Hang, T. T. N.; Nghi, D. H.; Phuc, N. X.; Quang, D. T. *Chem. Lett.* **2011**, *40*, 846–848.
62. McCarthy, J. R. *Nanomedicine* **2009**, *4*, 693–695.
63. Babes, L.; Denizot, B.; Tanguy, G.; Le Jeune, J. J.; Jallet, P. *J. Colloid Interface Sci.* **1999**, *212*, 474–482.
64. Mazumder, S.; Dey, R.; Mitra, M. K.; Mukherjee, S.; Das, G. C. *J. Nanomater.* **2009**, 815734.
65. Gibson, J.; Khanal, B.; Zubarev, E. *J. Am. Chem. Soc.* **2007**, *129*, 11653–11661.
66. Heo, D. N.; Yang, D. H.; Moon, H. J.; Lee, J. B.; Bae, M. S.; Lee, S. C.; Lee, W. J.; Sun, I.; Kwon, I. K. *Biomaterials* **2012**, *33*, 856–866.
67. Mirza, A. Z.; Shamshad, H. *Eur. J. Med. Chem.* **2011**, *46*, 1857–1860.
68. Qian, X.; Peng, X. H.; Ansari, D. O.; Yin-Goen, Q.; Chen, G. Z.; Shin, D. M.; Yang, L.; Young, A. N.; Wang, M. D.; Nie, S. *Nat. Biotechnol.* **2008**, *26*, 83–90.
69. Elbialy, N.; Abdelhamid, M.; Youssef, T. *J. Biomed. Nanotechnol.* **2010**, *6*, 687–693.
70. Soto, E.; Ostroff, G. *NSTI Nanotech 2007 Technical Proceedings* **2007**, *2*, 378–381.
71. Kay, M. A.; Manno, C. S.; Ragni, M. V.; Larson, P. J.; Couto, L. B.; McCleland, A.; Glader, B.; Chew, A. J.; Tai, S. J.; Herzog, R. W.; Arruda, V.; Johnson, F.; Scallan, C.; Skarsgard, E.; Flake, A. W.; High, K. A. *Nat. Genet.* **2000**, *24*, 257–261.

72. Flotte, T. R.; Brantly, M. L.; Spencer, L. T.; Byrne, B. J.; Spencer, C. T.; Baker, D. J.; Humphries, M. *Hum. Gene Ther.* **2004**, *15*, 93–128.
73. Wagner, J. A.; Nepomuceno, I. B.; Messner, A. H.; Moran, M. L.; Batson, E. P.; Dimiceli, S.; Brown, B. W.; Desch, J. K.; Norbash, A. M.; Conrad, C. K.; Guggino, W. B.; Flotte, T. R.; Wine, J. J.; Carter, B. J.; Reynolds, T. C.; Moss, R. B.; Gardner, P. *Hum. Gene Ther.* **2002**, *13*, 1349–1359.
74. Mueller, C.; Flotte, T. R. *Gene Ther.* **2008**, *15*, 858–863.
75. Opie, S. R.; Warrington, K. H., Jr.; Agbandje-McKenna, M.; Zolotuhkin, S.; Muzyczka, N. *J. Virol.* **2003**, *77*, 6995–7006.

## Chapter 4

# Glyconanoparticles for Gene Delivery

**Marya Ahmed and Ravin Narain***

**Department of Chemical and Materials Engineering,**
**University of Alberta, Alberta Glycomics Centre,**
**University of Alberta, 116 St., Edmonton, AB, T6G 2G6, Canada**
***E-mail: narain@ualberta.ca**

Gene therapy has gained widespread interest due to its potential for treatment of many genetic diseases. The use of non-viral systems for delivery of nucleic acids are of particular interest as they can be engineered for high biocompatibility, specificity and targeted delivery. Carbohydrate-based non-viral nano-systems, termed as glyconanoparticles, have emerged as a unique class of gene delivery systems with the potential of having all of these characteristics. Carbohydrates provide a stealth layer to delivery carriers without compromising their cellular uptake. Furthermore, the targeting efficacies of the glyconanoparticles towards certain organs can be tuned either by incorporating specific ligands on the surface or by increasing the carbohydrate densities. Herein, an overview of the synthesis of different glyconanoparticles and their use for gene expression is discussed. Modification of polymeric nanoparticles, liposomes, gold and magnetic nanoparticles, quantum dots and carbon nanotubes with carbohydrate residues have been achieved and used for *in vitro* and *in vivo* delivery.

In Nanomaterials for Biomedicine; Nagarajan, R.;
ACS Symposium Series; American Chemical Society: Washington, DC, 2012.

# Introduction

The field of gene therapy has received substantial of attention since its emergence in the late 1900s (*1*, *2*). The simplicity of this technique and its potential to treat genetic disorders such as cystic fibrosis, haemophilia, cancer, and diabetes, inspired several researchers to produce a variety of cationic gene delivery vectors and study their gene expression efficacies. The practical uses of this strategy is, however, much more difficult than predicted. Some of the known potential barriers that exist in this context are protection of DNA from enzymes and nucleases, efficient complexation and release, cellular uptake and specificity, endosomal escape and nuclear entry. To overcome these issues, a variety of cationic systems has been synthesized and explored for their gene expression *in vitro* and *in vivo* (*1*, *2*). The advances in the field of nanotechnology has allowed the synthesis of unique nanomaterials for biomedical applications (*3*, *4*). These colloidal nanocarriers are interesting for gene delivery applications, due to their high stability in solution, in addition to their response to external stimuli and controlled release of biomolecules (*5*).

The essential features of nanoparticles include their nanoscale dimensions, facile control over size, high surface area, and unique electronic, magnetic and optical properties. The high surface to volume ratio of metallic nanoparticles also make them highly reactive as compared to the bulk metals, hence passivation of nanoparticles with biomolecules is necessary (*6*). In addition, the major drawback of using cationic vectors for gene expression is their high toxicities, renal clearance, non-specific uptake by cells, and induction of immune response in vivo (*1*, *2*). Hence, the incorporation of stealth layer on these gene delivery vectors is considered crucial to overcome these issues. Polyethylene glycol (PEG) is the most commonly used stealth layer for gene delivery vectors, it is found to considerably decrease the interaction of cationic vectors with serum proteins as well as to the cell surfaces, which translates into the lower uptake of PEG modified vectors and hence low gene expression (*1*, *2*). Alternatively, the use of carbohydrate ligands to stabilize the surface of nanomaterials as well as to reduce their non-specific interactions and to decrease their toxicities is found to be an excellent approach, without compromising their cellular uptake and gene expression (*3*, *7*). For example, sialic acid on cell membranes serves as antigenic determinant molecules and removal of sialic acid from red blood cells follows their rapid uptake by mononuclear phagocyte system (*8*). Glycosylation is an important step of post translational modification in cells. The cell surface and extracellular matrix contains a variety of carbohydrates in the form of glycoproteins and glycolipids, which play key role in cell-cell interactions, communication and recognition of antibodies, and hormones *via* multivalent interactions. The chemical diversity and complexity of carbohydrates indicate they have tremendous potential for encoding biological information for a variety of physiological and pathological processes (*9*). The concept of multivalency, that is the interaction of several ligands at one specific receptor are dominant in nature, however the detailed analysis of these interactions was not possible, until the development of nano-scaffolds for bio-applications (*9*). Hence, it is concluded that the surface chemistry of nanoparticles is critical in governing their interactions with living tissues. The passivation of nanoparticles with biocompatible ligands like carbohydrates can increase their cellular uptake, and impart targeting efficacies, by multivalent interactions with targeting receptors, which is dependent upon the extent of their glycosylation. In the context of gene delivery, most of the work of carbohydrates functionalized nanoparticles is focused on decreasing the toxicity of these systems. The natural polysaccharides such as dextran (*10*), and chitosan (*11*) are abundantly used to passivate the nanoparticles surface and to decrease the toxicities as gene delivery vectors. Some of these natural polysaccharides based nanoparticles are also studied for their targeting abilities (*6*). The limitations in the synthesis of complex carbohydrates, and the isolation of pure oligosaccharides from natural sources, pose major problems in understanding the role of sugar molecules for targeting purposes (*9*).

With the advances in the field of polymer chemistry, the facile synthesis well defined polymers is now possible (*12*). Living radical polymerization is a free radical polymerization, which can polymerize a variety of different vinyl monomers, in both organic and aqueous conditions and in the presence of a range of functional groups. Reversible addition-fragmentation chain transfer polymerization (RAFT) has allowed the synthesis of variety of glycopolymers and their copolymers, of controlled molecular weights and architecture, with pendant hydroxyl groups (*7*). These polymers are also used to surface functionalize nanomaterials including gold nanoparticles (*13*, *14*), quantum dots (*15*) and carbon nanotubes (*16*, *17*) and their cellular localization and gene delivery efficacies are studied. With these remarkable synthetic techniques, it is therefore possible to produce well-defined glycopolymers of varying compositions and architectures to study the interaction with living cells. Galactose (*5*) and mannose (*18*) are well studied monosaccharides due to their targeting abilities towards certain living cells *in vitro* and *in vivo*. The specificity of galactose towards liver cells (*5*) and mannose for the targeting of immune cells such as dendritic cells, macrophages (*18*) is discussed in the literature. Mannosylated antigen targeting is used as an effective approach to develop new vaccines against immune system (*18*). The use of carbohydrates functionalized nanomaterials for gene delivery applications seems an excellent approach to overcome the toxicity issues, as well as to incorporate the targeting abilities to the gene delivery vectors. In contrast to polyplexes alone, high surface area of nanoparticles provides a scaffold for the display of large a number of carbohydrates on the surface. In addition, the interactions between carbohydrates and nucleic acid *via* hydrogen bonding is also studied (*19*) and it is found that facile complexation of DNA on glyconanoparticles surface is possible in the presence of minimum cationic component (*20*). It is thought that glyconanoparticles will serve as potent gene delivery vectors, due to their low toxicities, enhanced DNA complexation efficacies, high cellular interactions and targeting (depending upon the extent of glycosylation). The complexation of plasmid DNA using glyconanoparticles, their cellular uptake and gene expression is depicted in figure 1 (*14*).

In addition, the optical, electronic and magnetic properties of the metallic and semiconductor nanomaterials can also provide a combination of imaging and delivery vectors. Herein is a brief review of glyconanoparticles used for gene expression in literature is provided.

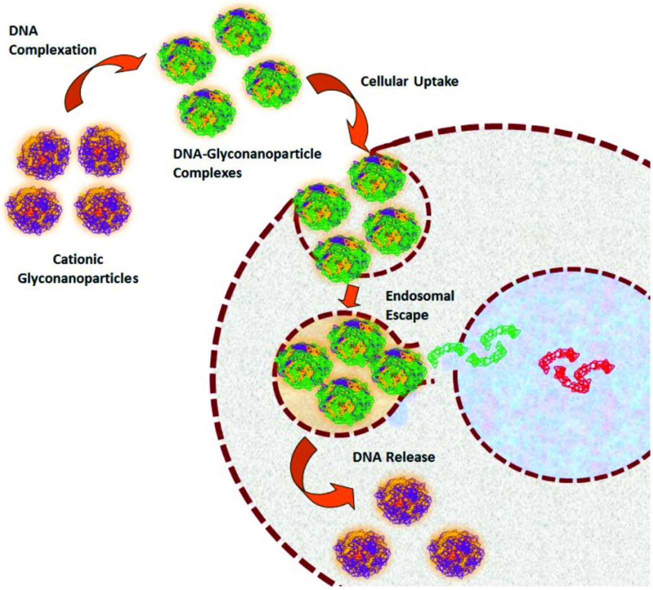

*Figure 1. Complexation of plasmid DNA by cationic glyconanoparticles, their cellular uptake, endosomal escape and gene expression (14).*

## Types of Glyconanoparticles

Polymeric nanoparticles and liposomes are extensively used for gene delivery purposes from last two decades (*1*, *2*). The advancement in the field of nanotechnology has provided nanometer sized scaffolds with large surface area to surface functionalize biomolecule, thus mimicking biological properties to these nanocarriers. Gold nanoparticles, magnetic nanoparticles, quantum dots and carbon nanotubes are few examples of nanomaterials. In addition to polymeric particles and liposomes, these nanoparticles will be discussed for their role in the field of gene delivery.

## Polymeric Glyconanoparticles

The colloidal polymeric carriers are interesting choice for various biological applications. Polymeric nanoparticles were prepared to complex DNA in their native supercoiled form. The encapsulation of DNA in the polymeric nanoparticles was obtained during the synthesis of nanoparticles. The synthesis of biocompatible polymeric spheres using biodegradable polysaccharides has been achieved by various methods and their gene expression has been studied (*6*). Plasmid encapsulated crosslinked chitosan nanoparticles were prepared in acidic solution in the presence of sodium sulphate (an initiator), the microparticles produced were tested for their ability to express reporter gene (*22*) and to induce cytokine expression *in vitro* (*11*). The gelatin based DNA encapsulated nanoparticles were prepared by ethanol precipitation and were tested for their gene expression *in vitro* and *in vivo* (*23*).

The surface modification of polymeric nanoparticles with polysaccharides can also be achieved by the following methods:

1. Adsorption
2. Incorporation
3. Co-polymerization

### *Adsorption*

Surface adsorption of carbohydrates on nanomaterials is achieved by non-covalent interactions such as electrostatic, and hydrophobic interactions on their surface (*6*). This technique is extensively used to coat liposomes and polymeric nanoparticles. The surface functionalization of polyisobutyl cyanoacrylate (PiBCA) nanoparticles with orosomucoid, a sialic acid based glycoprotein, was obtained at acidic pH. It was found that surface adsorption of carbohydrates on nanoparticles is governed by both electrostatic as well as hydrophobic interactions (*24*). However, due to the high hydrophilicity of polysaccharides, hydrophobic interactions between nanoparticles and polysaccharides is not always a method of choice, and complex modification of polysaccharides with hydrophobic groups are required. Polylactic acid (PLA) particles were coated with phenoxy dextran by hydrophobic interactions between phenoxy groups of modified dextran and hydrophobic surface of PLA nanoparticles (*25*). Alternatively, formation of poly(ε-caprolactone) (PCL) nanoparticles using cationic detergents and their sequential coating with hyaluronic acid *via* electrostatic interactions was an effective approach to yield glyconanoparticles of 250-500 nm sizes (*26*). The surface adsorption of carbohydrates on nanomaterials via electrostatic interactions and hydrophobic interactions suffers from several disadvantages, such as low yield, concentration dependent aggregation and displacement of surface layer in physiological conditions. Hence incorporation of carbohydrates on the surface of nanomaterials requires other chemical approaches which will be discussed in detail (*6*).

### *Incorporation*

Incorporation of carbohydrate residues during the synthesis of polymeric nanomaterials is another facile approach to yield glyconanoparticles by physical adsorption, in the absence of additional steps of surface functionalization. Chitosan coated poly(lactic-*co*-glycolic acid) (PLGA) nanoparticles were produced in which surface functionalization of nanoparticles with chitosan was obtained by the entanglement of chitosan with PLGA (*27*). The emulsion-solvent evaporation is another common method to prepare and coat nanoparticles in one step and involves dissolution of polymers in organic solvent-water emulsion in the presence of surfactants (*6*). To avoid the drawbacks of surfactants, dextran-PEG conjugates were synthesized and were used to stabilize PLGA particles in oil-water emulsion. The incorporation of PEGylated-dextran in PLGA chains produced nanoparticles with PEG anchored in the core of nanoparticles, while dextran extended on the surface (*28*). Similarly, hydrophobicized dextran were synthesized and used as stabilizer in oil-water emulsions as an alternative to poly(vinyl alcohol) (PVA) to stabilize PLA particles (*29*). Diafiltration method is another approach to yield carbohydrates modified nanomaterials. Poly(*L*-lysine)-*g*-dextran was prepared by reductive amination reaction. Subsequently formation of glyconanoparticles was obtained by dialysis of PLA with PLL-*g*-dextran for 48 hours, nanoparticles formed were collected by centrifuge and the interaction of nanoparticles with plasmid DNA was studied. It was found that increasing the grafting density of dextran improved the DNA complexation of nanoparticles (*20*).

## Co-Polymerization

### Emulsion Polymerization

Emulsion polymerization is another technique to produce polymeric nanoparticles. The polymerization of alkyl cyanoacrylate (ACA) *via* anionic polymerization in oil-water emulsion in the presence of polysaccharides produced carbohydrates functionalized PACA nanospheres. Cyclodextrin (*30*) and dextran (*24*) and chitosan (*31*) were used as stabilizer during the polymerization. Others suggested that hydroxyl groups of sugar molecules (dextran, cyclodextrin, chitosan) can also initiate the polymerization of alkyl cyanoacrylate (ACA), these sugar molecules then covalently bind to PACA and serve as stabilizer (*32*). The grafting density of carbohydrates on PACA spheres was dependent on pH of reaction, concentration and molecular weight of carbohydrates (*31*). Low pH, high molecular weight and high concentration of chitosan promoted highly stable glyconanoparticles (*31*).

### Radical Polymerization

Radical polymerization has gained a lot of attention due to the synthesis of carbohydrates based polymers in aqueous solution, in the absence of organic solvents and surfactant, which is desirable for the drug and gene delivery applications (*6*). Radical polymerization of monomers (such as MMA, ACA) in the presence of polysaccharides was initiated by cerium IV ions. The acidic condition leads to the block copolymer formation between polysaccharides and monomers by the cleavage of polysaccharides. The formation of nanoparticles with surface carbohydrate residues occurs in water due to the amphiphilic nature of block copolymers, these nanoparticles show high stability for a long period of time (*6*).

In contrast to conventional free radical polymerization, living radical polymerization (LRP) has allowed a facile control over the molecular weights, architecture of the polymers (*12*). The glycopolymers of varying molecular weights and architecture were synthesized via RAFT, in the absence of metallic catalyst and protected group chemistry (*7*). The presence of functional pendant moieties allows the facile functionalization of these glycopolymers on nanoscaffolds by surface grafting.

## Nanogels

The crosslinked, colloidal network of polymer chains with distinct core and corona morphology and stimuli-responsive properties including sponge effect, degradation and thermosensitivity are referred as nanogels (*33*). The nanogels are recently emerged as unique polymer based carriers which allow the encapsulation of biomolecules in their core, followed by their release upon external stimuli (*33*). Chitosan (*34*), dextran (*35*), hyaluronic acid (*36*) and PEGylated galactose functionalized nanogels (*37*) have been prepared by the crosslinking of polymer chains. The encapsulation of oligonucleotides and siRNA in the core of nanogels is obtained by imbibing of small molecules in the dried nanogels. The hyaluronic acid (HA) based nanogels were prepared by disulphide crosslinking of HA-SH in the presence of DNA. Glutathione (GSH) dependent release of DNA from nanogels was achieved *in vitro* (*36*). Photo-crosslinked chitosan based thermo-responsive, nanogels were prepared by incorporating diacrylated-pluronic F127 in glycidyl methacrylated chitosan along with DNA (*34*). The mixture was irradiated with UV light in the presence of photoinitiator Irgacure (I-2959) to obtain DNA encapsulation nanosized particles. The release of DNA from nanogels was achieved by the degradation of chitosan. The size of nanogels, release of DNA and crosslinking density was controlled by tuning the amount of chitosan and photo-irradiation time. In another study, chitosan oligomers were obtained by depolymerization of chitosan in the presence of $NaNO_2$. Chitosan oligomers and DNA were crosslinked in the presence of pentasodium tripolyphosphate, a crosslinking agent based, to yield plasmid loaded glyconanogels. The physiochemical properties of chitosan nanogels were optimized by tuning chitosan concentration, molecular weight, crosslinking density and DNA loading. It was found that low molecular weight chitosan oligomers based nanogels make small particles upon complexation with DNA and show high gene expression and low toxicity as compared to high molecular weight chitosan, both *in vitro* and *in vivo* (*38*). Dextran based degradable nanogels were prepared by inverse miniemulsion photopolymerization method. Dextran-hydroxyethyl methacrylate (Dex-HEMA) and [2-(methacryloyloxy)ethyl]-trimethyl-ammonium chloride (TMAEMA) were mixed in oil-water emulsion in the presence of emulsifier and initiator. The mixture was sonicated and exposed to UV light to initiate radical polymerization process. The cationic dextran based nanogels of 200-300 nm were obtained and were functionalized with siRNA in post loading step, by incubation of nanogels in siRNA solution. These nanogels showed high cellular uptake and gene silencing in hepatoma cells (*35*).

## Liposomes

The fusogenic potential of liposomes with cell membranes was identified in 1970s and in almost two decades after lipofection was used as an effective strategy to transfer genes into living systems (*1*). Some of the commonly used and commercially available liposomes are *N*-[1-(2,3-dioleyloxy)propyl]-*N,N,N*-trimethyl-ammonium chloride (DOTMA), 2,3-dioleyloxy-*N*-[2(sperminecarboxamido) ethyl] *N*,*N*-dimethyl-1-propanaminium trifluoroacetate (DOSPA) ,2-dioleoyl-3-trimethyl ammonium propane (DOTAP), and dioctadecylamido-glycylspermine (DOGS). The major drawback of liposomes based gene delivery vectors is their high toxicity. The functionalization of liposomes with polysaccharides has been used as a strategy to produce non-toxic lipofection agents. The modification of liposomes with carbohydrates can be obtained using different methods (*1*, *18*). The head group modification of liposomes produced aminoglycoside lipids, also called KanaChol, as these aminoglycoside lipid are synthesized from kanamycin, as shown in figure 2. The synthesis of aminoglycoside lipids was obtained by dissolving Kana-Chol 6 and DOPE in chloroform at ratio of 1:1. The chloroform was evaporated and lipid layer was suspended in buffer to form liposome (*39*). These aminoglycosides bind to the phosphodiester backbone of nucleic acid *via* hydrogen bonding interactions, with 1,3-hydroxyamine group and showed enhanced gene expression *in vitro* and *in vivo* (*40*).

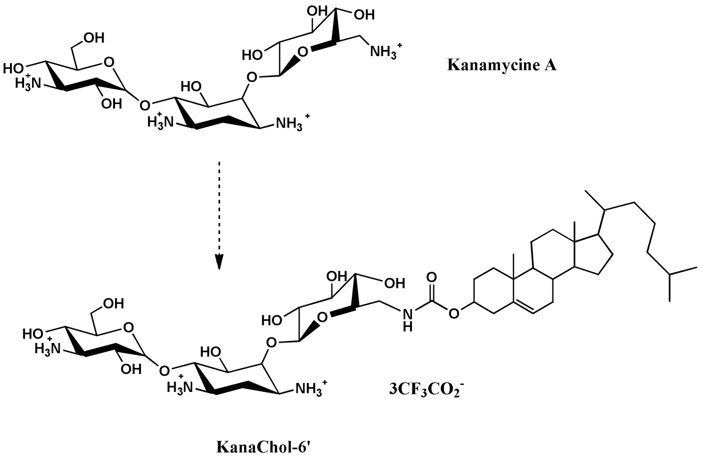

*Figure 2. The structure of cationic lipid KanaChol-6', obtained from Kanamycin (39).*

The physical adsorption of chitosan on DNA-liposome complexes was used to increase the stability and promote the gene expression of phospholipid-DNA vesicles (*41*). This, positively charged, biodegradable polysaccharide is known to bind biological membranes and increase the permeability of cargo across cell membrane. DNA was encapsulated in liposomes by dehydration-rehydration method. Chitosan coating of DNA-containing vesicles was obtained by physical desorption of chitosan solution on liposomes surface at 4 °C and at acidic pH, possibly by hydrophobic interactions. The chitosan functionalized vesicles were centrifuged to remove excess chitosan and chitosan content in supernatant was determined using optical rotatory dispersion spectra (λ = 220-650 nm) and cibacron red dye. The complexation of cibacron dye with chitosan can be detected by the UV spectra (λ = 450-650 nm). The surface functionalization of vesicles with chitosan is found to prevent their aggregation, and decrease their size, as well as provide the net positive charge and stability to these vesicles (*41*).

Cholesterol based lipids were modified to produce *N*-(4-aminobutyl)-(cholesten-5-yloxyl)formamide which was further reacted with 2-imino-2-methoxyethyl-1-thiogalactoside to yield cholesten-5-yloxyl-*N*-(4-((1-imino-2-*β-D*-thiogalactosylethyl)amino)butyl)formamide (Gal-4-Chol). It is found that galactosylated liposomes can successfully and selectively transfer gene of interest in liver *in vivo* (*42*). The covalent linking of mono- and oligosaccharides with hydrophobic alkyl chains is used as a strategy to produce amphiphilic glycolipids based structures (Figure 3).

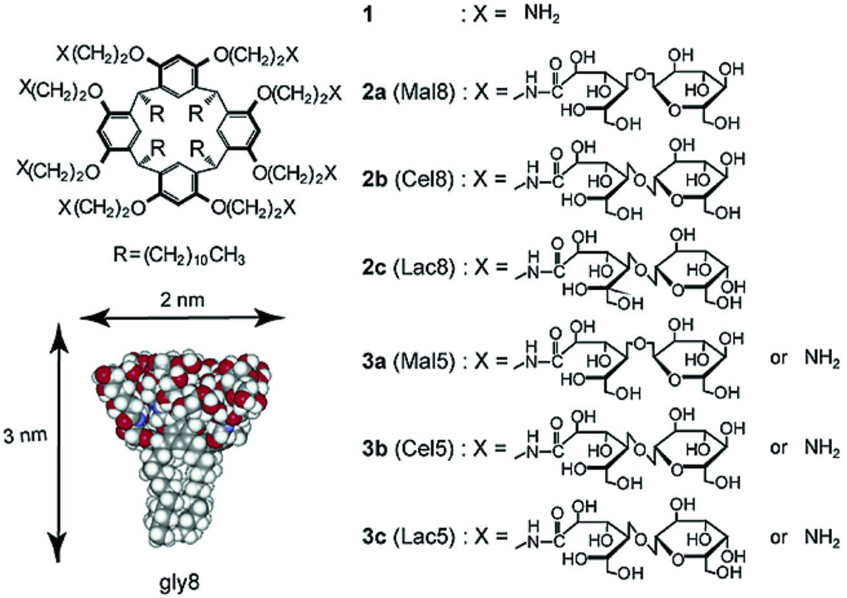

*Figure 3. Chemical structures of glycomonomers and oligomers to produce glycoamphiphiles, and an illustration of gly8 in the folded form (43).*

The addition of octamine in organic solution of lactone in inert atmosphere produced glycocluster amphiphiles by amide linkage. The incorporation of amine moieties along with eight saccharide moieties produced cationic glyco-amphiphile, indicated as gly8 in figure 3. These cationic glycoamphiphiles were used for DNA complexation and gene expression studies in Hela cells. The physicochemical properties of these glycolipids, as a function of surface carbohydrate residues and length of hydrophobic chain were studied. It was found that aggregation of glycolipid-DNA complexes was dependent on the size of carbohydrates, for example cellobiose based particles show less aggregation than maltose and lactose based nanoparticles (*43*).

Multifunctional envelope type nanodevices (MEND) were prepared and functionalized with sugar residues to increase their cellular uptake and nuclear entry in non-dividing cells. In MEND type devices, pDNA was complexed with polycations followed by the encapsulation with glycolipid envelope (*44*). Sugar cholesterol conjugates were prepared by the reaction of Cholest-5-en-3β-ol-p-toluenesulfonate with 3,4,5-tri-*O*-acetyl-1-thiophenyl-2-*N*-troc-*β-D*-glucopyranoside in organic solvent. The 11-(Cholest-5-en-3β-yloxy)-3,6,9-trioxaundecanyl-3,4,5-tri-*O*-acetyl-2-*N*-troc-β-D-glucopyranoside produced was deprotected to yield (Cholest-5-en-3β-yloxy)-3,6,9-trioxaundecanyl-2-*N*-acetyl-β-D-glucopyranoside (Figure 4).

Similarly, galactose and mannose based cholesterol conjugates were synthesized. MEND were then formulated using lipid hydration method, sugar-modified cholesterol was converted into a lipid film. pDNA was condensed with protamine, and lipid film was rehydrated in pDNA-protamine solution. These glyconanoparticles showed enhanced reporter gene expression in synchronized cell lines as compared to cholesterol based MEND particles in the absence of sugar moities (*44*). Mannosylated liposomes are found to be effective delivery carriers to target immune cells. Mannosylated liposomes can be obtained with the following methods. 1. Mannose functionalized lipids can be used as starting material to produce glycolipids. 2. Liposomes can be modified with mannose derivatives via covalent bonds. 3. Mannose can be physically adsorbed on the surface of liposomes. All of these methods involve in the formation of thin lipid layer, followed by the hydration of lipids in aqueous solution. In the first method, the mixture of lipids and mannosylated derivatives are mixed in organic solvent followed by the formation of film by the evaporation of organic liquid and hydration of glycoliposomes in aqueous solution. The covalent attachment of mannose derivatives (such as *p*-aminophenyl-α-D-mannopyranoside with phosphatidyl ethanolamine of liposomes) can be obtained using glutaraldehyde (*45*). The mannosylated liposomes are further used for gene expression *in vivo*. The DNA loaded [cholesten-5-yloxy- *N* -(4-((1-imino-2-β-D-thiomannosyl-ethyl)amino) butyl) formamide] (Man-C4-chol) were prepared according to the procedure discussed above and showed high gene expression *in vitro* as compared to plain liposomes (*46*). In mice, an injection of mannosylated liposomes showed high gene expression in liver cells. DNA immunization using mannosylated liposomes showed strong immune response against encoding antigen. Injection of OVA-encoding pDNA in mice produced strong induction of IL-2, IFN-γ and TNF-α in serum of animals as compared to plain liposomes. Mannosylated niosomes have been used for the oral delivery of plasmid vaccines against hepatitis B virus. These glyco-niosomes showed enhanced production of antibodies in mice after 2 weeks of injections and levels were high to provide protection against hepatitis B virus (*47*). Man-C4-Chol liposomes loaded with Gp100 coding plasmid (Gp 100 is a protein covalently bound to ubiquitin, pUb-M gene, to enhance its degradation by proteasome, and to regulate intracellular protein processing), induced high levels of pUb protein in antigen presenting cells (*48*). Mannosylated chitosan based nanoparticles were used for cytokine gene therapy to suppress cancer cells. In Balb/c mine intratumoral injection of IL-2 encoding DNA- mannosylated chitosan complexes suppressed tumour growth and angiogenesis (*49*).

The conjugation of carbohydrates on the surface of metallic and semiconductor nanoparticles provides a platform to produce hybrid materials with their gene delivery efficacies, in combination with unique properties of these nano-scaffolds.

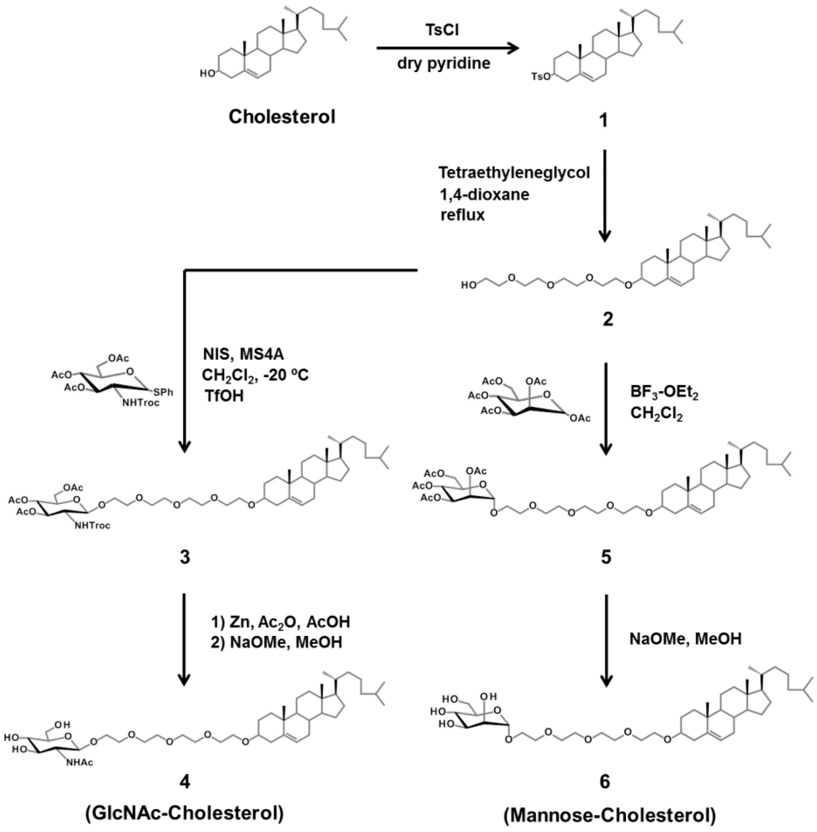
TsCl
dry pyridine
Cholesterol
1
Tetraethyleneglycol
1,4-dioxane
reflux
2
NIS, MS4A
$CH_2Cl_2$, -20 °C
TfOH
$BF_3$-$OEt_2$
$CH_2Cl_2$
3
5
1) Zn, $Ac_2O$, AcOH
2) NaOMe, MeOH
NaOMe, MeOH
4
(GlcNAc-Cholesterol)
6
(Mannose-Cholesterol)

*Figure 4. Synthetic steps to produce sugar-cholesterol conjugates. (Reproduced with permission from reference (44), copyright 2008 Elsevier).*

## Quantum Dots

Quantum dots (QDs) are semiconductor nanocrystals which present a good combination of therapeutics and diagnostics, due to their large surface area and superior photoluminescence properties. As compared to conventional fluorophores, QDs are stable towards photo-bleaching, possess higher quantum yield, narrow emission spectra and broad absorption bands. The conjugation of QDs with biological ligands is desirable to decrease their toxicities, and for the conjugation of other biomolecules (DNA/RNA) on the surface to produce self-tracking delivery agent. Biotinylated glycofunctionalized QDs were prepared and were shown to possess high stability in aqueous solution and low toxicity *in vitro* (*15*). The synthesis of statistical biotinylated glycopolymers of 2-gluconamidoethyl methacrylamide (GAEMA), N-(2-aminoethyl)biotinamide (BAEMA) and 2-aminoethyl methacrylamide (AEMA) was obtained *via* RAFT. The amine groups of biotinylated glycopolymer were conjugated to the surface of carboxyl functionalized QDs using EDC/NHS chemistry (Figure 5) (*15*).

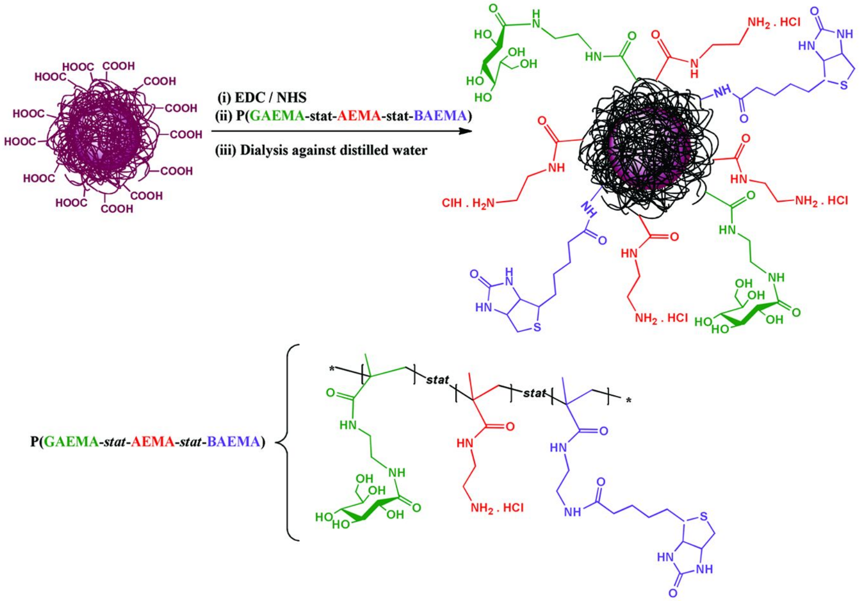
(i) EDC / NHS
(ii) P(GAEMA-stat-AEMA-stat-BAEMA)
(iii) Dialysis against distilled water
P(GAEMA-*stat*-AEMA-*stat*-BAEMA)
stat
stat

*Figure 5. Surface functionalization of QDs with poly(GAEMA-st-AEMA-st-BAEMA) using EDC/NHS chemistry (15).*

Chitosan functionalized QDs were prepared by the adsorption of cationic chitosan on the surface of anionic QDs and bioconjugates were analyzed using TEM and DLS. These fluorescent glyconanoparticles were then complexed with siRNA and were studied for their cellular uptake and gene knock down efficiencies. Furthermore, these glyconanoparticles were conjugated with HER2 antibody and specific uptake and expression of these negatively charged biocompatible QDs by HER2 cells was confirmed and was compared to other cell lines (*50*).

## Gold Nanoparticles

Gold nanoparticles (GNPs) are inert non-toxic biocompatible materials which can be easily functionalized with a variety of molecules. These characteristics make them ideal for delivery applications (*51*). Size and polydispersities of nanoparticles are key characteristics for biological applications (*14*). Gold nanoparticles of sizes of 1-150 nm can be successfully synthesized and surface functionalized for biological applications. The reduction of gold salts using $NaBH_4$, citrate, or photo reducing agents is well known strategy to produce monodisperse GNPs, in the absence or presence of stabilizing ligands. The size of the nanoparticles can be controlled by varying the concentration of gold salt, or amount of reducing agent used (*51*). The monolayer coverage of gold nanoparticles with biomolecules allows the passivation of their hydrophobic surface as well as tuning of surface charge to maximize transfection efficacy. The most commonly used surface chemistry to modify GNPs is by covalent linking of thiol containing molecules on gold by Au-S bond. The Au-S bonding is strong (34 kcal/mol) as compared to Au-N (4 kcal/mol) which has also been used to modify the gold surface. The incorporation of carbohydrates based amines on the surface of GNPs *via* Au-N bonding is found to improve their biological properties, including their stability in serum, and low toxicity (*13*, *14*). Cyclodextrin modified oligo(ethylenediamine) chains were used to functionalize GNPs. β-cyclodextrin conjugated oligo-ethylenediamine linker was modified to produce thiol functionality, using dicyclohexyl carbodiimide and lipoic acid, as shown in figure 6 (*51*).

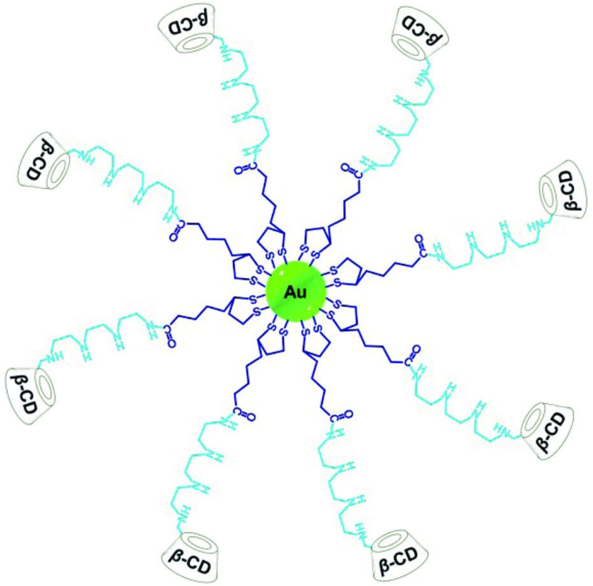

*Figure 6. Oligo(ethylenediamino)-β-cyclodextrin modified gold nanoparticles (51).*

The cationic glyconanoparticles were then synthesized in the presence of stabilizing ligands using NaBH4 reduction method. These glyconanoparticles showed moderate gene expression with low toxicity (*51*). The cationic glycopolymers produced by RAFT were used to functionalize gold nanoparticles, in one step photochemical strategy as shown in figure 7 (*13*). It was shown that gene expression of these cationic glycopolymers modified gold nanoparticles is size dependent process and GNPs of 40 nm diameter show high gene expression as compared to other sizes of GNPs (*14*). The conjugation of low molecular weight chitosan on GNPs surface was obtained by the reduction of gold salt in the presence of chitosan. These glyconanoparticles were found to be effective gene delivery agents.

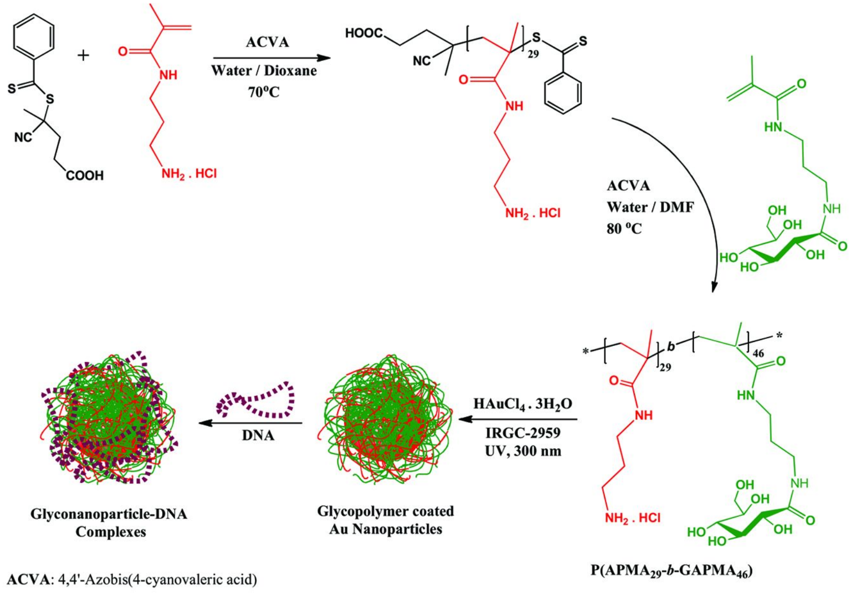
ACVA
Water / Dioxane
70°C
ACVA
Water / DMF
80 °C
HAuCl$_4$ . 3H$_2$O
IRGC-2959
UV, 300 nm
DNA
Glyconanoparticle-DNA Complexes
Glycopolymer coated Au Nanoparticles
P(APMA$_{29}$-*b*-GAPMA$_{46}$)

**ACVA**: 4,4'-Azobis(4-cyanovaleric acid)

*Figure 7. Synthesis of cationic glycopolymers via RAFT, cationic glycopolymer functionalized gold nanoparticles using photochemical initiator (I-2959), and their DNA complexation (13).*

The gene expression using chitosan based polymers is molecular weight dependent, high molecular weight chitosan show high gene expression but has poor physical properties including high viscosity and low solubility at neutral pH and slow dissociation of plasmid DNA. The conjugation of low molecular weight chitosan on gold surface is found to enhance the gene expression of the conjugates *in vitro* (*52*).

## Magnetic Nanoparticles (MNPs)

The synthesis of magnetic nanoparticles for delivery applications was first proposed in 1970s by Widder, Senyi and colleagues (*53*). The nanodimensions of these particles along with paramagnetic properties provide selectivity towards the uptake of these nanoparticles by cells or organs in the presence of a magnetic field. Magnetic nanoparticles can be synthesized by a variety of methods. Some of the commonly used methods are wet precipitation and co-precipitation, reverse micelle mechanism, chemical vapor condensation, thermal decomposition and reduction and liquid phase reduction. The core material of magnetic nanoparticles are iron based oxides such as magnetite $Fe_3O_4$, maghemite $Fe_2O_3$, and iron alloys such as $CoFe_2O_4$, $NiFe_2O_4$, and $MnFe_2O_4$ (*53*). Magnetite and maghemite possess high magnetic moments, are non-toxic materials and are currently used as MRI contrast agents. The coating of MNPs with natural polysaccharides is a common approach for their use for biomedical applications (*5*).

The polysaccharides functionalized MNPs can be obtained using various methods such as physical adsorption, and incorporation. Heparin based cationic polymers were physically adsorbed on the surface of anionic MNPs, it was found that co-administration of glyco-MNPs with HVJ (hemagglutinating virus of Japan) vector, significantly enhanced its gene expression in liver cells *in vivo* (*54*). Hexanoyl chloride modified chitosan modified MNPs were produced by the interactions between amine of polymer chains, as the nitrogen of amine groups contain free electrons which can chelate metal ions, and this modification was confirmed using X-ray diffraction (XRD) technique. These nanoparticles were used as hybrid vector with adenovirus to increase its cellular uptake in the presence of magnetic field and gene expression *in vitro* and *in vivo* (*55*, *56*). Super-paramagnetic iron oxide nanoparticles, capped with oleic acid were synthesized by thermal decomposition method. These nanoparticles were then functionalized with linoleic acid-modified chitosan polymers by ligand exchange mechanism (*57*). $Fe_2O_3$-DNA nanocomplexes were also prepared and stabilized with chitosan *via* electrostatic interactions, these nanoparticles showed gene expression *in vivo* in the presence of magnet (*58*). The incorporation of carbohydrates in iron oxide nanoparticles was obtained by co-precipitation of $Fe^{2+}$ and $Fe^{3+}$ salts in water in the presence of polysaccharides. The stability of these colloids in physiological solution was dependent upon the type of carbohydrates used during the synthesis. Moreover, the colloids grown in the presence of polymers showed higher stability than those prepared by post-functionalization of polysaccharides (*53*).

## Carbon Nanotubes

Carbon nanotubes (CNTs) have received substantial of attention in the field of biochemistry and biomedicines due to their unique electronic, physicochemical, thermal and structural properties. The surface functionalization of nanotubes with biomolecules increases their solubility in water, decreases their toxicity and provides a scaffold to produce novel nanomaterials. The functionalization of CNTs with carbohydrate residues can be achieved in two ways (*9*):

- Non-covalent functionalization
- Covalent- functionalization

## Non-Covalent Functionalization

The surface wrapping of CNTs with polysaccharides has been used as a tool to improve their solubility, and to decrease their toxicity, while maintaining their intrinsic properties. This technique involves the synthesis of amphiphilic glycopolymers, which can interact with the surface of nanotubes by hydrophobic interactions or π−π interactions. For example, mucin glycosylated polymers were prepared by modifying the backbone of α-*N*-acetylgalactosamine containing polymer with C18 lipid and these polymers were subsequently used to modify the surface of CNTs by hydrophobic interactions (*59*). The synthesis of biofunctional glycodendrimers containing pyrene tails were also synthesized and were used to functionalize nanotubes by π−π interactions (*60*). Schizophyllan glycopolymers (SPG) are interesting as they can dissociate into single strands in dimethyl sulfoxide (DMSO) and can be reconstituted in water. Using this property, SPG containing galactose appendages (Gal-SPG) were used to functionalize CNTs, by physical wrapping SPG on the surface of CNTs in DMSO (*61*). The fabrication of nanotubes with monosaccharides was also achieved by covalent modification of monosaccharides with lipids. The resulting glyco-lipids were attached to the surface of nanotubes by hydrophobic or π−π interactions (*62*). Cyclodextrin and other monosaccharides were adsorbed on the surface of nanotubes by using "high-speed vibration milling technique". Similarly, starch was helically wrapped on the surface of nanotubes, and the wrapping of nanotubes was temperature dependent mechanism, at high temperature nanotubes could be separated by mixing the functionalized nanotubes with glucosidase (*9*).

## Covalent Functionalization

The covalent functionalization of nanotubes with biomolecules is mainly obtained by the modification of carboxyl groups on the surface of nanotubes. These COOH groups are obtained by the oxidation of pristine nanotubes using strong acids. Amine functionalized glycomonomers are then grafted on the surface of the CNTs via amide linkages (*9*). The solubility of nanotubes was found to be dependent on the size of biomolecules used for stabilization, the high molecular weight sugars showed better stability of nanotubes than low molecular weight ones. The direct grafting of biomolecules on the surface of nanotubes in the absence of linker, can compromise the native structural properties of nanotubes (*9*). The grafting of long polymer chains containing reactive end groups is found to be a useful technique to modify the surface of carbon nanotubes. The synthesis of glycopolymers by RAFT (*12*) has successfully produced biomolecules of varying molecular weight with reactive functional groups that can be used to modify the surface of CNTs as shown in figure 8. Cationic glycopolymer modified CNTs had been used to encode green fluorescent protein (GFP) in Hela cells. These cationic glycopolymers modified CNTs showed high water solubility, stability in aqueous solution for a long period of time, high gene expression and low toxicity (*17*).

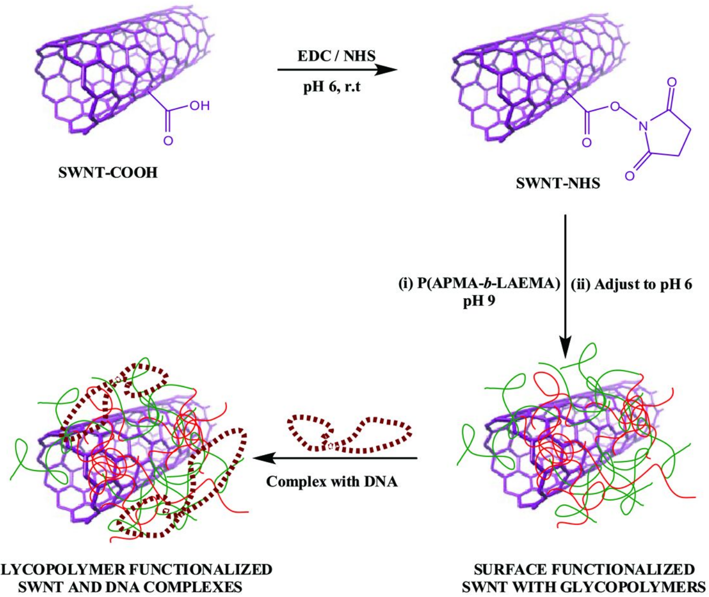

*Figure 8. Surface functionalization of carbon nanotubes with cationic glycopolymers using EDC/NHS chemistry and their complexation with plasmid DNA (17).*

## Mechanism of Uptake of Glyconanoparticles and Gene Expression

The mechanism of uptake of nanoparticles is critical in determining their endosomal escape, nuclear entry and gene expression. Non-viral vectors are transported to various cytosolic compartments depending upon their mechanism of uptake, and all these pathways demonstrate different levels of gene expression. Size, shape and surface chemistry of nanomaterials dictate the endocytic pathways of these materials in living cells (*21*). The sizes of DNA-nanoparticles complexes vary over time in the presence of serum proteins and nanoparticles of sizes 300-2000 nm can show successful gene expression in living cells. However, for systemic applications, nanoparticles of size 100 nm or less are considered ideal, as they must pass through capillary network to obtain high transfection efficiencies (*21*). The carbohydrates based gene delivery vectors show enhanced gene expression in the presence of serum proteins (*7*). It has also been shown that size of glyconanoparticles play critical role in their uptake mechanism and gene expression (*14*). Cationic glycopolymers functionalized gold nanoparticles are studied for their gene expression in Hela cells. It is shown that cationic glyconanoparticles of 40 nm in diameter show optimum gene expression, as compared to other sizes of nanoparticles (*14*). Nakai *et al.* has demonstrated that surface chemistry of nanoparticles is important in determining their aggregation and gene expression. Artificial glycoviruses prepared using different carbohydrates (lactose, cellobiose and maltose derivatives) and lipids showed aggregation dependent upon the presence of carbohydrate residues on the surface as shown in figure 9. The aggregation of glycoclusters in water is confirmed using dynmic light scattering (DLS) and gel permeation chromatography (GPC). Cellobiose derivatized glycoclusters show formulation of small (50 nm in diameter) particles and enhanced gene expression, as compared to other glycoclusters (*43*).

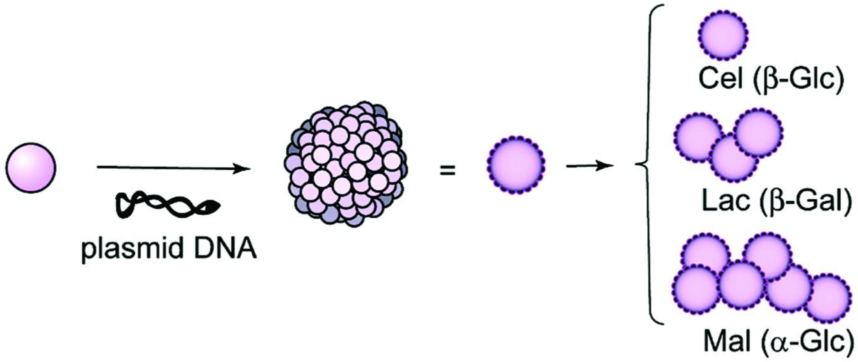

*Figure 9. Synthesis and self aggregation of carbohydrates based glycoclusters in the presence of plasmid DNA (43).*

Surface charge of DNA-nanoparticles complex is another important criteria that determines their mechanism of uptake and gene expression. Zeta potential of nanoparticles can also predict the stability of particles under physiological conditions. Positively charged DNA-nanoparticles complexes are generally believed to be better gene expressing agents due to thei interactions with negatively charged proteoglycans on the surface of cells. However, the interactions of positively charged particles with serum protein also leads to neutralization of their charge before their uptake by living cells. Hence preneutralization of cationic-nanoparticles DNA complexes has been used as a tool to optimize their gene expression (*21*).

## Characterization of Glyconanoparticles

The determination of amount of polysaccharides on the surface of nanoparticles is a direct approach to confirm the presence of carbohydrates on nanoparticles surface. Elemental analysis, high performance capillary electrophoresis and HPLC have been used to study the adsorption of polysaccharides on nanoparticles surface (*6*). Modification of polysaccharides with hydrophobic functional groups allows their facile analysis by UV-spectroscopy. For example phenoxy groups absorb at a wavelength of 269 nm, the adsorption of phenoxy modified dextran on a nanoparticle surface can be quantified (*25*). In addition, biodegradable properties of polysaccharides such as dextran were used to determine the content of dextran on nanoparticles. In this strategy dextran coated nanoparticles were incubated with endodextranase, an enzyme which selectively degraded dextran, the resulting dextran fragments were then assess using anthrone method (*63*).

# Physicochemical Techniques

## Zeta Potential

Surface charge of nanoparticles is dependent on its surface properties, hence surface modification of nanoparticles with polysaccharides and DNA can be confirmed by the change in zeta potential of nanoparticles before and after their surface functionalization (*6*).

## Hydrophobic Interaction Chromatography

The incorporation of polysaccharides on the surface of nanoparticles increases their hydrophilicity. This change in hydrophobic character of nanoparticles can be studied using hydrophobic interaction chromatography (*6*). For example, PiBCA nanoparticles show high retention in a column filled with propylamine agarose, in contrast orosomucoid coated PiBCA particles do not interact with column (*64*).

## Analysis of Chemical Compositions of Surface

X-ray photon spectroscopy (XPS), or electronic surface chemical analysis (ESCA) are widely used quantitative techniques to determine the composition of top layer of nanoparticles. The presence of dextran and other polysaccharides on the surface of nanoparticles has been confirmed using these techniques (*6*).

## Interaction with Proteins

The adsorption of serum proteins on the surface of nanoparticles is a major drawback in their use for biological applications. The polysaccharide coating on the surface of nanoparticles is found to effectively inhibit the interaction of serum proteins. This technique has also been used to confirm the presence of polysaccharides on the surface of nanoparticles. For example, bovine serum albumin (BSA) does not interact with dextran coated PLA particles and the amount of BSA present on dextran coated nanospheres is similar to PEG coated nanospheres, which are used as positive control (*25*).

Ultra-violet (UV) and Infra-red (IR) spectroscopy are used to identify the presence of functional groups on the surface of nanotubes. The pristine SWNTs show strong adsorption at 1400 and 1800 nm, and MWNT show adsorption at 214 nm. The surface functionalization of nanotubes leads to complete disappearance of these peaks (*9*).

NMR spectroscopy has been used to identify functional groups on the surface of colloidal nanomaterials. In addition, Raman spectroscopy is another powerful tool to characterize CNTs modifications. The degree of functionalization can be achieved by thermogravimetric analysis (TGA) (*9*).

## Characterization of Morphology of Nanoparticles

The most popular techniques of characterizing solid scaffolds such as nanotubes and nanoparticles are atomic force microscopy (AFM), transmission electron microscopy (TEM), and scanning electron microscopy (SEM). The surface morphology and three dimensional topography of nanomaterials is obtained using SEM, TEM and AFM. The height profile of AFM indicates the presence of functional groups on the sidewalls of nanotubes. TEM provides high quality images of nanomaterials but they cannot provide concrete evidences of presence of functional groups on the surface. Scanning tunneling microscopy (STM) has been used to image the organic modification on CNTs. STM can provide a direct image of both the atomic structure and electronic density of states. The complementary data on the morphology of CNTs can be obtained using high resolution TEM (HRTEM) and scanning transmission electron microscopy (STEM). There is no general technique to characterize nanomaterials completely. A combination of these techniques is required to confirm the functionalization of colloidal nanoparticles with polysaccharides (*9*).

## Targeting Efficacies of Glyconanoparticles

The emergence of glycobiology, glycotechnology and glycomics has provided a great insight in the role of protein and carbohydrate interactions. Carbohydrates based targeted gene delivery, also called ‘glycotargeting’ has been explored from the last two decades. Most of these targeting strategies involved multivalent interactions of carbohydrates with endogenous lectins. For example, asialoglycoprotein receptors (ASGPR) on the liver cells are extensively studied for targeting purposes, due to their specificity towards galactose or *N*-acetylgalactosamine residues and high density on liver cells (50,000-500,000 lectin/cell) (*64*). The alteration in cell surface lectins and their expression in diseases state, changes their specificity towards carbohydrate ligands. Liver fibrosis identified by the increased deposition of extracellular matrix is caused by the activation of hepatic stellate cells (HSC). HSC in diseases form show high density of mannose-6-phosphate/insulin like growth factor II (M6P/IGFII) receptors on their surface, and can be targeted specifically using mannose-6-phosphate functionalized nanoparticles. The degree of M6P-functionalization on the surface of carrier is critical to impart specificity towards HSC cells (*65*). This strategy was used to deliver triplex forming oligonucleotide (TFO) conjugated to mannose-BSA conjugates via disulphide bond. TFO can inhibit the transcription of collagen gene promoter in rats, and hence can inhibit the extracellular matrix deposition (*64*). Mannose based receptors are expressed on macrophages, immune cells and liver cells. The role of mannose based targeting for macrophages has been studied in detail. Mannose based conjugates show high gene expression in macrophages at low substitution degree (5%) (*18*).

The use of lactosylated-gene delivery carriers for cystic fibrosis has been studied. It is found that, as compared to mannosylated gene delivery vectors, lactosylated carriers showed high cellular uptake and gene expression in diseased airway tissues. Others have shown that galactosylated gene delivery vectors can specifically interact with pulmonary tissue, due to the presence of β-galactosidase binding lectins on cell surface. The selective expression of E-selectin on the surface of endothelial cells has been exploited for gene targeting applications. Sialyl-Lewis X (sLex) conjugated liposomes were synthesized and showed specific delivery of antisense oligonucleotides (ASODN) to inhibit the translation of ICAM-1 mRNA in vascular endothelial cells. The treatment of ASODN-encapsulated liposomes inhibited ICAM-1 protein expression in endothelial cells in concentration dependent manner (*64*).

The complexity in understanding multivalent interactions of carbohydrates and presence of similar receptors on the surface of cells, has considerably complicated the use of glyconanoparticles as delivery carriers. So far, galactose and mannose are two well-studied monosaccharides for gene targeting purposes. However, their specificity towards different organs is debatable, Galactose residues are found to target liver cells, pulmonary tissues, similarly mannose receptors are available on the immune cells surface, as well as hepatocytes. In addition, it is also found that, in general, glyconanoparticles show enhanced cellular uptake in cancer cells as compared to normal cells possibly due to the high number of cell surface receptors on malignant cells as compared to normal cells. For example, gelatin based polymeric nanoparticles showed enhanced gene expression in lung carcinoma cells as compared to normal cells (*24*). Hence, the major contribution of glyconanoparticles for gene delivery in literature is focused on serving as a stealth layer and decrease in the toxicities of cationic systems without compromising their cellular uptake and gene expression (*4*, *13*, *17*, *56*).

The modification of glyconanoparticles with cell specific receptors (antibodies, proteins) is shown to impart the targeting properties to these glyconanoparticles. For example, chitosan modified magnetic nanoparticles were conjugated with carcinoembryonic antigen (CEA) to target cancer cell line (A549). These magnetic nanoparticles showed enhanced gene expression in malignant cell line as compared to normal cells (WI-38) (*58*). Transferrin and KNOB-protein conjugated chitosan nanoparticles were prepared using bioconjugation techniques, to increase the uptake of chitosan based nanoparticles, which was found to be limited step in gene expression. It was found that conjugation of transferrin does not affect the gene expression of nanomaterials significantly, as compared to chitosan based nanoparticles. KNOB is a globular protein of adenovirus capsid. The conjugation of KNOB on chitosan nanoparticles *via* disulphide linkage, significantly increased the uptake and gene expression of chitosan nanoparticles. The chitosan nanoparticles showed high accumulation in liver and kidney of mice as shown from biodistribution analysis of nanoparticles (*22*). Similarly, linoleic acid functionalized chitosan nanoparticles are prepared for hepatocytes targeting. Linoleic acid accumulates in liver and plays a critical role in in cholesterol and triglycerides synthesis. These nanoparticles showed enhanced cellular uptake and gene expression in liver tissue (*57*). Hyaluronic acid based nanogels are shown to selectively interact with cancer cells due to the interactions of hyaluronic acid with over-expressed CD44 receptors in malignant cells (*36*). The surface functionalization of siRNA loaded dextran based cationic nanogels with fusogenic peptide is found to increase their gene knockdown efficacies as compared to controls (*35*). The carbohydrate residues are also thought to stimulate nuclear uptake of nanoparticles *via* lectin carbohydrate interactions with nuclear envelope. However, this effect of glyconanoparticles is not dependent on the type of sugars used for the gene delivery. These glyconanoparticles showed enhanced gene expression in synchronized cells as compared to their corresponding non-sugar derivatives (*44*).

## Conclusion and Future Directions

The chapter provides a concise overview on the synthesis of glyconanoparticles based gene delivery vectors and the study of their gene delivery efficacies. With the advances in the field of chemistry, glycobiology and nanotechnology, it is possible to design the gene delivery vectors of desired properties. The facile immobilization of carbohydrate based ligands on the surface of metallic and semiconductor nanoparticles, allowed the emergence of hybrid vectors, with gene therapeutic efficacies, as well as imaging capabilities, and hyperthermia properties. The glyconanoparticles based gene delivery vectors served as excellent biocompatible, non-toxic vectors, as compared to other stealth layers used to passivate the surface of gene delivery vectors. Due to the limited knowledge in the field of glycomics, and glycobiotechnology, the role of carbohydrate-based nano-vectors for targeting purposes is not fully understood. The functionalization of glyconanoparticles with other targeting moieties is found to increase their specificity considerably. Further work is required to understand the role of multivalency for targeting purposes.

## References

1. Mintzer, M. A.; Simanek, E. E. *Chem. Rev.* **2009**, *109*, 259–302.
2. Grigsby, C. L.; Leong, K. W. *J. R. Soc., Interface* **2010**, *7*, S67–S82.
3. De la Fuente, J. M.; Penades, S. *Biochim. Biophys. Acta* **2006**, *1760*, 636–651.
4. Shi, J.; Votruba, A. R.; Farokhzad, O. C.; Langer, R. *Nano Lett.* **2010**, *10*, 3223–3230.
5. Kami, D.; Takeda, S.; Itakura, Y.; Gojo, S.; Wattanabe, M.; Toyoda, M. *Int. J. Mol. Sci.* **2011**, *12*, 3705–3722.
6. Lemarchand, C.; Gref, R.; Couvreur, P. *Eur. J. Pharm. Biopharm.* **2004**, *58*, 327–341.
7. Ahmed, M.; Narain, R. *Biomaterials* **2011**, *32*, 5279–5290.
8. Schauer, R. *Trends Biochem. Sci.* **1985**, *10*, 357–360.
9. Gorityala, B. K.; Ma, J.; Wang, X.; Chen, P.; Liu, X-W. *Chem. Soc. Rev.* **2010**, *39*, 2925–2934.
10. Francis, M.; Lavoie, L.; Winnik, F.; Leroux, J. C. *Eur. J. Pharm. Sci.* **2003**, *56*, 337–346.
11. Akabuga, J.; Ozbas-Turan, S.; Erdogan, N. *Eur. J. Pharm. Biopharm.* **2004**, *58*, 501–507.

12. Boyer, C.; Bulmus, V.; Davis, T. P.; Ladmiral, V.; Liu, J.; Perrier, S. *Chem. Rev.* **2009**, *109*, 5402–5436.
13. Ahmed, M.; Deng, Z.; Liu, S.; Lafrenie, R.; Kumar, A.; Narain, R. *Bioconjugate Chem.* **2009**, *20*, 2169–2176.
14. Ahmed, M.; Deng, Z.; Narain, R. *ACS Appl. Mater. Interface* **2009**, *1*, 1980–1987.
15. Jiang, X.; Ahmed, M.; Deng, Z.; Narain, R. *Bioconjugate Chem.* **2009**, *20*, 994–1001.
16. Lane, L.; Housni, A.; Narain, R. *J. Polym. Sci., Part A: Polym. Chem.* **2006**, *44*, 6558–6568.
17. Ahmed, M.; Jiang, X.; Deng, Z.; Narain, R. *Bioconjugate Chem.* **2009**, *20*, 2017–2022.
18. Irache, J. M.; Salman, H. H.; Gamazo, C.; Espuelas, S. *Expert Opin. Drug. Delivery* **2008**, *5*, 703–724.
19. Eaton, P.; Ragusa, A.; Clavel, C.; Rojas, C. T.; Graham, P.; Duran, R. V.; Penades, S. *IEEE Trans. Nanobiosci.* **2007**, *6*, 309–318.
20. Maruyama, A.; Ishihara, T.; Kim, J-S.; Kim, W. S.; Akaike, T. *Colloids Surfaces., A* **1999**, *153*, 439–443.
21. Adler, A. F.; Leong, K. W. *Nano Today* **2010**, *5*, 553–569.
22. Mao, H-Q.; Roy, K.; Troung-Le, V. L.; Janes, K. A.; Lin, K. Y.; Wang, Y.; August, J. T.; Leong, K. W. *J. Controlled Release* **2001**, *70*, 399–421.
23. Kaul, G.; Amiji, M. *Pharm. Res.* **2005**, *22*, 951–961.
24. Couvreur, P.; Kante, B.; Roland, M.; Guiot, P.; Bauduin, P.; Speiser, P. J. *J. Pharm. Pharmacol.* **1979**, *31*, 331–332.
25. Rouzes, C.; Gref, R.; Leonard, M.; De Sousa Delgado, A.; Dellacherie, E. *J. Biomed. Mater. Res.* **2000**, *50*, 557–565.
26. Barbault-Foucher, S.; Gref, R.; Russo, P.; Guechot, J.; Bochot, A. *J. Controlled Release* **2002**, *83*, 365–375.
27. Janes, K. A.; Calvo, P.; Alonso, M. *J. Adv. Drug Delivery Rev.* **2001**, *47*, 83–97.
28. Coombes, A. G. A.; Tasker, S.; Lindblad, M.; Holmgren, J.; Hoste, K.; Toncheva, V.; Schacht, E.; Davis, M. C.; Ilum, L.; Davis, S. S. *Biomaterials* **1997**, *18*, 1153–1161.
29. Rouzes, C.; Durand, A.; Leonard, M.; Dellacherie, E. *J. Colloid Interface Sci.* **2002**, *253*, 217–223.
30. Duche^ne, D.; Ponchel, G.; Wouessidjewe, D. *Adv. Drug Delivery Rev.* **1999**, *36*, 29–40.
31. Yang, S. C.; Ge, H. X.; Hu, Y.; Jiang, X. Q.; Yang, C. Z. *Colloid Polym. Sci.* **2000**, *278*, 285–292.
32. Douglas, S. J.; Illum, L.; Davis, S. S. *J. Colloid Interface Sci* **1985**, *103*, 154–163.
33. Vinogradov, S. V. *Expert Opin. Drug Delivery* **2007**, *4*, 5–17.
34. Lee, J. I.; Kim, H. S.; Yoo, H. S. *Int. J. Pharma.* **2009**, *373*, 93–99.
35. Raemdonck, K.; Naeye, B.; Buyens, K.; Vandenbroucke, R. E.; Hogset, A.; Demeester, J.; De Smedt, S. C. *Adv. Funct. Mater.* **2009**, *19*, 1406–1415.
36. Lee, H.; Mok, H.; Lee, S.; Oh, Y-K.; Park, T. G. *J. Controlled Release* **2007**, *119*, 245–252.

37. Oishi, M.; Hayashi, H.; Itaka, K.; Kataoka, K.; Nagasaki, Y. *Colloid Polym. Sci.* **2007**, *285*, 1055–1060.
38. Csaba, N.; Koping-Hoggard, M.; Alonso, M. J. *Int. J. Pharma.* **2009**, *382*, 205–214.
39. Belmont, P.; Aissaoui, A.; Hauchecorne, M.; Oudrhiri, N.; Petit, L.; Vigneron, J.-P.; Lehn, J.-M.; Lehn, P. *J. Gene Med.* **2002**, *4*, 517–526.
40. Hendrix, M.; Alper, P. B.; Priestley, E. S.; Wong, C.-H. *Angew. Chem., Int. Ed.* **1997**, *36*, 95–98.
41. Kudsiova, L.; Arafiena, C.; Lawrence, M. J. *J. Pharma. Sci.* **2008**, *97*, 3981–3997.
42. Kawakami, S.; Fumoto, S.; Nishikawa, M.; Yamashita, F.; Hashida, M. *Pharma. Res.* **2000**, *17*, 306–313.
43. Nakai, T.; Kanamori, T.; Sando, S.; Aoyama, Y. *J. Am. Chem. Soc.* **2003**, *125*, 8465–8475.
44. Masuda, T.; Akita, H.; Nishio, T.; Niikura, K.; Kogure, K.; Ijiro, K.; Harashima, H. *Biomaterials* **2008**, *29*, 709–723.
45. Kole, L.; Das, L.; Das, P. K. *J. Infect. Dis.* **1999**, *180*, 811–820.
46. Kawakami, S.; Sato, A.; Nishikawa, M.; Yamashita, F.; Hashida, M. *Gene Ther.* **2000**, *7*, 292–299.
47. Hattori, Y.; Kawakami, S.; Suzuki, S.; Yamashita, F.; Hashida, M. *Biochem. Biophys. Res. Commun.* **2004**, *317*, 992–999.
48. Lu, Y.; Kawakami, S.; Yamashita, F.; Hashida, M. *Biomaterials* **2007**, *28*, 3255–3262.
49. Kim, T. H.; Jin, H.; Kim, H. W.; Cho, M-H.; Cho, C. S. *Mol. Cancer Ther.* **2006**, *5*, 1723–1732.
50. Tan, W. B.; Jiang, S.; Zhang, Y. *Biomaterials* **2007**, *28*, 1565–1571.
51. Wang, H.; Chen, Y.; Li, X-Y.; Liu, Y. *Mol. Pharmaceutics* **2007**, *4*, 189–198.
52. Zhou, X.; Zhang, X.; Yu, X.; Zha, X.; Fu, Q.; Liu, B.; Wang, X.; Chen, Y.; Shan, Y.; Jin, Y.; Wu, Y.; Liu, J.; Kong, W.; Shen, J. *Biomaterials* **2008**, *29*, 111–117.
53. McBain, S. C.; Yiu, H. H. P.; Dobson, J. *Int. J. Nanotech.* **2008**, *3*, 169–180.
54. Morishita, N.; Nakagami, H.; Morishita, R.; Takeda, S-I.; Mishima, F.; Terazono, B.; Nishijima, S.; Kaneda, Y.; Tanaka, N. *Biochem. Biophys. Res. Commun.* **2005**, *334*, 1121–1126.
55. Bhattarai, S. R.; Kim, S. Y.; Jang, K. Y.; Lee, K. C.; Yi, H. K.; Lee, D. Y.; Kim, H. Y.; Hwang, P. H. *Nanomed.: Nanotech. Biol. Med.* **2008**, *4*, 146–154.
56. Bhattari, S. R.; Kim, S. Y.; Jang, K. Y.; Lee, K. C.; Yi, H. K.; Lee, D. Y.; Kim, H. Y.; Hwang, P. H. *J. Virol. Methods* **2008**, *147*, 213–218.
57. Lee, C-M.; Jeong, H-J.; Kim, S-L.; Kim, E-M.; Kim, D. W.; Lim, S. T.; Jang, K. Y.; Jeong, Y. Y.; Nah, J. W.; Sohn, M-H. *Int. J. Pharma.* **2009**, *371*, 163–169.
58. Kumar, A.; Jena, P. K.; Behera, S.; Lockey, R. F.; Mohapatra, S.; Mohapatra, S. *Nanomed.: Nanotech. Biol. Med.* **2010**, *6*, 64–69.
59. Chen, X.; Tam, U. C.; Czlapinski, J. L.; Lee, G. S.; Rabuka, D.; Zettl, A.; Bertozzi, C. R. *J. Am. Chem. Soc.* **2006**, *128*, 6292–6293.

60. Wu, P.; Chen, X.; Hu, N.; Tam, U. C.; Blixt, O.; Zettl, A.; Bertozzi, C. R. *Angew. Chem., Int. Ed.* **2008**, *47*, 5022–5025.

61. Hasegawa, T.; Fujisawa, T.; Numata, M.; Umeda, M.; Matsumoto, T.; Kimura, T.; Okumura, S.; Sakurai, K.; Shinkai, S. *Chem. Commun.* **2004**, 2150–2151.

62. Sudibya, H. G.; Ma, J.; Dong, X.; Ng, S.; Li, L-J.; Liu, X-W.; Chen, P. *Angew. Chem., Int. Ed.* **2009**, *48*, 2723–2726.

63. Olivier, J-C.; Vauthier, C.; Taverna, M.; Ferrier, D.; Couvreur, P. *Colloids Surf., B* **1995**, *4*, 349–356.

64. Zhang, H.; Ma, Y.; Sun, X-L. *Med. Res. Rev.* **2010**, *3*, 270–289.

65. Beljaars, L.; Molema, G.; Weert, B.; Bonnema, H.; Olinga, P.; Groothuis, G. M.; Meijer, D. K.; Poelstra, K. *Hepatology* **1999**, *29*, 1486–1493.

## Chapter 5

# Bioconjugated Gold Nanoparticle for Rapid Capture and Targeted Photothermal Lysis of Pathogenic Bacteria

**Paresh Chandra Ray,* Sadia Afrin Khan, Anant Kumar Singh, Dulal Senapati, Zhen Fan, Teresa Demeritte, and Rajashekhar Kanchanapally**

**Department of Chemistry, Jackson State University,
1400 Lynch St., Jackson, Mississippi 39217, USA
*E-mail: paresh.c.ray@jsums.edu. Fax: 601-979-3674**

Outbreak of food poisoning by *Salmonella* and *E. coli* bacteria are very common in this world. On the other hand, multiple drug resistant *Salmonella enterica* serover typhimurium definitive type 104 (DT104) is at present an emerging threat worldwide. As a result, an ultrasensitive sensing technology for the rapid detection and new approaches for the treatment of infectious bacterial pathogens that do not rely on traditional therapeutic regimes is very urgently required in today's world. This book chapter discusses our recent report on bio-conjugated nanomaterial based strategies for the pathogen detection and photothermal applications. We have focused on the basic concepts and critical properties of the nanostructures that are useful for the pathogen sensing and killing.

## Introduction

Outbreaks of waterborne and food-borne pathogens like *Escherichia coli, Staphylococcus spp. and Salmonella spp.* regularly occur in the U.S and other developed countries (*1–9*). Since food production industry is worth about 578 billion U.S. dollars, often food recalls due to the presence of food-borne

In Nanomaterials for Biomedicine; Nagarajan, R.;
ACS Symposium Series; American Chemical Society: Washington, DC, 2012.

pathogens are becoming nightmare for US economical growth (*1–9*). On the other hand, due to the biological diversity of the harmful pathogens and quite low infection dose, it is a continual challenge to prevent infectious disease outbreaks. Infection disease is responsible for approximately one-third of global mortality and billion dollars of economical loss each year (*1–15*). Since current methods for the identification of pathogenic bacteria take several days to report the correct information, there is a huge demand for the development of rapid, sensitive, and reliable assay to identify the harmful pathogens selectively with high sensitivity (*1–15*). Gold nanomaterial-enabled detection strategies, which are currently in the infant stage, may be able to fulfill the demand (*10–30*). Due to the presence of large surface area, large number of target-specific recognition element such as antibody, aptamers and peptides can be attached to gold nanomaterial surface (*30–70*). As a result, bio-conjugated gold nanoparticle can be used for several pathogens simultaneously as well as selectively even at the single bacterium level, as shown in Scheme 1. Since last four years, our group has been developing gold nanomaterials based highly sensitive assay for highly selective and sensitive sensing of different pathogens (*15*, *20–23*, *30*). Current book chapter intended to illustrate the current status of the field mainly from our laboratory and also to spur possible future research in this area for the next generation scientific community.

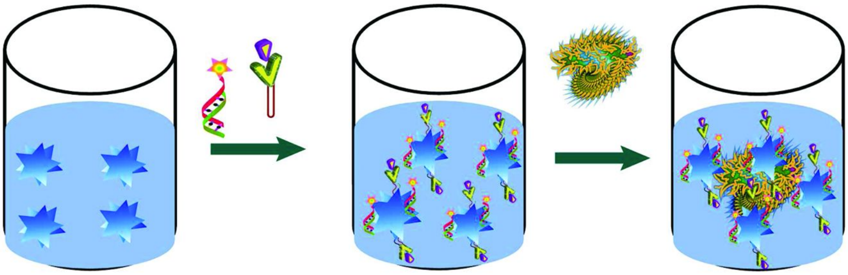

*Scheme 1. Schematic representation shows bio-conjugated gold nanotechnology-driven approach to selectively capture bacteria.*

Since the development of penicillin in the 1940s, antibiotics became economic powerhouses for our world society and also responsible for saving countless human lives (*1–10*). Only in the USA, there are around 42 billion U.S. dollars sales of antibiotics in 2009. It is almost 20% of drug expenditures among any therapeutic group of drugs (*1–9*). However, due to the intensive use of the antibiotics, world is now facing a tremendous problem and that is, human pathogens have become resistant to many available antibiotics (*1–10*). Multidrug resistance (MDR) in bacteria occurs by the accumulation of resistance plasmids or transposons of genes, with each coding responsible for resistance to a specific drug type (*1–10*). Due to the presence of multiple antimicrobial resistance genes like 1) *pse* for ampicillin resistance, 2) *floR* for chloramphenicol resistance, 3) *str* for streptomycin resistance, 4) *sulI* for sulfonamide resistance, and 5) *tetR* or *tetG* for tetracycline resistance, MDR *bacteria* are resistant to five mostly used ampicillin, chloramphenicol, streptomycin, sulfonamides, and tetracycline antibiotics. As a result, MDRB became the cause for the major sources of hospital-acquired infections and approximately sixty percent of nosocomial infections (*1–10*). According to the Infectious Diseases Society of America, we must deliver 10 new antibiotics by the year 2020 and it will not be easy in this world's economical condition. Similarly, according to World Health Organization (WHO) (*9*) there may be another 1-2 decades left for people to use the existing antibiotics and after that, the MDRB infectious diseases may not be cured using currently available antibiotics in the market. All the above facts clearly indicate that the new approaches for the treatment of infectious bacterial pathogens that do not rely on traditional therapeutic regimes, is very urgent for our society's health care. One promising method, still in its infant stage, is to use nanomaterial-based photothermal killing of harmful bacteria selectively (*17–23*). We and other groups have shown that unique size and shape dependent optical properties of gold nanomaterials can be used for the selective non-invasive photothermal lysis applications for MDRB and other pathogens (*17–23*). In this book chapter, we summarize recent promising reports mainly from our group and suggest future strategies to identify, target or destroy pathogens.

## Bio-Conjugated Gold Nanomaterial Based Sensing of Bacteria

Gold metal nanostructures attract much interest because they are easy to synthesize and they possess unique size or shape dependent properties (as shown in Figure 1-2), including large optical field enhancements resulting in the strong scattering and absorption of light (*10–71*). In case of noble metals, as the size is reduced to tens of nanometers scale, which is comparable to the wavelength of light, a new very strong absorption is observed, resulting from the collective oscillation of the electrons in the conduction band from one surface of the particle to the other and known as localized surface plasmon (LSP) (*10–71*). Due to the presence of LSP, electric fields near the particle's surface are greatly enhanced and the particle's optical extinction reaches maximum at the plasmon resonant frequency. It can be visible or NIR wavelength depending on size and shape of nanoparticles (*10–71*), as shown in Figure 1. Due to the huge surface plasmon enhancement, absorption cross-sections of noble gold nanoparticles are 5-7 orders of magnitude more than that of any available dye molecule (*10–71*). As a result, one can consider each metal nanoparticle as an optical probe equivalent to several million dye molecules, which will help to increase detection sensitivity tremendously (*10–71*). There is another advantage to use nanoparticle as a probe, which is, unlike dyes, metal nanoparticles are photostable and do not undergo photobleaching easily.

For biological applications, it is necessary to use near-infrared (NIR) light, especially 650−900 nm, since the absorption of physiological fluids and tissues and biological water is minimal in this region (*17–23*, *31–33*). One way of tuning the localized surface plasmon frequency is by changing the particle shape and size as shown in Figure 2. When an incident light couples with surface plasmon mode, it helps in the local increase of resonant electromagnetic fields over several orders of magnitude (*17–23*, *31–33*).

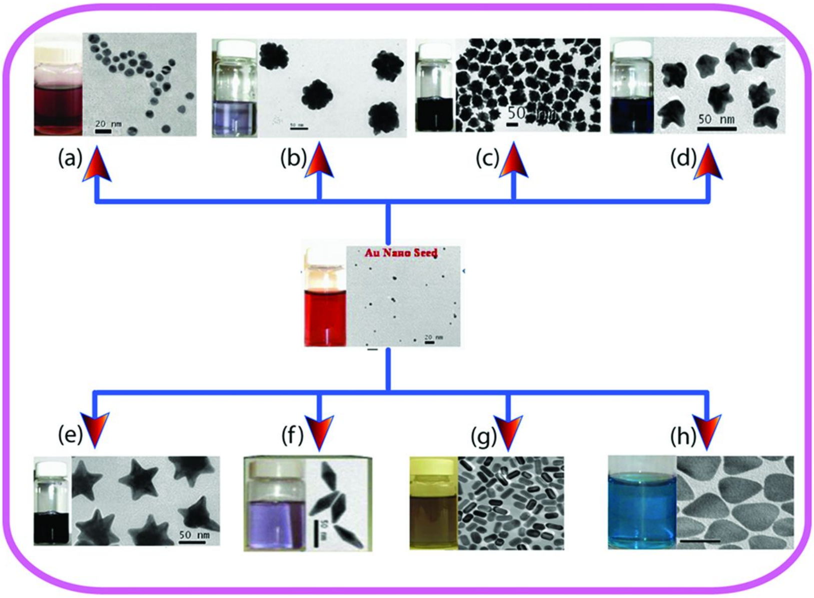

*Figure 1. Picture showing how one can synthesize gold nanoparticles of different shapes from gold seed by just varying the nature and concentration of surfactant (presence of (a) 0.0 M CTAB, (b) 0.001 M CTAB, (c) 0.003 M CTAB, (d) 0.01 M CTAB, (e) 0.03 M CTAB, (f) 0.4 M CTAB, (g) 0.1 M CTAB, (h) 0.14 M CTAB.*

This phenomenon enhances several radiative and non-radiative processes such as absorption, fluorescence, Raman scattering, hyper-Rayleigh scattering, and hyper-Raman scattering (*10–71*). As a result, these optical techniques have been used (*25–50*) for the recognition of pathogens by monitoring the change in the optical signal that occurs after the addition of pathogens on functionalized nanomaterials, as shown in Scheme 2. For the selective sensing and therapy, nanomaterials have been modified with different recognition elements like antibodies and aptamers to target antigen-presenting cells as epitopes present on pathogen surface (*10–25*). In the next section, we will focus on how various gold nanoparticle based surface plasmon enabled spectroscopies have been used by our groups for optical signal transduction to provide highly sensitive pathogen sensing (as shown in Scheme 2).

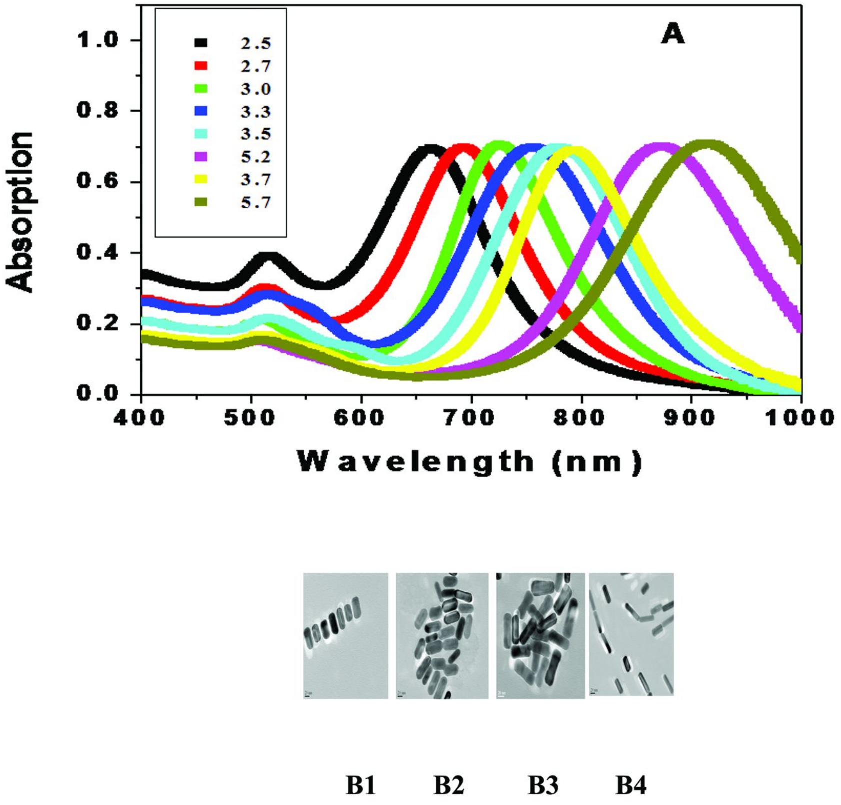

*Figure 2. Extinction profile of Au nanorods with aspect ratios varying from 2.0 to 5.7 (reprinted with permission from Ref. (60), Copyright 2008, Willey- VCH). E) TEM image of gold nanorods of average aspect ratios, B1: (σ) ≈2.0, B2: (σ) ≈2.8, b3: (σ) ≈4.0 and b4: (σ) ≈5.2. (reprinted with permission from Ref. (70), Copyright 2009, Willey- VCH).*

## Colorimetric Bacteria Sensing

Colorimetric assay for bacteria sensing will be ideal for the development of real life biosensor, because any layman can use these sensors using naked eyes. Since the colors of gold nanoparticle solutions are highly dependent on the interparticle distance of nanoparticles, the working principle of the gold nanoparticle based colorimetric sensor is based on the fact that when individual gold nanoparticles come into close proximity, due to the interparticle plasmon coupling, a distinct color change is usually observed (*10–70*). As a result, last several years (*10–23*) we and other groups have used this colorimetric change processes for ultrasensitive bacteria sensing. In 2005, Berry et. al. (*16*) reported that due to the strong electrostatic interactions, cetyltrimethylammonium bromide (CTAB)-functionalized gold nanorods can conformally deposit to form a monolayer on Bacillus cereus. We have reported (*20*) colorimetric detection of *E. coli* bacteria using gold nanorod. Our colorimetric bacteria identification is based on the fact that, *E. coli* bacteria are more than an order of magnitude larger in size (1−3 µm) than the anti-*E. coli* antibody-conjugated gold nanorods. In the presence of *E. coli* bacteria, several gold nanorods conjugate with one *E. coli* bacterium, as shown in Figure 3. As a result, anti-*E. coli* antibody-conjugated gold nanorods undergo aggregation (*20*). Due to the aggregation, a color change takes place (as shown in Figure 3C). This color change is mainly due the change in interparticle interaction resulting from the assembly of nanoparticles on the cell surface. This bioassay is rapid, takes less than 15 min from bacterium binding to detection and analysis, and is convenient and highly selective.

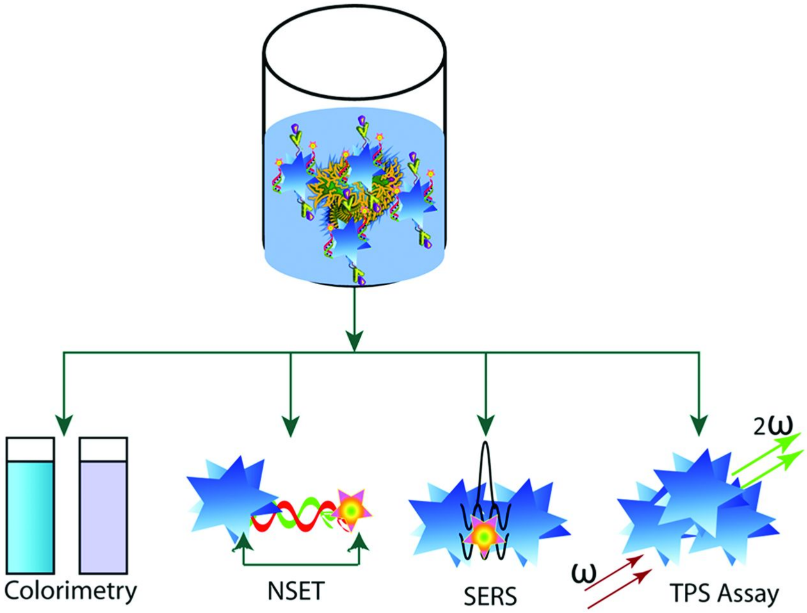

*Scheme 2. Schematic representation showing different gold nanotechnology based optical techniques for the selective sensing of pathogens.*

Recently we have reported (*21*) the development of bio-conjugated gold nanomaterial for the selective sensing of salmonella bacteria. For selective salmonella bacteria detection, at first we have modified the nanoparticles with anti-salmonella antibody (as shown in Figure 4A). Our reported experimental data have shown that the sensitivity of colorimetric assay for Salmonella detection is $10^4$ bacteria cells/mL (*21*), which is comparable with the detection limit ($10^4$–$10^5$cfu/mL) of ELISAs. We have also shown that gold nanoparticle based colorimetric assay is highly selective. As shown in Figure 4C, no color change has been observed even after the addition of $10^6$ *E. coli* bacteria. Similarly, we have not observed any color change when we added $10^6$ *Salmonella typhimurium* bacteria to anti *E. coli* antibody conjugated oval shape gold nanoparticles. On the other hand, distinct color changes have been observed when we added $10^6$ *E. coli* bacteria to anti-*E. coli* antibody conjugated oval shape gold nanoparticles.

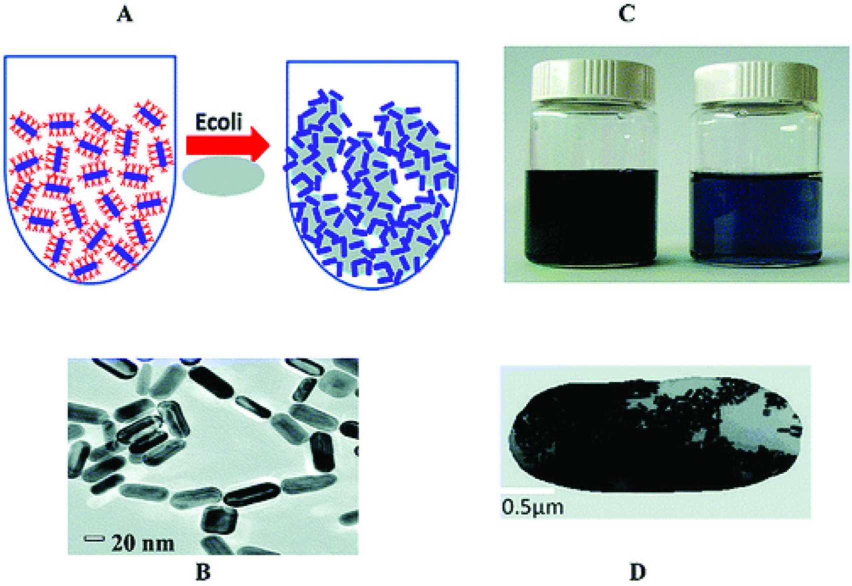

*Figure 3. (A) Schematic representation of anti-E. coli antibody-conjugated nanorod-based sensing of E. coli bacteria. (B) TEM image of anti-E. coli antibody-conjugated nanorods before the addition of E. coli bacteria. (C) Photograph showing colorimetric change upon the addition of E. coli bacteria ($10^4$ cfu/mL), and (D) TEM image demonstrating aggregation of the gold nanorods after the addition of E. coli bacteria ($10^3$ cfu/mL). (reprinted with permission from Ref. (20), Copyright 2009, American Chemical Society).*

Next to understand whether our gold nanotechnology based assay can detect MDRB from food sample, we have reported (*22*) the selectivity and sensitivity of our colorimetric assay using ampicillin, chloramphenicol, streptomycin, sulfonamides, and tetracycline antibiotics drug resistant (MDRB) *S. typhimurium DT104* (ATCC 700408) infected romaine lettuce. For this purpose, we purchased lettuce from Walmart and then chopped them into small pieces. After that chopped lettuces were infected them with Salmonella DT104. Figure 5 shows the selectivity and sensitivity of our colorimetric assay, when antibody-conjugated gold nanoparticles were mixed with various concentrations of MDRB *S. typhimurium DT104* infected lettuce samples. As shown in Figure 5, no color change has been observed even after the addition of lettuce sample infected by$10^6$ CFU/gm *Salmonella ser. Agona* or *E. coli* bacteria on to M3038 antibody conjugated popcorn shape gold nanoparticle. We have also tested for mixture of bacteria, as shown in Figure 5. Our result clearly shows that the color change is observed only when MDRB $10^3$ CFU/gm or above *Salmonella* DT104 is present. The sensitivity of this colorimetric assay was $10^3$ CFU/gm.

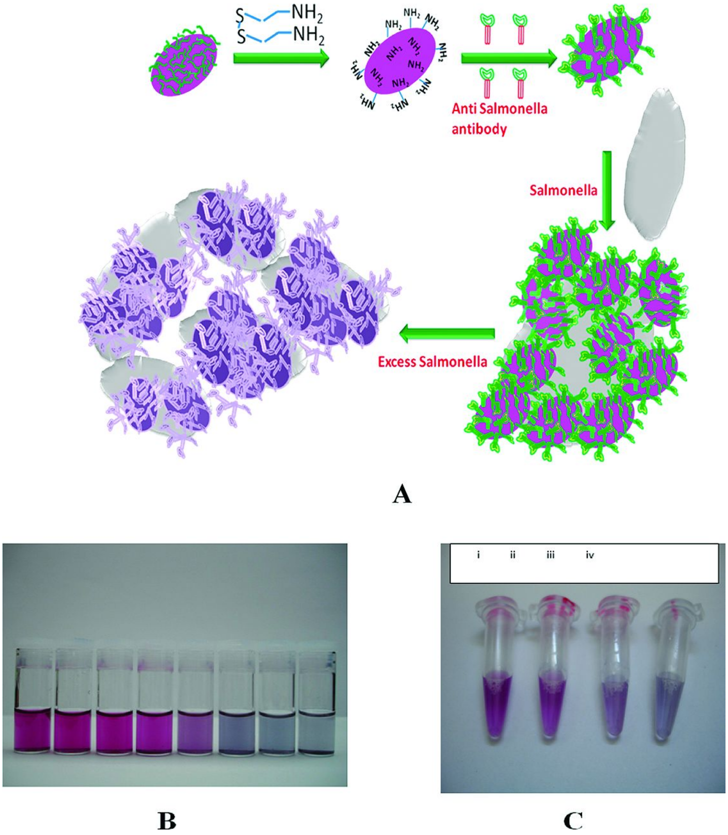

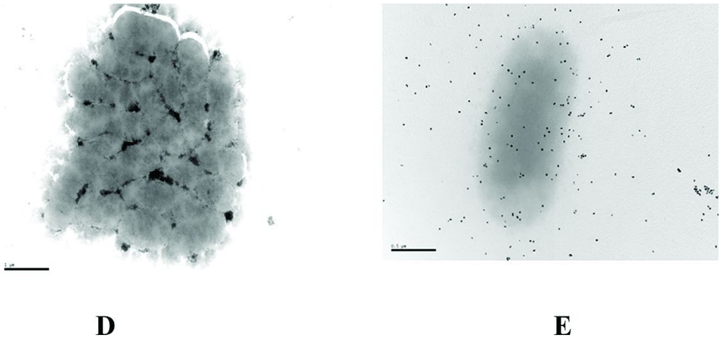

*Figure 4. A) Schematic representation showing antibody-conjugated nanotechnology-driven approach using oval shape gold nanoparticle to selectively target and destroy pathogenic bacteria. B) Photograph showing colorimetric change upon the addition of (from left to right) 10, 50, 100, 500, 1000, 5000, 10000, 50000, 100000, 500000 CFU/mL Salmonella bacteria. C) Photograph showing colorimetric change upon the addition of i) $10^6$ E. coli bacteria to anti salmonella antibody conjugated oval shape gold nanoparticles, ii) $10^6$ salmonella bacteria to anti E. coli antibody conjugated oval shape gold nanoparticles, iii) $10^3$ E. coli bacteria to anti E. coli antibody conjugated oval shape gold nanoparticles, iv) $10^6$ E. coli bacteria to anti E. coli antibody conjugated oval shape gold nanoparticles. D) TEM image demonstrating the formation of bigger microbial clusters in the presence $10^6$ cfu/mL salmonella bacteria. E) TEM image of salmonella bacteria in the presence of anti E.coli antibody conjugated oval shape gold nanoparticles. Our TEM image clearly demonstrates that the S. typhimurium bacterium cells are poorly labeled by the anti-E.coli antibody coated oval shape gold nanoparticles. (reprinted with permission from Ref. (21), Copyright 2010, Willey- VCH).*

## Two-Photon Rayleigh Scattering Assay for Bacteria Sensing

The two-photon Rayleigh light scattering or hyper-Rayleigh scattering can be observed from fluctuations in symmetry, caused by rotational fluctuations (*20*, *30*, *39*, *41*, *42*, *48*, *70–74*). This is a second harmonic generation experiment in which the light is scattered in all directions rather than as a narrow coherent beam (*20*, *30*, *39*, *41*, *42*, *48*, *70–74*). Two-photon scattering properties of nanostructured materials are drastically influenced by the quantum confinement effect and as a result, this is highly promising for biological and chemical sensing applications (*20*, *30*, *39*, *41*, *42*, *48*, *70–74*). Recently we have demonstrated (*20*) a fast and highly sensitive assay for *E. coli* bacteria detection using an antibody-conjugated gold nanorod based two-photon scattering technique. We have reported (*20*) that when anti *E. coli* antibody-conjugated nanorods were mixed with various concentrations of *E. coli* O157:H7 bacteria, the two-photon scattering intensity increased by about 40 times. This increment is based on the fact that when anti

*E. coli* antibody-conjugated nanorods were mixed with various concentrations of *Escherichia coli* O157:H7 bacteria, several gold nanorods conjugated with one *E. coli* bacterium and formed bio-conjugated gold nanorod aggregates, as shown in Figure 6. As a result, the two-photon scattering intensity increased by about 40 times. Due to the aggregation in the presence of *E. coli* bacteria, nanorods lost the center of symmetry. As a result, one can expect a significant amount of electric dipole contribution to the two-photon scattering intensity. Since electric dipole contributes several times higher than that of multipolar moments, we expect two-photon scattering intensity to increase with aggregation. Again, due to the aggregation, a new broad band appears around 200 nm, far from their longitudinal plasmon absorption band, as shown in Figure 6. As a result, the single photon resonance enhancement and two-photon luminescence factors are much larger for nanorod aggregates due to the closeness of $\lambda_{max}$ to the fundamental wavelength at 860 nm. This factor should increase the two-photon scattering intensity. Similarly, since size increases tremendously with aggregation, the two-photon scattering intensity is expected to increase with the increase in particle size. Our experimental results have shown that *E. coli* bacteria can be detected quickly and accurately without any amplification or enrichment at the 50 cfu/mL level with excellent discrimination against any other bacteria. Our report (*20*) clearly shows that our antibody-conjugated gold nanorod based two-photon scattering assay can provide a quantitative measurement of the *E. coli* bacteria concentration. To understand whether our assay is highly selective, we have also reported the two-photon scattering intensity changes upon the addition of *S. typhimurium* bacteria to anti-*E. coli* antibody-conjugated gold nanorods. As shown in Figure 6, two-photon scattering intensity changed by only 6% when we added the *S. typhimurium* bacteria to anti-*E. coli* antibody-conjugated gold nanorods. So our reported (*20*) data clearly show that our reported two-photon scattering assay is highly selective.

## Bacteria Sensing Using Gold Nanoparticle Based SERS Assays

The possibility of observing Raman signals, which are normally very weak, with enhancements on the order of $10^8$−$10^{14}$ allow SERS to be unique for ultrasensitive pathogen sensing (*22*, *33*, *35–40*, *50–65*). Several reports show (*22*, *33*, *35–40*, *50–65*) that very high selectivity and sensitivity can be offered by SERS. Very recently, we have reported Rh-6G modified antibody-conjugated popcorn shape gold nanoparticle-based SERS technique for the detection of MDRB Salmonella DT104 (*22*). In nano-popcorn, like nano-star, the central sphere acts as an electron reservoir while the tips are capable of focusing the field at their apexes, which provides huge field enhancement of scattering signal (*22*, *33*). Our result indicates that in the presence of drug resistant MDRB *Salmonella DT104*, antibody-conjugated gold nanoparticle undergoes aggregation, which helped to form several hot spots and provided ~ $10^9$ order of magnitude SERS signal enhancement through mainly electromagnetic field enhancement mechanism. Figure 7 shows the SERS enhancement in the presence of Salmonella DT104. The Raman modes at 236, 252, 273 and 376 cm$^{-1}$ are

N-C-C bending modes of ethylamine group of the Rh6G ring and the Raman modes at 615, 778, 1181, 1349 1366,1511, 1570, 1603 and 1650 cm$^{-1}$ are due to C-C-C ring in-plane bending, C-H out-of-plane bending, C-N stretching and C-C stretching, as we reported (*22*, *33*). As shown in Figure 7, the SERS intensity change was negligible in the presence of $10^6$ *Salmonella ser. Agona* bacteria/mL or *E.coli* bacteria, whereas a good enhancement has been observed even in the presence of only 10 CFU/gm MDRB *S. typhimurium* DT104. It is mainly due to the lack of strong interaction between antibody-conjugated popcorn shape gold nanoparticle and *Salmonella ser. Agona or E.coli* bacteria. Our reported result clearly indicates that our gold nanoparticle based SERS assay is highly selective and very sensitive.

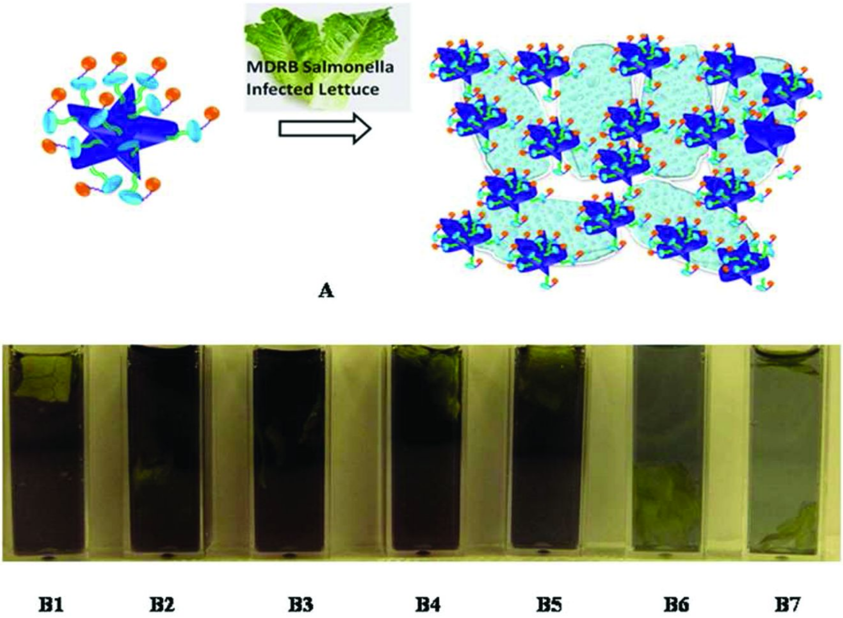

*Figure 5. A) Schematic representation showing our gold nanotechnology-driven colorimetric approach for rapid selective screening of MDRB Salmonella bacteria from infected lettuce. B) Photograph showing colorimetric change upon the addition of infected lettuce on antibody-conjugated gold nanoparticle. Lettuce was infected by B1) $10^2$CFU/gm MDRB Salmonella, B2) $10^6$ CFU/gm Salmonella ser. Agona bacteria, B3) $10^6$CFU/gm E. coli bacteria, B4) mixture of $10^6$CFU/gm Salmonella ser. Agona and $10^6$CFU/gm E.coli, B5) mixture of $10^6$CFU/gm Salmonella ser. Agona and $10^2$CFU/gm MDRB Salmonella, B6) mixture of $10^6$CFU/gm Salmonella ser. Agona and $10^3$CFU/gm MDRB Salmonella, B7) $10^3$CFU/gm MDRB Salmonella. C) Plot demonstrating SERS enhancement (SERS intensity change before and after addition of bacteria) due to the addition of different kinds of bacteria to monoclonal M3038 antibody-conjugated popcorn shape gold nanoparticle. (reprinted with permission from Ref. (22), Copyright 2011, Royal Society).*

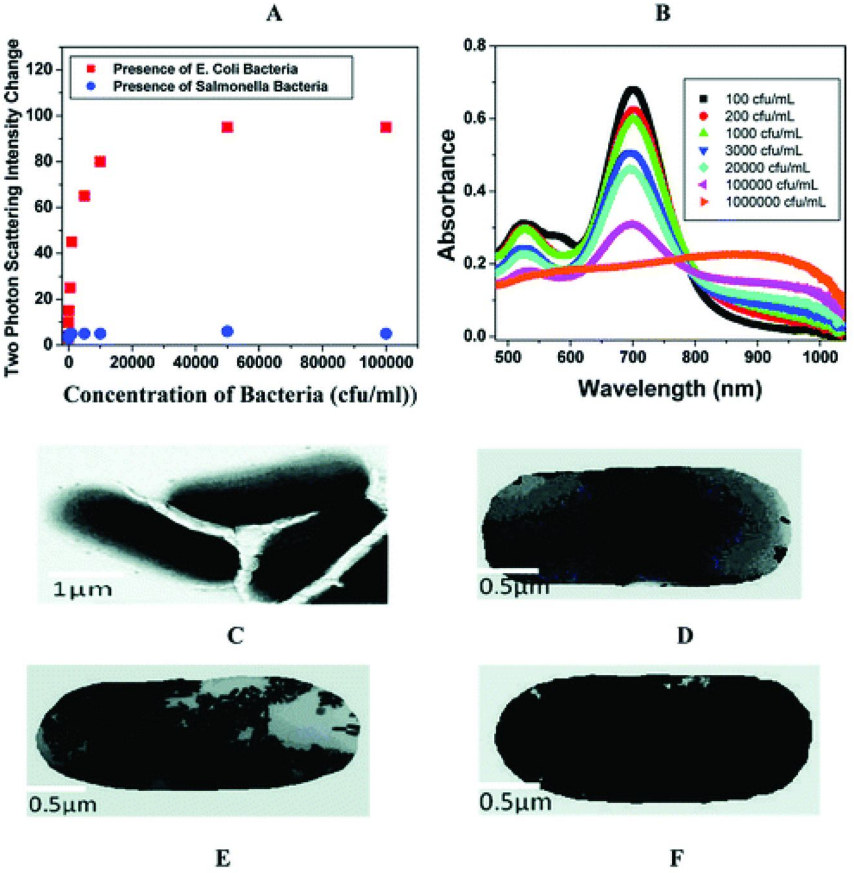

*Figure 6. (A) Plot demonstrating two-photon scattering intensity changes (by 40 times) due to the addition of E. coli bacteria to anti-E. coli antibody-conjugated gold nanorods. Two-photon scattering intensity changes very little upon the addition of Salmonella bacteria. (B) Absorption profile variation of anti-E. coli antibody-conjugated Au nanorods due to the addition of different concentrations of E. coli bacteria ($10^2$ to $10^7$ cfu/mL). The strong long wavelength band in the near-infrared region ($\lambda_{LPR}$ = 680 nm) is due to the longitudinal oscillation of the conduction band electrons. The short wavelength peak ($\lambda \approx 520$ nm) is from the nanorods' transverse plasmon mode. New band appearing around 950 nm, due to the addition of E. coli bacteria, demonstrates the aggregation of gold nanorods. (C) TEM image of E. coli bacteria before the addition of nanorod. (D) TEM image after the addition of $10^2$ cfu/mL E. coli bacteria. (E) TEM image demonstrating aggregation of gold nanorods after the addition of $8 \times 10^4$ cfu/mL E. coli bacteria. (F) TEM image demonstrating aggregation of gold nanorods after the addition of $10^7$ cfu/mL E. coli bacteria. (reprinted with permission from Ref. (20), Copyright 2009, American Chemical Society).*

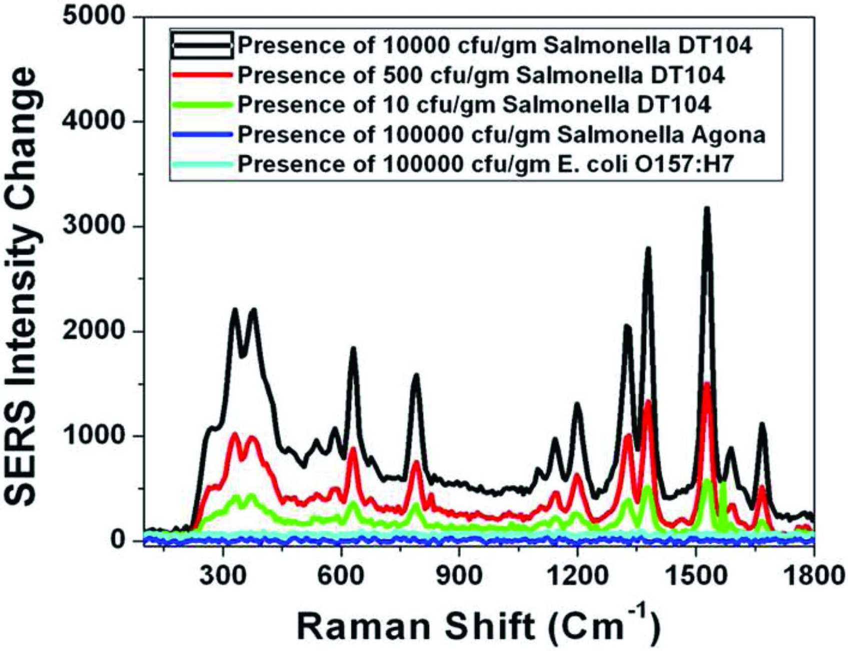

*Figure 7. Plot demonstrating SERS enhancement (SERS intensity change before and after the addition of bacteria) due to the addition of different kinds of bacteria to monoclonal M3038 antibody-conjugated popcorn shape gold nanoparticle. (reprinted with permission from Ref. (22), Copyright 2011, Royal Society).*

## Selective Bacteria Killing Using Bio-Conjugated Gold Nanomaterial

Gold nanoparticles of different sizes and shapes with optical properties tunable in the visible to near-infrared can be used for the hyperthermic destruction of MDRB using NIR light (*17–23*), as shown in Scheme 3. For photothermal destruction, gold nanoparticles serve as “light-directed nano heaters”, which is very useful for selective laser photothermolysis pathogens (*15–23*, *30–33*, *38*). Gold nanoparticles are known to absorb light several millions of times stronger than the organic dye molecules, as a result, in the presence of light of proper wavelength, due to the electron–phonon relaxation process, temperature rises on the order of a few tens of degrees (*15–23*, *30–33*, *38*). This photothermal hypothermia process produces sufficient heat for the destruction of MDRB via cell damage using different thermal effects, such as denaturation of proteins/enzymes, induction of heat-shock proteins, metabolic signaling disruption, endothelial swelling, microthrombosis, etc. (*15–23*, *30–33*, *38*). When the incident laser frequency overlapped with the plasmon absorption maximum of the gold nanoparticles conjugated pathogens, selective heating and destruction of MDRB can be achieved at a much lower laser powers than that required to destroy healthy bacteria to which bio-conjugated nanoparticles do not bind specifically. Zharov et. al. (*19*) reported localized killing of *S. aureus* in vitro by combining laser and photo-thermal technique. Later, Norman et. al. (*17*) reported photothermal killing using gold nanorods that have been covalently linked with antibodies to selectively destroy *Pseudomonas aeruginosa,* which was obtained from the upper respiratory tract of sinusitis patients.

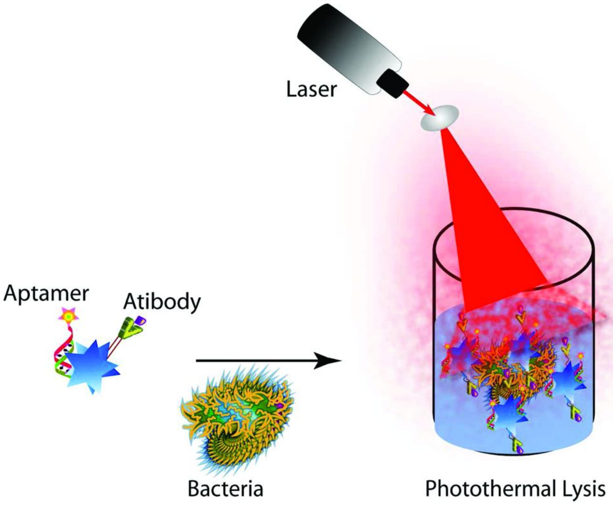

*Scheme 3. Schematic representation showing bacteria conjugated nanoparticle based photothermal hyperthermic destruction for MDRB.*

All initial studies did not demonstrate the selectivity of their assay with respect to other pathogens, which is very important before this technique can be used for real life sample. At 2010, we have reported selective photothermal killing of salmonella bacteria using antibody conjugated popcorn shape gold nanoparticle (*21*). As shown in Figure 8, our result shows that when oval shape gold nanoparticles are attached to bacterial cells, the localized heating that occurs during 670 nm irradiation is able to cause irreparable cellular damage. To understand whether our oval shape gold nanoparticle based photo thermal lysis assay is highly selective, we have also performed experiments to find out how our assay responds to the addition of $10^6$/ml *E. coli* bacteria to anti salmonella antibody conjugated oval shape gold nanoparticle. As shown in Figure 8, most of the *E. coli* bacteria remain alive even after 15 minutes of irradiation using 670 nm light. On the other hand, 97% bacteria are killed when we use salmonella bacteria instead of *E. coli* bacteria. So our experimental results clearly show that our bioconjugated oval shape gold nanoparticle based photo-thermal lysis process is highly selective (*21*).

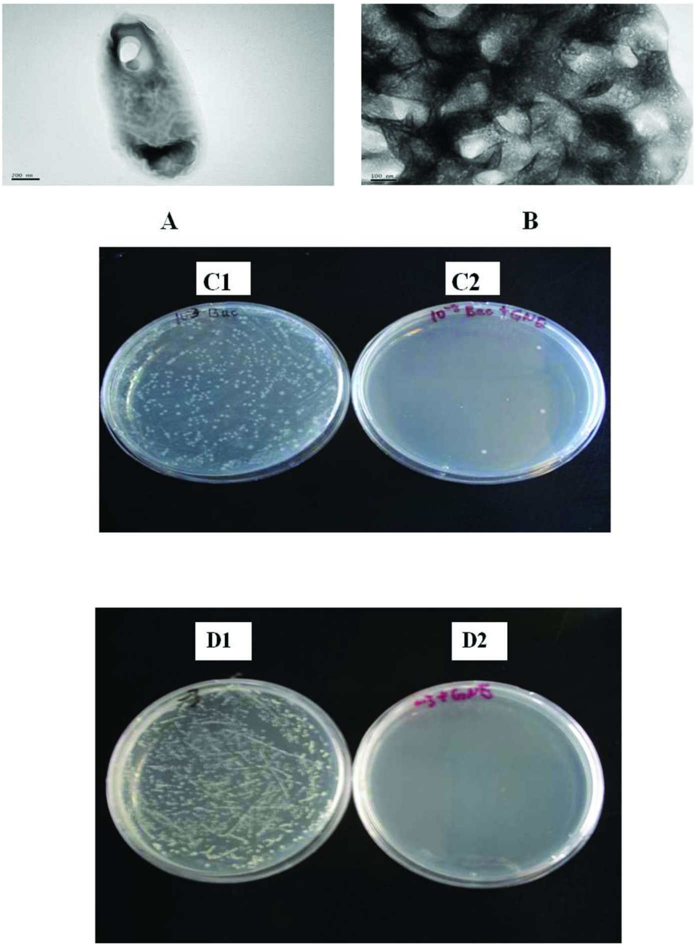

*Figure 8. TEM image demonstrating irreparable damage of single bacterial cell surface when anti–Salmonella antibody coated NP conjugated S. typhimurium bacterium were exposed to 676 nm NIR radiation for 10 minutes. B) TEM image demonstrating irreparable damage of cluster of bacterial cell surfaces when NP conjugated S. typhimurium bacterium were exposed to 676 nm NIR radiation for 10 minutes. C) Colonies of S. typhimurium bacteria demonstrating the presence of the live bacteria after exposure to 670 nm light for 10 minutes to C1) 5 x $10^4$ / ml S. typhimurium bacteria without NP. C2) 5 x $10^4$ / ml S. typhimurium bacteria in the presence of anti–Salmonella antibody coated NP. D) Colonies of bacteria demonstrating selectivity of our photo thermal lysis process. D1) $10^6$/ml E.coli bacteria in the presence of anti–Salmonella antibody coated NP. D2) $10^6$/ml S. typhimurium bacteria in the presence of anti–Salmonella antibody coated NP. (reprinted with permission from Ref. (21), Copyright 2010, Willey- VCH).*

After that, to demonstrate that our gold nanotechnology based assay can kill MDRB from food sample, we have reported (*23*) a photothermal assay to kill MDRB using MDRB *Salmonella DT104* infected romaine lettuce. Table 1 shows how laser irradiation time varies with the concentration of bacteria (CFU/gm) to kill 100% MDRB from MDRB infected lettuce sample. As shown in Table 1, 100 % of bacteria can be destroyed by 6 to 30 minutes laser irradiation treatment, depending on the MDRB concentration ($10^2$ -$10^7$ CFU/gm).

**Table 1. Laser irradiation time to kill 100% MDRB in lettuce samples. (reprinted with permission from Ref. (*23*), Copyright 2011, Royal Society)**

| *Concentration of MDRB (CFU/gm) in lettuce samples* | *Laser Irradiation Time (minutes) to Kill 100% Bcateria* |
|---|---|
| $10^2$ | 6 |
| $10^3$ | 9 |
| $10^4$ | 14 |
| $10^5$ | 20 |
| $10^6$ | 25 |
| $10^7$ | 30 |

## Conclusion and Outlooks

In this chapter, we have discussed the great potential of bio-conjugated nanomaterials for the possible application of MDRB diagnostics and photothermal treatment. We have shown that outstanding plasmonic properties of metal nanoparticles are useful for bacteria labeling, imaging and diagnosis. We have reported that bio-conjugated gold nanomaterials also can be served as "nanoscopic heaters" in the presence of suitable light, which are very useful for the selective killing of MDRB without antibiotics. Photothermal MDRB destruction strategies are completely different from conventional drug therapies, and as a result, its resistance is unlikely to happen soon. Though the use of bio-conjugated nanomaterial for MDRB sensing and killings are only just the beginning, it represents one of the highly promising areas of scientific inquiry into the biomedical clinical assay and food technology field. Since the prevalence of multiple drug resistant bacteria is on the rise, we and several other groups are continuing to explore this technology. We believe that it will likely lead to the development of exciting techniques or powerful combinations of existing ones for MDRB infection disease treatment.

While there are several advantages of using nanomaterial based assays, there still remain a number of challenges which needs to be solved before it will be useful for MDRB treatment. Problems such as nonspecific binding, aggregation, and environmental stability need to be addressed, before it can be used for sensing in complex environments with high background and the presence of competing targets. In parallel, and for each study, toxicity and side effects need to be addressed in a serious and systematic way as a function of nanoparticle size, shape, and surface coating. As a result, an understanding of biological response and environmental remediation is necessary before they can be used as new drug. Similarly, advancement in theoretical studies at nano-bio interfaces would be of great value and will probably need to grow rapidly as new and challenging experimental results are reported.

## Acknowledgments

Dr. Ray thanks NSF-PREM grant # DMR-0611539, NSF-CREST grant # HRD-0833178 and NSF-RISE grant # HRD-1137763 for their generous funding

## References

1. Nikaido, H. Multidrug Resistant in Bacteria. *Annu. Rev. Biochem.* **2009**, *78*, 119–146.
2. Andersson, D. I.; Hughes, D. Antibiotic resistant and its cost: is it possible to reverse resistant? *Nat. Rev.* **2010**, *8*, 260–271.
3. Ronholm, J.; Zhang, Z.; Cao, X.; Lin, M. Monoclonal Antibodies to Lipopolysaccharide Antigens of Salmonella enterica serotype Typhimurium DT104. *HYBRIDOMA* **2011**, *30*, 43–52.
4. Allen, H. K.; Donato, J.; Wang, H. H.; Cloud-Hansen, K. A.; Davies, J.; Handelsman, J. Call of the wild: antibiotic resistant genes in natural environments. *Nat. Rev. Microbiol.* **2010**, *8*, 251–259.
5. Chiu, C. H.; Su, L. H.; Chu, C. H.; Wang, M. H.; Yeh, C. M.; Weill, F. X.; Chu, C. Detection of Multidrug-Resistant Salmonella enterica Serovar Typhimurium Phage Types DT102, DT104, and U302 by Multiplex PCR. *J. Clin. Microbiol.* **2006**, *44*, 2354–2358.
6. Pignato, S.; Coniglio, M. A.; Faro, G.; Lefevre, M.; Weill, F.-X.; Giammanco, G. Molecular Epidemiology of Ampicillin Resistance in Salmonella spp. and Escherichia coli from Wastewater and Clinical Specimens. *Foodborne Pathog. Dis.* **2010**, *7*, 945–951.
7. Perron, G. G.; Quessy, S.; Letellier, A.; Bell, G. Genotypic diversity and antimicrobial resistance in asymptomatic *Salmonella enterica* serotype Typhimurium DT104. *Infect., Genet. Evol.* **2007**, *7*, 223–228.
8. Cabello, F. C. Aquaculture and florfenicol resistance in *Salmonella enterica* serovar Typhimurium DT104. *Emerging Infect. Dis.* **2009** (April), available from http://wwwnc.cdc.gov/eid/article/15/4/08-1171.htm.
9. World Health Organization, Tuberculosis (TB). Available from http://www.who.int/tb/challenges/mdr/en/index.html (accessed October 10, 2010).
10. Ram, S.; Vajpayee, P.; Shanker, R. Prevalence of Multi-Antimicrobial-Agent Resistant, Shiga Toxin and Enterotoxin Producing *Escherichia coli* in Surface Waters of River Ganga. *Environ. Sci. Technol.* **2007**, *41*, 7383–7388.

11. Smith, P. Aquaculture and florfenicol resistance in *Salmonella enterica* Typhimurium DT104. *Emerging Infect. Dis.* **2008**, *14*, 1327–8.
12. Patel, J. R.; Bhagwat, A. A.; Sanglay, G. C.; Solomon, M. B. Rapid detection of Salmonella from hydrodynamic pressure-treated poultry using molecular beacon real-time PCR. *Food Microbiol.* **2006**, *23*, 39–46.
13. Andersson, D. I. The biological cost of mutational antibiotic resistance: Any practical conclusions? *Curr. Opin. Microbiol.* **2006**, *9*, 461–465.
14. Vikesland, J.; Wigginton, K. R. Nanomaterial Enabled Biosensors for Pathogen Monitoring - A Review, Peter. *Environ. Sci. Technol.* **2010**, *44*, 3656–3669.
15. Khan, S. A.; Singh, A. K.; Senapati, D.; Fan, Z.; Ray, P. C. Nanomaterial for Targeted Detection and Photothermal Killing of Bacteria. *Chem. Soc. Rev.* **2012**in press.
16. Berry, V.; Gole, A.; Kundu, S.; Murphy, C. J.; Saraf, R. F. Deposition of CTAB-Terminated Nanorods on Bacteria to Form Highly Conducting Hybrid Systems. *J. Am. Chem. Soc.* **2005**, *127*, 17600–17602.
17. Norman, R. S.; Stone, J. W.; Gole, A.; Murphy, C. J.; Sabo-Attwood, T. L. Targeted Photothermal Lysis of the Pathogenic Bacteria, *Pseudomonas aeruginosa*, with Gold Nanorods. *Nano Lett.* **2008**, *8*, 302–306.
18. Wang, C.; Irudayaraj, J. Gold Nanorod probe for the Detection of Multiple Pathogens. *Small* **2008**, *4*, 2204–2208.
19. Zharov, V. P.; Mercer, K. E.; Galitovskaya, E. N.; Smeltzer, M. S. Photothermal Nanotherapeutics and Nanodiagnostics for Selective Killing of Bacteria Targeted with Gold Nanoparticles. *Biophys J.* **2006**, *90*, 619–627.
20. Singh, A. K.; Senapati, D.; Wang, S.; Griffin, J.; Neely, A.; Candice, P.; Naylor, K. M.; Varisli, B.; Kalluri, J. R.; Ray, P. C. Gold Nanorod Based Selective Identification of *Escherichia coli Bacteria* Using Two-Photon Rayleigh Scattering Spectroscopy. *ACS Nano* **2009**, *3*, 1906–1912.
21. Wang, S.; Singh, A. K.; Senapati, D.; Neely, A.; Yu, H.; Ray, P. C. Rapid Colorimetric Identification and Targeted Photothermal Lysis of Salmonella Bacteria by Using Bioconjugated Oval-shaped Gold Nanoparticles. *Chem. Eur. J.* **2010**, *16*, 5600–5606.
22. Khan, S. A.; Singh, A. K.; Senapati, D.; Fan, Z.; Ray, P. C. Targeted highly sensitive detection of multi-drug resistant salmonella DT104 using gold nanoparticles. *Chem. Commun* **2011**, *47*, 9444–9446.
23. Khan, S. A.; Singh, A. K.; Senapati, D.; Fan, Z.; Ray, P. C. Targeted highly sensitive detection of multi-drug resistant salmonella DT104 using gold nanoparticles. *J. Mater. Chem.* **2011**, *21*, 17705–17709.
24. Donath, E. Biosensors: Viruses for Ultrasensitive Assays. *Nat. Nanotech.* **2009**, *4*, 215–216.
25. Ravindranath, S. O.; Mauer, J. L.; Deb-Roy, C.; Irudayaraj, J. Biofunctionalized Magnetic Nanoparticle Integrated Mid-Infrared Pathogen Sensor for Food Matrixes. *Anal. Chem.* **2009**, *81*, 2840–2846.
26. Liu, X.; Dai, Q.; Austin, L.; Coutts, J.; Knowles, G.; Zou, J.; Chen, H.; Huo, Q. One-Step Homogeneous Immunoassay for Cancer Biomarker Detection Using Gold Nanoparticle Probes Coupled with Dynamic Light Scattering. *J. Am. Chem. Soc.* **2008**, *130*, 2780–2782.

27. Golightly, R. S.; Doering, W. E.; Natan, M. J. Surface-Enhanced Raman Spectroscopy and Homeland Security: A Perfect Match? *ACS Nano* **2009**, *3*, 2859–2869.
28. Kell, A. J.; Stewart, G.; Ryan, S.; Peytavi, R.; Boissinot, B.; Huletsky, A.; Bergeron, M. G.; Simard, B. Vancomycin-Modified Nanoparticles for Efficient Targeting and Preconcentration of Gram-Positive and Gram-Negative Bacteria. *ACS Nano* **2008**, *2*, 1777–1788.
29. Chen, T.; Wang, H.; Chen, G.; Wang, Y.; Feng, Y.; Teo, W. S.; Wu, T.; Chen, H. Hotspot-Induced Transformation of Surface-Enhanced Raman Scattering Fingerprints. *ACS Nano* **2010**, *4*, 3087–3094.
30. Ray, P. C. Size and Shape Dependent Second Order Nonlinear Optical Properties of Nanomaterials and Their Application in Biological and Chemical Sensing. *Chem. Rev.* **2010**, *110*, 5332–5365.
31. Huang, X.; El-Sayed, I. H.; Qian, W.; El-Sayed, M. A. Cancer Cell Imaging and Photothermal Therapy in the Near-Infrared Region by Using Gold Nanorods. *J. Am. Chem. Soc.* **2006**, *128*, 2115–2120.
32. Singh, A. K.; Lu, W.; Senapati, D.; Khan, S. A.; Fan, Z.; Senapati, T.; Demeritte, T.; Beqa, L.; Ray, P. C. Long-Range Nanoparticle Surface-Energy-Transfer Ruler for Monitoring Photothermal Therapy Response. *Small* **2011**, *7*, 2517–2525.
33. Lu, W.; Singh, A. K.; Khan, S. A.; Senapati, D.; Yu, H.; Ray, P. C. Gold Nano-Popcorn-Based Targeted Diagnosis, Nanotherapy Treatment, and In Situ Monitoring of Photothermal Therapy Response of Prostate Cancer Cells Using Surface-Enhanced Raman Spectroscopy. *J. Am. Chem. Soc.* **2010**, *132*, 18103–18114.
34. Kaittanis, C.; Santra, S.; Perez, J. M. Role of Nanoparticle Valency in the Nondestructive Magnetic-Relaxation-Mediated Detection and Magnetic Isolation of Cells in Complex Media. *J. Am. Chem. Soc.* **2009**, *131*, 12780–12791.
35. Xie, J.; Zhang, Q.; Lee, J. Y.; Wang, D. I. The Synthesis of SERS-Active Gold Nanoflower Tags for *In Vivo* Applications. *ACS Nano* **2008**, *2*, 2472–2480.
36. Rule, K. L.; Vikesland, P. J. Surface-Enhanced Resonance Raman Spectroscopy for the Rapid Detection of Cryptosporidium parvum and Giardia lamblia. *Environ. Sci. Technol.* **2009**, *43*, 1147–1152.
37. Li, F.; Zhao, Q.; Wang, C.; Lu, X.; Li, X. F.; Le, X. C. Detection of *Escherichia coli* O157:H7 Using Gold Nanoparticle Labeling and Inductively Coupled Plasma Mass Spectrometry. *Anal. Chem.* **2010**, *82*, 3399–3403.
38. Jain, P. K.; Huang, X.; El-Sayed, I. H.; El-Sayed, M. A. Noble Metals on the Nanoscale: Optical and Photothermal Properties and Some Applications in Imaging, Sensing, Biology, and Medicine. *Acc. Chem. Res.* **2008**, *41*, 1578–1586.
39. Lu, W.; Arumugam, S. R.; Senapati, D.; Singh, A. K.; Arbneshi, T.; Khan, S. A.; Yu, H.; Ray, P. C. Multifunctional Oval Shape Gold Nanoparticle Based Selective Detection of Breast Cancer Cells Using Simple Colorimetric and Highly Sensitive Two-Photon Scattering Assay. *ACS Nano* **2010**, *4*, 1739–1749.

40. Dasary, S. S. R.; Singh, A. K.; Senapati, D.; Yu, H.; Ray, P. C. Gold Nanoparticle Based Label-Free SERS Probe for Ultrasensitive and Selective Detection of Trinitrotoluene. *J. Am. Chem. Soc.* **2009**, *131*, 13806–13812.
41. Neely, A.; Perry, C.; Varisli, B.; Singh, A. K.; Arbneshi, T.; Senapati, D.; Kalluri, J. R.; Ray, P. C. Ultrasensitive and Highly Selective Detection of Alzheimer's Disease Biomarker Using Two-Photon Rayleigh Scattering Properties of Gold Nanoparticle. *ACS Nano* **2009**, *3*, 2834–284.
42. Griffin, J.; Singh, A. K.; Senapati, D.; Lee, E.; Gaylor, J.; Boone, J. J.; Ray, P. C. Sequence Specific HCV-RNA Quantification Using Size Dependent Nonlinear Optical Properties of Gold Nanoparticles. *Small* **2009**, *5*, 839–845.
43. Griffin, J.; Singh, A. K.; Senapati, D.; Rhodes, P.; Mitchell, K.; Robinson, B.; Yu, E.; Ray, P. C. Size and Distance Dependent NSET Ruler for Selective Sensing of Hepatitis C virus RNA. *Chem. Eur. J.* **2009**, *15*, 342–351.
44. Darbha, G. K.; Rai, U. S.; Singh, A. K.; Ray, P. C. Highly Selective detection of $Hg^{2+}$ ion using NLO properties of gold nanomaterial. *J. Am. Chem. Soc.* **2008**, *130*, 8038–8042.
45. Griffin, J.; Ray, P. C. Gold Nanoparticle Based NSET For Monitoring $Mg^{2+}$ Dependent RNA Folding. *J. Phys. Chem. B* **2008**, *112*, 11198–11201.
46. Schmucker, A. L.; Harris, N.; Banholzer, M. J.; Blaber, M. G.; Osberg, K. D.; Schatz, G. C.; Mirkin, C. A. Correlating Nanorod Structure with Experimentally Measured and Theoretically Predicted Surface Plasmon Resonance. *ACS Nano* **2010**, *4*, 5453–5463.
47. Darbha, G. K.; Ray, S.; Ray, P. C. Gold-nanoparticle-based miniaturized FRET Probe for rapid and ultra-sensitive detection of mercury in soil, water and fish. *ACS Nano* **2007**, *3*, 208–214.
48. Ray, P. C. Label-Free Diagnostics of single base-mismatch DNA hybridization on Gold Nano-particles using hyper-Rayleigh scattering technique. *Angew. Chem., Int. Ed.* **2006**, *45*, 1151–1154.
49. Wijaya, A.; Schaffer, S. B.; Pallares, I. G.; Kimberly, H.-S. Selective Release of Multiple DNA Oligonucleotides from Gold Nanorods. *ACS Nano* **2009**, *3*, 80–86.
50. Cao, Y. W. C.; Jin, R. C.; Mirkin, C. A. Nanoparticles with Raman spectroscopic fingerprints for DNA and RNA detection. *Science* **2002**, *297*, 1536–1540.
51. Nie, S.; Emory, S. R. Probing Single Molecules and Single Nanoparticles by Surface-Enhanced Raman Scattering. *Science* **1997**, *275*, 1102–1104.
52. Giljohann, D. A.; Seferos, D. S.; Prigodich, A. E.; Patel, P. C.; Mirkin, C. A. Gene regulation with polyvalent siRNA-nanoparticle conjugates. *J. Am. Chem. Soc.* **2009**, *131*, 2072–2073.
53. Porter, M. D.; Lipert, R. J.; Siperko, L. M.; Wang, G.; Narayanana, R. SERS as a bioassay platform: fundamentals, design, and applications. *Chem. Soc. Rev.* **2008**, *37*, 1001–1011.
54. Tiwari, V. S.; Oleg, T.; Darbha, G. K.; Hardy, W.; Singh, J. P.; Ray, P. C. Non-resonance SERS Effects of Silver Colloids with Different Shapes. *Chem. Phys. Lett.* **2007**, *446*, 77–82.

55. Casadi, F.; Leona, M.; Lombardi, J. R.; Van Duyne, R. Identification of Organic Colorants in Fibers, Paints, and Glazes by Surface Enhanced Raman Spectroscopy. *Acc. Chem. Res.* **2010**, *43*, 782–791.
56. Brus, L. Noble Metal Nanocrystals: Plasmon Electron Transfer Photochemistry and Single-Molecule Raman Spectroscopy. *Acc. Chem. Res.* **2008**, *41*, 1742–1749.
57. Pallaoro, A.; Braun, G. B.; Reich, N. O.; Moskovits, M. Mapping Local pH in Live Cells Using Encapsulated Fluorescent SERS Nanotags. *Small* **2010**, *6*, 618–622.
58. Baik, J. M.; Lee, S. J.; Moskovits, M. Polarized Surface-Enhanced Raman Spectroscopy from Molecules Adsorbed in Nano-Gaps Produced by Electromigration in Silver Nanowires. *Nano Lett.* **2009**, *9*, 672–676.
59. Yan, B.; Thubagere, A.; Premasiri, R. W.; Ziegler, L. D.; Negro, L. D.; Reinhard, B. M. Engineered SERS Substrates with Multiscale Signal Enhancement: Nanoparticle Cluster Arrays. *ACS Nano* **2009**, *3*, 1190–1202.
60. Lu, W.; Singh, A. K.; Khan, S. A.; Senapati, D.; Yu, H.; Ray, P. C. Gold Nano-Popcorn Based Targeted Diagonosis, Nanotherapy Treatment and In-Situ Monitoring of Photothermal Therapy Response of Prostate Cancer Cells Using Surface Enhanced Raman Spectroscopy. *J. Am. Chem. Soc.* **2010**, *132*, 18103–18114.
61. Lorenzo, L. R.; Javier, F.; Abajo, G.; Liz-Marzn, L. M. Surface Enhanced Raman Scattering Using Star-Shaped Gold Colloidal Nanoparticles. *J. Phys. Chem. C* **2010**, *114*, 7336–7340.
62. Khoury, C. G.; Vo-Dinh, T. Gold Nanostars For Surface-Enhanced Raman Scattering: Synthesis, Characterization and Optimization. *J. Phys. Chem. C* **2008**, *112*, 18849–18859.
63. Hu, Y. S.; Jeon, J.; Seok, T. J.; Lee, S.; Hafner, J. H.; Drezek, R. A.; Choo, H. Enhanced Raman Scattering from Nanoparticle-Decorated Nanocone Substrates: A Practical Approach to Harness In-Plane Excitation. *ACS Nano* **2010**, *4*, 5721–5730.
64. Dondapati, S. K.; Sau, T. K.; Hrelescu, C.; Klar, T. A.; Stefani, F. D.; Feldmann, J. Label-free Biosensing Based on Single Gold Nanostars as Plasmonic Transducers. *ACS Nano* **2010**, *4*, 6318–6322.
65. Song, H. M.; Wei, Q.; Ong, Q. K.; Wei, A. Plasmon-Resonant Nanoparticles and Nanostars with Magnetic Cores: Synthesis and Magnetomotive Imaging. *ACS Nano* **2010**, *4*, 5163–5173.
66. Zelada-Guillén, G. A.; Riu, J.; Düzgün, A.; Rius, F. X. Immediate Detection of Living Bacteria at Ultralow Concentrations Using a Carbon Nanotube Based Potentiometric Aptasensor. *Angew. Chem., Int. Ed.* **2009**, *48*, 7334–7337.
67. Antoine, I. R.; Benichou, E.; Bachelier, G.; Jonin, C.; Brevet, P. F. Multipolar Contributions of the Second Harmonic Generation from Silver and Gold Nanoparticles. *J. Phys. Chem. C* **2007**, *111*, 9044–9048.
68. Dadap, J. I.; Shan, J.; Eisenthal, K. B.; Heinz, T. F. Second-Harmonic Rayleigh Scattering from a Sphere of Centrosymmetric Materials. *Phys. Rev. Lett.* **1999**, *83*, 4045.

69. Chandra, M.; Indi, S.; Das, P. K. Depolarized Hyper-Rayleigh Scattering from Copper Nanoparticles. *J. Phys. Chem. C* **2007**, *111*, 10652–10656.
70. Darbha, G. K.; Rai, U. S.; Singh, A. K.; Ray, P. C. Gold Nanorod Based Sensing of Sequence Specific HIV-1 Virus DNA Using Hyper Rayleigh Scattering Spectroscopy. *Chem. Eur. J.* **2008**, *14*, 3896–3903.
71. Duboisset, I. R.-A.; Benichou, E.; Bachelier, G.; Jonin, C.; Brevet, P. F. Single Metallic Nanoparticle Sensitivity with Hyper Rayleigh Scattering. *J. Phys. Chem. C* **2009**, *113*, 13477–13481.
72. Clays, K.; Persoons, A. Hyper-Rayleigh Scattering in Solution. *Phys. Rev. Lett.* **1991**, *66*, 2980–2983.
73. Terhune, R. W.; Maker, P. D.; Savage, C. M. Measurements of Nonlinear Light Scattering. *Phys. Rev. Lett.* **1965**, *14*, 681.
74. Reeve, J. E.; Collins, A. H.; Mey, K. D.; Kohl, M. M.; Thorley, K. T.; Paulsen, O.; Clays, K.; Anderson, H. L. Modulated Conjugation as a Means of Improving the Intrinsic Hyperpolarizability. *J. Am. Chem. Soc.* **2009**, *131*, 2758–2759.

## Chapter 6

# Historical Overview of the First Two Waves of Bactericidal Agents and Development of the Third Wave of Potent Disinfectants

**J. Liu,[1,2] K. Chamakura,[3] R. Perez-Ballestero,[3] and S. Bashir*,[4]**

[1]**Department of Chemistry, Texas A&M University-Kingsville, MSC 161,**
**700 University Blvd., Kingsville, Texas 78363, U.S.A.**
[2]**Department of Chemistry, Texas A&M University, P.O. Box 30012,**
**College Station, Texas 77842-3012, U.S.A.**
[3]**Department of Biological and Health Sciences,**
**Texas A&M University-Kingsville, MSC 158, 700 University Blvd.,**
**Kingsville, Texas 78363, U.S.A.**
[4]**Chemical Biology Research Group, Texas A&M University-Kingsville,**
**MSC 161, 700 University Blvd., Kingsville, Texas 78363, U.S.A.**
***E-mail: br9@tamuk.edu**

Certain microorganisms could cause disease and morbidity. Disinfection science was used as a “shield” for protection of human health, including access and availability to clean water. Two broad strategies were used, physical separation, purification, chemical inhibition, and sterilization. In the field of chemical disinfection, three chemicals were widely used, alcohols, phenols and bleach. Adjunct to use of chemical disinfectants was the use of metals or metal oxides, such as silver or titania. Silver has been used for years and has recently been re-evaluated due to the advent of nanotechnology. Silver nanoparticles have been extensively used in the treatment of disease and purification and heralded the ‘second wave’ of disinfection science, the ‘first wave’ being physical and chemical disinfection based on organic and inorganic compounds or salts. Recent advances in structured or engineered surfaces like zeolites has enabled ultrahigh surface area and rapid sterilization through the use of metal organic

In Nanomaterials for Biomedicine; Nagarajan, R.;
ACS Symposium Series; American Chemical Society: Washington, DC, 2012.

frameworks (MOFs) as the ‘third wave’ of disinfection science. MOFs offer the same advantages as colloids but also have ultra-high surface area, long-term persistence and ultra-low doses, which will be applied toward water purification.

## Prelog: Disinfection Science

In this book chapter, only chemical disinfectants of bacteria will be discussed in the form of supplemental tables and summaries; with a brief overview of physical methods followed by chemical in general followed by halogen/ozone/hydrogen peroxide and finally use of metal nanoparticles and comparison with our current results. Following the introduction, a brief experimental design to assess bleach and phenol and silver nanoparticles will be described including characterization methods. The related results, advantages and disadvantages of each type of disinfectant will be stated, followed by a comparison with current literature. The context of the results will be discussed in terms of mechanisms of inhibition and our findings will be compared and contrasted with other literature findings of similar systems. Lastly, a new approach using metal organic frameworks will be briefly described and concluded with future trends in the area of disinfection science with particular emphasis of use of metal/metal-oxide nanoparticles and metal organic framework based disinfectants towards water purification, surface sterilization and possible uses in health care.

## Introduction

### Introduction to Disinfection Science: A Historical Overview

Between 1840-1857, three scientists, Ignaz Semmelweis (*1*), Louis Pasteur (*2*) and Joseph Lister (*3*) had demonstrated that microbes could cause disease and that disinfection through chemical means such as with bleach (Semmelweis used a mixture of calcium chloride hypochlorite, calcium hypochloride and calcium chloride) or heat treatment (pasteurization), or bandages treated with phenol greatly reduced the transmission of disease. Robert Koch (between 1876-1884) has set the foundation of the science of microbiology and evaluation of chemicals that could be used toward disinfection or disease-control as demonstrated by Rideal and Walker (*4*). The approach required for “standard “ *in vitro* “procedures (*5*)” using specific strains such as *Staphylococcus aureus* (ATCC 6538), *Pseudomonas aeruginosa* (ATCC 15422) using the proscribed dilution method (*6*), although other microorganism were also evaluated such as *Escherichia coli* (*7*). These protocols firmly established the profound benefits of sterilization (for inanimate matter (*8*)) and antisepsis (for living matter) (*9*). As early as 1900, a review of the literature in a report to the committee on disinfectants identified the following candidates: formaldehyde, mercuric chloride, chloride of lime [calcium (hydroxide/chloride/hypochlorite)], sulphurous acid, phenol, copper sulphate, zinc chloride, quick lime [calcium oxide ] and boiling of water (*10*), some of which are used today, which relay on chemical or physical methods (*11–15*) towards disinfection.

The effectiveness of a particular treatment has been quantified by using the decimal reduction time (D value, in units of time) defined as the time at fixed temperature and pressure required for one log reduction of a the initial colony forming units, for example plotting colony forming units (CFUs) versus time, the rate of decrease can be calculated. If the log decrease in CFU is repotted against time, the D value can be directly obtained from the gradient as the negative reciprocal. If the D value for the same microbe is plotted against changes in temperatures at fixed pressure, the "sensitivity" of the microbe to heat can also be determined, this value has been dubbed the Z value (in units of temperature) (*16*). The time and temperature for disinfection is dependent on the type of microbe, its growth cycle and with microbial spores requiring higher temperatures (*17*). The actual temperature/pressure profile is related to type of media (for example whether milk, fruit juice, alcohol is being used), but one general method that could apply to a broad range of food stuffs, medical equipment or storage containers is rapid heating at 150 °C for 10 seconds under steam convection or heating at 75 °C and cooling for an extended period of time for temperature-sensitive liquids, fabrics or equipment (*18*) by following standard operation procedures, such as outlined by the food and drug administration or other regulatory agencies (*19*).

## The First Wave Disinfectant: A Historical Overview

Chemical disinfectants are chemicals that inhibit and inactivate microbes. Since microbes are living biological organism, which may use oxygen as their terminal electron acceptor (aerobic respiration) or other, small molecules in the absence of oxygen (anaerobic respiration), possible intervention at physical or electrochemical disruption can lead to inhibition of growth and cellular inactivation. Inhibition can be achieved chemically, the specific disinfectant classified based on the functional group or mode of inhibition e.g. acid, base, detergent, respiration inhibitor respectfully, following published guidelines, set forth by the federal government or professional associations, such as association for professionals in infection control and epidemiology (*20*).

Citric fruit, such as oranges are known to spoil slowly unlike other fruits such as bananas and reason for this is thought to be due to citric acid, which has been used as a disinfectant. The principal advantages of acid based disinfectants are speed of action (almost immediate) and lower costs and negligible toxicity to humans (for weak acids).

The halogens (*21–25*) are potent oxidants, with chlorine being the most commonly used oxidants from the family. Chlorine, unlike iodine is a gas at room temperature and as a disinfectant is in the form of hypochlorite or hypochlorous anion, the most widely used being as the sodium salt of hypochlorite. As in the case of iodine, the disinfectant 'strength' is related to concentration of the oxidizing agent, whether the agent is in 'free' form, or whether it is slowly release as was shown for poviodine-iodine or as chloramines for release of chlorine. Sodium hypochlorite (bleach) is light yellow liquid with 5 % chlorine. Bleach is probably one of the most widely used forms of disinfection of water, medical equipment and households in the ppm range.

Peroxides (*26*) are compounds with the oxidation state for oxygen of minus one, are diamagnetic, and are similar to superoxide and ozonides, which have the same oxidation, state, and unlike peroxides are paramagnetic and prone to radical ion formation. Examples of peroxides include hydrogen or benzoyl peroxide, which is a strong oxidizing agent and is used in disinfection and sterilization including wound infection. Hydrogen peroxide is generally obtained as a dilute solution (< 5%) and rapidly decomposes and comes in a formulation with other chemical additives as stabilizers towards decomposition. Ozone is a gas which is known to absorb UV radiation, but can be used in the formation of reactive oxygen species including hydroxide radical and hydroperoxyl ($HO_2$) radicals, including peroxide and superoxide (oxidation state minus one-half), which cause microbial lysis. The peroxides are generally used at concentrations of less than 5% and slightly higher percentage as a bleaching agent, with higher percentages used for sterilization. As a disinfectant, hydrogen peroxide like bleach is fast acting and used in the ppm range, to reduce the microbial population by 90% (decimal reduction time, D) within minutes and may be used in gaseous or vapor form for disinfection of entire rooms. For disinfection of water, ozone is used in less than 1 ppm, with hydrogen peroxide in the low ppm is effective more against Gram-positive than Gram-negative microbes. The problem with these disinfectants are disinfection by-products, possible corrosion of the container, such as iron containers, slow acting of benozyl peroxide due to its low solubility in water or bleaching effect of hydrogen peroxide.

Phenol, one of the oldest chemical disinfectants (*27*, *28*) was used as an antiseptic spray was by Joseph Lister (1900s) in the form of triclosan, a mixture of salicylic acid and chloroxylenol and is a stronger acid than aliphatic alcohols. The formulation used is in the form of a micelle or detergent and are applied to a wide array of microbes and surfaces, generally in low ppm. Phenol itself is water-soluble and used as a standard disinfectant to which new forms of disinfectants are compared to in terms of D-value of phenol (P value coefficient). The general effectiveness of phenol as a disinfectant is against Gram-positive microbes. Since phenol or phenol-based disinfectants have been used in many settings for over a century, with over usage has led to some microbial resistance. Salicylic acid is a co-additive to the above, which is also an anti-inflammatory agent, in the form of antimicrobial soaps or detergents or cleaning agents, usually at 1000 ppm, have like phenols been used against a wide variety of microbes, particularly Gram-positive microbes (*21–23*, *26–29*).

## Mechanism of Inhibition of Chemical Disinfectants

The above introduction to chemical disinfectants (*30–32*) can be considered the '*first wave*' and have been shown to be effective for a wide-variety of uses including disinfection and sterilization. Review of Figure 1 indicates that inhibition is achieved through a number of different processes discussed above. Briefly, physical destruction of the cell wall, membrane or macromolecules can be achieved, or oxidation of cellular machinery such as nucleic acids or proteins or membrane glycoproteins would cause disruption of critical systems. Other processes are mechanical disruption of certain regions, such as introduction of cellular pores, cross-linking of amino acids or nucleotides would cause disruption and microbial inactivation.

The mechanism (*33–43*) by which acids inhibit microbe are varied, but can be generalized as follows: Strong acids (*33*) lead to total dissociation and a lower pH, the low acidic environment disrupts the electrical membrane potential (due to disruption of proton motive force), hijacking the normal machinery of the microbe for nutrient uptake and storage, in addition to modification and potential oxidation of surface lipids or proteins. For weak acids, the lowering of the pH is not an issue, since the pH is between 4-5, which may also be sufficient to disrupt the membrane potential, uptake, storage and utilization of essential nutrients, leading to disruption of ATP. Other disruptions may include mis-match in macromolecule synthesis, such as where proteins or nucleic acid are covalently cross-linked at specific amino acids, such as cysteine. This linking will eventually leading to disruption of oxidation phosphorylation and inhibition of respiration particularly with ester derivatives of the acids that may interaction with the microbial lipid structures more efficiently than acids. With bases, partial solubilization (*37*) of the membrane may occur due to occurrence of phospholipids, lipids and fatty acids. Disruption of the cell wall (for Gram-negative microbes) and plasma membrane will cause lysis, protein degradation, similar to processes involved with acids. Alcohols (*34*) assist with protein denaturation, cross-linking through hydrogen bonding and membrane lysis (*35*). Anilides and Diamides class (*36*) of disinfectants such as tribromsalan and propamidine respectfully are effective against Gram-positive bacteria (*37*), but have limited use as disinfectants. The former class inhibit through interaction with the plasma membrane leading to disruption of the lipid bilayer. The latter have been shown to be effective against gram-positive bacteria.

The mode of action of peroxides is through oxidation of the membrane or macromolecules, for example for chlorine the active species is the hypochlorous anion. The targets for oxidation are sulfhydryl groups in cysteine amino acids, and oxidation of other amino acids in general, membrane lipids, sugars and membrane proteins respectfully affecting oxidative phosphorylation leading to cell death. Oxidation can be achieved directly through donation (transfer) of oxygen, or acceptance of electrons. Since this process is mutually exclusive, the electron acceptor becomes reduced and the electron donor becomes oxidized. Common examples include the halogens (*38*), producing halogen anion (or trianion for iodine); mineral acids producing the oxide/dioxide; bleach, producing water and the halide anion; oxygen producing oxides, water and carbon dioxide; ozone producing oxidation by-products and water and permanganate producing the metal cation and/or metal oxide' and peroxides producing oxides and water (*39–42*).

Phenols (*43*) are known to increase the cell wall permeability through interaction with cell wall enzymes via the hydroxyl moiety of the parent molecule, leading to ion leakage and membrane lysis. Increased permeability will disrupt the membrane potential due to uncoupling of proton motive force and oxidative phosphorylation, in addition to disruption of key kinases, isomerases and decarboxylases. One example is that triclosan is known to inhibit enoyl reductase, in addition to membrane insertion into lipid components (*58*). Triclosan is a heterodimer of dichlorophenoxy and chlorophenol, while hexachlorophene and chloroxylenol are other derivatives, which have been used.

Lastly, since all living cells required chemical energy to reproduce, grow or undergo regeneration or repairs, chemical energy is obtained indirectly from raw materials via redox processes (*44*) or directly from sunlight, also using redox processes (*45*), albeit of a different kind and any disruption of these processes would be vital (*46*). These modes of action are in five groupings and are summarized in Figure 1.

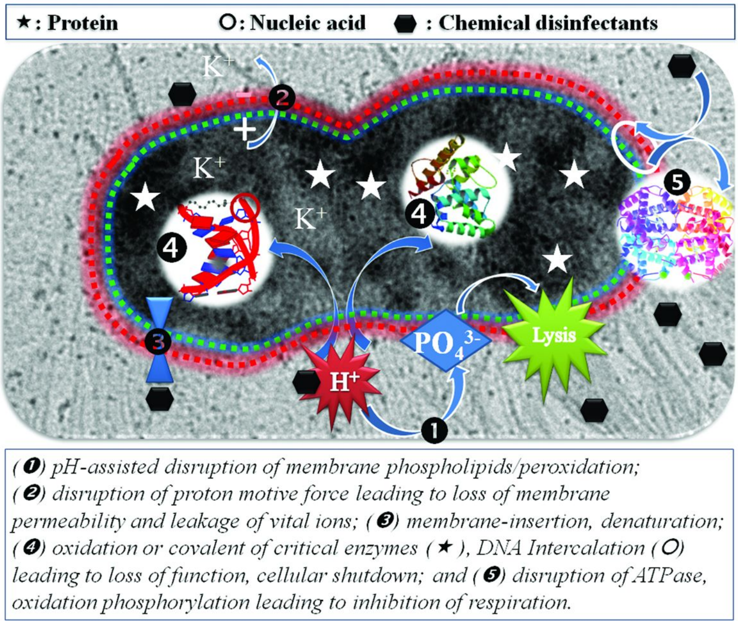

*(❶) pH-assisted disruption of membrane phospholipids/peroxidation; (❷) disruption of proton motive force leading to loss of membrane permeability and leakage of vital ions; (❸) membrane-insertion, denaturation; (❹) oxidation or covalent of critical enzymes (★), DNA Intercalation (O) leading to loss of function, cellular shutdown; and (❺) disruption of ATPase, oxidation phosphorylation leading to inhibition of respiration.*

*Figure 1. Chemical disinfectants interact through many avenues. Five general processes are: (1) pH-assisted disruption of membrane phospholipids/peroxidation leading to membrane rupture; (2) disruption of proton motive force leading to loss of membrane permeability and leakage of vital ions; (3) membrane-insertion, denaturation and loss of function; (4) oxidation or covalent of critical enzymes (star) such as enoyl reductase, kinases, decarboxylases and/or covalent modification of topoisomerases, DNA Intercalation (○, e.g at the minor groove) leading to loss of function, cellular shutdown; and (5) disruption of ATPase, oxidation phosphorylation leading to inhibition of respiration.*

## The Second Wave: A Historical Overview

Recently a newer approach as the '*second wave*' has been evaluated in the last four decades, using metal or metal oxides as disinfectants (*47–50*). Metals can be group into three categories, metals that in trace amounts are essential for metabolic processes, metals with in higher amounts are toxic and metals, which are toxic and not involved in biochemical, processes (*51*). Copper has historically been used by bakers as a sterilization agent in chimney fumes to inactivated any yeast and when accumulated can be toxic. Silver has been used in ancient times either as metal silver, or in the form of 1% silver sulfadiazine solution to prevent wound infection (*52*) or surface sterilization. Compared to their chemical disinfectants (*33–43*) metals have distinct advantages particularly when in emulsion/colloidal form. In recent times, silver has been reevaluated in the form of nanoparticles (*54–62*).

The use of small clusters of metals or colloids is not a recent phenomenon, Faraday (1850s) was fabricating colloidal-gold (3-30 nm) and realized that colloidal-gold in the nanometer range has chemical and physical properties not found in bulk gold (*63*). The reasons for the difference are due to the volume occupied by the electron. In metals, the electrons occupy a large volume, in that the separation between the valence (semi-conductor or insulator-like properties) and conductance (metal-like properties) is negligible, yielding a conducting material, with a very radius. If the separation were to increase or become slightly larger (than *kT*) semiconductor properties would be observed and further the separation then insulator properties would be observed. These electronic properties depend upon the relationship between the work function and the electron affinity or ionization of the atom or the dielectric constant. As the dimensions are reduced to slightly greater than Bohr radius, the work function is smaller than the ionization energy or electron affinity, the metal clusters are electronically stable because they have a particular separation which affords thermodynamic and electronic stability (e.g. clusters size of 13, 55 and so forth) (*64*) and large surface area to volume ratio, giving each atom within the cluster and 'active' surface for chemical reactions to occur (*65*), because unlike the bulk metal, the majority of atoms are exposed to the environment, in which the orbital symmetry and energy of each atom facilitate rapid catalysis (*66*), a fact well known since many catalysts are dispersed as fine powders. Optically reduction in size, will restrict the volume over which the electron moves (below the electron mean free path) resulting in coherent oscillations over the cluster with electromagnetic radiation of light, yielding visible colors (*67*). These surface plasmon absorption of noble metals have application in (photo)catalysis (*68*), optoelectronics (*69*) and storage devices (*70*), as well as sensors (*71*) and disinfectants (*72*). A consequence of this "down-sizing" is that many structural isomers can be constructed using the same number of atoms, many of which have similar binding energies (*73*), and that the final geometry is strongly dependent on the synthesis procedure (*74*). Through selective use of solvent polarity, pH, temperature, whether chemical (*75*) or radiolytic (*76*) reducing agent are employed, other dispersing agents, speed of mixing, and whether different cluster sizes or range of sizes and shapes (*77*). Use of zeolites (*78*) or polymer templates (*79*) can thus allow one, two and three-dimensional surfaces to be constructed, each of which is highly active (*80*). Their historical use as catalysts in synthesis have been supplemented as disinfectants, nothing that the cluster dimensions can be engineered to be smaller than or equal to the microbe. This has allowed bulk metals such as zinc, copper, silver to be reused as potent nano-bactericidal agents.

## Mechanism of Inhibition of Metal/Transition Metal Oxide Based Disinfectants

The mode of action of these metals is similar to chemical disinfectants (*34–42*, *53*), with a few subtle differences. Metal ions can diffuse into the membrane and disrupt cell membrane proteins, promoting metal-assisted catalysis of reactive oxygen species, such as hydroxyl radicals, in addition to nucleic acid binding, which is general to metal ions (*81*). Since the metal species is not consumed, its time of action (or persistence) can be considerably longer than chemical disinfectants such as bleach. In addition, silver is known to irreversibly-bind to cysteine, causing protein denaturation, changes in permeability of the cell and inhibition of respiration through disruption of cytochromes, proton motive force of the membrane and oxidative phosphorylation (*82*). In the form of silver sulfadiazine, additional wall damage is observed in the form of micro vesicle formation and nucleic acid denaturation. Titania is a transition metal oxide and has been extensively used in water purification and disinfection particularly with Gram-negative microbes through photocatalytic oxidation and generation of reactive oxygen species (ROS), usually coupled with ultraviolet radiation. The role of titania is to provide an active surface for catalysis to proceed and the role of UV to supply sufficient energy to break chemical bonds (*83*). The role of UV irradiation can be replaced through introduction of a metal center, such as silver, which would supply electrons to the titania to complete the catalysis and generation of ROS (*84*). Thus fabrication of nanocomposites such as silver-titania would enable disinfectant water under visible light conditions, primarily through ROS-mediated pathways.

The formulations of nanodisperant colloids (e.g. silver, titania and other transition metal/metal oxides) had led to a resurgence of interest in their application in water disinfection science (*54–62*). These '*second wave*' class of disinfectants has been evaluated against a vast array of microorganisms and appear to be effective at inhibiting microbes. This reevaluation is due to precise control of surfaces (both dimensionally and macroscopically) including formulation of defined optioelectrical and magnetic properties. Lastly, unlike certain chemical disinfectants, these nanocolloid systems have longer persistence and can be effective at much lower doses, thereby minimizing generation of potential disinfection by-products.

The mechanism by which inhibition is achieved is multifold but appears to involve cellular disruption either directly (membrane insertion/ change in cellular permeability/ nucleic acid or protein denaturation) or indirectly through generation of reactive oxygen species as summarized in Figure 2. Although a generalization, inhibition may be achieve using four approaches: membrane insertion and lysis of the cell wall (1), metal-catalyzed generation of reactive oxygen species (2) which also weaken the cell membrane, leading to protein (star) or nucleic acid (○) denaturation, disruption of membrane respiration enzymes (3) and inhibition of cellular replication through covalent modification of nucleic acid base-pairs (4).These four general methods may be employed towards microbial inactivation based on data from numerous studies (*54–62*).

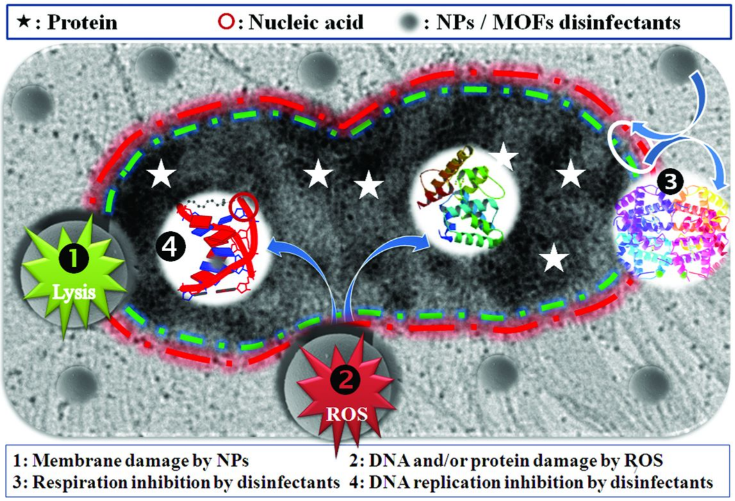
★: Protein
O: Nucleic acid
●: NPs / MOFs disinfectants
1
Lysis
2
ROS
3
4
1: Membrane damage by NPs
2: DNA and/or protein damage by ROS
3: Respiration inhibition by disinfectants
4: DNA replication inhibition by disinfectants

*Figure 2. Silver atoms or ions may be release (beginning of arrow 4), which may directly interact with phospholipids of the outer membrane, in addition to metal catalyzed generation of radical or reactive species, which cause lipid peroxidation; direct membrane insertion via membrane insertion leading to increased membrane permeability and loss of membrane potential (2); mechanical weakening of the cell wall through complexation of wall proteins, lipids and/or glycans leading to mechanical failure of the wall (1); once migrated into the cytoplasm, additional oxidation of critical proteins (star) and nucleic acids (○) leading to protein denaturation and nucleic acid fragmentation (end of arrow 4); binding to respiratory proteins inhibiting electron transport (3).*

## The Third Wave: A Historical Overview

The basic concept of using structured one-dimensional (colloids) (*85*), two-dimensional (films) (*86*), three-dimensional (cages, MOFs) (*87*) without additional supports or with structured supports such as nanotubes (*88*), chitosan (*89*), silica (*90*) and polymers (*91*) has been established for a wide variety of uses including disinfection and microbial inactivation (*92*). Structured arrays like metal organic frameworks are central metal ion coordinated within an organic lattice framework. This provides a very high internal surface area, structured internal pores that can retain solvent and enable coordinate between the MOF and microbe surfaces, in addition to the ability of the outer surface separately interacting with the microbe surface. This provides great flexibility and has recently been demonstrated first by the J. Liu Group in 2010 (*87*) and separately by another study (*93*). The former demonstrated using an octatopic framework with a cobalt central atom, while the latter used Ag-based organoboron framework with great promise for disinfection of model microorganism. Metal-MOF structures retains many of the advantages of nanocolloid such as silver-titania, in long term persistence, low doses (compared to chemical disinfectants such as bleach and even other colloids), size control and effectiveness under visible-light conditions. The added advantage of MOFs (elaborated in the following sections) is the ultrahigh surface area (greater than the use of an only a colloid) and not only use of the internal surface area but also the internal MOF area towards disinfection. The three-dimensional lattice can form a 'web-like' structure, which can surround the microbe and be effective from all-sides, whereas with colloids, between 20-50 would be required to surround the microbe, here considerably less MOF is required and each MOF exerts greater lethality than a single nanoclusters. For this reason and the structural differences, these are known as the '*Third wave*' of nanodisinfectants.

These motifs built upon are more flexible than zeolites framework of Si/Al (e.g. $Na_2Al_2Si_3O_{10}{\cdot}2H_2O$) (*94*). In these type of structures the aluminosilicates occupying tetrahedral geometry ($T_n$) bridged by oxygen atoms in the form of polygon rings (nMR), which in turn are connected to form larger small (<=8 MR), intermediate ((<=8 MR) and large (<=12 MR) pores sizes, noting that a 8-MR will have 16 atoms due to the intervening O-atoms (*95*). Therefore, these structures can give rise to two surfaces, an internal and external surface on which potentially ion exchange (*96*) and catalysis can occur (*97*). Metal organic frameworks motifs can thus extend the work done with zeolites in the fabrication of crystalline structures using ligands as building blocks, noting that in the former case, most templates are inorganic in nature and the templates are removed by oxidation (*98*). In the present case, the framework is generated using n-dentate ligands which form secondary building units (SBU, akin to a tertiary structure of a protein) and these SBU-template to form a net (akin to a tertiary structure of a protein) (*99*). The ligands can be bidentate (e.g. oxalic acid), tridentate (citric acid) or incorporate azoles or other sub-structures, generated using hydrothermal or solvothermal fabrication techniques (*100*). The ligands may also be cross-linked yielding more complex nets (akin to protein quaternary structure) with multiple tetrahedral linked via the ligands, square or modified octahedral cages can result (*101*). Since the solvents can be eliminated from the resulting pores, MOF have been used for trapping and storage of hydrogen, methane, carbon dioxide as well as catalysis (*102*).

In the present application, carboxylate-based frameworks can be used to generate tetra- and hextopic coordinate frameworks with a metal center. Either metal which are required in trace amounts could be used (e.g. Ca, Co, Cu, Fe, K, Mg, Mn, Mo, Na, Ni, Se, V and W) (*51*) or metals which are known to be toxic (e.g. Ag, Al, As, Au, Ge, Hg, Pb, Sb, Sn and Tl) (*51*) including $TiO_2$ a known bactericidal agent. Although heterocyclic frameworks with these metals as decorative metals, dopants or bridging atoms have been synthesized by various investigators (*77*, *103–114*), not every MOF-type system can be employed as a disinfectant, either due to air/water-sensitivity of the complex or innate toxicity of the central metal.

## Mechanism of Inhibition of MOF System

The mode of microbial inactivation is expected to be similar to nanocolloids (*cf.* Figure 2) in that reactive oxygen species (ROS) can be generated (*115*), disruption of membrane potential through redox recycling (*116*) or physical modification of macromolecules (*117*) .Where appropriate, the central atoms can be used for Fenton Type oxidation ((i) $Fe^0 + H_2O_2 \rightarrow Fe^{2+} + 2OH^-$ ; (ii) $Fe^{2+} + H_2O_2 \rightarrow Fe^{3+} + OH^- + {}^{\bullet}OH$, $Fe^0$ is oxidized using $H_2O_2$ to $Fe^{2+}$ defined by $^{k}{}_{1Fe}{}^{0}$, from which further oxidation result in formation of hydroxyl radicals set by $^{k}{}_{2Fe}{}^{2+}$ ) through adsorbent or surface interactions. Through these processes hydroxyl radicals are generated through using various sources ($Fe^{2+}/H_2O_2$, UV/$TiO_2$, Metal-$TiO_2$ and other metal/ transition metal oxide nanocomposites). The hydroxyl radicals will facilitate lipid peroxidation and degradation of organics (*118*). With our metal either as ions (*119*) or in zero-valent oxidation state (*120*) (in our case cobalt initiated specific biochemical interactions (*cf. Comparison with our and other published data section*) can be exploited such as alterations in iron utilization (*121*), or phosphate hydrolysis (*122*) and decreases in the fidelity of DNA synthesis (*123*) . Collectively, coupled with the ultrahigh surface area and numerous reactive sites, rapid disinfection of prokaryotic is expected similar to those observed with nanoparticle systems (*124*).

## Methodology: Bottom-Up Preparation of NP and MOF Disinfectants

### Preparation of Nanoparticle Disinfectants

Silver and Silver-doped $TiO_2$ nanoparticles were studied and prepared using bottom-up colloidal method (*85*) in this study (schematic shown in Figure 3). Briefly, silver nitrate ($AgNO_3$, 0.0071 moles) was dissolved in 30.00 mL of Milli-Q water. Arabic gum (AG, 3.00 %) solution was added to prevent the particles agglomeration. Various reducing agents, such as ascorbic acid ($C_6H_8O_6$), sodium citrate ($C_6H_5ONa_3$), sodium borohydride ($NaBH_4$), and dimethylamine borane (DMAB, $C_2H_{10}NB$) were used for the complete chemical reduction of silver cation ($Ag^+$). The titanium butoxide was used the starting materials and formed a colloid suspension, which was modified using Ag-NP suspension. Then the mixture was stirred for 30 min at 60 °C to derive the stable colloidal suspension, which was used as disinfectant. In this method, the particle agglomeration was successfully prevented using a green chemical, AG as surfactant. The synthetic sol process is schematically illustrated in Figure 3 and consists of sol-synthesis starting from the (1) appropriate metal alkoxide followed by the (2) reduction of the metal ion, which is (3) extracted using wet chemistry. Finally, the nanocolloid is characterized using (4) electron microscopy and x-ray spectroscopy.

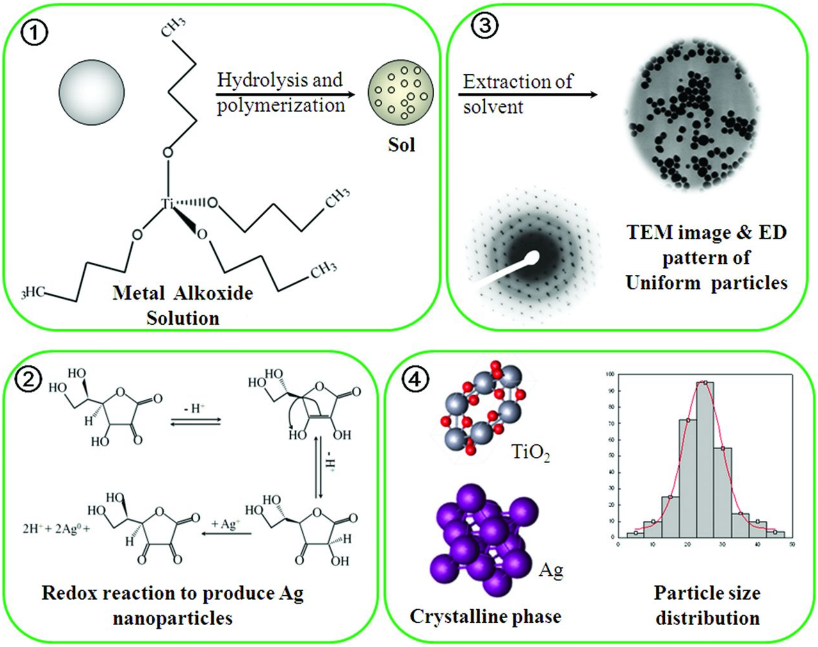
①
Hydrolysis and polymerization
Sol
CH3
Ti
3HC
Metal Alkoxide Solution
③
Extraction of solvent
TEM image & ED pattern of Uniform particles
②
- H+
+ Ag+
2H+ + 2Ag0 +
Redox reaction to produce Ag nanoparticles
④
TiO2
Ag
Crystalline phase
Particle size distribution

*Figure 3. Schematic representation of nanoparticles disinfectant preparation, (1) represents the $TiO_2$ colloid synthesis using $Ti(O^nBu)_4$ metal alkoxide as starting materials; (2) represents the Ag colloid synthesis through redox reaction; (3) represents the Ag-$TiO_2$ nanoparticle synthesis via extraction of solvents; and (4) represents the nanostructural characterization of the nanoparticles, such as crystalline structure, particle size and size distribution study.*

## Preparation of Metal Organic-Framework Disinfectants

The MOFs were generated through hydro-solvothermal approach to produce well-defined and highly crystallized organometallic compounds. The combinatorial approach allows for great flexibility in terms of physical, optical or electrical properties, the various parameters in the design, synthesis and fabrication of the metal organic framework where transition metals, such as iron (Fe), cobalt (Co), nickel (Ni) and silver (Ag) serve central element and ligand as organic linker. The nucleation of MOFs crystal units occurred at elevated temperatures. Combinatorial approach was used to optimize the fabrication variable and regulate size and stability of MOFs crystals (schematic shown in Figure 4a-c). With reference to Figure 4, fabrication is via the hydro-solvothermal due to the short reaction time and lower reaction temperature, via nucleation reaction between the active site of the ligand (**4a**) and metal through covalent bond coordination framework bottom-up (**4b**) process through which crystal geometry, porosity and atomic size can be controlled (**4c**).

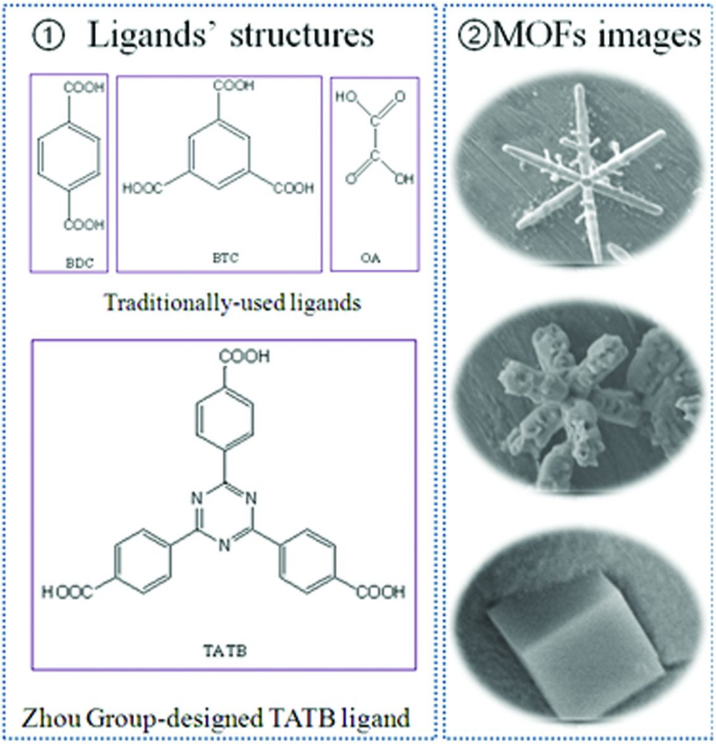
① Ligands' structures
COOH
COOH
BDC
COOH
HOOC
COOH
BTC
HO
O
O
OH
OA
Traditionally-used ligands
COOH
N
N
N
HOOC
COOH
TATB
Zhou Group-designed TATB ligand
②MOFs images

*Figure 4. Schematic of metal organic-framework synthesis using flexible combinatorial chemistry approach of variable metal (e.g. Fe, Ag, Co, Ni) and ligand (e.g. benzene-1,4-dicarboxylic acid, BDC; benzene-1,3,5-tricarboxylic acid, BTC; oxalic acid, OA; 4-[4,6-bis(4-carboxyphenyl)-1,3,5-triazin-2-yl](“tri”)benzoic acid, TATB) can be used to generate metal organic framework of defined porosity, dimension, reflectivity, permittivity and conductivity, (1) shows four selected ligands and (2) SEM images of MOFs typical morphology.*

## Methodology: Bactericidal Evaluation and Structural Characterization of Disinfectants

The bactericidal activity assays were performed as previously described (*85*). Briefly, *Escherichia coli (E. coli*) were used as the model organism. *E. coli* were cultured in nutrient broth for 16 h at 37°C. For the treatment a 3.75-fold dilution was used, which was further diluted by 60-fold and further incubated overnight. A similar procedure was performed with *Staphylococcus aureus* to assess the activity of the Ag-NPs on Gram-positive bacteria. The controls were identical except a solution of water was used instead of the chemical or nanoparticle.

The structure of *E. coli* was characterized as previously described (*110*). Briefly, untreated and treated cells were examined using fluorescent microscopy to determine wall/membrane integrity and high-resolution transmission microscopy (HR-TEM), equipped with X-ray energy dispersive spectroscopy (EDS) to obtain morphological images and elemental distribution as well as electron energy loss spectroscopy (EELS) to determine the distribution of the elemental composition. The actual staining was previously described (*85*) and used 2X Live/Dead BacLight reagent, inactivated bacteria appeared red, while viable microbes appeared green. For electron microscopy a FEI Tecnai $G^2$-F20 transmission electron microscope (TEM) equipped with Oxford X-ray energy dispersive spectrometer (EDS) was used, as previously described (*85*) to obtain nanostructure information and crystalline phase about the colloid-derived nanoparticles. The instrument was operated in the TEM, scanning TEM (STEM) modes to obtain chemical information. The TEM was also used in electron energy loss spectroscopy (EELS) mode using Gatan Imaging Filter, as previously described (*85*). Analysis of *in-situ* elemental mapping would allow the mechanism of bacteria inactivation to be inferred (Figures 1 and 2).

## Potency Evaluation of Three-Wave Disinfectants

The study indicates that all types of disinfectants evaluated were effective at inhibition of 100% of microbes; however some classes were more effective at lower doses. These trends are summarized in Figure 5. The study also highlights another interesting factor regarding silver nanoparticles that effectiveness is tangentially related to synthetic method, for example silver nanoparticles reduced with 1:1 molar ratio with citrate reducing agent were effective at 40 ppm, whereas similar particles reduced with a 1:2 molar ratio with citrate were not (Table 2 of Ref. (*85*)) or silver reduced with a stronger reducing agent dimethylamine borane were effective at lower concentration (1:2 NP: reducing agent, 100% inhibition using 10 ppm, Table 2 of Ref. (*85*)) whereas 10 ppm was ineffective when other reducing agents were used. The last formulation was the most effective in terms of speed and dosage, even when compared with other molar rations (e.g. 1:1 NP: reducing agent). The 1:1 ratio, at 10 ppm was effective after 4 hr, whereas the 1:2 ratio formulations, also at 10 ppm were effective in 2 hr (Table 3 of Ref (*85*)). In terms of incubation time, the longer the incubation time, the lower the dosage. Taking the results from Table 3 (of Ref. (*110*)), it can be seen that the progression from 2→4→6→8 hr incubation in terms of dosage in ppm is 40→10→2.5→0.6 for *E. coli* respectfully.

Lastly, the actual time/dosage is microbe-dependent; comparison to *S. aureus* show 2.5 ppm was the most effective dose (Table 4 of Ref. (*85*)). The results from Figure 5 are also separately summarized below for each class of disinfectant.

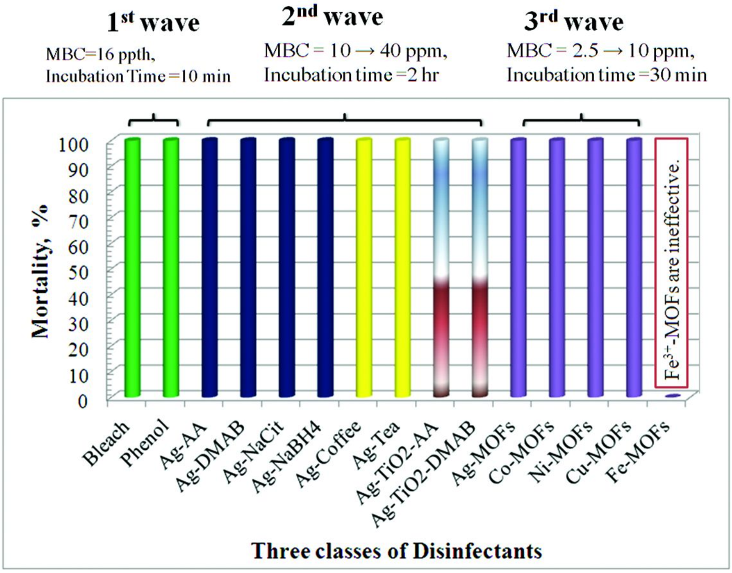

*Figure 5. Bactericidal potent of E. coli three classes of disinfectants. For each wave of disinfectant, the percent morbidity after a specified incubation time and disinfectant concentration is also indicated. (Adopted from Ref. (85), License Number: 2861490170097, Copyright Elsevier.)*

## Potency Evaluation of The 1st-Wave Disinfectants

The above Figure 5 indicated both phenol and bleach, act 12-fold quicker than silver NPs, however at 400-fold greater concentrations than what is effective with silver nanoparticles. Phenol and nanoparticles are effective over a greater time range than bleach, due to their greater stability towards oxidative decomposition.

## Potency Evaluation of The 2nd-Wave Disinfectants

The above comparison indicates a number of generalizations reported elsewhere in the literature that nanoparticles have lower concentration requirements for 100% microbial inhibition; which is microbe-type sensitive, thicker cell wall require higher concentrations than thinner cell walls; that with greater NP to microbe interaction, lower concentrations are required, which is not observed for either phenol or bleach, which appear to be incubation-time independent. Morphological changes examined by TEM in Figure 6 also indicate light and dark regions, (**6b**) plus a gap between the wall and membrane (**6c**) relative to a viable cell (**6a**) which is similar with silver (as shown in Ref. (*110*)), or silver-titania or MOFs.

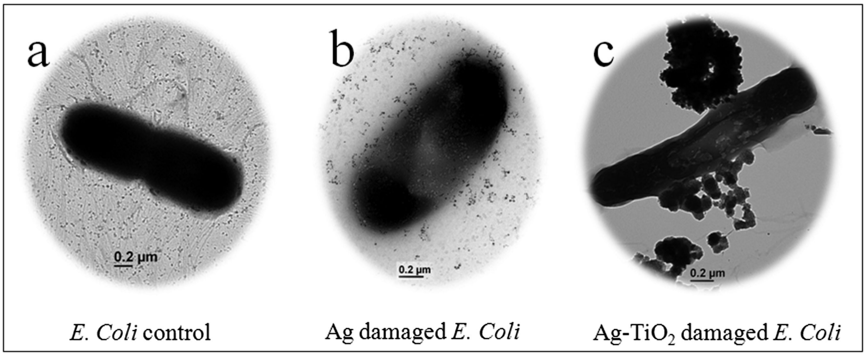

*E. Coli* control    Ag damaged *E. Coli*    Ag-$TiO_2$ damaged *E. Coli*

*Figure 6. The morphological analyses of bacteria treated using Ag and Ag-$TiO_2$ NPs disinfectants; a: E. coli control; b: Ag damaged E. coli; and c: Ag and Ag-$TiO_2$ damaged E. coli.*

BacLight staining (Figure 1 from Ref. (*85*)) also showed that microbial morphology was intact with silver nanoparticles, whereas with bleach, total cellular degradation was observed (Figure 1 of Ref. (*85*)). Elemental mapping (from Ref. (*78*)) for potassium ($L_3$ edge at 294 eV), silver (M4,5 edge at 367 eV) (Figure 4 of Ref. (*85*)) and P-block elements such as nitrogen (K edge at 401 eV), carbon (K edge at 284 eV), chlorine ($L_{2,3}$ edge at 200 eV), phosphorous ($L_{2,3}$ edge at 132 eV ), calcium (L3 edge at 346 (Ca), sulfur ($L_{2,3}$ edge at 165 eV, Supplement Figure 3 of Ref. (*85*)) established a number of plausible modes of inactivation consistent with older literature and illustrated in Figure 1.

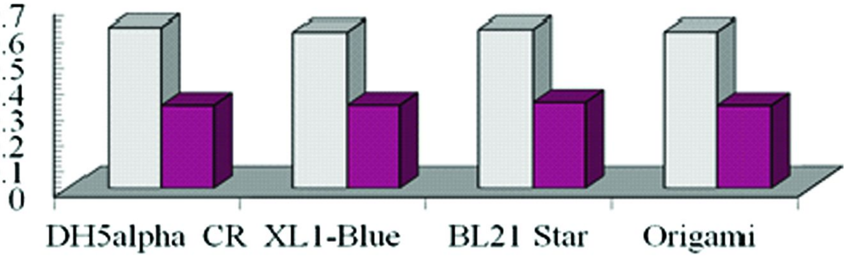

*Figure 7. Morbidity of different strains of E. coli using is Ag NPs derived from green chemistry synthesis. a (first column): gray plot represents the initial absorbance of E. coli; and b(or second column): red plot represents the final absorbance of E. coli.*

The only variation in lethality was incubation time between a Gram-negative/ positive microbe, which was attributed to differences in cell wall composition and thickness. Evaluation of different strains of a Gram-negative microbe no practical difference, suggesting that microbes resistant to antibiotics would be susceptible to nanoparticle type disinfectants. The relative morbidity of different *E. coli* strains with Ag nanoparticles is summarized in Figure 7.

## Potency Evaluation of The 3rd-Wave Disinfectants

Figure 5 also indicates that MOF class disinfectants have similar properties to both bleach and silver nanoparticles, the effectiveness is primarily due to the crystal nature, and the unit cell is shown in Figure 8a. Analysis of the cell also shows a fiber-like structure in bulk form (**8b**, lower insert shows crystal) and the effect of *E. coli* (**8c**) with extensive membrane damage, similar to that observed with bleach, in a similar time frame, except much lower dosage that that used for bleach, (*cf.* Figure 5).

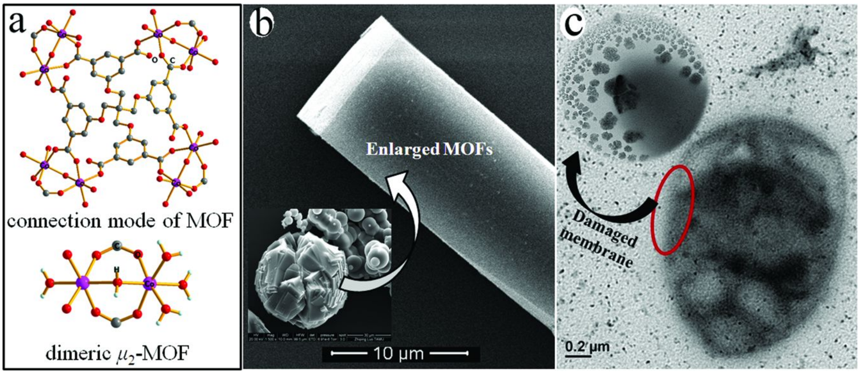

*Figure 8. Co-based MOFs used as disinfectant, a: X-ray single crystallographic data; b: SEM morphological image of Co-MOFs; and c: Bacteria cell wall of E. coli using Co-MOF disinfectant.*

The MOFs seem to act at a more rapid rate at a lower effective concentration than either bleach or nanoparticle disinfectants. Similar to silver nanoparticles, MOFs are equally effective with different strains of *E. coli*, in Figure 9, except was slightly more potent with all strains, except the DH5 alpha (DH5a) strain. This may be due to greater interaction at certain surfaces after long incubation times, which was not observed for nanoparticles (*cf.* Figure 7), since only nanoparticle to microbe interaction is possible, however with MOF two types of interactions are possible, one with the outer MOF surface, one with the inner surface

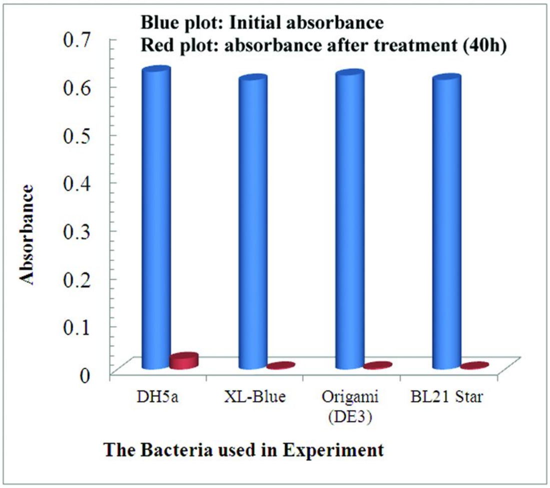

*Figure 9. MOFs with four formations (single time treatment) used as disinfectant, a (or first column): blue plot represents the initial absorbance of E. coli; and b(or second column): red plot represents the final absorbance of E. coli.*

## Comparison with Our and Other Published Data

Literature comparison to bulk silver, such as silver nitrate (*125*) indicate that nanosilver is more effective, particular due to antibiotic-resistance microbes has increased focus as a possible alternative treatment (*126*). Examination of the TEM micrographs (Figures 6, 8**c** current and Figure 2 from Ref. (*85*)) indicate light and dark regions within the cytoplasm, which demonstrated nucleic acid coalescence, strongly suggestive of either direct base-pair binding or inactivation (*127*) or reactive oxygen species induced oxidation and fragmentation (*128*) has been demonstrated with viral DNA. Electron Energy Loss Spectroscopy analysis of selected regions (of *E. coli* from Figure 4 of Ref. (*85*)) demonstrated no incorporation of silver suggesting that the phase contrast is due to nucleic acid fragmentation. The expected elements from DNA of C, N, P, and O were subsequently observed without Ag incorporation. Careful examination of the region between the cell wall and plasma membrane also showed a light and gray region, indicative of peeling, detachment of the membrane from the cell wall and shrinkage. This is indicative of damage and denaturation of phospholipids on the surface and integral membrane and porin proteins within the membrane, anchoring toward the plasma membrane and possible inhibition of respiratory proteins. If our hypothesis were correct, the morphological changes and associated widening of the cell wall and plasma membrane would be expected, as was observed in our study, in addition, elemental mapping would expect to show P and S in addition to N and O, close to the condensed gray regions. EELS mapping appeared to confirm these assumptions, since the above elements were observed. Sulfur is ordinarily not found in DNA, thereby allowing a differentiator between these macromolecules and suggesting that the interaction was towards the membrane and cytoplasmic side. One other possible explanation is that these atoms are from the reducing or binding agents used in the initial synthesis. Although a possibility, this is unlikely, since the samples was washed and since the reducing or biding agents do not contain any sulfur. Comparison with *S. aureus*, showed similar morphological changes to those observed for *E. coli*, except the phase contrast appeared to be darker. The more intense dark gray may be attributable to the presence of a thicker peptidoglycan cell wall in Gram-positive microbes, which are lacking in Gram-negative microbes. This may also partially explain why higher concentration of silver nanoparticles and greater incubation time was required for 100% inhibition, when compared to results from *E. coli*. A plausible explanation may be that the silver nanoparticle, interact with surface phospholipids and membrane-bound proteins possibly respiratory proteins, metal-assisted oxidative/reduction of protein thiols and nucleic material causes membrane to wall peeling and nucleic acid fragmentation, coupled to increase cell permeability resulting in leakage of potassium and calcium, ions critical in keeping the membrane potential for active diffusion of nutrients and ions. Our own (unreported in Ref. (*85*)) studies show that silver can interact with and bind to certain amino acids, which are promoter silver effectiveness (*129*) and certain amino acid are degrade the effectiveness (*130*) of silver, presumably through complexation. Both of these observations have also been reported in the literature, and mechanisms similar to ours, except in some cases incorporation of silver within the cytoplasm was also detected (*131*), in contrast to our EELS based findings, where no internal silver was detected (*85*). An additional factor (as stated earlier) was that the fabrication method (in our study, the reducing agent and NP-to-agent ratio) had an effect with respect to effective dosage, the formulation method having an indirect bearing on final particle size/volume, which ultimately would affect particle stability and surface area; the greater the surface area the lesser the expected dosage, which has also been reported elsewhere (*132*). In our study, a diameter of less than 25 nm was found to be effective, too large a diameter was prone to clustering and too small were unstable and also clustered, between 5-25 nm were stable without clustering and provided to be effective sizes for disinfection, has also been observed in other studies (*133*). In our study, although the NP diameter was varied slightly the cubic type shape was kept constant; however, unlike with phenol or bleach, which disperse within liquids, the shape of nanoparticles can be changed and has been examined and shown to be shape-dependent (*134*). The advantages of using silver nanoparticles either are clear, ultrahigh surface area, in the form of colloidal silver (*135*), or clustered within a matrix, such as a zeolite (*136*), organic framework (*137*), or dendrimer (*138*). These formulations enable silver to rapidly interact with the microbe at numerous points, thereby affecting rapid response; for example, it was shown an MBC of < 20 ppm from our study (*cf.* Figure 5, except for $Fe^{3+}$ MOF) and < 300 pm for Ag-framework (*139*). The inactivation is thought to be due to multiple interactions via the framework and inhibition of ribosomal subunits proteins

(*140*), disrupting phosphate uptake (*141*), irreversibly binding to protein thiols (*142*) inhibiting cell division (*143*) and respiration (*144*), resulting in cell lysis or membrane damage, increased permeability, inhibition of metabolite processes and inactivation which by-pass the usual inhibitory mechanisms employed toward antibiotics as was observed in Figures 7 and 9.

Future Direction of the research are to evaluate the MOFs fabricated which we believe will be effective against non-pathogenic and pathogenic microbes (such as *E. coli, S. aureaus*) but also against microbes which utilize ammonia (*Nitrosomonas*) and nitrites (*Nitrobacter*) and microbes which have a hydrophobic mycolate layer in their cell wall, such as *Mycobacteria* and unicellular heterotrophic protist. Other classes of organisms include Oomycetes, *Dictyosteliida, Protostelids*, parasitic worms; viruses, and prions found in water streams including waste water with the added advantage of using the MOF surface to promote possible oxidation and degradation of organics (e.g. pesticides, pharmaceuticals, fertilizers) and possible elimination of select heavy metals.

## Future Trends

The new applications focus on bimetallic composites for ease of removal from water (*139*) or for surface treatment (*144*) or embedded into various types of fibers toward wound healing (*145*) or water filtration (*146*). The NP exhibit a wide-spectrum of activity toward Gram-negative/positive microbes, fungi (*147*), algae (*148*) and viruses (*149*). Once concern is that over-reliance and usage of these engineered materials might lead to environmental contamination, particularly wastewater and sewage (*150*), which paradoxically is one motivator force in their initial use as water disinfectants. In this regards, careful usage and monitoring (*151*) is required to gauge potential cyto- and genotoxic effects in fish, reptiles and higher animals (*152*). The antimicrobial mechanisms have been discussed and provided to be effective against microbes, which are currently tolerant to antibiotics (*153*), but the possibility of metal-tolerance as demonstrated by some strains against silver sulfadiazine exists (*154*). The required dosage, duration and stability of the fabricated nanoparticles are related to nanoparticle diameter, nanoparticle shape, dimensionality and organism type. The ‘success’ against prokaryotic organisms has shifted attention to eukaryotic and mammalian cells with a view of utilizing similar structures and formulations towards treatment of wound infection (*155*), organ disease (e.g. eye infection) and cancer cells (*156*). In regards to the future of disinfection, it appears that engineered nanomaterials (*157*) offer a very real long lasting alternative to hydrogen peroxide, bleach and phenol as our longest-serving disinfectants, particularly with regards to water treatment, purification and beyond toward personal healthcare.

## Acknowledgments

The authors wish to thank the College of Arts & Sciences (CoA&S, Dr. Bashir, 160336-00002) and Welch Departmental Grant (AC-0006) at Texas A&M University-Kingsville (TAMUK) for funding and student support respectfully. The Microscopy and Imaging Center (MIC) at TAMU and the Department of Chemistry at TAMUK are also duly acknowledged for their technical support and nanostructure characterization. The Welch Foundation (AC-006) is duly acknowledged to facilitate the research and disseminate the results.

## Authors' Contribution

The research work referred to in part in the Results Section was undertaken by K. Chamakura R. Perez-Ballestero (microbial component) Z. Luo (acquired microscopy related data and analysis), S. Bashir (wrote first draft, Figure 1, supplemental tables 1A-H, partial experimental design, partial data analysis and funding) and J. Liu (who conceived of the research idea, scope, aims and thrust of the current book chapter as invited by the editor, completed the remaining experimental design, all other experimental work and analysis, editing of subsequent drafts and on-line submission) cited as Ref. (*110*).

## References

1. Wykilicy, H.; Skopec, M. *Infect. Control* **1983**, *4*, 367–370.
2. Debré P. In *Louis Pasteur*; Debré, P., Ed.; The John Hopkins University Press: Baltimore, MD, 1998; pp 219−256.
3. Maki, D. G. *N. Engl. J. Med.* **1976**, *294*, 1286–1287.
4. Ridel, S.; Walker, J. T. A. *J. R. Sanit. Inst.* **1903**, *24*, 424–441.
5. Association of Official Analytical Chemists (AOAC). *Official Methods of Analysis*, 15th ed.; AOAC: Arlington, VA, 1990.
6. Cole, E. C.; Rutala, W. A.; Nessen, L.; Wannamaker, N. S.; Weber, D. J. *Appl. Environ. Microbiol.* **1990**, *56*, 1813–1817.
7. Heimets, F.; Taylor, W. W.; Lehman, J. J. *J. Bacteriol.* **1954**, *67*, 5–12.
8. Holland, M. R. *Oral Surg. Oral Med. Oral Pathol.* **1955**, *8*, 788–795.
9. Larson, E. L. *Am. J. Infect. Control* **1995**, *23*, 251–69.
10. Robinson, F. C. *Public Health Pap. Rep.* **1900**, *26*, 151–68.
11. Agalloco, J.; Akers, J.; Madsen, R. *PDA J. Pharm. Sci. Technol.* **2009**, *63*, 89–102.
12. Lindboe, W. G.; Hayakawa, K. *J. Parenter. Sci. Technol.* **1993**, *47*, 138–41.
13. Goveia, V. R.; Pinheiro, S. M.; Graziano, K. U. *Rev. Lat. Am. Enfermagem* **2007**, *15*, 373–6.
14. Bruch, C. W. *Life Sci. Space Res.* **1964**, *16*, 100–4.
15. Elliott, R. P.; Michener, H. D. *Appl. Microbiol.* **1961**, *9*, 452–68.
16. Sutton, S. V.; Franco, R. J.; Porter, D. A.; Mowrey-McKee, M. F.; Busschaert, S. C.; Hamberger, J. F.; Proud, D. W. *Appl. Environ. Microbiol.* **1991**, *57*, 2021–6.
17. Miller, C. H. *Dent. Clin. North Am* **.1991**, *35*, 339–55.

18. Gould, G. W. *J. Appl. Microbiol.* **2006**, *101*, 507–13.
19. Sagripanti, J. L.; Bonifacino, A. *Appl. Environ. Microbiol.* **1999**, *65*, 4255–60.
20. Rutala, W. A. *Am. J. Infect. Control* **1996**, *26*, 153–5.
21. Fleischer, W.; Reimer, K. *Dermatology* **1997**, *195*, 3–9.
22. Deborde, M.; Gunten, U. von. *Water Res.* **2008**, *42*, 13–51.
23. Vandervelde, T. L.; Mallmann, W. L.; Moore, A. V. *Sanitarian* **1948**, 11, 47−9.
24. von Gunten, U. *Water Res.* **2003**, *37*, 1443–67.
25. von Gunten, U. *Water Res.* **2003**, *37*, 1469–87.
26. Greenberg, M.; Dodds, M.; Tian, M. *J. Agric. Food Chem.* **2008**, *56*, 11151–6.
27. Jones, R. D.; Jampani, H. B.; Lee, J. L. *Am. J. Infect. Control.* **2000**, *28*, 184–96.
28. Lilly, H. A.; Lowbury, E. J. *Br. Med. J.* **1971**, *3*, 674–6.
29. Russell, A. D. *Symp. Ser. Soc. Appl. Microbiol.* **2002**, *31*, 1S–3S.
30. Samuel, I. *Virologie* **1978**, *29*, 213–8.
31. Lowbury, E. J.; Lilly, H. A. *Br. Med. J.* **1973**, *1*, 510–5.
32. Winward, G. P.; Avery, L. M.; Stephenson, T.; Jefferson, B. *Water Res.* **2008**, *42*, 2260–8.
33. Mohammadi, Z.; Abbott, P. V. *Aust. Endod. J.* **2009**, *35*, 131–9.
34. Burch, T. M.; Stanger, B.; Mizuguchi, K.; A. Reid, D. *Anesth. Analg.* **2012**, *114*, 622–5.
35. Rutala, W. A.; Weber, D. J. *Emerg. Infect. Dis.* **2001**, *7*, 348–53.
36. Russo, A.; Viotti, P. L.; Vitali, M.; Clementi, M. *Am. J. Infect. Control* **2003**, *31*, 117–23.
37. Martin, K.; Laydet, E.; Canaud, B. *Adv. Renal Replacement Ther.* **2003**, *10*, 122–32.
38. Rutala, W. A.; Weber, D. J. *Clin. Microbiol. Rev.* **1997**, *10*, 597–610.
39. Estrela, C.; Silva, J. A.; Alencar, A. H.; de Leles, C. R.; Decurcio, D. A. *J. Appl. Oral Sci.* **2008**, *16*, 364–8.
40. Calzavara-Pinton, P. G.; Venturini, M.; Sala, R A. *J. Photochem. Photobiol., B* **2005**, *78*, 1–6.
41. Backer, H.; Hollowell, J. *Environ. Health Perspect.* **2000**, *108*, 679–84.
42. Kim, B. R.; Anderson, J. E.; Mueller, S. A.; Gaines, W. A.; Kendall, A. M. *Water Res.* **2002**, *36*, 4433–44.
43. Exon, J. H. *Vet. Hum. Toxicol.* **1984**, *26*, 508–20.
44. Russell, A. D. *Symp. Ser. Soc. Appl. Microbiol.* **2002**, *31*, 121S–135S.
45. Allen, J. F.; Harrison, M. A.; Holmes, N. G. *Biochimie* **1989**, *71*, 1021–8.
46. Barlow, K. *Nutr. Health* **1991**, *7*, 143–50.
47. Cottone, J. A.; Young, J. M.; Dinyarian, P. *Int. J. Prosthodontics* **1990**, *3*, 379–83.
48. Grass, G.; Rensing, C.; Solioz, M. *Appl. Environ. Microbiol.* **2011**, *77*, 1541–7.
49. Silvestry-Rodriguez, N.; Sicairos-Ruelas, E. E.; Gerba, C. P.; Bright, K. R. *Rev. Environ. Contam. Toxicol.* **2007**, *191*, 23–45.

50. Foster, H. A.; Ditta, I. B.; Varghese, S.; Steele, A. *Appl. Microbiol. Biotechnol.* **2011**, *90*, 1847–68.
51. Gadd, G. M. *FEMS Microbiol. Lett.* **1992**, *100*, 197–203.
52. Hollinger, M. A. *Crit. Rev. Toxicol.* **1996**, *26*, 255–60.
53. Mohammadi, Z.; Abbott, P. V. *Aust. Endod. J.* **2009**, *35*, 131–9.
54. Inoue, Y.; Hoshino, M.; Takahashi, H.; Noguchi, T.; Murata, T.; Kanzaki, Y.; Hamashima, H.; Sasatsu, M. *J. Inorg. Biochem.* **2002**, *92*, 37–42.
55. Balogh, L.; Swanson, D.; Tomalia, D.; Hagnauer, G.; McManus, A. *Nano Lett.* **2001**, *1*, 18–21.
56. Zhang, Y.; Peng, H.; Huang, W.; Zhou, Y.; Yan, D. *J. Colloid Interface Sci.* **2008**, *325*, 371–376.
57. Yoon, K.; Byeon, J.; Park, J.; Ji, J.; Bae, G.; Hwang, J. *Environ. Eng. Sci.* **2008**, *25*, 289–293.
58. Kim, J. *J. Ind. Eng. Chem.* **2007**, *13*, 718–722.
59. Smetana, A.; Klabunde, K.; Sorensen, C. *J. Colloid Interface Sci.* **2005**, *284*, 521–526.
60. Kvitek, L.; Panacek, A.; Soukupova, J.; Kolar, M.; Vecerova, R.; Prucek, R.; Holecova, M.; Zboril, R. *J. Phys. Chem. C* **2008**, *112*, 5825–5834.
61. Raffi, M.; Hussain, F.; Bhatti, T.; Akhter, J.; Hameed, A.; Hasan, M. *J. Mater Sci. Technol.* **2008**, *24*, 192–196.
62. Vertelov, G.; Krutyakov, Y.; Efremenkova, O.; Olenin, A.; Lisichkin, G. *Nanotechnology* **2008**, *19*, 355707-1–355707-7.
63. Faraday, M. *Philos. Trans. R. Soc.* **1857**, *147*, 145–181.
64. (a) Tomanek, D.; Mukherjee, S.; Bennemann, K. H. *Phys. Rev.* 1983, B28, 665−73; (b) *Phys. Rev.* **1984**, B29, 1076.
65. Brus, L. E. *J. Chem. Phys.* **1984**, *80*, 4403–09.
66. Garfunkel, E. L.; Minot, C.; Gavezzotti, A.; Simonetta, M. *Surf. Sci.* **1986**, *167*, 177–197.
67. Papavassiliou, G. C. *Prog. Solid State Chem.* **1979**, *12*, 185–271.
68. Evans, E. L.; Griffiths, R. J. M.; Thomas, J. M. *Science (Washington, DC)* **1971**, *171*, 174–5.
69. Homberger, M.; Simon, U. *Philos. Trans. R. Soc. A* **2010**, *368*, 1405–53.
70. Abbas, A.; Linman, M. J.; Cheng, Q. *Biosens. Bioelectron.* **2011**, *26*, 1815–24.
71. Tolaymat, T. M.; El Badawy, A. M.; Genaidy, A.; Scheckel, K. G.; Luxton, T. P.; Suidan, M. *Sci. Total Environ.* **2010**, *408*, 999–1006.
72. Alrousan, D. M. A.; Dunlop, P. S. M.; McMurray, T. A.; Byrne, J. A. *Water Res.* **2009**, *43*, 47–54.
73. Vajda, S.; Pellin, M. J.; Greeley, J. P.; Marshall, C. L.; Curtiss, L. A.; Ballentine, G. A.; Elam, J. W.; Catillon-Mucherie, S.; Redfern, P. C.; Mehmood, F.; Zapol, P. *Nat. Mater. (London)* **2009**, *8*, 213–16.
74. Turkevich, J.; Stevenson, P. C.; Hillier, J. *Discuss. Faraday Soc.* **1951**, *11*, 55–75.
75. Lu, X.; Rycenga, M.; Skrabalak, S. E.; Wiley, B.; Xia, Y. *Annu. Rev. Phys. Chem.* **2009**, *60*, 167–92.
76. Mills, G.; Henglein, A. *Radiat. Phys. Chem.* **1985**, *26*, 385–390.

77. Ahmadi, T.; Wang, Z. L.; Green, T. C.; Henglein, A.; El-Sayed, M. A. *Science (Washington, DC)* **1996**, *272*, 1924–6.
78. Sachtler, W. H. M.; Tzou, M. S.; Jiang, H. J. *Solid State Ionics* **1988**, *26*, 71–76.
79. Lim, B.; Xia, Y. *Angew. Chem., Int. Ed.* **2011**, *50*, 76–85.
80. Cao, G.; Liu, D. *Adv. Colloid Interface Sci.* **2007**, *136*, 45–64.
81. Wilkinson, L. J.; White, R. J.; Chipman, J. K. *J. Wound Care* **2011**, *20*, 543–9.
82. Kowaltowski, A. J.; de Souza-Pinto, N. C.; Castilho, R. F.; Vercesi, A. E. *Free Radicals Biol. Med.* **2009**, *47*, 333–43.
83. Ivask, A.; Bondarenko, O.; Jepihhina, N.; Kahru, A. *Anal. Bioanal. Chem.* **2010**, *398*, 701–16.
84. Valko, M.; Morris, H.; Cronin, M. T. *Curr. Med. Chem.* **2005**, *12*, 1161–208.
85. Chamakura, K.; Perez-Ballestero, R.; Luo, Z.; Bashir, S.; Liu, J. *Colloids Surf. B* **2011**, *84*, 88–96.
86. Rafiuddin, Z. Z. *Colloids Surf B Biointerfaces* **2012**, *90*, 48–52.
87. Chamakura, K.; Perez-Ballestereo, R.; Bashir, S.; Luo, Z.; Liu, J. *MRS Fall (December) Meeting*, Boston 2010, including private communications at discussion session.
88. Gunawan, P.; Guan, C.; Song, X.; Zhang, Q.; Leong, S. S.; Tang, C.; Chen, Y.; Chan-Park, M. B.; Chang, M. W.; Wang, K.; Xu, R. *ACS Nano* **2011**, *5*, 10033–40.
89. Don, T. M.; Chen, C. C.; Lee, C. K.; Cheng, W. Y.; Cheng, L. P. *J. Biomater. Sci. Polym. Ed.* **2005**, *16*, 1503–1519.
90. Le, N. T.; Nagata, H.; Aihara, M.; Takahashi, A.; Okamoto, T.; Shimohata, T.; Mawatari, K.; Kinouchi, Y.; Akutagawa, M.; Haraguchi, M. *Appl. Environ. Microbiol.* **2011**, *77*, 5629–34.
91. Medina-Ramirez, I.; Bashir, S.; Luo, Z.; Liu, J. L. *Colloids Surf., B* **2009**, *73*, 185–91.
92. Theron, J.; Walker, J. A.; Cloete, T. E. *Crit. Rev. Microbiol.* **2008**, *34*, 43–69.
93. Liu, Y.; Xu, X.; Xia, Q.; Yuan, G.; He, Q.; Cui, Y. *CrystEngComm* **2010**, *46*, 2608–2610.
94. Cundy, C. S.; Cox, P. A. *Chem. Rev.* **2003**, *103*, 663–701.
95. Baerlocher, C.; McCusker, L. B.; Olson, D. H. *Atlas of Zeolite Framework Types*, 6th ed.; Elsevier: Amsterdam, The Netherlands, 2007; pp13−392. (Also see Database of Zeolite Structures, Baerlocher, C., McCusker, L. B. Created 1996, Last Accessed July 2012 at URL http://www.iza-structure.org/databases/.)
96. Pérez-Ramírez, J.; Christensen, C. H.; Egeblad, K.; Christensen, C. H.; Groen, J. C. *Chem. Soc. Rev.* **2008**, *37*, 2530–42.
97. Abelló, S.; Montané, D. *ChemSusChem* **2011**, *4*, 1538–56.
98. Flytzani-Stephanopoulos, M.; Gates, B. C. *Annu. Rev. Chem. Biomol. Eng.* **2012**, *3*, 545–74.
99. James, S. L. *Chem. Soc. Rev.* **2003**, *32*, 276–88.
100. Eddaoudi, M.; Moler, D. B.; Li, H.; Chen, B.; Reineke, T. M.; O'Keeffe, M.; Yaghi, O. M. *Acc. Chem. Res.* **2001**, *34*, 319–30.
101. Stock, N.; Biswas, S. *Chem. Rev.* **2012**, *112*, 933–69.
102. Bradshaw, D.; Garai, A.; Huo, J. *Chem. Soc. Rev.* **2012**, *41*, 2344–81.

103. de Lill, D. T.; Bozzuto, D. J.; Cahill, C. L. *Dalton Trans.* **2005**, *21*, 2111–5.
104. Smaldone, RA.; Forgan, R. S.; Furukawa, H.; Gassensmith, J. J.; Slawin, A. M.; Yaghi, O. M.; Stoddart, J. F. *Angew. Chem., Int. Ed.* **2010**, *49*, 8630–4.
105. Moon, H. R.; Kobayashi, N.; Suh, M. P. *Inorg. Chem.* **2006**, *45*, 8672–6.
106. Sun, C.; Li, Y.; Wang, E.; Xiao, D.; An, H.; Xu, L. *Inorg. Chem.* **2007**, *46*, 1563–74.
107. Turner, D. L.; Stone, K. H.; Stephens, P. W.; Vaid, T. P. *Dalton Trans.* **2010**, *39*, 5070–5073.
108. Whalley, A. L.; Blake, A. J.; Collison, D.; Davies, E. S.; Disley, H. J.; Helliwell, M.; Mabbs, F. E.; McMaster, J.; Wilson, C.; Garner, C. D. *Dalton Trans.* **2011**, *40*, 10457–72.
109. Jiang, H. L.; Lin, Q. P.; Akita, T.; Liu, B.; Ohashi, H.; Oji, H.; Honma, T.; Takei, T.; Haruta, M.; Xu, Q. *Chemistry* **2011**, *17*, 78–81.
110. van de Water, L. G.; Zwijnenburg, M. A.; Sloof, W. G; van der Waal, J. C.; Jansen, J. C.; Maschmeyer, T. *ChemPhysChem* **2004**, *5*, 1328–35.
111. Mahmoudi, G.; Morsali, A.; Zeller, M. *J. Iran. Chem. Soc.* **2008**, *5*, 574–578.
112. Yang, E.-C.; Li, J.; Ding, B.; Liang, Q.-Q.; Wang, X.-G.; Zhao, X.-J. *CrystEngComm* **2008**, *10*, 158–161.
113. Fritsch, J.; Rose, M.; Wollmann, P.; Bohlmann, W.; Kaskel, S. *Materials* **2010**, *3*, 2447–2462.
114. Avendano, C.; Zhang, Z.; Ota, A.; Zhao, H.; Dunbar, K. R. *Angew. Chem., Int. Ed.* **2011**, *50*, 6543–7.
115. Harris, G. K.; Shi, X. *Mutat. Res.* **2003**, *533*, 183–200.
116. Fukuzumi, S.; Itoh, S. *Antioxid. Redox Signal* **2001**, *3*, 807–24.
117. Antos, JM.; Francis, M. B. *Curr. Opin. Chem. Biol.* **2006**, *10*, 253–62.
118. Toledo, L. C.; Silva, A. C. B.; Augusti, R.; Lago, R. M. *Chemosphere* **2003**, *50*, 1049–54.
119. Li, D.; Qu, J. *J. Environ. Sci. (China)* **2009**, *21*, 713–9.
120. Bergendahl, J. A.; Thies, T. P. *Water Res.* **2004**, *38*, 327–34.
121. Okamoto, S.; Eltis, L. D. *Metallomics* **2011**, *3*, 963–70.
122. Kimura, E. *Curr. Opin. Chem. Biol.* **2000**, *4*, 207–13.
123. Beyersmann, D.; Hartwig, A. *Toxicol. Appl. Pharmacol.* **1992**, *115*, 137–45.
124. Hrenovic, J.; Milenkovic, J.; Daneu, N.; Kepcija, R. M.; Rajic, N. *Chemosphere* **2012**, *88*, 103–7.
125. Klasen, H. J. *Burns* **2000**, *30*, 1–9.
126. Gemmell, C. G.; Edwards, D. I.; Frainse, A. P. *Chemotherapy* **2006**, *57*, 589–608.
127. Landsdown, A. B. G. *J. Wound Care* **2002**, *11*, 125–38.
128. Fox, C. L.; Modak, S. M. *Antimicrob. Agents Chemother.* **1974**, *5*, 582–8.
129. Kazachenko, A. S.; Legler, T. A. V.; Peryanova, T. O. V.; Vstavskaya, Y. A. *Pharm. Chem. J.* **2000**, *34*, 34–5.
130. Matsumura, Y.; Yoshikata, K.; Kunisaki, S. I.; Tsuchido, T. *Appl. Environ. Microbiol.* **2003**, *69*, 4278–81.
131. Sondi, I.; Salopek-Sondi, B. *J. Colloid Interface* **2007**, *275*, 177–82.
132. Morones, J. R.; Elechiguerra, J. L.; Camacho, A.; Ramirez, J. T. *Nanotechnology* **2005**, *16*, 2346–53.

133. Panacek, A.; Kvítek, L.; Prucek, R.; Kolar, M.; Vecerova, R.; Pizúrova, N.; Sharma, V. K.; Nevecna, T.; Zboril, R. *J. Phys. Chem.* **2006**, *110*, 16248–53.
134. Pal, S.; Tak, Y. K.; Song, J. M. *Appl. Environ. Microbiol.* **2007**, *27*, 1712–20.
135. Su, H. L.; Chou, C. C.; Hung, D. J.; Lin, S. H.; Pao, I. C.; Lin, J. H.; Huang, F. L.; Dong, R. X.; Lin, J. J *Biomaterials* **2009**, *30*, 5979–87.
136. Sadjadi, M. S.; Farhadyar, N.; Zare, K. *J. Nanosci. Nanotechnol.* **2009**, *9*, 1365–8.
137. Zhuang, W.; Yuan, D.; Li, J.-R.; Luo, Z.; Bashir, S.; Liu, J.; Zhou, H.-C. *Adv. Healthcare Mater.* **2012**, *1*, 225–238.
138. Dastjerdi, R.; Montazer, M. *Colloids Surf., B* **2001**, *79*, 5–18.
139. Huang, W. C.; Tsai, P. J.; Chen, Y. C. *Small* **2009**, *5*, 51–56.
140. Yamanaka, M.; Hara, K.; Kudo, J. *Appl. Env. Microbiol.* **2005**, *71*, 7589–93.
141. Rosenkranz, H. S.; Carr, H. S. *Antimicrob. Agents Chemother.* **1972**, *5*, 199–201.
142. Liau, S. Y.; Read, D. C; Pugh, W. J.; Furr, J. R.; Russell, A. D *Lett. Appl. Microbiol.* **1997**, *25*, 279–83.
143. Feng, Q. L.; Wu, J.; Chen, G. Q.; Cui, F. Z.; Kim, T. N.; Kim, J. O. *J. Biomed. Mater.* **2000**, *52*, 662–8.
144. Li, W. R.; Xie, X. B.; Shi, Q. S.; Zeng, H. Y.; Ou-Yang, Y. S.; Chen, Y. B. *Appl. Microbiol. Biotechnol.* **2001**, *85*, 1115–22.
145. Asz, J.; Asz, D.; Seigel, R. J.; Mallory, S. B.; Foglia, R. P. *J. Pediatr. Surg.* **2006**, *41*, e9–12.
146. Jain, P.; Pradeep, T. *Biotechnol. Bioeng.* **2005**, *90*, 59–63.
147. Durán, N.; Marcato, P. D.; Durán, M.; Yadav, A.; Gade, A.; Rai, M. *Appl. Microbiol. Biotechnol.* **2011**, *90*, 1609–24.
148. Narayanan, K. B.; Sakthivel, N. *Adv. Colloid Interface Sci.* **2011**, *169*, 59–79.
149. Galdiero, S.; Falanga, A.; Vitiello, M.; Cantisani, M.; Marra, V.; Galdiero, M. *Molecules* **2011**, *16*, 8894–918.
150. Fabrega, J.; Luoma, S. N.; Tyler, C. R.; Galloway, T. S.; Lead, J. R. *Environ. Int.* **2011**, *37*, 517–31.
151. Tolaymat, T. M.; El Badawy, A. M.; Genaidy, A.; Scheckel, K. G.; Luxton, T. P.; Suidan, M. *Sci. Total Environ.* **2010**, *408*, 999–1006.
152. Teow, Y.; Asharani, P. V.; Hande, M. P.; Valiyaveettil, S. *Chem. Commun.* **2011**, *47*, 7025–38.
153. Monteiro, D. R.; Gorup, L. F.; Takamiya, A. S.; Ruvollo-Filho, A. C.; Rde Camargo, E.; Barbosa, D. B. *Int J Antimicrob. Agents* **2009**, *34*, 103–10.
154. Hoffmann, S. *Scand. J. Plast. Reconstr. Surg.* **1984**, *18*, 119–26.
155. Chen, X.; Schluesener, H. J. *Toxicol. Lett.* **2008**, *176*, 1–12.
156. Grodzinski, P.; Silver, M.; Molnar, L. K. *Expert Rev. Mol. Diagn.* **2006**, *6*, 307–18.
157. Edwards-Jones, V. *Lett. Appl. Microbiol.* **2009**, *49*, 147–52.

## Chapter 7

# Application of Carbon Nanotubes to Wound Healing Biotechnology

**Trevor J. Simmons,[*,1,2,3,8] Christopher J. Rivet,[2,4]
Gurtej Singh,[2,5] Julie Beaudet,[1,2] Eric Sterner,[2,5]
Daniela Guzman,[9] Daniel P. Hashim,[10] Sang-Hyun Lee,[11]
Guoguang Qian,[6] Kim M. Lewis,[6] Pankaj Karande,[2,5]
Pulickel M. Ajayan,[10] Ryan J. Gilbert,[2,4] Jonathan S. Dordick,[2,3,4,5,7]
and Robert J. Linhardt[1,2,3,4,5,7]**

**[1]Department of Chemistry & Chemical Biology, [2]Center for Biotechnology & Interdisciplinary Studies, [3]Rensselaer Nanotechnology Center, [4]Department of Biomedical Engineering, [5]Department of Chemical & Biological Engineering, [6]Department of Physics, Applied Physics, and Astronomy, [7]Department of Biology,
Rensselaer Polytechnic Institute, Troy, New York 12180
[8]Coordinación para la Innovación y Aplicación de la Ciencia y Tecnología, [9]Departamento de Estomatología, Universidad Autónoma de San Luis Potosí, SLP México 78000
[10]Department of Mechanical Engineering & Materials Science,
Rice University, Houston, Texas 77005
[11]Department of Microbial Engineering, Konkuk University,
Seoul 143-701, Korea
[*]E-mail: simmot@rpi.edu**

Carbon nanotubes have remained at the center of nanotechnology research for the past two decades, and have been increasingly present in the areas of biology and biotechnology. While questions still remain about the toxicity of these materials, there is great interest in exploiting their unique properties to create innovative biotechnology applications. The application of carbon nanotubes to wound healing offers the possibility of dressings with enhanced functionality, controlled delivery of antiseptics, and real-time monitoring of healing events. By briefly examining the development of wound healing biotechnology, a context for

In Nanomaterials for Biomedicine; Nagarajan, R.;
ACS Symposium Series; American Chemical Society: Washington, DC, 2012.

the use of carbon nanotubes in modern medical practices can be established. Several applications have been evaluated by preliminary studies herein to provide a proof-of-concept demonstration of the potential of carbon nanotubes to be incorporated into wound healing biotechnology.

## Introduction

Carbon nanotubes (CNTs) are a quasi one-dimensional allotrope of carbon with an ever expanding range of applications. There are both single-walled nanotubes (SWNTs) and multi-walled nanotubes (MWNTs), and these nanotubes can be metallic, semi-metallic, or semiconducting depending on their chirality. Typically nanotubes have diameters of 1-50 nm depending on the number of $sp^2$-hybridized carbon walls, and lengths of several microns, giving them very high aspect ratios. These materials are exceedingly strong and flexible, showing superior mechanical properties compared to many conventional materials. Most applications of CNTs to date have been in materials science. CNTs are increasingly being considered for biomedical applications, although there are serious concerns over the toxicity of these materials. The medical application of CNTs been slowed by the complexity of the nano-bio interface and a common perception that such nanomaterials should be inherently toxic. This perception is based in part on lessons learned over the last century about the harmful effects of microparticulate and biopersistent materials such as asbestos. Despite these justifiable concerns, the application of CNTs to medicine, particularly as stable composites, offers potential benefits that require careful exploration. This chapter focuses on the application of CNTs to a model system, wound healing biotechnology.

## Wound Healing Biotechnology

The primary goal of wound care is to allow for rapid wound closure, prevent infection, and to improve the aesthetic appearance and maximize the functionality of the resulting scar tissue. The natural process of wound healing consists of three overlapping phases – inflammation, tissue formation, and tissue remodeling. For the sake of this study, we will focus on the first two stages of wound healing that are the primary foci of wound care strategies.

### Early Stages of Wound Healing

When a wound is sustained, typically there will be a disruption of blood vessels and surrounding tissues such as skin. Inflammation occurs in the early stage of wound healing, just after a clotting cascade where fibrin begins clotting to reestablish hemostasis while providing an extracellular matrix to enable cell migration. Platelets create a hemostatic plug while simultaneously releasing several wound healing mediators such as platelet-derived growth factor that both attracts and stimulates fibroblasts and macrophages. In the absence of hemorrhage, platelets are not believed to be essential to wound healing. Inflammatory leukocytes begin to work at the wound site while neutrophils cleanse the site of foreign matter and bacteria, with some undergoing phagocytosis by macrophages. Monocytes arrive at the wound site and become activated macrophages, which initiate the formation of granulation tissue. The macrophages continue phagocytosis to remove damaged tissues, foreign matter, and microbes. Inflammatory cytokines expressed at the wound site have effects such as the stimulation monocytes to become macrophages, promotion of colony formation, and the attraction of fibroblasts. Growth factors released by the monocytes and macrophages are also important, as reflected by defective wound repair in macrophage-depleted animals (*1*).

Tissue formation in the form of re-epithelialization begins to take place just hours from the initial injury. Epidermal cells from skin appendages such as hair follicles and sweat glands remove damaged stroma and clotted blood from the wound while undergoing phenotypic alterations. The epidermal and dermal cells no longer adhere to one another, as their hemidesmosomal links are dissolved. This allows for the lateral movement of the epidermal cells toward the center of the wound by following an ionic current known as the "current of injury" (*2*).The migrating epidermal cells dissect the wound, separating dried eschar from the viable tissues. The extracellular matrix begins to remodel as macrophages and fibroblasts use matrix metalloproteases to cut their way through the matrix and allow the epidermal cells to migrate between the collagenous dermis and the fibrin eschar. One to two days after the after the initial injury, the epidermal cells at the wound margin proliferate behind the migrating epidermal cells. The mechanism of cell migration is not clear, and several factors coordinate this activity (*3–5*). The epidermal cells eventually return to their normal phenotype during the remodeling phase, reattaching to the underlying dermis. The remodeling phase then continues for months to years, and the resultant scar tissue has reduced strength and functionality.

## Ancient Wound Care Techniques

Wound care may be one of the earliest forms of biotechnology. It is an animal instinct to lick wounds in an attempt to clean them and promote healing, and this can be observed in mammals such as dogs, cats, rodents, apes, and even humans. Prehistoric man should have noticed the connection between wound hygiene and recovery, and based on this likely began devising techniques to promote healing. Early hunter gatherers would surely have experimented with herbal and other natural remedies to aid wound healing and stop bleeding. One of the earliest wound care strategies is outlined in the Ebers Papyrus (*6*) ca. 1500 B.C., where a combination of grease from animal fat, cotton fibers, and honey was used for wound care. It is likely that this treatment was the result of trial and error and that the underlying mechanisms behind the success of the treatment were not completely understood at the time. The animal fats helped provide protection from the environment and kept the wound moist, the cotton fibers provided a fibrous matrix for clotting, and the honey was added as an antiseptic as well as perhaps a binder. Honey was one of the early antiseptic compounds placed on wounds, and while debate exists over its effectiveness (*7*), it continues to be used in modern medicine.

## Wound Care in the 19th and 20th Centuries

While wound care saw steady advances dating from prehistory, it was not until the 19th century that serious advances in medical science allowed for a revolution in wound care. One of the pioneers of medical hygiene was the American physician Oliver Wendell Holmes, an outspoken critic of medical practices of the 19th Century. He was criticized for his theories regarding the spread of puerperal fever, known today as septicemia, from doctor to patient. One critic, Charles D. Meigs, wrote (*8*) that doctors are gentlemen and that "…gentleman's hands are clean." The Hungarian obstetrician Ignaz Schemmelweis also supported the benefits of hand washing in maternal survival several years later in Vienna, and began using an analog of modern bleach as prophylaxis in 1847 to cleanse away "cadaverous particles" (*9*). This work was further developed in the 1860's by the British surgeon Joseph Lister, also known as the "Father of Modern Antisepsis", who developed several procedures and practices involving carbolic acid (phenol) solutions, non-porous materials in surgery, and the use of clean gloves (*10*). It was the early work of the French chemist Louis Pasteur that had motivated Joseph Lister, and this along with the work of Holmes and Schemmelweis helped establish the germ theory of disease, arguably the most significant advance in modern medicine. The German surgeons Ernst von Bergmann (*11*) and Paul Leopold Friedrich (*12*), would later introduce the heat sterilization of surgical instruments in 1886 and the excision of wound sites in 1898 respectively.

The 20th Century saw advances in synthetic polymers such as nylon, polyolefins, and polyvinyls. This provided a wide variety of new materials for the development of dressings and other wound care materials. During the mid-20th Century it was the work of the British doctor George D. Winter (*13*) that rediscovered the importance of moist wound healing, something noted by the Greek surgeon Galen of Pergamum ca. 120-200 A.D. (*14*). This is considered by many to be the dawn of modern wound care, with a significant enhancement of re-epithialization resulting in superior wound healing.

### *Antiseptics as a Double-Edged Sword*

The contributions of Holmes, Lister, and Schemmelweis involved the use of antiseptic chemicals to create a sterile environment in and around open wounds. While the development of such techniques has undoubtedly saved countless lives, it has been recognized that such antiseptics also pose the risk of causing undesirable effects as well. Bleach is an excellent disinfectant for surgical equipment, but is not recommended for cleaning wounds, as it has a deleterious affect on mammalian cells. The use of iodine tinctures has long been established as an effective topical antiseptic, and is generally considered non-toxic to humans. In fact some surgeries involve irrigation of the thoracic cavity with large quantities of povidone-iodine solution during surgery. Nevertheless, there have been reports of acute sensitivity in some patients causing serious complications (*15*). This suggests that to determine the suitability of an antiseptic, both the microbicidal activity and the cytotoxicity must be taken into consideration.

### Wound Care in the Modern Era

The rediscovery of moist wound healing by George D. Winter and Howard Maibach in the 1960's led researchers to design wound care strategies that more closely mimicked the human body. Superabsorbent polymers known as hydrogels were incorporated into treatments for burns and other wounds throughout the 1990's. Recent developments in tissue engineering have allowed for "living skin equivalents" to be created from cultured epithelial cells in a matrix such as a hydrogel or biopolymer. While these materials lack many of the components of whole living skin, they provide the potential for novel skin grafting techniques for extensive wounds.

## Use of Carbon Nanotubes in Biotechnology Applications

Since the emergence of carbon nanotubes in the early 1990's, there has been a steadily increasing interest regarding the application of these materials to existing technologies that had employed other carbonaceous materials such as graphite and charcoal, as well as to develop novel applications that would exploit the unique characteristics of these structures. While the actual number of carbon nanotube applications to biotechnology and other biologically centered fields of study is vast, they generally fit into one of several categories. The most commonly discussed categories are composites (*16*), interfaces (*17*), sensors (*18*), biomimetic actuators (*19*), drug delivery (*20*), and therapeutic agents (*21*). The present work encompasses several of these categories, namely composites, interfaces, sensors, and drug delivery.

### Elephant in the Room: Nanotoxicity

Although there are valid concerns about the safety of nanomaterials, their prudent use can result in remarkable improvements to existing technologies, and such possibilities cannot be ignored (*22*). Increasing attention has been focused on the impact of CNTs on cell growth, with results of some studies showing toxicity and others showing enhanced cell growth. These seemingly contradictory results can be rationalized by the various compositions, lengths, diameters, and levels of CNT purity, all of which can have a significant impact on their toxicity. Toxicity has been mainly attributed to the presence of metallic impurities, and to the presence of very small CNT fragments (*23*, *24*). The work presented here uses high purity CNT material (filtration allows for further reduction of amorphous carbon impurities and small CNT fragments) to create a novel conductive antiseptic bandage material. This material may enable the enhanced recovery of nervous and muscle tissue damage resulting from injury while preventing infection. Studies have shown that CNTs can be used effectively as scaffolds for the enhanced growth of mammalian cells such as neurons, stem cells, smooth muscle cells, and epithelial cells (*25*, *26*). These pre ious studies employed CNTs for cell growth substrates with no apparent toxicity, and provide motivation for the work presented herein.

## Carbon Nanotube-Based Antiseptic Bandages

Single wall carbon nanotubes (SWNTs) were combined with a water-based povidone-iodine (PVPI) complex as an aqueous suspension, which was then deposited as a film on a polytetrafluoroethylene (PTFE) filter membrane to form a three-dimensional nanocomposite network supported on PTFE. CNTs are routinely solubilized with povidone (also referred to as polyvinylpyrrolidone or PVP) by relying on a polymer wrapping mechanism that essentially encases the SWNT in a polymer monolayer (*27*) with a helical coil conformation, which is also the proposed structure of the povidone-iodine complex in water (*28*, *29*). The povidone-iodine complex (PVPI) has well-known antiseptic properties and is effective against a wide spectrum of pathogens, including *Escherichia coli* (*E. coli*) (*30*). Aqueous PVPI has been used as a topical antiseptic and surgical scrub for more than 40 years and microbial resistance has not yet been reported (*29*). Combining PVPI with SWNTs in water can allow for a stable water-based dispersion of SWNTs with iodine non-covalently bound to the surface. The film resulting from suction filtration onto a PTFE membrane is micro-porous, several microns thick, and has micron-length SWNTs randomly arranged within a polymer (povidone) coating. The SWNT–PVPI film (*31*) is highly flexible and remains bound to the PTFE membrane unless removed with an adhesive tape or similar adhesive material.

### *Synthesis of Antiseptic Bandage Material*

Comprehensive details (*31*) of the material synthesis and analysis are provided elsewhere, however selected procedures are restated here for clarity. Purified SWNTs, obtained from Swan Chemical, Inc., have less than 3.7% wt. ash content and less than 1.7% wt. iron content (the majority of which is encapsulated) according to the certificate of analysis from the manufacturer. An aqueous suspension of PVPI was obtained from Purdue L.P., as the product Betadine®. The SWNTs were solubilized in water by adding 10 mg SWNT to an aqueous solution that contained 1.5 mL PVPI solution (10% PVPI) and 18.5 mL deionized (DI) water, which is a ratio of approximately 150 mg PVPI to 10 mg SWNTs in 20 mL DI water, with a minority of stabilizing components present in Betadine® brand PVPI solution. The mixture is bath sonicated for 30 min to aid the suspension of SWNTs. The solution is then deposited onto a PTFE membrane with 1 μm pores (Millipore Omnipore JAWP-47mm) using vacuum filtration, after which the film is dried in an oven (60 °C) for several hours *in vacuo*. Analysis of the deposited material with scanning electron microscopy (SEM) revealed a tangled mat of CNT-PVPI fibers (Figure 1). The presence of iodine in the finished bandage material was confirmed using energy-dispersive X-ray spectroscopy (EDX) performed during the SEM imaging, which shows two substantial iodine peaks (Figure 2). Additional peaks from the polymer and the PTFE filter membrane were also observed. No peaks for iron catalyst impurities were observed, indirectly confirming the high purity of the material as claimed by the manufacturer.

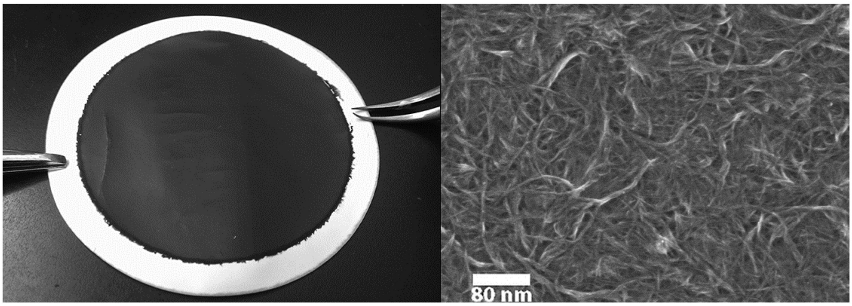

*Figure 1. Digital photograph (left) and field emission-scanning electron microscopy images of CNT–PVPI bandage material. The SWNTs in the bandage films are covered by a layer of PVPI, scale bar approximately 80 nm. Image (left) reproduced with permission from ref. (31). Copyright 2009 Elsevier.*

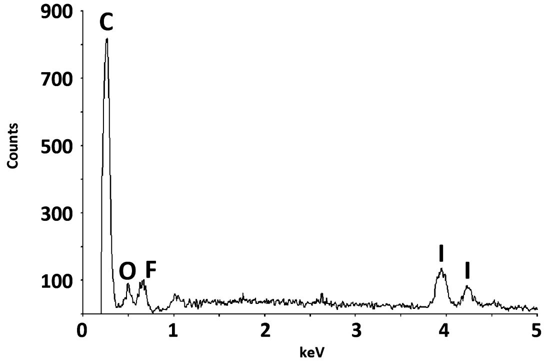

*Figure 2. Energy-dispersive X-ray spectroscopy data obtained during imaging in the electron microscope show peaks indicative of carbon, oxygen, fluorine, and iodine. Data reproduced with permission from ref. (31). Copyright 2009 Elsevier.*

## *Assessment of Antibacterial Properties with Escherichia Coli*

The antiseptic properties of the bandage were confirmed by applying the film to a bacterial culture for 48 h. *E. coli* BL-21 was transformed with pGFPuv (Clontech, CA, USA) by the standard calcium chloride method. The pGFPuv expresses β-galactosidase-GFPuv fusion protein that can be induced by isopropyl-β-D-1-thiogalactopyranoside (IPTG) and includes an ampicillin (amp) resistance gene [19]. Transformed *E. coli* was transferred on to the surface of Luria Broth (LB)/amp/IPTG agar and incubated at 37 °C for 24 h. Illuminating the agar surface with a UVA lamp, isolated green fluorescent colonies were picked and incubated in 10 mL LB/amp broth at 37 °C for 12 h. After centrifugation (5000 rpm, 10 min), the recombinant cells were washed with and resuspended in distilled water at a concentration of 104 CFU per mL. Then 0.1 ml of the cell suspension was spread on a LB/amp/IPTG agar plate. After drying for 30 min, CNT/PVP control and CNT/PVPI bandages were placed on the surface of separate agar plates and incubated at 37 °C for 48 h.

Upper images are bacterial cell cultures with the CNT material removed from the agar plates to reveal the amount of *E. coli* growth, with closer views of the CNT bandage material in the lower images. The control (A) shows a large number of *E. coli* colonies on the bandage material, while the CNT–PVPI sample (B) shows almost no colony formation on the bandage material after 48 h. The CNT–PVPI material significantly inhibited the growth of bacterial colonies, despite the growth medium containing a larger number of colonies than the control sample (Figure 3 & 4).

This material would be useful as a bandage for wounds where there is a significant risk of infection. PVPI solutions are routinely administered to gauze or other absorbent materials used as bandages and dressings, and placed on the wound site. This material is similar to conventional wound dressings that are both flexible and breathable, but unlike conventional dressings it is nanotextured and has a self-contained slow-release antiseptic with no known bacterial resistance. PVPI has been shown by numerous studies to have relatively low-toxicity to mammalian cells, although studies performed in our laboratories seem to contradict several studies that suggest PVPI will not slow wound healing or cell growth (*32–34*), and this point will be discussed in the following section of this chapter.

The most common method for the application of PVPI to wounds is to presoak standard bandage material prior to application. This method presents the possible hazard of causing burns to the skin from irritation caused by excess PVPI solution (*35*). The advantage of the CNT–PVPI bandage is that it is embedded with dry PVPI supported by SWNTs, and would be ready for immediate use, with no risk of burns from excess PVPI solution being trapped against the skin. The iodine is slowly released from the PVPI complex wrapping SWNTs (Figure 5), leaving behind PVP wrapped SWNTs in the bandage material, as they are strongly bound in the woven network of the bandage material.

The iodine is released from the SWNT-PVPI into the fluids at the wound site, as well as any unbound PVPI in the bandage material. PVP is a water soluble polymeric surfactant, and therefore there will not be any significant binding of tissue to the bandage material which is completely coated by the PVPI. When cellular adherence is desired, this can be controlled by the addition of a polymer such as poly-L-lysine (PLL). SWNTs which are not completely wrapped by the PVPI in solution are removed during the solution processing, and therefore all of the bandage material is covered with a layer of PVPI, and there is no significant amout of direct contact between CNTs and the cells at the wound site.

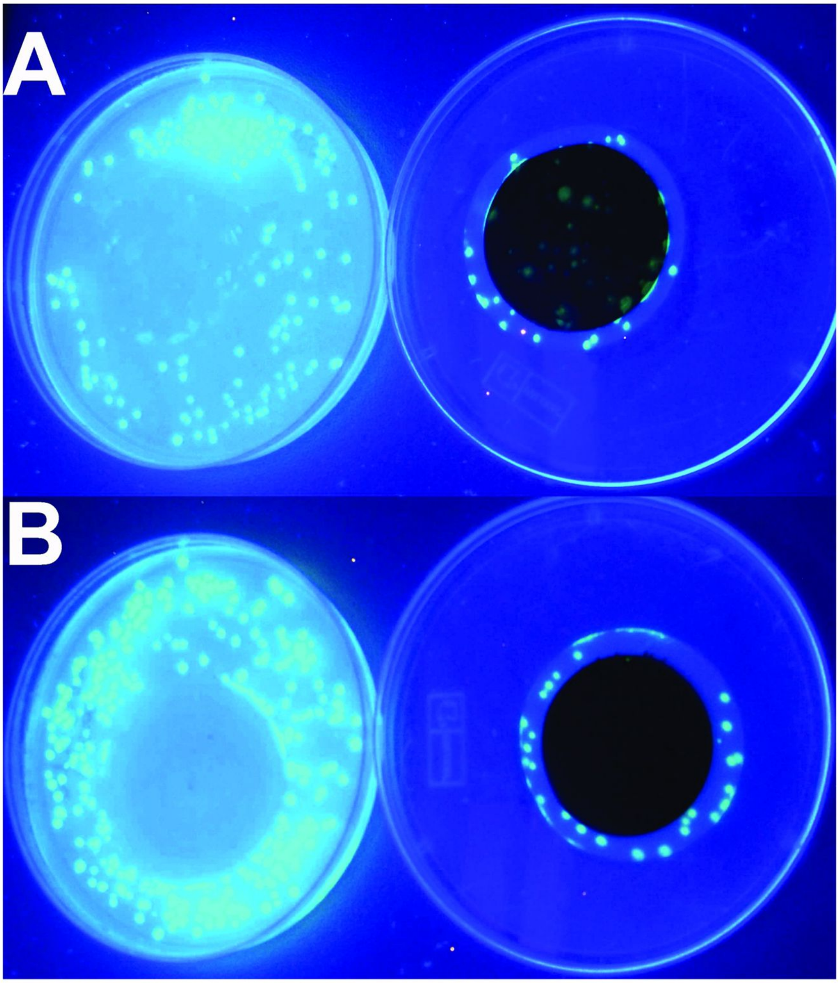

*Figure 3. Photographs of bacterial growth media (left) and bandage material (right). CNT–PVP control (A) and CNT–PVPI (B) on 47mm PTFE filter membranes, under UVA illumination. Images reproduced with permission from ref. (31). Copyright 2009 Elsevier. (see color insert)*

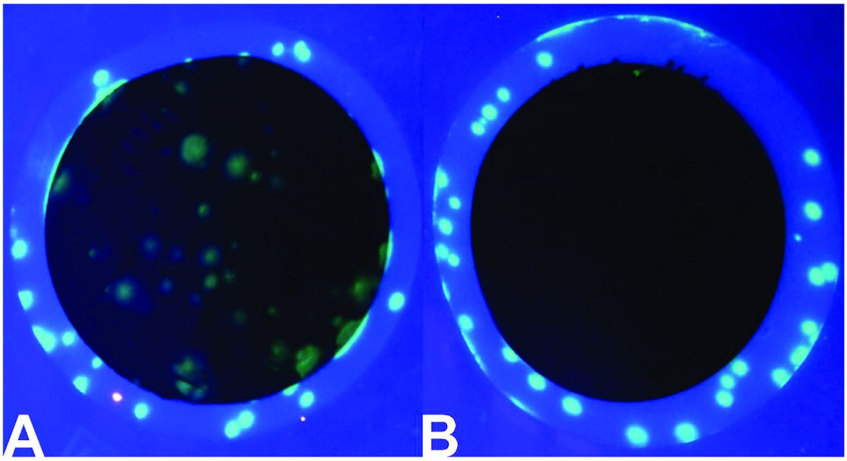

*Figure 4. Photograph showing the control (A) sample showing significant E. coli growth, while the iodine containing sample (B) shows virtually no E. coli growth. Images reproduced with permission from ref. (31). Copyright 2009 Elsevier. (see color insert)*

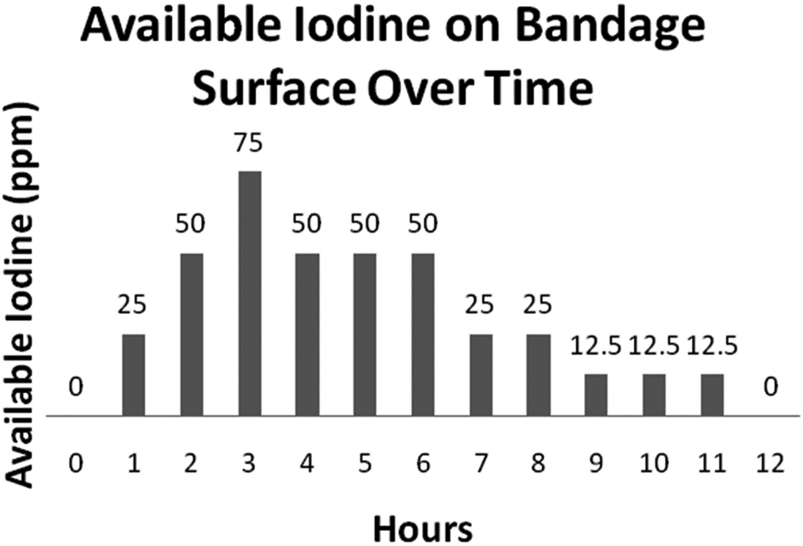

*Figure 5. Measurement of available iodine at the bandage surface using iodine test paper containing starch and potassium iodide. A bandage sample 1 cm$^2$ was soaked in 2 mL phosphate buffered saline (PBS) solution at 37° C, with the solution being changed after each measurement. Data reproduced with permission from ref. (31). Copyright 2009 Elsevier.*

### *Keratinocyte Growth Study*

Although there are numerous studies which suggest that PVPI is of low-toxicity to human keratinocytes and other cells (*32–34*), other studies have suggested the contrary. It has been shown (*36*) that even dilute PVPI solutions will inhibit the growth of human fibroblast cells. In light of these conflicting bodies of work, a study was carried out to evaluate the effect of PVPI containing CNT films on human keratinocyte growth. CNT-PVPI films were created as previously described, and one set of films was washed thoroughly with deionized water to remove excess PVPI and to reduce the overall iodine content of the film. Another set of films was prepared by substituting PVP (10 kDa, Aldrich) solution for the PVPI solution (equivalent concentration), to provide a control with no iodine content.

Human keratinocytes (HaCaT cell line) were generously donated by Dr. Torsten Wittmann at the University of California at San Francisco. These cells were cultured at 37°C in 5% $CO_2$ in Dulbecco's modification of Eagle's Medium (DMEM; Mediatech). It was additionally supplemented with 15% Fetal Bovine Serum (FBS; Thermo Scientific) and 1% penicillin/streptomycin (Mediatech). The culture media was changed every three days, and the cells were routinely passaged in 75 $cm^2$ tissue culture flasks, discarding after 20 passages. A solution of 0.25% Trypsin/ethylene diaminetetraacetic acid (EDTA) (Mediatech) was used to harvest the cells. These human keratinocytes were added onto the CNT-PVPI and CNT-PVP films at a density of 25,000 cells in a volume of 100 μL in wells of a 96-well plate. Experiments were carried out in duplicate. The cells were incubated for 24-48 h and then evaluated by confocal fluorescence microscopy. The positive and negative controls were seeded with identical cell concentrations and incubated under identical conditions. Bovine serum albumin (BSA) inhibits cell attachment to growth surface while PLL promotes cell attachment, and therefore these materials were chosen for the negative and positive controls repectively. The polystyrene well plates of the negative and positive controls were exposed to a 5g/100 mL PBS solution of BSA and PLL respectively for 3 hours, then rinsed with fresh PBS solution and seeded.

Cellular viability was assessed using calcein-AM, a fluorescent green dye that becomes activated upon cleavage by intracellular esterases in live cells, and propidium iodide which is a red nuclear stain that is membrane permeable only for dead cells. Cells were first stained with propidium iodide in PBS (2μg/mL) for 30 minutes and washed twice with fresh PBS. Cells were then stained with a solution of calcein-AM in PBS (2μg/mL) for 15 minutes, washed twice with fresh PBS and imaged using an Olympus DSU fluorescence microscope. All samples were imaged at 4x magnification using constant exposure times and electronic gain settings.

It was immediately clear that the iodine containing films, even the washed CNT-PVPI films, showed very few live cells (Figure 6). The control CNT-PVP films showed growth of living cells at 24h and substantial clusters of live cells after 48 h. The cellular population of PVPI containing films do seem to corroborate the studies that claim PVPI inhibits the growth of mammalian cells (*36*). The slow increase of live cell populations of PVPI containing films over 48 h seems to confirm that the iodine inhibits growth but is not acutely toxic, suggesting that PVPI does exhibit a low-toxicity to mammalian cells (*32–34*). The presence of polymer coated CNTs were not noticeably toxic to the cells, and this has also been reported in previous studies (*31*, *37*, *38*). The CNT-PVP film containing PLL showed results similar to the positive control (PLL coated cover glass). These findings suggest that the use of iodine in such CNT-PVP films should be limited in cases where the rapid establishment of keratinocytes and other mammalian cells is critical. If infection of the wound site by bacteria, fungi, or viruses is the key concern, then the use of iodine in such CNT-PVP films is acceptable. CNT-PVPI films would prevent the establishment of such infections, and eventually allow for the growth of keratinocytes and similar cells after a period of time. If the use of iodine-based antiseptics is indicated in a particular case, this study suggests that it would be acceptable to employ the CNT-PVPI bandage films to the wound site.

## Electrical Stimulation To Promote Wound Healing

Humans and other animals have bioelectric systems that help to coordinate wound healing. One example of this is in the red spotted newt (*2*), where a steady polarized ionic current is produced when a limb is amputated, and continues until the limb has regrown. This "current of injury" was discussed previously in the outline of early wound healing. Keratinocytes migrate toward the center of a wound by following the current of injury along with other cues, and for this reason it is possible to increase the cell mobility at a wound site with electrical stimulation. Directed movement of cells by electric currents is known as galvanotaxis, and has been shown to occur within 10-20 minutes of direct current (DC) stimulation (*39*).

### Electrical Stimulation of Keratinocytes with Carbon Nanotube Films

In addition to the antibacterial properties of this CNT-PVPI material, it is also a conductive material, showing a sheet resistance of approximately 10 kΩ/sq. Conductivity was determined by both 2-point and 4-point probe measurements, with an inter-probe distance of 1mm. The resistance determined was low enough to allow a significant electrical current to be passed through the material. This desirable electrical property makes it possible to explore enhanced cell growth through electrical stimulation, as electrical currents can enhance growth of cells such as neurons, keratinocytes, and fibroblasts (*40*). Liopo et al. showed that electrical stimulation through SWNT networks can help carry ionic currents that aid in the extension of neurites, and ultimately in building networks between nerve cells (*41*). Unfortunately it is contraindicated to use electrical currents in the presence of metals and certain elements, and this is especially important when antimicrobial metals like silver and elemental iodine may be present. It is for this reason that the electrical stimulation of cells should be performed only with CNT-PVP materials, and not CNT-PVPI materials. Therefore it will be necessary to develop alternative antiseptic agents if they are to be included in an electrical stimulation application.

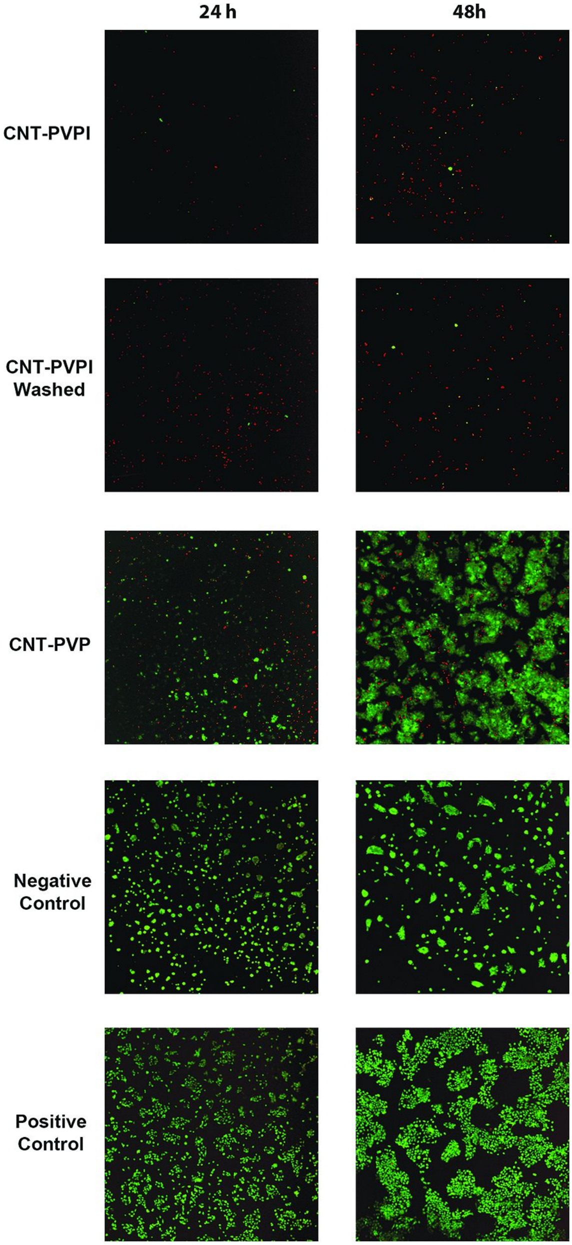
24 h
48h
CNT-PVPI
CNT-PVPI Washed
CNT-PVP
Negative Control
Positive Control

*Figure 6. Confocal fluorescence microscopy images of live (green) and dead (red) cells after 24 (left) and 48 (right) hours respectively. All samples showed live cells after 24 h and an increase in live cells after 48 h, but the iodine containing samples (top and middle sets) showed significantly less. The negative control was grown on a BSA coated polystyrene well, and the positive control was grown on a PLL coated polystyrene well. (see color insert)*

CNT-PVP films were evaluated as an electrically stimulating bandage for wound healing applications. Human keratinocytes cultured under conditions identical to those previously discussed in the cell viability study were seeded onto the carbon nanotube films at a density of 25,000 cells in a volume of 40 µL, creating a circular droplet. They were allowed to attach for a period of 3 h in a cell incubator. After 3 h of attachment, one of the carbon nanotube films was connected to a MPJA-14602PS DC power source with two gold-coated glass electrodes. The DC voltage supplied was set at 200 µV/mm at approximately 30 mA, which was calibrated to deliver approximately 50-100 µV/mm to the culture media containing the keratinocytes. The voltage was maintained between the electrodes with the keratinocytes in culture media in the middle of the carbon nanotube film avoiding direct contact with the electrodes (Figure 7).

The voltage was maintained for 1 h, with a drop in current from 30 mA to 20 mA over that time. During this time, an identical control sample, which received no electrical stimulation, was incubated in identical conditions. After the 1 h electrical stimulation, the cells on both the carbon nanotube films were then incubated for an additional 24 h before imaging. The same experiment was repeated with same cell seeding (25,000 cells), but in a volume of 100 µL, creating a relatively large circular droplet approximately 1 cm in diameter. These 100 µL cultures were allowed 3 h of attachment, 1 h of electrical stimulation, and 3 more h of growth. The effect of the electrical stimulation was examined by confocal fluorescence microscopy using calcein-AM to stain live cells (Figure 8).

As can be seen from the images, the cells in the electrically stimulated bandages (for both A and B, lower sets) are more widely distributed. There appears to be a directionality reflected in the growth pattern of the cells, with a larger proportion of the cells towards the direction of the cathode (+), which is the expected behavior for galvanotaxis of human keratinocytes subjected to DC current (*39*). This suggests that the CNT-PVP films were capable of delivering biologically relevant electrical stimulation to human keratinocytes. The smaller more evenly distributed cell clusters would allow for better coverage of an affected wound site, and increase the mobility of the keratinocytes. Increasing the mobility of keratinocytes is a critical component of wound healing, as this has been shown to minimize the effects of scarring (*42*).

## Wound Monitoring with CNT Bandage

Real-time monitoring of wounds *in situ* is an important technological goal that is gaining increasing attention from researchers. The wound healing process is a complex and dynamic series of events, making it difficult for a single treatment strategy to be applicable in every case. It would be preferred for medical professionals to have the ability to respond to changes in the wound environment as they occur, and not rely on invasive procedures such as bandage removal for periodic observation of wound sites. Reduction in bandage and dressing removal for wound assessment would be an additional benefit of such *in situ* wound monitoring, as it would it would reduce pain and limit the possibility of infection. Several optical strategies are currently being developed that rely on *in situ* immunofluorescence techniques targeting specific growth factors and proteins. In addition to such advanced techniques are complementary methods to detect changes in wound site conditions such as pH and moisture. These *in situ* wound monitoring techniques offer promise of a future where bandages can keep medical professionals updated on the status of a wound and deliver therapeutic agents at their discretion.

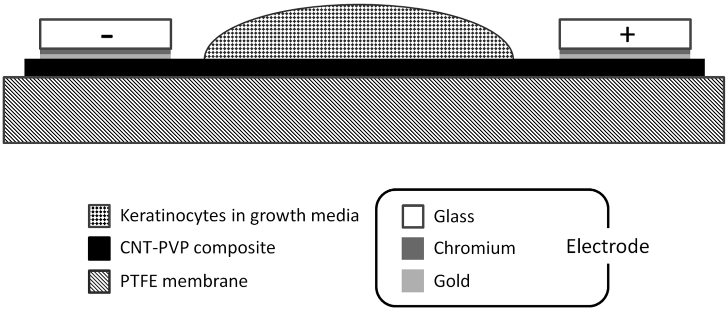

*Figure 7. Schematic diagram of electrical stimulation experimental setup. Keratinocytes in a liquid growth media are deposited on a CNT-PVP composite film supported on a PTFE membrane. Two gold coated glass electrodes are placed on either side of the CNT-PVP film. There is a layer of chromium primer on the glass that allows for greater adherence of the gold.*

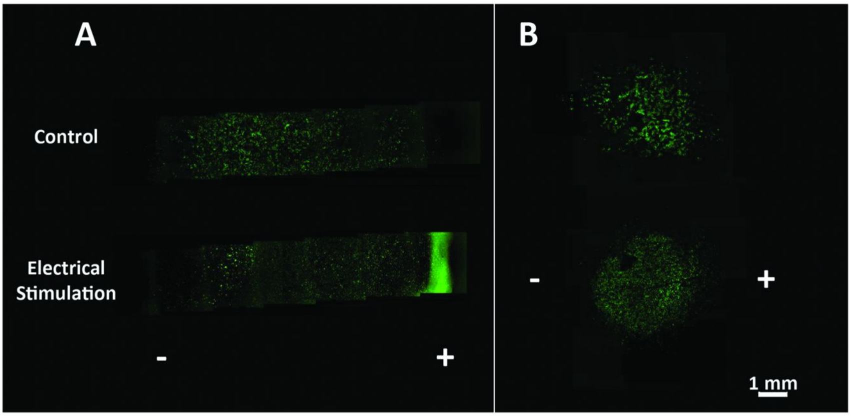

*Figure 8. Confocal fluorescence imaging of live human keratinocytes at 4x magnification. The samples of both the 7 h (A) and 28 h (B) total incubation times show that the control set presents larger clusters of cells, while the electrically stimulated set shows a larger number of smaller clusters. The large green band seen on the electrically stimulated 7 h sample (A, lower) was identified by energy dispersive X-ray spectroscopy as NaCl. (see color insert)*

## Real-Time Monitoring of Clot Drying as Proof-of-Concept

The electrical conductivity of carbon nanotubes was exploited to demonstrate a simple proof-of-concept for use of CNT-PVP films for *in situ* wound monitoring. A simulated clot was created by combining 1 mL of a 10 mg/mL solution of fibrinogen in Dulbecco's phosphate buffered saline (DPBS) solution with 48 µL of a 50 U/mL solution of thrombin in DPBS. These two solutions were combined on the center of bandage with the fibrinogen being added first. The initial electrical resistance of the film studied was approximately 600 Ω, and the addition of PBS to completely wet the film and the supporting PTFE membrane reduced this resistance to approximately 250 Ω. The CNT-PVP film wetted with PBS was given several minutes to equilibrate before testing began. The formation of the simulated clot on the surface of the bandage did not appreciably change the resistance. Once the clot formed, it was allowed to dry in ambient conditions (25 °C and 35% relative humidity). The studied was continued for 18 h and electrical measurements were digitally recorded by an automated LabVIEW program running on a desktop computer interfaced with a Keithley 2400 sourcemeter.

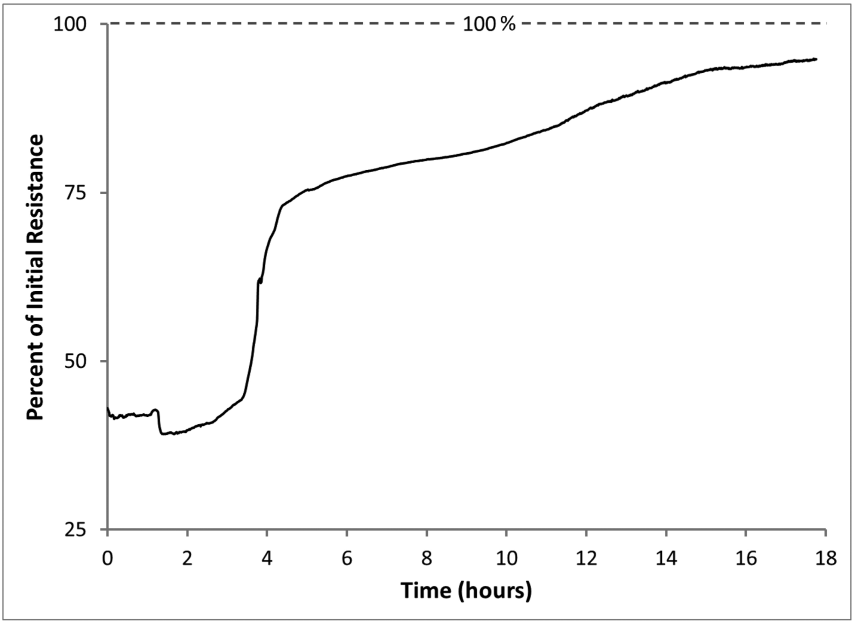

*Figure 9. Electrical resistance monitoring of drying of a CNT-PVP bandage film with a simulated clot. Drying of the clot at 25 °C shows a sharp increase in resistance at 4 h, returning quickly to approximately 75% of the initial resistance (~600 Ω).*

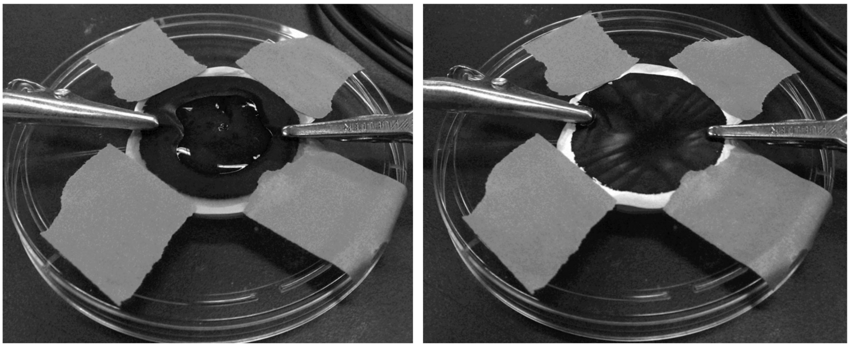

*Figure 10. Simulated clot (fibrinogen and thrombin in PBS) on CNT-PVP film before (left) and after (right) drying for 18 h at 25 °C.*

After remaining essentially constant for about 1 h, a sudden drop was noted, followed by a slow increase until about 3 h (Figure 9). The resistance significantly increased between 3h 15 m and 4 h 15 m, and then maintained a relatively steady increase for the remaining 14 h of the study. The final resistance at 18 h was approximately 95% the initial value, and the bandage material appeared to be completely dried with an obvious residue from the simulated clot remaining (Figure 10).

## Conclusions

In summary, we have developed a novel nanocomposite material from the combination of SWNTs with PVP in aqueous media. The filtration of this aqueous suspension creates a high purity micro-porous film that can have antiseptic iodine available on the surface of a network of SWNT wrapped in polymer. This material is strongly antiseptic and control samples lacking iodine had no noticeable microbicidal activity towards *E. coli*, which further supports the suitability of this material for use as an antiseptic bandage. This study showed that although PVPI is accepted as a low-toxicity antiseptic for mammals, the application of the CNT-PVPI material must be judicious, taking into account the inhibition of cell growth during the initial 48 hours. Electrical pulses sent through this SWNT composite material may allow for enhanced cell growth as in several previous studies, and possibly enable faster reconnection of damaged neuronal networks. When carefully employed, CNTs can be non-toxic to mammalian cells and therefore an extremely valuable addition to medicine, biotechnology, and therapeutics. Further studies will be needed to fully determine the efficacy of this bandage with regard to wound healing, and the effects of electrical stimulation on neuronal growth. Moreover, future experiments will be required to integrate both an antiseptic strategy with an electrical stimulation strategy in the same material. To accomplish this, an antiseptic other than iodine or silver must be identified, and incorporated with the CNT-PVP material. Ultimately the goal of materials development for modern wound care should be to develop “smart” bandages and dressings. These smart materials should both carry out *in situ* monitoring of wounds and deliver therapeutic agents at appropriate points in the wound healing process to accelerate recovery, reduce pain, and minimize scarring.

## Acknowledgments

Abigail Koppes provided helpful suggestions and expertise in the area of electrical stimulation of cells. Michael Figueroa led discussions on the affect of iodine on cellular growth and helped direct the aims of this work. Raymond Dove kindly provided guidance on the SEM imaging techniques used. TJS and PMA acknowledge previous financial support from National Science Foundation, Materials World Network: Fabrication of Polymer Composites and Sensors Using Doped Nanotubes, grant DMR-0801012. TJS also acknowledges support from JNC Corporation through the Rensselaer Nanotechnology Center. RJL acknowledges support from the National Institutes of Health, grant AI06578, and from the Rensselaer Nanotechnology Center. JB acknowledges the support of the National Institutes of Health, grant GM090257. ES acknowledges support from the National Institutes of Health Bioengineered Research Partnership grant HL096972. RJG and CJR acknowledge support from the National Institutes of Health through the National Institute of Neurological Disorders and Stroke, grant R21NS62392. KML and GQ acknowledge the support of the Department of Physics, Applied Physics, & Astronomy at Rensselaer Polytechnic Institute. DPH is grateful to the National Science Foundation for the Graduate Research Fellowship Award, grant 0940902.

## References

1. Leibovich, S. J.; Ross, R. *Am. J. Pathol.* **1975**, *78*, 71–100.
2. Jenkins, L. S.; Duerstock, B. S.; Borgens, R. B. *Dev. Biol.* **1996**, *178*, 251–262.
3. Nanney, L. B.; King, L. E., Jr. In *The molecular and cellular biology of wound repair*, 2nd ed.; Clark, R. A. F., Ed.; Plenum Press: New York; 1996; pp 171−194.
4. Abraham, J. A.; Klagsbrun, M. In *The molecular and cellular biology of wound repair*, 2nd ed.; Clark, R. A. F., Ed.; Plenum Press: New York; 1996; pp 195−248.
5. Werner, S.; Smola, H.; Liao, X.; Longaker, M. T.; Krieg, T.; Hofschneider, P. H.; Williams, L. T. *Science* **1994**, *266*, 819–22.
6. Ghalioungui, P. *The Ebers papyrus. A New English Translation, Commentaries and Glossary*; Academy of Scientific Research and Technology: Cairo, Egypt, 1987; Vol. 1, pp 1−298
7. Moore, O. A.; Smith, L. A.; Campbell, F.; Seers, K.; McQuay, H. J.; Moore, R. A. *BMC Complementary Altern. Med.* **2001**, *1*, 2.
8. Meigs, C. D. *On the Nature, Signs, and Treatment of Childbed Fevers*; Blanchard and Lea: Philadelphia, PA, 1854; Vol. 1, p 104.

9. Benedek I. *Ignaz Philipp Semmelweis: 1818-1865*; Corvina Kiadó: Budapest, Hungary, 1983.
10. Lister J. *Antiseptic Principle in the Practice of Surgery*, read by Joeseph Lister before the Surgical Section of the Annual Meeting of the British Medical Association in Dublin, August 9, 1867. Reprinted in *Br. Med. J.* **1967**, *2* (5543), 9–12.
11. Luther, B.; Wirth, I. *Zentralblatt für Chirurgie* **1986**, *111* (22), 1389–97.
12. Worm, V. *Zentralbl. Chir.* **1976**, 9.
13. Winter, G. D. *Nature* **1962**, *193* (4812), 293.
14. Carterand, M. J.; Fife, C. E. In *Microbiology of Wounds*; Percival, S., Cutting, K., Eds.; CRC Press: 2010; pp 345–372.
15. Campistol, J. M.; Abad, C.; Nogue, S.; Bertran, A. *J. Cardiovasc. Surg. (Torino)* **1988**, *28*, 410–412.
16. Yang, W. R.; Moghaddam, M.; Taylor, S.; Bojarski, B.; Wieczorek, L.; Herrman, J.; McCall, M. *Chem. Phys. Lett.* **2007**, *443*, 169–172.
17. Suehiro, J.; Ikeda, N.; Ohtsubo, A.; Imasaka, K. *Microfluid. Nanofluid.* **2008**, *5* (6), 741–747.
18. Lin, Y. H.; Lu, F.; Tu, Y.; Ren, Z. F. *Nano Lett.* **2004**, *4* (2), 191–195.
19. Vohrer, U.; Kolaric, I.; Haque, M. H.; Roth, S.; Detlaff-Weglikowska, U. *Carbon* **2004**, *42* (5−6), 1159–1164.
20. Bianco, A.; Kostarelos, K.; Prato, M. *Curr. Opin. Chem. Biol.* **2005**, *9*, 674–9.
21. Mashal, A.; Sitharaman, B.; Li, X.; Avti, P. K.; Sahakian, A. V.; Booske, J. H.; Hagness, S. C. *IEEE Trans. Biomed. Eng.* **2010**, *57* (8), 1831–1834.
22. Lacerda, L.; Bianco, A.; Prato, M.; Kostarelos, K. *Adv. Drug Delivery Rev.* **2006**, *58*, 1460–70.
23. Shvedova, A. A.; Castranova, V. *J. Toxicol. Environ. Health, Part A* **2003**, *66* (20), 1909–1926.
24. Monteiro-Riviere, N. A.; Nemanich, R. J.; Inman, A. O.; Wang, Y. Y.; Riviere, J. E. *Toxicol. Lett.* **2005**, *155*, 377–384.
25. Jan, E.; Kotov, N. A. *Nano Lett.* **2007**, *7* (5), 1123–1128.
26. MacDonald, R. A.; Laurenzi, B. F.; Viswanathan, G.; Ajayan, P. M.; Stegemann, J. P. *J. Biomed. Mater. Res. A* **2005**, *74A* (3), 489–96.
27. Bravo-Sanchez, M.; Simmons, T. J.; Vidal, M. A. *Carbon* **2010**, *48* (12), 3531–3542.
28. Simmons, T. J.; Hashim, D. P.; Vajtai, R.; Ajayan, P. M. *J. Am. Chem. Soc.* **2007**, *129* (33), 10088–10089.
29. Betadine® Microbicides (which contain povidone-iodine) Product Information. Purdue Products L.P., 2005.
30. Houang, E. T.; Gilmore, O. J. A.; Reid, C.; Shaw, E. J. *J. Clin. Pathol.* **1976**, *29* (8), 752–755.
31. Simmons, T. J.; Lee, S-H.; Park, T-. J.; Hashim, D. P.; Ajayan, P. M.; Linhardt, R. J. *Carbon* **2009**, *47*, 1561–1564.
32. Müller, G.; Kramer, A. J. *Antimicrob. Chemother.* **2008**, *61* (6), 1281–1287.
33. Zhou, L. H.; Nahm, W. K.; Badiavas, E.; Yufit, T.; Falanga, V. *Br. J. Dermatol.* **2002**, *146* (3), 365–74.
34. Banwell, H. *Dermatology* **2006**, *212* (S1), 66–76.

35. Nahlieli, O.; Baruchin, A. M.; Levi, D.; Shapira, Y.; Yoffe, B. *Burns* **2001**, *27* (2), 185–188.
36. Balin, A. K.; Pratt, P. *Dermatol. Surg.* **2002**, *28*, 3.
37. Monteiro-Riviere, N. A.; Inman, A. O.; Wang, Y. Y.; Nemanich, R. J. *Nanomedicine* **2005**, *1*, 293–299.
38. Firme, C. P., III; Bandaru, P. R. *Nanotechnol., Biol., Med.* **2010**, *6*, 245–256.
39. Fang, K. S.; Farboud, B.; Nuccitelli, R.; Isseroff, R. R. *J. Invest. Dermatol.* **1998**, *111*, 5.
40. McCaig, C. D.; Rajnicek, A. M.; Song, B.; Zhao, M. *Physiol. Rev.* **2005**, *85*, 943–978.
41. Liopo, A. V.; Stewart, M. P.; Hudson, J.; Tour, J. M.; Pappas, T. C. *J. Nanosci. Nanotechnol.* **2006**, *6* (5), 1365–74.
42. Park, J-. C.; Park, B. J.; Suh, H.; Park, B. Y.; Rah, D. K. *Yonsei Med. J.* **2011**, *42* (6), 587–594.

## Chapter 8

# Laser-Induced Rupture of Infrared Dye-Doped Liposomes

**Honoh Suzuki,[*] I-Yin Sandy Lee, and Takuro Sakai**

**Department of Chemistry, University of Toyama, 3190 Gofuku,
Toyama 930-8555, Japan
[*]E-mail: honoh@sci.u-toyama.ac.jp**

Near-infrared dyes can be used as a highly localized heat source in nanostructures. Laser irradiation to dye-doped liposomes causes giant temperature- and pressure-jumps at the lipid bilayer, resulting in the rupture of liposomes. This laser-induced process is promising in medical applications such as drug delivery and photodynamic therapy. Photoacoustic generation of a spherical pressure wave in microscopic domains also suggests the possibility of micro- or nano-implosion, which may offer a powerful mechanism for spontaneous focusing of photoacoustic energy in solution. In this chapter, we discuss laser-induced dynamics in liposome solutions studied by fluorometry and time-resolved phase-contrast microscopy. Microscopic snapshots suggest very fast and spherically symmetric rupturing dynamics that is consistent with Mie theoretical calculations and photoacoustic simulations.

## Introduction

Liposomes (lipid bilayer vesicles) have a history of research over half a century and are one of the most successful pharmaceutical carriers in drug delivery systems to date. Since its discovery in 1964, tremendous efforts have been made toward clinical realization, in such aspects as efficient drug encapsulation, protective coating, targeting, and controlled release. The FDA approval of Doxil (liposome coated with polyethylene glycol and encapsulating an anti-cancer drug, doxorubicin) in 1995 was certainly a landmark; other liposomal drugs are also used in clinical practice today (*1*).

In Nanomaterials for Biomedicine; Nagarajan, R.;
ACS Symposium Series; American Chemical Society: Washington, DC, 2012.

Liposome technology still has a lot of room for improvement, especially in active targeting and intelligent drug release. For example, attachment of antibodies to the lipid surface can lead to the active targeting for specific cancer cells (*2*). Incorporation of pH- or temperature-sensitive elements also makes 'smart' liposomes that can release the drug in response to environmental triggers (*3*, *4*). Rapid progress in the design of smart liposomes, including utilization of redox potentials and magnetic fields, can be found in recent reviews (*5*, *6*). The current bottleneck is, however, that the more precise engineering is necessary for the more complex systems to go through clinical trials. Biologically safer materials as well as novel approaches that have generality and wide applicability are desirable.

Among various drug activation triggers, use of laser light has shown remarkable success in recent years. Photodynamic therapy (PDT), the origin of which is also old (dates back to 1900), combines light and an administered photosensitizer (*e.g.* Haematoporphyrin Derivative and Photofrin) that serves to activate molecular oxygen, which in turn attacks target cancer cells. It received the first approval for cancer treatment in Canada in 1993, followed by approvals in several other countries shortly after that. Although not as ideal as smart targeting would be, fiber optical delivery of laser light offers convenience for local irradiation to near-surface tumors. Second and third generation photosensitizers, intended for improved activity, selectivity, and targeting, are now at a development stage (*7*).

In view of the success and further potentials of liposome-based therapeutics and PDT, it is natural to expect that a hybrid approach combining the two may also be fruitful. In particular, light can be used both to trigger the drug release and to activate it, possibly with a different wavelength for each functionality. This idea does not appear to have been extensively developed so far. In PDT, liposomal formulation is commonly utilized for solubilization of hydrophobic photosensitizers, in a similar way to emulsions, cyclodextrins, detergents, and lipoproteins. In such cases, the role of liposome is merely a solubilizer.

On the other hand, various types of light-sensitive smart liposomes have been proposed (*8–10*). In these studies, photo-induced structural changes of the dye molecule (spiropyran, rhodopsin, or azobenzene derivative) embedded in the bilayer are shown to alter the permeability across the membrane and trigger the drug release. The main drawback of this sophisticated approach is that the photon energy required for the structural change is relatively high: it is rather difficult to move into longer wavelengths that are convenient for biomedical applications.

The wavelength range of photons useful for biomedicine is primarily determined by the tissue transmittance. The red and near-infrared (NIR) region (800 - 1100 nm), in between hemoglobin and water absorption bands, is called the therapeutic window for deep penetration of light, where biological tissue shows low absorption and scattering with a typical penetration depth of 1 - 9 mm (*11*). This window mainly corresponds to photothermal processes rather than photochemical ones, so that it is most useful in laser-induced thermotherapy and surgery. PDT requires the photon energy considerably greater than 94 kJ $mol^{-1}$ (1270 nm) to generate singlet oxygen, and has difficulty in reaching this window; the current PDT practice uses 630 nm, and thus the penetration is not optimal.

To make the best use of the NIR window, one must resort to a multiphoton mechanism, such as two-photon PDT (*12*), unfortunately with the disadvantage of a low quantum yield.

In this chapter, we present some results from our attempt to use NIR laser pulses to trigger the drug release from liposomes. Lipids have little absorption in the therapeutic window, so that we need a photosensitizer. We have chosen a non-fluorescent NIR dye that converts photons into heat very effectively. It is well suited for photothermal and photoacoustic (as opposed to photochemical) processes, which are a sort of multiphoton events that accumulate and release photon energies as heat or pressure, and expected to carry impacts large enough to break the liposome. Fluorometry showed that this is actually the case. Time-resolved microscopy, together with photothermal and photoacoustic simulations, revealed that two mechanisms, implosion and cavitation, are operating in the microscopic region inside and outside of the spherical liposome. These two phenomena are well known in the fields of detonation and nuclear physics, sonochemistry, and medical ultrasonics, but quite new in drug delivery. The generality of the concept may benefit the future development of laser-assisted biomedicine.

The following sections are arranged as follows. First, we introduce optical properties of the NIR dye, and discuss possible design strategies for the NIR-sensitive liposomes. Second, experimental results are given to show the success of NIR laser-induced drug release. Third, laser-liposome interactions and the resulting events (photothermal and photoacoustic processes) are analyzed by Mie theory and simulations, which indicate the relevant time and length scales of each process as well as the possibility of micro-implosion. Fourth, snapshots from time-resolved microscopy are presented to reveal transient, microscopic bubble formation. Finally, we briefly suggest prospects for future directions.

## Design of NIR-Sensitive Liposomes

### NIR Dye

The dye of our choice, *N,N,N',N'*-tetrakis(*p*-diethylaminophenyl)-*p*-benzoquinone-bis(imonium) perchlorate (IRG-023, Nippon Kayaku), is a non-fluorescent NIR dye with a strong absorption band closely matching the Nd-YAG laser (Figure 1). It was originally developed as a singlet oxygen quencher to protect cyanine dyes in the industrial production of CD-R (Compact Disc Recordable) (*13*). An analogous dye with butyl groups and hexafluoroantimonate anion (IR-165, American Cyanamid) is used in laser-protective goggles, and its ultrafast photothermal dynamics has been studied in detail by picosecond laser spectroscopy (*14*). The dye can absorb tens of photons during a picosecond pulse, rapidly convert their energy into heat via vibronic couplings and phonon up-pumping, and generate huge temperature jumps (up to 720 K in the molecular hot spot and 70 K in the bulk solution); hence it is termed a 'molecular heater.' Our preliminary studies showed that IRG-023 is significantly more stable than IR-165 in aqueous liposome solution.

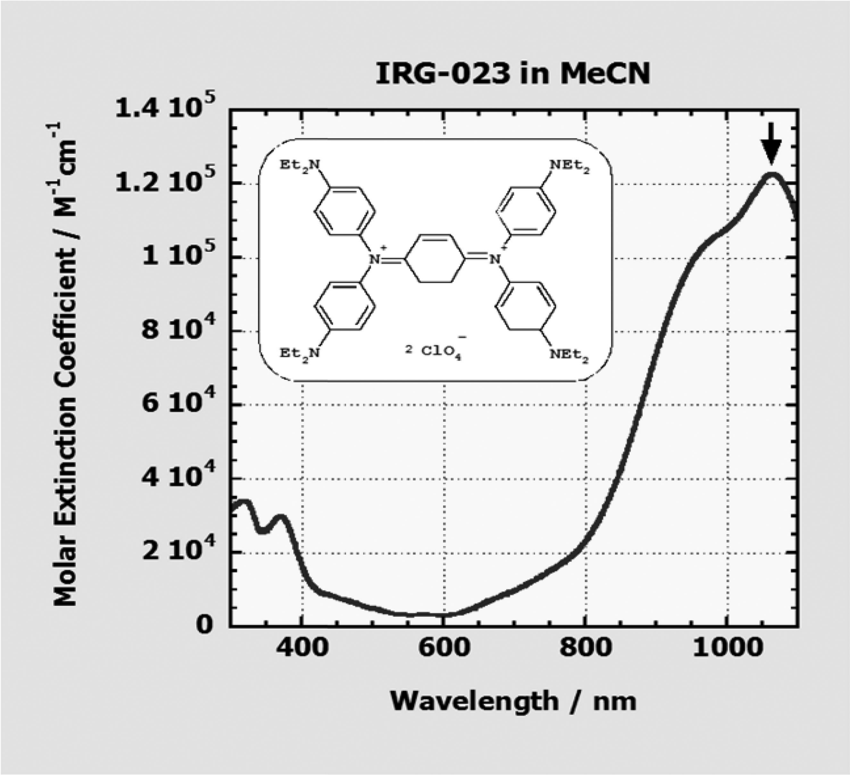

*Figure 1. Structure and absorption spectrum of the near-infrared dye IRG-023 in acetonitrile. The arrow indicates 1064 nm (Nd-YAG fundamental).*

The strong photothermal sensitization capability of the dye is advantageous in laser triggering in liposomes, allowing site-selective optical heating. Temporal (pico- and nanosecond) and spatial (molecular and nanometer-scale) localization of the temperature jump implies concentration of energy, which may maximize the effectiveness and minimize the side effects to the normal tissue.

## Design Strategy

There are two possible schemes for the incorporation of the dyes into liposomes: placing them in the inner phase or embedding them at the bilayer. Here we take the latter choice because of several reasons:

(1) Many dyes including IRG-023 are hydrophobic and spontaneously adsorbed or embedded in the bilayer. In contrast, to place them into the inner phase solution, one needs some sort of solubilization or modification of the chemical structure to make it hydrophilic.

(2) It is better to keep interference minimal between the drug in the inner phase and the dyes, so that complication arising from their interactions before and during laser irradiation can be avoided. This will allow more freedom in examining drug and photosensitizer candidates for clinical trials, and make life easier in future developments.

(3) When the laser pulse irradiates a liposome with the dyes doped in the bilayer, laser-induced heat and pressure may first build up at the spherical surface of the liposome, and then spread both inward and outward according to the laws of heat diffusion and pressure-wave (*i.e.* acoustic) propagation. The concentric wave propagation has a special property of self-amplification and is called *implosion*. If the wave proceeds inward, retaining its spherical symmetry, the pressure grows up and eventually becomes huge at the liposome center. Such a spontaneous energy concentration or focusing, if actually happens, may lower the required laser power and lessen the side effects.

There are also several possibilities as to laser irradiation. For example, we may use relatively strong, short pulses to induce violent rupture of liposomes. Alternatively, we may use weak pulses or continuous-wave (CW) laser sources to mildly heat the bilayer membrane, inducing the phase transition (gel to liquid crystalline state) in the bilayer and the permeability change for gradual and controlled drug release. Both are well worth investigating. We concentrate on the former here, because of our interest in laser-induced dynamics in the microscopic domain and possibility to utilize it as a new mechanism for laser-induced drug activation.

## Laser-Induced Rupture

### Liposome Preparation and Characterization

Liposomes can be classified according to their structures and sizes. Multi-lamellar vesicles (MLV) are most easily prepared, but small (< 100 nm) and large (> 100 nm) unilamellar vesicles (SUV and LUV) are preferable in model systems. The dye-doped LUV has been prepared by the reverse evaporation method (*15*). IRG-023 is practically insoluble in water and spontaneously embedded in the bilayer. The lipid was assayed according to the phosphomolybdate (Ames) method (*16*), and the dye content was estimated by the NIR absorbance. Because of the dicationic nature of the dye, the embedding efficiency strongly depends on the net charge of the lipid: a negatively charged lipid, *L*-α-dipalmitoylphosphatidyl-*DL*-glycerol (DPPG), is found to achieve the molecular embedding ratio up to dye/lipid ~ 1/150.

Dynamic light scattering indicated that the liposomes have a broad size distribution spanning from 200 nm to ~10 μm. It follows from a molecular packing consideration that a single liposome with the diameter of 210 nm typically consists of 380,000 lipid molecules, and may contain 2,500 dye units in the bilayer; it becomes a formidable NIR absorber as a whole.

## Fluorometry

Fluorometric probes (*e.g.* calcein) can be used for detecting release of the inner phase solution to the bulk (*17*). The dye-doped liposomes containing aqueous calcein solution have been prepared and gel-filtrated for the removal of excess calcein in the bulk. As calcein is self-quenched at a high concentration, the liposome solution is not fluorescent. Upon laser pulse irradiation, the fluorescence is recovered, indicating the calcein release (Figure 2).

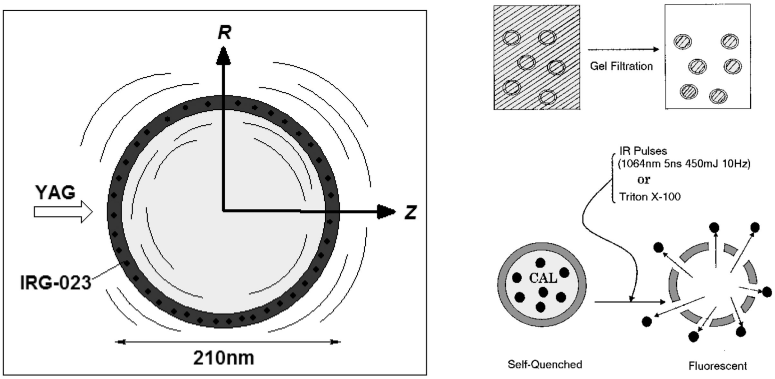

*Figure 2. Schematic drawing of the fluorometric experiments. Left: Interactions between the dye-doped liposome and laser pulses. Right: Rupture detection with the calcein probe in the inner phase.*

A typical time course of the fluorescence change is shown in Figure 3. Irradiation of unfocused, collimated laser pulses (wavelength 1064 nm, pulse duration 5 ns, spot diameter 2.6 mm, repetition rate 10 Hz, and pulse energy 161 mJ) causes fluorescence recovery. The fluorescence, however, reaches a plateau that is approximately half the intensity corresponding to the full release (observed by the addition of a surfactant Triton X-100), suggesting that a considerable portion of the liposomes are non-responsive to the laser triggering. Indeed, after passing the liposomes through an extruder with a porous polycarbonate filter and sizing them down below 1 μm, the response is completely lost. Accordingly, we conclude that the laser-induced release has a strong dependence on the liposome size; only the larger ones (> 1 μm) break.

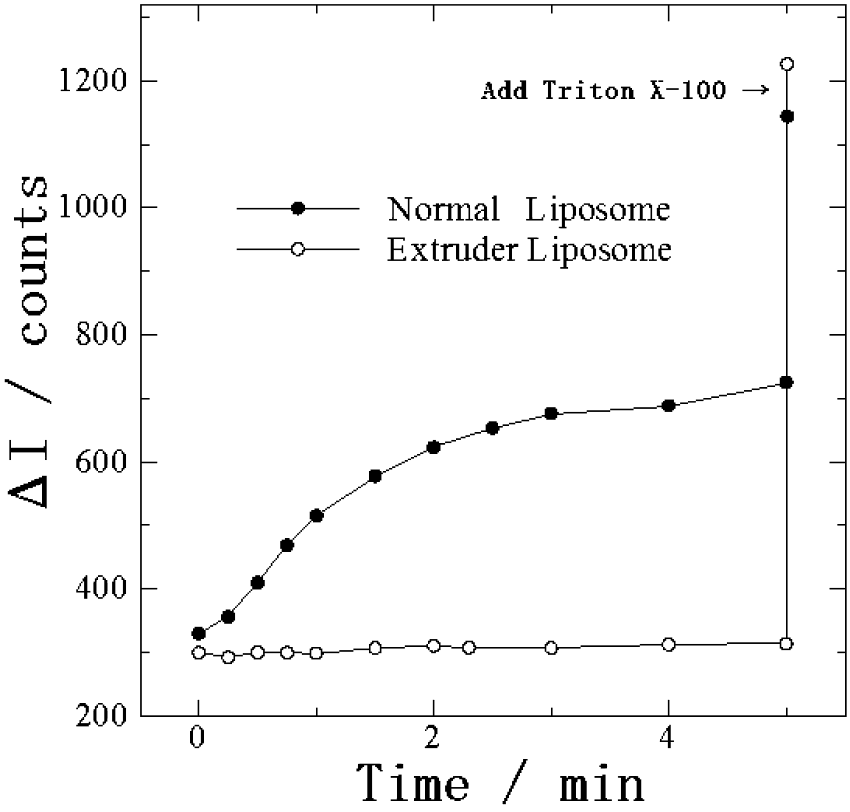

*Figure 3. Fluorescence recovery of the NIR dye-doped liposome solution containing calcein upon laser pulse irradiation.*

There are several possibilities that might explain this dependence. First of all, a larger liposome has more dyes on it and absorbs more photons, so that it is naturally expected to break more easily. Here, actually, some sort of collective mechanism -- accumulation of energy over a single liposome -- is tacitly assumed. It is not, however, clear whether the larger size is truly advantageous for the triggering or not, since the number of dyes per liposome scales as $r^2$ ($r$ = liposome radius) whereas the heat capacity scales as $r^3$; it is more difficult to heat up a larger one. On the other hand, if we assume that the laser-induced temperature jump is localized at the bilayer, and that the resulting effects on the liposome membrane (heat, pressure, chemical changes, etc.) locally alter the permeability or damage the bilayer structure, it would depend only on the number density of the embedded dyes on the surface (*i.e.*, the dye/lipid ratio). Although this ratio is, in principle, a function of the surface energy, or more rigorously, the small-system chemical potential (*18*), and depends on the surface curvature and thus on the liposome size, it is rather unlikely that such curvature effect would make a crucial difference in the case of LUV of the diameter as large as 1 μm.

To clarify the above issues and get insight into possible directions toward clinical developments, it is essential to understand the optical interactions between a laser pulse and a liposome, as well as their outcome of photothermal and photoacoustic processes. In particular, the following question is addressed: is it a local, molecular-scale event in the bilayer, or a global, 'liposome-wide' collective effect?

## Rupture Mechanism

### Mie Scattering: Mesoscopic Optical Field

When a collection of dyes form a mesoscopic (nano- and micrometer scale) structure, their interaction with light requires a careful treatment. The condition usually met in the case of a dilute homogeneous solution, *i.e.*, that the absorption and scattering of molecules occur in the optical mean field and independently of each other, is no longer valid. The electromagnetic field is deformed by one chromophore and also affects neighboring others, so that the Lambert-Beer law breaks down, and the interference and shadow effects often emerge. Computation of such systems typically involves sophisticated numerical approximation to the solution of the Maxwell equations.

Fortunately, if the structure is spherically symmetric, Mie theory gives an exact analytical expression for the optical field (*19*, *20*). We performed a model calculation of the dye-doped liposome, which showed that the interference and shadowing are minor, and that the embedded dyes in the bilayer are illuminated more or less uniformly under the laser field.

This result significantly simplifies our simulation of the resulting photothermal and photoacoustic processes, in which the bilayer is heated up uniformly according to the laser dose, and the evolution of the local temperature or pressure is computed as a function of the time and the distance from the liposome center. The relevant material properties of the bilayer (heat capacity, sound speed, and thermal expansion coefficient) are assumed to be the same as those of water, so that our modeled 'liposome' is actually a water ball, with the thin surface layer stained with the NIR dye, and embedded in the bulk water. Nanometer-scale optical heating is to occur in this hollow-sphere geometry.

### T-Jump: Photothermal Simulation

Time evolution of the laser-induced temperature jump can be simulated according to the standard partial differential equation of heat diffusion with a time-dependent heat source term (*21*). The numerical computation (Figure 4) showed that the temperature jump $\Delta T$ reaches 150 K at the bilayer during the 5-ns laser pulse irradiation, but rapidly dissipates down to 70 K in 10 ns and 25 K in 100 ns. The heat diffused into the inside of the liposome remains there forming a 'heat ball,' which cools down in less than 300 ns.

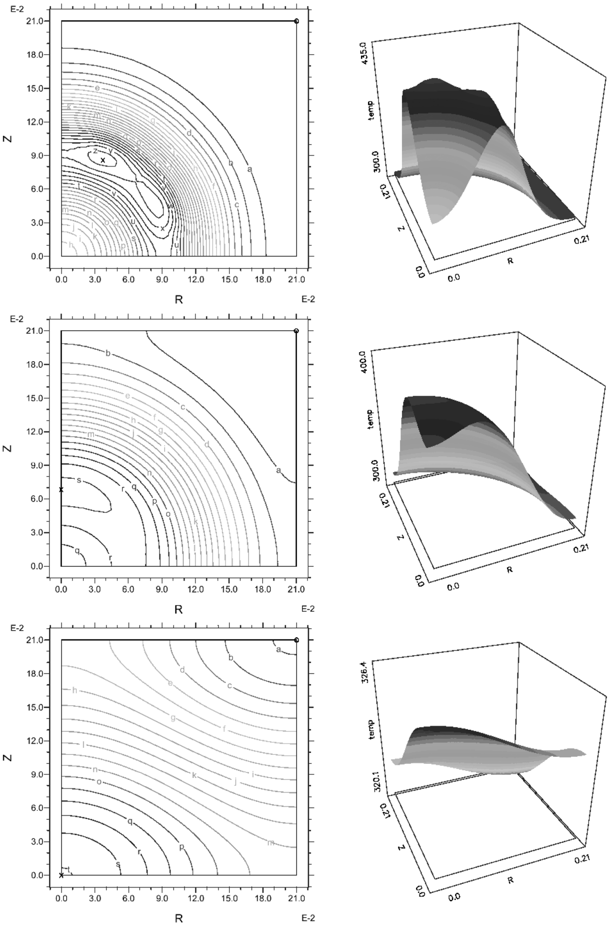

*Figure 4. Temperature distribution [K] inside and outside of the dye-doped liposome at t = 5 (upper), 10 (middle), and 90 ns (lower) after laser pulse irradiation. The cylindrical coordinate system (r, z) [μm] is depicted in Figure 2.*

Although the rise of 150 K should be more than enough to induce the permeability change and even boiling, it only lasts for a short time compared with typical time scales of the bilayer lipid dynamics (*22*), and may not offer a powerful triggering mechanism by itself. On the other hand, the heat ball concept can be useful in combination with thermal activation of drugs in the inner phase.

## P-Jump: Photoacoustic Simulation

Optical heating, if local or inhomogeneous, accompanies generation of a pressure (sound) wave. Thermal expansion of the heated volume and the resulting pressure build-up makes it a virtual hammer to the surrounding volume, and the generated sound propagates according to the acoustic wave equation. A linearized wave equation is adequate for small-signal photoacoustics well below the nonlinearity and shock-wave regimes (*23*):

$$v_s^{-2}\frac{\partial^2 P}{\partial t^2}-\nabla^2 P=\frac{\beta_v}{c_p}\frac{\partial Q}{\partial t} \tag{1}$$

where $v_s$ is the sound velocity, $P(r,\ t)$ the acoustic pressure, $\beta_v$ the thermal volume expansion coefficient, $c_p$ the heat capacity, and $Q(r,\ t)$ the absorbed photon energy per unit volume and time.

The simulation (Figure 5) showed that the photoacoustic process is inherently fast and far-reaching, compared with the photothermal one, because the acoustic wave runs much faster than the heat diffusion. It can also become violent. After the initial build-up at the bilayer, the spherical wave splits into two (incoming and outgoing) waves. The contracting wave is implosive and reaches the center with a huge energy density. In addition, after passing the origin, it suddenly flips its polarity and starts spreading out as a negative pressure wave. This, rather unexpected, phase inversion is a consequence of the boundary condition that the volume velocity must vanish at the origin (*24*), and may be understood in terms of momentum conservation.

The implosive character of the photoacoustic wave, generated in the hollow-sphere geometry, is intriguing in the context of drug delivery for two reasons. First, the huge energy concentration at the liposome center may offer a new mechanism for drug activation induced by the high pressure or even a shock wave. In spite that Equation (1) and our simulation are limited to linear acoustics, the huge pressure peak casts a possibility for shock wave generation. More elaborated nonlinear acoustics will be needed to test this idea.

The second point is equally or even more promising. When the negative pressure wave spreads out and passes across the bilayer, a strong pulling force is exerted on the membrane, which might cause a mechanical fracture and trigger the drug release. Besides, if the force surpasses the tensile strength of the bilayer or the aqueous media, cavitation should happen. It may break the liposome structure effectively and violently.

The implosion implies collective dynamics and spontaneous energy focusing over the liposome scale. Therefore, the dependence of the laser triggering sensitivity on the liposome size may well be explained. In fact, the simulation verified that a larger liposome has the capability of generating higher positive and negative pressure peaks at the center.

## Rupture Imaging

To examine the possibility of implosion and cavitation in the laser-induced rupture, we have performed time-resolved imaging experiments. A home-built microscope was equipped with a phase-contrast objective having a long working distance to allow enough space for the laser pulse to hit the liposome sample. A time resolution of 400 ns was achieved with a gated image intensifier and a xenon flash lamp. Details of the system are described elsewhere (*25*).

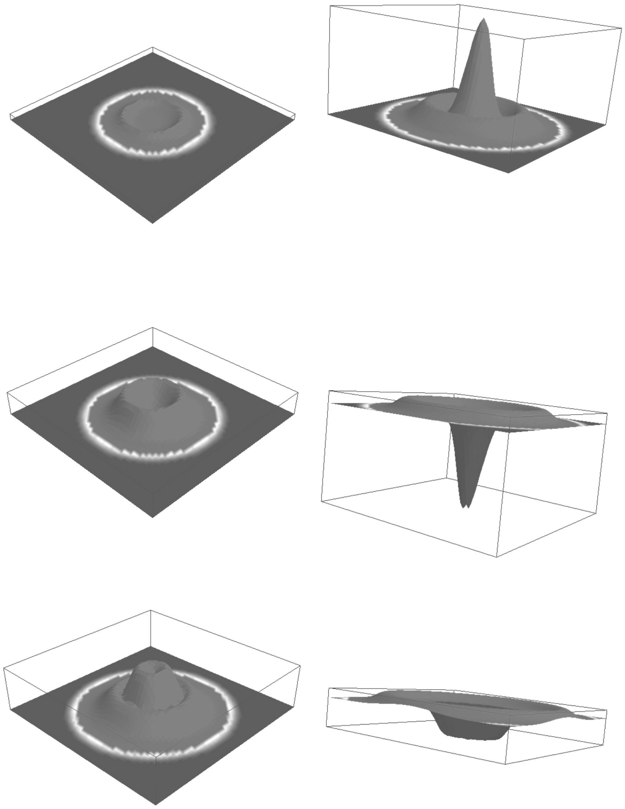

*Figure 5. Photoacoustic wave propagation indicating the phase inversion at the center of the liposome (r = 10 µm). From upper to lower and left to right: t = -2.8, 0, 2.8, 5.0, 9.5, and 13.9 ns; P(max) = 23 kbar, P(min) = -22 kbar.*

For an easy observation by optical microscopy, giant unilamellar vesicles (GUV) with the diameter of 10 to 50 µm were prepared according to the literature (*26*). A fresh sample of the dye-doped GUV on the glass slide was irradiated with a single-shot laser pulse, and the microscopic image after a varied delay time was captured.

The captured images clearly indicate the onset of microscopic cavitation (Figure 6). Upon the laser pulse irradiation, a swarm of embryonic microbubbles emerge almost instantaneously, and grow in size within a few µs. Most of the bubbles are transient and disappear long before we can notice them in real time. There is a statistical threshold in the laser pulse energy, above which the cavitation is very frequently observed, and below which it seldom occurs. The threshold seems to depend on the liposome size and on the dye content.

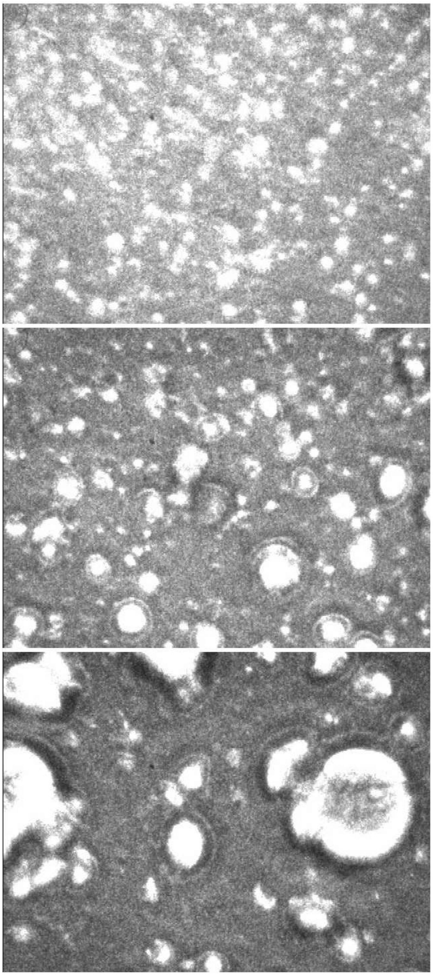

*Figure 6. Microscopic snapshots at t = 0 (upper), 400 (middle), and 1000 ns (lower) after laser pulse irradiation. The image width spans 240 µm. Note that each image represents an individual event (not a sequential time evolution).*

Because of the current limitation in time and image resolutions in our experiments, it is still an open question whether the cavitation indeed emerges from the liposome center as a result of the phase inversion of the implosive photoacoustic wave, or there is some other mechanism (*e.g.* photothermal boiling at the bilayer) responsible for it. Nevertheless, there is little doubt that cavitation is among the major causes of the laser-induced rupture, and the liposome-size dependence of the threshold supports the implosive mechanism as a likely candidate.

### Future Prospects

Our liposome needs many improvements and engineering. For example, the required laser pulse energy is by orders of magnitude higher than the clinically safe level; the liposome size suitable for triggering may also be too large for common use as a drug carrier (< 400 nm). Efficient incorporation of dyes into the bilayer by covalent bonding, as well as effective laser delivery and in situ focusing, may help.

The concept of implosion and cavitation is quite general and does not depend on the specific details of dyes or lipids. The wide applicability is clearly an advantage in clinical optimization. In addition, cavitation plays a dominant role in sonochemistry and medical ultrasonics: the bubble collapse induces extremely high temperature and pressure, and generates radicals and reactive oxygen species (ROS). The bubble also interacts and resonates with the acoustic wave, and can generate a shock wave (*25*). In contrast to ultrasonic bubbles, the laser-induced transient bubbles in our system are local and can be specific to the target tissue; they can be used as an *in situ* ROS generator or a micro-hammer.

Recently, optical heating of NIR absorbers (*e.g.* dyes, nanoparticles, and carbon nanotubes) is often utilized for phototherapy and molecular-targeted cancer therapy (*27*). The present approach considers the liposome not just as a delivery vehicle but also as a heating template, and thus a mesoscopic stage for cooperative phenomena. Such a view can lead to a variety of new mechanisms for laser-induced drug activation, such as the interplay among photons, heat, sound, and bubbles.

## Conclusion

NIR-Sensitive liposomes have been developed by incorporating a photothermal sensitizer into the bilayer. They can be triggered by laser pulses to release the drug, and are expected to be of use in a hybrid approach combining drug delivery and photodynamic therapy.

Micro-implosion and cavitation are identified as the crucial processes in the laser-induced liposome rupture. They originate from the bilayer-specific optical heating and the resulting photoacoustic wave dynamics in the hollow-sphere geometry. The self-concentration of energy may lead to a highly efficient laser action with a lower dose. The transient microbubbles can also be used as a powerful medical tool. The generality of the concept is advantageous in optimization efforts for clinical trials.

## Acknowledgments

This work is supported by the Japanese Ministry of Education, Science and Culture (Grant No. 23550010).

# References

1. Zhang, L.; Gu, F.; Chan, J.; Wang, A.; Langer, R.; Farokhzad, O. *Clin. Pharmacol. Ther.* **2007**, *83*, 761–769.
2. Sapra, P.; Allen, T. M. *Cancer Res.* **2002**, *62*, 7190–7194.
3. Weinstein, J. N. *Cancer Treat. Rep.* **1984**, *68*, 127–135.
4. Simões, S.; Moreira, J. N.; Fonseca, C.; Düzgüneş, N.; Pedroso de Lima, M. C. *Adv. Drug Delivery Rev.* **2004**, *56*, 947–965.
5. Ganta, S.; Devalapally, H.; Shahiwala, A.; Amiji, M. *J. Controlled Release* **2008**, *126*, 187–204.
6. Sawant, R. R.; Torchilin, V. P. *Soft Matter* **2010**, *6*, 4026–4044.
7. Bonnett, R. *Chemical Aspects of Photodynamic Therapy*; Gordon and Breach: 2000.
8. Sunamoto, J.; Iwamoto, K.; Mohri, Y.; Kominato, T. *J. Am. Chem. Soc.* **1982**, *104*, 5502–5504.
9. O'Brien, D. F. *Photochem. Photobiol.* **1979**, *29*, 679–685.
10. Kano, K.; Tanaka, Y.; Ogawa, T.; Shimomura, M.; Okahata, Y.; Kunitake, T. *Chem. Lett.* **1980**, *9*, 421–424.
11. Roggan, A.; Dörschel, K.; Minet, O.; Wolff, D.; Müller, G. In *LITT: Laser-Induced Interstitial Thermotherapy*; SPIE: 1995; pp 10−44.
12. Bhawalkar, J.; Kumar, N.; Zhao, C. F.; Prasad, P. N. *J. Clin. Laser Med. Surg.* **1997**, *15*, 201–204.
13. Yanagisawa, S.; Matsui, F.; Okazaki, T. *Nippon Kagaku Kaishi* **1992**, 1141–1143.
14. Chen, S.; Lee, I.-Y. S.; Tolbert, W. A.; Wen, X.; Dlott, D. D. *J. Phys. Chem.* **1992**, *96*, 7178–7186.
15. Szoka, F.; Olson, F.; Heath, T.; Vail, W.; Mayhew, E.; Papahadjopoulos, D. *Biochim. Biophys. Acta* **1980**, *601*, 559–571.
16. Ames, B. N. *Methods Enzymol.* **1966**, *8*, 115–118.
17. Straubinger, R. M.; Hong, K.; Friend, D. S.; Papahadjopoulos, D. *Cell* **1983**, *32*, 1069–1079.
18. Hill, T. L. *Thermodynamics of Small Systems*; Dover: 2002.
19. Bohren, C. F.; Huffman, D. R. *Absorption and Scattering of Light by Small Particles*; Wiley: 1983.
20. Suzuki, H.; Lee, I.-Y. S. *Int. J. Phys. Sci.* **2008**, *3*, 038–041. *Int. J. Phys. Sci.* **2009**, *4*, 615 (Errata).
21. Farlow, S. J. *Partial Differential Equations for Scientists and Engineers*; Dover: 1993.
22. Kates, M., Manson, L., Eds. *Biomembranes, Volume 12: Membrane Fluidity*; Plenum: 1984.
23. Zharov, V. P.; Letokhov, V. S. *Laser Optoacoustic Spectroscopy*; Springer-Verlag: 1986.
24. Blackstock, D. T. *Fundamentals of Physical Acoustics*; Wiley-Interscience: 2000.
25. Lee, I.-Y. S.; Hayama, Y.; Suzuki, H.; Osawa, T. *J. Phys. Chem. C* **2010**, *114*, 22392–22397.

26. Moscho, A.; Orwar, O.; Chiu, D. T.; Modi, B. P.; Zare, R. N. *Proc. Natl. Acad. Sci.* **1996**, *93*, 11443–11447.
27. Mitsunaga, M.; Ogawa, M.; Kosaka, N.; Rosenblum, L. T.; Choyke, P. L.; Kobayashi, H. *Nature Med.* **2011**, *17*, 1685–1691.

## Chapter 9

# Polysaccharide Functionalized Magnetic Nanoparticles for Cell Labeling and Tracking: A New Three-Dimensional Cell-Array System for Toxicity Testing

**Y. Miyamoto,[1,2,*] Y. Koshidaka,[1] H. Noguchi,[3] K. Oishi,[1] H. Saito,[4] H. Yukawa,[1] N. Kaji,[5] T. Ikeya,[6] H. Iwata,[7] Y. Baba,[5] K. Murase,[4] and S. Hayashi[1]**

**[1]Department of Advanced Medicine in Biotechnology and Robotics, Nagoya University Graduate School of Medicine, 65 Tsurumai-cho, Showa-ku, Nagoya 466-8550, Japan**
**[2]Department of Reproductive Biology, National Research Institute for Child Health and Development, 2-10-1 Okura, Setagaya-ku, Tokyo 157-8535, Japan**
**[3]Department of Gastroenterological Surgery, Transplant and Surgical Oncology, Okayama University Graduate School of Medicine, Dentistry and Pharmaceutical, 2-5-1 Shikata-cho, Okayama 700-8558, Japan**
**[4]Nagoya Research Laboratory, MEITO Sangyo Co., Ltd., 25-5, Kaechi, Nishibiwajima, Kiyosu 452-0067, Japan**
**[5]Department of Applied Chemistry, Nagoya University Graduate School of Engineering, Nagoya University, Furo-cho, Chikusa-ku, Nagoya 464-8603, Japan**
**[6]Photosensitive Materials Research Center, Toyo Gosei Co., LTD., 1603, Kamimyoden, Ichikawa 272-0012, Japan**
**[7]Department of Orthopaedic Surgery, Nagoya Kyoritsu Hospital, 1-172 Hokke, Nakagawa-ku, Nagoya 454-0933, Japan**
***E-mail: ymiyamoto@med.nagoya-u.ac.jp; myoshi1230@hotmail.com. Tel.: +81-3-5494-7047. Fax: +81-3-5494-7048**

Magnetic resonance imaging (MRI) using contrast agents has been widely used to diagnose vascular diseases, to visualize the internal structure of organs, and to monitor transplanted cells and tissues. We recently developed a novel contrast agent for MRI using polysaccharide-modified magnetic iron

In Nanomaterials for Biomedicine; Nagarajan, R.;
ACS Symposium Series; American Chemical Society: Washington, DC, 2012.

oxide nanoparticles. The polysaccharide-magnetic particle complex has an advantage of low toxicity to cells and tissues and slow blood clearance over conventional contrast agents. However, because the surface charge of the particles is negative, transplanted cells such as pancreatic islet cells are less labeled. To overcome this problem, a complex of a polysaccharide and a positively charged magnetic metallic compound has been developed. These newly designed magnetic nanoparticles were efficiently transduced into various cells (for example pancreatic islet cells, MIN6 cells, HepG2 cells, hepatocytes, and somatic stem cells). The present chapter mainly describes the establishment of a cytotoxicity test system using our polysaccharide-based magnetic iron oxide nanoparticles. As a promising cell evaluation system, a new three-dimensional cell culture system "cell-array system" has been established. In the future, the system will be useful as a powerful tool for drug development.

## Introduction

### Issues in Cell Therapy and Regenerative Medicine

In cell and organ transplantation, cells and tissues to be transplanted are usually evaluated by observing vital phenomenon that are associated with the normal functions of the cells and tissues. For example, the engraftment of transplanted pancreatic islet cells is indirectly evaluated by measuring the blood pressure of portal vein and by measuring of the amount of secreted insulin after transplantation into congenital type I diabetic patients (*1–3*). However, immediately after transplantation, the cells and tissues are not easy to be evaluated, and few such indirect evaluation methods are available for the monitoring of success at the early stages. Therefore, transplanted cells and tissues might be given inappropriate treatment, thus leading to the potential for adverse effects or to a lack of transplant survival. On the other hand, even if cells and tissues are successfully transplanted into patients, cell necrosis caused by immunorejection after transplantation and cell death caused by the damage may occur. For these reasons, adequate follow-up of transplanted cells and tissues after the surgery is strongly desired.

In addition, regenerative medicine has received much attention in recent years due to the progress in embryonic stem (ES) cell technology (*4*, *5*). Especially, cell therapy using various cells differentiated from the stem cells have been devised as promising treatments. Hematopoietic stem cell transplantation (*6*) has been most commonly used, and the treatment method using the cells enables patients with blood diseases such as leukemia and hypoplastic anemia to make normal blood from the donor stem cells. This type of transplantation includes bone marrow transplantation (BMT), cord blood stem cell transplantation (CBT), and peripheral blood stem cell transplantation (PBSCT). Among these methods, BMT has been most commonly used for the treatment of patients with intractable blood diseases such as leukemia and hypoplastic anemia. BMT involves injecting a donor's normal marrow cells into the vein of the affected patient. Adipose tissue-derived stem/progenitor cells (ASCs) (*7–10*) have also attracted attention as an alternative cell source of marrow stromal cells (MSCs). These medical treatments, however, require a large supply of human ASCs. In addition, there are several other candidate cell sources for transplantation, such as human amnion mesenchymal cells (*11*, *12*), other somatic stem cells, ES cells (*13*, *14*), and induced pluripotent stem (iPS) cells (*15–19*), and cell therapies using different cell sources are used for different purposes.

With regard to being able to observe them post-transplantation, cells and tissues can be labeled with magnetic metallic oxides, such as super-paramagnetic iron oxide (SPIO) before transplantation and then followed-up by magnetic resonance imaging (MRI) (*20–32*). As a result, the transplanted cells are able not only to be detected as tomographic images in the body but also as metabolic products of the cell. It is also possible to judge the viability of transplanted cells, and the function, proliferation, etc. can be analyzed by multilaterally extracting the data, and analyzing the physiological and physiochemical information provided on the biological tissue.

## Magnetic Nanoparticles for Cell Labeling and Tracking

The technology for visualizing therapeutic cells used by both regenerative medicine and the cell therapy is highly desired. Magnetic nanoparticles are taken into transplanted cells as methods to visualize therapeutic cells, and such transplanted cells can be tracked using the nuclear magnetic resonance (NMR) method. Figure 1 shows the basic concept of the noninvasive cell tracking technology using magnetic nanoparticles. First, transplanted cell is labeled with magnetic nanoparticles. In the case of liver disease as a target, hepatocytes are labeled with magnetic nanoparticles (Figure 1A). Then the labeled cells are transplanted into the patient's body. The cells reach the liver via the portal vein (Figure 1B). Finally, the doctor confirms the implantation site by MR imaging. The transplanted cell can thus be detected outside the patients body (Figure 1C).

We therefore propose the use of highly safe less-invasive medical treatments and diagnostics for patients in the transplant medical treatment.

We herein take a look at some examples of the main step to make a diagnosis of transplanted cells which are labeled by magnetic nanoparticles including: 1) the development of imaging magnetic nanoparticles that become embedded in cells and tissues, 2) *in vitro* toxic assessment, and 3) *in vivo* toxic assessment. The toxicity to the therapeutic cells is dramatically reduced, and it is also important to maintain the original cell functions. There are several factors affecting the cytotoxicity of magnetic nanoparticles, such as the characteristic features (particle size, zeta voltage, etc), cell uptake, cell viability, and the aggregation rate in magnetic nanoparticles.

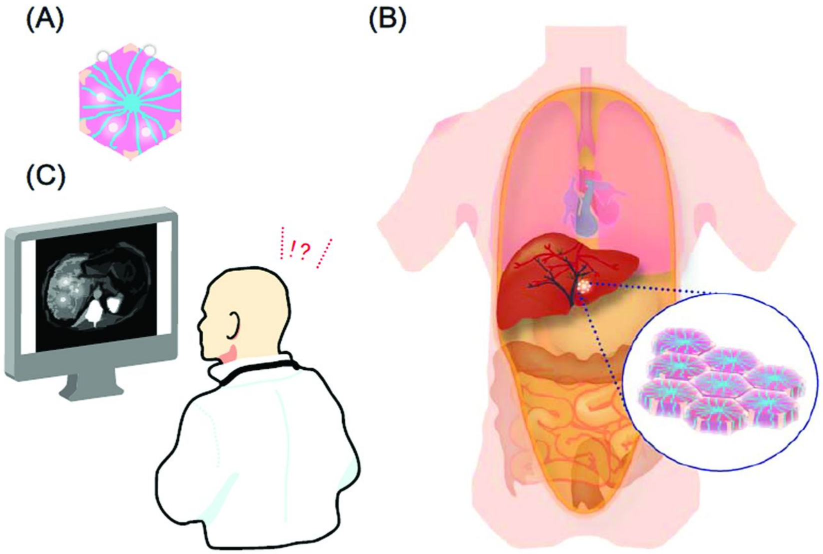

*Figure 1. The basic concept of the noninvasive cell tracking technology. (A) The cell is labeled by magnetic nanoparticles. (B) The cell is then transplanted inside the patient's body. (C) The transplanted cell can thus be confirmed from outside the patients body. (see color insert)*

To reduce the cytotoxicity of magnetic nanoparticles, it is necessary to evaluate magnetic nanoparticles according to the treatment protocol (*in vitro*), and to select the best nanoparticles in culture conditions for cell labeling. In the following sessions, we will introduce 1) development process of polysaccharide functionalized magnetic nanoparticles, 2) the current status regarding the assessment of cytotoxicity and cellular functions using polysaccharide-based magnetic iron oxide nanoparticles, 3) problems associated with magnetic nanoparticles that use iron and gadolinium, and 4) as a candidate cell evaluation examination system, a new three-dimensional cell culture system the "cell-array system".

## Magnetic Resonance Imaging and Contrast Agents for MRI

MRI is a method for visualizing internal body structures by using the nuclear magnetic resonance (NMR) phenomenon (*33*). The MR image is obtained based on the density and relaxation times (T1, T2) of specific atoms. Because the image is composed of physiological information and the signal strength can be changed by changing the pulse sequence and the imaging parameters, the contrast can be enhanced. To increase the signal intensity of MRI, gadolinium, manganese, iron, and chrome, can be used. The MRI contrast agents alter the relaxation times of tissues and body cavities where they are present.

The gadolinium contrast agents shorten the relaxation times required for protons excited by electromagnetic wave radiated energy to return to the original state by discharging energy. It improves the strength of the signal discharged from the atomic nucleus of hydrogen, and clarifies the focal location and range. Gd magnetic nanoparticles produce T1 contrast images, but not T2 contrast images. However, iron oxide magnetic nanoparticles produce not only T2 contrast images, but also T1 weak contrast images. Although gadolinium has cytotoxicity, this can be reduced by chelation with various chelators. Gd magnetic nanoparticles might cause side effects in renal disease patients. The gadolinium agents do not have high specificity for tissues and organs, because they distribute in the extracellular fluid after the intravenous (IV) push, and they are used to image the whole body. After the IV-push, many MRI contrast agents, of which the principal ingredient is iron, are taken into Kupffer cells of a liver. Because many malignant tumors that occur in the liver lack Kupffer cells, they have been used to detect liver cancer. Moreover, a powdered MRI contrast medium, of which the principal ingredient is iron, is also taken for abdominal MRI diagnosis. The MRI contrast agents that use gadolinium (Magnevist®, Primovist® etc.) and iron (Superparamagnetic iron oxide (SPIO): Resovist®, Feridex® etc.) are widely used in the clinic setting all over the world.

## Development Process of Polysaccharide Functionalized Magnetic Nanoparticles

As mentioned above, the cells are labeled with the magnetic nanoparticles, and the behavior of the transplanted cells is observed in the body. Because the patient's postoperative course can thus be monitored non-invasively, the safety of cell therapy and regenerative medicine is expected to be improved. It has been proposed that cells can be labeled using a complex with polysaccharides, such as magnetic metallic oxides-dextrans. The polysaccharide-magnetic particle complex has an advantage of low toxicity to cells and tissues and slow blood clearance. However, it is difficult to detect the labeled cells by MRI after transplantation, because the surface charge of the particles is negative, and thus, transplanted cells such as pancreatic islet cells are generally less labeled. A complex of a polysaccharide and a positively charged magnetic metallic compound was developed to overcome this problem. As an example, a magnetic metallic oxide nanoparticle covered with diethylamino-dextran was reported (*34*). Similarly, surface-modified iron oxide nanoparticles (ION) were obtained by co-precipitating a pullulan and its derivatives in an ammonium aqueous solution of $Fe^{2+}/Fe^{3+}$. By using the modified nanoparticles, labeled rat mesenchymal stem cells (MSC) could be detected by MRI (*35*).

We consider that conventional polysaccharides magnetic particle complexes form aggregates in culture medium, and as a result, they have a reduced labeling efficiency. To solve this problem, we examined the manufacturing process and the physical properties of various polysaccharide magnetic particle complexes (Figure 2) and thereby identified a polysaccharide magnetic particle complex which successfully achieves a specific aggregation level (*36–38*). Figure 2 illustrates the iron oxide nanoparticles coated with several dextran derivatives. The dextran coated nanoparticles are obtained by precipitation in the presence of dextran derivative solution. We prepared magnetic iron oxide nanoparticles coated with different amounts of cationic dextran derivatives and then optimized the coated amount to efficiently label the cells (*36–38*).

Resovist (ATDM), which has already been clinically approved for human use, are coated particles that appear to have an acceptable size (ranging from 45 nm to 60 nm). The other particle (CMEADM, TMADM) sizes range from 30 to 65 nm. The particle size and end-group of modified dextran (anionic or cationic substitution) influence the zeta potential of the magnetic iron oxide nanoparticles. These newly designed magnetic nanoparticles were efficiently transduced into cells because of positive-charge nanoparticles, since the cell surface is normally negatively charged. Thefore, it is important that the nanoparticles controlled the zeta potential (the positive-charge or negative-charge).

We continuously examined whether it was possible to use it for cell marking (*37*). Our experiments used MIN6 cells, a pancreatic β cell line, for the tests. MIN6 cells were incubated for 1 hour at 37°C with 150μg-Fe /mL nanoparticles, reconstituted in culture medium. 1st, TMADM-02, 03, and 04 were efficiently transduced into cells because of their positive charge. The iron content of the MIN6 cells labeled with each nanoparticle was measured by photon correlation spectroscopy (PCS), using the Nuclear Magnetic Resonance Sequence (NMR) (Bruker mq20 Series NMR Analyzer: Bruker, Milton, Ontario, Canada). 2nd, for comparison purposes unlabeled MIN6 cells were used as a control, the cell viability of MIN6 cells labeled with the nanoparticles was evaluated by trypan blue exclusion tests. Only a slightly significant difference was observed (>95%). 3rd, To test the stability of these four nanoparticles in culture medium, the relative aggregation rates were measured. TMADM-03 was stable and did not aggregate, while TMADM-02 and TMADM-04 did aggregate. In addition, the most suitable TMADM-03 for cell marking was determined. Regarding TMADM-03, the cell uptakes (6.0 μg-Fe /1×$10^6$ cells) were nearly twice that of the other magnetic nanoparticles. The physical properties of TMADM-03 demonstrate little difference in particle size in comparison to other nanoparticles. However, the zeta potential of TMADM-03 has a weak positive charge.

The polysaccharide particle complexes (TMADM-03) successfully labeled cells, were stable in culture medium, and thus produced a high contrast MRI image (*37*, *38*). TMADM-03 was taken up by MIN6 cells, and thereafter the labeled cells provided sufficient contrast for cell visualization in MR images ex vivo.

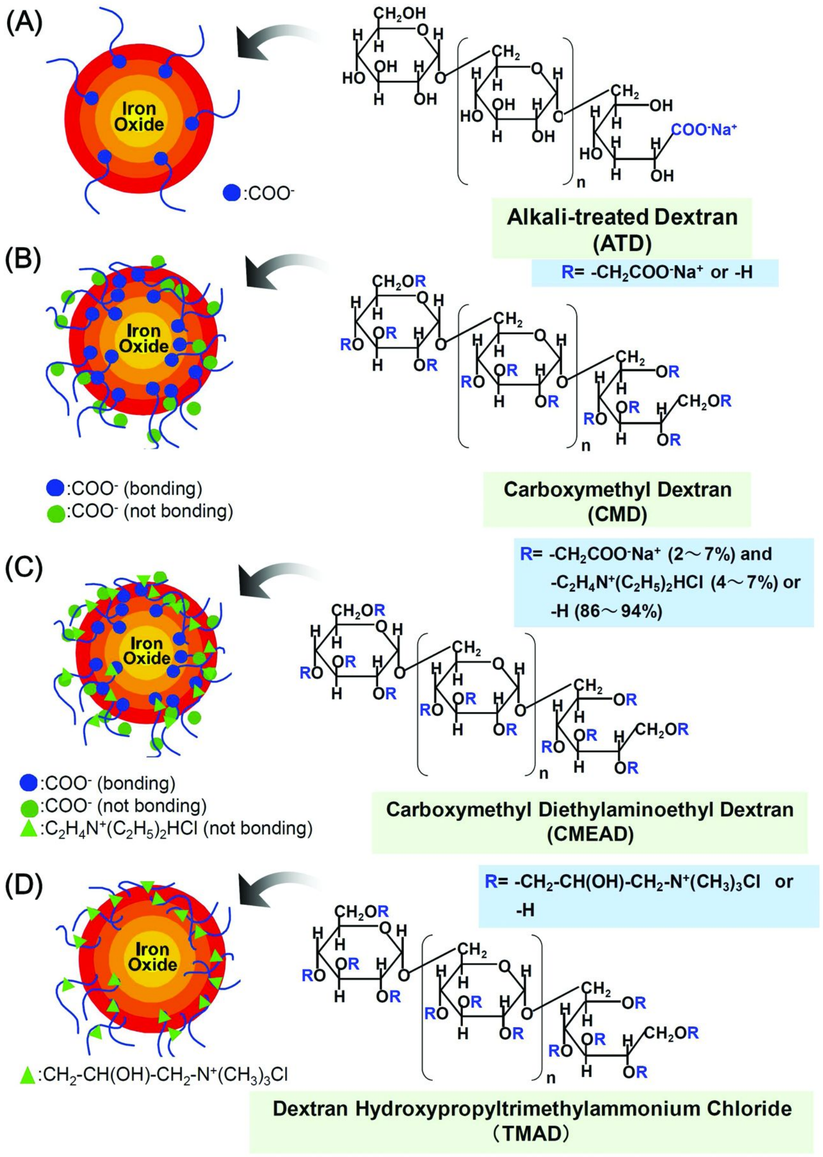
(A)
Iron Oxide
●:$COO^-$
Alkali-treated Dextran (ATD)
$COO^-Na^+$
(B)
Iron Oxide
●:$COO^-$ (bonding)
●:$COO^-$ (not bonding)
Carboxymethyl Dextran (CMD)
R= $-CH_2COO^-Na^+$ or -H
(C)
Iron Oxide
●:$COO^-$ (bonding)
●:$COO^-$ (not bonding)
▲:$C_2H_4N^+(C_2H_5)_2HCl$ (not bonding)
Carboxymethyl Diethylaminoethyl Dextran (CMEAD)
R= $-CH_2COO^-Na^+$ (2～7%) and
$-C_2H_4N^+(C_2H_5)_2HCl$ (4～7%) or
-H (86～94%)
(D)
Iron Oxide
▲:$CH_2-CH(OH)-CH_2-N^+(CH_3)_3Cl$
Dextran Hydroxypropyltrimethylammonium Chloride (TMAD)
R= $-CH_2-CH(OH)-CH_2-N^+(CH_3)_3Cl$ or -H
$CH_2OH$
$CH_2OR$
$CH_2$
n

*Figure 2. Iron oxide magnetic nanoparticles coated with anionic or cationic derivatives of dextran. (A) alkali-treated dextran (ATD), (B) carboxymethyl dextran (CMD), (C) carboxymethyl diethylaminoethyl dextran (CMEAD), (D) hydroxypropyl trimethylammonium dextran (TMAD) coated magnetic iron oxide nanoparticles. The nanoparticles were kindly provided by MEITO Sangyo Co., Ltd. (Kiyosu, Japan). (see color insert)*

## General Cytotoxicity Assessment

Cell toxicity tests are required for safety trials of medical devices that come in contact with tissues and blood in the body, and are used as supplementary tests for new drugs, such as for genotoxicity assays, etc. (*39*). Cytotoxicity in culture can indicate the potential of the compound to induce toxicity at the organ or organism levels, although the toxicity to a whole organism and cytotoxicity are not always correlated. Even if some substances do not have cytotoxicity based on standard Absorption, Distribution, Metabolism and Excretion (ADME) studies, their metabolic products might show cytotoxicity. Cytotoxicity tests are performed using culture cells as an initial screening for toxicity or as an alternative to animal tests. A high correlation has been shown between dermal irritancy and cytotoxicity in skin models obtained from cultured cells. Because of the current social conditions and regulations surrounding animal tests, their use is tightly regulated, and they are generally not conducted for preparations such as cosmetics. Cell toxicity testing using skin models thus often serves as a surrogate. On the other hand, the cytotoxicity can vary depending on the cell type. This is of particular importance in some cases, especially because anticancer drugs are required to show selective cytotoxicity to carcinoma cells, while inducing as little damage as possible to healthy cells. For these reasons, cell cytotoxicity testing is used as the first step in the screening of many new drugs.

Cytotoxicity is defined as the material properties and physical actions that induce cell death or that inhibit cell functions, including cell proliferation. Cytotoxicity is evaluated by the percentage of living cells and dead cells using cultured cells, or, the survival or mortality rates of the cells. Various methods have been developed to evaluate the cytotoxicity of floating or adherent cells for different purposes. The methods can be divided into counting cells directly, counting colonies of proliferating cells, and evaluating cell viability indirectly by quantifying the radio- or optical labeling of substances in cells.

The presence of damaged cell membranes is often used to detect dead or dying cells. The use of dyes, such as trypan blue stain, is able to identify dead cells, but not living cells, because living cells are able to block the penetration of the dyes, while dead cells can not do so. As a result, the living cells and the dead cells can be distinguished and counted under an optical microscope. Alternatively, substances leaked from the cytoplasm of dead cells can be used to assess cell viability. For example, the activity of lactic dehydrogenase (LDH) is frequently used to assess cell damage (*40–42*). Other cell counting methods as based on the products from living cells. For example, the MTT assay utilizes a method involving the reduction of tetrazolium salts (such as MTT) into a chromogenic substrate, such as formazan (*43–45*). Moreover, the survival rate can be determined by the detection of adenosine triphosphate (ATP), a substance found only in living cells (*46*). The method can measure the amount of ATP by luminescence from luciferase. A method using a radioactive substance can count the tritium labeled thymidines taken up into living cells. Besides the above described methods, the colony formation method to estimate cell proliferation is also used. In general, the 1st screening in cell toxicity testing is done by the techniques mentioned above.

## The Current Status Regarding the Assessment of Cytotoxicity and Cellular Functions Using Polysaccharide-Based Magnetic Iron Oxide Nanoparticles

Cytotoxicity was evaluated for the polysaccharide-based magnetic iron oxide nanoparticles that we developed and the findings were compared to the results obtained for commercially available nanoparticles (Resovist®: ATDM). We measured the cell viability using the MTT assay and trypan blue exclusion test. We used HepG2 cells, a human hepatocellular liver carcinoma cell line and MIN6 cells, for the tests, because the liver and pancreas are organs that are currently being targeted for cell therapy and transplantation. The dose of polysaccharide-based magnetic iron oxide nanoparticles administered was 150 μg-Fe/mL per 5 x $10^6$ cells, and this concentration could be detected by MRI (*38*). Cytotoxicity was not detected using either of the assays, and the cells incorporating the developed magnetic iron oxide nanoparticles (TMADM-03) maintained their original morphology (Fig 3). These magnetic iron oxide nanoparticles (TMADM-03) were stable even in culture medium, and they were efficiently taken up by the cells, and thereafter efficiently labeled the cells. Transmission electron microscopy (TEM) confirmed the presence of iron oxide nanoparticles inside the HepG2 cells. The nanoparticles were found in different cell structures and they were mainly observed in lysosomes (Figure 4A, B), the cell membrane (Figure 4B).

The primary screening for cytotoxicity (MTT, LDH assay etc) was performed. If no cytotoxicity or only limited cytotoxicity is observed, then the screening test is followed by an examination of the cell functions inhibited by the test agent.

Regarding the quality of the transplanted cells, it is important that the cells maintain their original cell function before or after adding the nanoparticles to the cell (*47–49*). Finally, if the original cell functions for transplanted cells must be maintained, we did not necessarily do the toxicity assessment.

When HepG2 cells were used in a test of the magnetic iron oxide nanoparticles modified with polysaccharides, the results should reflect the maintenance of the inherent functions of hepatocytes. For example, the test can measure the metabolic activity of cytochrome P450 (CYP3A) and the amount of albumin produced. We measured the effects of our nanoparticles on both of these factors and showed that there were no significant differences in the heptocyte functions between test samples with and without the magnetic iron oxide nanoparticles (TMADM-03) under optimized conditions for MR imaging (*50*). The success of these evaluations (lack of cytotoxicity and no impact on cellular functions) prompted us to perform subsequent animal tests in preparation for eventual clinical use of the nanoparticles. The magnetic particles were taken up by culture cells, then the cells were transplanted into mice, and the disposition of the nanoparticles was visualized 1-2 days after transplantation (*38*).

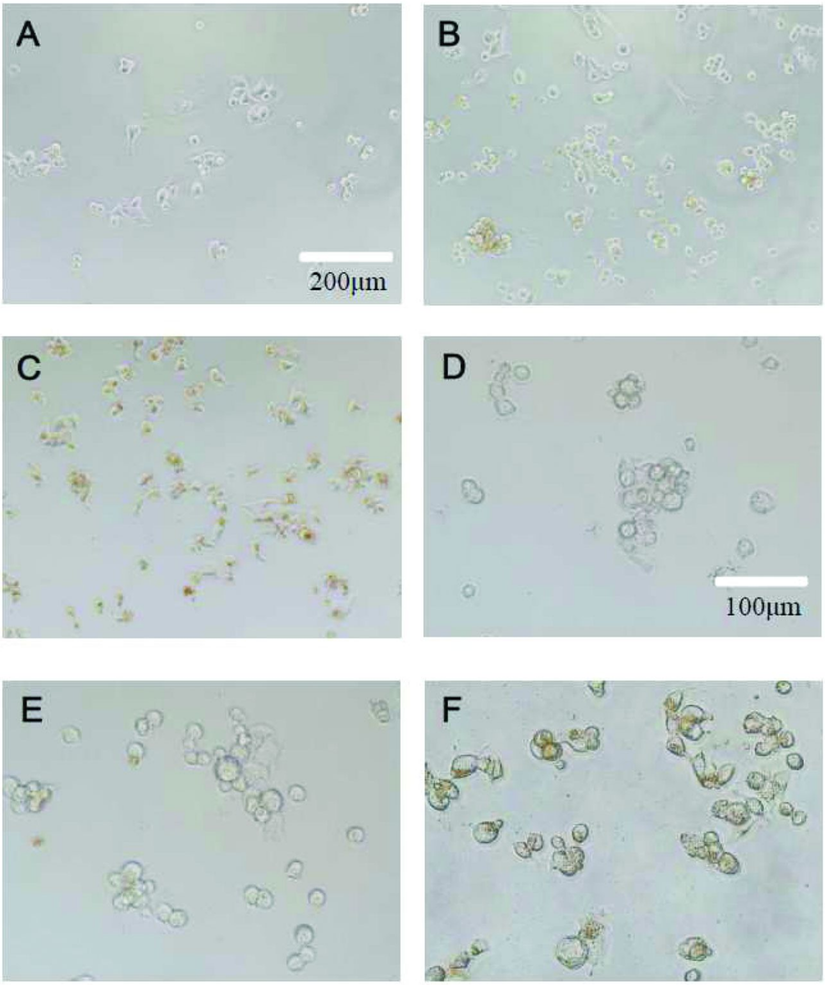

*Figure 3. Morphological observations of the HepG2 cells before (A, D) and after the addition of magnetic iron oxide nanoparticles (B, C, E, F). The HepG2 cells were cultured on cell culture dishs for 24 h after the inoculation. Scale bar: 200µm (A, B, C), and 100µm (D, E, F). Phase contrast micrograms of cells labeled with ATDM (B, E), and TMADM-03 (C, F). (see color insert)*

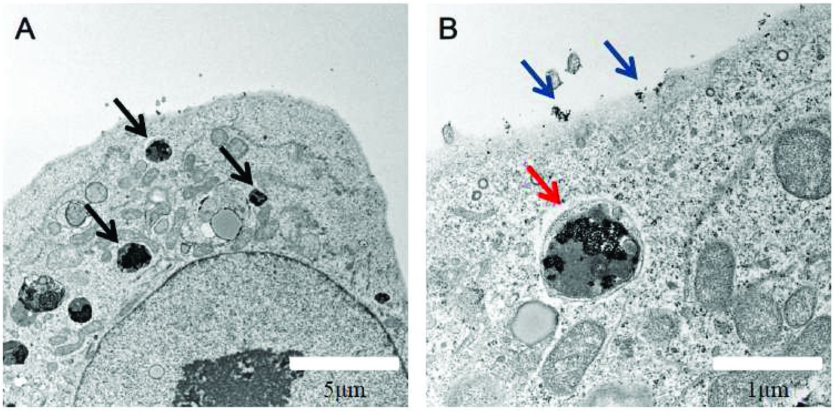

*Figure 4. Electron microscopy of HepG2 cells labeled with TMADM-03 (A) Morphology of HepG2 cells labeled with TMADM203. The arrows point to lysosomes containing the nanoparticles; ×4,860. (B) Nanoparticles (red arrow) detected in the lysosomes; Nanoparticles (blue arrows) attached to the cell membrane; ×18,400. (see color insert)*

## Problems Associated with Magnetic Nanoparticles That Use Iron and Gadolinium

Similar to other magnetic nanoparticles, target selective magnetic nanoparticles (*51*), cationic liposomes (*52*), and cationic coating magnetic nanoparticles (*53*) have also been developed. Target selective magnetic nanoparticles conjugated with specific antibodies accumulate at a specific site in the body after vascular injection. Their main disadvantages are the instability of such antibodies and their high cost. Cationic liposomes have been extensively studied by Kobayashi et al. Since cationic liposomes accommodate magnetic nanoparticles, and their magnetic strength tend to be stronger that that of other carriers. However, the liposomes are not very stable and they can be stored in a refrigirator for only a few days. As a result, it may be difficult to use them in normal clinical situations. Cationic coating magnetic nanoparticles are now being investigated and more data is needed regarding their biocompatibility. At present, the only magnetic nanoparticles that have been approved as a medicine are dextran coating magnetic nanoparticles (DM). DM of the cationic dextran coating are thus considered to be medically useful in the future.

Gd magnetic nanoparticles might cause side effects to renal disease patients. The nanoparticles cannot be used to stain cell aggregates in vitro, because they flow through blood vessels and might not be uptaken into cells. Gd magnetic nanoparticles are difficult to modify with cationic compounds, because chelators of the nanoparticles to reduce cytotoxities will interfere with such modification. At the present stage, the clinical use of Gd magnetic nanoparticles therefore still remains controversial.

## As a Candidate Cell Evaluation Examination System, A New Three-Dimensional Cell Culture System the “Cell-Array System"

As described above, the first stage that must be passed in order for the polysaccharide-based magnetic iron oxide nanoparticles to obtain authorization by official medical agencies is the successful completion of toxicity testing in cells and animals (preclinical trials) (*54*). Typically, the discovery and development of a new drug requires about 10 billion U.S. Dollars and it takes about 15-20 years. In addition, it has been reported that only about one in 20,000 candidate compounds evaluated for efficacy and toxicity might eventually receive approval for human clinical use.

We performed toxicity and safety trials using cell lines, but human cells should be evaluated for their potential clinical application (*10*, *55*, *56*). In particular, the cells used should address the major problems associated with the development of many drugs, such as hepatotoxicity. Because various factors, such as racial differences, age, gender, and case history, can impact the effects of a drug, the toxicity and safety of an agent to human primary hepatocytes should thus be verified in many samples. The evaluation of the hepatotoxicity of the polysaccharide-based magnetic iron oxide nanoparticles will be essential for their continued development, and metabolic tests (*57*) using human primary hepatocytes will also need to be performed to establish the metabolites of the compound.

As a candidate cell evaluation examination system, a new three-dimensional cell culture system the “cell-array system" has been established (*58*, *59*). Recently, three-dimensional (3D) culture systems have attracted attention in the fields of regenerative medicine, cell and tissue transplantation, and drug discovery research (*60–63*). Otsuka and Kataoka et al. demonstrated that multicellular spheroids comprising a combination of primary hepatocytes and endothelial cells (JCRB0099: HH) maintained stable liver-specific functions (*58*, *59*). The most important feature of the cell array is the formation of hepatocyte spheroids of a controlled size, ideally 100 μm in diameter, on a micropatterned surface with poly(ethylene glycol) brushes (Figure 5). We created cell adhesive (circle) and nonadhesive regions on a glass substrate using polyethylene glycol (PEG) derivatives as described in Figure 5. We next seeded and cultured hepatocytes on the patterned substrate and, as a result, three dimensional (3D) tissue constructs were thereby engineered. During this process, hepatocytes on nonadhesive regions move to adhesive regions and then formed multilayer aggregates.

**(A)** Micropatterned culture plates

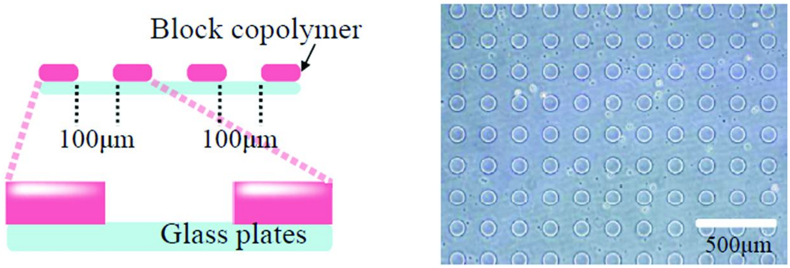
Block copolymer
100μm
100μm
Glass plates
500μm

**(B)** the 3D culture scheme of the endothelial cells and primary hepatocytes

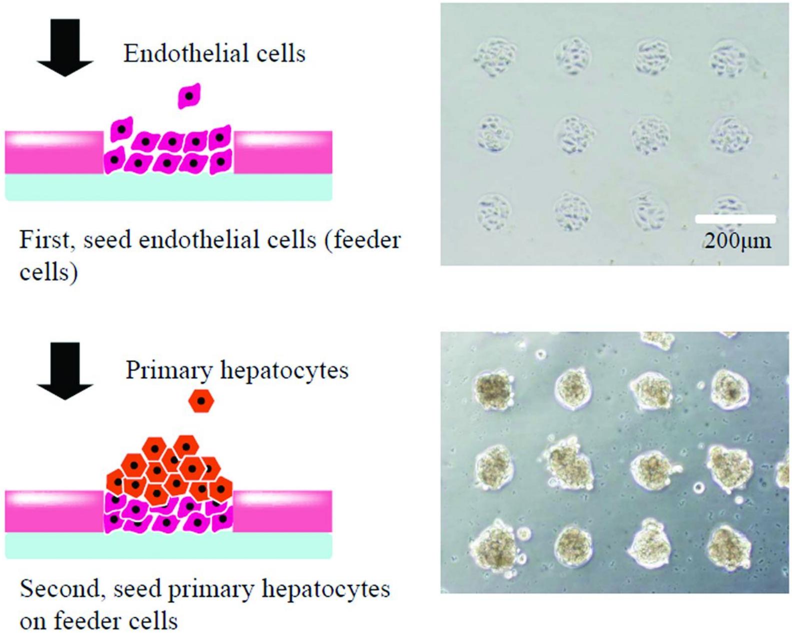
Endothelial cells
First, seed endothelial cells (feeder cells)
200μm
Primary hepatocytes
Second, seed primary hepatocytes on feeder cells

*Figure 5. A cell array system is one promising device for generating a 3D culture system. Scale bar: 500 and 200μm (A and B). (A) Micropatterned culture plates, (B) the 3D culture scheme of endothelial cells and primary hepatocytes. The Cell-able system was kindly provided by Transparent Inc. (Ichikawa, Japan). (see color insert)*

Spinner flasks or gyratory culture apparatuses are conventionally used to culture hepatocytes without making any contact with the surface of the apparatuses in order to thus promote cell aggregation. Culture devices modified with either low cell adhesive cationic compounds (*64*) or poly(2-hydroxyethyl methacrylate) (PHEMA) (*65*) are also used to culture hepatocytes, thus leading to cell aggregates (*64*). In addition to these culture devices, hollow fibers (*66*) and scaffolds (*67*) are employed to perform the three dimensional (3D) culture of hepatocytes. All of these culture methods minimize cell-materials interaction and give 3D cell constructs by cell aggregation. The cell constructs obtained by all the conventional methods have their own size distribution. The larger 3D cell constructs cause cell necrosis, because of the lower permeability of oxygen molecules and nutrients (*68*). The responses of hepatocytes are not reproducible when mixtures of 3D cell culture constructs for cell validation are used. To solve the problem, we developed a culture device with size-controlled cell adhesive and nonadhesive regions. While conventional hepatocyte cultures using a cationic polystyrene surface produced 3D cell constructs with diameter ranging from 20 to 300 μm for 14 days, our culture system thus resulted in 3D cell constructs measuring 100 μm in diameter.

An advantage of the 3D cell culture system is that hepatocytes can be cultured with less loss of cell functions in comparison to 2D culture. It is generally difficult to maintain the cell functions of hepatocytes in the traditional 2D culture. In the 2D culture, hepatocytes rapidly lose their functions hourly even immediately after being isolated (*69*). On the other hand, hepatocytes cultured in our 3D culture system maintained their synthesis activity of albumin and the metabolic activity of CYP for up to 2 months (*70*, *71*). To evalutate the 3D culture, the morphology of the construct is observed with either an optical microscope or a confocal laser microscope in more detail. Biochemical analysis methods using antibodies, dyes, and drugs are also commonly used to investigate the cell functions of 3D cell constructs (hepatocyte spheroids).

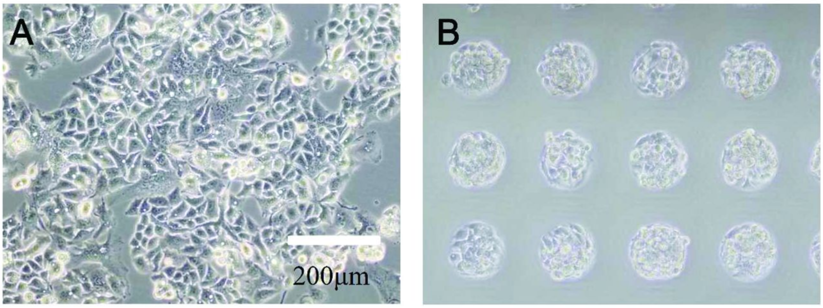

*Figure 6. Morphological observations of the HepG2 cell array. Scale bar: 200μm. Phase contrast micrograms of the (A) monolayer culture. (B) Cell-array system. Morphologically intact spheroids were observed (2 days after inoculation). (see color insert)*

The array system has been shown to be able to maintain the CYP activities and responsiveness to CYP inducers better than a monolayer culture system (*57*). For instance, the “Cell-able” mimics an environment close to natural tissues by allowing for the 3D culture of the cells. In the present study, we investigated 1) the preparation of spheroid arrays of HepG2 cells (Figure 6), and 2) the toxicity and functional evaluation of HepG2 spheroid arrays using our contrast agent (*50*). In the future, the results obtained using this evaluation system are expected to be used as a tool for the practical application of our contrast agent and also to examine the drug development applications of “Cell-able”.

## Acknowledgments

We thank Ms. Rina Yokota (Nagoya University) for her assistance. This work was supported in part by Health and Labor Sciences Research Grants from the Ministry of Health, Labour and Welfare (Tokyo, Japan); Research for Promoting Technological Seeds from Japan Science and Technology Agency; and a Grant-in-Aid for Scientific Research from the Japan Society for the Promotion of Science.

## References

1. Shapiro, A. M.; Lakey, J. R.; Ryan, E. A.; Korbutt, G. S.; Toth, E.; Warnock, G. L.; Kneteman, N. M.; Rajotte, R. V. *New Engl. J. Med.* **2000**, *343* (4), 230–238.
2. Shapiro, A. M.; Ricordi, C.; Hering, B. J.; Auchincloss, H.; Lindblad, R.; Robertson, R. P.; Secchi, A.; Brendel, M. D.; Berney, T.; Brennan, D. C.; Cagliero, E.; Alejandro, R.; Ryan, E. A.; DiMercurio, B.; Morel, P.; Polonsky, K. S.; Reems, J. A.; Bretzel, R. G.; Bertuzzi, F.; Froud, T.; Kandaswamy, R.; Sutherland, D. E.; Eisenbarth, G.; Segal, M.; Preiksaitis, J.; Korbutt, G. S.; Barton, F. B.; Viviano, L.; Seyfert-Margolis, V.; Bluestone, J.; Lakey, J. R. *New Engl. J. Med.* **2006**, *355* (13), 1318–1330.
3. Noguchi, H.; Iwanaga, Y.; Okitsu, T.; Nagata, H.; Yonekawa, Y.; Matsumoto, S. *Am. J. Transplant* **2006**, *6* (10), 2476–2482.
4. Zhang, F.; Citra, F.; Wang, D. A. *Tissue Eng., Part B* **2011**, *17* (2), 115–124.
5. Kiskinis, E.; Eggan, K. *J. Clin. Invest.* **2010**, *120* (1), 51–59.
6. Little, M. T.; Storb, R. *Nat. Rev. Cancer* **2002**, *2* (3), 231–238.
7. Gimble, J. M.; Katz, A. J.; Bunnell, B. A. *Circ. Res.* **2007**, *100*, 1249–1260.
8. Yoshimura, K.; Sato, K.; Aoi, N.; Kurita, M.; Hirohi, T.; Harii, K. *Aesthetic Plast. Surg.* **2008**, *32*, 48–55.
9. Yoshimura, K.; Sato, K.; Aoi, N.; Kurita, M.; Inoue, K.; Suga, H.; Eto, H.; Kato, H.; Hirohi, T.; Harii, K. *Dermatol. Surg.* **2008**, *34* (9), 1178–1185.
10. Miyamoto, Y.; Oishi, K.; Yukawa, H.; Noguchi, H.; Sasaki, M.; Iwata, H.; Hayashi, S. *Cell Transplant*, in press.
11. Sakuragawa, N.; Kakinuma, K.; Kikuchi, A.; Okano, H.; Uchida, S.; Kamo, I.; Kobayashi, M.; Yokoyama, Y. *J. Neurosci. Res.* **2004**, *78* (2), 208–214.

12. Parolini, O.; Alviano, F.; Bagnara, G. P.; Bilic, G.; Bühring, H. J.; Evangelista, M.; Hennerbichler, S.; Liu, B.; Magatti, M.; Mao, N.; Miki, T.; Marongiu, F.; Nakajima, H.; Nikaido, T.; Portmann-Lanz, C. B.; Sankar, V.; Soncini, M.; Stadler, G.; Surbek, D.; Takahashi, T. A.; Redl, H.; Sakuragawa, N.; Wolbank, S.; Zeisberger, S.; Zisch, A.; Strom, S. C. *Stem Cells* **2008**, *26* (2), 300–311.
13. Reubinoff, B. E.; Pera, M. F.; Fong, C. Y.; Trounson, A.; Bongso, A. *Nat. Biotechnol.* **2000**, *18*, 399–404.
14. Thomson, J. A.; Itskovitz-Eldor, J.; Shapiro, S. S.; Waknitz, M. A.; Swiergiel, J. J.; Marshall, V. S.; Jones, J. M. *Science* **1998**, *282*, 1145–1147.
15. Narazaki, G.; Uosaki, H.; Teranishi, M.; Okita, K.; Kim, B.; Matsuoka, S.; Yamanaka, S.; Yamashita, J. K. *Circulation* **2008**, *118*, 498–506.
16. Okita, K.; Ichisaka, T.; Yamanaka, S. *Nature* **2007**, *448* (7151), 313–317.
17. Takahashi, K.; Tanabe, K.; Ohnuki, M.; Narita, M.; Ichisaka, T.; Tomoda, K.; Yamanaka, S. *Cell* **2007**, *131*, 861–872.
18. Takahashi, K.; Yamanaka, S. *Cell* **2006**, *126*, 663–676.
19. Miyamoto, Y.; Noguchi, H.; Yukawa, H.; Oishi, K.; Matsushita, K.; Iwata, H.; Hayashi, S. *Cell Medicine*, in press.
20. Bulte, J. W.; Zhang, S.; van Gelderen, P.; Herynek, V.; Jordan, E. K.; Duncan, I. D.; Frank, J. A. *Proc. Natl. Acad. Sci. U.S.A.* **1999**, *96* (26), 15256–15261.
21. Dodd, C. H.; Hsu, H. C.; Chu, W. J.; Yang, P.; Zhang, H. G.; Mountz, J. D., Jr.; Zinn, K.; Forder, J.; Josephson, L.; Weissleder, R.; Mountz, J. M.; Mountz, J. D. *J. Immunol. Methods* **2001**, *256* (1−2), 89–105.
22. Dodd, S. J.; Williams, M.; Suhan, J. P.; Williams, D. S.; Koretsky, A. P.; Ho, C. *Biophys. J.* **1999**, *76* (1, Pt 1), 103–109.
23. Dousset, V.; Delalande, C.; Ballarino, L.; Quesson, B.; Seilhan, D.; Coussemacq, M.; Thiaudiére, E.; Brochet, B.; Canioni, P.; Caillé, J. M. *Magn. Reson. Med.* **1999**, *41* (2), 329–333.
24. Lewin, M.; Carlesso, N.; Tung, C. H.; Tang, X. W.; Cory, D.; Scadden, D. T.; Weissleder, R. *Nat. Biotechnol.* **2000**, *18* (4), 410–414.
25. Moore, A.; Sun, P. Z.; Cory, D.; Högemann, D.; Weissleder, R.; Lipes, M. A. *Magn. Reson. Med.* **2002**, *47* (4), 751–758.
26. Tai, J. H.; Foster, P.; Rosales, A.; Feng, B.; Hasilo, C.; Martinez, V.; Ramadan, S.; Snir, J.; Melling, C. W.; Dhanvantari, S.; Rutt, B.; White, D. J. *Diabetes* **2006**, *55* (11), 2931–2938.
27. Evgenov, N. V.; Medarova, Z.; Dai, G.; Bonner-Weir, S.; Moore, A. *Nat. Med.* **2006**, *12* (1), 144–148.
28. Jirák, D.; Kríz, J.; Herynek, V.; Andersson, B.; Girman, P.; Burian, M.; Saudek, F.; Hájek, M. *Magn. Reson. Med.* **2004**, *52* (6), 1228–1233.
29. Evgenov, N. V.; Medarova, Z.; Pratt, J.; Pantazopoulos, P.; Leyting, S.; Bonner-Weir, S.; Moore, A. *Diabetes* **2006**, *55* (9), 2419–28.
30. Barnett, B. P.; Arepally, A.; Karmarkar, P. V.; Qian, D.; Gilson, W. D.; Walczak, P.; Howland, V.; Lawler, L.; Lauzon, C.; Stuber, M.; Kraitchman, D. L.; Bulte, J. W. *Nat. Med.* **2007**, *13* (8), 986–991.

31. Kriz, J.; Jirák, D.; Girman, P.; Berková, Z.; Zacharovova, K.; Honsova, E.; Lodererova, A.; Hajek, M.; Saudek, F. *Transplantation* **2005**, *80* (11), 1596–1603.
32. Saudek, F.; Jirák, D.; Girman, P.; Herynek, V.; Dezortová, M.; Kríz, J.; Peregrin, J.; Berková, Z.; Zacharovová, K.; Hájek, M. *Transplantation* **2010**, *90* (12), 1602–1606.
33. Barker, P. B.; Bizzi, A.; Stefano, N. D.; Gullapalli, R.; Lin, D. D. M. *Clinical MR Spectroscopy: Techniques and Applications*; Cambridge University Press, West Nyack, NY, 2009; Vol. 1, pp 1−274.
34. Chouly, C.; Pouliquen, D.; Lucet, I.; Jeune, J. J.; Jallet, P. *J. Microencapsul.* **1996**, *13* (3), 245–255.
35. Jo, J.; Aoki, I.; Tabata, Y. *J. Controlled Release* **2010**, *142* (3), 465–473.
36. Oishi, K.; Noguchi, H.; Saito, H.; Yukawa, H.; Miyamoto, Y.; Murase, K.; Hayashi, S. *Cell Transplant* **2010**, *19* (6), 887–892.
37. Oishi, K.; Noguchi, H.; Saito, H.; Yukawa, H.; Miyamoto, Y.; Ono, K.; Murase, K.; Sawada, M.; Hayashi, S. *Cell Medicine*, in press.
38. Saito, H.; Murase, K.; Uchida, H.; Hayashi, S.; Noguchi, H. JP Patent, P2010-30915A, 2010.
39. Spielmann, H.; Liebsch, M. *Toxicol. In Vitro* **2001**, *15*, 585–590.
40. Korzeniewski, C.; Callewaert, D. M. *J. Immunol. Methods* **1983**, *64* (3), 313–320.
41. Sasaki, T.; Kawai, K.; Saijo-Kurita, K.; Ohno, T. *Toxicol. In Vitro* **1992**, *6* (5), 451–457.
42. Goergen, J. L.; Marc, A.; Engasser, J. M. *Cytotechnology* **1993**, *11* (3), 189–195.
43. Slater, T. F.; Sawyer, B.; Strauli, U. *Biochim. Biophys. Acta* **1963**, *77*, 383–393.
44. Mosmann, T. *J. Immunol. Methods* **1983**, *65* (1−2), 55–63.
45. Yamaue, H.; Tanimura, H.; Nakamori, M.; Noguchi, K.; Iwahashi, M.; Tani, M.; Hotta, T.; Murakami, K.; Ishimoto, K. *Dis. Colon Rectum* **1996**, *39* (4), 416–422.
46. Cree, I. A.; Andreotti, P. E. *Toxicol. In Vitro* **1997**, *11* (5), 553–556.
47. Jasmin, T. A. L.; Nunes, H. M.; Passipieri, J. A.; Jelicks, L. A.; Gasparetto, E. L.; Spray, D. C.; Campos de Carvalho, A. C.; Mendez-Otero, R. *J Nanobiotechnology* **2011**, *9*, 4.
48. Fan, C.; Gao, W.; Chen, Z.; Fan, H.; Li, M.; Deng, F.; Chen, Z. *Int. J. Pharm.* **2011**, *404* (1−2), 180–190.
49. Barnett, B. P.; Ruiz-Cabello, J.; Hota, P.; Ouwerkerk, R.; Shamblott, M. J.; Lauzon, C.; Walczak, P.; Gilson, W. D.; Chacko, V. P.; Kraitchman, D. L.; Arepally, A.; Bulte, J. W. *Contrast Media Mol. Imaging* **2011**, *6* (4), 251–259.
50. Miyamoto, Y.; Koshidaka, Y.; Saito, H.; Kagami, Y.; Murase, K.; Kaji, N.; Yukawa, H.; Noguchi, H.; Iwata, H.; Ikeya, T.; Baba, Y.; Hayashi, S. 2010 International Chemical Congress of Pacific Basin Societies (PACIFICHEM 2010): New Aspects of Chemical Glycobiology toward Development of new Diagnostics and Therapeutics Symposium, Honolulu, HI, 2010.
51. John, R.; Boppart, S. A. *Curr. Med. Chem.* **2011**, *18* (14), 2103–2114.

52. Yanase, M.; Shinkai, M.; Honda, H.; Wakabayashi, T.; Yoshida, J.; Kobayashi, T. *Jpn. J. Cancer Res.* **1998**, *89* (4), 463–469.
53. Ito, A.; Ino, K.; Kobayashi, T.; Honda, H. *Biomaterials* **2005**, *26* (31), 6185–6193.
54. LoRusso, P. M.; Boerner, S. A.; Seymour, L. *Clin. Cancer Res.* **2010**, *16* (6), 1710–1718.
55. Miyamoto, Y.; Suzuki, S.; Nomura, K.; Enosawa, S. *Cell Transplant* **2006**, *15*, 911–919.
56. Miyamoto, Y.; Teramoto, N.; Hayashi, S.; Enosawa, S. *Cell Transplant* **2010**, *19*, 701–706.
57. Hewitt, N. J.; Lech, M. J.; Houston, J. B.; Hallifax, D.; Brown, H. S.; Maurel, P.; Kenna, J. G.; Gustavsson, L.; Lohmann, C.; Skonberg, C.; Guillouzo, A.; Tuschl, G.; Li, A. P.; LeCluyse, E.; Groothuis, G. M.; Hengstler, J. G. *Drug Metab. Rev.* **2007**, *39*, 159–234.
58. Otsuka, H.; Hirano, A.; Nagasaki, Y.; Okano, T.; Horiike, Y.; Kataoka, K. *ChemBioChem* **2004**, *5* (6), 850–855.
59. Miyamoto, Y.; Ikeya, T.; Enosawa, S. *Cell Transplant* **2009**, *18* (5), 677–681.
60. Miyamoto, Y.; Enosawa, S.; Takeuchi, T.; Takezawa, T. *Cell Transplant* **2009**, *18*, 619–626.
61. Huang, H.; Hanada, S.; Kojima, N.; Sakai, Y. *Cell Transplant* **2006**, *15*, 799–809.
62. Kinoshita, T.; Miyajima, A. *Biochim. Biophys. Acta* **2002**, *1592*, 303–312.
63. Lee, J. I.; Nishimura, R.; Sakai, H.; Sasaki, N.; Kenmochi, T. *Cell Transplant* **2008**, *17*, 51–59.
64. Peshwa, M. V.; Wu, F. J.; Sharp, H. L.; Cerra, F. B.; Hu, W. S. *In Vitro Cell. Dev. Biol.: Anim.* **1996**, *32* (4), 197–203.
65. Walker, T. M.; Rhodes, P. C.; Westmoreland, C. *Toxicol. In Vitro* **2000**, *14* (5), 475–485.
66. Sullivan, J. P.; Gordon, J. E.; Bou-Akl, T.; Matthew, H. W.; Palmer, A. F. *Artif. Cells, Blood Substitutes, Immobilization Biotechnol.* **2007**, *35* (6), 585–606.
67. Feng, Z. Q.; Chu, X.; Huang, N. P.; Wang, T.; Wang, Y.; Shi, X.; Ding, Y.; Gu, Z. Z. *Biomaterials* **2009**, *30* (14), 2753–2763.
68. Glicklis, R.; Merchuk, J. C.; Cohen, S. *Biotechnol. Bioeng.* **2004**, *86* (6), 672–680.
69. O'Brien, P. J.; Chan, K.; Silber, P. M. *Chem. Biol. Interact.* **2004**, *150* (1), 97–114.
70. Takahashi, Y.; Joumura, Y.; Kozeki, E.; Ikeya, T. *Tissue Culture Res. Commun.* **2011**, *30*, 42–43.
71. Enosawa, S.; Miyamoto, Y.; Hirano, A.; Suzuki, S.; Kato, N.; Yamada, Y. *Drug Metab. Rev.* **2007**, *39* (Suppl. 1), 342.

## Chapter 10

# Halloysite Nanoclay for Controlled Release Applications

**Christopher J. Ward,[1] Megan DeWitt,[2] and Edward W. Davis*,[1]**

**[1]Auburn University, Department of Polymer and Fiber Engineering,
115 Textile Building, Auburn, Alabama 36849
[2]Current address: University of Rochester, Department of Chemical
Engineering, 500 Joseph C. Wilson Blvd., CPU Box 274379,
Rochester, New York 14627
*E-mail: ewd0001@auburn.edu**

Nanoclays have shown great potential in the field of controlled release. In particular, the cylindrical geometry and surface chemistry of halloysite nanotubes make them attractive for use as nanocarriers. Halloysite's tubular cavity can be filled with drug which later diffuses out of the lumen, enabling controlled release behavior over several hours. When halloysite is incorporated into polymer matrices, such as polyvinyl alcohol (PVOH) and poly(methyl methacrylate) (PMMA), release has been shown to be extended even further, on the order of days. In this chapter, the principles and mechanisms used in controlled release applications are presented, and recent studies of controlled release from halloysite nanotubes are reviewed. Particular attention is paid to two studies on the incorporation of tetracycline-loaded halloysite into polymer films to prepare monolithic controlled release systems. Factors affecting the release from halloysite are explored, particularly loading method and material properties.

## Introduction

Controlled delivery involves releasing drugs for extended periods of time or in a targeted manner. This is very important, considering that conventional drug delivery usually involves administration of high doses of drug to guarantee

In Nanomaterials for Biomedicine; Nagarajan, R.;
ACS Symposium Series; American Chemical Society: Washington, DC, 2012.

that a sufficient amount of drug reaches the affected site. The two most used methods, oral administration and injection, typically utilize high initial doses, often resulting in unwanted side effects. In addition, when single doses are administered, normal metabolic processes result in the need for repeated dosing to maintain the drug level within the therapeutic range. Lack of patient compliance with the dosing schedule decreases the effectiveness of the treatment and is a major issue in medicine.

Controlled release devices solve these problems by incorporating the drug into structures that are capable of protecting the drug until the desired site is reached, or by continuously releasing the drug over time. Nanomaterials are one of the more interesting classes of materials under evaluation today for controlled release applications. These materials have several benefits, including the ability to improve effective solubility by complexation or encapsulation (the small size allowing for the uptake of the carrier system by cells), the ability to integrate methods to target the release to a specific site or under specific physiological conditions, and the ability to integrate methods to track the nanoscale release system to confirm accumulation in the target location. Accumulation at a specific location in the body allows for targeted treatment utilizing compounds that may be very toxic to normal tissue, for example cancer therapy.

Among the different types of nanostructures available, nanoclays have garnered increasing interest due to high availability and low cost: resulting from their natural origins. Halloysite, in particular, has been the subject of much study. Halloysite is mined commercially and is currently used as an additive to fine china. Its naturally rolled structure creates a pore that can be filled with bioactive agents. Recent studies have suggested that drugs loaded into the lumen of halloysite can have extended release, especially when a polymer matrix is applied to the outside of the nanotubes. These clay/polymer nanocomposites have shown great promise in the design of controlled release devices.

## Controlled Release

The concept of controlled release of medications was first developed in the mid 1800's by Lafargue, who developed a system of releasing morphine directly to affected sites via lancets (*1*). This technique fell out of favor with the widespread adoption of intravenous injections. The idea was briefly revived again in the early 1920's with the use of pure drug pellets implanted into the body (*2*). Due to the difficulties associated with instability in areas of the body undergoing constant motion and the requirement of surgery to insert and remove the pill in case of overdoses, it once again fell into disuse (*1*). Interest in controlled release reemerged in the late 1950's and early 1960's. During this time there were studies performed concerning the release of penicillin from penicillin-sulfonamide tablets (*3*). In addition, there was growing interest in controlled release for pesticides and agricultural agents (*4*). In 1965, the first successful commercial study on the use of nitroglycerin tablets for the treatment of angina was initiated. Today, millions of patients use nitroglycerin tablets for this purpose, with the result of many saved lives. Since then, many other commercial products have been developed with controlled release technologies: gel capsules, where the outer layer slowly dissolves away, releasing the drug within the small intestine (*5*); transdermal patches that help with nicotine addictions and motion sickness (*6*, *7*); and structures that can be implanted into the body to slowly release compounds such as anti-rejection medication and growth hormones (*8*).

The two traditional routes of drug delivery are injection (intravenous, subcutaneous, or intramuscular) and oral (ingested tablets or liquids). In both cases, relatively high levels of medications have to be introduced to the body to ensure that a proper dosage of the medication reaches the active site (the location within the body where the drug acts). For example, when the drug has a short half-life, a high dose is required to ensure that degradation through metabolic processes during transport does not result in too low a drug concentration at the intended site. High concentrations of many drugs can cause adverse reactions and unwanted side effects. The excess drug that is not adsorbed is wasted; likewise, the fraction metabolized by the body before reaching the active site is wasted and can cause adverse side effects.

The route through the digestive system can take as long as six hours: too long for some short half-life drugs and too long when the drug needs to arrive at an active site in a short time. Thus, these drugs are administered by injection directly into the bloodstream or into a location where they can be adsorbed quickly (*9*, *10*). While bypassing the digestive system is one of the main reasons for utilizing injections, this approach does not always eliminate the need for high doses. These medications are degraded by metabolic processes, adsorbed by the liver, and eliminated through the kidneys. Thus, often, a high dose is required to maintain therapeutic levels.

The oral route is even more inefficient for transporting drugs. As the drug enters the digestive system, it is subjected to different degradation mechanisms that act to begin to eliminate the drug supply. These mechanisms include hydrolysis in the stomach, enzymatic digestion in the intestines, metabolism at the walls of the digestive organs, and further degradation within the colon (*11–13*). All of these processes limit the amount of drug available for adsorption and transport to the desired area of the body. To enable a sufficient supply of drug to reach the small intestine, where a majority of the absorption takes place, a much higher dose than is eventually needed has to be introduced to the body to account for both the degradation in the digestive tract and metabolism after adsorption. Often these doses increase irritation of the digestive system and can cause unwanted side effects such as allergic reactions (called hypersensitivity), drug dependence (*14*), and possibly death (*15*). While there are numerous problems associated with oral delivery of drugs, this method of delivery is still the preferred method due to its ease and widespread use.

Medications are effective within a, sometimes narrow, window of concentration: too high of a concentration can result in complications such as irritation or allergic reactions, while too low of a concentration results in no therapeutic value of the drug. Due to metabolic processes, the concentration of drug changes with time after administration. Too ensure that a proper level of the medication is maintained, repeated doses over time must be administered (*9*, *16*). Figure 1 shows the concentration of drug within the body as a function of time, with repeated doses for a typical orally administered drug. As the drug is adsorbed in the small intestine, the level of drug in the body rises. After adsorption slows, metabolic processes decrease the level of drug in the body over time. The drug stays within the optimal concentration window for only a portion of the time. Dosing levels have to be carefully calculated and monitored so that a patient does not unintentionally overdose on medications (*16*, *17*). This problem can be partially solved by introducing more frequent dosing with lower levels of drug. This reduces the problem of toxicity and damage to the body during the initial period of high drug levels; however, patient compliance becomes an issue. As the number and frequency of doses increases, the patient will either grow tired of the treatment and disregard treatment instructions or the patient will forget to take the medication. Concentration of the drug within the body will then drop below effective levels.

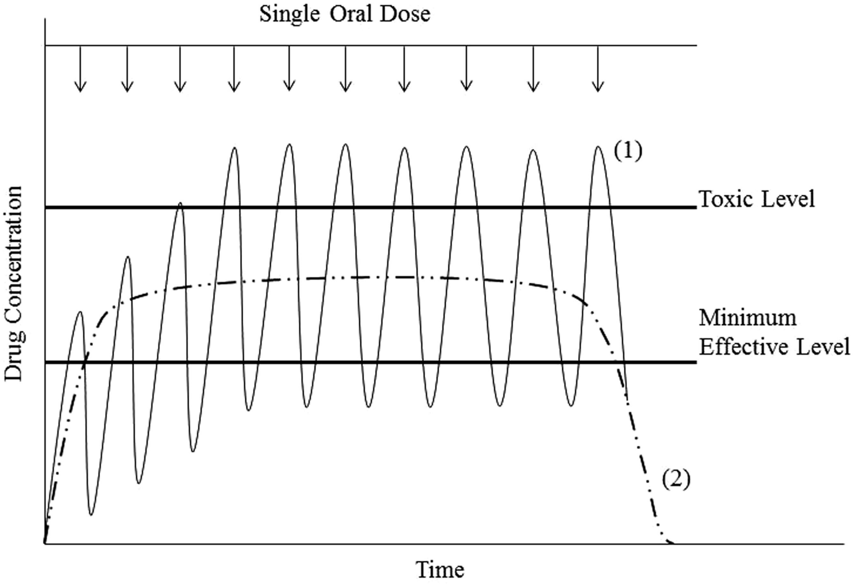

*Figure 1. Typical curves of concentration vs. time for (1) oral doses and (2) controlled release. The curve of injections would appear very similar to the oral dose curve, except that initial concentration would be high, followed by cyclic drops as injections are repeated to keep medication levels high enough.*

The problems associated with the traditional drug delivery methods have resulted in the development of controlled release systems for drug delivery. There are several advantages to controlled release of medications: i) a consistent level of medication present within the body or at a particular site (Figure 1), ii) longer release duration for those drugs with shorter lifespans, iii) reduction of side effects and unintentional overdose, and iv) increased patient compliance due to the elimination of repeated doses or injections (*1*, *18*). Indeed, the last point is extremely important, as the issue of patients refusing or forgetting to take regular oral tablets or injections is a very common problem. Multiple studies have shown that degrading patient compliance can lead to problems such as lingering or increasing illness, mortality from original illness, as well as increased cost of medical care (low patient compliance results in longer treatments, thus higher costs) (*19*). In order to eliminate the need for successive doses to keep medication levels high enough to be effective, controlled release methods need to be developed with the capability of releasing the correct level of medication over long periods of time. However, releasing the drug at a location away from the target site means that higher levels of medication are required to account for transport losses and effectively deliver treatment. Thus, controlled release systems often incorporate targeting mechanisms that allow for release of drugs only when and where the drug is required (*1*, *11*, *20*).

Controlled release can be categorized in several ways: the mechanism of release, the targeting method, and the delivery route. The mechanism of release refers to the physical or chemical mechanism by which the drug is released from the device. There are several classes of mechanisms, including mechanical and osmotic pumps, and polymer systems where the release is controlled by chemical degradation or diffusion (*21*). Another method of categorization is through targeting methods. This refers to the way the device responds to the local environment, allowing the release to occur only at the target site or only under a particular set of physiological conditions. Targeting includes chemical manipulation of the drug, surface modification of the delivery system to allow recognition of the local environment and affect release, and systems that respond to gross changes in pH or salinity (*20*). The delivery route refers to the route of administration of medications to the body. By far the most prevalent are injection and oral, but others can include transdermal, buccal, rectal, nasal, pulmonary, ocular, and implantable (*20*).

## Mechanism of Release

There are three main mechanisms used for the development of controlled release systems: pump-based systems, systems which utilize the degradation of a monolith or film, and systems that utilize the diffusion from a monolith or through a film. The main principles, including introduction to the body, mechanism of release, and then removal (if necessary), behind all three release mechanisms are shown in Figure 2.

One major drawback to pump-based systems is that surgery is required both for implantation and removal. There are two main types of pump systems used for controlled release: mechanical and osmotic. The advantage of pumps is that the drug can be administered very slowly for long periods of time and that the pump outlet can be adjacent to the target site. This type of release can be very beneficial in treatments that utilize medications with significant side effects. One example is chemotherapy of liver cancer. Other examples include situations where constant doses that respond to body conditions are required (e.g. the release of heparin and insulin to the bloodstream) (*21*). Osmotic pumps are designed with a polymer membrane surrounding a water-soluble drug. As water permeates the polymer membrane, hydrostatic pressure builds up inside the membrane, forcing the drug solution through the opening into the body (*9*, *16*, *21*). Osmotic pumps are currently popular for the dispensing of pain relievers like hydromorphone. Release has been shown to be able to occur for many days (*22*). While they can be miniaturized, even the most modern osmotic pumps are still rather large, especially compared to the nanoscale controlled release systems currently under development (*23*). Mechanical pumps can be based on the swelling of a material on one side of a membrane pushing the membrane and forcing drug from a reservoir on the other side of the membrane, in which case the entire system can be implanted. More commonly, electrically driven pumps located external to the body with a catheter leading from the pump to the target site are used. Osmotic pumps are typically implanted.

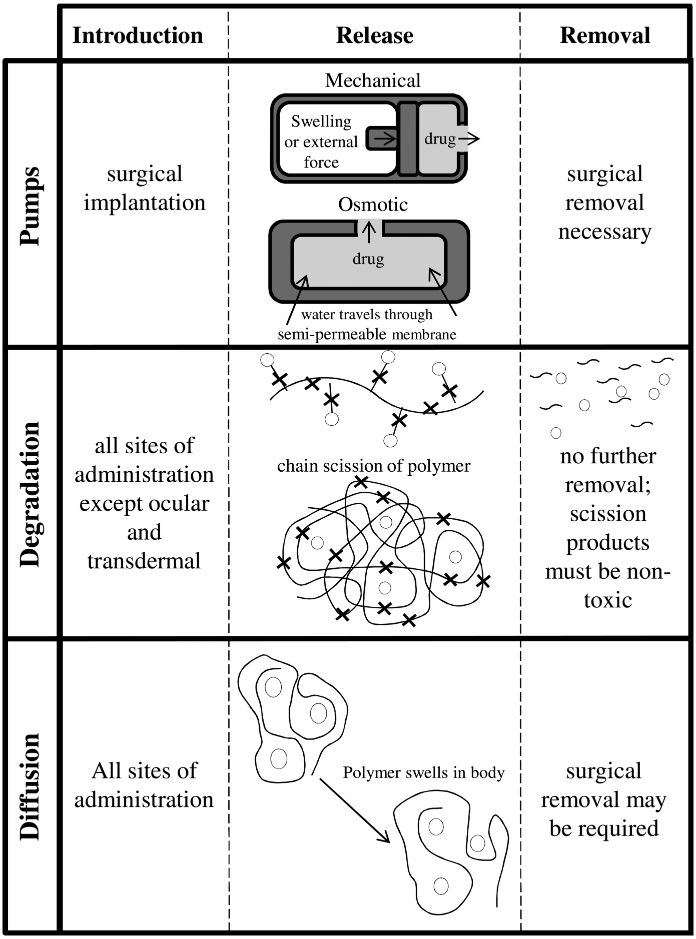
Introduction
Release
Removal
Pumps
surgical implantation
Mechanical
Swelling or external force
drug
Osmotic
drug
water travels through semi-permeable membrane
surgical removal necessary
Degradation
all sites of administration except ocular and transdermal
chain scission of polymer
no further removal; scission products must be non-toxic
Diffusion
All sites of administration
Polymer swells in body
surgical removal may be required

*Figure 2. Primary mechanisms of controlled release.*

Degradation of polymers is another mechanism used for controlled release. In these systems, the drug is either physically mixed with a polymer or chemically bound to the polymer chain, either physiochemically or covalently. The latter case can provide better protection for the drug from metabolic process due to the added difficulty of breaking the connecting bonds. As the polymer backbone, or the bond holding the drug to the side group, is cleaved by hydrolysis or enzymatic reactions, the drug is released from the system (*16*, *21*). One key requirement is that the polymer and products of the degradation process must be nontoxic. There is no need for surgical removal, although surgical implantation can be required, and the cost of such materials is comparatively low. One issue is that some systems degrade more by bulk degradation than by surface degradation (*24*). Bulk degradation results in relatively quick release profiles as the entire structure degrades somewhat simultaneously. Of this type, polyesters are the most studied for controlled release, particularly poly(lactic-co-glycolic acid) (PLGA). It predictably degrades in aqueous liquids with hydrolysis of ester links in its backbone. Controlled release structures that are created from PLGA are typically designed to self-catalyze during degradation, further increasing the rate of degradation and release (*25*, *26*). To control degradation, and thus release, factors such as degree of crystallinity, glass transition temperature, and molecular weight can be manipulated. Polymers such as polyanhydrides typically degrade through a surface erosion process due to their hydrophobic nature (water does not penetrate to cleave the chains in the bulk), and can be used to design systems that exhibit zero order release as well as more complicated release profiles (*25*). Hydrolysis products of polyanhydrides are water soluble and considered by most to be biocompatible (*25*). Poly(ortho esters) have also been utilized in release devices where bulk degradation is undesired. These devices are controlled by adding basic or acidic components which act to catalyze or further retard degradation and, thus, extend release of the drug (*25*, *27*).

In diffusion-based systems, the drug is contained within a reservoir inside the material or dispersed within the material. In this system, the aqueous fluid in the body diffuses into the matrix. The drug then diffuses out of the system. There are two main types of diffusion systems: i) the fluids of the body and the drug do not affect the material and transport takes place through molecular diffusion through the swollen polymer; and ii) the fluids of the body swell the material and diffusion occurs through the resultant micropores instead of the material (*9*, *16*, *21*, *28*, *29*). In the second case, the important factor is that release is controlled through solubility in the liquid medium instead of the polymer.

## Targeting Methods

Targeting the release to a specific location within the body can be achieved through two broad methods. The drug can be modified to be inactive before it is introduced to the body, after which a known and controllable transformation then activates the drug at the target site. (*20*, *30*). The prodrug approach is one example. In this case, the modified inactive compound is activated once in the body by the introduction of a secondary compound (*31*). Unfortunately, this technique cannot deliver to a specific site, only a specific area. Another method is through the use of a chemical delivery system, where the inactive, modified drug, released into the body, will undergo predictable chemical and enzymatic reactions along the way to the intended site. Once reaching the intended site, the predicted number of chemical changes will have occurred and the drug will be back to its normal state, capable of then treating the desired area (*20*).

The final method involves the use of a carrier that "protects" the drug from the body during transport and prevents the release of the drug until the target site is reached. The carriers used to transport the drug can be macromolecules, microspheres, nanoparticles, or liposomes. Macromolecules, microspheres, and nanoparticles have been shown to be particularly effective (*20*). Release from these small particles occurs through: i) diffusion through the surface of the particles, ii) diffusion through the incorporation matrix, iii) erosion of the particle, or iv) erosion of the incorporating matrix (*9*). The release from these carriers can be targeted in several ways. Materials that degrade under a temperature gradient are used in systems where the release is activated by intentional inflammation at the active site or through the use of low-level radiation. By utilizing magnetic materials as the carrier or adding magnetic material to a polymer microsphere, an outside magnetic field can hold the drug-releasing microsphere in the desired area for the duration of the release. In addition, microspheres can be used for passive targeting, in which no attempt is made at targeting except through size of the spheres. Depending on the size of the spheres, they will lodge in different size capillaries to release in different areas of the body (*20*, *32*), shown in Figure 3. Nanoscale particles can even lodge in the membrane pores of cells themselves: for example, drug carriers that penetrate the leaky vasculature typically associated with cancer tumors and lodge in the tumor cells themselves (*32*).

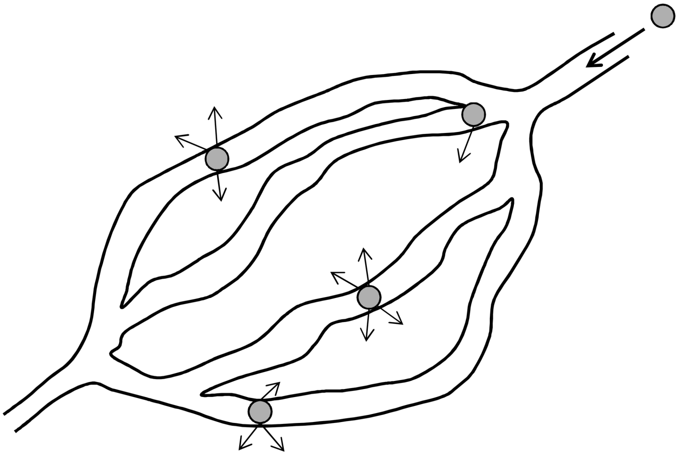

*Figure 3. Drug targeting achieved through size of micro (or nano) particles. Particles are lodged into the capillaries and begin to release.*

## Delivery Routes

There are many delivery routes that can be conceived for the delivery of controlled release systems. Table 1 provides a summary of the factors associated with these sites and some examples of controlled release systems currently under development or in current commercial use. Some of these lend themselves to the use of polymer, film-based systems (buccal, sublingual, transdermal, ocular, and implantable) while others (injection, oral, nasal, and pulmonary) do not.

Drugs administered between the cheek and gums, buccal, as well as under the tongue, sublingual, bypass the gastrointestinal tract and enter general circulation through the jugular vein. This administration site can be more effective than oral (*1*, *11*, *20*). Typically, drug release in these areas of the body is very short-acting due to short contact times. It has been shown, however, that some saliva-activated, adhesive-controlled release structures can be utilized to provide for sustained release (*20*, *33*).

Transdermal delivery systems also rely on a short path to the circulatory system. The drug is introduced to the skin were it is absorbed by the large number of blood vessels in the dermis and hypodermis layers (*1*, *11*, *20*, *34*). There are several advantages to using the skin as the route for drug delivery: i) avoiding the gastrointestinal tract and commensurate degradation, ii) allowing for the use of short half-life drugs, due to quick application and then absorption, iii) vast improvement of patient compliance, this being one of the least invasive techniques, and iv) quick removal of the controlled release agent if necessary (*20*). Because of the skin's high barrier properties, primarily the epidermis, drugs that enhance the absorption of the initial treatment drug are often incorporated in the controlled release system, resulting in a higher level of design complexity (*1*, *20*). Transdermal controlled release systems can be described as either membrane-controlled or monolithic. Essentially, membrane-controlled systems have a reservoir that holds the drug separated from the skin by a membrane that allows for the slow diffusion of the drug to the epidermis layer of the skin. Monolithic systems are those systems that are applied directly to the skin, with little to no rate-determining properties (*9*, *11*). Some current commercial applications of membrane-transdermal controlled release systems include the treatment of motion sickness by the release of scopolamine (*7*), the treatment of angina by the release of nitroglycerine (*35*), and smoking cessation patches that release small amounts of nicotine (*6*). Currently, research is underway for the development of patches that release anesthesia for the relief of pain following surgery or from chronic conditions (*11*).

Traditional ocular treatments involve drug solutions that are applied topically to the eye at high concentrations and are usually used for treatment of ocular problems. Due to the cleansing mechanisms of the eye, controlled release methods are needed. Recent advances in controlled release contact lenses have shown great promise. Instead of relying on a liquid or viscous material to provide release of a drug, the drug is incorporated into the polymer of contact lenses, providing a support against the body's protective measures (*43*). Issues such as the drainage, tears, and automatic blinking of the eyelids are still an issue, but with a structure present beneath the eyelid that cannot be washed away, continuous release is possible (*11*, *20*, *36*).

**Table 1. Drug administration routes, their key aspects, and experimental and commercial controlled release systems utilizing the route**

| *Route* | *Key Points* | *Experimental Systems* | *Commercial Systems* | *Reference* |
|---|---|---|---|---|
| ***Capable of using films or monoliths*** | | | | |
| **Buccal and Sublingual** | bypasses digestive process, enter the body through the jugular vein | saliva-activated adhesive systems | nitroglycerine tablets for angina | (*1*, *11*, *20*, *33*) |
| **Transdermal** | large surface area for absorption, high barrier properties of epidermis | patch that releases anesthesia for pain relief | patches that release scopolamine, nitroglycerine, and nicotine | (*1*, *6*, *7*, *11*, *34*, *35*) |
| **Ocular** | protective actions of the eye make sustained release difficult | controlled release contact lenses | | (*11*, *20*, *36*) |
| **Implantable** | requirement of surgery for implantation and sometimes removal | biodegradable polymer implants that release treatment for bone infections and bone growth | drug-eluting, biodegradable implants | (*9*, *37*, *38*) |
| ***Do not utilize polymeric films or monoliths*** | | | | |
| **Injection** | subcutaneous, intramuscular, and intravenous | hydrogels, microparticles, and polymers to release proteins and polypeptides | polymer nanoparticles to release prostate cancer drugs | (*39*, *40*) |
| **Oral** | small intestine most effective release site, difficult to travel through digestive process | flotation tablets, bioadhesive polymers | erodible tablets and capsules, natural polymer matrices that swell | (*1*, *11*, *16*, *20*) |

*Continued on next page.*

**Table 1. (Continued). Drug administration routes, their key aspects, and experimental and commercial controlled release systems utilizing the route**

| | | | | |
|---|---|---|---|---|
| ***Do not utilize polymeric films or monoliths*** | | | | |
| **Nasal** | ease of deployment, sinus cavities have high absorption capability | mucoadhesive release of anti-Parkinson drugs | | (*11*, *20*) |
| **Pulmonary** | large absorption area in lungs | microspheres for the release of steroids | inhaled insulin-releasing treatment | (*20*, *41*, *42*) |

Implants are surgically inserted into the body at the site of treatment and have been demonstrated to release drug over more than 30 days (*22*). Traditionally, this type of device is designed to release the drug through one of the two diffusion mechanisms, or through a degradation mechanism. In the case of diffusion-based systems, the device is surgically removed after treatment (*9*). Researchers in Turkey have experimented with the use of biodegradable implants composed of polyhydroxyalkanoate to release antibiotics to treat implant-related osteomyeletis, or bone infection (*37*). Results have shown that release was sustainable and efficiency of the antibiotic proved to be very high. In addition, within six weeks of implantation (drug completed eluting after one week), the implant began to degrade and disappear. In a collaborative study performed in U.S. universities, a biodegradable poly-(dl-lactide/glycolide) scaffold has been developed for the release of osteotropic factors, compounds that promote bone growth (*38*).

Additional drug delivery routes that, while not typically suitable for delivery from films, are commonly used include injection, oral, nasal, and pulmonary. Injection includes subcutaneous, intramuscular, and most commonly, intravenous. Continuously injecting certain medications into the human body requires continuous monitoring and intense use of medical equipment, usually resulting in hospitalization. Significant progress has been documented, however, in creating biodegradable microspheres that will slowly degrade and release active agents. As noted, these systems can be designed to lodge in certain areas of the body by controlling the sphere diameter, Larger microspheres, 25 micrometers and larger, will be trapped almost instantly and begin to release at the site of injection, while smaller microsphere can be transported much further (*11*, *20*). Due to the capillary and lymphatic vessels located in the muscle tissues, drug release and adsorption to the circulatory system can be faster than waiting for the drug to be absorbed through the gastrointestinal tract (*1*, *11*, *20*, *44*).

Oral administration is a very common and simple method for administering medications. Some disadvantages of oral administration of controlled release systems are degradation in the gastrointestinal tract and liver, gastric emptying, and intestinal motility (*1*, *11*, *20*). Among researchers, it is generally agreed that the small intestine is the most desirable site for absorption of the drug. Unfortunately, however, travel time to and through this part of the human body is around three hours, leaving sustained release difficult. Studies have examined the possibility of twelve hours of release through flotation tablets, bioadhesive polymers, and certain drugs that will slow gastric emptying and intestinal motility. However, slowing gastiric emptying can cause other issues and is generally considered undesirable (*1*, *11*).

Due to the relative ease of deployment and noninvasive nature, the sinus cavity is an attractive site for the administration of drugs. The sinus cavity has a very high absorption capability; however, controlled release systems need to be designed with particles of large enough size to ensure that the particles do not travel to the lungs and will remain lodged in the nasal cavity during release (*11*, *20*, *45*). Unfortunately, issues such as reproducibility and mucus interaction are still unsolved.

While the absorption area is huge for the lungs, usually little drug reaches the lungs due to loss by absorption in the mouth or stomach (*20*). This results in the fact that high doses need to be utilized to guarantee sufficient delivery. To make this a viable release method, mechanisms need to discovered whereby the controlled release vehicle can be delivered successfully to the lung and then be bound to the tissue in high enough concentrations via aerosols or nebulizers (*20*). Due to these constraints, this method will be unlikely to be put into practice for very many applications.

## Nanotechnology in Drug Release

The National Nanotechnology Initiative defines Nanotechnology as the understanding and control of matter at the nanoscale, at dimensions between approximately 1 and 100 nanometers, where unique phenomena enable novel applications. Historically, there is a trend to miniaturize routes of drug delivery, i.e. making pills smaller and injections less traumatic. Utilizing nanoscale systems can resolve some of the common problems of current drug release technologies. For one, solubility, often affected by physiological conditions, of the drugs can be increased. To allow for drug transport in cases of poor solubility, the drug can be contained within a nanocarrier that will go into solution (*46*). Second, specific surface area is increased, allowing for quicker release. This results in quicker absorption, increasing the efficacy (*46*). On the other hand, nanoparticle systems can be designed to sustain release for more extended periods of time than most traditional methods, with less risks to the patient (*46*). The reduced risks result from decrease in strength and number of doses and the commensurate reduction in side effect frequency. Presently, one of the few techniques for sustaining a flow of drugs to a patient is through constant intravenous flow, mandating that the patient is constantly monitored by physicians. Nanoscale systems within the body will be able to affect the same drug release and the less invasive administration improves patient compliance. Finally, one of the more important benefits of nanotechnology is the possibility of targeting the drug release (*46*). While there are some targeting methods that are applicable for macroscale drug release systems, targeting methods are much more common and functional for micro- and nanoparticles. The properties of the nanoparticles, such as chemical composition, charge, magnetism, etc, provide ways for each specific type of system to utilize targeting methods. There are a multitude of different kinds of nano-scale systems for drug release. Generally, however, they can be summarized by the following categories: i) metallic nanoparticles, ii) lipid-based nanoparticles, iii) polymer-based nanoparticles, and iv) dendritic materials (*47*). In addition, a very promising nanotechnology for drug release includes the developing field of nanoclays.

Metallic nanoparticles include those systems made from materials such as metal oxides, gold, silver, silicate, calcium phosphate, and magnetic materials. Usually, these systems are comprised of an inner shell composed of silicon, containing the drug to be released, and an outer shell composed of the selected metallic material (*47*). Traditionally, however, metal-based nanoparticles are utilized more for their usefulness in targeting and tracking (*47*, *48*). Magnetic particles can be included in polymeric-based carriers to provide the ability to remotely activate release. The magnetic properties are used to track the particles and the release activated by other methods. Metallic nanoparticles are also useful for activating release under specific physiological conditions. Gold and silver can be conjugated with proteins and antibodies to provide control of where the nanoparticles travel and when and where the carriers will release (*47*). Due to its ease of functionalization, it is also possible to couple silica to many biological compounds and molecules, such as proteins, DNA, antibodies, oligonucleotides, and oligopeptides. Silica can be functionalized with fluorophores, enabling tracking through fluorescence (*47*, *49*).

In aqueous solutions, lipids form structures similar to polymer micelles called liposomes; hydrophobic tails are concentrated together and hydrophilic groups interact with the aqueous solution (*47*), shown in Figure 4. The typical size of liposomes used for medical research ranges from 20 to 500 nanometers (*50*). Depending on the structure, both hydrophilic and hydrophobic drugs can be incorporated (*25*, *46*, *48*, *49*). The inherent problems with this technique, however, are that lipids and thus liposomes react with lipoproteins present in the body, a critical concentration of lipid is required before the structure is stable, and the supply of medical-grade lipids at an acceptable price is limited (*25*, *46*, *47*, *49*).

Block copolymers form micelles that are capable of entrapping drugs as shown in Figure 4 (*25*, *47*, *49*). Sizes for these small particles can range from 50 to 150 nanometers, when encapsulating release compounds (*51*). A benefit of the use of block copolymer micelles over lipid-based systems is that a much lower critical concentration is required to stabilize the micelle structure. Micelle structures have been shown to be very effective for drug and gene-controlled release (*25*, *48*, *49*, *52–54*). The hydrophilic shell, or outer layer, is stable in the body and serves to protect the drug from metabolism. Micelle properties can be tailored by incorporating crosslinks in the structure. Crosslinking increases stability, increases the level of protection the micelle offers the drug, and slows release, thereby increasing release duration. Common polymers used for the hydrophobic block are from the poly(ortho esters) class; for the hydrophilic block, polyethylene oxide is popular. Unlike lipids, which can carry both hydrophobic and hydrophilic payloads, micelles can only be used with hydrophobic drugs (*25*, *49*). The small size and hydrophilic shell make micelles particularly useful in intravenous administration by prolonging circulation time. In addition, drugs that are incorporated into polymeric micelles have been shown to accumulate, to a greater extent, in tumors. This behavior lends their use to targeted delivery of anticancer therapies. This occurs due to the perivascular accumulation of colloidal drug carriers in tumor tissues (*48*). An example of this is the novel micelle system created from amphiphilic pH-responsive poly(N-isopropylacrylamide) (PNIPAM) incorporating anti-tumor drugs such as doxorubicin or aluminum chloride phthalocyanine (*46*, *55*).

Dendrimers are a newer class of polymers that are created from a process of repetitive reactions that create three-dimensional structures. Studies have confirmed that some dendrimers are capable of being created as small as three nanometers in diameter (*56*). The benefit of such a structure for controlled release is that the three-dimensional structure is capable of entrapping drug compounds. The branches of these structures can either be structured around the drug and be created outward (divergent) or polymerized inward to create the shell around the drug (convergent). The complexity of the branches and size of the dendrimers can be easily controlled, allowing the design of release rates based on local porosity and crosslink density to allow for the tailoring of release (*25*, *47–49*). One type of drug that has been shown to be very effective with dendrimers is 5-Fluorouracil, a promising anti-tumor treatment. Unfortunately, it has very toxic side effects. Thus, poly(amido amine) (PAMAM) dendrimers can be conjugated with 5-Flurouracil after acetylation (*48*, *57*). This prevents the treatment from interacting with the rest of the body until it reaches the tumor site. There, after hydrolysis, the drug is released.

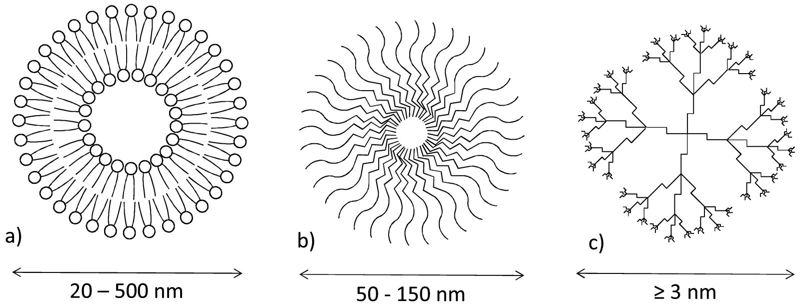

*Figure 4. a) Liposome composed of a bilayer of hydrophilic (circles) and hydrophilic tails (lines), b) Polymeric micelle composed of a diblock polymer with hydrophobic sections towards the inside (zigzag lines) and hydrophilic sections towards the outside (curved lines), c) Dendrimer with branches capable of trapping desired compounds.*

## Halloysite Nanoclays for Controlled Release

Nanoclays are a mined product with natural origin and have a wide availability. There are four basic groups of nanoclays widely available: kaolinite, smectite, illite, and chlorite (*58*). However, the main group of interest for controlled release is the smectite group (*58*). Smectite clays are characterized by their layering configuration, which is composed of tetrahedral sheets of silica fused to an octahedral sheet of alumina (*59*). This group includes montmorillonite, laponite, halloysite, hectorite, beidillite, nontronite, and saponite. Nanoclays have exhibited many beneficial properties upon their incorporation into polymers. These properties include an increase in tensile strength, bending strength, and modulus (or stiffness) (*60*), changes in rheological properties with nanoclay concentration (*59*, *61*), decrease of diffusion rates due to the creation of tortuous pathways (*62*), and reduced thermal transfer (*63*). Additional benefits include a reduced coefficient of thermal expansion, increased ability for char formation to prevent flame transfer (*64*), and the ability to absorb liquids in galleries between layers or inside the lumen in nanotubes (*65*).

Found in numerous places around the world, montmorillonite is formed through the reaction of certain volcanic ash with the addition of water and the presence of sufficient amounts of magnesium (*66*). Montmorillonite has the formula $(Na,Ca)0.33(Al,Mg)_2(Si_4O_{10})(OH)_2{\cdot}nH_2O$. The morphology of this clay consists of a stacked array of sheets similar to a deck of cards. Each sheet is composed of three layers, two of silica and one of alumina (*59*). The silica layers are formed of tetrahedral sheets with an octahedral sheet of alumina sandwiched in between (*58–60*). Montmorillonite was the first clay used in commercial polymer nanocomposite systems; montmorillonite reinforced nylon was used by Toyota in automotive fan housings in 1988 (*67*). In these applications the normal morphology is disrupted and the individual sheets, roughly one nanometer in thickness, are dispersed throughout polymer. Montmorillonite was also the first nanoclay studied for its use in controlled release. In these applications the stacked layer is typically maintained and the drug loaded in the interstitial space between the individual sheets. This loading is possible due to the ionic nature of the silica layers providing substantial cation exchange capacity that can be used to ionically bond the drug to the sheet surfaces. Cationic clays such as montmorillonite are very common in nature and are composed of negatively charged alumino-silicate layers. It should be noted that while anionic clays are not commonly found in nature (hydrotalcite is one notable exception) they can be readily synthesized and can be used in a similar fashion to load anionic compounds (*68*). The bound drug often “swells” the structure, resulting in increased gallery spacing between the sheets. This phenomenon is called intercalation. The layers of the clay are still associated together, but the spacing is much larger. In recent years, research has focused on the controlled release of drugs such as ibuprofen, 5-flourouracil, promethazine chloride, buformin hydrochloride, sertraline, timolol maleate, and tetracycline hydrochloride (*69*).

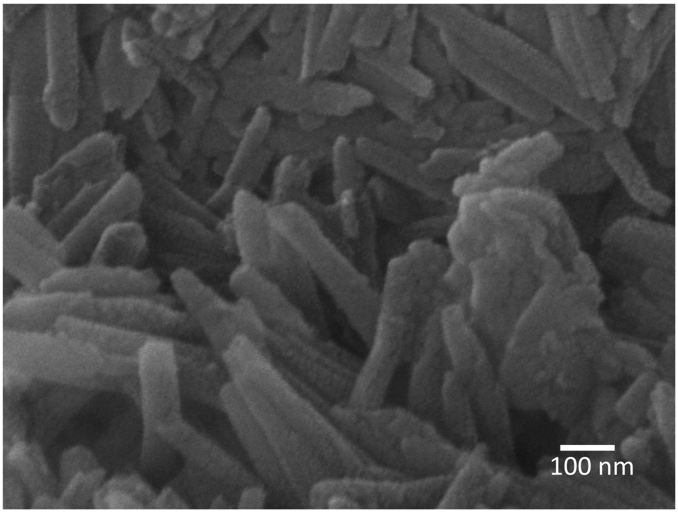

*Figure 5. SEM of halloysite nanotubes.*

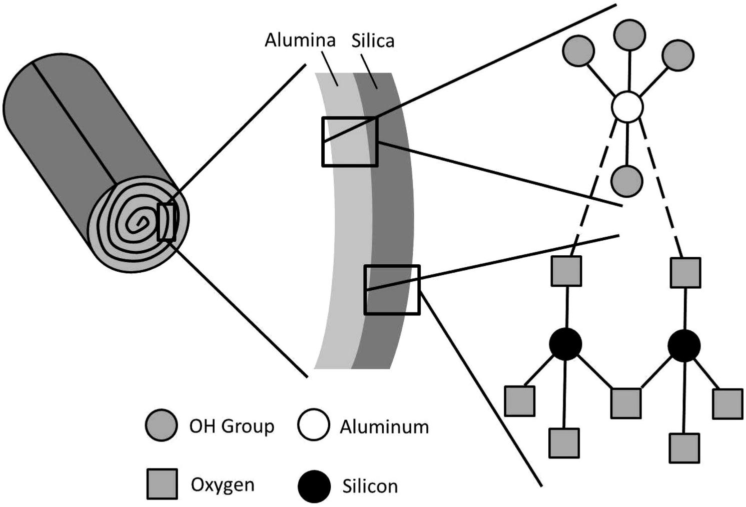

*Figure 6. Schematic of halloysite structural hierarchy. The alumina layer is on the concave side of the rolled sheet. The silica layer is located on the convex surface. These layers are bound together through a layer of oxygen. The outer surface of the twinned layers is covered with charged oxygen and hydroxyl groups that allow for binding of adsorbed species.*

Of more recent interest, however, are those nanoclays that have a nanocylinder morphology. In halloysite, one such material, each sheet is composed of one layer of silica and one layer of alumina with a chemical formula of ($Al_2Si_2O_5(OH)_4$ x $nH_2O$). One of the most common morphologies of this nanoclay is a rolled form, a tubular structure consisting of many concentric layers (*70–76*). The tube-like shape of halloysite is shown in Figure 5 and the hierarchal structure of the tube layers is shown in Figure 6. These tubes vary in length from 500 to 1000 nanometers, in diameter from 15 to 300 nanometers, and have an average density of 2.59 g/cm$^3$ (*73*, *74*, *76*). While the reason for the rolling of the halloysite layers has not been fully explained, the main theories concern the water of hydration. As the alumina and silicate layers are weathered, the water of hydration causes a packing disorder which is relieved by the layers rolling (*71*, *73–75*). Partial proof for this theory is that as the water of hydration changes (namely, as the value of n changes), the distance between rolled layers also changes. The completely dehydrated form of halloysite (n = 0) has an average layer spacing of 0.72 nanometers with about 15 to 20 layers in total (*74*). Another theory concerns the structure of the tube walls. The inside of the walls is composed of the alumina layers. These layers have hydroxide groups that are not attached to anything else. On the other side of the wall, the silica layer contains oxygen groups that compose the backbone of the walls. This attached structure on one side of the wall versus the unattached structure on the other side will cause the wall to roll. In addition to controlled release, halloysite has been used for various other purposes, including utilizing its catalytic properties for petroleum cracking, using the interlumen space as nanoreactors to fabricate nanowires and nanoparticles, and taking advantage of its ion exchange capacity to absorb such materials as dyes, stains, chemicals, and pollutants (even breaking down some pollutants into smaller molecules) (*70*). Like other smectite nanoclays, one of the characteristics that makes halloysite useful for controlled release is the charge found on the nanoclays. The high cation exchange capacity of halloysite allows for the attachment of charged species, such as drugs and other molecules. Species can also be bound to the inside surface by interactions that can occur through the hydroxyl functional groups located along the inside of the lumen of the tubes.

One potential issue with the use of nanomaterials for medical applications is biocompatibility. Vergaro et al. performed a study on this topic, examining the viability of cells upon the introduction of halloysite (*77*). This study indicates that up to a 75 mg/ml concentration, roughly 1000 times the toxic level of asbestos, has no serious effects on cell viability. The difference is that biocompatibility may be related to length. Individual halloysite tubes are much shorter than asbestos and can be removed from the body more easily by macrophages.

It should be noted that a "synthetic" halloysite, imogolite, can be produced by the reaction of silicic acid with hydroxyaluminum cations (*78*, *79*). However, imogolite consists of a single wall, not the multiple walls found in natural halloysite. The average outer diameter of these tubes is 2.3 to 2.7 nanometers with an inner diameter of 1 nanometer. The average length of these tubes is only about 100 nanometers (*78*, *79*). One study describes that the tubes pack very closely with only a 2.7 nanometer distance from center to center of the tubes (*78*).

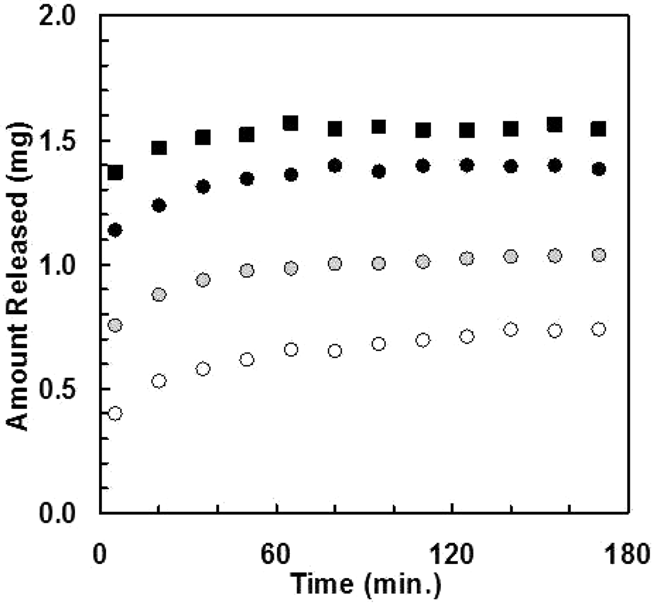

*Figure 7. Mass released of tetracycline hydrochloride from halloysite based on number of loading cycles and method of loading. Black squares are prepared from Method 1, while circles represent Method 2. Black represents four loading cycles, shaded represents three, and open represents two. Reprinted with permission from (88), Christopher J. Ward, Shang Song, and Edward W. Davis J. Nanosci. Nanotechnol. vol.10, pp.6641-6649 (2010). Copyright©American Scientific Publishers.*

Halloysite has been studied for numerous uses related to controlled release. Fields such as paint additives, pesticides, herbicides, lubricants, and cosmetics could easily utilize halloysite in controlled release techniques (*70*). For example, to enhance the efficacy of anticorrosion treatments and to allow for extended periods of time before reapplication, halloysite has been studied as a nanocarrier for anti-corrosion chemicals such as benzotriazole, even creating end stoppers of copper complexes to extend release (*70*, *75*, *80–83*). Similarly, bioprotection agents, such as iodobutylpropyl carbonate (IBPC), have been evaluated for controlled release from halloysite nanotubes to combat marine fouling (*70*, *73*). More closely related to the medical field, Abdullayev et al. have studied the possibility of creating silver nanorods inside halloysite protection for antibacterial applications, such as in coatings and paints (*84*).

**Table 2. Initial burst amounts, time of full release, and extent of release for pharmaceutical compounds utilized in controlled release studies**

| *Drug* | *Initial Burst (%)* | *Time of Release (hrs.)* | *Extent of Release (%)* | *Reference* |
|---|---|---|---|---|
| ***tetracycline hydrochloride – two loadings*** | 27 - 41 | 2.3 - 37 | 75 - 95 | (*87*, *88*) |
| ***tetracycline hydrochloride – three loadings*** | 12 - 57 | 2 – 10 | 75 - 80 | (*85*, *88*) |
| ***tetracycline hydrochloride – four loadings*** | 69 | 1.3 | 75 | (*88*) |
| ***propranolol hydrochloride*** | 27 | >8 | >90 | (*86*) |
| ***diltiazem hydrochloride*** | 98 | 0.6 | 100 | (*86*) |
| ***nifedipine*** | 6 | >5 | >70 | (*73*, *74*, *89*) |
| ***furosemide*** | 10 | >5 | >70 | (*73*, *74*, *89*) |
| ***dexamethasone*** | 8 | >5 | >70 | (*73*, *74*, *89*) |
| ***khellin*** | 1 | 195 | 10 | (*85*) |
| ***nicotinamide adenine dinucleotide*** | 20 | 6 | 87 | (*85*) |

The first study directly evaluating halloysite as a drug-delivery vehicle examined the release tetracycline HCl, a hydrophilic antibiotic, and khellin, a hydrophobic vasodialator (*85*). In the case of tetracycline HCl, release occurred over the course of ten hours while for the khellin, release occurred for a week. Since that initial report, researchers have begun to evaluate halloysite as a controlled release nanoparticle for other drugs, including diltiazem hydrochloride, propranolol hydrochloride, nifedipine (antianginal), furosemide (antihypertension), and dexamethasone (corticosteroid) (*74*, *86–89*). One study has been performed releasing diltiazem hydrochloride and propranolol hydrochloride through chitosan-coated halloysite. Results indicate that drug release is significantly delayed, with the reduction of the burst effect (*86*). Burst is the term used for the rapid initial release that often appears with several nanoparticle-based systems. To further retard release, halloysite has been coated with polymers (chitosan and gelatin) using a layer by layer approach; release rates were reduced by 75% (*90*). Tetracycline hydrochloride-loaded halloysite nanotubes have been evaluated for the treatment of periodontitis in canines (*87*). Halloysite loaded with drug was incorporated into a polyethylene glycol gel that, once injected into the mouth as a liquid, solidifies and slowly releases drug as it diffuses from the halloysite. By incorporating the drug loaded halloysite into a polymer matrix, the overall release can be made to last on the order of several days or weeks (*87*, *88*). One study demonstrated the ability of halloysite nanotubes to simultaneously improve mechanical properties of bone cement and release drug (*91*).

One of the key benefits of halloysite for controlled release is its tubular structure. This structure allows the drug to be loaded inside the tube where it can be released through a combination of diffusion along the length of the tube and ionic adsorption/desorption processes with the inner wall. However, the small diameter of the tube and the fact that it is filled with air in the dried purified state poses an issue for drug loading. Upon immersion in a drug solution, capillary forces trap this air in the tubes, limiting the ability of drug-laden solution from reaching the tube pore. The key to the potential use of halloysite as a controlled release system is the initial packing of this tubular space with drug.

Loading of the halloysite with a drug is done by one of two main methods (*88*). The first method utilizes an excess of a saturated drug solution, which is mixed with ground, sieved, and dried halloysite. With the application of a vacuum to the suspension, air trapped inside the lumen of the tubes is pulled from the tubes with the result of bubbles on the surface of the suspension. Upon rapid release of the vacuum, the drug solution is then pulled inside the tubes, replacing the air. This procedure is repeated two to three more times to fully fill the tubes with drug solution. Following the final vacuum cycle, the mixture is centrifuged, the solution is decanted, and the nanotubes dried under vacuum. The second method also utilizes saturated drug solution (pH 3.8). Instead of an excess, however, the drug solution is mixed with the halloysite in equal portions by weight. The result is a thick paste, not a suspension. Once again, the mixture is placed under a vacuum and then pressure released for two to three cycles. The mixture is then dried directly under vacuum. Additional drug solution is applied and the cycle is repeated until dry. The benefits of the second method are that there is no waste of drug or drug solution and that the amount of drug added to the halloysite can be directly calculated without analysis of a supernatant.

As can be seen in Figure 7, the release profiles, measured by UV spectrophotometry, of tetracycline hydrochloride-loaded halloysite, were very similar regardless of loading method selected. In this work, a 20 mg/ml tetracycline HCl ethanol:water (90:10) solution was used. Either an excess of solution (5:1 drug solution halloysite or greater) was used for each loading cycle, method 1, or an equal mass of drug solution and halloysite was used in each loading cycle, method 2. Release was determined by placing 0.02 grams of the drug loaded halloysite into 40 ml of a 10 mmolar phosphate buffer, pH 6.8, kept at 37 °C. Release was tracked using UV spectrophotometry. The amount of material released/loaded increased as the number of loading cycles increased. The values ranged from approximately 35 to approximately 70 mg drug/gram of halloysite by using four loading cycles versus two loading cycles. The amount released was similar for four cycles of method 1 versus four cycles of method 2 despite the use of over 5 times the amount of saturated drug solution.

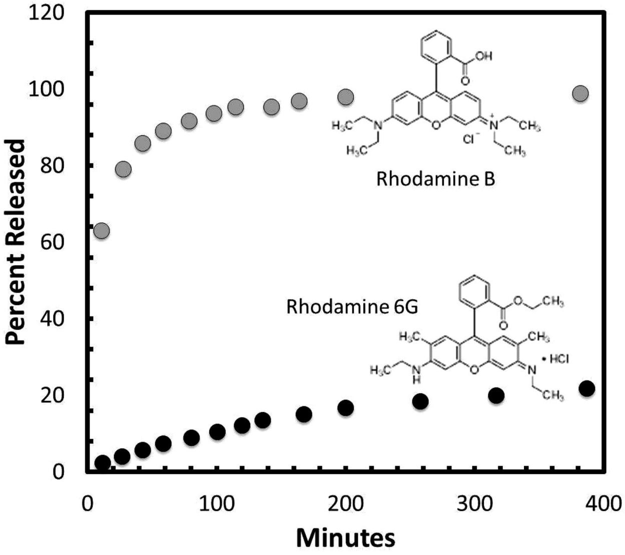

*Figure 8. Percent released of rhodamine B and rhodamine 6G from halloysite. Black circles represent rhodamine 6G and shaded circles represent rhodamine B.*

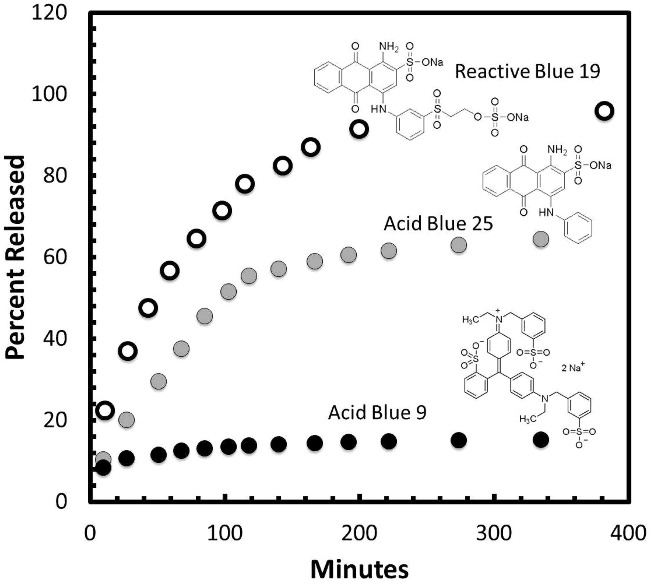

*Figure 9. Release as a function of size and charge. Black circles represent acid blue 9; shaded circles, acid blue 25; and open circles, reactive blue 19.*

A significant portion of the release can occur as an initial burst within the first five minutes. Table 2 compares the amount released during the initial burst, the time of release, and the total percent of loaded material released for various drugs released from halloysite and reported in the literature. The values range from less than 5% released during the initial burst to a high of almost 100% of the loaded drug being released during the burst phase. The data from Ward et. al. indicates that the burst increases as the number of loading cycles increased. Correspondingly, final release percentages increased with the number of loading cycles. The fraction of drug loaded which was released varied: 10% for khellin (a drug with low solubility in aqueous media), 70 - 90% for drugs such as nifedipine and tetracycline HCl, and 100% for diltiazem hydrochloride (a small molecule drug with high solubility in aqueous media). The duration of release ranged from 0.6 hours to 5 hours. One report in the literature indicated release of over 37 hours (*87*). However, the data from Ward et. al. indicates a much shorter release duration of 2.3 hours for the same system. The time of release and the fraction of drug released are related to the strength of the interaction between the halloysite and the drug, the size of the drug, and the solubility of the drug in the release environment.

The burst effect can be explained based on the fact that there are three places that drugs can be loaded or associated with in relation to halloysite: i) loaded inside the nanotube, ii) bound to the outside of the nanotube through electrostatic forces, and iii) existing as crystallites in the interstitial spaces between the nanotubes. The initial burst can be thought of as release of the drug crystallized in the interstitial areas. As loading cycles are repeated, less drug can be loaded into the nanotube or coated on the outside. There is a fixed volume inside the tube and the amount of drug capable of associating with the surface of the tube is determined by the cation exchange capability of the nanotubes. Thus, the fraction of unbound or poorly bound tetracycline increases as the number of loading cycles increases. As a result, there is an increase in the fraction of drug released during the burst phase as the number of loading cycles increases. After the initial burst, a more gradual release occurs, resulting from release of the drug bound on the outside (more rapid) and that bound inside the tube (less rapid).

Ward et. al. used washing protocols to determine if the release during the burst phase could be reduced or eliminated. In the first protocol, the drug loaded halloysite was rinsed by placing 0.2 grams on the surface of vacuum filter paper and rinsing with 100 ml of DI water. In the second protocol, 0.2 grams of drug loaded halloysite was mixed with 40 ml of DI water for ~1 min., centrifuged for 5 min., decanted, and the process repeated with a second 40 ml aliquot of DI water. After filtration or centrifugation, both materials were vacuum dried. Examining the release profiles of “washed” drug loaded halloysite, it was found that approximately the same amount of drug is removed that “burst” in a release test (*88*). The release profiles are smoother with a significantly reduced burst of release.

The release of compounds loaded into the interlumen space depends on factors associated with solubility, surface interaction with the halloysite surface, and diffusion rates. These factors can include, size, charge, and polarity of the compound. An example of the effects of the loaded compound properties is shown in Figure 8. Two similar dyes, rhodamine B and rhodamine 6G, were loaded at similar rates into halloysite. The dye-loaded halloysite was then placed in a buffer solution and the release followed over time by UV spectrophotometry. In rhodamine 6G, a $C_2H_5$ side group sterically interferes with hydrogen bonding of the carboxylic acid group, resulting in lower solubility in the aqueous medium. Despite the quaternary ammonium cation, which would be expected to bind rhodamine B to the silica surface, rhodamine B releases significantly faster than rhodamine 6G. The significant effect of solubility on the release of compounds from halloysite shown here has also been reported by Levis et. al. for two cationic drugs with different solubilities in water, diltiazem hydrochloride and propranolol hydrochloride, and in the original work conducted by Lvov et. al. (*85*, *86*). The higher the solubility of the release compound, the easier it is dissolved in the release medium and the quicker it escapes the nanotubes.

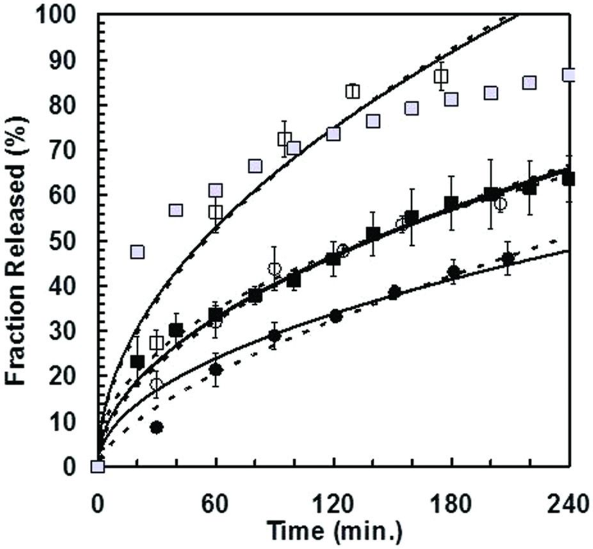

*Figure 10. Release from four PVOH films. Films containing pure tetracycline are shown as squares, while films containing drug-loaded halloysite are shown as circles. Open symbols represent only tetracycline or drug-loaded halloysite while filled symbols indicates the data is from films that also contained 5 wt% montmorillonite. The shaded squares are for films prepared from pure tetracycline and unloaded halloysite. Solid lines are fits to Higuchi, while dashed lines are fits to the Ritgar-Peppas model. Reprinted with permission from Ref. (88), Christopher J. Ward, Shang Song, and Edward W. Davis J. Nanosci. Nanotechnol. vol.10, pp.6641-6649 (2010). Copyright©American Scientific Publishers.*

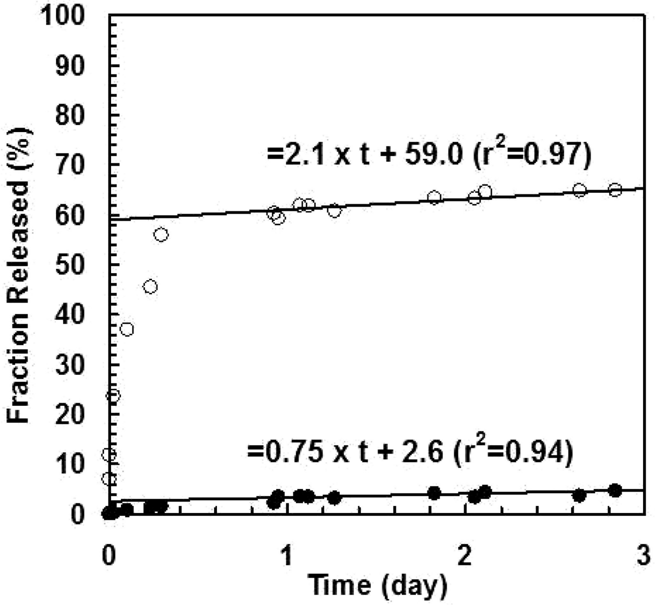

*Figure 11. Release of tetracycline from PMMA Films. Films with pure tetracycline are open circles, and films with dug-loaded halloysite are shaded circles. Linear fits are applied only to the data collected after 10 hours. Reprinted with permission from Ref. (88), Christopher J. Ward, Shang Song, and Edward W. Davis J. Nanosci. Nanotechnol. vol.10, pp.6641-6649 (2010). Copyright©American Scientific Publishers.*

Charge and size are also important factors. Charge affects the ionic interaction with the silica surface of the tube. Size influences diffusion rate. Figure 9 provides an example of the effects of charge and size. Reactive blue 19 and Acid Blue 25 differ in that Reactive Blue 19 is larger and carries a second negatively charged group. The size would be expected to slow release by diffusion through the tube, however the extra negative charge creates a strong unfavorable interaction with the clay surface which drives the release of the compound from the system. As a result, the release of Reactive Blue 19 is faster. Acid Blue 9 is similarly sized to Reactive Blue 19, but it contains three negative charges and one positive charge on the molecule, for a net charge of -2. Despite its size and overall negative charge, Acid Blue 9 releases much slower than either Reactive Blue 19 or Acid Blue 25. This effect is due to favorable interactions between the cation and the clay surface and the formation of complexes that result from the interaction between ionic groups of neighboring molecules. Figure 9 also provides an example of the effect of molecular charge on the release kinetics. Reactive blue 19 possesses two negative charges, while acid blue 25 has one negative charge and acid blue 9 has three negative charges and one positive charge. Shchukin et. al. also explored the effect of size and found that larger globular enzymes released slower than smaller enzymes from halloysite (*92*).

Few studies have been performed concerning the incorporation of drug-loaded halloysite into polymer films (*87*, *88*). However, incorporation of drug-loaded halloysite in polymer systems is one method for the development of halloysite-based controlled release devices. These materials have potential uses as wound packing or dressing materials, as transdermal patches, or as implantable controlled release systems. Kelly et. al. evaluated the use of drug loaded halloysite for the treatment of canine periodontitis (*87*). They utilized a composite material consisting of a polymeric matrix encapsulating tetracycline loaded halloysite. They found positive results with a significant reduction in the disease process for dogs treated with the controlled release technology versus those treated with traditional therapies.

Ward et. al. explored the use of halloysite in polymer films based on polyvinyl alcohol (PVOH) or poly(methyl methacrylate) (PMMA) (*88*). Both of these materials have biomedical uses but differ significantly in their behavior in an aqueous environment. PVOH swells significantly while PMMA has a much lower degree of swelling. In both cases, the films were prepared by a solvent cast technique. Films were prepared with drug contents ranging from 2.4 mg tetracycline per gram of film to 7.2 mg tetracycline per gram of film. Films were produced in which the tetracycline was first loaded into halloysite and, for comparison, films were produced where the tetracycline was loaded directly into the film. Compared to the release from films in which the drug is loaded directly into the solvent casting solution, the release from the systems where the drug is loaded into halloysite is slower, shown in Figure 10. A similar effect is obtained by adding 5 wt.% montmorillonite to the systems in which the drug is loaded directly into the film. One might attribute the reduction in release with the addition of montmorillonite to the reduction in diffusion rate that results from the tortuous path created by the montmorillonite. However, halloysite is tubular and not capable of creating the same tortuous path as montmorillonite. Thus, the reduction in release rates is due to release from the halloysite itself and not only to changes in diffusion rates. To understand the release mechanisms involved, two models were fit to the data in Figure 10. Higuchi's model, Equation 1, describes the release of a compound based purely on Fickian diffusion. The Ritgar-Peppas model, Equation 2, is similar to Higuchi's model, except that 0.5 is replaced by n, related to transport mechanism and geometry. For the first two cases, where tetracycline is loaded directly into the film and loaded in halloysite, the Higuchi model best fits the results, indicating that diffusion dominates the release. However, when montmorillonite is added, the Ritgar-Peppas model better fits the data, with n > 0.5, indicating that other phenomena affect the release. This suggests that it is the adsorption/desorption phenomena that occurs at the surface of montmorillonite and not just the increase in diffusion path length that is responsible for the reduction in release from these systems.

$$\frac{M_t}{M_\infty} = kt^{1/2} \tag{1}$$

$$\frac{M_t}{M_\infty} = kt^n \qquad (2)$$

PMMA films, in direct comparison to PVOH films, do not swell in the release medium. Figure 11 shows release from PMMA films incorporated with pure tetracycline and drug-loaded halloysite. It can be seen that pure tetracycline films consist of an initial burst of roughly 60 percent during the first ten hours of release. On the other hand, virtually no burst effect is seen with the drug-loaded halloysite film. After the first ten hours of release, for both films, there is a linear release, with the release of pure tetracycline around three times that of tetracycline from the drug-loaded halloysite film.

## Conclusion

Halloysite nanotubes have been shown to exhibit very promising properties in regards to the extended release of drugs. Loading of the drug in the lumen of the tubes is facilitated by vacuum and total amount loaded can be controlled over a wide range of levels by adjusting the number of loading cycles used and the concentration of drug in the loading solution. Release from the tubes is dependent on the nature and magnitude of interaction with the halloysite silica surface, as well as the molecular solubility. Compounds with high solubility, unfavorable ionic interactions with the surface, or that are small in size release faster. With the added complexity of dispersion of the drug-loaded tubes in a polymer matrix, release can be extended and tailored by controlling the rate of diffusion through the matrix. Release can be extended over the course of days or weeks by this method.

## References

1. Ballard, B. E. In *Sustained Controlled Release Drug Delivery*; Robinson, J. R., Ed.; Marcel Dekker, Inc.: New York, 1978; Vol. 6, pp 1−69.
2. Florence, A. T. In *Controlled Release in Oral Drug Delivery*; Wilson, C. G., Crowley, P. J., Eds.; Controlled Release Society: London, 2011; pp 1−26.
3. Millar, J. F.; Lindner, G. GB Patent 823,914, 1959.
4. Jung, J. *Z. Pflanzenernaehr.* **1960**, *91*, 122–130.
5. Alhaique, F.; Santucci, E.; Carafa, M.; Coviello, T.; Murtas, E.; Riccieri, F. M. *Biomaterials* **1996**, *17* (20), 1981–1986.
6. Fiore, M. C.; Smith, S. S.; Jorenby, D. E.; Baker, T. B. *J. Am. Med. Assoc.* **1994**, *271* (24), 1940–1947.
7. Nachum, Z.; Shupak, A.; Gordon, C. R. *Clin. Pharmacokinet.* **2006**, *45* (6), 543–566.
8. Cascone, M. G.; Sim, B.; Sandra, D. *Biomaterials* **1995**, *16* (7), 569–574.
9. Venkatraman, S.; Davar, N.; Chester, A.; Kleiner, L. In *Handbook of Pharmaceutical Controlled Release Technology*; Wise, D. L., Ed.; Marcel Dekker, Inc.: New York, 2000; pp 431−463.

10. Franklin, M. R. In *Remington: the Science and Practice of Pharmacy*, 21st ed.; Troy, D. B., Ed.; Lippincott Williams & Wilkins: Baltimore, MD, 1995; pp 1142−1170.
11. Berner, B.; Dinh, S. In *Treatise on Controlled Drug Delivery*; Kydonieus, A., Ed.; Marcel Dekker, Inc.: New York, 1992; pp 1−35.
12. Gupta, P. K.; Robinson, J. R. In *Treatise on Controlled Drug Delivery*; Kydonieus, A., Ed.; Marcel Dekker, Inc.: New York, 1992; pp 255−313.
13. Nilsson, T. In *International Encyclopedia of Ergonomics and Human Factors*, 2nd ed.; Karwowski, W., Ed.; CRC Press: Boca Raton, FL, 2006; Vol. 1, pp 412-424.
14. Comer, R. J. In *Abnormal Psychology*; Worth Publishers: New York, 2004; pp 359−398.
15. Edlin, G.; Golanty, E. *Health and Wellness*; Jones and Bartlett Publishers, LLC: Sudbury, U.K., 2010.
16. Kydonieus, A. F. In *Controlled Release Technologies: Methods, Theory, and Applications*; Kydonieus, A. F., Ed.; CRC Press: Boca Raton, FL, 1980; Vol. 1, pp 1−19.
17. Martini, L. G.; Crowley, P. J. In *Controlled Release in Oral Drug Delivery*; Wilson, C. G.; Crowley, P. J., Eds.; Springer Science + Business Media, LLC: New York, 2011; pp 49−70.
18. Lee, P. I.; Good, W. R. In *ACS Symposium Series*; American Chemical Society: Washington, DC, 1987; pp 1−13.
19. Cramer, J. A.; Roy, A.; Burrell, A.; Fairchild, C. J.; Fuldeore, M. J.; Ollendorf, D. A.; Wong, P. K. *Value in Health* **2008**, *2* (1), 44–47.
20. Li, V. H. K.; Lee, V. H. L.; Robinson, J. R. In *Controlled Drug Delivery*; Robinson, J. R., Lee, V. H. L., Eds.; Marcel Dekker, Inc.: New York, 1987; Vol. 29, pp 3−94.
21. Bruck, S. D. In *Controlled Drug Delivery*; Bruck, S. D., Ed.; CRC Press, Inc.: Boca Raton, FL, 1983; Vol. 1, pp 1−13.
22. Dash, A.; Cudworth, G., II. *J. Pharmacol. Toxicol. Methods* **1998**, *40* (1), 1–12.
23. Theeuwes, F.; Yum, S. I. *Ann. Biomed. Eng.* **1976**, *4* (4), 343–353.
24. Uhrich, K. E.; Cannizzaro, S. M.; Langer, R. S.; Shakesheff, K. M. *Chem. Rev.* **1999**, *99* (11), 3181–3198.
25. Betancourt, T.; Doiron, A.; Homan, K. A.; Brannon-Peppas, L. In *Nanotechnology in Drug Delivery*; de Villiers, M. M., Aramwit, P., Kwon, G. S., Eds.; American Association of Pharmaceutical Scientists: New York, 2009; pp 283−312.
26. Galeska, I.; Kim, T.-K.; Patil, S. D.; Bhardwaj, U.; Chatttopadhyay, D.; Papadimitrakopoulos, F.; Burgess, D. J. *AAPS J.* **2005**, *7* (1), 231–240.
27. Daniels, A. U.; Andriano, K. P.; Smutz, W. P.; Chang, M. K.; Heller, J. *J. Appl. Biomater. Biomech.* **1994**, *5* (1), 51–64.
28. Davis, E. W.; Mukkamala, R.; Cheung, H. M. *Langmuir* **1998**, *14* (4), 762–767.
29. Schmuhl, N.; Davis, E. W.; Cheung, H. M. *Langmuir* **1998**, *14* (4), 757–761.
30. Boder, N. *Adv. Drug Res.* **1984**, *13*, 255.

31. Bundgaard, H. In *Topics in Pharmaceutical Sciences 1983*; Breimer, D. D., Speiser, P., Eds.; Elsevier Science Publishers: New York, 1983; pp 329−343.
32. Burger, J. J.; Tomlinson, E.; Mulder, E. M.; McVie, J. G. *Int. J. Pharm.* **1985**, *23*, 333.
33. Davis, S. S.; Daly, P. B.; Kennerley, J. W.; Frier, M.; Hardy, J. G.; Wilson, C. G. *Adv. Pharmacother. I* **1982**, *17*.
34. Odland, G. F. In *Biochemistry and Physiology of the Skin*; Goldsmith, L. A., Ed.; Oxford University Press: New York, 1983; pp 3−63.
35. Reichek, N.; Priest, C.; Zimrin, D.; Chandler, T.; Sutton, M. S. J. *Am. J. Cardiol.* **1984**, *54* (1), 1–7.
36. Trueblood, J. H.; Rossomondo, R. M.; Carlton, W. H.; Wilson, L. A. *Arch. Ophthalmol.* **1974**, *91*, 313.
37. Gürsel, İ.; Korkusuz, F.; Türesin, F.; Gürdal Alaeddinolu, N.; Hasırcı, V. *Biomaterials* **2000**, *22* (1), 73–80.
38. Whang, K.; Goldstick, T. K.; Healy, K. E. *Biomaterials* **2000**, *21* (24), 2545–2551.
39. Pitt, C. G. *Int. J. Pharm.* **1990**, *59* (3), 173–196.
40. Wischke, C.; Schwendeman, S. P. In *Fundamentals and Applications of Controlled Release Drug Delivery*; Siepmann, J., Siegel, R. A., Rathbone, M. J., Eds.; Springer Science and Business Media, LLC: New York, 2012; pp 171−228.
41. Karmouty-Quintana, H.; Tamimi, F.; McGovern, T. K.; Grover, L. M.; Martin, J. G.; Barralet, J. E. *Biomaterials* **2010**, *31* (23), 6050–6059.
42. Andrews, D. A.; Ben-Jebria, A.; Langer, R. *J. Appl. Physiol.* **1998**, *85* (2), 379–385.
43. Tieppo, A.; White, C. J.; Paine, A. C.; Voyles, M. L.; McBride, M. K.; Byrne, M. E. *J. Controlled Release* **2011**, *157* (3), 391–397.
44. Abramson, D. I. *Blood Vessels and Lymphatics*; Academic Press: New York, 1962; pp 61−83.
45. Rabbe, O. G.; Yeh, H. C.; Newton, G. J.; Phalen, R. F.; Velasquez, D. J. *Inhaled Particles IV, Part I*; British Occupational Hygiene Society: Edinburgh, Scotland, 1977; p 3.
46. Jain, K. K. In *Drug Delivery Systems*; Jain, K. K., Ed.; Humana Press: Totowa, NJ, 2008; pp 1−50.
47. Fulekar, M. H. *Nanotechnology: Importance and Applications*; I.K. International Publishing House Pvt. Ltd.: New Delhi, India, 2010; pp 48−69.
48. Sahoo, S. K.; Labhasetwar, V. *Drug Discovery Today* **2003**, *8* (24), 1112–1120.
49. Thassu, D.; Pathak, Y.; Deleers, M. In *Nanoparticle Drug Delivery Systems*; Thassu, D.; Pathak, Y.; Deleers, M., Eds.; Informa Healthcare USA, Inc.: New York, 2007; pp 1−32.
50. Storm, G.; Crommelin, D. J. A. *Pharm. Sci. Technol. Today* **1998**, *1* (1), 19–31.
51. Liu, J.; Zeng, F.; Allen, C. *Eur. J. Pharm. Biopharm.* **2007**, *65* (3), 309–319.
52. Nishiyama, N.; Kataoka, K. *Adv. Exp. Med. Biol.* **2004**, *519* (155-177).

53. Kataoka, K.; Harada, A.; Nagasaki, Y. *Adv. Drug Delivery Rev.* **2001**, *47* (1), 113–131.
54. Rosler, A.; Vandermaulen, G. W.; Klok, H. A. *Adv. Drug Delivery Rev.* **2001**, *53* (1), 95–108.
55. Dufreshne, M. H.; Garrec, D. L.; Sant, V.; Leroux, J. C.; Ranger, M. *Int. J. Pharm.* **2004**, *277* (1−2), 81–90.
56. Donald, A. T. *Prog. Polym. Sci.* **2005**, *30* (3–4), 294–324.
57. Tripathi, P. K.; Khopade, A. J.; Nagaich, S.; Shrivastava, S.; Jain, S.; Jain, N. K. *Pharmazie* **2002**, *57* (4), 261–264.
58. Uddin, F. *Metall. Mater. Trans. A* **2008**, *39A* (12), 2804–2814.
59. Patel, H. A.; Somani, R. S.; Bajaj, H. C.; Jasra, R. V. *Bull. Mater. Sci.* **2006**, *29* (2), 133–145.
60. Patil, N. V. *Adv. Mater. Processes* **2005**, *163* (12), 39–40.
61. Franchini, E.; Galy, J.; Gérard, J.-F. *J. Colloid Interface Sci.* **2009**, *329* (1), 38–47.
62. Xu, B.; Zheng, Q.; Song, Y.; Shangguan, Y. *Polymer* **2006**, *47* (8), 2904–2910.
63. Maiti, M.; Mitra, S.; Bhowmick, A. K. *Polym. Degrad. Stab.* **2008**, *93* (1), 188–200.
64. Das, G.; Karak, N. *Polym. Degrad. Stab.* **2009**, *94* (11), 1948–1954.
65. El-Sherif, H.; El-Masry, M. *Polym. Bull.* **2010**, *66* (6), 721–734.
66. Kamena, K. *Funct. Fillers Plast.* **2005**, 163–174.
67. Takayanagi, M. *Kobunshi* **1984**, *33* (8), 615–19, 24.
68. Vaccari, A. *Catal. Today* **1998**, *41* (1−3), 53–71.
69. Joshi, G. V.; Kevadiya, B. D.; Patel, H. A.; Bajaj, H. C.; Jasra, R. V. *Int. J. Pharm.* **2009**, *374* (1–2), 53–57.
70. Du, M.; Guo, B.; Jia, D. *Polym. Int.* **2010**, *59* (5), 574–582.
71. Hedicke-Hoechstoetter, K.; Lim, G. T.; Altstaedt, V. *Compos. Sci. Technol.* **2009**, *69* (3−4), 330–334.
72. Li, C.; Liu, J.; Qu, X.; Yang, Z. *J. Appl. Polym. Sci.* **2009**, *112* (5), 2647–2655.
73. Lvov, Y. M.; Price, R. R. *Bio-Inorg. Hybrid Nanomater.* **2008**, 419–484.
74. Lvov, Y. M.; Shchukin, D. G.; Mohwald, H.; Price, R. R. *ACS Nano* **2008**, *2* (5), 814–820.
75. Shchukin, D.; Lamaka, S. V.; Yasakua, K. A.; Zheludkevich, M. L.; Ferreira, M. G. S.; Moehwald, H. *J. Phys. Chem. C* **2008**, *112* (4), 958–964.
76. Zhou, Y. *Open Nanosci. J.* **2008**, *2*, 1–5.
77. Vergaro, V.; Abdullayev, E.; Cingolani, R.; Lvov, Y.; Leporatti, S. *Biomacromolecules* **2010**, *11* (3), 820–826.
78. Bursill, L. A.; Peng, J. L.; Bourgeois, L. N. *Philos. Mag. A* **2000**, *80* (1), 105–117.
79. Guimaraes, L.; Enyashin, A. N.; Frenzel, J.; Heine, T.; Duarte, H. A.; Seifert, G. *ACS Nano* **2007**, *1* (4), 362–368.
80. Shchukin, D.; Mohwald, H. *Adv. Funct. Mater.* **2007**, *17*, 1451–1458.
81. Shchukin, D.; Zheludkevich, M.; Yasakau, K.; Lamaka, S.; Ferreira, M. G.; Mohwald, H. H. *Adv. Mater.* **2006**, *18*, 1672–1678.

82. Abdullayev, E.; Price, R.; Scchukin, D.; Lvov, Y. *Appl. Mater. Interfaces* **2009**, *1* (7), 1437–1443.
83. Abdullayev, E.; Lvov, Y. *J. Mater. Chem.* **2010**, *20*, 6681–6687.
84. Abdullayev, E.; Sakakibara, K.; Okamoto, K.; Wey, W.; Ariga, K.; Lvov, Y. *ACS Appl. Mater. Interfaces* **2011**, *3*, 4040–4048.
85. Price, R.; Gaber, B.; Lvov, Y. *J. Microencapsulation* **2001**, *18*, 713–723.
86. Levis, S. R.; Deasy, P. B. *Int. J. Pharm.* **2003**, *253*, 145–157.
87. Kelly, H. M.; Deasy, P. B.; Ziaka, E.; Claffey, N. *Int. J. Pharm.* **2004**, *274*, 167–183.
88. Ward, C. J.; Song, S.; Davis, E. W. *J. Nanosci. Nanotechnol.* **2010**, *10* (10), 6641–6649.
89. Veerabadran, N.; Price, R.; Lvov, Y. *NANO* **2007**, *2*, 215–222.
90. Veerabadran, N.; Lvov, Y.; Price, R. *Macromol. Rapid Commun.* **2009**, *24*, 99–103.
91. Wei, W.; Abdullayev, E.; Hollister, A.; Mills, D.; Lvov, Y. *Macromol. Mater. Eng.* **2012**, *297*.
92. Shchukin, D.; Price, R.; Lvov, Y. *Small* **2005**, *1*, 510–513.

## Chapter 11

# Development of Porous Nanomaterials for Applications in Drug Delivery and Imaging

**Ashish Datt, Nicholas Ndiege, and Sarah C. Larsen***

**Department of Chemistry, University of Iowa, Iowa City, Iowa 52242**
***E-mail: sarah-larsen@uiowa.edu**

Microporous and mesoporous materials, such as zeolites and mesoporous silica, are emerging as important materials for applications in drug delivery and imaging. The advantages of zeolites and mesoporous silica for biomedical applications include biocompatibility, low toxicity, large surface areas and the ability to control the physicochemical properties. In this chapter, the loading and release of the model drug, aspirin, from zeolite-Y with varying silica/alumina ($SiO_2/Al_2O_3$) ratios and from MCM-41 functionalized with amine groups will be discussed. Positron emission tomography (PET) imaging applications with modified zeolite and mesoporous silica materials will also be discussed.

## Introduction

Porous nanomaterials, such as microporous zeolites and mesoporous silica, are emerging materials for biomedical applications, such as drug delivery (*1*, *2*), imaging (*3–7*) and theranostics (*8*, *9*). Zeolites are microporous, crystalline aluminosilicates (or silicates) with pore sizes typically ranging from 5-10 Å (*10*). Mesoporous silica is a related porous material that has larger pore dimensions of >20 Å and amorphous walls (*11–13*). The structures of zeolite Y with the faujasite structure and a mesoporous silica, MCM-41 (Mobil Crystalline Material) are shown in Figure 1. The advantages of synthetic zeolites and mesoporous silica, with respect to biomedical applications are biocompatibility, low toxicity, large surface areas and the ability to control the properties through surface

In Nanomaterials for Biomedicine; Nagarajan, R.;
ACS Symposium Series; American Chemical Society: Washington, DC, 2012.

functionalization (*14–18*). Biomedical applications of zeolites and mesoporous silica in drug delivery (*19–22*), bloodclotting (*23*) and imaging (*5*, *7*, *24–26*) have been reported.

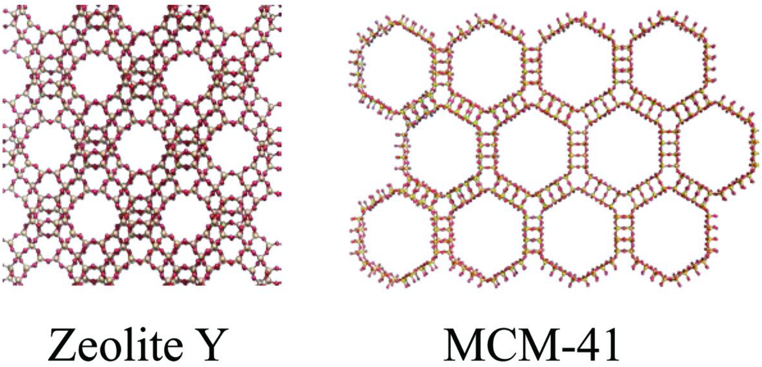

*Figure 1. Representative structures of porous materials: NaY zeolite (left) and MCM-41 mesoporous silica (right).*

Zeolites and mesoporous silica can be synthesized with crystal sizes of 100 nm or less giving these materials two dimensions on the nanoscale- the pore size and the crystal size. Nanoscale zeolites and mesoporous silica have large surface areas due to appreciable internal and external surface areas (*27*, *28*). The external surface area of nanoscale zeolites is up to an order of magnitude larger than the external surface area for micron-sized zeolites and provides an additional surface for reaction or functionalization (*29–31*). The external surface of nanoscale zeolites has been functionalized with organic functional groups for use in biomedical applications, such as imaging (*32*) and drug delivery (*1*). Due to the larger pore sizes, mesoporous silica can be functionalized on both the internal and external surfaces for applications in catalysis (*20*), imaging (*6*, *33*, *34*) and drug delivery (*2*, *21*).

Mesoporous silica has been more widely explored relative to zeolites for applications in drug delivery and imaging due to the larger pore size of mesoporous silica compared to zeolites. However, recent studies have shown that zeolites share many of the favorable properties of mesoporous silica materials particularly for applications involving small molecule drugs and imaging agents (*17*, *18*). In this book chapter, recent results on the applications of porous nanomaterials (zeolites and mesoporous silica) in drug delivery and imaging will be presented. Specific examples involving loading and release of aspirin from zeolite Y and MCM-41 will be presented as well as the results of a recent study involving gallium-exchanged zeolites for future use in positron emission tomography (PET).

## Applications of Zeolites and Mesoporous Silica in Drug Delivery

A major issue of interest for both material and medical science is the incorporation of drugs into inorganic systems to deliver an active compound. Over the past few decades there has been rapid expansion in controlled drug delivery in the field of modern medication and pharmaceuticals since a controlled release can bring both therapeutic and commercial value to health-care products. Controlled drug release should optimize drug efficiency and reduce adverse effects. In this work, porous materials, zeolites and mesoporous silica, were used as hosts for the small drug molecule, aspirin.

Zeolites are crystalline, inorganic materials with narrow pore size distributions and have silicon, aluminium and oxygen atoms in their framework (*10*). Zeolites can be synthesized with a large variety of framework types exhibiting different pore sizes and connectivities. The stability of zeolites varies depending on the framework, the Si/Al ratio and the types of charg-compensating cations. Synthetic zeolites have advantages over naturally occurring zeolites in that they can be obtained in pure form and also their morphology can be controlled. Due to selectivity, zeolites can be used for ion exchange and adsorption processes. The presence of well-defined porosity affords a more homogeneous environment for matrix-drug complexes and hence a better control of the drug release rate.

There are several examples of biomedical applications of zeolites reported in the literature including imaging (*5*, *24–26*), wound treatment (*23*), and drug delivery (*35–40*). These examples demonstrate that different zeolites can be exchanged with cations, functionalized or loaded with drug molecules for specific biomedical applications. In examples of drug-loading, Zeolite Y/magnetite nanocomposites have been loaded with doxorubicin molecules (*35*) and paraquat molecules have been loaded into trimethylsilyl functionalized zeolite Y (*36*). Recently, the adsorption of sulfonamide antibiotics on zeolite Y has been investigated (*37*, *38*). Release of drug molecules from zeolites is controlled by a number of factors such as the pore size, the identity of any grafted functional groups or exchangeable cations and the nature of intermolecular interactions (*39*, *40*). The loading and release of anthelminthics and other drugs from zeolites have produced a controlled release of these molecules (*39*). For example, dealuminated zeolite Y has been successfully used in the controlled delivery of ibuprofen (*40*). Additional research is needed to understand fundamental zeolite and drug molecule interactions so that the loading and release of the drug molecules can be better controlled.

Mesoporous silica materials are inorganic materials, which are synthesized in the presence of surfactants that act as templates for the polycondensation of silica species (*11–13*). Mesoporous silica materials are porous with pore sizes ranging from 2-15 nm. The pore size can be varied during synthesis by varying time, temperature and the choice of the surfactant. High surface areas and large pore sizes make mesoporous silica an ideal material for hosting molecules of different sizes, shapes, and functionalities. Recently, mesoporous silica materials have received much attention in the fields of catalysis, adsorption, separation, sensing and biomedicine. There are many examples of drug molecules loaded onto mesoporous silica materials reported in the literature (*2*, *19–21*, *41*, *42*). Ibuprofen has been extensively studied as a model drug adsorbed on the mesoporous silica materials, MCM-41, SBA-15 and hexagonal mesoporous silica (HMS) materials (*40*, *43*, *44*). MCM-41, SBA-15 and HMS are different types of mesoporous silica which differ in their pore diameter range, thickness of their walls and their nature of the synthesis conditions (*9*, *21*, *45*, *46*). In addition, many anti-cancer drugs, such as doxorubicin and camptothecin, have also been studied for controlled release using mesoporous silica materials. Lin and coworkers studied the release of a drug cargo using capped mesoporous silica materials (*2*, *20*, *21*). Recently, rattle type mesoporous silica $Fe_3O_4@SiO_2$ have also attracted a great deal of attention for drug delivery (*42*). Drug delivery using mesoporous silica materials largely depends on the textural properties of these materials, such as pore diameters, pore volumes, particle morphology and surface modifications.

There has been interest in exploring controlled drug delivery systems with mesoporous silica due to several attractive features, such as, high surface area, tunable pore sizes with narrow distributions, well-defined surface properties, low toxicity and very good biocompatibility. In this study, zeolitic and mesoporous systems are the hosts during the loading and release of a small drug molecule. In order to compare the adsorption and release of the drug, modified versions of both zeolites and mesoporous silica were used.

Aspirin (Figure 2) was chosen as a model drug due to its small molecular size, good pharmacological activity, and short biological half-life (*47*, *48*). Also, it has a carboxyl group which can interact with surface silanol groups or the amino groups on the pore walls and may be useful for the drug-controlled release. Aspirin is one of the most widely used medications and was the first discovered member of the class of drugs known as nonsteroidal anti-inflammatory drugs (NSAIDs). It is an anti-inflammatory drug used as analgesia in the relief of minor pain and in the treatment of cardiovascular diseases (*47*, *48*). It is also used as medication which can prevent blood clots, heart attacks and strokes due to its antiplatelet effect.

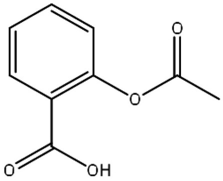

*Figure 2. Structure of aspirin.*

## Loading and Release of Aspirin from Zeolite HY

In the first example, the loading and release of aspirin from zeolite HY with silica to alumina ($SiO_2/Al_2O_3$) ratios varied from 5, to 30, to 60 was investigated. As the silica to alumina ratio increases, the hydrophobicity of the zeolite increases. In a typical aspirin drug loading experiment, the zeolite was stirred in ether with a known concentration of aspirin for 24-48 hours. The aspirin loaded solid zeolites collected after centrifugation were characterized using thermal gravimetric analysis (TGA) and nitrogen adsorption, as well as solid state magic angle spinning nuclear magnetic resonance (MAS NMR).

The information listed in Table 1 provides a summary of physiochemical data acquired before/after aspirin loading. The surface area and pore volume both decrease after the aspirin loading which is attributed to the presence of aspirin molecules inside the zeolite pores. For instance, for zeolite HY-5, the surface area and the pore volume decrease by approximately 60% after aspirin loading. Table 1 also lists the amount of the aspirin loaded inside the zeolite matrices which was calculated using TGA data. The zeolite with the highest aluminum content (HY-5) has the maximum amount of aspirin loaded most likely due to the presence of maximum bridging –OH sites responsible for hydrogen bonding with the aspirin. The aspirin to supercage loading is calculated to be 1 for HY-5 and ~0.6 for zeolites HY-30 and HY-60. Overall, the aspirin loading decreases with increasing silica to alumina ratio which corresponds to an increase in hydrophobicity.

**Table 1. Physicochemical properties of zeolite-Y before and after aspirin loading**

| | *$SiO_2/Al_2O_3$* | *$V_{pore}$, before (after)[a] ($cm^3/g$)* | *SA, before (after)[a] ($m^2/g$)* | *Aspirin loading (mg/g)* | *Aspirin after release (mg/g)* |
|---|---|---|---|---|---|
| HY-5 | 5 | 0.26 (0.11) | 594 (232) | 100 | -- |
| HY-30 | 30 | 0.30 (0.18) | 688 (440) | 78 | 29 |
| HY-60 | 60 | 0.31 (0.16) | 711 (396) | 69 | 23 |

[a] Before aspirin loading (after aspirin loading).

$^{13}C$ MAS NMR was used to gain a better understanding of the structure and motion of aspirin loaded in zeolite Y. The $^{13}C$-$^{1}H$ cross polarization (CP) MAS NMR spectra of a) a physical mixture of aspirin and HY-5 and b) aspirin loaded HY-5 are shown in Figure 3. In Figure 3a, the peak at ~18 ppm corresponds to the $–CH_3$ of the aspirin molecule, the peaks in the range of 100-155 ppm are assigned to the aromatic carbons and the peaks at ~170 ppm correspond to the C=O group carbons (*49*). The peaks labeled with asterisks in the Figure 3a represent the spinning side bands due to the chemical shift anisotropy in the sample. Closer inspection of the NMR spectrum in Figure 3b clearly shows broader line widths for the aspirin peaks relative to the physical mixure in Figure 3a and this is attributed to decreased motion of the aspirin when it is occluded in the zeolite pores. In addition, the aromatic carbons are shifted by ~10 ppm relative to the physical mixture due to the phenyl group interaction with the zeolite walls which is comparable to what has been observed previously for polymeric hosts (*49*).

For aspirin release experiments, a known amount of aspirin loaded zeolite was stirred with phosphate buffer maintained at physiological conditions of pH 7.4 and 37 °C. Aliqouts were collected after successive time intervals and the supernatants were analyzed with UV-Vis spectroscopy with absorbance maxima at 296 nm. The release data is shown in Figure 4.

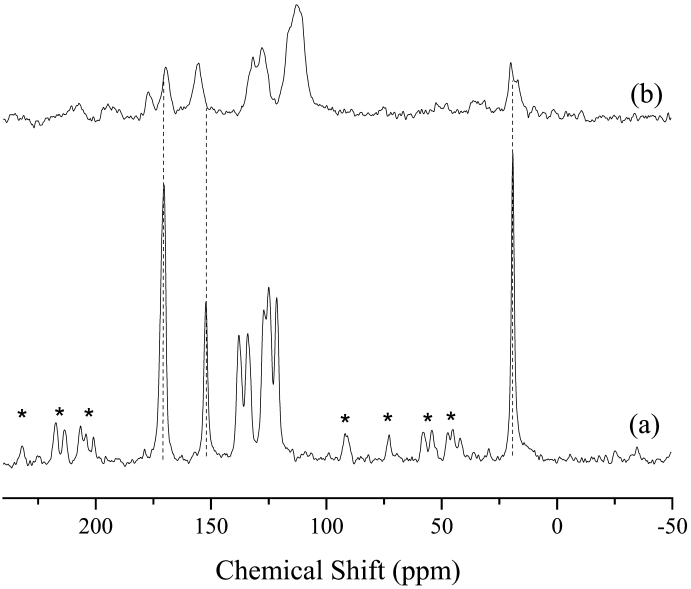

*Figure 3. Representative $^{13}C$-$^{1}H$ CP-MAS NMR spectra of (a) physical mixture of zeolite Y (HY-5) with aspirin, (b) zeolite Y (HY-5) loaded with aspirin. The asterisks indicate spinning sidebands.*

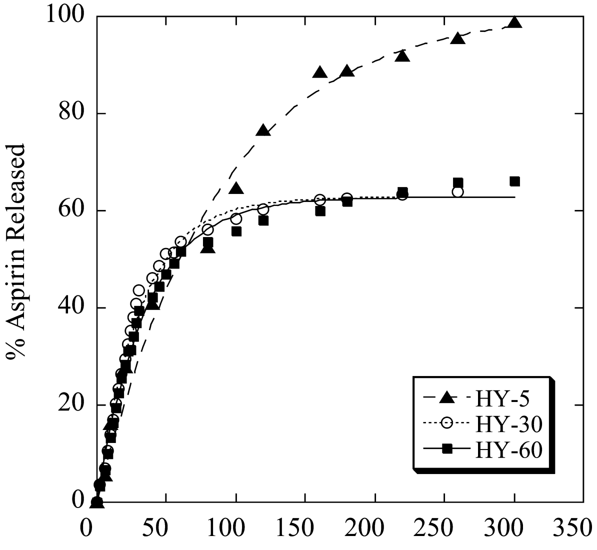

*Figure 4. Aspirin release kinetics from HY-5, HY-30 and HY-60. The least squares fits to [1] are shown by the solid lines.*

The drug release follows the first-order kinetic exponential decay model (*50*, *51*), with the equation represented as:

$$Q=Q_{max}(1-\exp(-k_1t)) \qquad [1]$$

where Q is the amount of drug released in time t, $Q_{max}$ is the maximum amount of drug released and $k_1$ is the first order release constant. The parameters $Q_{max}$ and $k_1$ obtained after fitting the release data with [1] in Figure 4 are listed in Table 2. $Q_{max}$ was ~100% for HY-5 and 63% for HY-30 and HY-60. The first order release rate constant, $k_1$, was 0.011, 0.032 and 0.028 $min^{-1}$ for HY-5, HY-30 and HY-60, respectively.

**Table 2. Fitted Kinetic Release Parameters for Aspirin Release from HY[a]**

| *Sample* | *$Q_{max}$, %* | *$k_1$ ($min^{-1}$)* |
|---|---|---|
| HY-5 | 101±4 | 0.011±0.001 |
| HY-30 | 63±1 | 0.032±0.001 |
| HY-60 | 63±1 | 0.028±0.001 |

[a] $Q_{max}$=maximum aspirin released (%); $k_1$=release rate constant.

For all the aspirin loaded zeolites, a burst release was observed during the first hour of release which corresponds to the presence of weak hydrogen bonding between aspirin and the zeolite matrices. The aspirin release showed an interesting trend amongst zeolites with different $SiO_2/Al_2O_3$ ratios. The highest aluminum content zeolite (HY-5) showed a faster release whereas the lesser aluminum content lead to the slower release profile and this is attributed to the differences in hydrophobicity with varying $SiO_2/Al_2O_3$. In addition, the HY samples contain extraframework or octahedrally coordinated aluminum which has previously been shown to be an important factor in the loading of ibuprofen in zeolite HY (*40*). In future work, the role of aluminum will be elucidated using aluminum MAS NMR.

### Loading and Release of Aspirin from Amine-Functionalized Mesoporous Silica

In the second example, the mesoporous silica material, MCM-41, was functionalized with amine groups and then the loading and release of aspirin was investigated. The rationale for modifying these materials was to enhance the aspirin loading capacity through an acid-base interaction, since the aspirin is a weak acid and amine groups act as bases. For comparison, the drug release was also investigated for the parent mesoporous silica. MCM-41 was synthesized according to published procedures in the literature (*46*). In a typical synthesis, MCM-41 was prepared with 2 g CTAB dissolved in 460 ml deionized water, then 7 ml NaOH solution (2 M) was added to the surfactant solution. The solution was then stirred for 30 min at 80°C and then 9.2 ml tetraethoxysilane

(TEOS) was added. The white precipitate was filtered, washed with deionized water and dried overnight at 80°C. Calcination of the material was performed at 550°C for 5 h to remove the surfactant. Two different methods, co-condensation (CC) and post-synthesis (PS) grafting were used to functionalize MCM-41 with aminopropyltriethoxy silane (APTES) according to the schemes shown in Figure 5 (*52–54*).

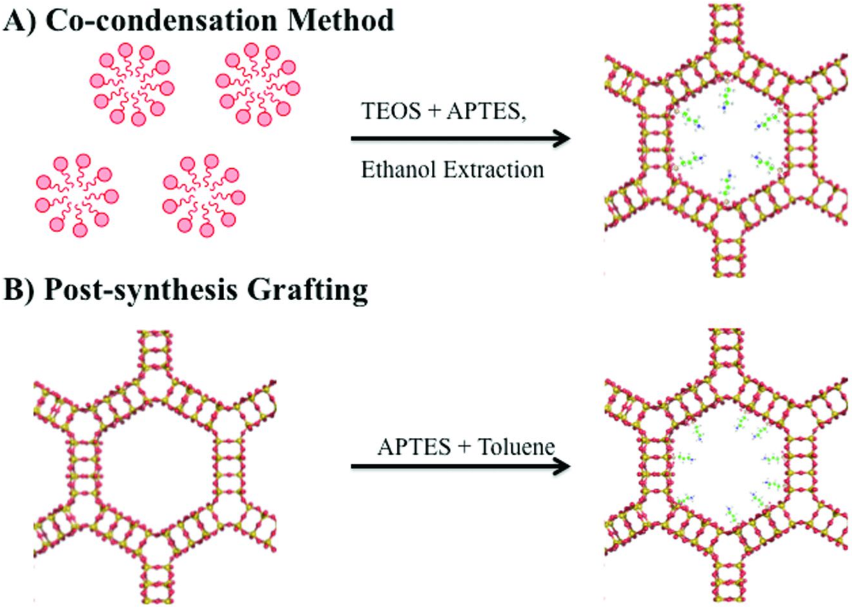

*Figure 5. Schematic diagram illustrating the functionalization of MCM-41 by A) co-condensation and B) post synthesis grafting.*

For the co-condensation procedure, the APTES functional group was added during the MCM-41 synthesis. For the post-synthesis grafting method, the APTES was added to the calcined MCM-41 material after synthesis. As illustrated in Figure 5, the co-condensation method results in a more uniform but lower overall loading of the functional group compared to the post-synthesis method (*12*). Samples prepared by the post-synthesis grafting method may be less homogeneous due to preferential reaction of the organic group at the pore mouth (*12*). MCM-41 samples with 2 different loadings of APTES were prepared and will be labeled "1" for the lower loaded sampled and "2" for the higher loaded sample which refers to the mL of APTES added during modification. The functionalized MCM-41-CC and MCM-41-PS were characterized using various techniques, such as powder x-ray diffraction (XRD) and TGA.

The aspirin in ether was loaded into the MCM-41 materials. The loading increased from 100 mg aspirin/g for the parent MCM-41 material to 120 mg aspirin/g for the modified MCM-CC-1 and MCM-PS-1. The aspirin loading increased as the APTES loading increased for both PS and CC samples but the increase was proportionately higher for the MCM-41-CC sample.

The $^{13}C$-$^{1}H$ CPMAS NMR spectra for a) aspirin, b) aspirin loaded MCM-CC-1 and c) aspirin loaded MCM-PS-1 are shown in Figure 6. The $^{13}C$-$^{1}H$ CPMAS NMR spectrum of aspirin exhibits the characteristic aspirin peaks with resonances attributed to the carbonyl group at around 170 ppm and resonances in the 116 - 150 ppm region corresponding to the aromatic carbons of the phenyl system in aspirin (*49*). The peak from the methyl group of aspirin is observed at ~19 ppm. For the APTES modified MCM-41 (Fig 6b and 6c), two additional peaks attributed to the propyl chain of the aminopropyltriethoxy silane moiety are also observed at ~ 8 and 41 ppm as well as an overlapping peak at 20 ppm. Just as for aspirin loaded in zeolite Y, the aromatic resonances shift by approximately 10 ppm relative to the pure aspirin suggesting that the aromatic ring of aspirin interacts with the MCM-41 surface.

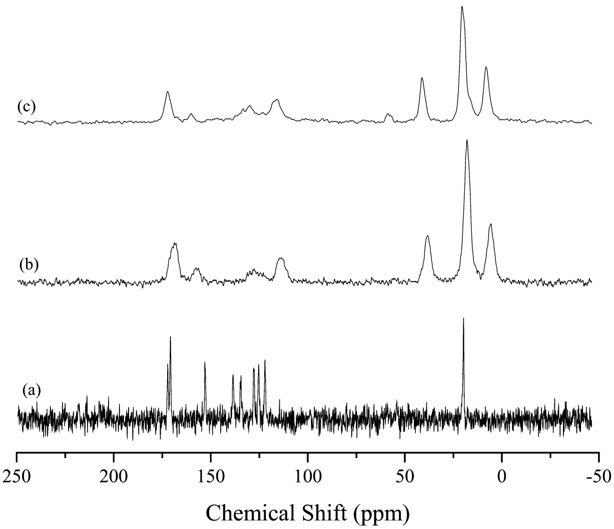

*Figure 6. $^{13}C$ CP-MAS NMR spectrum of (a) pure aspirin, (b) co-condensed MCM-41 with amine and aspirin, (c) post-synthesis grafting with amine and aspirin.*

Analogous to the zeolite aspirin release experiments, the aspirin loaded MCM-41 materials were mixed in a phosphate buffer solution at pH 7.4 and 37 °C. Small aliquots were taken at regular intervals of time and the supernatants were analyzed using UV-Vis spectroscopy. The aspirin release was nearly complete for the parent MCM-41. For the APTES functionalized MCM-41 materials, the aspirin release was incomplete after 5 hours. The release profiles are shown in Figure 7 and the release data for the functionalized MCM-41 samples obtained from fits to the first order kinetic exponential decay model (Equation 1) is listed in Table 4. The aspirin release profile for the parent MCM-41 could not be fit very well using the first order kinetic model [1] and therefore, the Power law model was used (*50*). The Power Law model is given below:

$$M_t/M_\infty=at^n+b \qquad [2]$$

$M_t/M_\infty$ is the fractional release of the drug. For Fickian diffusion, n=0.5 and b accounts for the burst effect in the release process (*50*). The parent MCM-41 data could be fit using this model with n=0.5 indicating Fickian diffusion and with a y-intercept which indicates a burst effect. The data and the fit are shown in Figure 7. The diffusion of the drug molecules from the pores is largely dependent on the nature of interaction of the drug molecule with the pore and the intrinsic mobility of the drug molecules inside the pores. The modifications of the samples with functional groups causes steric hindrance for the dissolution medium as a result of which the diffusion deviates from the Fick's law.

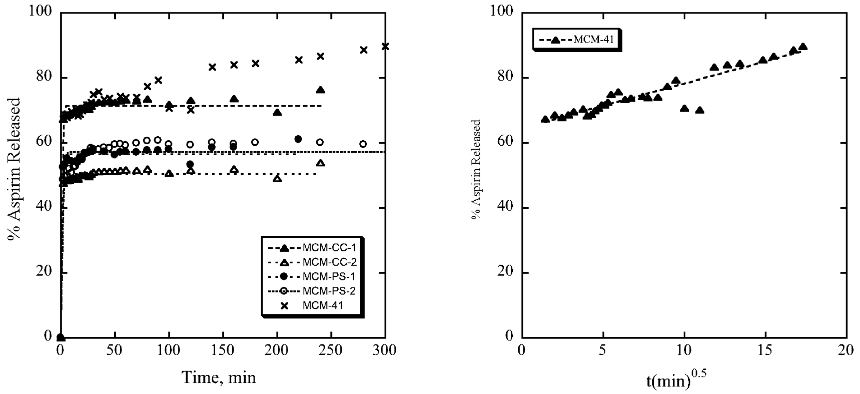

*Figure 7. Aspirin release kinetics from MCM-CC-1 (filled triangle), MCM-CC-2 (open triangle), MCM-PS-1 (closed circle) and MCM-PS-2 (open circles) are shown in the graph on the left. The least squares fits to [1] are shown by the solid lines. The graph on the right shows the power law fit to the data for the parent MCM-41.*

The source of burst release is a combination of several factors namely physiochemical characteristics of the host material, nature of the drug-host interactions (surface adsorption), morphology as well as the porous nature of the material (*55*). The release results suggest that an initial burst release occurs for each MCM-41 sample. After the burst release, the release from the parent MCM-41 follows Fickian diffusion. For post-synthesis and co-condensation samples, after the initial burst release, first order kinetics according to [1] are followed. The higher amine content results in the slower drug release for MCM-PS samples which can be attributed to the presence of amine groups at the pore entrances which hinders and slows the release process. In case of co-condensation, the release rate was not correlated with the loading of amine groups and this can be attributed to the more regular distribution of functional groups in the mesopores. As a result, the release rate does not vary significantly with the amount of amine loading for the MCM-CC.

When comparing the two methods of functionalization (Table 3 and 4), for the same overall amine loading level (MCM-CC-2 and MCM-PS-1), the aspirin loading is higher for the MCM-CC-2, but the rate constants are similar. The amount released is slightly higher for MCM-PS-1 relative to MCM-CC-2. The loading levels and release rates reflect the different distributions of amine groups on the MCM-41 samples. The slower release rate for MCM-PS-2 is attributed to the higher loading which results in steric hindrance due to functional groups located at the pore entrances which restrict diffusion. In the absence of organic functionali groups, the release kinetics for the parent MCM-41 follow the burst release and Fickian diffusion.

**Table 3. Physicochemical properties of the MCM-41 before and after aspirin loading**

| *Sample* | *SA before (after)[a] ($m^2/g$)* | *$V_{pore}$ before (after)[a] ($cm^3/g$)* | *APTES loading, (mmol/g)* | *Aspirin loading (mg/g)* | *Aspirin after release (mg/g)* |
|---|---|---|---|---|---|
| MCM-41 | 1120(810) | 0.91 (0.67) | -- | 100 | 10 |
| MCM-CC-1 | 803 (661) | 0.68 (0.53) | 0.45 | 120 | 44 |
| MCM-CC-2 | 744 (520) | 0.41 (0.28) | 0.54 | 170 | 120 |
| MCM-PS-1 | 757 (618) | 0.48 (0.35) | 0.54 | 120 | 59 |
| MCM-PS-2 | 729 (518) | 0.46 (0.31) | 0.60 | 130 | 71 |

[a] Before aspirin loading (after aspirin loading).

**Table 4. Fitted Kinetic Release Parameters for Aspirin Release from MCM-41[a]**

| *Sample* | *$Q_{max}$, %* | *$k_1$ ($min^{-1}$)* |
|---|---|---|
| MCM-PS-1 | 56.6±0.4 | 1.3±0.2 |
| MCM-PS-2 | 57.3±0.6 | 0.78±0.1 |
| MCM-CC-1 | 71.4±0.4 | 1.4±0.2 |
| MCM-CC-2 | 50.4±0.3 | 1.4±0.2 |

[a] $Q_{max}$=maximum aspirin released (%); $k_1$=release rate constant.

In Nanomaterials for Biomedicine; Nagarajan, R.;
ACS Symposium Series; American Chemical Society: Washington, DC, 2012.

## Comparison of Aspirin Loading on Zeolite Y and Mesoporous Silica

Aspirin was studied as a model drug to investigate the factors that control the loading and release from zeolites and mesoporous silica materials. In the case of zeolite Y, the maximum aspirin loading that was achieved was ~106 mg/g (aspirin/zeolite). The drug loading was largely dependent on the aluminum content in the zeolite. The aluminum content also appeared to be the dominating factor in the cumulative aspirin release profiles with the highest aluminum containing zeolite showing the faster release profile. This loading release behavior was attributed to the increasing hydrophilicity with increasing aluminum content which favors aspirin loading. As the aluminum content decreases, the zeolite becomes more hydrophobic and provides a steric hindrance for the release of aspirin molecules from the zeolite. Solid state NMR was instrumental in understanding the restricted motion of the aspirin molecules in the zeolite. The line broadening and shifts of the aromatic resonances provided evidence of aspirin/zeolite interactions.

In case of mesoporous silica materials, the aspirin loading was largely dependent on the orientation and the distribution of APTES moieties. For the parent MCM-41, the maximum amount of the aspirin loaded was 100 mg/g (aspirin/mesoporous silica) whereas the amount increased to 120 mg/g for the amine modified samples. For the co-condensed sample, the aspirin further increased with an increased amine loading, but only a moderate loading increase was observed for the post-synthesis grafting sample with the higher loading. This is attributed to the differences in the distributions of amine groups on the modified MCM-41 materials. For the post-synthesis grafting method, the amine groups are preferentially located at the pore entrances, so even if the amine loading is increased, the increase in aspirin loading is moderate due to steric effects. The release profiles reflect the different distributions of the amine groups in the co-condensed versus the post-synthesis modification.

A direct comparison of the overall loading and release for aspirin on HY and MCM-41 can be made using the data in Tables 1 and 3 and graphed in Figure 8. The data shows that the aspirin loadings for HY-5 and the parent MCM-41 are comparable and the highest loadings are achieved for the MCM-41 samples with the highest APTES loadings, MCM-PS-2 and MCM-CC-2 samples. When comparing the release amounts, the parent MCM-41 and the HY-5 exhibit the most complete release. The MCM-PS condensed samples have similar release amounts independent of the amine loading and this was attributed to the location of the amine groups at the pore mouths. For the MCM-CC samples, the higher loading leads to lower overall release. Taken together, these results suggest that the loading and release depends on the characteristics of the porous host, such as aluminum content, and both the level of surface modification and the method of surface modification.

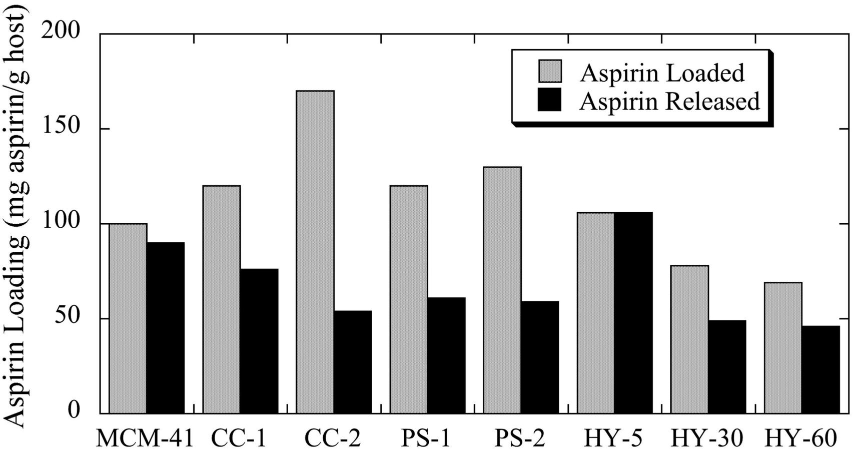

*Figure 8. Comparison of the amount of aspirin loaded (gray) and released (black) for HY zeolites and MCM-41.*

## Applications of Zeolites and Mesoporous Silica in Imaging

Porous nanomaterials, such as zeolites and mesoporous silica, are also being investigated for applications in biomedical imaging, such as Magnetic Resonance Imaging (MRI) and Positron Emission Tomography (PET). Zeolites and mesoporous silica are high surface area materials that can be functionalized with molecules (e.g., peptides, aptamers) designed for high-affinity binding to *in vivo* molecular targets (such as cell surface receptors). In addition, the radionuclides and contrast agent metals for applications in MRI (*5–7*, *24*, *56–59*) and PET (*60–62*) can be adsorbed onto these porous materials. The development of these porous nanomaterials provides opportunities for the preparation of multifunctional nanoparticles that can be used for targeted molecular imaging (*33*, *62*, *63*).

Porous nanomaterials have recently emerged as promising candidates for applications in biomedical imaging, drug delivery, sensing, catalysis and separations. Zeolites and mesoporous silica are desirable for these applications due to their uniform pore structure, high surface area, low toxicity, biocompatibility and chemical tailorability (*64*, *65*). Functionality can be imparted to zeolites by grafting with organic groups, such as amines, thiols, and carboxylates that allow selective ligation to take place (*29*, *31*, *66*). In addition, aluminosilicate zeolites can be ion-exchanged with cations that can be loaded into the zeolite resulting in increased sensitivity (*10*).

Cu(I)-catalyzed "click" chemistry is a technique that has recently proven to be a versatile method for chemically anchoring enzymes and proteins onto surfaces of porous materials (*67–72*). Cu(I)-catalyzed "click" chemistry is a 1,3-dipolar cycloaddition of organic azides to alkynes where conjugation of the binding partners occurs via 1,2,3-triazole linkage. Relative to other ligation techniques, Cu(I)-catalyzed click chemistry exhibits higher yields, favorable thermodynamics and compatibility with many different functional groups.

Ion exchange of zeolites has traditionally been utilized for catalytic applications (e.g. hydrocarbon cracking). Recently, this feature has been extended further such that the cation exchanged into the zeolite serves as a chemical probe or contrast agent. One example is $Gd^{3+}$ exchange into zeolite Y for use as an MRI (magnetic resonance imaging) agent (*7*, *24*, *56*, *57*). Recently, Tsotsalas and coworkers showed that $^{111}In$ could be encapsulated in functionalized zeolite L in which the channels were blocked with a stopcock molecule to prevent leakage of the $^{111}In$ (*61*, *62*). The study also demonstrated that the stability of the zeolite L *in vivo* was very high.

In the example discussed here, the cation exchange of NaY zeolites and Cu(I)-catalyzed "click" chemistry were combined to yield a bifunctional zeolite (Figure 9) that can be functionalized with a variety of molecular targeting vectors (e.g., peptides, aptamers), while maintaining cation-absorptive characteristics that enable high efficiency labeling with radionuclides and contrast agent metals for imaging applications (*73*).

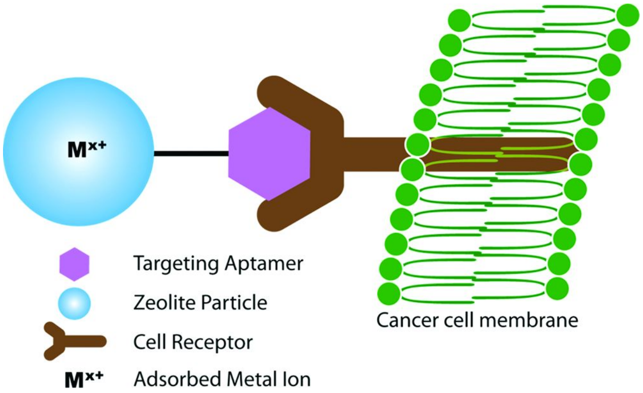

*Figure 9. Overall strategy for use of the bifunctional zeolite in targeted imaging applications. (Reproduced with permission from reference (73). Copyright 2011, American Chemical Society)*

The potential advantages of bifunctional-zeolite-based molecular targeting vectors is two-fold. First, because of their high surface area, zeolite particles enable addition of multiple targeting vectors per particle. Secondly, the porous nature of the material enables labeling of the targeting vectors with a significantly higher concentration of contrast-agent metal or radionuclide than traditional molecular imaging agents, which generally employ stoichiometric chelator additions to single targeting vector moieties (ie., a single chelator per peptide) (*74*). These properties could, in principle, lead to higher contrast of malignancies that can provide for earlier detection of tumors, more rapid assessments of response to therapies and more precise targeted delivery of drugs.

## Functionalization of Zeolite Y for PET Imaging Applications

In this study, a "clickable" zeolite platform for targeted imaging applications was designed and synthesized (*73*). The objective was to prepare an azide-functionalized zeolite that could be readily modified with molecular targeting vectors, while preserving the capability for high labeling efficiency with radiometals and contrast agent metals. Generator produced $^{68}$Ga, a positron-emitting radionuclide with a half-life of 68 minutes, was used to demonstrate the potential for application in PET imaging (*75*). A commercial zeolite, NaY (Zeolyst) was functionalized to prepare an azide-terminated zeolite surface (NaY-AZPTS) that was then reacted with an acetylene moiety in the presence of Cu(I) as shown schematically in Figure 10.

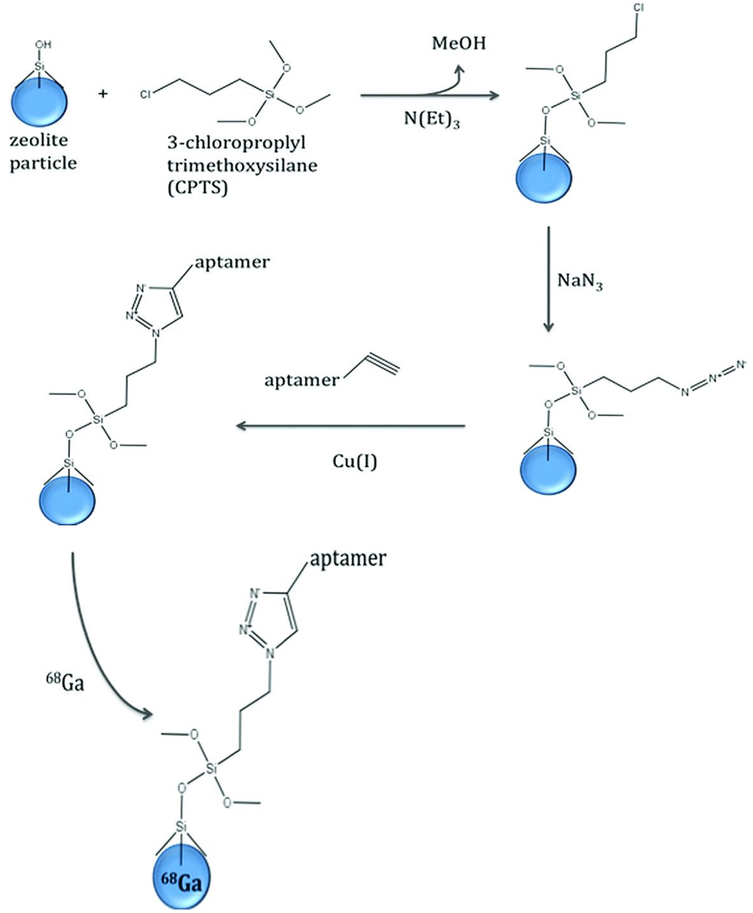

*Figure 10. Reaction scheme for functionalization of zeolite NaY with CPTS and AZPTS followed by click chemistry with a model alkyne. (Reproduced with permission from reference (73). Copyright 2011, American Chemical Society).*

Then, the “clicked” zeolite was loaded with gallium ($^{68}$Ga) by traditional aqueous ion-exchange methods to prepare Ga-exchanged NaY-AZPTS. The ion-exchange capacity of aluminosilicate zeolites, such as zeolite Y, is key to the success of this project and represents a major advantage of zeolites relative to other silicate materials, such as mesoporous silica. The stability of the nanocrystalline Y under physiological conditions (pH=7.4) is another important factor and has been investigated by us previously (*65*). Gallium will serve as a representative imaging or contrast agent that could be replaced by indium or gadolinium for other imaging applications. The extent of surface functionalization was varied in order to optimize the preparation of the bifunctional GaY-AZPTS. Importantly, our results indicated that the incorporation of $^{68}$Ga can be accomplished at room temperature, which will allow preparation of radiolabeled nanoparticles using molecular targeting vectors that may be susceptible to degradation at high temperatures usually required for $^{68}$Ga-chelator coupling reactions (*74*, *76*). Future studies will demonstrate the *in vivo* application of these materials.

## Conclusions

Porous nanomaterials, such as zeolites and mesoporous silica, are promising materials being developed for biomedical applications, such as drug delivery and imaging. The high surface area, low toxicity and biocompatibility of zeolites and mesoporous silica are all desirable properties when considering biomedical applications. The ability to vary the chemical properties of zeolites and mesoporous silica through synthesis and surface modification provides a further avenue for tailoring the zeolites and mesoporous silica for these applications.

## Acknowledgments

This material is based upon work partially supported by the National Science Foundation under Grant CHE-0847974, CHE-0840371. Daryl Fields, Izz El-Mazaawi, Renugan Raidoo (all undergraduate students) are acknowledged for experimental assistance. Summer support for undergraduates DF and IEM was provided by NSF CHE-0754738 and the SROP/McNair program. NN acknowledges support from Grant Number UL1RR024979 from the National Center for Research Resources (NCRR), a part of the National Institutes of Health (NIH). Its contents are solely the responsibility of the authors and do not necessarily represent the official views of the CTSA or NIH. RR acknowledges financial support from Iowa Biosciences Advantage National Institutes of Health (NIGMS 58939).

## References

1. Pearce, M. E.; Mai, H. Q.; Lee, N.; Larsen, S. C.; Salem, A. K. *Nanotechnology* **2008**, *19*, 175103.
2. Trewyn, B. G.; Giri, S.; Slowing, I. I.; Lin, V. S. Y. *Chem. Commun.* **2007**, 3236–3245.

3. Tsai, C. P.; Hung, Y.; Chou, Y. H.; Huang, D. M.; Hsiao, J. K.; Chang, C.; Chen, Y. C.; Mou, C. Y. *Small* **2008**, *4*, 186–191.
4. Matheoud, R.; Secco, C.; Ridone, S.; Inglese, E.; Brambilla, M. *Phys. Med. Biol.* **2008**, *53*, N137–N148.
5. Li, W. S.; Li, Z. F.; Jing, F. Y.; Yang, X. G.; Li, X. J.; Pei, F. K.; Wang, X. X.; Lei, H. *Acta Chim. Sinica* **2007**, *65*, 2029–2033.
6. Lin, Y. S.; Hung, Y.; Su, J. K.; Lee, R.; Chang, C.; Lin, M. L.; Mou, C. Y. *J. Phys. Chem. B* **2004**, *108*, 15608–15611.
7. Balkus, K. J.; Shi, J. M. *Langmuir* **1996**, *12*, 6277–6281.
8. Xie, J.; Lee, S.; Chen, X. Y. *Adv. Drug Delivery Rev.* **2010**, *62*, 1064–1079.
9. Ambrogio, M. W.; Thomas, C. R.; Zhao, Y. L.; Zink, J. I.; Stoddartt, J. F. *Acc. Chem. Res.* **2011**, *44*, 903–913.
10. Breck, D. W. *Zeolite Molecular Sieves: Structure, Chemistry, and Use*; Wiley-Interscience: New York, 1974.
11. Davis, M. E. *Nature* **2002**, *417*, 813–821.
12. Hoffmann, F.; Cornelius, M.; Morell, J.; Froba, M. *Angew. Chem., Int. Ed.* **2006**, *45*, 3216–3251.
13. Raman, N. K.; Anderson, M. T.; Brinker, C. J. *Chem. Mater.* **1996**, *8*, 1682–1701.
14. Thomas, J. A.; Ballantyne, B. *Int. J. Toxicol.* **1992**, *11*, 259–273.
15. Anton Petushkov, N. N.; Salem, A. K.; Larsen, S. C. *Adv. Mol. Toxicol.* **2010**, *4*, 223–266.
16. Garcia-Bennett, A. E. *Nanomedicine* **2011**, *6*, 867–877.
17. Kralj, M. *Period. Biol.* **2003**, *105*, 99–107.
18. Kralj, M.; Pavelic, K. *EMBO Rep.* **2003**, *4*, 1008–1012.
19. He, Q.; Shi, J. *J. Mater. Chem.* **2011**, *21*, 5845–5855.
20. Huh, S.; Wiench, J. W.; Trewyn, B. G.; Song, S.; Pruski, M.; Lin, V. S. Y. *Chem. Commun.* **2003**, 2364–2365.
21. Slowing, I. I.; Trewyn, B. G.; Giri, S.; Lin, V. S. Y. *Adv. Funct. Mater.* **2007**, *17*, 1225–1236.
22. Vallet-Regi, M.; Balas, F.; Arcos, D. *Angew. Chem., Int. Ed.* **2007**, *46*, 7548–7558.
23. Galownia, J.; Martin, J.; Davis, M. E. *Microporous Mesoporous Mater.* **2006**, *92*, 61–63.
24. Bresinska, I.; Balkus, K. J. *J. Phys. Chem.* **1994**, *98*, 12989–12994.
25. Young, S. W.; Qing, F.; Rubin, D.; Balkus, K. J.; Engel, J. S.; Lang, J.; Dow, W. C.; Mutch, J. D.; Miller, R. A. *J. Magn. Reson. Imaging* **1995**, *5*, 499–508.
26. Platas-Iglesias, C.; Elst, L.; Zhou, W.; Muller, R. N.; Geraldes, C.; Maschmeyer, T.; Peters, J. A. *Chem. Eur. J.* **2002**, *8*, 5121–5131.
27. Song, W.; Grassian, V. H.; Larsen, S. C. *Chem. Commun.* **2005**, 2951–2953.
28. Song, W.; Justice, R. E.; Jones, C. A.; Grassian, V. H.; Larsen, S. C. *Langmuir* **2004**, *20*, 4696–4702.
29. Song, W.; Woodworth, J. F.; Grassian, V. H.; Larsen, S. C. *Langmuir* **2005**, *21*, 7009–7014.
30. Barquist, K.; Larsen, S. C. *Microporous Mesoporous Mater.* **2008**, *116*, 365–369.

31. Zhan, B.-Z.; White, M. A.; Lumsden, M. *Langmuir* **2003**, *19*, 4205–4210.
32. Lerouge, F.; Melnyk, O.; Durand, J. O.; Raehm, L.; Berthault, P.; Huber, G.; Desvaux, H.; Constantinesco, A.; Choquet, P.; Detour, J.; Smaihi, M. *J. Mater. Chem.* **2009**, *19*, 379–386.
33. Liong, M.; Lu, J.; Kovochich, M.; Xia, T.; Ruehm, S. G.; Nel, A. E.; Tamanoi, F.; Zink, J. I. *ACS Nano* **2008**, *2*, 889–896.
34. Rieter, W. J.; Kim, J. S.; Taylor, K. M. L.; An, H. Y.; Lin, W. L.; Tarrant, T.; Lin, W. B. *Angew. Chem., Int. Ed.* **2007**, *46*, 3680–3682.
35. Arruebo, M.; Fernandez-Pacheco, R.; Irusta, S.; Arbiol, J.; Ibarra, M. R.; Santamaria, J. *Nanotechnology* **2006**, *17*, 4057–4064.
36. Zhang, H.; Kim, Y.; Dutta, P. K. *Microporous Mesoporous Mater.* **2006**, *88*, 312–318.
37. Braschi, I.; Gatti, G.; Paul, G.; Gessa, C. E.; Cossi, M.; Marchese, L. *Langmuir* **2010**, *26*, 9524–9532.
38. Braschi, I.; Blasioli, S.; Gigli, L.; Gessa, C. E.; Alberti, A.; Martucci, A. *J. Hazardous Mater.* **2010**, *178*, 218–225.
39. Dyer, A.; Morgan, S.; Wells, P.; Williams, C. *J. Helminthol.* **2000**, *74*, 137–141.
40. Horcajada, P.; Márquez-Alvarez, C.; Rámila, A.; Pérez-Pariente, J.; Vallet-Regí, M. *Solid State Sci.* **2006**, *8*, 1459–1465.
41. Gao, Q.; Xu, Y.; Wu, D.; Shen, W.; Deng, F. *Langmuir* **2010**, *26*, 17133–17138.
42. Lu, J.; Liong, M.; Zink, J. I.; Tamanoi, F. *Small* **2007**, *3*, 1341–1346.
43. Zhu, Y.; Shi, J.; Li, Y.; Chen, H.; Shen, W.; Dong, X. *Microporous Mesoporous Mater.* **2005**, *85*, 75–81.
44. Andersson, J.; Rosenholm, J.; Areva, S.; Lindén, M. *Chem. Mater.* **2004**, *16*, 4160–4167.
45. Zhao, D. Y.; Feng, J. L.; Huo, Q. S.; Melosh, N.; Fredrickson, G. H.; Chmelka, B. F.; Stucky, G. D. *Science* **1998**, *279*, 548–552.
46. Trewyn, B. G.; Slowing, I. I.; Giri, S.; Chen, H. T.; Lin, V. S. Y. *Acc. Chem. Res.* **2007**, *40*, 846–853.
47. Ridker, P. M.; Cook, N. R.; Lee, I. M.; Gordon, D.; Gaziano, J. M.; Manson, J. E.; Hennekens, C. H.; Buring, J. E. *New Engl. J. Med.* **2005**, *352*, 1293–1304.
48. Catella-Lawson, F.; Reilly, M. P.; Kapoor, S. C.; Cucchiara, A. J.; DeMarco, S.; Tournier, B.; Vyas, S. N.; FitzGerald, G. A. *New Engl. J. Med.* **2001**, *345*, 1809–1817.
49. Vachon, M. G.; Nairn, J. G. *Eur. J. Pharm. Biopharm* **1998**, *45*, 9–21.
50. Costa, P.; Lobo, J. M. S. *Eur. J. Pharm. Sci.* **2001**, *13*, 123–133.
51. Nieto, A.; Colilla, M.; Balas, F.; Vallet-Regi, M. *Langmuir* **2010**, *26*, 5038–5049.
52. Asefa, T.; MacLachlan, M. J.; Coombs, N.; Ozin, G. A. *Nature* **1999**, *402*, 867–871.
53. Vinu, A.; Hossain, K. Z.; Ariga, K. *J. Nanosci. Nanotechnol.* **2005**, *5*, 347–371.
54. Bruhwiler, D. *Nanoscale* **2010**, *2*, 887–892.
55. Huang, X.; Brazel, C. S. *J. Controlled Release* **2001**, *73*, 121–136.

56. Young, S. W.; Qing, F.; Rubin, D.; Balkus, K. J.; Engel, J. S.; Lang, J.; Dow, W. C.; Mutch, J. D.; Miller, R. A. *J. Magn. Reson. Imaging* **1995**, *5*, 499–508.
57. Csajbok, E.; Banyai, I.; Vander Elst, L.; Muller, R. N.; Zhou, W. Z.; Peters, J. A. *Chem. Eur. J.* **2005**, *11*, 4799–4807.
58. Taylor, K. M. L.; Kim, J. S.; Rieter, W. J.; An, H.; Lin, W. L.; Lin, W. B. *J. Am. Chem. Soc.* **2008**, *130*, 2154–2155.
59. Taylor, K. M. L.; Rieter, W. J.; Lin, W. B. *J. Am. Chem. Soc.* **2008**, *130*, 14358–14359.
60. Matheoud, R.; Secco, C.; Ridone, S.; Inglese, E.; Brambilla, M. *Phys. Med. Biol.* **2008**, *53*, N137–N148.
61. Tsotsalas, M. M.; Kopka, K.; Luppi, G.; Wagner, S.; Law, M. P.; Schafers, M.; De Cola, L. *ACS Nano* **2010**, *4*, 342–348.
62. Tsotsalas, M.; Busby, M.; Gianolio, E.; Aime, S.; De Cola, L. *Chem. Mater.* **2008**, *20*, 5888–5893.
63. Kim, J.; Kim, H. S.; Lee, N.; Kim, T.; Kim, H.; Yu, T.; Song, I. C.; Moon, W. K.; Hyeon, T. *Angew. Chem., Int. Ed.* **2008**, *47*, 8438–8441.
64. Petushkov, A.; Intra, J.; Graham, J. B.; Larsen, S. C.; Salem, A. K. *Chem. Res. Toxicol.* **2009**, *22*, 1359–1368.
65. Petushkov, A.; Freeman, J.; Larsen, S. C. *Langmuir* **2010**, *26*, 6695–6701.
66. Cheng, C. H.; Bae, T. H.; McCool, B. A.; Chance, R. R.; Nair, S.; Jones, C. W. *J. Phys. Chem. C* **2008**, *112*, 3543–3551.
67. Chassaing, S.; Kumarraja, M.; Sido, A. S. S.; Pale, P.; Sommer, J. *Org. Lett.* **2007**, *9*, 883–886.
68. Kolb, H. C.; Finn, M. G.; Sharpless, K. B. *Angew. Chem., Int. Ed.* **2001**, *40*, 2004–2021.
69. Moses, J. E.; Moorhouse, A. D. *Chem. Soc. Rev.* **2007**, *36*, 1249–1262.
70. Chassaing, S.; Sido, A. S. S.; Alix, A.; Kumarraja, M.; Pale, P.; Sommer, J. *Chem. Eur. J.* **2008**, *14*, 6713–6721.
71. Schlossbauer, A.; Schaffert, D.; Kecht, J.; Wagner, E.; Bein, T. *J. Am. Chem. Soc.* **2008**, *130*, 12558–12559.
72. Huang, L.; Dolai, S.; Raja, K.; Kruk, M. *Langmuir* **2010**, *26*, 2688–2693.
73. Ndiege, N.; Raidoo, R.; Schultz, M. K.; Larsen, S. *Langmuir* **2011**, *27*, 2904–2909.
74. Virgolini, I.; Ambrosini, V.; Bomanji, J. B.; Baum, R. P.; Fanti, S.; Gabriel, M.; Papathanasiou, N. D.; Pepe, G.; Oyen, W.; De Cristoforo, C.; Chiti, A. *Eur. J. Nucl. Med. Mol. Imaging* **2010**, *37*, 2004–2010.
75. Fani, M.; Andre, J. P.; Maecke, H. R. *Contrast Media Mol. Imaging* **2008**, *3*, 53–63.
76. Zhernosekov, K. P.; Filosofov, D. V.; Baum, R. P.; Aschoff, P.; Bihl, H.; Razbash, A. A.; Jahn, M.; Jennewein, M.; Rosch, F. *J. Nucl. Med.* **2007**, *48*, 1741–1748.

## Chapter 12

# Nanostructures Conjugated to Nucleic Acids and Their Applications

**Vanesa Sanz and Jesus M. de la Fuente***

**Instituto de Nanociencia de Aragon-Universidad de Zaragoza,
C/ Mariano Esquillor s/n, Zaragoza 50018, Spain
*E-mail: jmfuente@unizar.es**

The use of nucleic acids such as DNA and RNA in the construction of nanostructures has been widely reported in recent years. Combination of the excellent properties of nucleic acids with the intrinsic characteristics of nanomaterials will further the development of new devices in the field of nanoscience and nanotechnology. This review presents an extensive description of nanostructures conjugated to DNA and RNA and the potential applications of these constructs.

## Introduction

In recent years nanotechnology has emerged as a new discpline offering multiple applications in several fields of research. Progress in nanotechnology can benefit many sectors, such as the production of electronic devices, the development of more effective energy storage products, the design of smart delivery and tissue regeneration systems for biomedical applications, advances in sensor design for highly sensitive detection, and also improvements of manufacturing procedures in the industrial sector (*1–4*). Nanomaterials have been prepared with a range of materials and have been conjugated to various types of molecule to provide an array of properties and applications. The use of nucleic acids in the fabrication of nanostructures is a leading-edge advance in the field of material science (*5*). Nucleic acids, acting both as biological components themselves and as elements with particular properties, have been combined with nanomaterials for the development of specific devices, and even as components to enhance nanomaterial synthesis (*6–8*) (Figure 1). The optical, electrical and magnetic properties of DNA have been exploited for the development of nanodevices for technological applications. These nucleic acid-based nanostructures have been applied in many fields and show a wide range of applications, such as the fabrication of bio-electronic and optical devices for biosensing purposes, the development of artificial networks, the construction of biological recognition tools, and the development of nanoparticle-based gene delivery systems (*9*). The characteristic molecular structure of nucleic acids determines their interaction with nanomaterials and thus the development of procedures for the binding of these molecules but also governs their use as building blocks for the construction of nanodevices (*10*). DNA, because of its structure and molecular recognition properties, is a promising template to pattern materials with nanoscale precision. DNA also has potential applications in the development of innovative memory and communication devices (*11*). The field of nucleic acid nanotechnology is growing and it promises to make significant breakthroughs in material sciences and biology. In this review, we will discuss the relevance of nucleic acids in nanoscience, with a focus on the characteristics of the nucleic acid-nanoscience interface, the methods devised, and the development of novel devices and further advances in nanotechnology. In the following sections we will address these aspects and explore the current state-of-the-art of these methodologies and the search for potential applications for the interface between DNA and nanotechnology.

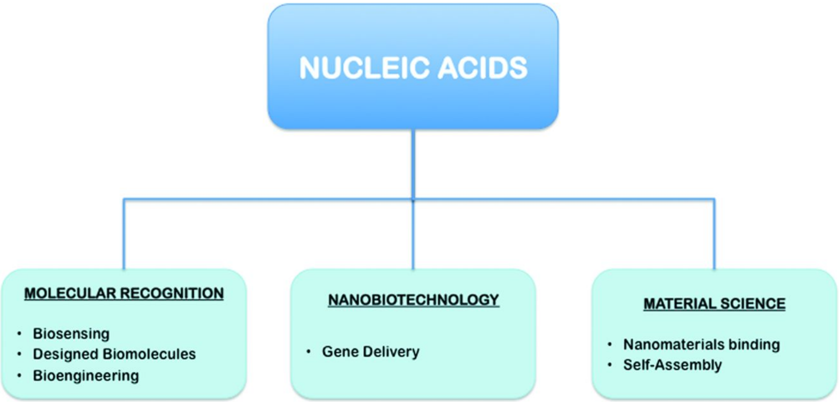

*Figure 1. Combination of nucleic acids with nanostructures.*

## Binding Nucleic Acids to Nanomaterials

The development of procedures to attach nucleic acids to nanomaterials is crucial for multiple applications, such as the construction of bio-electronic and optical devices for biosensing, and gene carrier and delivery systems. In these devices, DNA and RNA are bound to nanomaterials to provide a system for biological recognition and also as cargos for delivery purposes. Several procedures, covalent and non-covalent, have been used to attach DNA to nano surfaces (Figure 2); however, the method selected is determined by the type of nanomaterial. In the case of gold, the most widely used technique involves a covalent bond between a thiol group of a thiol-terminated DNA and gold (*12*) as the variables that influence DNA coverage on a gold surface have been fully characterized (*13*). Quaternary ammonium-functionalized gold nanoparticles also have the capacity to bind DNA with high affinity through ionic interactions (*14*). DNA has also been attached to other materials by means of ionic interactions with charged nanomaterials, hydrophobic interactions, covalent binding to a pre-activated surface, or through adsorption of biotinylated oligonucleotides on avidin-coated surfaces (*15*, *16*). For example, CdS nanoparticles have been assembled with DNA by means of ionic interactions to create semiconductor nanocrystal arrays (*17*), and peptide nucleic acids (PNAs) have been bound to silicon nanowires (*18*) and silica nanoparticles (*19*) through the avidin-biotin interaction. DNA wraps carbon nanotubes through π-π stacking interactions (*20*, *21*) and amine-functionalized DNA wraps carboxyl- functionalized carbon nanotubes through covalent binding (*22*). These findings opened the door to carbon nanotube-based applications in nanotechnology. DNA has also been bound to metals and semiconducting nanoparticles by the formation of nucleation sites along DNA molecules followed by metal or semiconductor deposition by chemical reduction of the corresponding salt (*23*). Furthermore, DNA binds to other kinds of materials carrying cationic groups, such as dendrimers (i.e. polyamidoamine (PAMAM) (*24*), alkylated polypyridylphenylene yielding quaternized pyridinium cations (*25*)), nanoparticles based on a positively charged polysaccharide such as chitosan (*26*) and lipid-based nanoparticles (*27*).

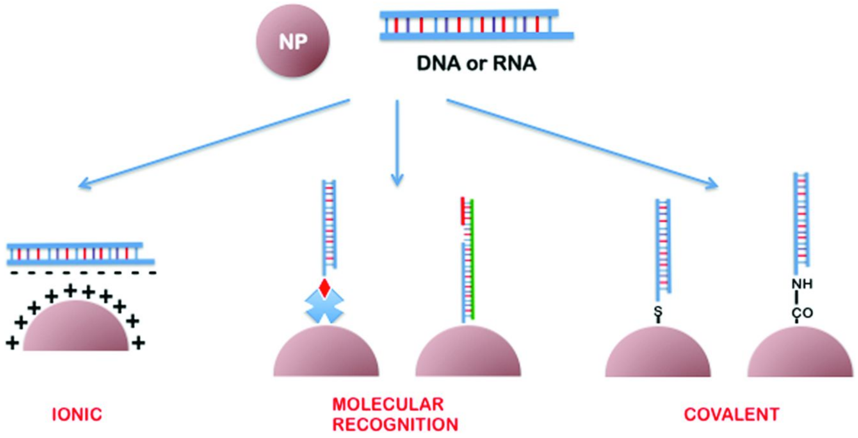

*Figure 2. Strategies to functionalize nanomaterials with nucleic acids.*

## Nanostructures Based on Nucleic Acids

In addition to the capacity of DNA to bind to surfaces through various interactions, it is also possible to take advantage of its regular and characteristic structure for the construction of nanodevices through self-assembly of DNA strands (*28*). These structures precisely position proteins, nanoparticles, metals, and other functional components into designed patterns. They can also act as templates for the growth of nanowires, assist in the structural determination of proteins, and offer new platforms for genomics applications.

Each segment along a given strand can be programmed to pair with a different partner. In this regard, the antiparallel double crossover motif, where two double helices are held in parallel by two pairs of antiparallel strand exchanges, has emerged as a useful tool for the construction of networks of native DNA. One of the advantages of this methodology, known as DNA origami (*29*), is the availability of biologically evolved polymerases that efficiently catalyze sequence-complementary monomer addition for correct replication of long DNA strands. 1D organization of gold nanoparticles was demonstrated by Alivisatos by labeling these particles with DNA strands, thus determining their exact position on complementary single-stranded DNA templates (*30*). 2D structures of gold nanoparticles by the same approach have also been described (*31–33*), where it is also possible to assemble a range of molecules onto the 2D DNA array (*34*). DNA sheets can be programmed to roll along their helical axes into tube-like structures, such as six-helix bundles (*35*) and prisms with three, four, or six flat-origami faces (*36*). These domains can be combined to form wireframe polyhedra with open faces, such as an icosahedron built from six-helix struts that is 100 nm in diameter (*37*) or a box with a controllable lid (*38*). Multilayer structures from sheets of DNA helices can be buil to give greater rigidity or complex 3D cavities (*39*). Further design versatility can be achieved by introducing structures whose helical axes supertwist and bend (*40*). DNA origami has been applied to the construction of nanoarray-based sensor devices (*41*, *42*), as information-bearing seeds for templating algorithmic assembly (*43*, *44*), to template protein guest (*45*) for the template-directed nucleation and growth of inorganic nanoparticles (*46*), and to self-assemble a cross-junction of carbon nanotubes in a field-effect transistor (*48*). This origami also has uses in the field of super-resolution optical microscopy (*47*) . Precisely positioned 2D DNA and protein nanoarrays have practical applications in many fields, such as genomics, proteomics, diagnosis, and tissue engineering. These structures have the capacity to precisely position proteins, nanoparticles, metals, and other functional components into designed patterns. In this regard, it is possible to incorporate synthetic molecules into DNA in order to create branched DNA structures with organic corner units (*49–51*), to create DNA foldamers when incorporating aromatic molecules (*52*), to replace the termini of DNA strands with ligands for metal coordination (*53*) , and even to expand the genetic alphabet by replacing the DNA bases (*54*). In the case of metal coordination, metal complexes can present optical, electronic, magnetic and catalytic properties that can be applied in multimetallic catalysis, sensing, artificial photosynthesis, data storage, nano-optics and nano-electronics. The combination of proteins on DNA templates can serve to generate enzyme arrays and substrates for proteomics and to study protein-protein interactions. For example, the biotin-avidin system has been applied to generate an alternating assembly of streptavidin groups onto a DNA array (*55*). Hybrid DNA-metal nanostructures have a plenty of applications in catalysis, sensing, data storage, nano-optics and nano-electronics (*56*, *57*). More complex systems with 3D assemblies have even allowed the construction of systems for controlled drug release, regulation of the folding and activity of encapsulated proteins, and encaging of nanomaterials, as well as the development of catalysis methods (*58–61*). The synthesis of molecule-responsive DNA materials able to change their structure upon the addition of specific DNA strands has also been reported, such as cyclic DNA dynamic scaffolds for the organization of gold nanoparticles and 3D DNA cages (*56*, *57*). These methodologies have promising applications and illustrate the potential of DNA as a template to position materials with nanoscale precision. Further research is required to be able to develop systems capable of amplifying and scaling up the synthesis of these structures, for example, using biological machinery.

DNA can be used to control the crystallization of inorganic nanoparticle-oligonucleotide conjugates (*60*). It is possible to guide the assembly of inorganic nanoparticles into defined crystalline states by using diverse DNA sequences. Apart from the DNA sequence bound to the nanoparticle building block, the presence of a non-bonding single-base flexor regulates this process. Carbon nanotubes, which are crucial for the development of complex geometries for nanodevices with field-effect transistor behavior, have also been self-assembled into 2D structures using DNA templates (*62*). Two lines of single-stranded DNA in a cross pattern serve as sequence-specific binding sites for two types of carbon nanotubes wrapped with a different DNA linker molecule.

## Applications

### Biosensors (Photonics and Photo-Electronics)

#### *Electrochemical Sensors*

Nucleic acids have been widely used in the development of biosensors. DNA is a self-assembled structure with properties of interest for the purposes of nanodevices. The electric conduction, doping and electronic states of DNA make it a suitable material for the construction of nano-electronic materials. DNA has been described as an insulator, semiconductor or as a metal being water molecules attached to the DNA (*63*). Doped DNA in a vacuum could be used as a nano-scale electron transport material, and DNA in air as a nano-scale ion transport material. The combination of these DNA properties with those of nanomaterials offers excellent prospects for the development of bio-electronic devices that merge biological recognition events with electronic signal transduction. Surfaces modified with nanomaterials have emerged as an excellent option for the development of more selective and sensitive DNA sensors. The detection of specific sequences of DNA has important implications for several fields, such as diagnosis of pathogenic and genetic diseases, forensic analysis, and the screening of specific agents. These sensors detect DNA and RNA targets, single-nucleotide polymorphisms and DNA methylation. A number of strategies for signal transduction for nucleic acid sensors have been described. The first approach consisted of the DNA hybridization sensor, where the binding of complementary DNA strands is transduced to electrochemical signals. These signals have also been obtained by biomolecular recognition events, such as conformational changes, which lead to reagentless, highly sensitive and selective biosensors. Given that several kinds of DNA-based electrochemical sensors have been developed, we consider it pertinent to describe and compare their features.

The first generation DNA electrochemical sensors (*64*) consists of a stem-loop (hairpin) DNA structure that contains a reporter probe, usually redox labels, immobilized on a gold surface acting as electrode and these devices take advantage of a distance-dependent electron transfer (Figure 3). In this approach, DNA hybridization induces a conformational change that moves the reporter redox probe further from the gold surface, thereby producing a decrease in electron transfer. This methodology uses a hairpin DNA structure with a thiol end in order to bind to the gold surface and a redox molecule to the other end, i.e. ferrocene, anthraquinone, ruthenium and osmium tetroxide. Parallel detection of multiple target DNA sequences has been performed using segments complementary to the target DNA sequences labeled with redox probes whose electrochemical signal can be followed separately (*65*). These electrochemical DNA sensors are reusable and they can be miniaturized and also integrated into electrochemical detectors at a low cost. CdTe nanoparticle-modified hairpin probes for sensitive electrochemical detection of DNA have also been reported (*66*). In this method, CdTe nanoparticles are covalently bound to the stem-loop structures and impedance spectroscopy is used for the detection of the electron transfer on the gold electrode upon DNA hybridization. This technique achieves fentomolar levels of sensitivity.

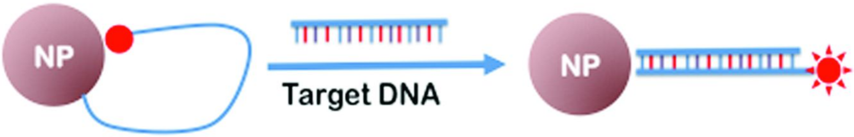

*Figure 3. DNA sensor using a hairpin DNA. One end of the DNA is covalently linked to a gold nanoparticle by a Au-S bond. The other end is labeled with a redox or a fluorescent label. A conformational change caused by DNA hybridization produces a decrease in electron transfer (64–66).*

Another alternative for DNA electrochemical sensors is based on the use of a target-responsive electrochemical aptamer switch strategy (*67*). In this approach, the analyte is a molecule that specifically interacts with its aptamer. A thiolated aptamer is bound to the gold electrode and is labeled with a redox reporter molecule. In the presence of the analyte, a tertiary aptamer structure is stabilized, separating the duplex from releasing the cDNA and approaching the redox reporter to the electrode surface, thus producing a measurable electrochemical signal. In order to further increase the sensitivity of these methodologies, a new technique based on an enzyme-based electrochemical DNA sensor has emerged (*68*). In this case, the hairpin probe is labeled with digoxigenin (DIG) and biotin at the 5′ and 3′ ends, the biotin ending being used to bind to a streptavidin- modified gold surface. A peroxidase-linked-anti DIG is applied to generate an electrochemical signal based on steric hindrance. In the presence of the complementary strand, hybridization breaks the hairpin structure and produces a linear duplex structure that allows the binding of the peroxidase-linked-antiDIG to the duplex and the electrochemical signal. The hybridization event activates a peroxidase enzyme that catalyzes the reduction of hydrogen peroxide. This enzymatic reaction amplifies the electrochemical signal, thus increasing the sensitivity of the method, lowering the detection limit compared to the non-enzyme-based electrochemical biosensor by 3 orders of magnitude. Other modalities of electrochemical DNA sensors involve, for example, the use of a thermal gradient detection method (*69*). In this approach, the typical profile of redox current versus temperature is split into multiple steps by tuning the hybridization temperature, which allows the discrimination of a target sequence from single nucleotide mismatches. In addition to DNA, RNA has also been detected by an electrochemical method based on hairpin probes and steric hindrance suppression signals (*70*). The method is characterized for endogenous interleukin-8 mRNA, obtaining a low basal signal, a large dynamic range, and fentomolar levels of detection. The DNA hybridization process has served to amplify biosensing applications in a method called hybridization chain reaction (*71*). In this approach, two stable species of DNA hairpins assemble in the presence of an initiator strand that triggers a cascade of hybridization events. The use of magnetic nanoparticles labeled with metal tags, colloidal gold tags, semiconductor quantum dot tracers, or polymeric carrier beads introduces new alternatives for electrochemical DNA detection strategies. The application of magnetic nanoparticles lowers the detection limits thanks to the possibility of magnetic separation (*72*). A method has been proposed that uses high sensitivity of anodic stripping analysis for zinc ions with magnetic separation for removing the non-specific adsorption that affects the DNA hybridization analysis (*73*). In this approach, single-stranded DNA is covalently bound to magnetic nanoparticles and oligonucleotide labeled with ZnS nanoparticles is used as a probe to detect the target single-stranded DNA. The hybridization process is followed by the dissolution of the ZnS nanoparticles, and zinc ions are determined by anodic stripping voltammetry. The latter method combined with carbon fiber ultramicroelectrode and polymer-modified glassy carbon electrode have also been applied for sensitive electrochemical detection assays for DNA hybridization using silver nanoparticles and lead sulphide nanoparticles, respectively (*74*, *75*). The quantum dots also have applications for DNA electrochemical detection (*76*). Multiple DNA targets have been simultaneously detected using distinct types of quantum dots (Figure 4) (*77*). Three nanoparticles were used for this purpose, zinc sulphide, cadmium sulphide and lead sulphide, to obtain a range of signals for three DNA targets by stripping voltammetry of the metal dissolution products. Magnetic removal of the non-hybridized targets is again used for higher sensitivity and selectivity. Gold nanoparticles have been reported for the electrochemical detection of nucleic acids (*78*). These systems involve thiolated DNA probes stuck to the gold nanoparticles; however, the non-specific adsorption of DNA on gold caused by the weak interaction between the metal and DNA bases is one of the major limitations of this method. The formation of mixed self-assembled monolayers (SAMs) with mercaptohexanol adsorption significantly inhibits non-specific DNA adsorption and orientates the DNA probes for highly effective hybridization (*79*). This assembly procedure has applications in the development of several electrochemical DNA sensors. However, the mercaptohexanol passivation layer does not prevent the non-specific adsorption of proteins. Non-fouling surfaces by the use of poly(ethylene glycol) in the SAM have been synthesized to increase the applicability of these electrochemical DNA sensors (*80*). It was also found that the incorporation of poly(ethylene glycol) in the SAM enhances electron transfer across the monolayer (*81*). The sensitivity of DNA sensors can be increased by amplification of the signal corresponding to a single DNA hybridization event by incorporating nanoparticle amplifiers (*82*). Electrochemical detection of nucleic acids with amplification strategies based on streptavidin-coated gold nanoparticles have also been described (*83*).

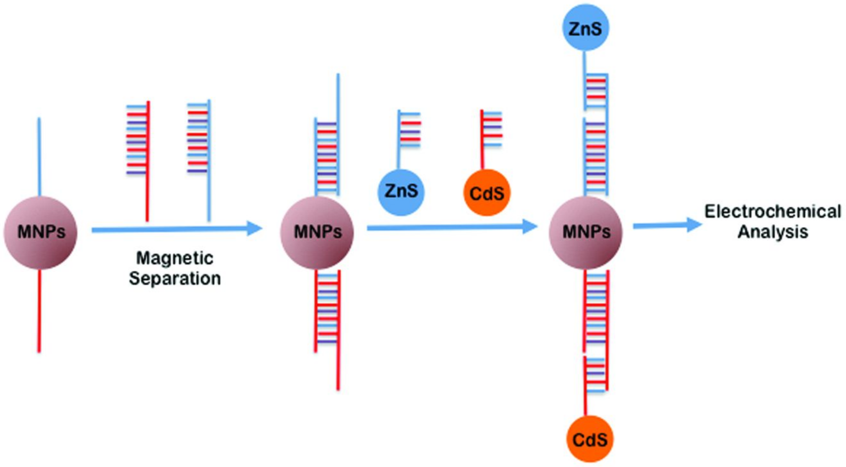

*Figure 4. The use of magnetic nanoparticles (MNPs) can enhance sample treatment and increase the sensitivity of an analytical method. The combination of magnetic nanoparticles with distinct compositions and DNA strands provides a multianalyte biosensor (77).*

Another strategy highly sensitive for the detection of DNA hybridization in a short time is based on a genomagnetic assay (*84*). This approach involves the immobilization of biotinylated inosine-substituted capture probe onto streptavidin-coated magnetic beads, followed by hybridization with the target

DNA. Electrochemical detection can be performed by the dissociation of the DNA hybrid in alkaline media and the voltammetric signal of guanine oxidation, or by magnetic separation based on an electrode containing a small magnet. Genomagnetic electrochemical detection has also been improved by using enzyme labels for the amplification (*85*). The enzyme streptavidin-alkaline phosphatase and magnetic nanoparticles labeled a probe that hybridized with a biotinylated DNA target. The α-naphthol product of the enzymatic reaction was measured by pulse voltammetry.

The use of carbon nanotubes for the electrochemical detection of DNA has received considerable attention (*86*). Extensive research has been performed on transistor-based systems for nucleic acid detection (*87*). In this modality, semiconductor carbon nanotubes are held between a source and drain and a difference in voltage is applied. The conductivity of the carbon nanotube changes in function of alterations in environmental conditions caused by specific interactions with molecules attached to the tube. In the case of DNA detection, aptamers are widely used because of their small Debye length, which enhances sensitivity (*88*). Various configurations have been implemented for field-effect transistors based on carbon nanotubes. The selection of a carbon nanotube network field-effect transistor has lead to low cost, simple and highly sensitive and accurate design of devices for nucleic acid detection (*89*). In this regard, a number of strategies have been reported for the amplification of the analytical signal obtained with these devices. Most changes in the current between the source and the drain and in the conductance occur in the modulation of the Schottky barrier in the nanotube-metal contact (*90*). Thus the sensitivity is enhanced by increasing the Schottky contact area in order to hold a higher number of biorecognition events. In these conditions, the detection limit has been improved 4 orders of magnitude over conventional devices. Procedures to achieve wide-tapered Schottky connections have been developed by angle-evaporation of gold in order to produce a larger Schottky contact area to immobilize a greater number of receptors. The changes in conductivity with these devices, apart from the modulation of the Schottky barrier in the nanotube-metal contact, is due to chemical gating on the nanotube channel (*91*). In nanotube-metal contacts, the single-stranded DNA adheres onto the carbon nanotubes with more efficiency than doble-stranded. In this way, hybridization with the DNA is less favorable in the nanotube than in nanotube-metal contact. The addition of divalent cations, such as $Mg^{2+}$, $Co^{2+}$, $Ca^{2+}$ and $Hg^{2+}$, enhances a higher adsorption of DNA onto nanotube metal.

### *Mechanical Sensors*

Biosensors based on microcantilevers have become a promising tool for the detection of biomolecular interactions. The transduction of the molecular recognition event by microcantilevers is in the form of a nanomechanical motion, which is usually coupled to an optical or piezo-resistive detection system. The biomolecule binds to the cantilever as a result of the recognition event, thus producing a resonant frequency shift that can be detected by the systems stated above. One of the advantages of these systems is that they allow simultaneous detection using arrays of cantilevers. The cantilever-based sensor principle for monitoring chemical and biological interactions has been applied for the detection of biomolecules, including specific DNA sequences (*92*). Thiolated DNA have been used to modify gold-coated microcantilever-based optical deflection devices for the discrimination of DNA mismatches (*93*). The hybridization of complementary target oligonucleotides results in a positive deflection of the cantilever, while hybridization with targets containing one or two mismatches produces a negative deflection. Microarray cantilevers have the capacity to detect multiple DNA targets (*94*). The sensitivity of the method reaches femtomoles of DNA on the cantilever, the mechanical motion being originated from a steric hindrance effect and related to the concentration of DNA. The use of inkjet printing has been introduced as a rapid method for the controlled deposition of functional layers on cantilever arrays for DNA detection (*95*). The inkjet method is straightforward, fast, versatile and scalable. Microcantilever-based mechanical resonance DNA detection using gold nanoparticle-modified probes has been also reported (*96*). In this procedure, thiolated DNA strands are bound to the gold surface of the cantilever and, after hybridization with the target DNA, the gold nanoparticles labeled with DNA are hybridized to the other end of the target DNA through complementary interactions. The growth of silver on the gold nanoparticles produces an increase in the effective mass on the microcantilever, thereby causing a frequency shift in the microcantilever, which can be detected.

### *Optical Sensors*

Nucleic acid detection can be achieved based on the optical properties of metal nanoparticles. The surface plasmon resonance (SPR) of gold nanoparticles has been widely used for the optical detection of DNA (*97*). Gold nanoparticles with a diameter of 13 nm exhibit an SPR absorption band at 520 nm in the UV-Vis spectrum, thus a solution of these nanoparticles appears red. When these nanoparticles aggregate, there is a shift in the SPR from 520 nm to 574 nm, turning the solution purple (Figure 5). This property of gold nanoparticles has been exploited to design optical methods for DNA detection. Thus specific DNA targets to promote the aggregation of these gold nanoparticles can be used to generate an optical analytical signal for the detection of DNA (*98*, *99*). Furthermore, the hybridization temperature together with the optical properties of this system allows the detection of mismatches (*100*). Taking advantage of this methodology, other kinds of nanoparticles with distinct SPR bands have been used for DNA detection. For example, silver-gold core-shell nanoparticles have been implemented for these purposes (*101*). These nanoparticles appear yellow in solution and black when aggregated in the presence of target DNA. In this way, a second working wavelength, in addition to that of the gold nanoparticles, can be selected for multidetection purposes. The distinct SPRs of nanoparticles according to their size has been also used for multidetection purposes (*102*). The main problem of these methodologies based on target-DNA mediated nanoparticle aggregation is their limited sensitivity.

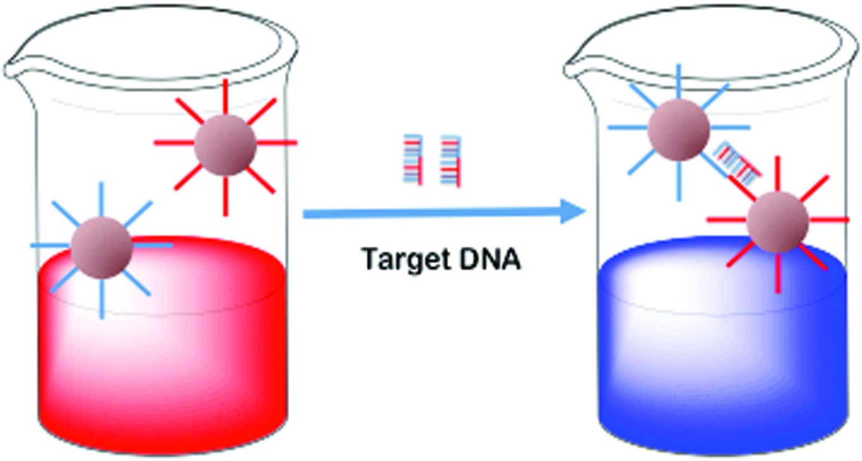

*Figure 5. Aggregation of gold nanoparticles caused by DNA hybridization is one of the most used nanosensors. A change in the color of the solutions occurs as a result of nanoparticle aggregation (97–100).*

In order to increase the sensitivity of these methodologies, the general trend was to develop microarray technology with the capacity to detect hundreds to thousands of nucleic acid sequences, both DNA and RNA, in a single assay (*103*). DNA microarrays have excellent features: they are relatively inexpensive, flexible, universal, rapid and user-friendly. The development of highly sensitive readout methods for these microarrays was achieved through complementing them with nanotechnology advances. The first approach was the scanometric assay, which uses DNA-functionalized gold nanoparticle probes (*104*). The properties displayed by gold nanoparticles (small label size, established bioconjugation chemistry, optical and electrical properties) offer advantages over conventional detection methods (based, for example, on molecular fluorophores, real-time PCR and enzyme-linked immunoassays), such as time efficiency, high sensitivity, miniaturization and cost-efficient detection. In this regard, a silver development step has been introduced to improve the optics of the systems and increase sensitivity (*105*). This step precipitates silver around the nanoparticle probes bound to the test slide, thereby improving the ability to scatter light by several orders of magnitude. In the assay, light is delivered to the test slide and the resulting evanescent wave excites the silver-amplified gold nanoparticles, the scattered light is then measured by a photosensor. Other detection systems based on silver precipitation on gold nanoparticles consist of silver metal dissolution in acidic solution and determination by anodic stripping voltammetry (*106*). Based on electrical detection strategies, further advances using gold nanoparticle probes have been made by functionalizing microelectrode gaps with intervening target capture sequences for the detection of sandwiched targets (*107*). This system allows miniaturization by using smaller electrode gaps thanks to techniques such as photolithography, electron beam lithography, dip-pen nanolithography and ink-jet printing to generate covalently anchored, nanoscale patterns of oligonucleotides on both metallic and insulating substrates (*108*).

Surface-enhanced Raman spectroscopy (SERS) also has applications as a readout method in these systems (*109*). In these assays, gold nanoparticles are functionalized with the target nucleic acid sequence and a Raman active molecule. The labeling with the Raman active molecule allows a specific wavelength for the Raman detection. In these systems, silver enhancement is used prior to SERS measurement. The use of Raman active molecules provides several advantages over fluorescent labels, such as narrower spectral bands in a broad spectral window, thereby allowing the possibility of a more selective and a higher number of analytes for multidetection purposes, and each Raman label can be excited with the same laser while in fluorescence several lasers are generally required.

Another optical detection system is based on the use conformation-associated quenching or energy transfer. For example, thiolated oligonucleotides labeled with a fluorophore at the other end and bound to a gold nanoparticle have been used for these purposes (*110*). The conformation of the oligonucleotide brings the fluorophore into proximity with the gold surface being quenched by the nanoparticle. However, after target binding, the conformation of the oligonucleotide is more rigid and opens, thus detaching the fluorophore from the gold surface and resulting in increased fluorescence. This system is highly sensitive. Another conformation-associated change in fluorescence has emerged called the molecular beacon (*111*). Molecular beacons are oligonucleotides designed to form a stem loop conformation and they are labeled at 5′ and 3′ ends with a fluorophore and a quencher, respectively. In this conformation, no fluorescence is obtained because of the quenching effect. However, after hybridization of the target oligonucleotide with the molecular beacon, fluorescence intensifies as a result of the increase in the distance between the quencher and fluorophore. Biotinylated molecular beacons have also been synthesized for immobilization onto avidin-functionalized surfaces (*112*). It was found that the stem part of the molecular beacon is the best anchoring point to link biotin in order to minimize the effects of biotin on fluorescence and hybridization with the DNA target. Molecular beacons have also been combined with nanoparticles to improve the analytical procedure. For example, these probes have been combined with gold nanoparticles to take advantage of their optical properties, thus allowing the development of new biosensors (*113*). In these systems, the organic quencher is replaced by gold, resulting in an increase in sensitivity of two orders of magnitude. However, these systems have some drawbacks, such as the physicochemical stability of the metal clusters, their ligand shell, and the chemical linkage between the clusters and the DNA. DNA hybridization has been controlled using gold nanoparticle-molecular beacons inductively coupled to a radio-frequency magnetic field (RFMF) (*114*). In this approach, the gold nanoparticle increases the local temperature, thus inducing denaturation. Hybrid systems composed of CdSe-ZnS core-shell quantum dots as donors and gold nanoparticles as quencher combined to molecular beacons have also been reported (*115*).

Optical sensors for DNA hybridization detection have also been developed using carbon nanotubes (*116*). These nanotubes have a photostable fluorescence in the near infrared region where human tissue and biological fluids are transparent to their emission. DNA hybridization is detected on the surface of dispersed single-walled carbon nanotubes through their band gap fluorescence. The hybridization of an oligonucleotide on the surface of the nanotube produces a hypsochromic shift in the near infrared fluorescence spectra. The sensitivity of the method is in the order of nM, although the response time of the sensor is high. However, the functionalization of the nanotube surface in order to attach the specific ligands for analyte recognition while preserving the optical properties of these nanomaterials remains a great challenge in the field. Quantum dots, as inorganic fluorophores, are more resistant to photodegradation than organic fluorophores, as occurs with carbon nanotubes. Furthermore, their broad absorption spectra and narrow emission peaks allow the simultaneous excitation of various quantum dots at a single wavelength for multidetection purposes (*117*). Due to their tunable narrow band emission and broad excitation spectra, quantum dots are excellent donors for fluorescence resonance energy transfer-based biosensors. Cy3-labeled single-stranded DNA has been used as an acceptor in these kinds of biosensors. Quantum dot-DNA conjugates have been also exploited for the development of surface plasmon enhanced fluorescence sensors (*118*). Using the microarray format where the labeled quantum dots are organized in individual surface spots, it is possible to perform simultaneous determination of DNA strands.

A major challenge in DNA detection is the development of amplification systems that do not require polymerase chain reaction (PCR). The bio-barcode assay consists of a gold nanoparticle-based system that introduces an amplification event for each target molecule labeled (*119*). This system has shown high sensitivity for the detection of proteins. This methodology uses magnetic microparticle probes with antibodies that specifically recognize the target protein, and nanoparticle probes carrying DNA strands and antibodies for the target protein. Thus the target protein can be sandwiched between the magnetic microparticles and the nanoparticles carrying DNA. After magnetic separation of the complexed probes and target, dehybridization of the oligonucleotides and the detection of the oligonucleotides released allow detection of the target protein. As the nanoparticle probe carries a large amount of oligonucleotides, one protein recognition event is amplified, thus sensitivity is in the attomolar level. The bio-barcode assay can be extended to detect any target capable of being sandwiched between the two probes. In this regard, DNA has been detected at zeptomolar concentrations, PCR amplification being unnecessary (*120*). The barcodes are oligonucleotides of up to 10 nucleotides that can be easily synthesized and chemically modified with functional groups. Nanowires have been also implemented for DNA detection without the need for amplification (*18*). In these systems, the surface of silicon nanowires are modified with peptide nucleic acid receptors designed to recognize specific genes. Femtomolar levels of sensitivity are achieved. Silicon nanowires present electrical properties and sensitivity that can be tuned reproducibly by controlling the dopant concentration and nanowire diameter. Furthermore, the functionalization of the silicon oxide surfaces to bind biological receptors has been widely studied.

A new approach for ultrasensitive detection of DNA and RNA is based on nanoparticle-amplified SPR (*98*). SPR imaging is a surface-sensitive spectroscopic technique for the measurement of interactions between biological molecules and receptors bound to the surface. For the hybridization adsorption of both DNA and RNA oligonucleotides, detection limits of nM have been reported. Peptide nucleic acids immobilized on a gold-capped nanoparticle layer substrate have been used in SPR-based sensors (*121*). The nanoparticle layer was prepared on a gold-deposited glass substrated by the surface-modified silica nanoparticles using silane-coupling reagent. The detection limit was in the order of pM for the target DNA. Protein biomarkers have been detected by SPR with RNA aptamer microarrays, where amplification is achieved by enzymatic reaction (*122*). Proteins are detected by the aptamer-protein-antibody complex on the RNA microarray. The SPR signal is amplified by a localized precipitation reaction catalyzed by the enzyme horseradish peroxidase conjugated to the antibody. Amplification with the enzyme reaction systems reaches detection limits in the fentomolar range.

## Aptamers, DNAzymes, and Aptazymes

The discovery of short single-stranded DNAs or RNAs with characteristic 3D structures that bind targets ranging from small organic molecules, and proteins, to cells and viruses with high affinity and specificity paved the way for the development of new functional nucleic acid based-nanodevices (*123*). These molecules, called aptamers, have been applied as sensing material with different configurations and have several advantages over antibodies as recognition systems (*124*). For example, they have high binding affinities for their targets and high flexibility for signal transduction and detection, they are characterized by their lack of immunogenicity, and they are stable against biodegradation and denaturation. Nanomaterial-assisted aptasensors (NAAs), which combine the advantages of aptamers with novel nanomaterials, are sensing platforms with high selectivity and sensitivity (*125*). Optical NAAs are able to transduce and magnify the aptamer recognition event into measurable signals, for which several detection methods such as colorimetry, fluorescence, surface-enhanced Raman scattering and SPR are used. A range of nanomaterials such as gold nanoparticles (*126*, *127*), quantum dots (*128*), carbon nanotubes (*88*), iron oxide nanoparticles (*129*), and silica nanoparticles (*130*), have been implemented for the aptamers conjugation using covalent and non-covalent approaches.

A further advance in the development of functional DNA was the use of catalytic DNA or DNAzymes (*131*). DNAzymes are DNA-based biocatalysts capable of performing chemical transformations that are not found in nature but that can be isolated by *in vitro* selection. This new function of DNA has been applied in biosensing thanks to the fact that the change in the chemical or physical properties of the material as a response to a chemical or biological stimuli can be detected with high sensitivity and selectivity (*132*). The exceptional sensitivity of DNAzyme-based nanodevices is based on their inherent capacity to generate amplification effects as a consequence of their turnover reactions. Examples of the use of DNAzymes in the development of sensors and for the removal of errors in nanomaterial assemblies can be found in the literature (*133*). The coupling of micro- and nanofluidic devices with the DNAzyme approach has relevant implications in advancing sensor design as this strategy could allow the analysis of low-volume samples with potential multi-array detection (*134*). An important and novel application of DNAzymes is the construction of molecular motors with open-close motions and walking motions (*135–137*). When the DNAzyme is free of substrate, the device is in the closed state, whereas hybridization by the substrate causes the device to open, to later close as a result of DNAzyme cleavage and product release. Finally, the combination of DNAzymes with aptamers has generated a new class of functional nucleic acids called allosteric DNAzymes or aptazymes (*138–140*).

## Gene Delivery Systems

Nucleic acids have applications in gene delivery systems. Gene therapy approaches for the treatment of human diseases rely on advances in the design of suitable gene delivery systems. Although naked DNA has been delivered to certain kinds of tissues, such as liver, solid tumors, epidermis, and skeletal and cardiac muscle cells, it shows low efficiency (*141*). The limiting factor in gene-based therapies is the lack of a suitable carrier with the capacity to deliver the therapeutic genes to the target cells, thus allowing their expression. Traditionally, gene delivery vehicles have been classified into two categories, namely viral or synthetic vectors (Figure 6). Viruses such as oncoretroviruses, lentiviruses, AAVs, adenoviruses and herpes viruses, can be transformed into gene-delivery vehicles by replacing part of their genome with a therapeutic gene (*142*). Viruses are usually highly efficient as their primary activity is to carry their genome into the target cell, navigate to the cell nucleus, and initiate the expression of their genome for self-replication. The main drawback when using viruses as transfection vectors, apart from their high manufacturing costs, is the safety concerns associated with their immunogenic character and the possibility that the virus reverts to a wild-type virion. The modification of the virus with synthetic polymers may reduce their immune responses without reducing their infectivity (*143*). Furthermore, viral transfection vectors have limitations in cell targeting as they are usually internalized through non-specific receptors, for example CAR receptor for adenoviruses or heparin sulfates for Herpes Simplex Virus (*144*). Alternatives to overcome this problem may be provided by the attachment of a targeting ligand to the viral capsid by chemical conjugation or by genetic engineering; however, these two methods may inactivate the virus (*145*).

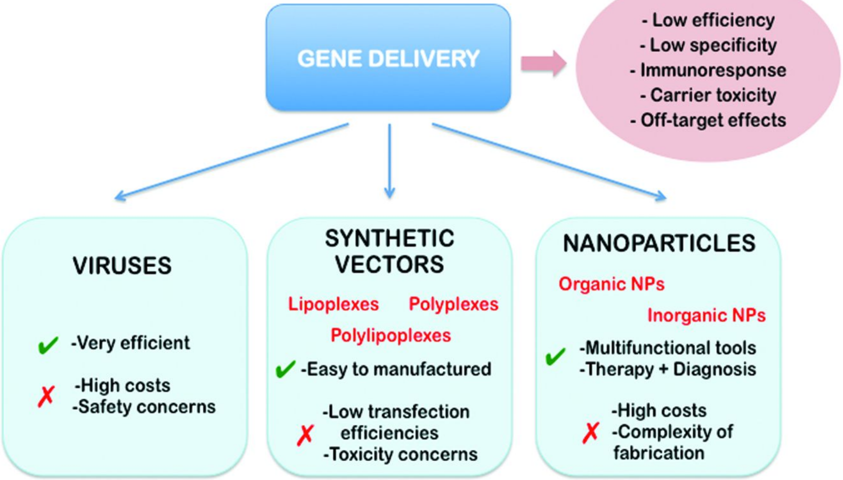
GENE DELIVERY
- Low efficiency
- Low specificity
- Immunoresponse
- Carrier toxicity
- Off-target effects
VIRUSES
✔ -Very efficient
✗ -High costs
-Safety concerns
SYNTHETIC VECTORS
Lipoplexes
Polyplexes
Polylipoplexes
✔ -Easy to manufactured
✗ -Low transfection efficiencies
-Toxicity concerns
NANOPARTICLES
Organic NPs
Inorganic NPs
✔ -Multifunctional tools
-Therapy + Diagnosis
✗ -High costs
-Complexity of fabrication

*Figure 6. Gene delivery vehicles.*

## Lipoplexes, Polyplexes, and Polylipoplexes

Synthetic vectors provide new alternatives for improved safety, greater flexibility and more facile manufacturing. These vectors can be classified as lipoplexes, polyplexes, or a combination of both, called polylipoplexes. Lipoplexes are usually associated with poor preparation reproducibility and *in vitro* and *in vivo* toxicity (*146*). Polyplexes have a more flexible chemistry allowing multiple functionalization and they are more easily manufactured. Non-viral vectors are characterized by their low transfection efficiencies and thus one of the main problems is the high concentration required for therapeutic purposes. Although the toxicity of synthetic vectors has been reported, in general they are assumed to have low immunogenic potential.

Cationic lipids have a hydrophobic moiety, which can comprise either one or two fatty acids or alkyl chains, or a cholesteryl group, and a polar head, which can be a single or a multiple amine function. The hydrophobic part assembles into bilayer vesicles in aqueous media, exposing the amine head groups for DNA binding through electrostatic interactions. Parameters such us the strength of the DNA binding, which is determined by the number of amine groups per molecule, and the conformational flexibility, stability and biodegradability, which is determined by the linker between the attached DNA and the hydrophobic core, are very important to establish the transfection effectiveness with lipoplexes. Lipoplexes range from 50 nm to 1 µm in size and are internalized by endocytosis. That is why neutral lipids such as DOPE and cholesterol have been incorporated in the lipoplex to improve *in vitro* transfection by promoting endosomal escape (*147*). When administrated via the intravenous route, these carriers are rapidly cleared by plasma and accumulate in lung tissue (*148*). However, lipoplexes are effective via the intratracheal route as they prevent DNA degradation during aerosolization (*149*). Liposomes were the first generation of colloidal carriers to be developed. Apart from their high cost of preparation, liposomes are also associated with cell toxicity, aggregation at high concentrations and *in vivo* instability. Although cationic lipid emulsions (CLEs) composed of a hydrophobic oil phase surrounded by the cationic lipid have a higher stability in physiological conditions and better transfection efficiencies, they lack reproducibility and well-defined formulation (*150*). Solid lipid nanoparticles (SLNs), which are colloidal particles of a lipid matrix that is solid at body temperature, represent another alternative to liposomes as gene carriers (*151*). Although their transfection efficiencies seem to be similar, SLNs have the capacity to prevent the degradation of the cargo and are easier to manufacture at a lower cost. Finally, modification of liposomes with peptides, such as octaarginine, not only enhances cellular uptake but also promotes lysosomal escape with minimum cytotoxicity (*152*).

Polyplexes are complexes of polymers bearing cationic groups with the negatively charged DNA. Polyethylenimine (PEI) is one of the most effective cationic polymers thanks to its proton-sponge properties, which facilitate endosomal escape (*153*). The main problem with PEI is its relatively high cytotoxicity. When PEI polyplexes are injected intravenously, transfection occurs mainly in the lung, but PEGylation allows transfection in distal tumor sites. The transfection efficiency obtained with polylysine (PLL) is much lower but its biodegradable nature makes it suitable for *in vivo* applications (*154*). The conjugation of histidine, which confers endosomolytic properties, to ε-lysine residues of PLL increases its transfection efficiency (*155*). High molecular weight PLL is more suitable for gene delivery via systemic injection as low molecular weight PLLs do not form stable complexes and are cleared by the complement system. Imidazole-containing polymers exhibit proton-sponge properties and biocompatibility (*156*). In this regard, homopolymers of histidine and gluconic acid or lysine and vinyl polymers with pendant imidazole moieties have been tested for gene delivery purposes. Chitosan is a biodegradable and biocompatible aminopolysaccharide that complexes DNA, although its delivery efficiency is generally low (*157*). However, chitosan/DNA complexes have been successfully applied in oral and nasal gene delivery systems thanks to the mucoadhesive properties of chitosan. The latest approaches to improve chitosan transfection efficiency involve the synthesis of novel chitosan derivatives, such as aminoethyl-chitin, thiolated-chitosan, chitosan-methoxy polyethylene glycol-cholesterol and low molecular weight alkylated chitosans. Cyclodextrins (CDs) are cup-shaped molecules with a hydrophilic exterior and hydrophobic interior that form inclusion complexes with small and hydrophobic compounds. Polycations containing pendant CDs can self-assemble with nucleic acids, the CD size, charge centre (amidine or quaternary ammoniums), and charge density being the parameters that affect gene delivery efficiency and polymer toxicity (*158*). A key feature of CD-containing polyplexes is that the complexes can be readily surface-modified by inclusion-complex formation. For example, PEGylation of these polyplexes can be achieved by modification with adamantane-PEG conjugates such as adamantane and CDs form inclusion complexes with high association constants (*159*). Biodegradable polycations have been tested for gene delivery purposes to reduce the cytotoxicity of the vector (*160*). Nevertheless, although they showed less toxicity, their efficiency was lower. Examples of these degradable polycations include cationic polyesters such as poly[α-(4-aminobutyl)-L-glycolic acid] (PAGA) or poly(β-amino esters). Synthetic peptides with membrane-disruptive properties have been developed (*161*). These peptides are protonated at acidic pH and become fusogenic with the endosomal membrane, thus allowing the delivery of the genetic material into the cytoplasm. However, given the potential of these peptides to trigger undesirable immune responses, several acid-responsive polymers have been designed to enhance the efficiency of polyplexes and lipoplexes. These polymers contain pH-responsive functionalities, such as carboxylic groups and hydrophobic groups, for interaction with the endosomal membrane, and become hydrophobic when protonated. Examples of these pH-responsive polymers include α-alkyl acrylic acids, maleic anhydride... Other variants of these membrane-disruptive polymers include pyridyl disulphide acrylate-containing polymers, which additionally provide a way to conjugate thiol-terminated oligonucleotides for the release of the genetic material in the cytosol after endosome escape mediated by the polymer (*162*). The implementation of dendrimers in gene delivery implies the use of those with a cationic net surface charge such as PAMAM and PPI dendrimers (*163*). There are some implications of the star shape of the dendrimer as DNA appears to interact with the surface primary amines, thus leaving the internal tertiary amines available for the neutralization of the acid pH in the endocytic vesicles, thereby leading to the dendrimer-gene release into the cytoplasm (*164*). The size and diameter of dendrimers determine their transfection efficiency, the efficiency of high generation dendrimers being higher than low generation ones. Partially degraded PAMAM dendrimers are reported to have more flexible structures that interact more efficiently with DNA and enhance the transfection efficiency. Size is a key determinant of dendrimer cytotoxicity. Higher dendrimer generation and a big number of charged groups decrease their viability. The nature of the complex depends on the stoichiometry and concentration of the DNA phosphates and dendrimer amines and also on the solvent properties, such as pH, salt concentration and buffer strength. Dendrimers also protect DNA from degradation. Novel technologies are emerging based on the use of recombinant polymers that are genetically engineered to overcome the extra- and intracellular barriers that prevent efficient gene delivery (*165*, *166*). Compared to synthetic polymers, recombinant polymers have higher homogeneity, versatility and flexibility, the most important concern being their capacity to activate the immune system. These genetically engineered protein-based polymers incorporate peptide motifs, such as elastin, silk and collagen, to produce materials with desired composition that confer particular properties to the polymer, such as responsiveness to microenvironmental stimuli, controlled biodegradation and presentation of informational motifs for cellular and subcellular interactions. For example, the introduction of histidine or imidazole reduces cytotoxicity and enhances transfection efficiency as a result of the proton sponge effect; the introduction of cystein residues reduces cytotoxicity and increases transfection efficiency (*167*); silk-elastin-like block copolymers provide mechanical strength and the DNA release is strongly affected by the ionic strength of the medium.

A novel intelligent system for gene delivery is based on diblock copolymers designed by recombinant DNA cloning technology and composed of oligolysine and a thermosensitive elastin-like polypeptide that aggregates above a temperature phase transition (*168*). This characteristic allows the development of methods for hyperthermic targeting of the genetic material conjugated with the polymer.

Lipopolyplexes have been prepared by condensing DNA with a polycation such as poly-L-lysine, PEI, spermidine, or spermine, and entrapping this polyplex within anionic or neutral liposomes (*169*). This method of DNA packaging has lower toxicity and can have a higher efficiency owing to its protection of DNA compared to liposomes alone. Polymeric vesicles for gene delivery have been produced by the modification of the cationic polymers poly-L-lysine and poly-L-ornithine by covalent attachment of both hydrophobic (palmitoyl) and hydrophilic (methoxy polyethylene glycol) groups in the presence of cholesterol.

## Nanoparticles for Gene Delivery

Nanoparticles have also been used for the condensation of nucleic acids to be biodelivered to control gene expression. The functionalization of these carriers allows their preferential accumulation at tumor sites by means of targeting ligands, thus providing a powerful tool for cancer gene therapy. Various kinds of nanoparticles have been implemented for these purposes. Gold nanoparticles have been used as gene carriers as they are inert and non-toxic and their functionalization procedures have been extensively studied. One of the main advantages of gold nanoparticles as delivery agents is that the gold-thiolate binding of the cargos allows regulation of transfection capacity by manipulating intracellular glutathione levels. Positively charged groups have been attached to gold nanoparticles to bind negatively charged nucleic acids. For example, lysine groups have been bound to gold nanoparticles to obtain higher *in vitro* transfection efficiencies than with polylysine alone (*170*). A layer-by-layer technique has been also employed to prepare charge-reversal functional gold nanoparticles for small interfering RNA (siRNA) delivery to cancer cells (Figure 7) (*171*). Complexes of gold nanoparticles with lipids and plasmid DNA (*172*) and gold nanoparticles with PEI and plasmid DNA (*173*) have been also exploited for gene delivery purposes. In addition to gold nanoparticles, other kinds of inorganic nanoparticles have been tested as gene carriers. Nanorods have applications as gene carriers as their composition, size and multifunctionality can be precisely controlled. Au/Ni nanorods in which plasmid DNA and targeting ligands are compacted on the nanorod in a spatially defined manner have been described (*174*). Fluorescent silica nanotubes synthesized through a sol-gel reaction have been filled with plasmid DNA and have been shown to deliver green fluorescence gene into mammalian cells (*175*). Quantum dots have been exploited to deliver siRNA to test gene silencing and to act as multi color probes (*176*). Quantum dots have also been coated with proton-sponge polymers to enhance the delivery of siRNA by overcoming several biological barriers, such as cellular penetration, endosomal release, carrier unpacking and intracellular transport (*177*). In addition, these systems have been used as fluorescent labels of gene carrier vectors, such as carbon nanotubes (*178*). Magnetic nanoparticles also have applications in gene delivery. In this kind of nanoparticles, the technique used for gene delivery is called magnetofection. In this strategy, the magnetic nanoparticles carrying the gene are incubated with the cell culture and exposed to a magnetic field gradient, increasing the sedimentation of the nanoparticles and the transfection yield (*179*). This method has potential applications for *in vivo* gene therapy, as the magnetic field can target the therapeutic agents to the target organs. Magnetic nanoparticles offer the possibility of magnetic resonance imaging (*180*).

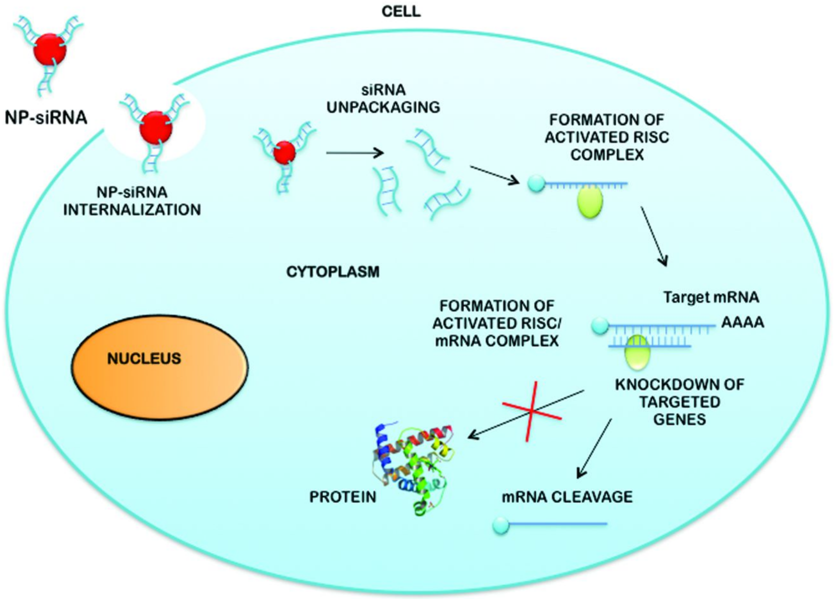
CELL
NP-siRNA
NP-siRNA INTERNALIZATION
siRNA UNPACKAGING
FORMATION OF ACTIVATED RISC COMPLEX
CYTOPLASM
NUCLEUS
FORMATION OF ACTIVATED RISC/ mRNA COMPLEX
Target mRNA
AAAA
KNOCKDOWN OF TARGETED GENES
PROTEIN
mRNA CLEAVAGE

*Figure 7. siRNA machinery.*

The use of carbon nanotubes for gene delivery requires the development of methods to bind DNA or RNA. Several procedures based on covalent and non-covalent techniques have been reported for this purpose (*181*, *182*). Carbon nanotubes provide excellent gene delivery systems because of their nano proportions, biocompatibility, low cytotoxicity and capacity to cross the cell membrane. Encouragingly, carbon nanotubes localize in tumors in mice, probably because of the increased vascularization inherent in tumors, thus making tumor targeting a feasible approach. Several approaches for gene delivery mediated by carbon nanotubes have been developed. For example, plasmid DNA expressing β-galactosidase was condensed on ammonium-functionalized carbon nanotubes by ionic interactions and the levels of gene expression in CHO cells was found to be 5 to 10 times higher than plasmid alone (*183*). Amino-functionalized multi-walled carbon nanotubes were also found to efficiently deliver plasmid DNA encoding green fluorescent protein gene into mammalian cells (*184*).

siRNA has also been delivered into cells by carbon nanotubes functionalized with ammonium groups bound to telomerase reverse transcriptase siRNA by ionic interactions (*185*). Furthermore, covalent approaches based on binding nucleic acids to carbon nanotubes have also been tested. For example, siRNA was covalently bound to carbon nanotubes using a cleavable disulfide bond (*186*). Recently, an alternative physical method of gene delivery called nanotube spearing has been reported (*187*). In this method, carbon nanotubes contain nickel particles in their tips, thus allowing them to respond to a magnetic field.

## Implications of Extracellular and Intracellular Barriers in the Design of Gene Delivery Systems

Extracellular barriers are the hurdles that genetic material encounters from the point of injection to the surfaces of the cellular target of interest. The systemic stability of the gene delivery system in the bloodstream strongly depends on the global charge of the DNA-carrier complex and is essential for extended circulation times (*188*). Highly charged carriers rapidly aggregate in high ionic strength solutions. In addition, positively charged systems interact with the extracellular matrix, cell surfaces and plasma proteins, all negatively charged, which may produce rapid clearance by phagocytic cells of the reticuloendothelial system or may activate the complement system. In contrast, negatively charged systems are cleared by phagocytosis via the macrophage polyanion receptor. Modification of the carriers with polymers such as PEG, N-(2-hydroxypropyl)methacrylamide (HPMA) poly(oxazoline), polyvinyl alcohol, poly(glycerol), poly-N-vinylpyrrolidone, poly(amino acid)s and sugars reduces these processes by creating a hydrophilic layer that decreases self, non-self and non-specific interactions (*189*). However, this modification may affect the internalization and intracellular trafficking of the carrier, a major barrier to internalization and endosomal escape. One way to address this problem may be the use of an environment-responsive removable coating. For example, chemical bonds display pH-dependent hydrolytic degradation such as acetals, vinyl ether, ortho esters and hydrazones, which allow the shielding of destabilization upon endosomal and lysosomal internalization (*190*). Other approaches include reduction-induction shedding by using disulfide bonds that are stable in plasma but reduced to thiol in the cytosol (*191*), or the proteolysis-induced shedding triggered by proteolytic enzymes encountered in the endo/lysosomal compartment (*192*). Furthermore, targeting of the vector can be achieved by means of proteolytic enzymes, such as lysozymes, cathepsins and matrix metallo proteinases, localized extracellularly in pathological sites such as inflammatory and malignant areas (*193*). The presence of charges on the complex also has aimplications on cytotoxicity. It has been suggested that the cytotoxicity of the complex is related to ionic interactions between anionic domains on the cell surface and cationic moieties on the vector that lead to an accumulation of aggregates that alters membrane function (*194*). Structural parameters of the vector, such as degree of branching, cationic charge density, type of cationic functionality, size, conformation and flexibility, determine the degree of cytotoxicity. The stabilization of complexes must allow the targeting of specific cell types by the interaction between surface receptors and ligand-containing gene delivery systems. A number of targeting moieties have been tested in this regard, such as glycosidic moieties, folate, asialoorosomucoid, transferrin, epidermal growth factor, antibodies or antibody fragments, and integrin-binding sequences (*195*). The success of a targeting strategy depends on the conjugation chemistry, the length of spacer between ligand and carrier, the ligand-receptor binding strength, and the number of targeting ligands per carrier. Furthermore, the presence of targeting ligands may induce immune responses which produce problems when repeating administrations, shedding being a solution to circumvent these drawbacks.

Once the carrier reaches its target it can be internalized by several mechanisms, receptor-mediated endocytosis being the most common, but also through non-specific pathways, such as ionic interaction with membrane-bound proteoglycans, lipophilic interaction with phospholipid membrane, and endocytosis (see Figure 4). Uptake mediated by cell-penetrating peptides, which are typically 5-40 amino acids in length, positively charged, and amphipathic in nature, facilitate membrane translocation (*196*). In these processes the vector carrying the genetic material is brought into the cytoplasm in vesicular compartments that deliver their contents to degradative vesicles called lysosomes. Release from these vesicles is required to prevent DNA degradation and has been achieved by different means, for example, the use of protonable amines that buffer the endosome pH through a proton sponge effect. Endosomal release peptides that undergo a structural transformation at acidic pH, can achieve cytosol by their interactions with membrane receptors. Another option is the use of alkylated carboxylic acids, such as poly(propylacrylic acid), which have membrane lytic properties induced by a decrease in pH. Another important intracellular barrier is the transport toward and into the nucleus. Nuclear transport has been enhanced in several ways, such as by nuclear localization signal peptides or nucleotide sequences (*197*) with nuclear targeting capacity on the genes themselves, or specific carbohydrates that are recognized by their respective intracellular receptor or lectin to direct the transport of the gene delivery system (*198*). Several approaches have been described to promote dissociation of the gene from the vector within the nucleus in order to further enhance the expression of the gene (*199*). Thermoresponsive polymers that undergo a reversible coil-to-globule phase transition such as poly(N-isopropylacrylamide) (NIPAM) have been used for this purpose, although high expression levels have not been achieved (*200*). Cleavable disulphide bonds that can be reduced and cleaved to thiol by the cytosolic glutathione or hydrolytically-sensitive ester bonds have been tested, although premature cleavage occurs before reaching the target in physiological environments (*201*).

The use of higher ordered macromolecular structures, such as interlocked, multi-component supramolecules or 2D and 3D scaffolds, could allow the design of improved vectors (*202*). The option of delivering naked DNA or polyplexes from implantable surface-erodible substrates is a way to overcome serum instability and clearance from the bloodstream associated with systemic injection. Implanted substrate near the targeted cells whose release can be controlled requires less DNA or polyplex loading. Examples of substrate-mediated gene delivery systems include DNA-eluting films developed by the layer-by-layer film deposition technology and porous and biodegradable 2D and 3D scaffolds that can also encourage cell ingrowth. Polyplexes incorporated into poly(lactide-co-glycolide) (PLGA) scaffolds have longer and greater levels of gene expression compared to systemic administration of polyplexes and scaffolds embedded with uncondensed DNA. This observation evidences the advantages of these implanted systems to overcome biological barriers in order to improve transfection efficiencies. Combinatorial chemistry has emerged as another potent tool for the design of new gene delivery systems (*203*). These methods can be used to model and predict the biological response of each compound in a combinatorial library, thereby avoiding the need to synthesize and evaluate each compound individually.

## Acknowledgments

This work was partially financed by the European Commission via ERA-NanoScience grant NanoTruck awarded to Dr. J.M. de la Fuente. This study is supported by ERC-Starting Grant 239931-NANOPUZZLE and the Spanish MEC project MAT2011-26851-C02-01. Jesus M. de la Fuente thanks ARAID for funding.

## References

1. Peer, D.; Karp, J. M.; Hong, S.; Farokhzad, O. C.; Margalit, R.; Langer, R. *Nat. Nanotechnol.* **2007**, *2*, 751–760.
2. Appell, D. *Nature* **2002**, *419*, 553–555.
3. LaVan, D. A.; McGuire, T.; Langer, R. *Nat. Biotechnol.* **2003**, *21*, 1184–1191.
4. Mironova, V.; Kasyanova, V.; Markwalda, R. R. *Trends Biotechnol.* **2008**, *26*, 338–344.
5. Kwon, Y.-W.; Lee, C. H.; Choi, D.-H.; Jin, J.-I. *J. Mater. Chem.* **2009**, *19*, 1353–1380.
6. Kawakami, S.; Higuchi, Y.; Hashida, M. *J. Pharm. Sci.* **2008**, *97*, 726–745.
7. Taniguchia, M.; Kawai, T. *Phys. E* **2006**, *33*, 1–12.
8. Deng, Z.; Mao, C. *Nano Lett.* **2003**, *3*, 1545–1548.
9. Abu-Salah, K. M.; Ansari, A. A.; Alrokayan, S. A. *J. Biomed. Biotechnol.* **2010**, 715295.
10. Aldaye, F. A.; Palmer, A. L.; Sleiman, H. F. *Science* **2008**, *321*, 1795–1799.
11. Dwyer, C.; Poulton, J.; Taylor, R.; Vicci, L. *Nanotechnology* **2004**, *15*, 1688.
12. Hwang, J. S.; Hwang, S. W.; Ahn, D. *Superlattices Microstruct.* **2003**, *34*, 433–438.
13. Hurst, S. J.; Lytton-Jean, A. K. R.; Mirkin, C. A. *Anal. Chem.* **2006**, *78*, 8313–8318.
14. McIntosh, C. M.; Esposito, E. A.; Boal, A. K.; Simard, J. M.; Martin, C. T.; Rotello, V. M. *J. Am. Chem. Soc.* **2001**, *123*, 7626–7629.

15. Pathak, S.; Choi, S. K.; Arnheim, N.; Thompson, M. E. *J. Am. Chem. Soc.* **2001**, *123*, 4103–4104.
16. Niemeyer, C. M.; Adler, M.; Gao, S.; Chi, L. *Angew. Chem., Int. Ed.* **2000**, *39*, 3056–3059.
17. Torimoto, T.; Yamashita, M.; Kuwabata, S.; Sakata, T.; Mori, H.; Yoneyama, H. *J. Phys. Chem. B* **1999**, *103*, 8799–8803.
18. Hahm, J. I.; Lieber, C. M. *Nano Lett.* **2004**, *4*, 51–54.
19. Zhao, X.; Tapec-Dytioco, R.; Tan, W. *J. Chem. Am. Soc.* **2003**, *125*, 11474–11475.
20. Dwyer, C.; Guthold, M.; Falvo, M.; Washburn, S.; Superfine, R.; Erie, D. *Nanotechnology* **2002**, *13*, 601–604.
21. Sanz, V.; Borowiak, E.; Lukanov, P.; Galibert, A. M.; Flahaut, E.; Coley, H. M.; Silva, S. R. P.; McFadden, J. *Carbon* **2011**, *49*, 1775–1781.
22. Hazani, M.; Naaman, R.; Hennrich, F.; Kappes, M. M. *Nano Lett.* **2003**, *3*, 153–155.
23. Dittmer, W. U.; Simmel, F. C. *Appl. Phys. Lett.* **2004**, *85*, 633–635.
24. Qamhieh, K.; Nylander, T.; Ainalem, M. L. *Biomacromolecules* **2009**, *10*, 1720–1726.
25. Shifrina, Z. B.; Kuchkina, N. V.; Rusanov, A. L.; Izumrudov, V. A. *Dokl. Chem.* **2007**, *416*, 213–216.
26. Jayakumar, R.; Chennazhi, K. P.; Muzzarelli, R. A. A.; Tamura, H.; Nair, S. V.; Selvamurugan, N. *Carbohydr. Polym.* **2010**, *79*, 1–8.
27. Li, W.; Szoka, F. C. *J. Pharm. Res.* **2007**, *24*, 438–449.
28. Shih, W. M.; Lin, C. *Curr. Opin. Struct. Biol.* **2010**, *20*, 276–282.
29. Rothemund, P. W. K. *Nature* **2006**, *440*, 297–302.
30. Alivisatos, A. P.; Johnsson, K. P.; Peng, X. G.; Wilson, T. E.; Loweth, C. J.; Bruchez, M. P.; Schultz, P. G. *Nature* **1996**, *382*, 609–611.
31. Pinto, Y. Y.; Le, J. D.; Seeman, N. C.; Musier-Forsyth, K.; Taton, A.; Kiehl, R. A. *Nano Lett.* **2005**, *5*, 2399–2402.
32. Zheng, J.; Constantinou, P. E.; Micheel, C.; Alivisatos, A. P.; Kiehl, R. A.; Seeman, N. C. *Nano Lett.* **2006**, *6*, 1502–1504.
33. Sharma, J.; Chhabra, R.; Liu, Y.; Ke, Y.; Yan, H. *Angew. Chem., Int. Ed.* **2006**, *45*, 730–735.
34. Yan, H.; Park, S. H.; Finkelstein, G.; Reif, J. H.; LaBean, T. H. *Science* **2003**, *301*, 1882–1884.
35. Douglas, S. M.; Chou, J. J.; Shih, W. M. *Proc. Natl. Acad. Sci. U.S.A.* **2007**, *104*, 6644–6648.
36. Endo, M.; Hidaka, K.; Kato, T.; Namba, K.; Sugiyama, H. *J. Am. Chem. Soc.* **2009**, *131*, 15570–15571.
37. Douglas, S. M.; Dietz, H.; Liedl, T.; Högberg, B.; Graf, F.; Shih, W. M. *Nature* **2009**, *459*, 414–418.
38. Andersen, E. S.; Dong, M.; Nielsen, M. M.; Jahn, K.; Subramani, R.; Mamdouh, W.; Golas, M. M.; Sander, B.; Stark, H.; Oliveira, C. L. P.; Pederson, J. S.; Birkedal, V.; Besenbacher, F.; Gothelf, K. V.; Kjems, J. *Nature* **2009**, *459*, 73–76.
39. Ke, Y.; Douglas, S. M.; Liu, M.; Sharma, J.; Cheng, A.; Leung, A.; Liu, Y.; Shih, W. M.; Yan, H. *J. Am. Chem. Soc.* **2009**, *131*, 15903–15908.

40. Dietz, H.; Douglas, S. M.; Shih, W. M. *Science* **2009**, *325*, 725–730.
41. Ke, Y.; Lindsay, S.; Chang, Y.; Liu, Y.; Yan, H. *Science* **2008**, *319*, 180–183.
42. Ke, Y.; Nangreave, J.; Yan, H.; Lindsay, S.; Liu, Y. *Chem. Commun.* **2008**, *43*, 5622–5624.
43. Barish, R. D.; Schulman, R.; Rothemund, P. W. K.; Winfree, E. *Proc. Natl. Acad. Sci. U.S.A.* **2009**, *106*, 6054–6059.
44. Fujibayashi, K.; Hariadi, R.; Park, S. H.; Winfree, E.; Murata, S. *Nano Lett.* **2008**, *8*, 1791–1797.
45. Shen, W.; Zhong, H.; Neff, D.; Norton, M. L. *J. Am. Chem. Soc.* **2009**, *131*, 6660–6661.
46. Stearns, L. A.; Chhabra, R.; Sharma, J.; Liu, Y.; Petuskey, W. T.; Yan, H.; Chaput, J. C. *Angew. Chem., Int. Ed.* **2009**, *48*, 8494–8496.
47. Steinhauer, C.; Jungmann, R.; Sobey, T. L.; Simmel, F. C.; Tinnefeld, P. *Angew. Chem., Int. Ed.* **2009**, *48*, 8870–8873.
48. Maune, H. T.; Han, S. P.; Barish, R. D.; Bockrath, M.; Goddard, W. A.; Rothemund, P. W. K.; Winfree, E. *Nat. Nanotechnol.* **2010**, *5*, 61–66.
49. Shi, J. F.; Bergstrom, D. E. *Angew. Chem., Int. Ed.* **1997**, *36*, 111–113.
50. Shchepinov, M. S.; Mir, K. U.; Elder, J. K.; Frank-Kamenetskii, M. D.; Southern, E. M. *Nucleic Acids Res.* **1999**, *27*, 3035–3041.
51. Scheffler, M.; Dorenbeck, A.; Jordan, S.; Wüstefeld, M.; von Kiedrowski, G. *Angew. Chem., Int. Ed.* **1999**, *38*, 3312–3315.
52. Wang, W.; Wan, W.; Zhou, H. H.; Niu, S.; Li, A. D. Q. *J. Am. Chem. Soc.* **2003**, *125*, 5248–5249.
53. Goritz, M.; Kramer, R. *J. Am. Chem. Soc.* **2005**, *127*, 18016–18017.
54. Chaput, J. C.; Switzer, C. *Proc. Natl. Acad. Sci. U.S.A.* **1999**, *96*, 10614–10619.
55. Yan, H.; Park, S. H.; Finkelstein, G.; Reif, J. H.; LaBean, T. H. *Science* **2003**, *301*, 1882–1884.
56. Aldaye, F. A.; Sleiman, H. F. *J. Am. Chem. Soc.* **2007**, *129*, 4130–4131.
57. Aldaye, F. A.; Sleiman, H. F. *J. Am. Chem. Soc.* **2007**, *129*, 13376–13377.
58. Chen, J. H.; Seeman, N. C. *Nature* **1991**, *350*, 631–633.
59. Goodman, R. P.; Heilemann, M.; Doose, S.; Erben, C. M.; Kapanidis, A. N.; Turberfield, A. J. *Nat. Nanotechnol.* **2008**, *3*, 93–96.
60. Park, S. Y.; Lytton-Jean, A. K. R.; Lee, B.; Weigand, S.; Schatz, G. C.; Mirkin, C. A. *Nature* **2008**, *451*, 553–556.
61. Nykypanchuk, D.; Maye, M. M.; van der Lelie, D.; Gang, O. *Nature* **2008**, *451*, 549–552.
62. Eskelinen, A. P.; Kuzyk, A.; Kaltiaisenaho, T. K.; Timmermans, M. Y.; Nasibulin, A. G.; Kauppinen, E. I.; Törm, P. *Small* **2011**, *7*, 746–750.
63. Gervasio, F. L.; Carloni, P.; Parrinello, M. *Phys. Rev. Lett.* **2002**, *89*, 108102–108106.
64. Fan, C.; Plaxco, K. W.; Heeger, A. J. *Proc. Natl. Acad. Sci. U.S.A.* **2003**, *100*, 9134–9137.
65. Fojta, M.; Kosteka, P.; Trefulka, M.; Havran, L.; Paleek, E. *Anal. Chem.* **2007**, *79*, 1022–1029.
66. Kjällman, T. H.; Peng, H.; Soeller, C.; Travas-Sejdic, J. *Analyst* **2010**, *135*, 488–494.

67. Zuo, X.; Song, S.; Zhang, J.; Pan, D.; Wang, L.; Fan, C. *J. Am. Chem. Soc.* **2007**, *129*, 1042–1043.
68. Liu, G.; Wan, Y.; Gau, V.; Zhang, J.; Wang, L.; Song, S.; Fan, C. *J. Am. Chem. Soc.* **2008**, *130*, 6820–6825.
69. Mao, Y.; Luo, C.; Ouyang, Q. *Nucleic Acids Res.* **2003**, *31*, e108.
70. Wei, F.; Wang, J.; Liao, W.; Zimmermann, B. G.; Wong, D. T.; Ho, C. M. *Nucleic Acids Res.* **2008**, *36*, e65.
71. Dirks, R. M.; Pierce, N. A. *Proc. Natl. Acad. Sci. U.S.A.* **2004**, *101*, 15275–15278.
72. Wang, J.; Kawde, A. N. *Electrochem. Commun.* **2002**, *4*, 349–352.
73. Zhu, N.; Zhang, A.; He, P.; Fang, Y. *Electroanalysis* **2004**, *16*, 1925–1930.
74. Cai, H.; Xu, Y.; Zhu, N.; He, P.; Fang, Y. *Analyst* **2002**, *127*, 803–808.
75. Zhu, N.; Zhang, A.; Wang, Q.; He, P.; Fang, Y. *Electroanalysis* **2004**, *16*, 577–582.
76. Pumera, M.; Castaneda, M. T.; Pividori, M. I.; Eritja, R.; Merkoci, A.; Alegret, S. *Langmuir* **2005**, *21*, 9625–9629.
77. Wang, J.; Liu, G.; Merkoçi, A. *J. Am. Chem. Soc.* **2003**, *125*, 3214–3215.
78. Luo, X.; Morrin, A.; Killard, A. J.; Smyth, M. R. *Electroanalysis* **2006**, *18*, 319–326.
79. Herne, T. M.; Tarlov, M. J. *J. Am. Chem. Soc.* **1997**, *119*, 8916–8920.
80. Zhang, J.; Lao, R.; Song, S.; Yan, Z.; Fan, C. *Anal. Chem.* **2008**, *80*, 9029–9033.
81. Li, D.; Song, S.; Fan, C. *Acc. Chem. Res.* **2010**, *43*, 631–641.
82. Li, J.; Song, S.; Liu, X.; Wang, L.; Pan, D.; Huang, Q.; Zhao, Y.; Fan, C. *Adv. Mater.* **2008**, *20*, 497–500.
83. Wang, J.; Xu, D.; Kawde, A.-N.; Polsky, R. *Anal. Chem.* **2001**, *73*, 5576–5581.
84. Erdem, A.; Pividori, M. I.; Lermo, A.; Bonanni, A.; del Valle, M.; Alegret, S. *Sens. Actuators, B* **2006**, *114*, 591–598.
85. Wang, J.; Xu, D.; Erdem, A.; Polsky, R.; Salazar, M. A. *Talanta* **2002**, *56*, 931–938.
86. Wang, J.; Liu, G. D.; Jan, M. R. *J. Am. Chem. Soc.* **2004**, *126*, 3010–3011.
87. Tang, X.; Bansaruntip, S.; Nakayama, N.; Yenilmez, E.; Chang, Y. L.; Wang, Q. *Nano Lett.* **2006**, *6*, 1632–1636.
88. So, H. M.; Won, K.; Kim, Y. H.; Kim, B. K.; Ryu, B. H.; Na, P. S.; Kim, H.; Lee, J. O. *J. Am. Chem. Soc.* **2005**, *127*, 11906–11907.
89. Star, A.; Tu, E.; Niemann, J.; Gabriel, J. C. P.; Joiner, C. S.; Valcke, C. *Proc. Natl. Acad. Sci. U.S.A.* **2006**, *103*, 921–926.
90. Byon, H. R.; Choi, H. C. *J. Am. Chem. Soc.* **2006**, *128*, 2188–2189.
91. Lu, F.; Gu, L.; Meziani, M. J.; Wang, X.; Luo, P. G.; Veca, L. M.; Cao, L.; Sun, Y. P. *Adv. Mater.* **2009**, *21*, 139–152.
92. Marie, R.; Jensenius, H.; Thaysen, J.; Christensen, C. B.; Boisen, A. *Ultramicroscopy* **2002**, *91*, 29–36.
93. Hansen, K. M.; Ji, H. F.; Wu, G.; Datar, R.; Cote, R.; Majumdar, A.; Thundat, T. *Anal. Chem.* **2001**, *73*, 1567–1571.

94. McKendry, R.; Zhang, J.; Arntz, Y.; Strunz, T.; Hegner, M.; Lang, H. P.; Baller, M. K.; Certa, U.; Meyer, E.; Güntherodt, H. J.; Gerber, C. *Proc. Natl. Acad. Sci. U.S.A.* **2002**, *99*, 9783–9788.
95. Bietsch, A.; Zhang, J.; Hegner, M.; Lang, H. P.; Gerber, C. *Nanotechnology* **2004**, *15*, 873–880.
96. Su, M.; Li, S.; Dravid, V. P. *Appl. Phys. Lett.* **2003**, *82*, 3562–3565.
97. Elghanian, R.; Storhoff, J. J.; Mucic, R. C.; Letsinger, R. L.; Mirkin, C. A. *Science* **1997**, *277*, 1078–1080.
98. He, L.; Musick, M. D.; Nicewarner, S. R.; Salinas, F. G.; Benkovic, S. J.; Natan, M. J.; Keating, C. D. *J. Am. Chem. Soc.* **2000**, *122*, 9071–9077.
99. Jin, R.; Wu, G.; Li, Z.; Mirkin, C. A.; Schatz, G. C. *J. Am. Chem. Soc.* **2003**, *125*, 1643–1654.
100. Storhoff, J. J.; Elghanian, R.; Mucic, R. C.; Mirkin, C. A.; Letsinger, R. L. *J. Am. Chem. Soc.* **1998**, *120*, 1959–1964.
101. Cao, Y. W.; Jin, R.; Mirkin, C. A. *J. Am. Chem. Soc.* **2001**, *123*, 7961–7962.
102. Reynolds, R. A., III; Mirkin, C. A.; Letsinger, R. L. *J. Am. Chem. Soc.* **2000**, *122*, 3795–3796.
103. Brown, P. O.; Botstein, D. *Nature Genetics* **1999**, *21*, 33–37.
104. Taton, T. A.; Mirkin, C. A.; Letsinger, R. L. *Science* **2000**, *289*, 1757–1760.
105. Bao, Y. P.; Huber, M.; Wei, T. F.; Marla, S. S.; Storhoff, J. J.; Müller, U. R. *Nucleic Acids Res.* **2005**, *33*, e15.
106. Chu, X.; Fu, X.; Chen, K.; Shen, G. L.; Yu, R. Q. *Biosens. Bioelectron.* **2005**, *20*, 1805–1812.
107. Park, S. J.; Taton, T. A.; Mirkin, C. A. *Science* **2002**, *295*, 1503–1506.
108. Demers, L. M.; Ginger, D. S.; Park, S. J.; Li, Z.; Chung, S. W.; Mirkin, C. A. *Science* **2002**, *296*, 1836–1838.
109. Cao, Y. W. C.; Jin, R. C.; Mirkin, C. A. *Science* **2002**, *297*, 1536–1540.
110. Maxwell, D. J.; Taylor, J. R.; Nie, S. *J. Am. Chem. Soc.* **2002**, *124*, 9606–9612.
111. Fang, X.; Li, J. J.; Perlette, J.; Tan, W.; Wang, K. *Anal. Chem.* **2000**, *72*, 747A–753A.
112. Fang, X.; Liu, X.; Schuster, S.; Tan, W. *J. Am. Chem. Soc.* **1999**, *121*, 2921–2922.
113. Mao, X.; Xu, H.; Zeng, Q.; Zeng, L.; Liu, G. *Chem. Commun.* **2009**, *21*, 3065–3067.
114. Niemeyer, M. C.; Adler, M. *Angew. Chem., Int. Ed.* **2002**, *41*, 3779–3783.
115. Yeh, H. Y.; Yates, M. V.; Mulchandani, A.; Chen, W. *Chem. Commun.* **2010**, *46*, 3914–3916.
116. Jeng, E. S.; Moll, A. E.; Roy, A. C.; Gastala, J. B.; Strano, M. S. *Nano Lett.* **2006**, *6*, 371–375.
117. Peng, H.; Zhang, L.; Kjällman, T. H. M.; Soeller, C.; Travas-Sejdic, J. *J. Am. Chem. Soc.* **2007**, *129*, 3048–3049.
118. Robelek, R.; Niu, L.; Schmid, E. L.; Knoll, W. *Anal. Chem.* **2004**, *76*, 6160–6165.
119. Nam, J. M.; Thaxton, C. S.; Mirkin, C. A. *Science* **2003**, *301*, 1884–1886.
120. Nam, J. M.; Stoeva, S. I.; Mirkin, C. A. *J. Am. Chem. Soc.* **2004**, *126*, 5932–5933.

121. Endo, T.; Kerman, K.; Nagatani, N.; Takamura, Y.; Tamiya, E. *Anal. Chem.* **2005**, *77*, 6976–6984.
122. Li, Y.; Lee, H. J.; Corn, R. M. *Anal. Chem.* **2007**, *79*, 1082–1088.
123. Ellington, A. D.; Szostak, J. W. *Nature* **1990**, *346*, 818–822.
124. Zayats, M.; Huang, Y.; Gill, R.; Ma, C. A.; Willner, I. *J. Am. Chem. Soc.* **2006**, *128*, 13666–13667.
125. Wanga, G.; Wanga, Y.; Chena, L.; Choo, J. *Biosens. Bioelectron.* **2010**, *25*, 1859–1868.
126. Medley, C. D.; Smith, J. E.; Tang, Z. W.; Wu, Y. R.; Bamrungsap, S.; Tan, W. T. *Anal. Chem.* **2008**, *80*, 1067–1072.
127. Wang, W.; Chen, C.; Qian, M.; Zhao, X. S. *Anal. Biochem.* **2008**, *373*, 213–219.
128. Cheng, A. K. H.; Su, H.; Wang, Y. A.; Yu, H. Z. *Anal. Chem.* **2009**, *81*, 6130–6139.
129. Yigit, M. V.; Mazumdar, D.; Lu, Y. *Bioconjugate Chem.* **2008**, *19*, 412–417.
130. Song, Y.; Zhao, C.; Ren, J.; Qu, X. *Chem. Commun.* **2009**, *15*, 1975–1977.
131. Breaker, R. R. *Nature* **2004**, *432*, 838–845.
132. Liu, J. W.; Lu, Y. *J. Fluoresc.* **2004**, *14*, 343–354.
133. Liu, J.; Lu, Y. *J. Am. Chem. Soc.* **2003**, *125*, 6642–6643.
134. Shaikh, K. A.; Ryu, K. S.; Goluch, E. D.; Nam, J. M.; Liu, J.; Thaxton, C. S.; Chiesl, T. N.; Barron, A. E.; Lu, Y.; Mirkin, C. A.; Liu, C. *Proc. Natl. Acad. Sci. U.S.A.* **2005**, *102*, 9745–9750.
135. Chen, Y.; Wang, M.; Mao, C. *Angew. Chem., Int. Ed.* **2004**, *43*, 3554–3557.
136. Chen, Y.; Mao, C. *J. Am. Chem. Soc.* **2004**, *126*, 8626–8627.
137. Tian, Y.; He, Y.; Chen, Y.; Yin, P.; Mao, C. *Angew. Chem., Int. Ed.* **2005**, *44*, 4355–4358.
138. Soukup, G. A.; Breaker, R. R. *Trends Biotechnol.* **1999**, *17*, 469–476.
139. Liu, J.; Lu, Y. *Anal. Chem.* **2004**, *76*, 1627–1632.
140. Wang, D. Y.; Lai, B. H. Y.; Sen, D. *J. Mol. Biol.* **2002**, *318*, 33–43.
141. Herweijer, H.; Wolff, J. A. *Gene Therapy* **2003**, *10*, 453–458.
142. Kay, M. A.; Glorioso, J. C.; Naldini, L. *Nat. Med.* **2001**, *7*, 33–40.
143. Kreppel, F.; Kochanek, S. *Mol. Ther.* **2007**, *16*, 16–29.
144. Bergelson, J. M.; Cunningham, J. A.; Droguett, G.; Kurt-Jones, E. A.; Krithivas, A.; Hong, J. S.; Horwitz, M. S.; Crowell, R. L.; Finberg, R. W. *Science* **1997**, *275*, 1320–1323.
145. Parrott, M. B.; Adams, K. E.; Mercier, G. T.; Mok, H.; Campos, S. K.; Barry, M. A. *Mol. Ther.* **2000**, *1*, 96–104.
146. Pack, D. W.; Hoffman, A. S.; Pun, S.; Stayton, P. *Nat. Rev. Drug Discovery* **2005**, *4*, 581–593.
147. Farhood, H.; Sebina, N.; Huang, L. *Biochim. Biophys. Acta, Biomembr.* **1995**, *1235*, 289–295.
148. Sakurai, F.; Nishioka, T.; Yamashita, F.; Takakura, Y.; Hashida, M. *Eur. J. Pharm. Biopharm.* **2001**, *52*, 165–172.
149. Guillaume, C.; Delépine, P.; Droal, C.; Montier, T.; Tymen, G.; Glaude, F. *Biochem. Biophys. Res. Commun.* **2001**, *286*, 464–471.
150. Nam, H. Y.; Park, J. H.; Kim, K.; Kwon, I. C.; Jeong, S. Y. *Arch. Pharm. Sci. Res.* **2009**, *32*, 639–646.

151. Joshi, M. D.; Müller, R. H. *Eur. J. Pharm. Biopharm.* **2009**, *71*, 161–172.
152. Khalil, I. A.; Kogure, K.; Futaki, S.; Harashima, H. *J. Biol. Chem.* **2006**, *281*, 3544–3551.
153. Boussif, O.; Lezoualc'h, F.; Zanta, M. A.; Mergny, M. D.; Scherman, D.; Demeneix, B.; Behr, J. PO. *Proc. Natl. Acad. Sci. U.S.A.* **1995**, *92*, 7297–7301.
154. Park, T. G.; Jeong, J. H.; Kim, S. W. *Adv. Drug Delivery Rev.* **2006**, *58*, 467–468.
155. Benns, J. M.; Choi, J. S.; Mahato, R. I.; Park, J. S.; Kim, S. W. *Bioconjugate Chem.* **2000**, *11*, 637–645.
156. Pack, D. W.; Putnam, D.; Langer, R. *Biotechnol. Bioeng.* **2000**, *67*, 217–223.
157. Köping-Höggard, M.; Tubulekas, I.; Guan, H.; Edwards, K.; Nilsson, M.; Varum, K. M.; Artursson, P. *Gene Ther.* **2001**, *8*, 1108–1121.
158. Davis, M. E.; Bellocq, N. C. *J. Inclusion Phenom. Macrocyclic Chem.* **2002**, *44*, 17–22.
159. Pun, S. H.; Davis, M. *Bioconjugate Chem.* **2002**, *13*, 630–639.
160. Lim, Y. B.; Kim, S. M.; Lee, Y.; Lee, W.-K.; Yang, T. G.; Lee, M.-J.; Suh, H.; Park, J.-S. *J. Am. Chem. Soc.* **2001**, *123*, 2460–2461.
161. Morris, M. C.; Chaloin, L.; Heitz, F.; Divita, G. *Curr. Opin. Biotechnol.* **2000**, *11*, 461–466.
162. Bulmus, V.; Woodward, M.; Lin, L.; Stayton, P. S.; Hoffman, A. S. *J. Controlled Release* **2003**, *93*, 105–120.
163. Dufès, C.; Uchegbu, I. F.; Schätzlein, A. G. *Adv. Drug Delivery Rev.* **2005**, *57*, 2177–2202.
164. Morille, M.; Passirani, C.; Vonarbourg, A.; Clavreul, A.; Benoit, J. P. *Biomaterials* **2008**, *29*, 3477–3496.
165. Dandu, R.; Ghandehari, H. *Prog. Polym. Sci.* **2007**, *32*, 1008–1030.
166. Haider, H.; Hatefi, A.; Ghandehari, H. *J. Controlled Release* **2005**, *109*, 108–119.
167. Read, M. L.; Bremner, K. H.; Oupicky, D.; Green, N. K.; Searle, P. F.; Seymour, L. W. *J. Gene Med.* **2003**, *5*, 232–245.
168. Chen, T. H. H.; Bae, Y.; Furgeson, D. Y. *Pharm. Res.* **2008**, *25*, 683–691.
169. Guo, W. J.; Lee, R. J. *Biosci. Rep.* **2000**, *20*, 419–432.
170. Ghosh, P. S.; Kim, C. K.; Han, G.; Forbes, N. S.; Rotello, V. M. *ACS Nano* **2008**, *25*, 2213–2218.
171. Guo, S.; Huang, Y.; Jiang, Q.; Sun, Y.; Deng, L.; Liang, Z.; Du, Q.; Xing, J.; Zhao, Y.; Wang, P. C.; Dong, A.; Liang, X. J. *ACS Nano* **2010**, *4*, 5505–5511.
172. Rhim, W. K.; Kim, J. S.; Nam, J. M. *Small* **2008**, *4*, 1651–1655.
173. Thomas, M.; Klibanov, A. M. *Proc. Natl. Acad. Sci. U.S.A.* **2003**, *100*, 9138–9143.
174. Sameli, K. A.; Searson, P. C.; Leong, K. W. *Nat. Mater.* **2003**, *2*, 668–671.
175. Chen, C. C.; Liu, Y. C.; Wu, C. H.; Yeh, C. C.; Su, M. T.; Wu, Y. C. *Adv. Mater.* **2005**, *17*, 404–407.
176. Chen, A. A.; Derfus, A. M.; Khetani, S. R.; Bhatia, S. N. *Nucleic Acids Res.*, *33*, e190.
177. Yezhelyev, M. V.; Qi, L.; O'Regan, R. M.; Nie, S.; Gao, X. *J. Am. Chem. Soc.* **2008**, *130*, 9006–9012.

178. Jia, N.; Lian, Q.; Shen, H.; Wang, C.; Li, X.; Yang, Z. *Nano Lett.* **2007**, *7*, 2976–2980.
179. Dobson, J. *Gene Ther.* **2006**, *13*, 283–287.
180. Choi, H.; Choi, S. R.; Zhou, R.; Kung, H. F.; Chen, I.-W. *Academic Radiology* **2004**, *11*, 996–1004.
181. Singh, R.; Pantarotto, D.; McCarthy, D.; Chaloin, O.; Hoebeke, J.; Partidos, C. D.; Briand, J. P.; Prato, M.; Kostarelos, K. *J. Am. Chem. Soc.* **2005**, *127*, 4388–4396.
182. Baker, S. E.; Cai, W.; Lasseter, T. L.; Weidkamp, K. P.; Hammers, R. J. *Nano Lett.* **2002**, *2*, 1413–1417.
183. Pantarotto, D.; Singh, R.; McCarthy, D.; Erhard, M.; Briand, J. P.; Prato, M.; Kostarelos, K.; Bianco, A. *Angew. Chem., Int. Ed.* **2004**, *43*, 5242–5246.
184. Gao, L.; Nie, L.; Wang, T.; Qin, Y.; Guo, Z.; Yang, D.; Yan, X. *ChemBioChem* **2005**, *7*, 239–242.
185. Shang, Z.; Yang, X.; Zhang, Y.; Zeng, B.; Wang, S.; Zhu, T.; Roden, R. B. S.; Chen, Y.; Yang, R. *Clin. Cancer Res.* **2006**, *12*, 4933–4939.
186. Kam, N. W. S.; Liu, Z.; Dai, H. *J. Am. Chem. Soc.* **2005**, *127*, 12492–12493.
187. Cai, D.; Huang, Z.; Carnahan, D.; Mataraza, J. M.; Chiles, T. C.; Qin, Z. H.; Huang, J.; Kempa, K.; Ren, Z. *Nat. Methods* **2005**, *2*, 449–454.
188. Dash, P. R.; Read, M. L.; Barrett, L. B.; Wolfert, M. A.; Seymour, L. W. *Gene Ther.* **1999**, *6*, 643–650.
189. Romberg, B.; Hennink, W. E.; Storm, G. *Pharm. Res.* **2008**, *25*, 55–71.
190. Ganta, S.; Devalapally, H.; Shahiwala, A.; Amiji, M. *J. Controlled Release* **2008**, *126*, 187–204.
191. Saito, G.; Swanson, J. A.; Lee, K. D. *Adv. Drug Delivery Rev.* **2003**, *55*, 199–215.
192. Koblinski, J. E.; Ahram, M.; Sloane, B. F. *Clin. Chim. Acta* **2000**, *291*, 113–135.
193. Vihinen, P.; Kähäri, V. M. *Int. J. Cancer* **2002**, *99*, 157–166.
194. Fischer, D.; Li, Y.; Ahlemeyer, B.; Krieglstein, J.; Kissel, T. *Biomaterials* **2003**, *24*, 1121–1131.
195. Schätzlein, A. G. *J. Biomed. Biotechnol.* **2003**, *2003*, 149–158.
196. Howl, J.; Nicholl, I. D.; Jones, S. *Biochem. Soc. Trans.* **2007**, *35*, 767–769.
197. Escriou, V.; Carrière, M.; Scherman, D.; Wils, P. *Adv. Drug Delivery Rev.* **2003**, *55*, 295–306.
198. Grosse, S.; Aron, Y.; Honoré, I.; Thévenot, G.; Danel, C.; Roche, A. C.; Monsigny, M.; Fajac, I. *J. Gene Med.* **2004**, *6*, 345–356.
199. Pollard, H.; Remy, J. S.; Loussouarn, G.; Demolombe, S.; Behr, J. P.; Escande, D. *J. Biol. Chem.* **1998**, *273*, 7507–7511.
200. Alarcon, C. D. L. H.; Pennadam, S.; Alexander, C. *Chem. Soc. Rev.* **2005**, *34*, 276–285.
201. Saito, G.; Swanson, J. A.; Lee, K. D. *Adv. Drug Delivery Rev.* **2003**, *55*, 199–215.
202. Shea, L. D.; Smiley, E.; Bonadio, J.; Mooney, D. J. *Nat. Biotechnol.* **1999**, *17*, 551–554.
203. Green, J. J.; Langer, R.; Anderson, D. G. *Acc. Chem. Res.* **2008**, *41*, 749–759.

## Chapter 13

# Nanobased Technological Applications for Central Nervous System Injuries

**Ana Dede, Yuan Yin, and Anjana Jain***

**Biomedical Engineering Department, Worcester Polytechnic Institute,**
**100 Institute Road, Worcester, Massachusetts 01605**
***E-mail: ajain@wpi.edu**

Injuries to the central nervous system (CNS) can have long-term devastating consequences. Due to the permanent loss of motor, sensory and cognitive function, it has become imperative to develop diagnostic technology that can identify the degree of injury prior to significant loss of neurons and function. The development of diagnostic and therapeutic strategies for CNS injuries has predominantly been nano-technologically based. This chapter discusses the current technologies being researched for diagnostics and therapeutics.

## Introduction

Nano-based technology has significant implications in promoting neuroprotection and repair after injury to the central nervous system (CNS). The CNS is responsible for processing critical information from sensory receptors throughout the body, as well as directing all somatic and autonomic actions, including the control of motor and cognitive functions. The CNS is incapable of spontaneous regeneration; therefore injuries result in permanent neuronal loss leading to deficits in motor and cognitive function which impact a person's quality of life (*1*). This chapter will focus on the nano-strategies utilized for diagnostics and treatment after trauma to the CNS, particularly spinal cord injury (SCI) and traumatic brain injury (TBI).

It is estimated that 12,000 new patients suffer from SCI every year in the United States with most injuries occurring between the ages of 16 and 30 (*2*). The lifetime treatment cost for patients varies according to the severity of injury. For tetraplegia, the lifetime cost accumulates over $4 billion, considering an injury

In Nanomaterials for Biomedicine; Nagarajan, R.;
ACS Symposium Series; American Chemical Society: Washington, DC, 2012.

at 25 years of age. The lifetime cost of paraplegias at the same age is over $2 billion (*2*). In 2005, about 40% of reported SCI cases had occurred from vehicular accidents while about 30% are a result of falls. Sports-related injuries consist of 10% of all cases, and have become more prevalent in the recent years (*2*).

For TBI, there are approximately 1.7 million documented cases every year and approximately 15-20% of these individuals will suffer from long-term disabilities (*3*). In the U.S., it is the leading cause of morbidity and mortality in individuals under the age of 45 (*3*, *4*). Two percent of the population in the US lives with disabilities resultant from TBI and 52,000 deaths are attributed to TBI annually, costing $56 billion dollars each year (*5*). The most common causes of TBI include motor vehicle incidents, sports related injuries, and falls (*3*). Additionally, TBI is a common occurrence in combat due to the shrapnel and the concussive force of blast related injuries. It has been reported that 18% of all soldiers returning from active duty have suffered some degree of TBI (*4*). It is imperative to develop diagnostics and therapeutic strategies to repair the devastating permanent consequences of CNS injuries.

## Pathology of CNS Injury

The progression of SCI and TBI occurs in two stages, referred to as the initial injury and secondary injury. The initial physical insult encompasses the acute damage that results from mechanical trauma, during which there is an immediate loss of cells mainly by necrosis (*6*). The secondary injury includes a cascade of events leading to further neuronal loss (*7*). It is the misregulation of the microenvironment that exacerbates the local cellular loss, causing permanent impairment of cognitive and motor function (*6*, *8–10*). Persistent cellular loss in the form of apoptosis is present in the secondary injury and it is one of the most important factors in mediating further damage after injury (*11*).

This damage is perpetuated by the body's own immune and wounding healing response. Directly after injury, the extravasation of T leukocytes in the CNS parenchymal causes the activation of endogenous microglia and astrocytes (*12*). Resident microglia have a similar role as migrating macrophages in the CNS. Once activated by the incorporation of MHC class I/II proteins, these cells gain the ability to directed endocytosis of apoptotic cells and other debris, as well as the ability to secrete pro-inflammatory factors, leading to additional microglia aggregation and activation (*13*). The combination of activated microglia and migrated macrophages secreting various bioactive molecules activates intrinsic and extrinsic apoptosis cascades resulting in further neuronal loss after injury (*14*).

Furthermore, the formation of the glial scar that occurs within the CNS prevents axonal outgrowth by both physical and chemical inhibition. Astrogliosis, otherwise known as the activation and proliferation of resident astrocytes by macrophages and T leukocytes, contributes to the majority of the glial scar (*15*). The development of astrogliosis and additional secretion of neuronal growth inhibitors, such as chondroitin sulfate proteoglycans (CSPGs), the activation of the reactive astrocytes causes significant inhibition of neuronal regeneration and outgrowth (*16*). Additional molecular mediators found in high concentrations near the injury cite, like the family of transforming growth factor β (TGF-β) continue to stimulate reactive astrocytes and other immune cells to release proteoglycans (*17*). This cascade not only creates an environment rich in inhibitory molecules, but with significant secretion and modifications to the extracellular matrix (ECM), creating a physical barrier for axonal outgrowth. These pro-apoptotic conditions after injury present a significant challenge when developing a treatment strategy.

Another aspect that makes managing the CNS injury a complex challenge is the physical isolation of the tissue from the systemic circulation. The brain and spinal cord are restricted from the blood flow through the blood-brain-barrier (BBB) and blood-spinal-cord-barrier (BSCB), which are formed through tight junctions of endothelial cells (*18*). In normal physiology these barriers serve a protective role to allow for high selectivity of agents found in the blood (*19*, *20*). However, in the treatment of the injury this creates additional challenges in the delivery of therapeutic agents through conventional routes like systemic injection.

This intricate pathology of CNS injury highlights the need for 1) diagnostics that are able to track the progression of not only the initial insult, but also of the secondary injury, and 2) targeted treatment modalities capable of reaching the site of injury.

## Current Diagnostics and Treatments

While medicine has significantly evolved in recent years, clinical diagnostic procedures and therapeutic approaches for CNS injuries have remained relatively unchanged. Several scoring systems continue to be the standard method for assessing the condition of the CNS, such as the Glasgow Coma Scale, ASIA impairment scale, and the Rancho Los Amigos Scale (*21–23*). However, these rating systems only assess the degree of cognitive and functional loss at the time of initial diagnosis, and offer no conclusive strategy to depict the prognosis of the injury and monitor its development. Like current diagnostic systems, current clinical interventions for the treatment of CNS injuries only target the acute damage and presenting symptoms. Surgical procedures are performed to relieve intracranial or vertebral pressure, to remove any penetrating debris, and to stabilize the tissue (*24*, *25*). Though these procedures prevent further damage to the CNS, they fail to address the irreversible functional and cognitive deficits that arise during the secondary injury phase. Furthermore, diuretics, steroids, anti-inflammatory agents, and other pharmaceuticals are administered to reduce the negative effects of the immune system response (*26*). However, this approach faces several drastic limitations in: 1) the amount of therapeutic agents that can reach the site, 2) the timeframe during which therapeutics can be effectively delivered, and 3) the methods of delivery available to healthcare providers treating CNS injuries. These factors show a clinical need for diagnostic tools that allow monitoring of the progression of the injury, and for effective therapeutic delivery systems capable of suppressing further damage and allowing for regeneration.

## Nanotechnology-Based Diagnostics for CNS injuries

Diagnostic tools are necessary to accurately assess and monitor after injury and for progression of the secondary injury. Recent advancements in nano-scale sensors, electronics, and molecular contrast agents have allowed for the development of such tools with promising results.

## Biosensors for Diagnostics

One of the biggest challenges of monitoring patients with CNS injuries is the inability to predict the onset and progression of the secondary cascade, which can arise, days to weeks after the initial damage. Continuous monitoring after injury allows for immediate therapeutic administration to minimize neuronal loss (*27–30*). For patients with severe CNS injuries, besides the visible and immediate symptoms, monitoring can be achieved with invasive cerebral microdialysis, where a catheter is directly inserted in the cerebrospinal fluid (CSF) at the injury site to continually sample the CSF for specified agents (*28*, *31*, *32*). Monitoring levels of oxygenation, temperature, pH, and other parameters change due to CNS injury allows for appropriate therapeutic intervention and the ability to provide a detailed prognosis for each patient. However, this technique cannot be applied towards patients suffering from mild or moderate injury, as they do not exhibit symptoms immediately from their injury. Therefore, these patients would benefit from a continuous monitoring system for slowly developing symptoms that have equally damaging effects.

The implantable biosensor; a nanotechnology based platform, recently developed for use in minimally invasive measuring of different physiological parameters, such as metabolite levels, pressure, gas exchange, temperature, and electrical signaling (*33*). Utilizing photoelectrical, piezoelectric, electrochemical, and other detection methods, biosensors are able to convert distinct biological readings into measurable and quantifiable data (*34–36*). For example, a novel biosensor based on a lab-on-a-tube spiral design, compacts multiple sensors, capable of measuring pH, oxygen, pressure, and other analytes in an attempt to diagnose and provide an accurate prognosis for CNS injury patients (*37*, *38*).

For temperature, thin-film transistor temperature sensors are locally implanted within the brain to measure temperature changes that result directly from neuronal activity and cerebral blood flow (*39*). Continuous blood pH monitoring of patients has been used to the viability of injured brain tissue (*39*). Fiber optic and electrochemical sensors have been found to accurately measure pH levels when implanted in the brains of Sprague-Dawley rats (*40*). Utilizing an oxidation-reduction reaction of an analyte, the electricochemical biosensor is capable of collecting electrical signals proportional to the concentration of the specified analyte (*41*). Amperometric adenosine biosensors with xanthine oxidase, purine nucleoside phosphorlase, and adenosine deaminase integrated on a platinum electrode have also been able to measure the changes in ATP energy metabolism within the CNS (*42*). When implanted in the spinal cord of Xenopus embryo the biosensor showed localization and concentration of ATP, with 100% activity after 5 days of implantation. Additionally, recent development of a platinum microelectrode with glucose oxidase immobilized on the surface was found to have 100% recovery of analyte *in vitro,* and when implanted into the rat brain it was seen to have high sensitivity to glucose, limited bio-fouling, and minimal interference (*43–46*). For measurements based on enzymatic reactions, this is accomplished by measuring electrons utilized during the reduction of flavin adenine dinucleotide (FAD) and the further reduction of oxygen to hydrogen peroxide (*47*). Utilizing these strategies, it is possible to create a monitoring biosensor for parameters implicated in CNS injury, allowing for on-demand monitoring and accurate prognosis.

## Nanotechnology for Diagnostic Imaging

Another diagnostic modality for CNS injuries utilizes clinical imaging applications. The release of inhibitory chemical cues and the influx of compounds that are normally restricted through the BBB and BSCB, further exacerbate cellular loss in the local populations (*48*). By utilizing MRI contrast agents like the ones represented in Figure 1 to target specific receptors, molecules, or other antagonists present in the injury site, it is possible to track the progression of the injury, deliver therapeutic interventions, and provide a better prognosis for CNS injuries.

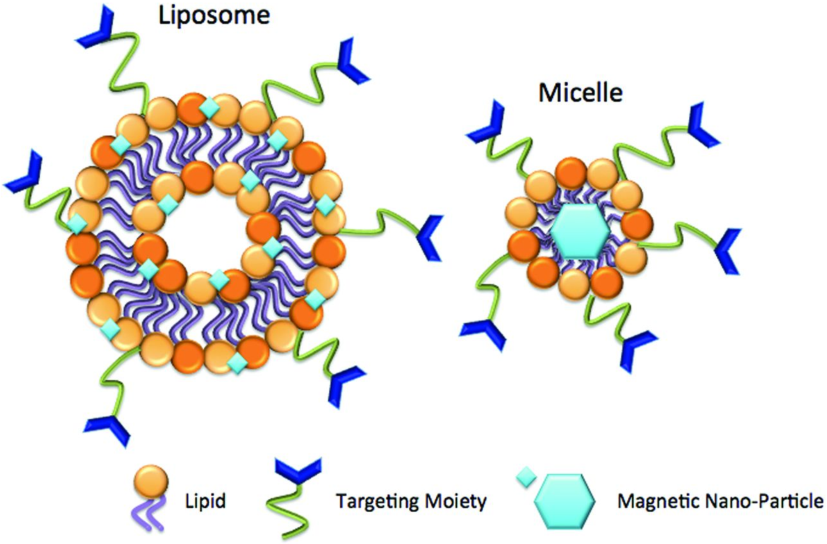

*Figure 1. Schematic of nanotechnology based molecular contrast agents. Paramagnetic liposome contrast agent and superparamagnetic micelle contrast agent, both with targeting moiety capabilities.*

Current standards used for diagnostics for patients with CNS injuries include imaging techniques such as X-ray computed tomography (CT), magnetic resonance imaging (MRI) and ultrasound. These modalities are able to detect the fracture, laceration or penetrating damage in the initial insult. However, these tools are not able to track the progression of the secondary damage, nor the type of damage that is occurring, such as the effected cell type. The advances in biocompatible nanotechnology and nanomaterials have allowed for the development of imaging modalities based on molecular contrast agents designed to have low cellular toxicity, to increase circulation time, and to allow for selective targeting (*49*). Moieties including liposomes, dendrimers, and other polymers can be combined with paramagnetic, superparamagnetic metallic agents, radioactive markers, and even fluorescent agents to allow for the development of *in vivo* imaging systems (*50–52*).

The most recent injectable contrast agents have both positive "hot spot" and negative "cold spot" enhancement capabilities; increasing imaging resolution of the target of interest, as well as increasing imaging enhancement of the surrounding tissue respectively. The most common types of non-targeted modalities are based on gadolinium; a paramagnetic contrast agent that allows for positive enhancement (*53*). Furthermore, superparamagnetic agents like super iron oxides (SPIO) increase relaxation times in the surrounding areas and tissue, allowing for negative enhancement at the site of interest (*54*). For example, nonspecific SPIO nanoparticles are preferentially phagocytosed by macrophages and are utilized for the assessment of general inflammation through the tracking of macrophage infiltration into brain tissue (*55*). Additionally, dextran-coated SPIO and micelle formulations allows for faster clearance and less internal aggregation (*56*). Binding ferromagnetic conjugants to polyamidoamine dendrimers also showed promising results in enhancing MRI imaging, while preventing the toxic effects of high concentrations of the chelates (*56*).

Initial research into creating targeted contrast agents for MRI relied on direct conjugation of chelate to antibodies, but offered minimal gains in image enhancement (*57*). It was found that the incorporation of multiple *d*iethylene*t*riamine*p*ent*a*cetate (Gd-DTPA) chelates in liposomes allowed for a significant increase in positive image enhancement, while still maintaining a low concentration (*58*). Utilizing this targeted contrast approach, researchers conjugated the Abetal-40 peptide to SPIO nanoparticles to generate enhancement of lesions within the brain after transient opening of the BBB with mannitonl (*59*). The 100-200nm diameter of liposome, micelle and dendrimer-based contrast agents allows for extravasation into injury sites. The increased half-life allows for image enhancement of down to the micron level and even single cell resolution capabilities. These types of nanotechnology-based contrast agents allow for the tracking of specific markers, agents, and cells implicated in the secondary injury cascade in the CNS injury.

## Nanotechnology-Based Treatments for CNS Injury

Aside from diagnostics, the field of nanotechnology has created a field of strategy regimes for CNS injury. Altering and enhancing biocompatible materials on the nanoscale has led to the formulation of different approaches to protect the undamaged surrounding cells and the creation of new neuronal networks that aid in regaining function.

An experimental approach for the reconstruction and regeneration of the damaged spinal cord and brain utilizes bioscaffolds (*60*, *61*). Two main categories of bioscaffolds that are relevant to the nervous system are: 1) hydrogels, which are crosslinked polymer networks, and 2) fibrous scaffolds, which are networks formed with interconnected fibers. These constructs are designed to support cellular migration, axonal extension, cell transplantation, and/or as drug delivery systems. The main goal of using a scaffold is to provide the advantage of bridging the gap created by the CNS injury, as well as to prevent scar tissue formation, thus leading to an overall environment that is more accommodating of tissue regeneration (*61*). There are a few parameters that need to be considered when designing scaffolds for regeneration of function after injury. These aspects are summarized in Figure 2 and will be discussed in detail in this chapter.

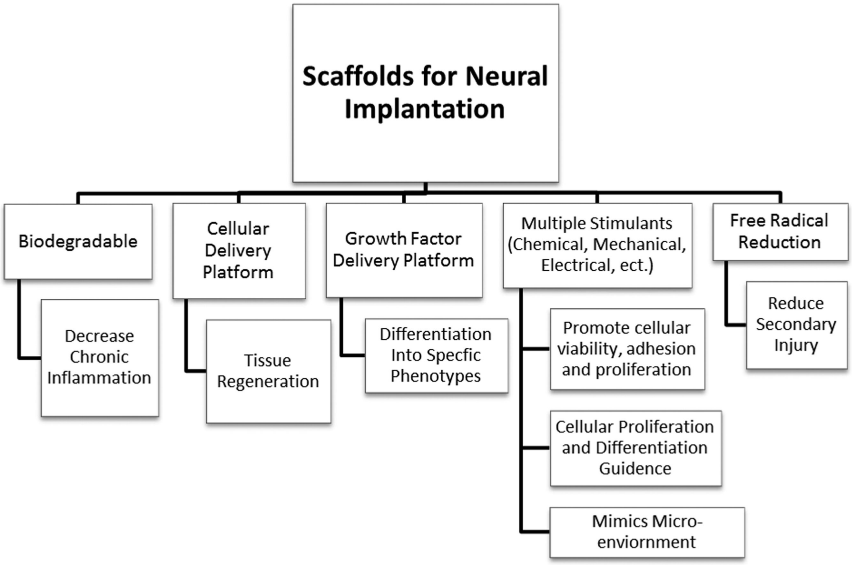
Scaffolds for Neural Implantation
Biodegradable
Decrease Chronic Inflammation
Cellular Delivery Platform
Tissue Regeneration
Growth Factor Delivery Platform
Differentiation Into Specfic Phenotypes
Multiple Stimulants (Chemical, Mechanical, Electrical, ect.)
Promote cellular viability, adhesion and proliferation
Cellular Proliferation and Differentiation Guidence
Mimics Micro-enviornment
Free Radical Reduction
Reduce Secondary Injury

*Figure 2. Ideal properties of scaffolds used for neural engineering. The schematic shows design criteria which when incorporated into the scaffold produce optimal results. Adopted with permission from (93). Copyright 2009 BioMed Central.*

## Modified Hydrogels

Hydrogels have been studied in depth for tissue engineering applications, including scaffolds to repair after CNS injury (*62–67*). Hydrogels can consist of crosslinked natural or synthetic polymer materials with water content of up to 98% (*61*, *68*). Natural hydrogel scaffolds have been formed with collagen, alginate, agarose, chitosan or methylcellulose, while synthetic polymer scaffolds include polyethylene glycol (PEG), poly(lactic-co-glycolic acid) (PLGA), poly(2-hydroxyethyl methacrylate) (PHEMA), poly (2-hydroxypropyl)-methacrylamide (PHPMA), and poly-[beta]-hydroxybutyrate.

Hydrogels have been studied extensively as vehicles for local cell delivery. In the treatment of CNS injury transplantation of cells is an extremely desirable therapeutic strategy. Delivering new cells in the damaged site serves to replace lost cell population, and furthermore, facilitate regeneration of neuronal networks to regain function. Embryonic stem cells, neural stem cells (NSCs), neural progenitor cells, induced pluripotent stem cells, olfactory ensheathing cells and Schwann cells have all been explored for repair post-injury.

However, the transplantation of these cells alone by injection in the area has been shown to lead to very low survival rates, as low as 0.2%-10% of the original cell graft (*69–71*). By embedding the cells in a hydrogel scaffold, the survival rate can be improved greatly (*72–74*). The effect of nanotechnology in the design of efficient hydrogel treatment strategies has been tremendous. While the overall hydrogel is a macro size structure, the scaffold can be modified on the nanometer level using proteins or signaling sequences to create effective therapeutic systems (*75–79*). Figure 3 illustrates the concept of a functionalized, implantable hydrogel in the case of SCI. This system is capable of filling any voids left by trauma to the CNS and the enhancing its regenerative and neuro-protective features.

Each of the aforementioned polymeric materials used to make hydrogels offers major advantages for use in clinical applications. For example, natural hydrogels tend to elicit less of an inflammatory response than synthetic ones, whereas the synthetic hydrogels are more easily tunable than natural ones as their mechanical properties can be easily modified for the desired parameters. One of the major draw backs of most hydrogels that have been developed, however, rests in the adhesive characteristics of the gels. In order to be an effective means of cell therapy in the CNS, a hydrogel scaffold needs to have properties that make it highly attractive to cells and proteins, so that 1) native cells can infiltrate the scaffold, 2) the delivered cells can survive, proliferate, differentiate and 3) matrix surrounding the cells can be reformed. These three aspects can develop a hydrogel system to be highly effective therapy in the regaining of function post-SCI and TBI, and the key lies in modifying the gel. To illustrate this concept one can consider hydrogels made out of agarose. Agarose, a natural polymer derived from red algae, is a very promising biomaterial due to its biocompatibility and ease in synthesis; however, its negative charge inhibits protein and cell adhesion. This property has been modified on the nanoscale with the insertion of bioactive molecules that behave as cell attractants. Many approaches have been developed to create such functionalized hydrogels and a summary of the most common ones, targeted towards CNS repair, as shown in Table 1. *In vivo* application of agarose hydrogel scaffold to bridge the gaps in the spinal cord has demonstrated to be conducive (*80*), especially when combined with drug delivery vehicles delivering bioactive agents that promote axonal outgrowth (*81*). For example, thermostabilized chondroitanase ABC was delivered from an agarose-microtuble hydrogel system *in vivo*, which resulted in sustained degradation of CSPG and showed significant locomotor improvement in rodent models (*82*). Another natural hydrogel that has been shown to be conducive for neural engineering is chitosan. Chitosan can be modified to be thermally responsive (*83*), as well as photocrossinkable (*84*), which are highly advantageous when developing in situ gelling hydrogel scaffolds for post-injury applications.

**Table 1. A summary of natural and synthetic materials that have been studied as functionalized scaffolds with bioactive molecules**

| ***Hydrogel material*** | ***Advantage*** | ***Disadvantage*** | ***Modifications*** | ***Source*** |
|---|---|---|---|---|
| *Natural* | | | | |
| Agarose | Biocompatible with many cell types | Not biodegradable | Laminin<br>Fibronectin<br>GRGDS | Bellamkonda et al. (*89*)<br>Luo et al. (*90*)<br>Jain et al. (*80*)<br>Yu et al. (*85*) |
| Alginate | Biodegradable, biocompatible, hydrophillic | Net negative charge which inhibits protein adsorption and cellular adhesion | RGD<br>Laminin<br>Fibronectin<br>collagen | Novikova et al. (*88*)<br>Kataoka et al. (*174*)<br>Freier et al. (*175*)<br>Suzuki et al. (*176*) |
| Xyloglucan | Easily tunable<br>Biodegradable | Low cell adhesion | Poly-L-lysine | Nisbet et al. (*177*)<br>Shirakawa et al. (*178*) |
| Methylcellulose | Biocompatible | Not bioactive<br>Non-biodegradable<br>Natural gellation temperature is outside the physiological range | Laminin<br>PDGF | Kobayashi et al. (*179*)<br>Tate et al. (*180*)<br>Stabenfeldt et al. (*86*)<br>Wells et al. (*181*) |
| Hyaluronan | Anti-inflammatory | Net negative charge inhibits cellular adhesion | Polylysine<br>Esterification<br>Gelatin<br>Collagen<br>PEG<br>Nogo | Seckel et al. (*182*)<br>Tian et al. (*99*)<br>Benedetti et al. (*103*)<br>Leach et al. (*105*)<br>Burdick et al. (*104*)<br>Shu et al. (*108*)<br>Segura et al. (*106*) |

*Continued on next page.*

**Table 1. (Continued). A summary of natural and synthetic materials that have been studied as functionalized scaffolds with bioactive molecules**

| ***Hydrogel material*** | ***Advantage*** | ***Disadvantage*** | ***Modifications*** | ***Source*** |
|---|---|---|---|---|
| Chitosan | Positive charge which allows for good cell adhesion<br>Biodegradable | Causes inflammatory response | Polylysine | Chenite et al. (*183*)<br>Nishimura et al. (*184*)<br>Peluso et al. (*185*)<br>Crompton et al. (*186*) |
| Matrigel™ | Biocompatable with multiple cell types, promotes cellular adhesion | Derived from mouse tumor cells | FGF<br>EGF<br>NGF | Tominaga et al. (*187*)<br>Toman et al. (*188*)<br>Ferri et al. (*189*) |
| *Synthetic* | | | | |
| Methacrylate-based | Easy to manufacture | No cellular adhesion | Collagen,<br>CDPGYIGSR,<br>CQAASIKVAV<br>FGF-1<br>NGF<br>NT-3 | Yu et al. (*190*)<br>Gianetti et al. (*191*)<br>Tsai et al. (*192*)<br>Kapur et al. (*193*)<br>Moore et al. (*194*)<br>Midha et al. (*194*) |
| Polyethylene glycol | Non-toxic<br>Suppresses oxidative stress | Weak cellular and protein adhesion | RGDS, IKVAV and YIGSR | Gunn et al. (*195*)<br>Piantino et al. (*196*)<br>Burdick et al. (*104*) |

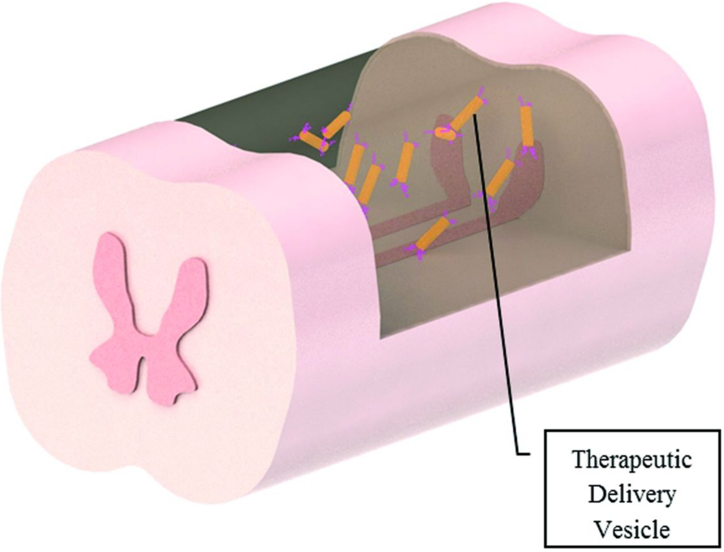

*Figure 3. Schematic of a modified hydrogel implant in spinal cord cavity. CNS injury modeled by dorsal-over hemisection implanted with functionalized hydrogel scaffold with drug delivery vehicle to elicit both neural protective and neural regenerative effects.*

The most common molecules that behave as cell attractants are ECM proteins such as collagen, laminin and fibronectin. These proteins are nano-molecules, as one dimension is on the order of less than 100 nm. They contain bioactive properties, which allow for improved cell adhesion, thus proving to be advantageous for neural repair. In an *in vitro* study laminin was coupled to agarose hydrogels using a crosslinking reagent, which resulted in a significant enhancement of neurite extensions (*85*). Laminin has also been incorporated in methylcellulose hydrogels, where it was observed to increase the overall bioactivity of the gels (*86*, *87*). In one of these studies, it was found that axonal outgrowth increased direct proportionally as a function of dose-dependent response to the density of laminin, whereas the viability of neurons increased until a laminin density threshold was met (*87*). Similarly, modifications with fibronectin were shown to improve cell adhesion in agarose scaffolds (*88*).

Along with embedding whole ECM proteins like laminin, fibronectin or collagen, small oligopeptides derived from these molecules have been used as well (Table 2). With the purpose of improving cell adhesion in hydrogels, Laminin-derived oligopeptides were functionalized to the agarose scaffold backbone, which promoted neurite extension (*89*, *90*). The use of fibronection-derived amino acid sequence RGD demonstrated promising results as a cell adhesion motif (*78*, *91*, *92*). For example, immobilization of RGD was studied with synthetic MHPMA hydrogels, where it was seen to promote not only adhesion and proliferation of neurons and astrocytes inside the gel, but also an enhanced integration of the hydrogel itself with the host tissue (*78*).

**Table 2. Peptide sequences used as modifications to enhance effectiveness of the scaffold**

| *Peptide Sequences* | *Function* | *Reference* |
|---|---|---|
| **RGD** | Cell Adhesion | Ruoslahti et al. (*197*) |
| **YIGSR** | Cell Adhesion and migration | Iwamoto et al. (*198*)<br>Tong et al. (*199*) |
| **IKVAV** | Neurite Extension | Silva et al. (*130*)<br>Tashiro et al. (*200*) |
| **RNIAEIIKDI** | Neurite Extension | Graner et al. (*201*)<br>Hager et al. (*202*) |
| **KHIFSDDSSE** | Astrocyte Adhesion | Kam et al. (*203*)<br>Hama et al. (*204*) |

Other peptides, including laminin-derived peptides, IKVAV and YIGSR have been shown to make hydrogels more conducive for cell adhesion and migration (*93–95*). Cui et al. showed that the incorporation of IKVAV to PHPMA hydrogel provided the hydrogel with desired properties to promote cell migration in the repair of the TBI in adult rats (*96*). A scanning electron microscopy image of the PHPMA-IKVAV hydrogel is shown in Figure 4. As can be seen in this picture, due to the nanoscale size of the immobilized sequence, the hydrogel remains highly porous, which is one of the factors that plays a role in the migration of cells (*96*).

Another hydrogel material used in the repair of CNS is hyaluronan. Also referred to as hyaluronic acid, this polymer has anti-inflammatory characteristics that make it very desirable (*97–101*). Hyaluronan alone has limited capabilities as a scaffold due to its negative charge; however, modifying it with bioactive agents can make it a more desirable choice. Wei et al. used the IKVAV sequence to functionalize the hydrogel and demonstrated desirable levels of axonal growth (*94*). In another study, incorporating poly-L-lysine molecules in hyaluronan hydrogels allowed for better adherence of native neurons and astrocytes in the injured brain (*99*).

Another innovative strategy of nano-modification of hyaluronan for CNS repair employs Nogo receptor antibodies. Although Nogo has a crucial role in neural development, it is another inhibitory molecule against axonal outgrowth. Incorporating antibodies against Nogo to the hydrogel allows binding to the Nogo receptor, thus inhibiting the binding of myelin glycoproteins, an event which is known to prevent neural repair (*99*, *102*). Other modifications of hyaluronan on the nanoscale include esterification, self-crosslinking and crosslinking with PEG, which can improve the stability and degradation rate of the scaffold (*103–107*). However, Shu et al. demonstrated that binding of hyaluronan with gelatin was able to mimic the ECM and support cell attachment and migration to provide a biocompatible and biodegradable scaffold (*108*).

Other hydrogel materials that have also gained significant interest include commercially available products such as Matrigel™ and NeuroGel™. Matrigel™ consists of basement membrane proteins, such as laminin and collagen. Its complex matrix composition and natural formation allows it to be extremely favorable to cellular attachment. The incorporation of Schwann cells into Matrigel has shown to significantly increase axonal outgrowth (*109*). When Schwann cells were mixed into the PAN/PVC tube along with Matrigel™ and implanted into a transected rodent spinal cord, a tissue bridge that contained Schwann cells, axons, vessels had reconnected the spinal cord after 1 month (*110*). NeuroGel™ is a crosslined variant of N-2-(hydroxypropyl) methacrylamide and when this substrate is inserted into the spinal cord after contusion injury, there was evidence of axonal infiltration into the hydrogel, promoting motion (*79*). An additional capability of NeuroGel™ to reduce glial scar formation when implanted into spinal cords has made it a specific material of interest for use within the CNS (*111*).

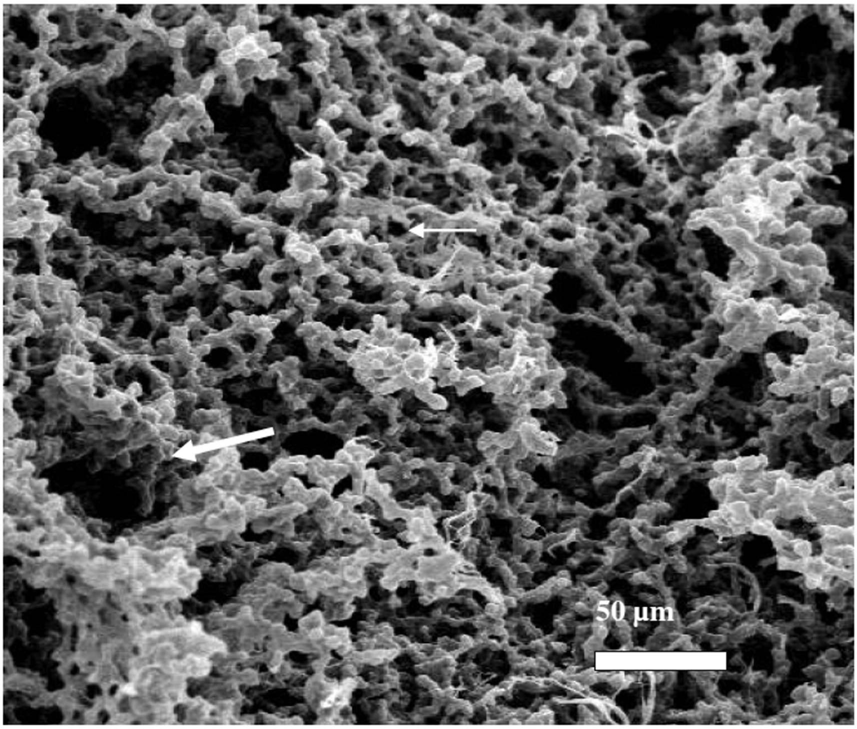

*Figure 4. Scanning electron microscope (SEM) image of a PHPMA hydrogel, functionalized with the IKVAV sequence. The arrows point to interconnected pores of various sizes in the hydrogel, which permit the migration of embedded cells. Reprinted with permission from (96). Copyright 2003 Sage Publications.*

## Fiber-Based Scaffolds

In addition to hydrogels, another approach that is being explored for the construction of neural engineering scaffolds is with the use fiber-based structures. While these scaffolds can be formed with macroscopic dimensions, the more advanced designs consist of nano-scale fibers. There are several strategies for the synthesis of fiber-based scaffolds, such as: electrospinning, self-assembly, drawing out (thermally induced phase separation) and catalytic synthesis (*112–114*). Electrospinning and self-assembly designs will be discussed in more detail in this section.

For fiber-based scaffolds, there are three design aspects that have a crucial role: 1) the diameter of the fibers, 2) the number of fibers, and 3) the alignment of fibers. Compared to microfibers, nanofibers display a higher potential for cellular attachment, proliferation, migration and, in the case of NSCs, nanofibers displayed a faster rate of differentiation (*115*). It has been suggested nanofibers mimic the ECM better due to their structural size of 600-800 nm (*43*, *44*, *116*). The role of the number of fibers in the scaffold or density is not yet fully understood, with relationship between cellular viability and proliferation yet to be determined (*117*, *118*). Lastly, the alignment of fibers is crucial in axonal outgrowth and neurite extensions, and will be discussed in greater detail below.

In electrospun scaffolds, specifying the pattern or direction of fibers has played a major role for the effectiveness of the scaffold in the axonal outgrowth, because it provides topographical directional cues for cell migration. For example, aligned poly-L-lactic acid (PLLA) nanofibers assisted in the neurite outgrowth and neuronal differentiation of neural stem cells, compared to nanofibers lacking alignment (*115*). Because PLLA is biodegradable, over time neuronal networks will take the place of the fibers over time, helping in the regeneration of function after injury. Similar results were observed with aligned electrospun nanofibers of poly-epsilon-caprolactone, a collagen/poly-epsilon-caprolactone blend or poly-L-lactate (*119*, *120*), whereas nanofiber scaffolds that have crossed fibers were detrimental to axonal outgrowth (*121*).

The second type of fibrous scaffolds consists of self-assembling nanofibers. The principle behind the self-formation is the existence of repeating sequences of positive and negative L-amino acids (*64*). The main advantage of these scaffolds rests in the fact that they can be injected in the liquid phase in the injury site and exposure to saline in the microenvironment will induce gelation and form stable nanofibers, which will provide support for cell attachment and differentiation (*64*). Research has been done to modify the bioactivity, surface chemistry and morphology of these fibers, as well as to control the mode of self-assembly (*122–124*).

Just like hydrogels, nanofibers can be modified with proteins and peptides on the surface to promote cellular adhesion. Integrin receptor binding sites RGD and IKVAV have previously been explored (*125–129*). Tysseling et al. suggested that embedding IKVAV sequence on self-assembling peptide amphiphile (PA) molecules played a key role in minimizing glial scar formation and promoting growth of axons in SCI (*125*). The same approach was observed to suppress differentiation of neural progenitor cells into astrocytes and promote differentiation into neurons (*130*). Another peptide scaffold modified with RADA16-I sequences supported the growth of PC12 cells and the formation of functional synapses *in vitro* using rat primary hippocampal neurons (*131*).

A sub-class of fiber scaffolds is carbon nanofibers that has demonstrated great promise. Due to their electroconductivity, carbon nanofibers have been shown to increase neuronal growth and decrease the astrocyte adhesion (*64*). One approach of nanotechnology that has shown significant progress in terms of neuronal guidance is the use of carbon-based nanoparticles, tubes or fibers. These strategies are able to guide neuronal axon regeneration of endogenous cells and implanted cells, taking advantage of the mechanical and electrical properties of the nano-material. Due to the conductivity and mechanical compliance of carbon nano-tubes, it is possible to electrically and mechanically condition regenerating neurons and differentiating NSCs into a functional network. After the first successfully cultured neurons on carbon nanotubes it was found that this type of substrate was able to increase neurite extension, branching, and overall electrical signaling within the network (*101*). Further treatment of nano-scale tubes with chemoattractants like positively charged surface modifications and anti-inflammatory coatings can increase the ability to direct neuronal regeneration towards areas of interest, as well as create a functional neuronal network at the site of injury. Carbon nanofibers have been fabricated in specific patterns, where neurons preferably attach and interconnect to form neural lattices that were implanted to repair the injured tissue with intact neural network, allowing for a fully functional neuronal graft, preconditioned and ready to conduct signals directly after implantation to aid in functional recovery (*116*).

## Delivery of Bioactive Molecules

The hydrogel and fiber-based scaffolds that have been described in the previous section can also be used as a medium for the delivery of neurotrophins and growth factors, such as nerve growth factor, brain-derived growth factor, and neurotrophin-3, which play a key role in the development of neuronal networks in the human body (*132–134*). Majority of the transplanted stem cells in the CNS differentiate into astrocytes and oligodendrocytes and only a minimal number of cells differentiate into a neuronal lineage (*135–141*). The presence of neurotrophins in the scaffold serves to promote differentiation of transplanted cells into a neuronal lineage, as well as to protect and encourage axonal outgrowth from endogenous neurons. There is evidence of a spontaneous increase of neurotrophins post-trauma, but these levels were found to be insufficient for regeneration (*142*). On the other hand, deliberate modification of the neurotrophin levels shows promising results, however, in order to be effective in the regeneration of function post-injury, these molecules needs to be delivered for an extended period of time (weeks to months) (*81*, *143–145*).

Delivery of neurotrophins and other bioactive molecules to the CNS is not an easy task. The BBB and BSCB make it nearly impossible to deliver molecules to the brain and spinal cord via systemic injection, because very few molecules can cross these barriers. With this consideration, the delivery of molecules for the treatment of SCI and TBI can be accomplished through different methods: 1) transplanting genetically engineered cells expressing the desired bioactive agent, 2) embedding bioactive molecules directly into a scaffold, and 3) loading the bioactive molecules on a carrier and embedding the carrier into the scaffold.

Delivery of genetically modified cells has shown promise in regenerating neurons, however, the concern with this therapeutic method remains significant because it requires a cellular transfection accomplished through a retroviral vector

(*146–152*). The second alternative, embedding bioactive factors directly in a scaffold carries less of the safety concern. One interesting approach that has been explored is delivery of chondroitanase ABC into the spinal cord lesion through Gelfoam: an insoluble gelatin sponge. When transplanted into animals, this delivery system showed improved axonal regeneration (*153*). However, delivery of molecules using this approach has not been most effective, predominantly due to the molecules not being delivered deep into the tissue, but remain around the surface of the scaffold (*154*). Release of the neurotrophin on the outside of the cell also means that the neurotrophin has to find new means of entering the cell (*155*). Furthermore, a typical exponential release profile is experienced as opposed to the desired linear, sustained profile (*156*).

The third alternative, the use of nanotechnology in the delivery systems, has been proven as the most effective approach. This strategy is generally administered through the basis of a degradable hydrogel, but it differs from the second method because it employs a special carrier for the neurotrophin, which is usually on the nanometer scale. It is advantageous in the fact that it allows for several advanced design requirements: stability, degradability, controlled release and specific targeting capabilities. Several carriers have been developed to support delivery of neurotrophins, such as nanoparticles, nanotubes, liposomes, micelles which will be discussed in more detail below.

A new research area incorporates concepts of molecular delivery to improve the performance of biosensors as diagnostic techniques. In order to reduce the inflammatory response, hydrogels can be embedded with anti-inflammatory agents, such as steroids continue to promote wound healing (*157*). The slow release of these molecules will counter the cascade of events prevalent in the secondary injury. Concurrently with the anti-inflammatory agents, angiogenesis-inducing molecules can be delivered from the hydrogel. This will ensure vascularization into the injury site, which is an extremely important factor for regaining lost function. This combinatorial delivery mechanism was utilized to deliver dexamethasone (DX), an anti-inflammatory glucocorticoid (*158*), and vascular endothelial growth factor (VEGF), which directs the development of blood vessels (*159*). The molecules were delivered in two ways: by PLGA microspheres embedded in the hydrogel, or through the hydrogel itself. Utilizing the microspheres produced a more sustained release profile, while direct delivery from the hydrogel resulted in a larger overall release of the two agents (*159*). Such parallel delivery of agents from implantable hydrogel systems has great potential for neuro repair, as well as the regaining of lost function.

## Nanoparticle Carriers

Nanoparticles are small sphere-like structures sized under 100 nm. They allow for efficient delivery of bioactive molecules because they are stable and have good carrier capacities for both hydrophilic and hydrophobic molecules. Furthermore they can easily be modified for targeted delivery. Targeted nanoparticles contain surface modification, such as conjugated ligands, which allow the nanoparticle to bind to a specific cell receptor and become endocytosed.

Nanoparticles of different materials and properties have been developed. The first study to perform release of neurotrophins from nanoparticles for treatment of SCI involved PLGA nanoparticles affected both neural and glial cells for extended periods of time. They encouraged neuronal regeneration, thus proving to be a strong delivery system the treatment of CNS injury. Cerium oxide, yttrim oxide and auto-catalysitcal ceria treated nanoparticles with various growth factors and neurotrophins have been developed since, and have shown neuroprotective capabilities, aiding in the survival of cells and retention of function after injury (*160*, *161*). Another delivery system designed by Reddy et al. used PLGA nanoparticles loaded with superoxide dismutase which was particularly beneficial in reducing oxidative stress post-injury (*162*). In study done by Kang et al. a hyaluronic acid hydrogel system with embedded PLGA nanoparticles was used to deliver FGF to models of CNS injury (*163*). The study showed promising results, particularly on the rate of angiogenesis near the injury site.

Advancement in understanding of the injury and advancements in the field of nanotechnology have shaped the designs of these delivery systems. In a recent study a HA-MC composite hydrogel was used with nanoparticle delivered NT-3 (*164*). Recognizing that the harsh chemical environments utilized in the formulation of nanoparticles can damage the encapsulated neurotrophin, this study was innovative because it incorporated protective molecules during each stage of the formulation. Modifications with trehalose, methyl cellulose, PEG and MgCO3 resulted in improved stability and bioactivity of NT-3, while encapsulated in the nanoparticle (*164*).

## Nanotube Carriers

Nanotubes have similar properties to nanoparticles, except they contain the shape of tubes. Just as with nanoparticles, neurotrophins can be encapsulated in the nanotubes and several studies have shown successful results. Carbon nanotubes in particular have been proved to be excellent delivery systems in TBI and SCI. They are not degradable, thus they provide long term supply of extracellular cues, which is particularly important in the secondary damage of CNS injury persistent days to weeks after the initial insult. Modifications of nanotubes can also be employed to increase their efficacy. For example, Hu et al. used a chemical charge modifier to make the surface of the nanotubes more acceptable in the injury environment, to support neuronal outgrowth. Compared to nanoparticles, the shape difference in nanotubes has allowed for novel approaches for delivery. Instead of encapsulating the biomolecule inside the nanotubes, a new strategy developed by Matsumoto et al. implemented a coating on the surface of carbon nanotubes with NGF and BDNF. This resulted in an increase in the biological activity level of the neurotrophins, and eventually lead to a considerable neuronal outgrowth (*165*).

Nanocarriers provide a significant advantage for the release of bioactive molecules, however before these approaches can be applied in the clinical setting further experimentation and analysis is required. One of the major areas that is still unclear is the fate of the carrier once they are released in the body. Because their dimensions are on the nanoscale, macrophages in the body are able to attack the carrier particles and engulf them because they are recognized as foreign (*166*). This process can exert a toxic effect on macrophages and limit their ability to target other cells in the body. One approach that has been suggested as a solution to this issue is the functionalization of the surface of the nanocarrier with a molecule that is recognized as "self", such as CD47, a protein that is present in the surface of all cells in the body (*167*). This protein is known to inhibit the activation of macrophages, thus serves as a plausible approach to minimize the nanocarrier uptake by macrophages.

## Nanoparticles for Labeling Transplanted Cells

These imaging modalities allow for not only tracking and diagnosing CNS but also for tracking cellular regeneration. *In vivo* cell transplantation therapies are limited by the inability to track and monitor the cell graft. The advancements in the research of nanoparticle contrast agents have made it possible to monitor these cells *in vivo*. Stem cell labeling with magnetically conjugated contrast agents allow for on demand tracking of injectable cell therapies, and visualization of the cellular regeneration progress (*168–171*). Super paramagnetic iron oxide particles have been developed as magnetodendrimers to label mammalian cells, including neural stem cells and mesenchymal stem cells (*172*). The long half-life of these magnetodendrimers and their affinity for cellular membranes allow for the accurate *in vivo* tracking of implanted cells. In the case of neural regeneration, crosslinked iron oxide-labeled neural stem cells (NSCs) have been successfully transplanted into rodent brains. Their migration, differentiation and incorporation into the native neuronal network has been visualized using long term MRI imaging studies (*173*). Labeling of NSCs with iron-based nanoparticles has no adverse effects on the cell survival, proliferation or differentiation, and the cells behaved identically to those grown in the same conditions but without nanoparticle modification (*169*).

## Future Opportunities

With the current trends of advancements in nanotechnology, understanding of neural anatomy, and neural pathophysiology, applications in diagnosing, neural protection and neural regeneration have gained significant progress in recent years. Recent literature and research has shown numerous approaches to in vitro studies on neurons. With further research into nanotechnology applications in the CNS, there will be extraordinary affects with direct clinical implications. Not only will nanotechnology revolutionize the methods by which these injuries are diagnosed, but the ability to further protect from secondary damage prevalent in CNS injuries and also elicit regenerative capabilities to regain the lost cognitive and motor function loss. The intermeshing of molecular biology with nanotechnology will surely continue to develop further applications to further the field of neural science and CNS injury studies. This will not only reduce the morbidity and mortality of these injuries, but also allow affected individuals to get back to their normal lives and lessen the treat of subsequent secondary injury and the debilitating ailments after the initial insult.

# References

1. y Cajal, S. R. *Degeneration & regeneration of the nervous system*; Oxford University Press, Humphrey Milford: Oxford, 1928; Vol. 1.
2. National Spinal Cord Injury Statistical Center. *Spinal Cord Injury Facts and Figures at a Glance*; University of Alabama: Birmingham, Alabama, 2011.
3. Bruns, J., Jr.; Hauser, W. A. *Epilepsia* **2003**, *44* (Suppl 10), 2–10.
4. Werner, C.; Engelhard, K. *Br. J. Anaesth.* **2007**, *99* (1), 4–9.
5. McGarry, L. J.; Thompson, D.; Millham, F. H.; Cowell, L.; Snyder, P. J.; Lenderking, W. R.; Weinstein, M. C. *J. Trauma* **2002**, *53* (6), 1152–9.
6. Borgens, R. B.; Liu-Snyder, P. *Q. Rev. Biol.* **2012**, *87* (2), 89–127.
7. Fitch, M. T.; Silver, J. *Exp. Neurol.* **2008**, *209* (2), 294–301.
8. Ozdemir, M.; Attar, A.; Kuzu, I. *Curr. Stem Cell Res. Ther.* **2012**, *7* (5), 364–369.
9. Livecchi, M. A. *Continuum (Minneap Minn)* **2011**, *17* (3 Neurorehabilitation), 568–83.
10. Fitch, M. T.; Doller, C.; Combs, C. K.; Landreth, G. E.; Silver, J. *J. Neurosci.* **1999**, *19* (19), 8182–98.
11. Juurlink, B. H.; Paterson, P. G. *J. Spinal Cord Med.* **1998**, *21* (4), 309–34.
12. Fabry, Z.; Raine, C. S.; Hart, M. N. *Immunol. Today* **1994**, *15* (5), 218–24.
13. Becher, B.; Prat, A.; Antel, J. P. *Glia* **2000**, *29* (4), 293–304.
14. Zhang, X.; Chen, Y.; Jenkins, L. W.; Kochanek, P. M.; Clark, R. S. *Crit. Care* **2005**, *9* (1), 66–75.
15. Bush, T. G.; Puvanachandra, N.; Horner, C. H.; Polito, A.; Ostenfeld, T.; Svendsen, C. N.; Mucke, L.; Johnson, M. H.; Sofroniew, M. V. *Neuron* **1999**, *23* (2), 297–308.
16. Ridet, J. L.; Malhotra, S. K.; Privat, A.; Gage, F. H. *Trends Neurosci.* **1997**, *20* (12), 570–7.
17. Horner, P. J.; Gage, F. H. *Nature* **2000**, *407* (6807), 963–70.
18. Abbott, N. J. *Cell. Mol. Neurobiol.* **2005**, *25* (1), 5–23.
19. Morganti-Kossmann, M. C.; Rancan, M.; Stahel, P. F.; Kossmann, T. *Curr. Opin. Crit. Care* **2002**, *8* (2), 101–5.
20. Schwartz, E. D. *Am. J. Neuroradiol.* **2005**, *26* (7), 1609–10.
21. Marion, D. W.; Carlier, P. M. *J. Trauma* **1994**, *36* (1), 89–95.
22. Marino, R. J.; Ditunno, J. F., Jr.; Donovan, W. H.; Maynard, F., Jr. *Arch. Phys. Med. Rehabil.* **1999**, *80* (11), 1391–6.
23. Shiel, A.; Horn, S. A.; Wilson, B. A.; Watson, M. J.; Campbell, M. J.; McLellan, D. L. *Clin. Rehabil.* **2000**, *14* (4), 408–16.
24. Fehlings, M. G.; Perrin, R. G. *Spine* **2006**, *31* (11) (Suppl), S28–35 discussion S36.
25. Piek, J. *Curr. Opin. Crit. Care* **2002**, *8* (2), 134–8.
26. Hurlbert, R. J. *Spine* **2006**, *31* (11) (Suppl), S16–21 discussion S36.

27. van Santbrink, H.; Maas, A. I.; Avezaat, C. J. *Neurosurgery* **1996**, *38* (1), 21–31.
28. Hillered, L.; Persson, L.; Nilsson, P.; Ronne-Engstrom, E.; Enblad, P. *Curr. Opin. Crit. Care* **2006**, *12* (2), 112–8.
29. Zweifel, C.; Lavinio, A.; Steiner, L. A.; Radolovich, D.; Smielewski, P.; Timofeev, I.; Hiler, M.; Balestreri, M.; Kirkpatrick, P. J.; Pickard, J. D.; Hutchinson, P.; Czosnyka, M. *Neurosurg. focus* **2008**, *25* (4), E2.
30. Stiefel, M. F.; Spiotta, A.; Gracias, V. H.; Garuffe, A. M.; Guillamondegui, O.; Maloney-Wilensky, E.; Bloom, S.; Grady, M. S.; LeRoux, P. D. *J. Neurosurg.* **2005**, *103* (5), 805–11.
31. Hillered, L.; Vespa, P. M.; Hovda, D. A. *J. Neurotrauma* **2005**, *22* (1), 3–41.
32. Meixensberger, J.; Kunze, E.; Barcsay, E.; Vaeth, A.; Roosen, K. *Neurol. Res.* **2001**, *23* (8), 801–6.
33. Dale, N.; Hatz, S.; Tian, F.; Llaudet, E. *Trends Biotechnol.* **2005**, *23* (8), 420–8.
34. Thompson, M.; Krull, U. J. *Anal. Chem.* **1991**, *63* (7), 393A–405A.
35. Vaddiraju, S.; Tomazos, I.; Burgess, D. J.; Jain, F. C.; Papadimitrakopoulos, F. *Biosens. Bioelectron.* **2010**, *25* (7), 1553–65.
36. Zhang, X.; Guo, Q.; Cui, D. *Sensors (Basel)* **2009**, *9* (2), 1033–53.
37. Li, C.; Wu, P. M.; Jung, W.; Ahn, C. H.; Shutter, L. A.; Narayan, R. K. *Lab Chip* **2009**, *9* (14), 1988–90.
38. Williams, J. *Lab Chip* **2009**, *9* (14), 1987.
39. Kim, I.; Fok, H. H.; Li, Y.; Jackson, T. N.; Gluckman, B. J. *Conf. Proc. IEEE Eng. Med. Biol. Soc.* **2011**, *2011*, 3286–9.
40. Grant, S. A.; Bettencourt, K.; Krulevitch, P.; Hamilton, J.; Glass, R. *Crit. Rev. Biomed. Eng.* **2000**, *28* (1-2), 159–63.
41. Newman, J. D.; Setford, S. J. *Mol. Biotechnol.* **2006**, *32* (3), 249–68.
42. Llaudet, E.; Botting, N. P.; Crayston, J. A.; Dale, N. *Biosens. Bioelectron.* **2003**, *18* (1), 43–52.
43. Ma, Z.; Kotaki, M.; Inai, R.; Ramakrishna, S. *Tissue Eng.* **2005**, *11* (1-2), 101–9.
44. Ma, Z.; Kotaki, M.; Yong, T.; He, W.; Ramakrishna, S. *Biomaterials* **2005**, *26* (15), 2527–36.
45. Lowry, J. P.; Miele, M.; O'Neill, R. D.; Boutelle, M. G.; Fillenz, M. *J. Neurosci. Methods* **1998**, *79* (1), 65–74.
46. Lowry, J. P.; O'Neill, R. D.; Boutelle, M. G.; Fillenz, M. *J. Neurochem.* **1998**, *70* (1), 391–6.
47. Wang, J. *Chemical reviews* **2008**, *108* (2), 814–25.
48. Bartanusz, V.; Jezova, D.; Alajajian, B.; Digicaylioglu, M. *Ann. Neurol.* **2011**, *70* (2), 194–206.
49. Morawski, A. M.; Lanza, G. A.; Wickline, S. A. *Curr. Opin. Biotechnol.* **2005**, *16* (1), 89–92.
50. Mulder, W. J.; Strijkers, G. J.; van Tilborg, G. A.; Griffioen, A. W.; Nicolay, K. *NMR Biomed.* **2006**, *19* (1), 142–64.
51. Thorek, D. L.; Chen, A. K.; Czupryna, J.; Tsourkas, A. *Ann. Biomed. Eng.* **2006**, *34* (1), 23–38.

52. Caruthers, S. D.; Winter, P. M.; Wickline, S. A.; Lanza, G. M. *Methods Mol. Med.* **2006**, *124*, 387–400.
53. Caravan, P. *Acc. Chem. Res.* **2009**, *42* (7), 851–62.
54. Bonnemain, B. *J. Drug Target.* **1998**, *6* (3), 167–74.
55. Kim, J.; Kim, D. I.; Lee, S. K.; Kim, D. J.; Lee, J. E.; Ahn, S. K. *Acta Radiol.* **2008**, *49* (5), 580–8.
56. Venditto, V. J.; Regino, C. A.; Brechbiel, M. W. *Mol. Pharmaceutics* **2005**, *2* (4), 302–11.
57. Gupta, A. K.; Naregalkar, R. R.; Vaidya, V. D.; Gupta, M. *Nanomedicine (Londom)* **2007**, *2* (1), 23–39.
58. Kabalka, G. W.; Davis, M. A.; Moss, T. H.; Buonocore, E.; Hubner, K.; Holmberg, E.; Maruyama, K.; Huang, L. *Magn. Reson. Med* **1991**, *19* (2), 406–15.
59. Wadghiri, Y. Z.; Sigurdsson, E. M.; Sadowski, M.; Elliott, J. I.; Li, Y.; Scholtzova, H.; Tang, C. Y.; Aguinaldo, G.; Pappolla, M.; Duff, K.; Wisniewski, T.; Turnbull, D. H. *Magn. Reson. Med.* **2003**, *50* (2), 293–302.
60. Schwab, M. E. *Science* **2002**, *295* (5557), 1029–31.
61. Hejcl, A.; Lesny, P.; Pradny, M.; Michalek, J.; Jendelova, P.; Stulik, J.; Sykova, E. *Physiol. Res.* **2008**, *57* (Suppl 3), S121–32.
62. Donnelly, E. M.; Lamanna, J.; Boulis, N. M. *Stem Cell Res. Ther.* **2012**, *3* (4), 24.
63. Huang, H.; Xi, H.; Chen, L.; Zhang, F.; Liu, Y. *Cell Transplant.* **2012**, *21* (Suppl 1), S23–31.
64. Kubinova, S.; Sykova, E. *Regener. Med.* **2012**, *7* (2), 207–24.
65. Tsuji, O.; Miura, K.; Fujiyoshi, K.; Momoshima, S.; Nakamura, M.; Okano, H. *Neurotherapeutics* **2011**, *8* (4), 668–76.
66. Kan, E. M.; Ling, E. A.; Lu, J. *Curr. Med. Chem.* **2010**, *17* (36), 4492–510.
67. Zurita, M.; Otero, L.; Aguayo, C.; Bonilla, C.; Ferreira, E.; Parajon, A.; Vaquero, J. *Cytotherapy* **2010**, *12* (4), 522–37.
68. Zhong, Y.; Bellamkonda, R. V. *J. R. Soc., Interface* **2008**, *5* (26), 957–75.
69. Hiraoka, M.; Kato, K.; Nakaji-Hirabayashi, T.; Iwata, H. *Bioconjugate Chem.* **2009**, *20* (5), 976–83.
70. Bakshi, A.; Keck, C. A.; Koshkin, V. S.; LeBold, D. G.; Siman, R.; Snyder, E. Y.; McIntosh, T. K. *Brain Res.* **2005**, *1065* (1-2), 8–19.
71. Kallur, T.; Darsalia, V.; Lindvall, O.; Kokaia, Z. *J. Neurosci. Res.* **2006**, *84* (8), 1630–44.
72. Walker, P. A.; Aroom, K. R.; Jimenez, F.; Shah, S. K.; Harting, M. T.; Gill, B. S.; Cox, C. S., Jr. *Stem Cell Rev.* **2009**, *5* (3), 283–300.
73. Little, L.; Healy, K. E.; Schaffer, D. *Chem. Rev.* **2008**, *108* (5), 1787–96.
74. Cooke, M. J.; Vulic, K.; Shoichet, M. S. *Soft Matter* **2010**, *6*, 4988–4998.
75. Loh, N. K.; Woerly, S.; Bunt, S. M.; Wilton, S. D.; Harvey, A. R. *Exp. Neurol.* **2001**, *170* (1), 72–84.
76. Pakulska, M. M.; Ballios, B. G.; Shoichet, M. S. *Biomed Mater* **2012**, *7* (2), 024101.
77. Teng, Y. D.; Lavik, E. B.; Qu, X.; Park, K. I.; Ourednik, J.; Zurakowski, D.; Langer, R.; Snyder, E. Y. *Proc. Natl. Acad. Sci. U.S.A.* **2002**, *99* (5), 3024–9.

78. Woerly, S.; Pinet, E.; de Robertis, L.; Van Diep, D.; Bousmina, M. *Biomaterials* **2001**, *22* (10), 1095–111.
79. Woerly, S.; Doan, V. D.; Evans-Martin, F.; Paramore, C. G.; Peduzzi, J. D. *J. Neurosci. Res.* **2001**, *66* (6), 1187–97.
80. Jain, A.; Kim, Y. T.; McKeon, R. J.; Bellamkonda, R. V. *Biomaterials* **2006**, *27* (3), 497–504.
81. Jain, A.; McKeon, R. J.; Brady-Kalnay, S. M.; Bellamkonda, R. V. *PloS One* **2011**, *6* (1), e16135.
82. Lee, H.; McKeon, R. J.; Bellamkonda, R. V. *Proc. Natl. Acad. Sci. U.S.A.* **2010**, *107* (8), 3340–5.
83. Crompton, K. E.; Goud, J. D.; Bellamkonda, R. V.; Gengenbach, T. R.; Finkelstein, D. I.; Horne, M. K.; Forsythe, J. S. *Biomaterials* **2007**, *28* (3), 441–9.
84. Valmikinathan, C.; Mukhatyar, V.; Jain, A.; Karumbaiah, L.; Dasari, M.; Bellamkonda, R. *Soft Matter* **2012**, *8*, 1964–1976.
85. Yu, X.; Dillon, G. P.; Bellamkonda, R. B. *Tissue Eng.* **1999**, *5* (4), 291–304.
86. Stabenfeldt, S. E.; Garcia, A. J.; LaPlaca, M. C. *J. Biomed. Mater. Res., Part A* **2006**, *77* (4), 718–25.
87. Stabenfeldt, S. E.; LaPlaca, M. C. *Acta Biomater.* **2011**, *7* (12), 4102–8.
88. Novikova, L. N.; Mosahebi, A.; Wiberg, M.; Terenghi, G.; Kellerth, J. O.; Novikov, L. N. *J. Biomed. Mater. Res., Part A* **2006**, *77* (2), 242–52.
89. Bellamkonda, R.; Ranieri, J. P.; Aebischer, P. *J. Neurosci. Res.* **1995**, *41* (4), 501–9.
90. Luo, Y.; Shoichet, M. S. *Nat. Mater.* **2004**, *3* (4), 249–53.
91. Hejcl, A.; Sedy, J.; Kapcalova, M.; Toro, D. A.; Amemori, T.; Lesny, P.; Likavcanova-Masinova, K.; Krumbholcova, E.; Pradny, M.; Michalek, J.; Burian, M.; Hajek, M.; Jendelova, P.; Sykova, E. *Stem Cells Dev.* **2010**, *19* (10), 1535–46.
92. Cui, F. Z.; Tian, W. M.; Hou, S. P.; Xu, Q. Y.; Lee, I. S. *J. Mater. Sci.* **2006**, *17* (12), 1393–401.
93. Subramanian, A.; Krishnan, U. M.; Sethuraman, S. *J. Biomed. Sci.* **2009**, *16*, 108.
94. Wei, Y. T.; Tian, W. M.; Yu, X.; Cui, F. Z.; Hou, S. P.; Xu, Q. Y.; Lee, I. S. *Biomed Mater* **2007**, *2* (3), S142–6.
95. Dhoot, N. O.; Tobias, C. A.; Fischer, I.; Wheatley, M. A. *J. Biomed. Mater. Res., Part A* **2004**, *71* (2), 191–200.
96. Cui, F. Z. T. W. M.; Fan, Y. W.; Hou, S. P.; Xu, Q. Y.; Lee, I.-S. *J. Bioact. Compat. Polym.* **2003**, *18*, 413–432.
97. Wang, X.; et al. *Interface* **2012**, *2* (3), 278–291.
98. Hahn, S. K.; Jelacic, S.; Maier, R. V.; Stayton, P. S.; Hoffman, A. S. *J. Biomater. Sci., Polym. Ed.* **2004**, *15* (9), 1111–9.
99. Tian, W. M.; Hou, S. P.; Ma, J.; Zhang, C. L.; Xu, Q. Y.; Lee, I. S.; Li, H. D.; Spector, M.; Cui, F. Z. *Tissue Eng.* **2005**, *11* (3-4), 513–25.
100. Fang, J. Y.; Chen, J. P.; Leu, Y. L.; Hu, J. W. *Eur. J. Pharm. Biopharm.* **2008**, *68* (3), 626–36.
101. Kim, M. R.; Park, T. G. *J. Controlled Release* **2002**, *80* (1-3), 69–77.

102. Wei, Y. T.; He, Y.; Xu, C. L.; Wang, Y.; Liu, B. F.; Wang, X. M.; Sun, X. D.; Cui, F. Z.; Xu, Q. Y. *J. Biomed. Mater. Res., Part B* **2010**, *95* (1), 110–7.
103. Benedetti, L.; Cortivo, R.; Berti, T.; Berti, A.; Pea, F.; Mazzo, M.; Moras, M.; Abatangelo, G. *Biomaterials* **1993**, *14* (15), 1154–60.
104. Burdick, J. A.; Chung, C.; Jia, X.; Randolph, M. A.; Langer, R. *Biomacromolecules* **2005**, *6* (1), 386–91.
105. Baier, Leach, J.; Bivens, K. A.; Patrick, C. W., Jr.; Schmidt, C. E. *Biotechnol. Bioeng.* **2003**, *82* (5), 578–89.
106. Segura, T.; Anderson, B. C.; Chung, P. H.; Webber, R. E.; Shull, K. R.; Shea, L. D. *Biomaterials* **2005**, *26* (4), 359–71.
107. Zheng Shu, X.; Liu, Y.; Palumbo, F. S.; Luo, Y.; Prestwich, G. D. *Biomaterials* **2004**, *25* (7-8), 1339–48.
108. Shu, X. Z.; Liu, Y.; Palumbo, F.; Prestwich, G. D. *Biomaterials* **2003**, *24* (21), 3825–34.
109. Nisbet, D. R.; Crompton, K. E.; Horne, M. K.; Finkelstein, D. I.; Forsythe, J. S. *J. Biomed. Mater. Res., Part B* **2008**, *87* (1), 251–63.
110. Xu, X. M.; Guenard, V.; Kleitman, N.; Bunge, M. B. *J. Comp. Neurol.* **1995**, *351* (1), 145–60.
111. Woerly, S.; Doan, V. D.; Sosa, N.; de Vellis, J.; Espinosa-Jeffrey, A. *J. Neurosci. Res.* **2004**, *75* (2), 262–72.
112. Ma, P. X.; Zhang, R. *J. Biomed. Mater. Res.* **1999**, *46* (1), 60–72.
113. Xing, X.; Wang, Y.; Li, B. *Opt. Express* **2008**, *16* (14), 10815–22.
114. McKenzie, J. L.; Waid, M. C.; Shi, R.; Webster, T. J. *Biomaterials* **2004**, *25* (7-8), 1309–17.
115. Yang, F.; Murugan, R.; Wang, S.; Ramakrishna, S. *Biomaterials* **2005**, *26* (15), 2603–10.
116. Dzenis, Y. *Science* **2004**, *304* (5679), 1917–9.
117. Yoshii, S.; Oka, M. *J. Biomed. Mater. Res.* **2001**, *56* (3), 400–5.
118. Ngo, T. T.; Waggoner, P. J.; Romero, A. A.; Nelson, K. D.; Eberhart, R. C.; Smith, G. M. *J. Neurosci. Res.* **2003**, *72* (2), 227–38.
119. Schnell, E.; Klinkhammer, K.; Balzer, S.; Brook, G.; Klee, D.; Dalton, P.; Mey, J. *Biomaterials* **2007**, *28* (19), 3012–25.
120. Corey, J. M.; Lin, D. Y.; Mycek, K. B.; Chen, Q.; Samuel, S.; Feldman, E. L.; Martin, D. C. *J. Biomed. Mater. Res., Part A* **2007**, *83* (3), 636–45.
121. Wang, H. B.; Mullins, M. E.; Cregg, J. M.; Hurtado, A.; Oudega, M.; Trombley, M. T.; Gilbert, R. J. *J. Neural Eng.* **2009**, *6* (1), 016001.
122. Hartgerink, J. B. E; Stupp, S. *Proc. Natl. Acad. Sci. U.S.A.* **2002**, *99* (8), 5133–5138.
123. Seidlits, S. K.; Lee, J. Y.; Schmidt, C. E. *Nanomedicine (London)* **2008**, *3* (2), 183–99.
124. Horii, A.; Wang, X.; Gelain, F.; Zhang, S. *PloS One* **2007**, *2* (2), e190.
125. Tysseling-Mattiace, V. M.; Sahni, V.; Niece, K. L.; Birch, D.; Czeisler, C.; Fehlings, M. G.; Stupp, S. I.; Kessler, J. A. *J. Neurosci.* **2008**, *28* (14), 3814–23.
126. Xu, H.; Shao, Z.; Wu, Y.; Deng, C.; Yu, X.; Ding, F.; Zhang, B.; Xu, W. *Chin. J. Biotechnol. (Beijing, China, English Edition)* **2009**, *25* (2), 292–8.

127. Wu, B.; Zheng, Q.; Wu, Y.; Guo, X.; Zou, Z. *J. Huazhong Univ. Sci. Technol., Med. Sci.* **2010**, *30* (2), 178–82.
128. Wang, Y. Y.; Lu, L. X.; Feng, Z. Q.; Xiao, Z. D.; Huang, N. P. *Biomed. Mater.* **2010**, *5* (5), 054112.
129. Paletta, J. R.; Bockelmann, S.; Walz, A.; Theisen, C.; Wendorff, J. H.; Greiner, A.; Fuchs-Winkelmann, S.; Schofer, M. D. *J. Mater. Sci.: Mater. Med.* **2010**, *21* (4), 1363–9.
130. Silva, G. A.; Czeisler, C.; Niece, K. L.; Beniash, E.; Harrington, D. A.; Kessler, J. A.; Stupp, S. I. *Science* **2004**, *303* (5662), 1352–5.
131. Holmes, T. C.; de Lacalle, S.; Su, X.; Liu, G.; Rich, A.; Zhang, S. *Proc. Natl. Acad. Sci. U.S.A.* **2000**, *97* (12), 6728–33.
132. Blesch, A.; Lu, P.; Tuszynski, M. H. *Brain Res. Bull.* **2002**, *57* (6), 833–8.
133. Ernsberger, U. *Cell Tissue Res.* **2009**, *336* (3), 349–84.
134. Bregman, B. S.; Coumans, J. V.; Dai, H. N.; Kuhn, P. L.; Lynskey, J.; McAtee, M.; Sandhu, F. *Prog. Brain Res.* **2002**, *137*, 257–73.
135. Gage, F. H.; Coates, P. W.; Palmer, T. D.; Kuhn, H. G.; Fisher, L. J.; Suhonen, J. O.; Peterson, D. A.; Suhr, S. T.; Ray, J. *Proc. Natl. Acad. Sci. U.S.A.* **1995**, *92* (25), 11879–83.
136. Fricker, R. A.; Carpenter, M. K.; Winkler, C.; Greco, C.; Gates, M. A.; Bjorklund, A. *J. Neurosci.* **1999**, *19* (14), 5990–6005.
137. Herrera, D. G.; Garcia-Verdugo, J. M.; Alvarez-Buylla, A. *Ann. Neurol.* **1999**, *46* (6), 867–77.
138. Shihabuddin, L. S.; Horner, P. J.; Ray, J.; Gage, F. H. *J. Neurosci.* **2000**, *20* (23), 8727–35.
139. Chow, S. Y.; Moul, J.; Tobias, C. A.; Himes, B. T.; Liu, Y.; Obrocka, M.; Hodge, L.; Tessler, A.; Fischer, I. *Brain Res.* **2000**, *874* (2), 87–106.
140. Enzmann, G. U.; Benton, R. L.; Talbott, J. F.; Cao, Q.; Whittemore, S. R. *J. Neurotrauma* **2006**, *23* (3-4), 479–95.
141. Cao, Q. L.; Zhang, Y. P.; Howard, R. M.; Walters, W. M.; Tsoulfas, P.; Whittemore, S. R. *Exp. Neurol.* **2001**, *167* (1), 48–58.
142. Widenfalk, J.; Lundstromer, K.; Jubran, M.; Brene, S.; Olson, L. *J. Neurosci.* **2001**, *21* (10), 3457–75.
143. Novikova, L. N.; Novikov, L. N.; Kellerth, J. O. *J. Comp. Neurol.* **2002**, *452* (3), 255–63.
144. Bradbury, E. J.; Khemani, S.; Von, R.; King; Priestley, J. V.; McMahon, S. B. *Eur. J. Neurosci.* **1999**, *11* (11), 3873–83.
145. Hiebert, G. W.; Khodarahmi, K.; McGraw, J.; Steeves, J. D.; Tetzlaff, W. *J. Neurosci. Res.* **2002**, *69* (2), 160–8.
146. Grill, R. J.; Blesch, A.; Tuszynski, M. H. *Exp. Neurol.* **1997**, *148* (2), 444–52.
147. Menei, P.; Montero-Menei, C.; Whittemore, S. R.; Bunge, R. P.; Bunge, M. B. *Eur. J. Neurosci.* **1998**, *10* (2), 607–21.
148. Lu, P.; Jones, L. L.; Snyder, E. Y.; Tuszynski, M. H. *Exp. Neurol.* **2003**, *181* (2), 115–29.
149. Jin, Y.; Fischer, I.; Tessler, A.; Houle, J. D. *Exp. Neurol.* **2002**, *177* (1), 265–75.
150. Tuszynski, M. H.; Murai, K.; Blesch, A.; Grill, R.; Miller, I. *Cell Transplant.* **1997**, *6* (3), 361–8.

151. Grill, R.; Murai, K.; Blesch, A.; Gage, F. H.; Tuszynski, M. H. *J. Neurosci.* **1997**, *17* (14), 5560–72.

152. Tuszynski, M. H.; Grill, R.; Jones, L. L.; Brant, A.; Blesch, A.; Low, K.; Lacroix, S.; Lu, P. *Exp. Neurol.* **2003**, *181* (1), 47–56.

153. Yick, L. W.; Cheung, P. T.; So, K. F.; Wu, W. *Exp. Neurol.* **2003**, *182* (1), 160–8.

154. Krewson, C. E.; Saltzman, W. M. *Brain Res.* **1996**, *727* (1-2), 169–81.

155. Patapoutian, A.; Reichardt, L. F. *Curr. Opin. Neurobiol.* **2001**, *11* (3), 272–80.

156. Babensee, J. E.; McIntire, L. V.; Mikos, A. G. *Pharm. Res.* **2000**, *17* (5), 497–504.

157. Patil, S. D.; Papadimitrakopoulos, F.; Burgess, D. J. *Diabetes Technol. Ther.* **2004**, *6* (6), 887–97.

158. Beer, H. D.; Fassler, R.; Werner, S. *Vitam. Horm.* **2000**, *59*, 217–39.

159. Norton, L. W.; Tegnell, E.; Toporek, S. S.; Reichert, W. M. *Biomaterials* **2005**, *26* (16), 3285–97.

160. Schubert, D.; Dargusch, R.; Raitano, J.; Chan, S. W. *Biochem. Biophys. Res. Commun.* **2006**, *342* (1), 86–91.

161. Das, M.; Patil, S.; Bhargava, N.; Kang, J. F.; Riedel, L. M.; Seal, S.; Hickman, J. J. *Biomaterials* **2007**, *28* (10), 1918–25.

162. Reddy, M. K.; Wu, L.; Kou, W.; Ghorpade, A.; Labhasetwar, V. *Appl. Biochem. Biotechnol.* **2008**, *151* (2-3), 565–77.

163. Kang, C. E.; Baumann, M. D.; Tator, C. H.; Shoichet, M. S. *Cells Tissues Organs* **2012**.

164. Stanwick, J. C.; Baumann, M. D.; Shoichet, M. S. *J. Controlled Release* **2012**, *160* (3), 666–75.

165. Matsumoto, K.; Sato, C.; Naka, Y.; Kitazawa, A.; Whitby, R. L.; Shimizu, N. *J. Biosci. Bioeng.* **2007**, *103* (3), 216–20.

166. Yoo, J. W.; Irvine, D. J.; Discher, D. E.; Mitragotri, S. *Nat. Rev. Drug Discovery* **2011**, *10* (7), 521–35.

167. Tsai, R. K.; Discher, D. E. *J Cell Biol.* **2008**, *180* (5), 989–1003.

168. Hinds, K. A.; Hill, J. M.; Shapiro, E. M.; Laukkanen, M. O.; Silva, A. C.; Combs, C. A.; Varney, T. R.; Balaban, R. S.; Koretsky, A. P.; Dunbar, C. E. *Blood* **2003**, *102* (3), 867–72.

169. Guzman, R.; Uchida, N.; Bliss, T. M.; He, D.; Christopherson, K. K.; Stellwagen, D.; Capela, A.; Greve, J.; Malenka, R. C.; Moseley, M. E.; Palmer, T. D.; Steinberg, G. K. *Proc. Natl. Acad. Sci. U.S.A.* **2007**, *104* (24), 10211–6.

170. Jendelova, P.; Herynek, V.; Urdzikova, L.; Glogarova, K.; Kroupova, J.; Andersson, B.; Bryja, V.; Burian, M.; Hajek, M.; Sykova, E. *J. Neurosci. Res.* **2004**, *76* (2), 232–43.

171. Ahrens, E. T.; Flores, R.; Xu, H.; Morel, P. A. *Nat. Biotechnol.* **2005**, *23* (8), 983–7.

172. Bulte, J. W.; Douglas, T.; Witwer, B.; Zhang, S. C.; Strable, E.; Lewis, B. K.; Zywicke, H.; Miller, B.; van Gelderen, P.; Moskowitz, B. M.; Duncan, I. D.; Frank, J. A. *Nat. Biotechnol.* **2001**, *19* (12), 1141–7.

173. Song, M.; Moon, W. K.; Kim, Y.; Lim, D.; Song, I. C.; Yoon, B. W. *Korean J. Radiol.* **2007**, *8* (5), 365–71.
174. Kataoka, K.; Suzuki, Y.; Kitada, M.; Ohnishi, K.; Suzuki, K.; Tanihara, M.; Ide, C.; Endo, K.; Nishimura, Y. *J. Biomed. Mater. Res.* **2001**, *54* (3), 373–84.
175. Freier, T.; Montenegro, R.; Shan Koh, H.; Shoichet, M. S. *Biomaterials* **2005**, *26* (22), 4624–32.
176. Suzuki, Y.; Kitaura, M.; Wu, S.; Kataoka, K.; Suzuki, K.; Endo, K.; Nishimura, Y.; Ide, C. *Neurosci. Lett.* **2002**, *318* (3), 121–4.
177. Nisbet, D. R.; Crompton, K. E.; Hamilton, S. D.; Shirakawa, S.; Prankerd, R. J.; Finkelstein, D. I.; Horne, M. K.; Forsythe, J. S. *Biophys. Chem* **2006**, *121* (1), 14–20.
178. Shirakawa, M.; Yamatoya, K.; Nishinari, K. *Food Hydrocolloids* **1998**, *12* (1), 25–28.
179. Kobayashi, Y.; Hoshi, T.; Anzai, J. *Chem. Pharm. Bull.* **2001**, *49* (6), 755–7.
180. Tate, M. C.; Shear, D. A.; Hoffman, S. W.; Stein, D. G.; LaPlaca, M. C. *Biomaterials* **2001**, *22* (10), 1113–23.
181. Wells, M. R.; Kraus, K.; Batter, D. K.; Blunt, D. G.; Weremowitz, J.; Lynch, S. E.; Antoniades, H. N.; Hansson, H. A. *Exp. Neurol.* **1997**, *146* (2), 395–402.
182. Seckel, B. R.; Jones, D.; Hekimian, K. J.; Wang, K. K.; Chakalis, D. P.; Costas, P. D. *J. Neurosci. Res.* **1995**, *40* (3), 318–24.
183. Chenite, A.; Chaput, C.; Wang, D.; Combes, C.; Buschmann, M. D.; Hoemann, C. D.; Leroux, J. C.; Atkinson, B. L.; Binette, F.; Selmani, A. *Biomaterials* **2000**, *21* (21), 2155–61.
184. Nishimura, K.; Nishimura, S.; Seo, H.; Nishi, N.; Tokura, S.; Azuma, I. *J. Biomed. Mater. Res.* **1986**, *20* (9), 1359–72.
185. Peluso, G.; Petillo, O.; Ranieri, M.; Santin, M.; Ambrosio, L.; Calabro, D.; Avallone, B.; Balsamo, G. *Biomaterials* **1994**, *15* (15), 1215–20.
186. Crompton, K. E.; Tomas, D.; Finkelstein, D. I.; Marr, M.; Forsythe, J. S.; Horne, M. K. *J. Mater. Sci., Mater. Med.* **2006**, *17* (7), 633–9.
187. Tominaga, M.; Kamo, A.; Tengara, S.; Ogawa, H.; Takamori, K. *Br. J. Dermatol.* **2009**, *161* (5), 1028–37.
188. Toman, R. E.; Payne, S. G.; Watterson, K. R.; Maceyka, M.; Lee, N. H.; Milstien, S.; Bigbee, J. W.; Spiegel, S. *The J. Cell Biol.* **2004**, *166* (3), 381–92.
189. Ferri, R. T.; Levitt, P. *Development* **1995**, *121* (4), 1151–60.
190. Yu, T. T.; Shoichet, M. S. *Biomaterials* **2005**, *26* (13), 1507–14.
191. Giannetti, S.; Lauretti, L.; Fernandez, E.; Salvinelli, F.; Tamburrini, G.; Pallini, R. *Neurol. Res.* **2001**, *23* (4), 405–9.
192. Tsai, E. C.; Dalton, P. D.; Shoichet, M. S.; Tator, C. H. *J. Neurotrauma* **2004**, *21* (6), 789–804.
193. Kapur, T. A.; Shoichet, M. S. *J. Biomater. Sci., Polym. Ed.* **2003**, *14* (4), 383–94.
194. Moore, K.; MacSween, M.; Shoichet, M. *Tissue Eng.* **2006**, *12* (2), 267–78.
195. Gunn, J. W.; Turner, S. D.; Mann, B. K. *J. Biomed. Mater. Res., Part A* **2005**, *72* (1), 91–7.

196. Piantino, J.; Burdick, J. A.; Goldberg, D.; Langer, R.; Benowitz, L. I. *Exp. Neurol.* **2006**, *201* (2), 359–67.
197. Ruoslahti, E.; Pierschbacher, M. D. *Science* **1987**, *238* (4826), 491–7.
198. Iwamoto, Y.; Robey, F. A.; Graf, J.; Sasaki, M.; Kleinman, H. K.; Yamada, Y.; Martin, G. R. *Science* **1987**, *238* (4830), 1132–4.
199. Tong, Y. W.; Shoichet, M. S. *Biomaterials* **2001**, *22* (10), 1029–34.
200. Tashiro, K.; Sephel, G. C.; Weeks, B.; Sasaki, M.; Martin, G. R.; Kleinman, H. K.; Yamada, Y. *J. Biol. Chem.* **1989**, *264* (27), 16174–82.
201. Graner, E.; Mercadante, A. F.; Zanata, S. M.; Forlenza, O. V.; Cabral, A. L.; Veiga, S. S.; Juliano, M. A.; Roesler, R.; Walz, R.; Minetti, A.; Izquierdo, I.; Martins, V. R.; Brentani, R. R. *Brain Res. Mol. Brain Res.* **2000**, *76* (1), 85–92.
202. Hager, G.; Pawelzik, H.; Kreutzberg, G. W.; Zieglgansberger, W. *Neuroscience* **1998**, *86* (4), 1145–54.
203. Kam, L.; Shain, W.; Turner, J. N.; Bizios, R. *Biomaterials* **2002**, *23* (2), 511–5.
204. Hama, H.; Hara, C.; Yamaguchi, K.; Miyawaki, A. *Neuron* **2004**, *41* (3), 405–15.

Downloaded by ILLINOIS STATE UNIV on December 8, 2012 | http://pubs.acs.org
Publication Date (Web): December 7, 2012 | doi: 10.1021/bk-2012-1119.ix002

# Subject Index

**A**

Adeno-associated virus, 73, 74*f*, 75*f*
Alternative surface receptor binding repertoire, 31
Antiseptic bandages, CNT applications, 160, 161*f*, 163*f*, 164*f*, 167*f*
Aspect ratios, bioconjugated AuNP, 111*f*
Aspirin
  mesoporous silica, 245, 247*f*, 248*f*, 249*t*
  zeolites, 242, 243*t*, 244*f*, 245*t*

**B**

Bacteria sensing, 109, 110*f*
  colorimetric, 111
  SERS assays, 116, 119*f*
  two-photon Rayleigh scattering assay, 115
Bactericidal agents
  bottom-up preparation, 139
    metal organic-framework disinfectants, 140, 141*f*
    nanoparticle disinfectants, 139, 140*f*
  chemical disinfectants, inhibition mechanism, 132, 134*f*
  disinfectant evaluation, 141
  disinfection science, 130
  first wave disinfectant, 131
  future trends, 148
  metal/transition metal oxide based disinfectants, inhibition mechanism, 136, 137*f*
  MOF disinfectants, 139
  MOF system, inhibition mechanism, 139
  overview, 129
  potency evaluation, 142, 143*f*, 144*f*
    first wave, 143
    second wave, 143
    third wave, 145, 145*f*, 146*f*
  published data, 146
  second wave, 135
  structural characterization, 141
  third wave, 137
β-glucan based drug delivery, 60
Bioactive molecule delivery, CNS injuries, 303
Biobarcode assay, 10*f*
Bioconjugated gold nanoparticle
  aspect ratios, 111*f*
  bacteria sensing, 109, 110*f*
  colorimetric bacteria sensing, 111
  laser irradiation time, MDRB killing, 122*t*
  overview, 107
  schematic representation, 108*s*, 112*s*, 113*f*, 114*f*, 117*f*
  selective bacteria killing, 119, 120*s*, 121*f*
  SERS assays, bacteria sensing, 116, 119*f*
  two-photon Rayleigh scattering assay, bacteria sensing, 115
  two-photon scattering intensity changes, 118*f*
Biosensors
  CNS injuries, 292
  electrochemical sensors, 263, 264*f*
  mechanical sensors, 267
  optical sensors, 268

**C**

Carbon nanotubes (CNT), 95
  applications
    antiseptic bandages, 160, 161*f*, 163*f*, 164*f*, 167*f*
    clot drying, 170, 170*f*, 171*f*
    electrical stimulation, 166
    keratinocytes, 166, 169*f*
    nanotoxicity, 159
    overview, 155
    wound healing biotechnology, 156
    wound monitoring, 168
  covalent functionalization, 96, 97*f*
  non-covalent functionalization, 96
Cell-array system, 202, 203*f*, 204*f*
Cell labeling, 193
Cell therapy, 192
Cell tracking, 193, 194*f*
Cellular functions, polysaccharide functionalized magnetic nanoparticles, 199, 201*f*
Central nervous system (CNS) injuries, nanobased technological applications
  bioactive molecule delivery, 303
  biosensors, 292
  diagnostic imaging, 293
  diagnostics, 291
  fiber-based scaffolds, 301
  modified hydrogels, 295, 297*t*, 299*f*, 301*f*

    molecular contrast agents, 293*f*
    nanoparticle carriers, 304
    nanotube carriers, 305
    neural implantation, 295*f*
    overview, 289
    pathology, 290
    peptide sequences, 300*t*
    transplanted cell labeling, 306
    treatments, 291, 294
Clot drying, CNT applications, 170, 170*f*, 171*f*
CNS injuries. *See* central nervous system (CNS) injuries, nanobased technological applications
CNT. *See* carbon nanotubes (CNT)
Cytotoxicity assessment, polysaccharide functionalized magnetic nanoparticles, 198, 199, 200*f*

D

DNA hybridization, 269*f*
DNAzymes, 272

E

Electrical stimulation, CNT applications, 166
Electrospun virus-polymer composite nanofibers, 32
Extracellular diagnostic applications, SNA, 8

F

Fiber-based scaffolds, 301

G

Gadolinium, polysaccharide functionalized magnetic nanoparticles, 201
Gene delivery systems, 273, 274*f*
    extracellular barriers, 279
    intracellular barriers, 279
    lipoplexes, 274
    polylipoplexes, 274
    polyplexes, 274
Gene expression, glyconanoparticle, 97, 98*f*
Glucan particles (GP)
    applications, 66
        adeno-associated virus, 73, 74*f*, 75*f*
        gold nanoparticles, 69, 70*f*
        magnetic iron oxide nanoparticles, 70, 71*f*, 72*f*
        quantum dots, 67, 67*f*, 68*f*, 69*f*
    β-glucan based drug delivery, 60
    nanoparticle design, drug delivery, 59
    nanoparticle loading strategies, 62
        encapsulated nanoparticles, 63, 64*f*
        nanoparticle binding, outer GP surface, 65, 66*f*
        in situ synthesis, 64, 65*f*
    overview, 57
Glyconanoparticle co-polymerization, 86
    emulsion polymerization, 86
    nanogels, 87
    radical polymerization, 86
Glyconanoparticles
    characterization, 98
    CNT, 95
        covalent functionalization, 96, 97*f*
        non-covalent functionalization, 96
    co-polymerization, 86
        emulsion polymerization, 86
        nanogels, 87
        radical polymerization, 86
    gene expression, 97, 98*f*
    gold nanoparticles, 93, 93*f*, 94*f*
    liposomes, 88, 88*f*, 89*f*, 91*f*
    MNP, 94
    morphology characterization, 100
    overview, 81
    physicochemical techniques, 99
        electronic surface chemical analysis, 99
        hydrophobic interaction chromatography, 99
        protein interaction, 99
        zeta potential, 99
    plasmid DNA complexation, 84*f*
    polymeric, 84
        adsorption, 85
        incorporation, 85
    quantum dots, 92, 92*f*
    targeting efficacies, 100
    types, 84
Gold nanoparticles, 69, 70*f*, 93, 93*f*, 94*f*
    bioconjugated
        aspect ratios, 111*f*
        bacteria sensing, 109, 110*f*
        colorimetric bacteria sensing, 111
        laser irradiation time, MDRB killing, 122*t*
        overview, 107

Downloaded by ILLINOIS STATE UNIV on December 8, 2012 | http://pubs.acs.org
Publication Date (Web): December 7, 2012 | doi: 10.1021/bk-2012-1119.ix002

    - schematic representation, 108*s*, 112*s*, 113*f*, 114*f*, 117*f*
    - selective bacteria killing, 119, 120*s*, 121*f*
    - SERS assays, bacteria sensing, 116, 119*f*
    - two-photon Rayleigh scattering assay, bacteria sensing, 115
    - two-photon scattering intensity changes, 118*f*
- GP. *See* glucan particles (GP)

**H**

- Halloysite nanoclay
  - controlled release, 210, 212*f*, 223, 227*t*, 229*f*
    - delivery routes, 217, 218*t*
    - release mechanism, 213, 214*f*
    - targeting methods, 215, 216*f*
  - nanotechnology, drug release, 220, 222*f*
  - overview, 209
  - PVOH films, 231*f*
  - rhodamine B, 229*f*
  - rhodamine 6G, 229*f*
  - SEM, 224*f*
  - structural hierarchy, 224*f*
  - tetracycline hydrochloride mass release, 226*f*
  - tetracycline release, 232*f*

**I**

- Infrared dye-doped liposomes
  - laser-induced rupture, 179
    - characterization, 179
    - fluorometry, 180, 180*f*, 181*f*
    - liposome preparation, 179
  - NIR-sensitive, 177
    - design strategy, 178
    - NIR dye, 177, 178*f*
  - overview, 175
  - rupture imaging, 184, 186*f*
  - rupture mechanism, 182
    - Mie scattering, 182
    - pressure jump, 183, 185*f*
    - temperature jump, 182, 183*f*
- Intracellular applications, SNA, 11
- Iron, polysaccharide functionalized magnetic nanoparticles, 201

**K**

- Keratinocytes, CNT applications, 166, 169*f*

**L**

- Laser-induced rupture, liposomes, 179
  - characterization, 179
  - fluorometry, 180, 180*f*, 181*f*
  - liposome preparation, 179
- Laser irradiation time, MDRB killing, 122*t*
- Lipoplexes, 274
- Liposomes, 88, 88*f*, 89*f*, 91*f*. *See* infrared dye-doped liposomes
  - infrared dye-doped

**M**

- Magnetic iron oxide nanoparticles, 70, 71*f*, 72*f*
- Magnetic nanoparticles (MNP), 94
- M13 bacteriophage, 35*f*, 36*f*, 37*f*
- Mesoporous silica, nanomaterials development, 241, 246*f*, 251
  - aspirin, 245, 247*f*, 248*f*, 249*t*
- Mie scattering, 182
- MNP. *See* magnetic nanoparticles (MNP)
- Modified hydrogels, 295, 297*t*, 299*f*, 301*f*
- Morphology characterization, glyconanoparticle, 100
- MRI contrast agents, 194
- Multivalent nanosized vaccines, 26

**N**

- Nanoflare technology operation, SNA, 13*f*
- Nanoparticle design, drug delivery, 59
- Nanoparticle loading strategies, 62
  - encapsulated nanoparticles, 63, 64*f*
  - nanoparticle binding, outer GP surface, 65, 66*f*
  - in situ synthesis, 64, 65*f*
- Nanotemplates, virus particle assembly
  - 3D structure, 23*f*
  - genetic modifications, 26
    - alternative surface receptor binding repertoire, 31
    - multivalent nanosized vaccines, 26
    - RGD motif insertion, cell adhesion, 27, 27*t*
  - hierarchical assembly, 32

Downloaded by ILLINOIS STATE UNIV on December 8, 2012 | http://pubs.acs.org
Publication Date (Web): December 7, 2012 | doi: 10.1021/bk-2012-1119.ix002

Downloaded by ILLINOIS STATE UNIV on December 8, 2012 | http://pubs.acs.org
Publication Date (Web): December 7, 2012 | doi: 10.1021/bk-2012-1119.ix002

    - direct cell outgrowth, 34
    - electrospun virus-polymer composite nanofibers, 32
    - TMV alignment, 39, 41*f*
  - M13 bacteriophage, 35*f*, 36*f*, 37*f*
  - mammalian cells, 37*f*, 38*f*
  - non-collagenous matrix proteins, 31*t*
  - optical images, 36*f*
  - overview, 21
  - regioselective chemical modifications, 25
  - schematic illustration, 25*f*
  - self-assembly, capillary tube, 40*f*
  - TMV mutants, 28*f*, 29*f*, 30*f*
  - TMV-PVA nanofibers, 33*f*
- Neural implantation, 295*f*
- Non-collagenous matrix proteins, 31*t*
- Nucleic acids conjugated nanostructures
  - applications, 263
    - biosensors, 263
  - aptamers, 272
  - aptazymes, 272
  - binding, 260, 261*f*
  - combination, 260*f*
  - DNA hybridization, 269*f*
  - DNAzymes, 272
  - functionalization strategy, 261*f*
  - gene delivery systems, 273, 274*f*
    - extracellular barriers, 279
    - intracellular barriers, 279
    - lipoplexes, 274
    - polylipoplexes, 274
    - polyplexes, 274
  - magnetic nanoparticles, 266*f*
  - overview, 259
  - siRNA machinery, 278*f*

**P**

- Peptide-antisense, 15*f*
- Physicochemical techniques, glyconanoparticle, 99
  - electronic surface chemical analysis, 99
  - hydrophobic interaction chromatography, 99
  - protein interaction, 99
  - zeta potential, 99
- Plasmid DNA complexation, glyconanoparticle, 84*f*
- Polylipoplexes, 274
- Polymeric glyconanoparticle, 84
  - adsorption, 85
  - incorporation, 85
- Polyplexes, 274
- Polysaccharide functionalized magnetic nanoparticles
  - cell labeling, 193
  - cell therapy, 192
  - cell tracking, 193, 194*f*
  - cell-array system, 202, 203*f*, 204*f*
  - cellular functions, 199, 201*f*
  - cytotoxicity assessment, 198, 199, 200*f*
  - development process, 195, 197*f*
  - gadolinium use, 201
  - iron use, 201
  - MRI contrast agents, 194
  - overview, 191
  - regenerative medicine, 192
- Porous nanomaterials development, drug delivery
  - mesoporous silica, 241, 246*f*, 251
    - aspirin, 245, 247*f*, 248*f*, 249*t*
  - overview, 239
  - structures, 240*f*
  - zeolite vs. mesoporous silica, 250, 251*f*
  - zeolites, 241, 251
    - aspirin, 242, 243*t*, 244*f*, 245*t*
    - PET imaging, 252*f*, 253, 253*f*

**Q**

- Quantum dots, 67, 67*f*, 68*f*, 69*f*, 92*f*

**R**

- Regenerative medicine, 192
- Regioselective chemical modifications, 25
- Rhodamine B, 229*f*
- Rhodamine 6G, 229*f*

**S**

- Scanometric assay, SNA, 11*f*
- Scavenger receptor-mediated endocytosis, SNA, 7*f*
- Selective bacteria killing, bioconjugated AuNP, 119, 120*s*, 121*f*
- SiRNA machinery, 278*f*
- SNA. *See* spherical nucleic acids (SNA)
- SNA-AuNP. *See* spherical nucleic acid-gold nanoparticle conjugate (SNA-AuNP)
- Spherical nucleic acid-gold nanoparticle conjugate (SNA-AuNP), 3*f*, 8, 8*f*, 12*f*
- Spherical nucleic acids (SNA)

aggregates, 5*f*
architectures, 14
AuNP, 3*f*, 8, 8*f*, 12*f*
biobarcode assay, 10*f*
chemical properties, 4
dimensionality, 2
extracellular diagnostic applications, 8
intracellular applications, 11
nanoflare technology operation, 13*f*
overview, 1
peptide-antisense, 15*f*
physical properties, 4
scanometric assay, 11*f*
scavenger receptor-mediated endocytosis, 7*f*
structure, 3*f*
synthesis, 2
whole genome expression analysis, 8*f*

**T**

Targeting efficacies, glyconanoparticle, 100
Tetracycline hydrochloride mass release, 226*f*
TMV alignment, 39, 41*f*
TMV mutants, 28*f*, 29*f*, 30*f*
TMV-PVA nanofibers, 33*f*
Transplanted cell labeling, 306
Two-photon scattering intensity changes, bioconjugated AuNP, 118*f*

**W**

Whole genome expression analysis, SNA, 8*f*
Wound healing biotechnology, CNT applications, 156
Wound monitoring, CNT applications, 168

**Z**

Zeolites, nanomaterials development, 241, 251
aspirin, 242, 243*t*, 244*f*, 245*t*
PET imaging, 252*f*, 253, 253*f*

Downloaded by ILLINOIS STATE UNIV on December 8, 2012 | http://pubs.acs.org
Publication Date (Web): December 7, 2012 | doi: 10.1021/bk-2012-1119.ix002